



Aalborg Universitet

AALBORG UNIVERSITY
DENMARK

Integration of a magnetocaloric heat pump in energy flexible buildings

Johra, Hicham

Publication date:
2018

Document Version
Publisher's PDF, also known as Version of record

[Link to publication from Aalborg University](#)

Citation for published version (APA):
Johra, H. (2018). *Integration of a magnetocaloric heat pump in energy flexible buildings*. Aalborg Universitetsforlag.

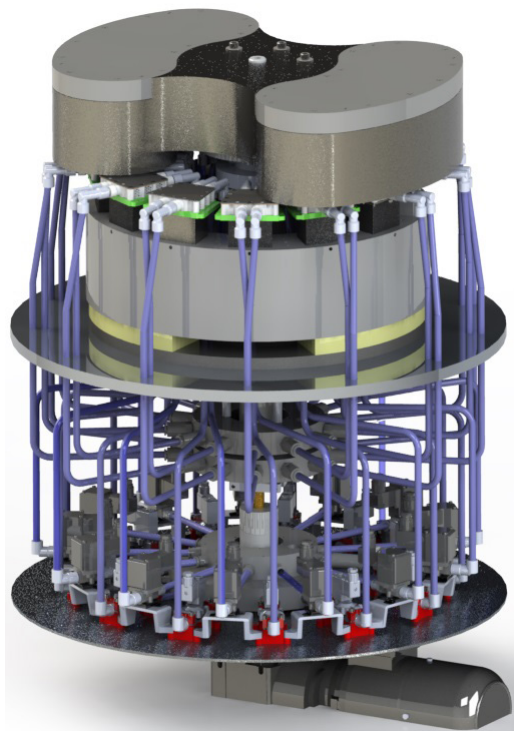
General rights

Copyright and moral rights for the publications made accessible in the public portal are retained by the authors and/or other copyright owners and it is a condition of accessing publications that users recognise and abide by the legal requirements associated with these rights.

- Users may download and print one copy of any publication from the public portal for the purpose of private study or research.
- You may not further distribute the material or use it for any profit-making activity or commercial gain
- You may freely distribute the URL identifying the publication in the public portal -

Take down policy

If you believe that this document breaches copyright please contact us at vbn@aub.aau.dk providing details, and we will remove access to the work immediately and investigate your claim.



INTEGRATION OF A MAGNETOCALORIC HEAT PUMP IN ENERGY FLEXIBLE BUILDINGS

**BY
HICHAM JOHRA**

DISSERTATION SUBMITTED 2018



AALBORG UNIVERSITY
DENMARK

INTEGRATION OF A MAGNETOCALORIC HEAT PUMP IN ENERGY FLEXIBLE BUILDINGS

by

Hicham Johra



AALBORG UNIVERSITY
DENMARK

Dissertation submitted

Dissertation submitted: March 2018

PhD supervisor: Prof. Per K. Heiselberg,
Aalborg University

PhD committee: Associate Professor Kjeld Svidt (chairman)
Aalborg University

Professor Dirk Saelens
KU Leuven

PhD Jaume Salom
IREC

PhD Series: Faculty of Engineering and Science, Aalborg University

Department: Department of Civil Engineering

ISSN (online): 2446-1636
ISBN (online): 978-87-7210-181-1

Published by:
Aalborg University Press
Langagervej 2
DK – 9220 Aalborg Ø
Phone: +45 99407140
aauf@forlag.aau.dk
forlag.aau.dk

© Copyright: Hicham Johra

Printed in Denmark by Rosendahls, 2018

CV

Personal Information

Name: Hicham Johra
Date of Birth: 07.11.1988
Nationality: French
Email: johra.hicham@gmail.com
Phone: +45 53 82 88 35



Education

Feb 2014 – Jan 2018 Ph.D. student, Civil Engineering Department, Aalborg University, Denmark

Sep 2010 – Aug 2011 Master of Engineering, Indoor Environment and Energy Engineering, Aalborg University, Denmark

Sep 2009 – Aug 2011 Master of Engineering, Civil Engineering and Urban Planning, National Institute of Applied Sciences of Rennes (INSA-Rennes), France

Sep 2006 – Aug 2009 Bachelor of Engineering, Civil Engineering and Urban Planning, National Institute of Applied Sciences of Rennes (INSA-Rennes), France

Professional Experience

Feb 2014 – Jan 2018 Ph.D. student, Civil Engineering Department, Aalborg University, Denmark

Aug 2011 – Feb 2014 Research assistant, Civil Engineering Department, Aalborg University, Denmark

Research Areas

Building energy flexibility

Magnetocaloric heat pumps

Heating systems

Building energy storage

Building thermal inertia

Phase change materials

Building thermodynamics

Building simulation

Energy efficient and sustainable buildings

ENGLISH SUMMARY

To prevent future energy crisis and tackle the problems of climate change, modern society must promote a radical evolution in our energy systems. The building sector, and in particular its heating needs, have clearly been identified as one of the main targets for the reduction of the global energy usage. In addition, buildings are a key actor for the development of renewable energy sources.

The main objective of this research study is to investigate and demonstrate the possibility of integrating a magnetocaloric heat pump in a single-family house under Danish weather conditions. Moreover, the study includes a numerical analysis to increase the understanding of the heating energy flexibility potential of residential buildings using thermal storage in the indoor environment.

The magnetocaloric heat pump is an innovative technology employing the magnetocaloric effect of certain materials in active magnetic regenerator thermodynamic cycles generating a heat transfer from a heat source to a heat sink. Numerical investigations performed in this study demonstrated that this device can be implemented in a low-energy residential building in Denmark and provide for its indoor space heating needs. When coupled to a ground source heat exchanger and a radiant under-floor heating system in a single hydronic loop, the magnetocaloric heat pump can operate at maximum capacity with an appreciable coefficient of performance of 3.93. A control strategy taking advantage of the building heating energy flexibility potential has been developed for optimum operation of the magnetocaloric heating system in a multi-zone dwelling. The thermal energy is stored in the indoor environment, which allows a shift and a concentration of the heating loads in time and thus a maximization of the heat pump full-load operation time. Consequently, the maximum average coefficient of performance of the magnetocaloric heating system ranges from 2.90 to 3.51, which is comparable with conventional vapour-compression heat pumps.

More generally, energy flexibility strategies can be employed to adapt the energy usage of buildings to the grid requirements. They can therefore help to control Smart Energy Grids dominated by intermittent renewable energy sources. Among these strategies, the thermal energy storage in the built environment by means of indoor temperature set point modulation was found to be a cost-effective solution. This research study focussed on heating energy flexibility potential of residential buildings in Denmark. This energy flexibility is defined here as the ability of a dwelling to shift its heating use in time by accumulating and retrieving thermal energy. The numerical analysis showed that even though effective thermal inertia determines the maximum heat storage capacity of the building, the insulation level of the envelope sets the storage efficiency and is the most important building parameter with respect to heating energy flexibility potential. Well-insulated

dwelling can thereby shift heating loads over long periods of time and poorly insulated buildings can only shift heating use over short periods of time. However, the latter can move a total amount of energy four times larger than high-insulation houses and thus have a larger impact on the energy grids.

This research project has also looked into the influence of additional thermal mass from indoor content items and furniture elements on the building thermodynamics and heating energy flexibility potential. Passive latent heat thermal storage solutions such as phase change materials integrated in wallboards or in furniture elements were found to significantly increase the total effective heat storage capacity of light-weight structure buildings. Moreover, it was demonstrated that assuming the indoor space to be an empty volume is not appropriate for dynamic energy simulations of houses with low structural thermal inertia. Transient thermal behaviour, building time constant, total heat storage capacity and therefore heating energy flexibility can be significantly influenced by the presence of indoor content and furniture in the built environment. To address that matter, this study reviewed the different methods for modelling items and furnishing elements present in the building indoor space. In addition, suggestions were made for choosing material characteristics of these indoor content elements.

DANSK RESUME

For at forhindre en fremtidig energikrise og håndtere problemerne ved klimaforandring er det moderne samfund nødt til at fremme en radikal evolution af vores energisystemer. Byggesektoren og i særdeleshed dennes varmebehov er blevet tydeligt identificeret som et af hovedmålene i reduktionen af det globale energiforbrug. Desuden er bygninger en hoveddaktør for udviklingen af vedvarende energikilder.

Hovedformålet for denne afhandling er at undersøge og påvise muligheden for at integrere en magnetokalorisk varmepumpe i et enfamiliehus under danske vejrforhold. Ydermere inkluderer afhandlingen en numerisk analyse for at øge forståelsen af potentialet for varmeenergifleksibilitet for boliger der bruger varmeopsamling i indeklimaet.

Den magnetokalorisk varmepumpe er en innovativ teknologi, der anvender en magnetokalorisk effekt af bestemte materialer i termodynamiske kredsløbsprocesser som benytter aktiv magnetisk regeneration og genererer varmeoverførsel fra en varmekilde til et varmeskjold. De numeriske undersøgelser der er udført i denne afhandling påviser, at dette apparat kan implementeres i en lavenergibolig i Danmark og sørge for dennes indendørs varmebehov. Når den er sammensluttet med et jordvarmeanlæg og et gulvopvarmningssystem i et enkelt vandbaseret kredsløb kan den magnetokalorisk varmepumpe operere på et maksimalt niveau med en mærkbar præstationskoefficient på 3.93. Der udvikles en kontrolstrategi der udnytter potentialet for varmeenergifleksibilitet i bygningen til optimal drift af det magnetokalorisk varmesystem i en multi-zone bolig. Den termiske energi opbevares i indeklimaet, hvilket muliggør et skift og en koncentration af varmebelastninger i tid og derved en maksimering af varmepumpens fuldlasttimer. Derfor rangerer den maksimale gennemsnits præstationskoefficient af de magnetokalorisk varmesystemer fra 2.90 til 3.51, hvilket er sammenligneligt med konventionelle varmepumper med dampkompression.

Mere generelt set, så kan strategierne for energifleksibilitet anvendes til tilpasse energiforbruget i bygninger til energinettets funktion krav. De kan derved hjælpe med kontrollen af Smart Energinet der domineres af irregulære vedvarende energikilder. Blandt disse strategier blev det afgjort, at den termiske energiopbevaring i det menneskeskabte miljø ved hjælp af modulering af indetemperatur setpunkt er en rentabel løsning. Denne afhandling fokuserede på potentialet for varmeenergifleksibilitet for boliger i Danmark. Denne energifleksibilitet defineres her som værende boligens evne til at skifte dens varmeforbrug i tid ved at akkumulere og hente termisk energi. Den numeriske analyse viste, at selv om effektiv termisk træghed bestemmer den maksimale varmeopbevaringsevnen i boligen, så fastsætter isolationsniveauet for enheden

effektiviteten af opbevaringen og er det vigtigste bygningsparameter hvad angår potentiale for varmeenergifleksibilitet. Boliger der er godt isolerede kan derved skifte varmebelastninger over lange tidsperioder og dårligt isolerede boliger kan kun ændre varmekonsum over korte tidsperioder. Dog kan det sidstnævnte flytte en total energimængde fire gang større end højisolerede huse og derved have større indvirkning på energinettet.

Denne afhandling har ligeledes undersøgt indflydelsen af yderligere termisk masse fra indendørs elementer og møbelementer på bygningens termodynamik og potentialet for varmeenergifleksibilitet. Løsninger til termisk opbevaring af passivt latent varme så som faseændrings materialer der er integrerede i vægplader eller i møbelementer viste sig at øge kapaciteten for den totale effektive varmeenergiopbevaring for bygninger af letvægtsstruktur. Ydermere blev det påvist, at hvis man antager indendørsarealet er af tom volumen er det ikke passende til dynamiske energisimulationer af huse med lav strukturelt termisk træghed. Kortvarig termisk opførsel, byggetidskonstant, total varmeopbevaringskapacitet and derved varmeenergifleksibilitet kan blive betydeligt påvirket af tilstedeværelsen af indendørs elementer og møbler i det menneskeskabte miljø. For at henvende til denne sag har afhandlingen inkluderet gennemgang af forskellige metoder for modellering af genstande og møbelementer i boligens indendørsareal. Desuden kommer der med forslag til valget af materialekarakteristika for disse indendørs elementer.

PREFACE

In the last year of my engineering studies at the National Institute of Applied Sciences of Rennes (France), I had the opportunity to come to Denmark. I was very enthusiastic about living in another place, exploring a different culture and getting to learn about a country which is well known for being one of the happiest in the world and highly committed to improve its sustainability. I obviously liked it very much as this one-year Erasmus exchange was followed by six years of work in Denmark.

I really enjoyed the work and life conditions, the team work and the problem based approach for learning at Aalborg University. Courses are engaging and students are very much implicated in research projects conducted by motivated professors. This made me gain a great interest in the world of scientific research. After obtaining my Master's Degree in Civil Engineering, I was given the chance to continue working at Aalborg University and start my professional scientific career as research assistant/laboratory engineer and then Ph.D. fellow.

We often hear that it is at the end of your Ph.D. that you know how you should have conducted your Ph.D. This is probably true. The scientific research is a long learning process. You actually never finish learning. That is what makes it so exiting. A Ph.D. project is so much more than just three or four years of academic work. For most of us, it is the first time that we are fully responsible for such a long term project. It is an intense life experience, an ambitious adventure, and definitely not a normal job. A lot of time and efforts are required. A lot of frustration and anxiety are generated. This feeling of being lost in the middle of an ocean of knowledge and scientific publications. The first year of Ph.D. is not easy. The second year is probably worst. Fortunately, after months of work, guided by my supervisor, supported by my friends and colleagues, I have managed to complete my scientific investigations and publish my first papers.

This Ph.D. thesis is a great accomplishment for me, and a major milestone in my scientific career. This Ph.D. project has challenged me and has deeply changed me (hopefully for the best). I have chosen the research field of energy efficiency for sustainable buildings because I truly think it can have a major positive impact on our society and our environment. I am very proud of contributing modestly to make our buildings more sustainable, comfortable and healthy, to develop innovative efficient energy systems, and therefore make this world a better place to be for the current and future generations.

ACKNOWLEDGEMENTS

The research study presented in this Ph.D. thesis was financed by the ENOVHEAT project, which is funded by the Innovation Fund Denmark (contract no 12-132673). The financial support is greatly appreciated. In addition, these scientific investigations were carried out partly within the framework of IEA EBC Annex 67 Energy Flexible Buildings.

Firstly, I would like to thank my supervisor, Prof. Per K. Heiselberg, for giving me the opportunity of undertaking this Ph.D. project, and for all these years of constructive and inspiring supervision and guidance. In addition, I would like to thank all the collaborators of the ENOVHEAT project, especially Konstantin Filonenko, Christian T. Veje, Tian Lei, Stefano Dall'Olio, Kurt Engelbrecht, Christian R.H. Bahl, Henrique Neves Bez and Andrea R. Insinga. Furthermore, I would like to express my sincere appreciation to all the participants of IEA EBC Annex 67 "Energy Flexible Buildings" project for sharing their knowledge with me. Major thanks are especially directed towards Jérôme Le Dréau for the fruitful discussions, help and collaborations. I would also like to thank Line Karlsen and Martin B. Østergaard for the pleasant collaborations we had.

I am very glad and thankful for all these years in the nice environment of Aalborg University, surrounded by kind and dedicated colleagues, always being supportive and friendly with good advice, help and interesting conversations. Thank you to all my colleagues from the Civil Engineering department and especially from the division of Architectural Engineering. Special thanks to Rasmus L. Jensen and Maria Alberdi-Pagola for all the support and help. My sincere appreciation also goes to all the secretarial staff and technical staff of the Civil Engineering Department, especially Lars, Henrik, Lasse, Mette, Pernille, Vivi, Linda and Anja.

Last, but not least I would like to thank my family from France and from Morocco, my mother, my father, my brother, my grandparents, all my friends from France, Denmark and all around the world, and my flatmates.

I had the chance to meet many amazing and inspiring people. One way or another, you all have impacted my life and have contributed to this Ph.D. project, to what I am today and where I am today. Thank you very much for that.

Cette thèse est dédiée à ma famille de France et du Maroc, à ma mère, à mon père, à mon frère, à mes grands-parents, à mes amis, à ce beau pays de France qui m'a vu naître, à cette merveilleuse Bretagne qui m'a vu grandir, et ce fantastique pays du Danemark qui m'a accueilli.

Hicham Jebra
Aalborg, 2018

A handwritten signature in blue ink, consisting of a stylized 'H' followed by a long horizontal stroke that extends to the right.

TABLE OF CONTENTS

Chapter 1. Introduction.....	23
1.1. General Background and problematics of the current energy situation	23
1.2. Building sector: a key target for a sustainable energy development strategy	24
1.3. ENOVHEAT project: development of an innovative magnetocaloric heat pump	25
1.4. Building energy flexibility	29
1.5. Objectives of the thesis	31
1.6. Thesis outline	32
Chapter 2. Literature review	33
2.1. Magnetocaloric heat pumps	33
2.1.1. Operation principle of the magnetocaloric heat pump	33
2.1.2. History of the magnetocaloric technology	38
2.2. Additional thermal mass of the indoor content / furniture and phase change materials for building thermal energy sotrage.....	39
2.2.1. Impact of the indoor content / furniture on the building thermodynamics and indoor environment	40
2.2.2. Modelling indoor content / furniture thermal mass	41
2.2.3. Phase change materials for building thermal energy storage in the indoor environment	45
Chapter 3. Magnetocaloric heat pump and building systems models	49
3.1. Characteristics of the magnetocaloric heat pump.....	49
3.2. Numerical modelling of the magnetocaloric heat pump	51
3.3. Building study cases.....	54
3.3.1. ENOVHEAT project study case for the integration of a magnetocaloric heat pump in houses	54
3.3.2. Building cases for the study of building energy flexibility in danish dwellings	57
3.4. Numerical modelling of the building systems.....	60
3.4.1. Multi-zone building model.....	60
3.4.2. Heating systems	62
3.4.3. Indoor content / furniture elements	64

3.4.4. Latent heat thermal energy storage.....	65
Chapter 4. Heating energy flexibility potential of residential buildings.....	67
4.1. Building energy flexibility index	68
4.2. Heat storage control strategy	70
4.3. Results and discussion.....	71
4.3.1. Impact of additional indoor thermal mass on the building time constant	71
4.3.2. Influence of the maximum activation time on the building energy flexibility	73
4.3.3. Impact of the building parameters on the energy flexibility.....	74
4.3.4. Impact of additional indoor thermal mass on the building energy flexibility	76
4.3.5. Parametric sensitivity analysis	77
4.4. Conclusion	80
Chapter 5. Integration of a magnetocaloric heat pump in residential buildings with energy flexibility control strategy.....	82
5.1. Implementation of the magnetocaloric heat pump in the hydronic heating system	82
5.2. Performance of the magnetocaloric heat pump with simple controller	83
5.3. Energy flexibility control strategy.....	88
5.4. Performance of the magnetocaloric heat pump with energy flexibility control strategy	90
5.5. Conclusion	95
Chapter 6. Conclusions of the thesis.....	97
Chapter 7. Future work.....	100
References.....	101
Publications for the thesis.....	111
Appendices.....	113

TABLE OF FIGURES

Figure 1-1: In few centuries from now, fossil fuels will be depleted and only renewable energy sources will be left [Courtesy of Vestas Wind Systems A/S].	23
Figure 1-2: Global renewable electricity production by region over the recent years: historical and projected (Courtesy of © OECD/IEA) [15].	24
Figure 1-3: Evolution of the building energy regulation in Denmark (the yearly space heating need is assessed with an indoor temperature set point of 20 °C) [21].	25
Figure 1-4: Logo of the ENOVHEAT project [28].	26
Figure 1-5: CAD model of the magnetocaloric heat pump prototype of the ENOVHEAT project: “MagQueen” [32].	28
Figure 1-6: Illustration (fictitious) of the mismatch between instantaneous power demand and renewable energy production (mostly wind power) in Denmark.	29
Figure 1-7: Example of demand side management strategy with peak shaving and load shifting.	30
Figure 2-1: Temperature – Entropy diagram of an ideal vapour-compression cycle.	33
Figure 2-2: Temperature – Entropy diagram of an active magnetic regenerator cycle.	34
Figure 2-3: Example of adiabatic temperature change due to the magnetocaloric effect (magnetization from 0 to 1 Tesla in gadolinium) [29]	35
Figure 2-4: Active magnetic regenerator cycle consisting of four processes: (b) adiabatic magnetization; (c) cold-to-hot blow; (d) adiabatic demagnetization; (e) hot-to-cold blow [31].	37
Figure 2-5: General categorization of phase change materials [67].	46
Figure 2-6: Compilation of phase change materials thermal properties found in the literature: latent heat of phase transition as function of temperature of phase transition [67].	47
Figure 3-1: Detailed description of the magnetocaloric heat pump prototype of the ENOVHEAT project: “MagQueen” (section view) [32].	49

Figure 3-2: CAD model of the two-pole magnet assembly. _____ 50

Figure 3-3: CAD model of the regenerator for the magnetocaloric heat pump prototype (dimensions are indicated in millimeters) [31]. _____ 50

Figure 3-4: Schematic of the hydronic circuit of the magnetocaloric heat pump prototype. _____ 51

Figure 3-5: Plan view of the house study case [21]. _____ 54

Figure 3-6: Integration of a conventional vapour-compression heat pump with ground source heat exchanger, hot water storage tank and water-based radiant under-floor heating system [21]. _____ 57

Figure 3-7: Example of a RC network for a wall construction element [21]. _____ 61

Figure 3-8: General scheme of the resistance network for the ϵ -NTU method [125] _____ 63

Figure 3-9: Enthalpy / temperature function for modelling phase change materials [21]. _____ 66

Figure 4-1: Example of indoor temperature set point modulation with price control and maximum activation time of 6 hours for low-insulation light structure house with radiator [151]. _____ 71

Figure 4-2: Change of building time constant with additional internal thermal mass [151]. _____ 72

Figure 4-3: Example of yearly indoor space heating use repartition as function of maximum activation time (light-weight structure low-insulation house with PCM wallboard) [151]. _____ 73

Figure 4-4: Building energy flexibility as function of maximum activation time (radiator: convective radiator; UFH: under-floor heating) [151]. _____ 74

Figure 4-5: Evolution of the building energy flexibility as function of the thermal inertia for different insulation levels and heating systems [151]. _____ 75

Figure 4-6: Change of building heating energy flexibility with additional indoor thermal mass (radiator heating system cases with maximum activation time of 24 hours) [151]. _____ 76

Figure 5-1: Integration of a magnetocaloric heat pump in single hydronic loop with ground source and under-floor heating system [31].	83
Figure 5-2: Heating power output and power usage of the magnetocaloric heat pump as function of fluid volumetric flow rate [31].	85
Figure 5-3: COP of the magnetocaloric heat pump and the entire heating system as function of the fluid volumetric flow rate [31].	85
Figure 5-4: Temperatures of the building system as function of time during the four-month heating test period [31].	86
Figure 5-5: Daily average COPs of the magnetocaloric heat pump as function of time during the four-month heating test period [31].	87
Figure 5-6: Example of heat storage strategy control for MCHP: (a) temperatures in the house (with and without heat storage strategy); (b) activation of the MCHP (with heat storage strategy); (c) fluid volumetric flow rate of the MCHP (with and without heat storage strategy); (d) COP of the MCHP (with and without heat storage strategy) [32].	89
Figure 5-7: Full-load operation time share of the MCHP during the four-month heating test period [32].	91
Figure 5-8: Box plot diagram of the heat pump COP as a function of heat storage temperature span and building thermal inertia (MCHP on the left, conventional vapour-compression heat pump on the right) [32].	93
Figure 5-9: Temperature variability (difference between 5th and 95th percentile of the house temperature) during the four-month heating test period (MCHP on the left, conventional vapour-compression heat pump on the right) [32].	94

TABLE OF TABLES

Table 2-1: Properties of the representative indoor content material categories [81].42

Table 3-1: Parameters of the building base case study [31]. _____ 55

Table 3-2: Main characteristics of the building cases for investigation of the heating energy flexibility potential [21]. _____ 59

Table 4-1: Significance ranking of the building parameters regarding heating energy flexibility [151]. _____ 77

Table 4-2: Sensitivity analysis of the additional indoor thermal mass parameters [151]. _____ 78

Table 4-3: Significance ranking of the additional thermal mass parameters regarding heating energy flexibility [151]. _____ 79

NOMENCLATURE-ABBREVIATIONS

A_c :	Cross sectional area [m ²]
a_s :	Specific surface area [m ² /m ³]
<i>AMR</i> :	Active magnetic regenerator
<i>ANOVA</i> :	Analysis of variance
c :	Specific heat capacity [J/kg.K]
c_H :	Specific heat capacity of a magnetocaloric material at constant magnetic field [J/kg.K]
<i>CAD</i> :	Computer-aided design
<i>CFD</i> :	Computational fluid dynamics
<i>COP</i> :	Coefficient of performance [-]
d_h :	Hydraulic diameter [m]
<i>DRY</i> :	Danish reference year weather data
F :	Building energy flexibility index [%]
<i>FDM</i> :	Finite difference method
<i>FVM</i> :	Finite volume method
<i>GSHE</i> :	Ground source heat exchanger
H :	Internal magnetic field [Tesla]
<i>HVAC</i> :	Heating ventilation and air conditioning
k :	Thermal conductivity [W/m.K]
<i>LHTES</i> :	Latent heat thermal energy storage

\dot{m}_f :	Fluid mass flow rate [kg/s]
<i>MCE</i> :	Magnetocaloric effect
<i>MCHP</i> :	Magnetocaloric heat pump
<i>MCM</i> :	Magnetocaloric material
<i>Nu</i> :	Nusselt number [-]
<i>P</i> :	Pressure [Pa]
<i>PCM</i> :	Phase change material
<i>PEX</i> :	Cross-linked polyethylene
<i>PI</i> :	Proportional Integral controller
<i>Q</i> :	Thermal power [W]
q_v :	Volumetric heat source [W/m ³]
<i>RC</i> :	Thermal Resistance-Capacitance
<i>RES</i> :	Renewable energy sources
<i>s</i> :	Specific entropy [J/K]
<i>t</i> :	Time [sec]
<i>T</i> :	Temperature [K]
<i>TABS</i> :	Thermally activated building system
<i>TES</i> :	Thermal energy storage
<i>U-tube</i> :	Pipe with a U-shape
<i>U-value</i> :	Thermal transmittance of a building element [W/m ² .K]
<i>UFH</i> :	Under-floor heating
<i>VCHP</i> :	Vapour-compression heat pump

W :	Power use [W]
x :	Axial position in the regenerator [m]

Greek symbols

$\Delta\delta$:	Finite control volume thickness [m]
Δt :	Simulation time step size [sec]
ε :	Porosity of the regenerator bed [%]
ε - NTU :	Effectiveness-Number of Transfer Unit
ρ :	Density [kg/m ³]

Other symbols

<i>%High</i> :	Percentage of the yearly thermal energy used during high energy price periods [%]
<i>%Medium</i> :	Percentage of the yearly thermal energy used during medium energy price periods [%]

Subscripts

<i>compressor</i> :	Compressor of the conventional vapour-compression heat pump
<i>disp</i> :	Axial dispersion
<i>f</i> :	Fluid coolant
<i>heating</i> :	Heating power delivered by the heat pump
<i>magnetic</i> :	Magnetic field generated by the two-pole magnet assembly
<i>motor</i> :	Motor driving the rotation of the rotor of the magnetocaloric heat pump

<i>pressureloss:</i>	Pressure losses in the hydronic circuit and in the regenerators
<i>pump:</i>	Hydraulic circulation pump
<i>ref:</i>	Reference case for the calculation of the building energy flexibility index
<i>s:</i>	Solid refrigerant magnetocaloric material
<i>stat:</i>	Static
<i>system:</i>	Entire heating system including heat pump, ground source and under-floor heating
<i>valve:</i>	Solenoid valves regulating the flow in the regenerators

CHAPTER 1. INTRODUCTION

1.1. GENERAL BACKGROUND AND PROBLEMATICS OF THE CURRENT ENERGY SITUATION

Following the coal-driven industrial revolution of the 19th century, the oil-fuelled machines radically changed the face of the world during the 20th century; reshaping our civilizations and economical systems. Unfortunately, the era of seemingly endless cheap fossil fuels is now over. If these carbonated combustibles have greatly contributed to the development and prosperity of the previous generations, they have now become the burden of the 21st century.

It has been well established that our addiction to fossil fuels causes climate change, global warming, sea level rising, ocean acidification, more occurrences of extreme weather event [1], various forms of pollution [2], and geopolitical tensions [3]. These result in increase of diseases [4], premature deaths [5], decline of food production [6][7], ecological and economical disasters [8], energy supply insecurity [9], massive migrations [10] and enhanced risks of armed conflicts [11].

Moreover, our planet is a finite volume and fossil fuels (including nuclear fissile fuels) will necessarily come to an end. If our societies keep the same enormous appetite for these energy resources, it is quite certain that they will be depleted within the next couple of centuries [12]. At that point, only renewable energy sources (RES) will be left, and countries still relying on fossil fuels will then inevitably be struck by a major energy crisis.



Figure 1-1: In few centuries from now, fossil fuels will be depleted and only renewable energy sources will be left [Courtesy of Vestas Wind Systems A/S].

However, the Earth's climate has already reached a tipping point. If the greenhouse gas emissions are not drastically reduced within the next few decades, dramatic and possibly irreversible climate changes will occur. We cannot postpone further the decarbonification of our energy systems without exposing our societies to pay a much greater cost in the near future [1].

In order to address all these problems and enable a brighter future for the upcoming generations, a radical paradigm shift is needed in our way of producing, transporting and using energy. Fortunately, policymakers are reaching global agreements [13] and financing research and development projects aiming for a large deployment of renewable energy sources. It is reassuring to observe that increasing public support is shown towards efficiency strategies intending to decrease our fossil fuel dependency and overall energy needs [14].

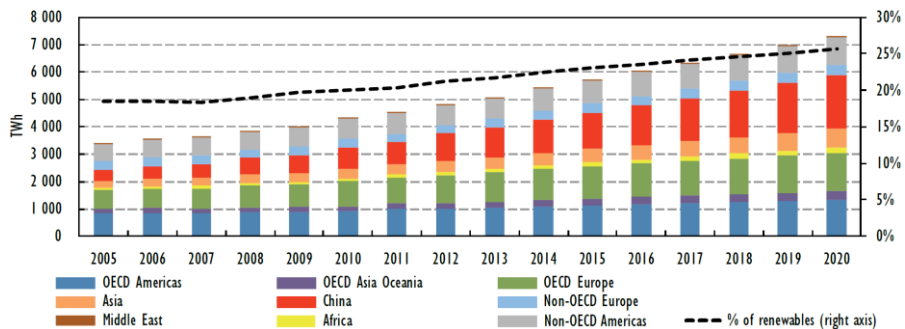


Figure 1-2: Global renewable electricity production by region over the recent years: historical and projected (Courtesy of © OECD/IEA) [15].

1.2. BUILDING SECTOR: A KEY TARGET FOR A SUSTAINABLE ENERGY DEVELOPMENT STRATEGY

The cleanest energy is the one you do not need to supply. Any long-term strategy for a transition towards low-carbon societies requires significant global energy savings.

In most countries, the building sector is the largest energy end-user. It accounts for nearly one-third of the worldwide final energy use and it is responsible for about one-third of the global CO₂ emissions [16]. In Europe, buildings are even more predominant: they represent more than 40% of the total final energy needs, followed by transportation with 33% [17]. Moreover, indoor space heating accounts for nearly 70% of the European building energy needs and a large share of it can be cut down [17]. The building sector has therefore been clearly identified as a key target for reaching essential energy and environmental objectives [18].

Buildings' envelope performance must be increased and efficiency of space heating systems and other heating/ventilation/air conditioning (HVAC) equipment must be improved to meet the goals of sustainable low-energy buildings with comfortable and healthy indoor environment. This is technically possible but it requires considerable investments, together with a serious implication and coordination of the policymakers and the different actors of the building sector. However, return on investment resulting from energy savings and healthy built environment are expected on the medium and long-term [16].

A general tightening of the building energy regulations towards the Zero Energy Building concept [19] can be observed for new constructions (see *Figure 1-3*). Nevertheless, the renewal of the building stock is only about 1% per year. In 2050, it is thus estimated that more than half of the current building stock will still be standing. It is therefore vital to conduct an extensive renovation campaign for improving the envelope performance of the existing buildings and swap conventional fossil fuel heating systems for RES [20].

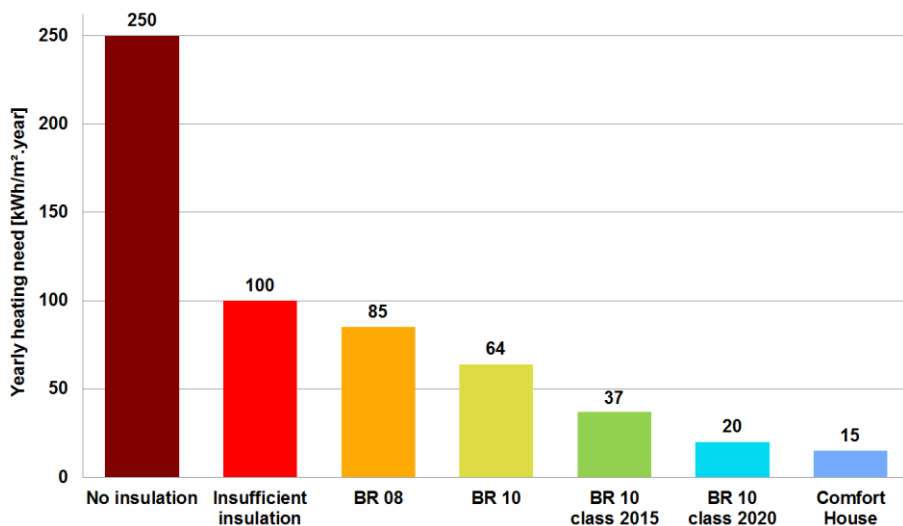


Figure 1-3: Evolution of the building energy regulation in Denmark (the yearly space heating need is assessed with an indoor temperature set point of 20 °C) [21].

1.3. ENOVHEAT PROJECT: DEVELOPMENT OF AN INNOVATIVE MAGNETOCALORIC HEAT PUMP

As mentioned before, major attention should be given to energy savings in heat production for buildings (indoor space heating and domestic hot water supply).

Studies have found that heat pumps are among the best heating supply solutions with regards to greenhouse gas emissions, energy efficiency, integration of RES and total costs for countries with heating dominated climate such as Denmark, Germany or the United Kingdom [22][23][24].

Heat pump systems are mechanical devices which transfer thermal energy from a cold reservoir with low exergy (heat source) to a warmer environment with higher exergy (heat sink). This heat transfer is performed by employing heating/cooling thermodynamic cycles (typically a vapour-compression cycle). Most of the conventional heat pumps are electrically driven and can operate with a high coefficient of performance (COP), usually ranging from 3 to 5 [25][26].

The great benefits of the heat pump technology have generated a large public interest. It became a key component of the energy development strategies in many countries. The heat pump market is therefore very vigorous with a rapid increase of installed units over the last decade and significant growth perspectives in the upcoming twenty years [27]. Consequently, industries and research groups strive to design new cost-effective technical solutions to market. In that sense, the ENOVHEAT project [28] aims at developing, building and testing the prototype of an innovative heat pump device based on the active magnetic regenerator (AMR) principle (see *Figure 1-5*). The heat transfer is performed here by cooling/heating thermodynamic cycles generated from the reversible magnetocaloric effect of the materials used as solid refrigerants (the magnetocaloric materials). Due to the reversible nature of the magnetocaloric effect, the AMR technology has great potential for high COP. Moreover, magnetocaloric devices have the advantage of a more silent operation, an absence of greenhouse or toxic gases, and the potentiality for recycling the magnets and the magnetocaloric materials (MCM) [29].



Figure 1-4: Logo of the ENOVHEAT project [28].

Magnetocaloric heat pumps (MCHP) have some undeniable assets. However, they have yet to prove their competitiveness in building applications compared to mature technologies such as conventional vapour-compression heat pumps (VCHP) [30].

The main objective of the ENOVHEAT project is thus to demonstrate that a MCHP can be integrated in a building and provide for its heating needs.

Residential buildings account for 75% of the total European building stock surface area, among which 64% are single-family houses [17]. Therefore, the ENOVHEAT project focusses on developing a machine which can supply the necessary heat power to sustain indoor space conditioning of low-energy single-family dwellings under Danish weather conditions. The MCHP is thus solely used for indoor space heating, excluding domestic hot water production. This restriction is due to the fact that domestic hot water production requires a higher temperature span, which is out of the scope of the current project. Nevertheless, the ENOVHEAT project is the first one aiming at demonstrating the viability of the AMR devices for the heat production in buildings. It is an encouraging starting point for further development of this promising technology [31].

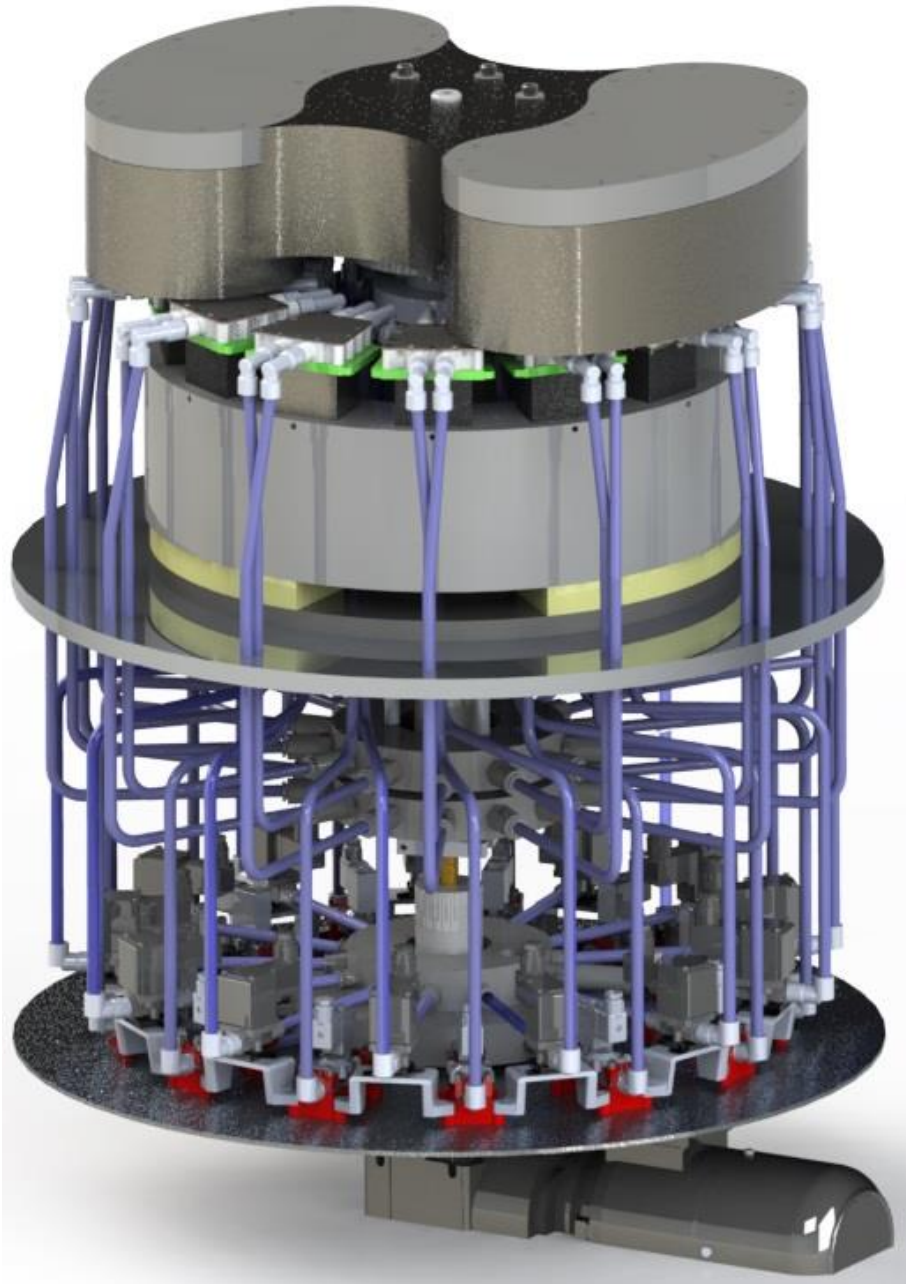


Figure 1-5: CAD model of the magnetocaloric heat pump prototype of the ENOVHEAT project: “MagQueen” [32].

1.4. BUILDING ENERGY FLEXIBILITY

Concerning the energy production, a global trend emerges among the current and future national energy development strategies. Most countries in the world have planned a large expansion of their RES. A vast deployment of wind and photovoltaic power is foreseen in numerous European countries [32]. In Denmark, for instance, wind power is expected to cover 50% of the annual energy needs in 2020. In 2050, Denmark aims at being completely fossil fuel free and covering its entire energy needs with RES [34].

Apart from hydroelectric dams, the main problems of RES are the intermittence of their production and their lack of power modulation. The important expansion of these intermittent RES may thus induce a serious mismatch between instantaneous energy use and production (see *Figure 1-6*). This can significantly compromise the stability of electrical grids, causing overloading of power lines and transformers, or provoking harmful voltage and frequency fluctuations [35]. Similarly, district heating networks with a large share of intermittent RES can also suffer from these instabilities [36].

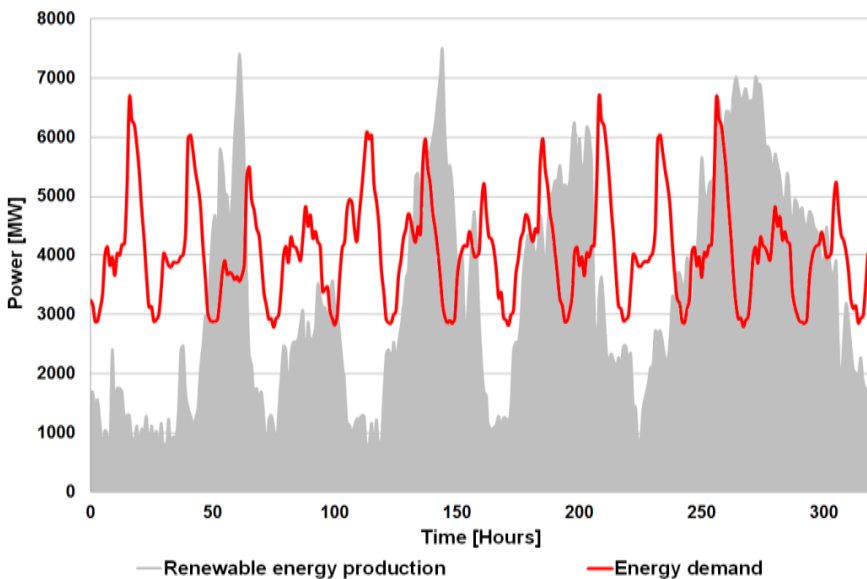


Figure 1-6: Illustration (fictitious) of the mismatch between instantaneous power demand and renewable energy production (mostly wind power) in Denmark.

To tackle the aforementioned problems, increasing efforts have been dedicated to develop a Smart Energy Grid technology able to bear a 100% renewable energy system [37]. The coupling of electrical grids, thermal grids, gas grids, various energy storage solutions, electric transportations, industries and buildings within a smart metering and control network system can allow a fine management of the energy demand and RES-dominated production. Demand side management strategies can thus help to reduce the mismatch between instantaneous power demand and renewable energy production. Diverse kinds of energy storage system and load shifting solution can be ingeniously employed to accumulate or overconsume energy when there is an overproduction of it, and retrieve or conserve energy when there is a shortage of it. Peak shaving and load shifting can be performed accordingly to modulate the power usage profile and make it fit with the requirements of the energy grids (see *Figure 1-7*) [38].

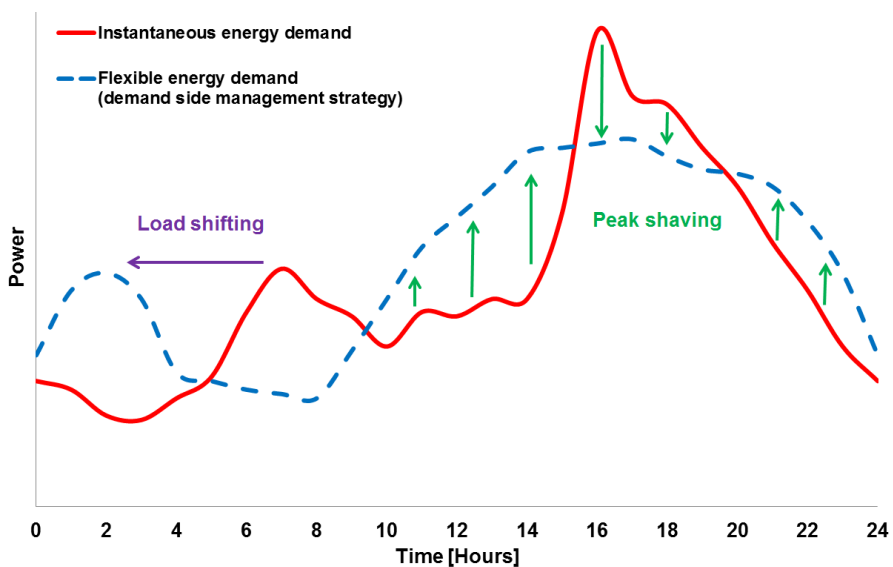


Figure 1-7: Example of demand side management strategy with peak shaving and load shifting.

In that context, the building sector operates a paradigm shift. As mentioned before, it is the largest energy end-user. In addition, buildings can modulate their own energy usage to a certain extent. Consequently, the building stock should not be perceived as a simple passive consumer anymore, but on the contrary, it should be considered as a major interactive actor. It has great potential for adjusting and shifting its power use, but also storing and sometimes producing energy (building prosumers), in order to facilitate the management of the grids and compensate for the RES intermittence

[38]. Buildings can reshape their energy use profile by means of thermal storage in hot water accumulation tanks or in the indoor environment and building structure [39], electricity storage in the batteries of electric vehicles and charging scheduling [40], power output adjustment of HVAC systems, or electrical plug-load shifting [41]. These various demand side management measures are commonly denominated as “Building Energy Flexibility” strategies [38].

1.5. OBJECTIVES OF THE THESIS

The framework of the ENOVHEAT project includes several different work-packages focusing on particular aspects of the magnetocaloric heat pump technology. Various theoretical, numerical and experimental investigations have been carried out on the following topics:

- Development, characterization and modelling of the magnetocaloric effect in new magnetocaloric material compounds.
- Design of optimum permanent magnet assemblies.
- Enhancement of the heat transfer between the magnetocaloric material and the coolant fluid in the active magnetic regenerator.
- Development and test of the general design of the entire magnetocaloric heat pump.
- Modelling of the heat pump system and study of its different configurations.
- Integration of the magnetocaloric device in a building as a heating system with efficient control strategy.

Although all the work-packages are connected and collaborating closely with each other, the research study presented in this thesis is targeting the last aforementioned topic. This Ph.D. project especially addressed the challenges related to the integration of the ENOVHEAT magnetocaloric heat pump in a low-energy house in Denmark, and the development of an efficient control strategy using the heating energy flexibility potential of the building.

The main objective of this research study is to numerically demonstrate that this magnetocaloric device can be used as an efficient space heating solution for single-family Danish houses with good insulation level. Investigations are carried out to determine how to integrate and operate this innovative heat pump into a house heating system, and what is the impact of the building design on the MCHP performance. In addition, researches are conducted to increase knowledge about the influence of the main building parameters on the heating energy flexibility potential of a dwelling using thermal storage in the indoor environment.

1.6. THESIS OUTLINE

Chapter 1 exposes the background and challenges of this research topic and the objectives of this Ph.D. research project.

Chapter 2 provides a literature review regarding the operating principles of the magnetocaloric heat pump technology and the influence and modelling technics of the indoor content thermal mass for building thermal storage.

Chapter 3 presents the different models of the magnetocaloric heat pump, HVAC and building systems used in this study.

Chapter 4 investigates the influence of the main building characteristics on its heating energy flexibility potential for thermal storage in the indoor space and structural elements.

Chapter 5 details how to integrate the magnetocaloric heat pump in a low-energy dwelling and discusses the performance of this innovative heating system when controlled with a building energy flexibility strategy.

Chapter 6 provides general conclusions drawn from the current research study.

Chapter 7 gives recommendations for further research work on the topics of this Ph.D. project.

Appendix A-F contains the collection of the published journal and conference articles, the journal articles currently under review and a published technical report which refer to the research study.

CHAPTER 2. LITERATURE REVIEW

This chapter presents a literature review about two major topics of this research project: the operating principles of the magnetocaloric heat pump technology and the influence and modelling technics of the indoor content thermal mass for building thermal storage.

2.1. MAGNETOCALORIC HEAT PUMPS

The operation principle of the magnetocaloric heat pump is firstly introduced and then followed by an historical summary of the magnetocaloric effect and magnetocaloric devices.

2.1.1. OPERATION PRINCIPLE OF THE MAGNETOCALORIC HEAT PUMP

Most of the conventional heat pumps and air-conditioning units are based on vapour-compression irreversible thermodynamic cycles (see *Figure 2-1*).

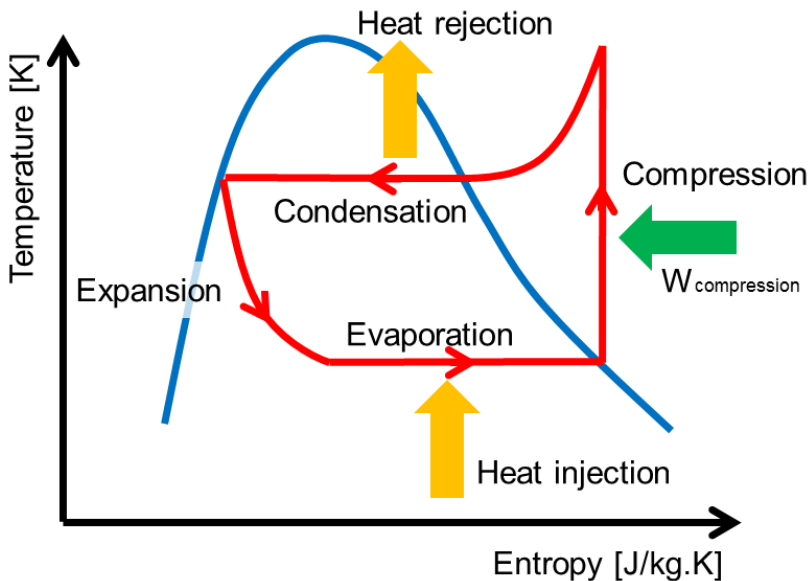


Figure 2-1: Temperature – Entropy diagram of an ideal vapour-compression cycle.

In recent years, there was an increasing interest for the magnetocaloric effect (MCE) applied to near room-temperature cooling as an interesting alternative to conventional vapour-compression systems. In the ENOVHEAT project, the MCE is used to develop a magnetocaloric heat pump for building space heating. In this innovative device, the heat transfer is thus generated from the MCE employed to perform several magnetic cooling/heating cycles, also known as the active magnetic regenerator (AMR) cycles (see *Figure 2-2*) [31].

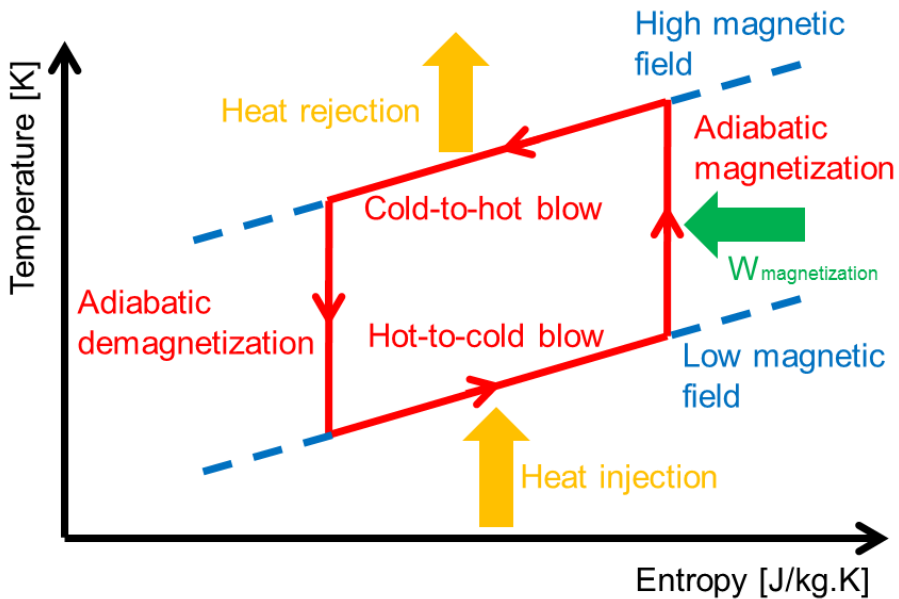


Figure 2-2: Temperature – Entropy diagram of an active magnetic regenerator cycle.

The magnetocaloric effect is a reversible temperature change experienced by a magnetic substance (the magnetocaloric material) when subjected to adiabatic magnetization or demagnetization (see *Figure 2-3*) [29]. The reversible magnetization (applying a magnetic field) of the MCM leads to a decrease of its magnetic entropy and consequently an increase of its temperature. Reciprocally, the demagnetization (removing a magnetic field) of the MCM induces an increase of its magnetic entropy and thus a decrease of its temperature. This MCM is therefore used here as a solid refrigerant exhibiting a thermal response when the applied magnetic field varies. There are various types of magnetocaloric materials and compounds. They present a specific maximum magnetocaloric response at their respective ferro-to-paramagnetic phase transition occurring at the so-called “Curie temperature”. The reference material for the MCE at room-temperature is

Gadolinium [31]. Comprehensive explanation of the magnetocaloric effect, materials and systems can be found in the publications of Smith et al. [29] and Kitanovski et al. [42].

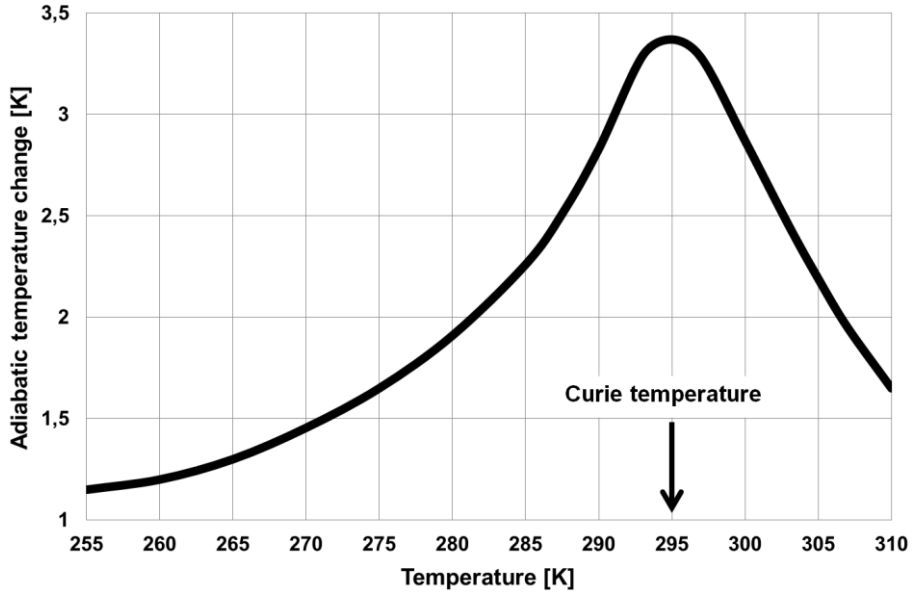


Figure 2-3: Example of adiabatic temperature change due to the magnetocaloric effect (magnetization from 0 to 1 Tesla in gadolinium) [29]

As mentioned before, the active magnetic regenerator cycle is at the core of the magnetocaloric heat pump operation for performing heat transfer from the heat source (cold side) to the heat sink (hot side). The magnetocaloric solid refrigerant is contained as a porous media in a regenerator casing. The latter allows bi-directional circulation of the coolant fluid transferring the thermal energy from the cold side to the hot side of the AMR device. The MCM is alternatively magnetized and demagnetized with an external magnetic field source such as a rotating permanent magnet [31].

One can see in *Figure 2-4* the details of the AMR cycle. At the beginning of the cycle, no magnetic field is applied but there is already a temperature gradient over the regenerator length resulting from the previous cycles: *Figure 2-4(a)*. The cycle starts with an adiabatic magnetization of the MCM leading to a decrease of the solid refrigerant entropy and a temperature increase over the length of the regenerator: *Figure 2-4(b)*. An isomagnetic heat transfer is then performed by circulating the coolant fluid from the cold side to the hot side of the AMR (cold-to-hot blow). The

hotter fluid rejects the heat to the heat sink and the regenerator is cooled down at constant magnetic field: *Figure 2-4(c)*. The magnetic field is removed and the regenerator is subjected to an adiabatic demagnetization inducing an increase of the MCM solid refrigerant entropy and a temperature decrease over the length of the regenerator: *Figure 2-4(d)*. At the end of the cycle, the fluid is moved back from the hot side to the cold side of the AMR (hot-to-cold blow) under zero-magnetic field, re-heating the bulk of the regenerator (heat regeneration process): *Figure 2-4(e)*. Once the heat transfer fluid and the magnetocaloric refrigerant reached local thermal equilibrium, the temperature distribution across the regenerator length is the same as at the initial state of the AMR cycle *Figure 2-4(f)* [31]. The active magnetic regenerator cycle is described in more detail in the articles of Engelbrecht et al. [43] and Lei et al. [44].

Due to the reversible nature of the magnetocaloric effect, the AMR-based magnetocaloric heat pump has great potential for high COP. Moreover, this innovative device has the benefit of a more silent operation, an absence of greenhouse or toxic gases, and the possibility for recycling the magnets and the magnetocaloric materials at end-of-life [29].

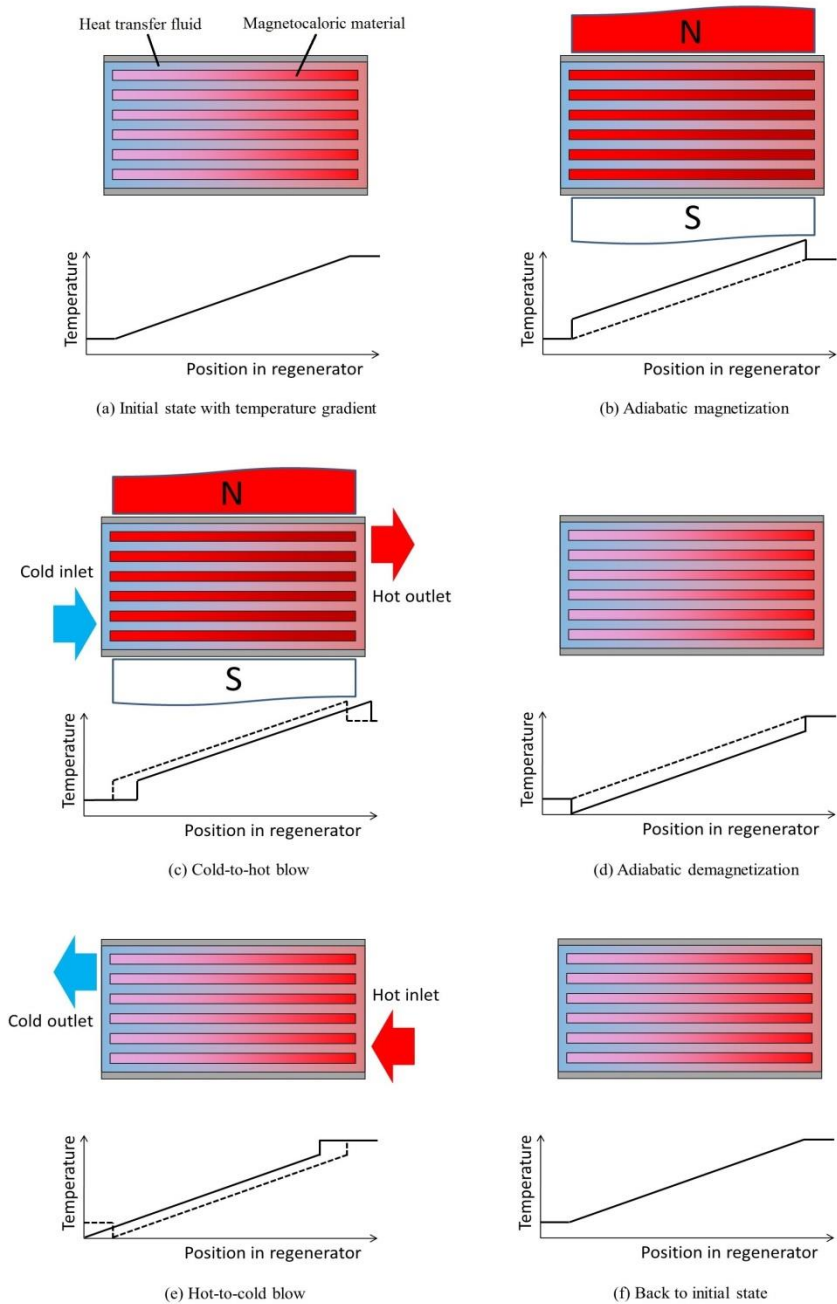


Figure 2-4: Active magnetic regenerator cycle consisting of four processes: (b) adiabatic magnetization; (c) cold-to-hot blow; (d) adiabatic demagnetization; (e) hot-to-cold blow [31].

2.1.2. HISTORY OF THE MAGNETOCALORIC TECHNOLOGY

The magnetocaloric effect was discovered in 1918 by Weiss and Piccard who observed for the first time that a reversible change in temperature occurs in nickel when a strong magnetic field (1.5 Tesla) is applied in the vicinity of the Curie temperature (354 °C) [29][45]. The phenomenon was later explained thermodynamically by Weiss et al. [46] and Debye [47] in 1926. Debye [47] and Giaque [48] suggested that the magnetocaloric effect could be used for very low temperature cooling applications. By the mid-1930s, magnetocaloric cooling was a standard laboratory technique to achieve absolute temperatures below 1 K [49].

In 1935, Urbain et al. [50] discovered that Gadolinium presents a Curie temperature (maximum MCE) which is near room-temperature. However, it was only in 1976 that Brown experimentally demonstrated that a magnetocaloric device using Gadolinium as refrigerant could be used near room-temperature applications [51]. In 1982, Barclay and Steyert developed and patented the active magnetic regenerator cycle [52]. In this new configuration, the MCM is employed for its MCE adiabatic temperature change but also as a thermal regenerator. It thus allowed a simplification of the magnetocaloric device together with a significant increase of the total temperature span above the temperature change of the MCE alone [29]. This active magnetic regenerator design is considered to be the most thermodynamically efficient for magnetocaloric heat pump devices [53]. It has therefore been the founding principle of almost all the following magnetocaloric cooling and heating systems ever since [29].

Then the magnetocaloric technology rapidly gained popularity and several research laboratories started building and testing their AMR prototypes. In 1998, Zimm et al. [54] reported COPs above 6 for a near room-temperature magnetic refrigerator using superconducting magnets. More recently, other research groups have investigated the performances of AMR near room-temperature cooling prototypes using permanent magnets. In 2012, Engelbrecht et al. [43] presented a rotary AMR device operating with a no-load temperature span of 25.4 K and a maximum cooling capacity of 1010 W. Rotary devices have either their regenerators or magnets spinning around an axis to generate the alternating magnetic field. This configuration is an interesting evolution from the early AMR design using a translation motion [52]. In 2013, a Japanese research team reported the performances of a device operating at a COP of 2.5 with a temperature span of 5 K [55]. In 2014, Jacobs et al. presented a prototype achieving 2502 W of cooling power with a 12 K temperature span and a COP above 2. Moreover, the device could reach up to 3042 W of cooling power at a zero-temperature span [56]. In 2016, several research groups have published the performances of their magnetocaloric devices. A maximum zero-span cooling power of 150 W, a maximum no-load temperature span of 12 K, and a thermal load of 80.4 W for a COP of 0.54 and a temperature span of 7.1 K were reported at the Federal

University of Santa Catarina [57]. A maximum no-load temperature span of 11.9 K and a maximum COP of 2.5 for a thermal load of 200 W were reported at the University of Salerno [58]. A research laboratory at the Technical University of Denmark tested and presented an AMR device capable of reaching 81.5 W of cooling power with a COP of 3.6 and a 15.5 K temperature span [30].

This research topic gains ever-increasing attention encompassing specific aspects and sub-components of the AMR devices with aim to improve their design and performance. In line with this, new magnetocaloric materials and compounds are developed characterized and modelled [59][60]. Among other things, the use of nanofluids is tested to improve heat transfer in the regenerators [61], the configurations of the permanent magnets are optimized [62][63], and different regenerator geometries are developed to enhance heat transfer to the coolant fluid and minimize pressure losses at the same time [64][65][66]. Finally, novel designs and configurations of the magnetocaloric machines are created to improve the overall operation performances and reduce parasitic losses in the system [30][57]. All these considerations have been taken into account for the development of the ENOVHEAT magnetocaloric heat pump prototype which is tested in this research project.

For further information, please refer to Appendix C. Paper III: “Integration of a magnetocaloric heat pump in a low-energy residential building”.

2.2. ADDITIONAL THERMAL MASS OF THE INDOOR CONTENT / FURNITURE AND PHASE CHANGE MATERIALS FOR BUILDING THERMAL ENERGY SOTRAGE

Interest is growing for accurate building energy assessment, prediction of indoor overheating, demand side management strategies, building energy flexibility measures, thermal energy storage (TES) in the indoor space, model predictive control, etc. All these topics need accurate dynamic simulation tools for building energy and indoor environment calculation. When modelling a building, the main parameters such as envelope properties, structural thermal inertia, solar gains, infiltration rate, etc, are always taken into account. However, the indoor space is very often assumed to be an empty volume, which is not the case for an occupied building in the real world. Indoor content items, such as furniture elements, are often ignored because of the complexity and variety of their shapes and material properties. This simplification can lead to noticeable errors when simulating transient indoor environment and building thermodynamics. This chapter firstly reviews several publications showing the importance of considering indoor content /

furniture in building simulations. Different modelling technics of the indoor content found in the literature are then presented. Finally, insight is given about phase change materials (PCM) and their integration in the indoor space for TES purpose.

2.2.1. IMPACT OF THE INDOOR CONTENT / FURNITURE ON THE BUILDING THERMODYNAMICS AND INDOOR ENVIRONMENT

Items contained in the indoor space but which are not part of the walls, ceilings and floors, are often ignored in building simulations. Furnishing elements, clothes, books, indoor plants, appliances, decoration accessories, etc. come in various shapes and are made of very different materials (wood, plastic, metals, ceramics, stone, textile, paper, polymer foam, etc) with very different thermophysical properties. They are usually not described in the building blue prints and therefore generally disregarded in building simulations. This simplification is suitable for basic energy calculations with constant boundaries conditions, but it can be problematic if one wants to accurately simulate the dynamics of buildings [67].

Most of the publications related to the influence of the indoor content and furniture on the built environment are focused on the indoor air quality and the chemical compounds emission from furnishing materials [68]. Other publications emphasize the significant impact of interior partitions, furniture elements and other indoor items on daylight conditions [69] and building acoustics [70]. However, the following review focuses on the indoor thermal comfort, the building thermal dynamics and energy issues.

Mortensen et al. [71] experimentally demonstrated the significant impact of the furnishing elements positioned near cold walls on local indoor micro-climate increasing the risks of condensation inside buildings. Yang et al. [72] performed a full-scale experiment to assess the moisture buffering ability of the furniture in rooms. They indicated that the presence of furnishing elements could decrease the indoor humidity variation by up to 12%. Because of their important effective surface areas, indoor items can hold a large amount of water vapour and increase the moisture buffering capacity of the room by up to 54.6%. Computational fluid dynamics (CFD) analysis pointed out that furniture elements can strongly interact with ventilation and air-conditioning emitters and can thus induce complex flow recirculations leading to high local air velocities, air jet obstruction or local draft [73][74].

Furnishing, carpets and interior decoration elements are positioned directly on the internal surfaces of the rooms. Because their large surface area screens the construction element beneath them, they can significantly change the radiative and convective heat exchange conditions, which can decrease the efficiency of radiant heating and cooling systems [75]. Zhao et al. [76] conducted numerical and experiment tests showing the interaction of chairs and benches with radiant floor

cooling system exposed to high solar load in a high-ceiling building. The surfaces shadowed by the furniture were local cold spots which had their cooling power reduced by 83% and presented high risks of moisture condensation. Similarly, Corcione et al. [77] numerically demonstrated that furniture in buildings could significantly decrease the heat transfer efficiency of radiant floor heating systems and thereby affect the indoor operative temperature. Fontana [78] corroborated these conclusions with small-scale experimental setups. The author concluded that a 40% furniture cover of the radiant floor heating surface can reduce its heat transfer to the room by up to 30%.

Concerning the building thermal dynamics, some researches emphasized the significant role of the furniture thermal mass in the total effective thermal inertia of the building. Antonopoulos and Koronaki [79] calculated that furniture accounts for 7.4% of the total effective thermal inertia of a typical Greek house. Moreover, their numerical simulations showed that this additional furniture thermal inertia can increase the building time constant by up to 15%. Wolisz et al. [80] conducted numerical investigations about the significance of modelling furniture and floor cover when simulating a building with dynamic indoor temperature set points. The results showed that the temperature increase can be delayed by up to 7 hours for a fully furnished room compared to an empty one. In addition, the furnishing and floor covering can change the cool-down time by up to 2 hours when using periodic set point modulation. After conducting a survey in some Danish buildings, Johra et al. [67] calculated that indoor content items and furniture elements can represent up to 40% and 36% of the total hourly effective thermal inertia of a light-weight and heavy-weight structure building, respectively. Moreover, it can account for up to 28% and 11% of the total daily effective thermal inertia of a light-weight and heavy-weight structure building, respectively.

One can see from this literature review that the empty room assumption might not be suitable for accurate dynamic building simulations. It is important to consider the modelling of the indoor content and furniture elements in the built environment. This research study addresses that issue by integrating the indoor items in its building models and evaluating their impact on the building time constant and heating energy flexibility potential.

2.2.2. MODELLING INDOOR CONTENT / FURNITURE THERMAL MASS

The first problem with modelling indoor space content and furniture is that no clear guideline can be found about their quantification and their thermophysical characteristics. To tackle this problem, Johra et al. [67] conducted a simple survey on 6 bedrooms, 3 living rooms and 3 single office rooms in different Danish buildings. Systematic mass and size measurements together with material identifications were performed for each piece of indoor content. The objective of this survey was to propose a reasonable range of values for the quantity and

characteristics of the indoor content elements. The thermophysical properties of 4 representative material categories and an equivalent fictitious indoor content material are presented in *Table 2-1*. The suggested average value of each parameter is followed by the lower and higher bounds in parentheses.

Table 2-1: Properties of the representative indoor content material categories [81].

Material category	Room mass content (kg/m ² floor area)	Surface area (m ² /m ² floor area)	Material density (kg/m ³)	Material thermal conductivity (W/m.K)	Material specific heat capacity (J/kg.K)	Planar element thickness (cm)	Daily effective thermal inertia (kJ/K.m ² floor area)
Light material	7 (0.5–14)	0.3 (0.1–0.6)	80 (20–140)	0.03	1400	10 (0.5–24)	3 (0.2–7)
Wood / plastic material	30 (8–80)	1.4 (0.5–2)	800 (400–1200)	0.2 (0.1–0.3)	1400	1.8 (1–5)	26 (9–45)
Concrete / glass material	1 (0.5–2)	0.03 (0.01–0.04)	2000 (1500–2500)	1.25 (0.5–2)	950	1 (0.2–2)	0.1 (0.05–0.2)
Metal material	2 (1–5)	0.02 (0.01–0.03)	8000	60	450	0.2 (0.1–0.3)	0.1 (0.05–0.4)
Equivalent indoor content material	40 (10–100)	1.8 (0.8–2.8)	600 (150–1500)	0.3 (0.1–0.5)	1400	4 (1–10)	30 (10–50)

Different modelling technics can be found in scientific publications attempting to account for indoor content in building simulations. There are presented hereafter in increasing level of detail and complexity.

First order RC network building model

Thermal networks, also known as Resistance – Capacitance (RC) network models, are commonly used to simulate an entire thermal zone of a building in a simple way. The simplest RC model contains x resistances and only 1 capacitance ($xRIC$). The single capacitance aggregates all the effective thermal inertia of the thermal zone, including indoor air volume, interior partition walls, envelope elements and the additional thermal mass of the indoor content and furniture. Therefore, the assumption is made that the entire thermal mass is isothermal at all time and with constant thermal resistance coefficients. One can find the description of a $5RIC$ model in the ISO standard 13790:2008 [82].

Higher order RC network building model

The dynamic behaviour of the simple $xRIC$ network can be improved by dissociating the thermal mass elements with dissimilar thermal diffusivities and model them independently with several distinct lumped capacitance nodes. The construction elements and the air volume of the indoor space can be separated to

create a $xR2C$ model. The RC network can then be expended further by increasing the number of resistances and capacitances ($xRyC$) and segregating the thermal mass from internal partition walls, envelope walls or heavy concrete structural elements.

The additional thermal mass from indoor content and furniture can then be merged with different lumped capacitances. If it is assumed that the indoor content items are isothermal and in thermal equilibrium with the indoor air, then their thermal inertia is added to the thermal capacitance of the indoor air node [83][84]. On the other hand, if it is assumed that the indoor air and the indoor content are not isothermal, the latter can be included in the thermal capacitance of the inner surface envelope walls or in the interior partition walls [83][85]. The internal thermal mass node can be subdivided further more into a $2R2C$ sub-network to take into account its temperature inhomogeneity.

Distinct capacitance for thermal mass of indoor content / furniture

The thermal diffusivity, surface heat exchange coefficient and Biot number of the indoor content / furniture elements may significantly differ from the ones of the other internal surfaces of a room. Therefore, the indoor items, the indoor air node and the other building elements can present significant temperature differences. This would justify a separate modelling of the indoor content with a dedicated lumped capacitance. In the TRNSYS software, an additional fictitious furniture thermal capacitance node can be added to the star network scheme for convection / radiation heat exchange calculations [84]. It is a non-geometrical heat balance calculation where no specific location is set for the fictitious element. Therefore, no real calculation for solar radiation distribution and long-wave radiation heat exchange is performed here. However, a proper equivalent surface area for the fictitious indoor content element must be stated. This can be done with a simplified calculation method provided by the ISO standard 13790:2008 [82]. Alternatively, a new method has been proposed by Li et al. [86] to lump the indoor content items with irregular shapes into a single capacitance thermal node with an adequate equivalent surface area.

Equivalent virtual sphere model

In RC models, each capacitance thermal node represents a sub-system which is assumed to be isothermal. It is a reasonable assumption if the Biot number of these elements is smaller than 0.1. However, this is not the case for most of the indoor content items [67]. Consequently, the lumped capacitance method is not appropriate to accurately model the thermal dynamics of the additional indoor thermal mass [87]. Gao et al. [88] and Zhou et al. [89] suggested the use of the virtual sphere method to overcome that problem. The different shapes of the indoor items are aggregated into a single sphere with a radius calculated as the characteristic length of the equivalent element. An effective convection heat transfer coefficient is used to account for the temperature inhomogeneity in the equivalent element. This modelling method is suitable for Biot numbers ranging from 0 to 20, which typically

fits all indoor content items [67]. However, no radiation heat exchange is taken into account.

Equivalent virtual planar element model

A common modelling technic for the indoor content items is to aggregated them all into a single equivalent planar element [79][80][87][90][91]. This equivalent slab is assumed to be made of a single homogeneous representative material with constant thermal properties. The thickness of the planar element is considered negligible compared to its length and width. Consequently, the heat transfer by conduction and the temperature profile within the slab are assumed to be one-dimensional. One can thus easily calculate the thermodynamics of this system with a 1-D finite difference method (FDM) or finite volume method (FVM) formulation. The main limitation of this modelling technic is that the planar element does not have a geometric representation or a location in the thermal zone. Therefore, the calculations of the internal solar distribution and the long-wave radiation heat exchange do not take the presence of the slab into account.

Equivalent geometric planar element model

Raftery et al. [92] have implemented in the Energy Plus software an equivalent planar element model with space location and geometric representation. The presence and geometry of the slab is thus fully accounted for the computation of the direct and diffuse internal solar repartition. The presence of the planar element is also taken into account for the radiosity calculation of the view factors used for the computation of the long-wave radiation heat exchange and the mean radiant temperature. Shading on the inner surfaces is modelled accordingly which improves the realism of the radiant systems' behaviour.

Detailed explicit furniture model

The aforementioned modelling methods aggregate all the indoor content / furniture elements into a single equivalent object. It can be justified because of the unknowns about the characteristics of an occupied building content and the great complexity to represent it in details. Nonetheless, some CFD [73][74] and daylight [69] numerical studies used very detailed representations of the interior environment with explicit locations and geometries of the items inside buildings. In the field of building energy simulation, a library of indoor content items such as chairs, tables, bookcases, light fittings, stairs, etc, has been developed by Hand [93] for the ESP-r software. The elements have realistic geometries and thermophysical properties, and can be placed precisely in the indoor environment. Internal solar radiation distribution, surface shading and view-factors are computed accordingly without restriction on the geometric complexity.

In the case of this research study, it is chosen to model the indoor content / furniture elements with an equivalent virtual planar element in each thermal zone of the building.

2.2.3. PHASE CHANGE MATERIALS FOR BUILDING THERMAL ENERGY STORAGE IN THE INDOOR ENVIRONMENT

Common building materials subjected to normal conditions (conditions which are commonly encountered in the built environment) do not experience major change in their micro-structure at ambient temperature. Therefore the variation of internal energy induced by temperature change is correlated to their specific heat capacity. These materials store thermal energy as “sensible heat”. On the other hand, some materials operate a phase transition near ambient temperature and can thus store thermal energy as “latent heat” with a limited temperature variation. These materials are commonly named “phase change material”. The most famous PCM is water, which has a phase transition occurring at 0 °C. The following discussion is restricted to PCM with solid-liquid phase transition taking place at temperatures ranging from 10 °C to 60 °C, which are the most commonly used for building thermal storage applications [67][94].

In recent years, PCMs became popular among the scientific community striving to develop new thermal energy storage systems for buildings. Indeed, latent heat thermal energy storage (LHTES) systems using PCM have a volumetric heat storage capacity which is 5 to 14 times more important than sensible heat storage materials like water or concrete [95]. Several publications investigated the integration of PCM in hot water storage tanks to improve the performance of heat pumps [96] and solar water heating systems [97]. Concerning passive LHTES, most researches focused on the integration of PCM in construction elements offering a large surface of exchange with the indoor environment such as inner surfaces of walls, ceilings and floors. Several experimental studies showed that PCM wallboards are easy to install and present significant potential to insure indoor temperature stability, reduce risks of overheating, and lessen cooling and heating peak loads [98][99][100][101]. The incorporation of PCM into concrete has also been tested experimentally. The results showed that no significant amount of PCM can be properly integrated in concrete without serious mechanical deterioration and large decrease of thermal conductivity, which limits the overall effective thermal inertia [102]. PCMs can also be directly integrated in between glazing panes to create translucent windows. Because of the semi-transparent properties of certain PCMs, this system can provide a source of natural light where there is no need for direct visual contact to the outdoor environment. The PCM is therefore directly activated by solar radiation, insuring a maximum use of its latent heat storage capacity [103]. Internal shutters and solar protections integrated in façade windows can also comprise PCM to store thermal energy during the day and release it to the indoor environment during the night [104][105]. Finally, some research and development groups suggested that the large surface area of the furniture elements could also be employed to integrate PCM. This solution could therefore increase the effective thermal inertia and heat storage capacity of the built environment without the need for construction work [67][81][106][107].

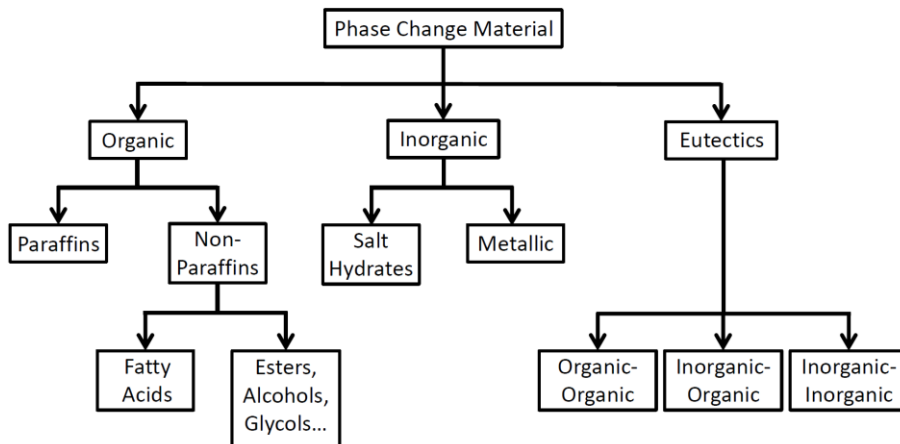


Figure 2-5: General categorization of phase change materials [67].

Relevant phase change materials for LHTES application in buildings can be classified into three main groups: organic, inorganic and eutectics (see *Figure 2-5*). Among them, paraffins, fatty acids, salt hydrates and their eutectic mixtures appear to be the most suitable for passive TES in the indoor environment [67]. The qualities of a good PCM for such purpose are listed hereafter:

- Melting / solidification temperature within the range of human's thermal comfort: 19 °C - 25 °C (see *Figure 2-6*).
- High volumetric latent heat of phase transition for maximum storage density.
- High specific heat capacity to provide additional sensible heat storage.
- High thermal conductivity of both liquid and solid phase for high activation and fast charging/discharging of the PCM.
- Small volume change between the liquid and solid phase and low vapour pressure to avoid containment failure.
- Congruent melting and reversible phase transition for stable storage capacity over time.
- High nucleation to avoid sub-cooling of the liquid phase.
- Non-corrosive to the containment materials.
- Non-flammable, non-explosive and non-toxic.
- Low-cost with possibility for recycling at end-of-life.

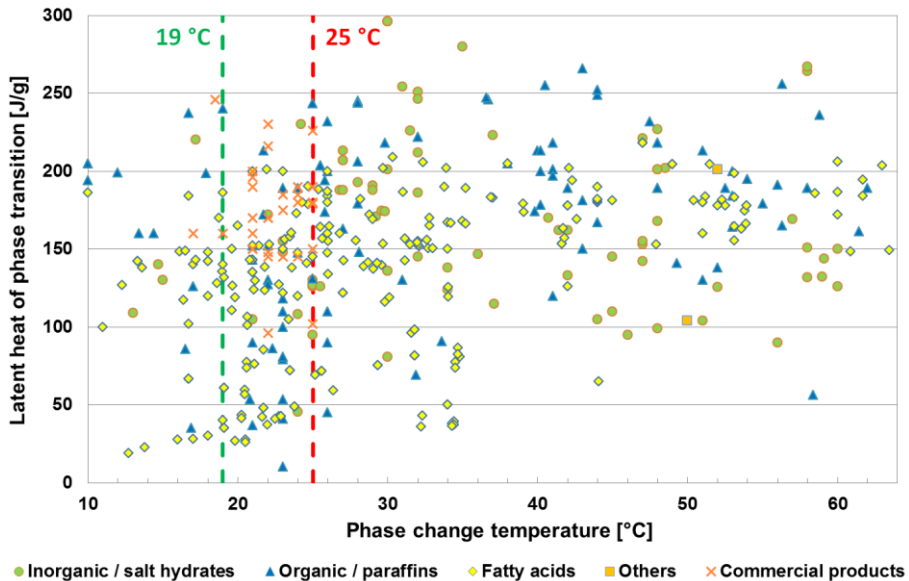


Figure 2-6: Compilation of phase change materials thermal properties found in the literature: latent heat of phase transition as function of temperature of phase transition [67].

The most interesting PCMs with a phase transition temperature suitable for TES in the indoor environment present a maximum latent heat between 200 J/g and 250 J/g. However, there are a number of methods to tune the chemical composition of a given PCM in order to shift its phase transition temperature. The main limitation of the PCMs is due to their low thermal conductivity. Fortunately, the incorporation of highly conductive particles, metallic foams or carbon nanostructures can significantly improve the global thermal conductivity of PCMs. Organic PCMs such as paraffins and fatty acids present a very good chemical and thermal stability with congruent melting and limited or no sub-cooling. On the contrary, inorganic products such as salt hydrates suffer from cycling instability, sub-cooling and high reactivity to metals [67].

According to this literature review, it appears that organic PCMs are the most appropriate solutions for near-room TES application in buildings. Consequently, the well-known Energain® [109] stable form PCM is chosen as study case for the thermal storage in the indoor environment strategy of this research study. This commercial product is composed of 60 % mass micro-encapsulated paraffin (organic PCM) incorporated in a polyethylene matrix (40 % mass).

For further information, please refer to Appendix A. Paper I and Appendix B. Paper II: “Influence of internal thermal mass on the indoor thermal dynamics and integration of phase change materials in furniture for building energy storage: A review” and “Numerical analysis of the impact of thermal inertia from the furniture / indoor content and phase change materials on the building energy flexibility”.

CHAPTER 3. MAGNETOCALORIC HEAT PUMP AND BUILDING SYSTEMS MODELS

This chapter presents the characteristics of the ENOVHEAT magnetocaloric heat pump prototype and the different building study cases used in these numerical investigations. In addition, a detailed description of the building systems and MCHP models is provided together with information about the validation process of the latter.

3.1. CHARACTERISTICS OF THE MAGNETOCALORIC HEAT PUMP

The ENOVHEAT magnetocaloric heat pump prototype is a rotary active magnetic regenerator device (see *Figure 3-1*). 13 active magnetic regenerators are mounted on an iron ring constituting the vertical stator.

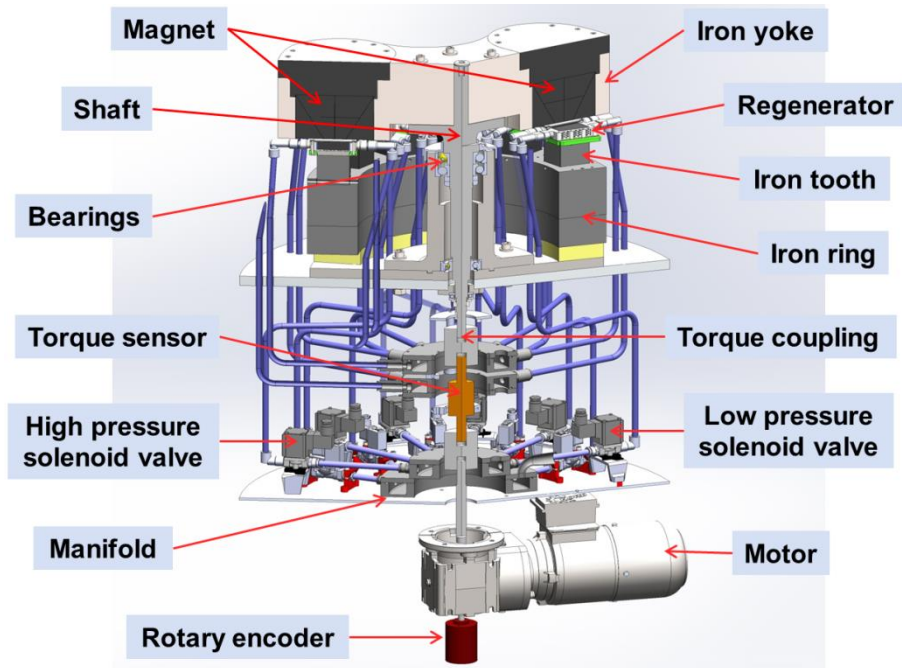


Figure 3-1: Detailed description of the magnetocaloric heat pump prototype of the ENOVHEAT project: “MagQueen” (section view) [32].

A two-pole magnet assembly, composed of 28 permanent magnet elements for each pole, is placed on the vertical rotor (see *Figure 3-2*). The latter is connected to an electric motor by a shaft. The rotation of the magnets creates a varying magnetic field in the regenerators with a maximum value of 1.46 Tesla. The rotation frequency of the device can vary from 0.5 Hz to 2 Hz.

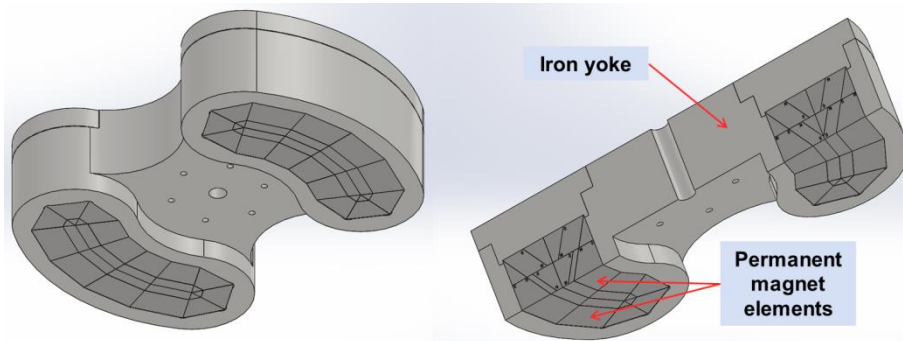


Figure 3-2: CAD model of the two-pole magnet assembly.

The MCM solid refrigerant is Gadolinium. The prototype contains a total of 2.8 kg of it. The MCM is arranged as packed bed spheres (450 μm diameter) inside the trapezoidal shaped-cassette regenerators (see *Figure 3-3*). An epoxy layer holds the packed bed spheres in place.

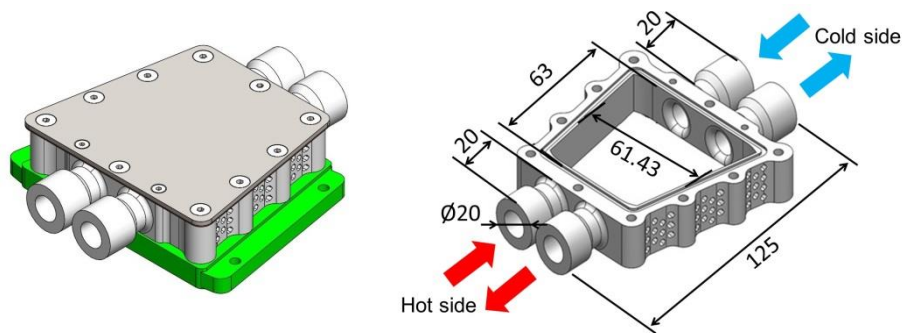


Figure 3-3: CAD model of the regenerator for the magnetocaloric heat pump prototype (dimensions are indicated in millimeters) [31].

The 13 magnetic active regenerators are connected to 2 manifold collectors and 2 manifold distributors. One collector and one distributor are on the cold side of the

regenerators and similarly on the hot side (see *Figure 3-4*). For each of the regenerators there are two solenoid valves: a low pressure valve on the stream towards the hot side manifold collector and a low pressure valve on the stream from the hot side manifold distributor. The valves are synchronized with the position of the magnet via an absolute encoder. They allow bi-directional circulation of the heat transfer fluid (20%vol ethylene glycol and 80%vol water) through the individual MCM porous media beds [31]. A single centrifugal pump circulates the coolant fluid from the heat source to the heat sink (maximum volumetric flow rate of 2100 L/h) [110].

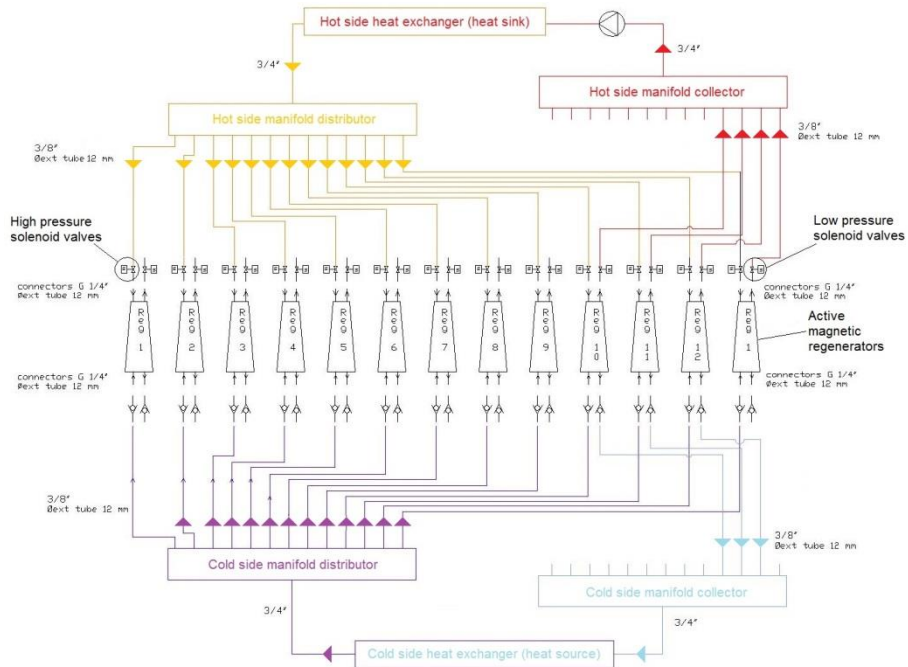


Figure 3-4: Schematic of the hydronic circuit of the magnetocaloric heat pump prototype.

3.2. NUMERICAL MODELLING OF THE MAGNETOCALORIC HEAT PUMP

The foundation for the modelling of the ENOVHEAT magnetocaloric heat pump prototype is the original dynamic one-dimensional numerical model of an AMR system created by Engelbrecht [111][112] and further developed by Lei et al. [65]. Some reasonable assumptions on the regenerator's geometry, external heat losses and demagnetization losses are made. Heat losses inside the regenerator due to

internal axial conduction are accounted for. Heat losses through the external walls of the regenerators are neglected. Losses from the demagnetization are calculated by determining the internal magnetic field in the magnetocaloric refrigerant. To that matter, an average demagnetization factor (which has been found to be 0.58) is used for the entire regenerator bed which is assumed to be a rectangular solid. The demagnetizing field effect is implemented in the model as described by Engelbrecht et al. [113]. The time-dependent fluid temperature distribution in the AMR can thus be calculated with the two following coupled partial differential equations:

$$\begin{aligned} & \frac{\partial}{\partial x} \left(k_{\text{disp}} A_c \frac{\partial T_f}{\partial x} \right) - \dot{m}_f c_f \frac{\partial T_f}{\partial x} - \frac{Nuk_f}{d_h} a_s A_c (T_f - T_s) + \left| \frac{\partial P}{\partial x} \frac{\dot{m}_f}{\rho_f} \right| \\ & = A_c \varepsilon \rho_f c_f \frac{\partial T_f}{\partial t} \end{aligned}$$

(Equation 3-1)

$$\begin{aligned} & \frac{\partial}{\partial x} \left(k_{\text{stat}} A_c \frac{\partial T_s}{\partial x} \right) + \frac{Nuk_f}{d_h} a_s A_c (T_f - T_s) \\ & = A_c (1 - \varepsilon) \rho_s \times \left[c_H \frac{\partial T_s}{\partial t} + T_s \left(\frac{\partial s_s}{\partial H} \right)_{T_s} \frac{\partial H}{\partial t} \right] \end{aligned}$$

(Equation 3-2)

Where k , T , ρ , c and s are the thermal conductivity, temperature, density, specific heat, and specific entropy; A_c , d_h , a_s , ε , x , t , \dot{m}_f , and H are the cross sectional area, hydraulic diameter, specific surface area, porosity of the regenerator bed, axial position, time, fluid mass flow rate and internal magnetic field; $\partial P / \partial x$ and Nu are the pressure drop and the Nusselt number. The subscripts f and s represent fluid and solid refrigerant, respectively. k_{disp} is the thermal conductivity of the fluid due to axial dispersion, k_{stat} is the static thermal conductivity of regenerator and fluid, and c_H is the specific heat capacity of the MCM at constant magnetic field [31]. The Nusselt number, k_{disp} and k_{stat} are calculated using correlations which are described in detail by Nielsen et al. [114]. An implicit finite volume method scheme

is used to solve these equations within the MATLAB software environment [115]. This numerical model has been successfully validated by Lei et al. with experimental data from an AMR prototype [116].

However, this detailed AMR model is too computationally demanding for the purpose of entire building simulations. The magnetocaloric heat pump operates relatively fast and its output can thus rapidly reach a quasi-steady state within about a minute. The detailed MCHP model is used to generate around 1600 quasi-steady state output points mapping the variation of the 4 input variables: operation frequency, volumetric fluid flow rate, cold side temperature input and hot side temperature input. The MCHP operation is thus approximated by several 5-dimensional lookup tables compiling the output data points and providing fluid temperatures, heating and cooling powers, COP, magnetic work and fluid pressure losses through the regenerators as functions of the inlet fluid temperatures, operation frequency and fluid mass flow rate to the heat pump. The lookup tables are native MATLAB-Simulink block functions. The simplified MCHP model can thus be run with very little computation time, making it adequate for building simulations with a time step size of 60 seconds.

Apart from the AMRs themselves, the additional components of the magnetocaloric heat pump are modelled in a simple way. The average electrical power consumption of the set of valves has been measured directly on the ENOVHEAT prototype. The average total power usage of the 26 solenoid valves is 63 W. It should be noted that some heat generated by the operation of the solenoid valves would be absorbed by the coolant fluid on the hot end of the AMR. This would slightly increase the heating power of the magnetocaloric device. Nevertheless, this heat surplus is very limited. Therefore, neglecting it is a conservative assumption to avoid over estimation of the system's performance. The magnetic work of the MCHP is employed to calculate the electrical power use of the device's motor with the assumption that the efficiency factor of the latter is equal to 0.65. The work of the hydraulic circulation pump is modelled with a polynomial function fitting the operation data provided by the pump manufacturer [110].

For further information, please refer to Appendix C. Paper III: "Integration of a magnetocaloric heat pump in a low-energy residential building".

3.3. BUILDING STUDY CASES

Within the framework of the ENOVHEAT project, a multi-zone building model has been created with the MATLAB-Simulink software environment in order to numerically study the integration of a magnetocaloric heat pump in a residential building. This building model is also used for investigating the heating energy flexibility potential of dwellings in Denmark.

3.3.1. ENOVHEAT PROJECT STUDY CASE FOR THE INTEGRATION OF A MAGNETOCALORIC HEAT PUMP IN HOUSES

A single-story dwelling with 126 m² of heated floor surface area is chosen as base study case for this research project (see *Figure 3-5*) [21]. This detached house has a typical geometry of modern single-family residential buildings in Denmark.

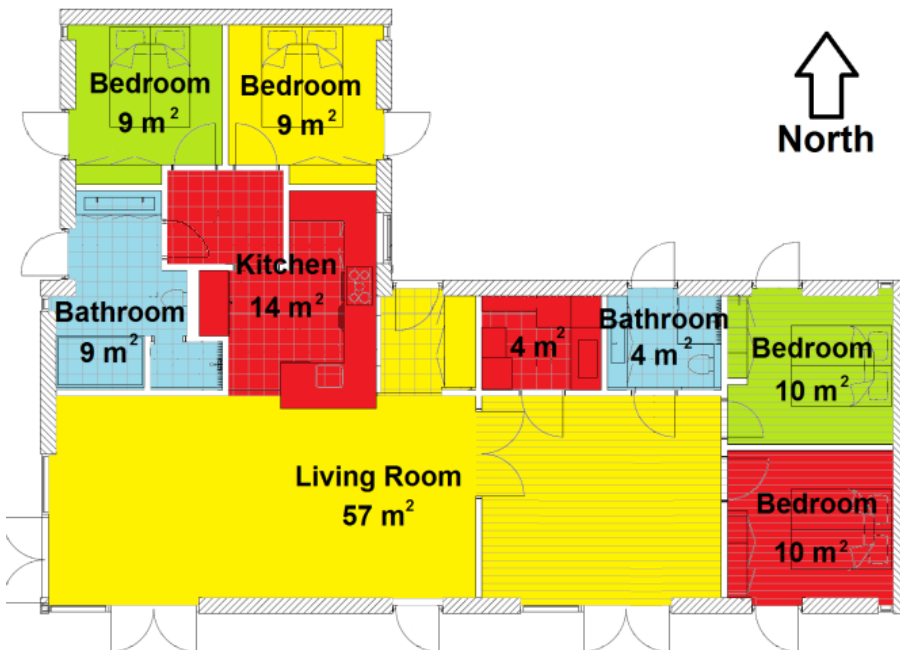


Figure 3-5: Plan view of the house study case [21].

The house has been designed to have a yearly indoor space heating needs of 16 kWh/m². It thus fulfills the low-energy requirements of a newly built dwelling “class 2020” of the Danish building regulation [117]. Moreover, it almost reaches the

“Comfort House” level [118]. The main building parameters of the house study case can be found in *Table 3-1*.

Table 3-1: Parameters of the building base case study [31].

Total ground floor area including walls [m ²]	150
Heated floor area [m ²]	126
Heated net volume [m ³]	309
External walls U-value [W/m ² .K]	0.11
Floor U-value [W/m ² .K]	0.071
Roof U-value [W/m ² .K]	0.081
Doors and windows U-value [W/m ² .K]	1
Glazing transmittance [%]	0.63
Infiltration rate [h ⁻¹]	0.1
Air change rate (without infiltration) [h ⁻¹]	1.2
Ventilation heat recovery [%]	85
Heating temperature set point [°C]	22
Heating energy need (set point = 20 °C) [kWh/m ² . year]	16

With regards to the integration of heat pump systems for space heating in Danish dwellings, the most energy efficient configuration is to couple a ground source heat exchanger (GSHE) as high temperature heat source with a water-based (hydraulic) radiant under-floor heating (UFH) system as low temperature heat sink [119]. The water-based brine heat transfer fluid is chosen to be 20%vol ethylene glycol and 80%vol water, which is commonly used for GSHE, heat pump and UFH installations.

Two different types of ground heat source are considered: a horizontal ground source loop and a vertical borehole. The two GSHE collectors are designed and sized according to manufacturer's technical guidelines [120] and international standards [121][122]. The soil and underground where the GSHE collectors are located are assumed to be composed of humid clayey sand (typical case in Denmark) with the following properties: density of 1900 kg/m³, thermal conductivity of 1.5 W/m.K, specific heat capacity of 1400 J/kg.K. The grouting material is assumed to have the following properties: density of 1500 kg/m³, thermal conductivity of 1.4 W/m.K, specific heat capacity of 1670 J/kg.K. Consequently, the

horizontal GSHE is sized to be a 194 m long single collector with a serpentine layout. It is composed of PEX pipes with 33 mm inner diameter and 40 mm outer diameter. The collector pipes are placed at a depth of 1.5 m under the ground surface. The spacing between the pipe legs is 1.5 m. The collector covers a total ground surface area of 291 m². The vertical borehole GSHE is a single collector consisting of a double U-tube pipe. It is composed of PEX pipes with 37 mm inner diameter and 44 mm outer diameter. The borehole has a depth (vertical length) of 100 m and a diameter of 160 mm. The spacing between the 2 U-tube legs is 80 mm. The borehole collector has a total pipe length of 200 m.

The water-based radiant under-floor heating system is designed according to manufacturer's technical guidelines [123] and international standards [124][125]. The UFH hydronic loops are composed PE-Xa pipes with 13 mm inner diameter and 16 mm outer diameter. They are embedded in a 100 mm thick concrete screed, 60 mm below the top surface. The spacing between the pipe legs is 300 mm.

For the sake of comparing the performance of the MCHP with a conventional reference heating system, a water-to-water vapour-compression heat pump is implemented in the same building study case with the same UFH system and GSHE. The VCHP has characteristics similar to the model TWM036 of ClimateMaster® [126]. With a nominal fluid flow rate of 2052 L/h in both heat source and heat sink, this heat pump has a heating power output of 8.28 kW with a COP of 4.51 (heat source at 5 °C and heat sink at 35 °C). A 250 L hot water storage tank, 3 circulation pumps (hydraulic circulation pumps Grundfos ALPHA2 L 15-40 [127]) and a mixing valve are added to form the reference heating system (see *Figure 3-6*). The hot water tank temperature is regulated by an ON/OFF controller connected to a temperature sensor placed at the top third of the tank and with a temperature set point of 35 °C.

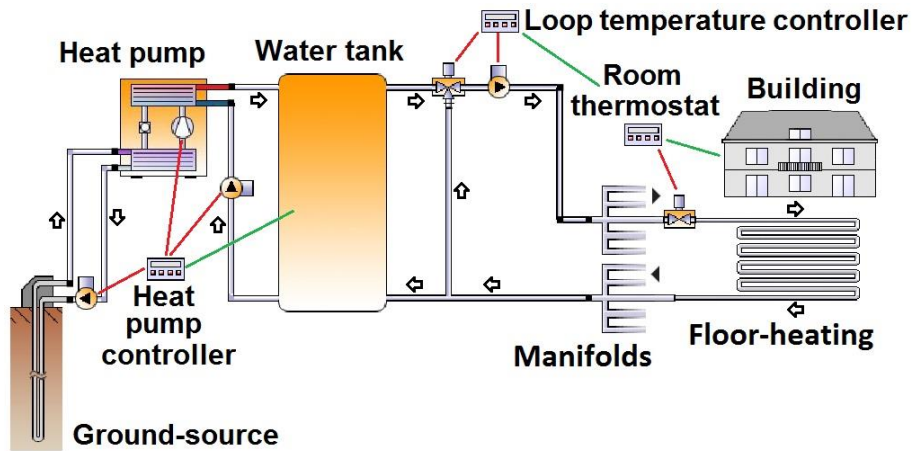


Figure 3-6: Integration of a conventional vapour-compression heat pump with ground source heat exchanger, hot water storage tank and water-based radiant under-floor heating system [21].

The outdoor weather boundary conditions such as air and ground temperature, solar radiation, atmospheric pressure, wind speed and direction, cloud cover, relative humidity and long wave radiation from the sky are extracted from the national reference Danish weather file DRY 2013 [128]. The house is thus considered to be located in an open field around Copenhagen. It is assumed that 4 persons are occupying the house according to a fixed weekly schedule. The equipment and people load time profiles are based on typical people occupancy and equipment usage schedule for a residential house in Denmark [129].

3.3.2. BUILDING CASES FOR THE STUDY OF BUILDING ENERGY FLEXIBILITY IN DANISH DWELLINGS

The aforementioned building configuration is used as basis to elaborate the study cases for the numerical investigations on the heating energy flexibility of dwellings and the control of the MCHP with an energy flexibility strategy.

As the influence of structural thermal inertia, additional indoor content thermal mass, envelope insulation level and type of heating system are investigated, a total of 144 different versions of the house base case are generated with variations of these four building parameters.

Two categories of building envelope performance are considered; namely, low-insulation house from the 80's and high-insulation passive house. The insulation thickness and its thermal conductivity, the infiltration and ventilation rate, the

windows' characteristics and surface area, and the HVAC systems' performance of the original base case are adjusted to reach these two insulation levels. The low-insulation case corresponds to a Danish house built in the years 1980 with relatively poor thermal performances: yearly indoor space heating needs around 160 kWh/m². The high-insulation case corresponds to a "Comfort House" which reaches the energy efficiency of the Passive House standard [118]: yearly indoor space heating needs around 13 kWh/m².

The material properties of the external and internal layers of the house's walls, ceilings and floors are varied from the original base case in order to generate three structural thermal inertia building classes (defined according to the recommendations of the ISO 13790:2008 standard [82]) with three different sub-variations in each of them.

- Light-weight structure house; daily effective thermal inertia: 30 Wh/K.m², 40 Wh/K.m² and 45 Wh/K.m².
- Medium-weight structure house; daily effective thermal inertia: 50 Wh/K.m², 60 Wh/K.m² and 70 Wh/K.m².
- Heavy-weight structure house; daily effective thermal inertia: 90 Wh/K.m², 100 Wh/K.m² and 110 Wh/K.m².

Four additional indoor thermal mass configurations are considered: empty room (only filled with air), additional indoor content / furniture, furnishing elements with integrated PCM panels, PCM wallboards placed on the inner surfaces of the house's walls and ceilings.

Two types of heating system are integrated in the different building cases: convective radiator and water-based radiant under-floor heating system. The UFH hydronic circuit is integrated in a wooden floor for the light-weight structure houses, and integrated in a 100 mm concrete screed for the medium and heavy-weight structure houses.

One can find the main information about the different building cases in *Table 3-2*.

Table 3-2: Main characteristics of the building cases for investigation of the heating energy flexibility potential [21].

Building envelope category	House 1980's			Passive House		
	Light	Medium	Heavy	Light	Medium	Heavy
Structural thermal mass category						
Effective thermal mass: Cm 24h (Wh/K.m ² gross floor)	30 - 40 - 45	50 - 60 - 70	90 - 100 - 110	30 - 40 - 45	50 - 60 - 70	90 - 100 - 110
Building envelope heat losses (W/K.m ² gross floor)	1.12	1.13	1.13	0.37	0.37	0.37
U-value windows (W/m ² .K)	1.7			0.78		
g-value windows (-)	0.63			0.5		
Ratio windows / gross floor area (m ²)	16.70%			26.90%		
Windows area (m ²)	25.1			40.39		
Air infiltration (ACH)	0.2			0.07		
Ventilation (ACH)	0.4			0.4		
Heat recovery (-)	0			0.8		
Air flow heat losses (W/K)	64			15.6		
Air flow heat losses (W/K.m ² gross floor)	0.43			0.1		
Yearly radiator heating need with set-point at 22°C (kWh/m ² net floor.year)	164	160	155	14	13	12
Maximum radiator heating power (W/m ²)	75			25		
Under-floor heating type	Type G wood floor	Concrete screed	Concrete screed	Type G wood floor	Concrete screed	Concrete screed
Yearly under-floor heating need with set-point at 22 °C (kWh/m ² net floor.year)	160	151	157	15	13.5	13
Nominal water flow per UFH loop (l/h)	170			125		
UFH maximum inlet water temperature (°C)	47	43	43	35	30	30

For the study of the MCHP controlled with an energy flexibility strategy, three building cases are generated with three different structural thermal inertia classes:

- Light-weight structure building: daily effective thermal inertia of 30 Wh/K.m².
- Medium-weight structure building: daily effective thermal inertia of 60 Wh/K.m².
- Heavy-weight structure building: daily effective thermal inertia of 100 Wh/K.m².

All the three cases have the envelope performance level of the house base case (yearly indoor space heating needs of 16 kWh/m²) and are equipped with a vertical borehole GSHE and a hydronic radiant UFH system. As mentioned before, the UFH hydronic circuit is integrated in a wooden floor for the light-weight structure houses,

and integrated in a 100 mm concrete screed for the medium and heavy-weight structure houses. No additional indoor content thermal mass is present in these cases and the rooms are assumed empty (only filled with air) [32].

3.4. NUMERICAL MODELLING OF THE BUILDING SYSTEMS

Numerical models of the different aforementioned building study cases have been created with the MATLAB-Simulink software environment and validated with standard procedures, well-known commercial simulation software and experimental test data. This chapter gives an overview of the modelling technics employed to create the different model components of the building system and its HVAC sub-systems.

3.4.1. MULTI-ZONE BUILDING MODEL

A detailed multi-zone numerical model is created with the MATLAB-Simulink software environment for each of the different building cases. Similarly to the HAM-tools [130] the heat transfer by conduction through the planar construction elements is calculated with a one-dimensional finite control volume method using an explicit formulation to solve the heat equation:

$$\rho c \frac{\partial T}{\partial t} = \nabla \cdot (k \nabla T) + q_v$$

(Equation 3-3)

Where ρ , c , T , k , and q_v are the density, specific heat capacity, temperature, thermal conductivity and volumetric heat source, respectively. In the interest of fast computation, the number of finite control volumes in the construction elements is kept small. This modelling method is therefore commonly named “Resistance-Capacitance network” or “RC network” (see *Figure 3-7*).

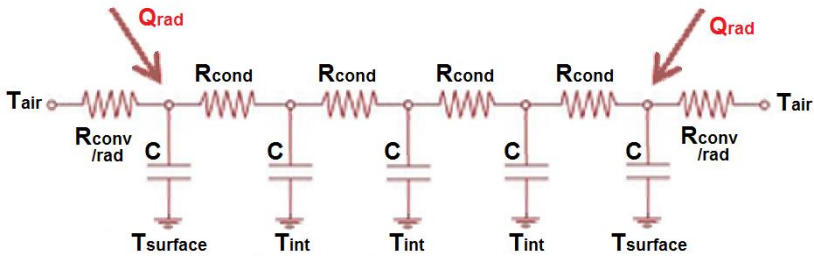


Figure 3-7: Example of a RC network for a wall construction element [21].

External wall, internal wall, ceiling and roof elements are subdivided into 5 thermal nodes in the direction normal to the main surface plan. 2 nodes are assigned to the outermost material layers (plaster, wood, brick or concrete). 3 nodes are assigned to the insulation layer (mineral wool). Floor elements (including the soil under the house, the expanded polystyrene insulation layer and the concrete screed or wooden slab containing the UFH pipes) are subdivided into 9 nodes.

Inside each thermal zone, a star network configuration connects all the surfaces facing the indoor space to the indoor air node with constant mixed convection/radiation thermal resistance coefficients [131]. Constant thermal resistances are used to model thermal bridges, ventilation, air infiltration and windows heat losses. For the external surfaces, the direct and diffuse solar radiation and the long-wave radiation to the sky are calculated as a function of the local weather conditions and the surface orientation.

Concerning internal heat gains, 70% of the people and equipment loads are considered fully convective and thus applied directly to the air node of the thermal zone. The remaining 30% are modeled as radiative and distributed over all the inner surfaces of the planar construction elements with respect to their surface area. Regarding the internal solar gains, 55% are modelled to go to the floor, 30% to go to the vertical walls and 15% to go directly to the air node of the thermal zone [131].

The 10 different thermal zones of the building (9 rooms and an attic) are connected together to form the house multi-zone model. Doors in between the rooms are considered closed at all time and therefore no direct air exchange between the different thermal zones occurs. The ventilation heat recovery is activated during the heating season and turned off if the inlet air temperature is above 22 °C. In case of over-heating during summer period, natural ventilative cooling is simulated by increasing the ventilation rate without any heat recovery.

In this model, the heat equation is solved with an explicit scheme. The size of the simulation time step should therefore be fine enough to avoid any numerical

instability. It is thus set constant to 60 seconds, which is small enough to satisfy the following stability criteria in every finite control volume of the model:

$$\Delta t \leq \frac{1}{2} \times \frac{\rho \cdot c \cdot \Delta \delta^2}{k}$$

(Equation 3-4)

Where Δt is the time step size, $\Delta \delta$, k , ρ and c are the thickness, the thermal conductivity, the density and the specific heat capacity of a finite control volume.

Each sub-component of the building model has been validated against well-known commercial software COMSOL Multiphysics and BSim. The average absolute difference between the MATLAB - Simulink multi-zone building model and the BSim reference model is 0.12 °C for indoor temperature, 0.5 W/m² for the heating power need and 0.88% for the total energy use [21]. In addition, the multi-zone building model has been validated as a whole with a BESTEST procedure [21][132].

3.4.2. HEATING SYSTEMS

Two types of heating emitters are modelled: a convective radiator and a hydronic radiant under-floor heating system. A first order transfer function with a time constant of 10 minutes is employed to model the radiator [133]. 30% of the heating power output is emitted by radiation and 70% by convection. A PI controller is used as a thermostat to regulate the radiator output in each thermal zone.

The hydronic radiant under-floor heating system is modeled as a horizontal heat exchanger embedded in a slab by coupling a “plug flow” model of a pipe with the ϵ -NTU method. The dynamics of the incompressible brine moving through a pipe at variable flow rate is accounted by the plug flow principle [134]. At each time step, a fluid cell is queued at the beginning (inlet) of the pipe. The size of the new fluid cell is calculated according to volume flow rate and the pipe’s diameter. Because of the principle of volume conservation, all the other queued incompressible fluid cells are pushed towards the pipe’s outlet. The outlet fluid temperature is computed as the volume-weighted average temperature of the fluid cells exiting the pipe at each time step. A no-mixing condition between adjacent fluid cells is assumed. This is reasonable as the brine is circulating with a fairly high velocity in the pipes. Moreover, the temperature difference between each neighboring cell remains limited. Consequently, the fluid cells solely exchange heat by convection with the walls of the surround pipe. The heat transfer between the fluid cells, the walls of the pipe and the rest of the UFH slab is calculated with the ϵ -NTU method [125][135].

This modelling technic collapses the complex three-dimensional heat transfer occurring in the slab where the heat exchanger is embedded into a simplified one-dimensional RC star network (see *Figure 3-8*). The calculated effectiveness of the equivalent heat exchanger also accounts for the interaction between the legs of the pipe circuit. The slab surrounding the pipe circuit is sub-divided into 3 thermal nodes. A PI controller regulating a mixing valve is used to adjust the inlet water temperature of the UFH distribution manifold.

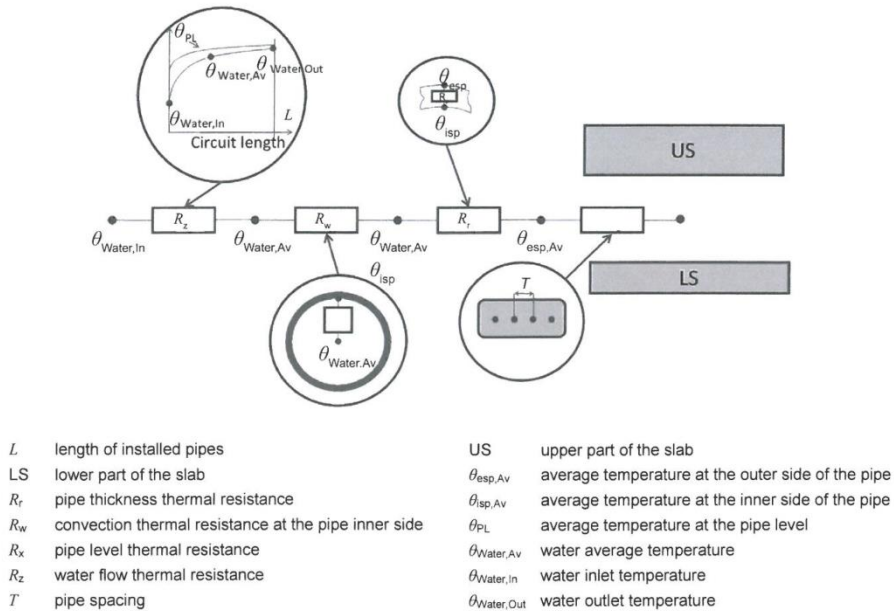


Figure 3-8: General scheme of the resistance network for the ε -NTU method [125]

The horizontal ground source heat exchanger is modelled in the same way as the UFH system with a plug flow model coupled to the ε -NTU method. The ground surrounding the horizontal GSHE is modelled as a one-dimensional domain with a state-space function [21]. The bottom temperature boundary condition of the ground domain (30 m depth) is set constant to 9.4 °C. The boundary conditions of the top ground surface are determined by the outdoor air temperature, wind speed and global solar radiation of the weather data file [128]. The boundary conditions on the sides of the soil domain are following the temperature time variations of an undisturbed ground in Denmark [21].

Two plug flow / ε -NTU method pipe heat exchanger models are coupled together to simulate the dynamic behavior of the vertical borehole GSHE. One pipe model is

accounting for the inlet leg of the U-pipe collector and the second pipe model accounts for the outlet leg of the collector. The complex interaction between the two legs of the collector, the filling grout of the borehole and the surrounding soil are modelled with a triangular thermal RC network presented by Diersch et al. [136]. Similarly to the horizontal GSHE, the ground surrounding the vertical borehole is modeled as a one-dimensional finite domain with a state-space function. The boundary conditions of the top ground surface are determined by the weather data file [128]. The boundary conditions on the sides of the soil domain are following the temperature time variation of an undisturbed ground in Denmark. The bottom temperature boundary condition of the ground domain (100 m depth) is set constant to 10.1 °C [21].

Similarly to the magnetocaloric heat pump, the reference conventional vapour-compression heat pump is modelled with a 4-dimensional lookup table compiling steady state operation data provided by the VCHP manufacturer [126]. The outlet temperatures from the evaporator and condenser, the heating and cooling power and the electrical consumption of the compressor are interpolated according to the inlet temperature and fluid mass flow rate to the evaporator and the condenser. The 250 L hot water storage tank model is a simplified version of that presented by Angrisani et al. [137]. The tank has a cylindrical shape: 58 cm diameter and 95 cm height. It is insulated with 5 cm of polyurethane foam and the heat losses to the ambient are therefore 1.356 W/K.

For all the aforementioned hydronic systems, the convective heat transfer coefficient of the brine circulating in the pipe is calculated according to the fluid flow rate and temperature, Reynolds number, and other temperature dependent thermophysical properties of the brine

The different components of heating system have been validated against the well-known commercial software BSim and with experimental test data [21].

3.4.3. INDOOR CONTENT / FURNITURE ELEMENTS

For each thermal zone of the building, the indoor content and furniture elements are aggregated in an equivalent fictitious planar element. The thermophysical properties of the equivalent material composing this planar element are chosen according to the suggestions presented before [67][81]. The equivalent element has a thickness of 4.7 cm with a mass corresponding to 60 kg/m² of the room's floor surface area. The surface area of each side of the element is equal to 1.8 times the room's floor surface area. Because the element does not have a real geometrical representation in the thermal zone, it is considered that 50% of the radiative share of the equipment, people, solar and radiator heating loads are absorbed by its surface. The element is coupled to the air node of the zone with a constant mixed convection/radiation surface thermal resistance of 0.13 m².K/W [131].

The thermodynamics of the planar element is calculated with a fully implicit (unconditionally numerically stable) one-dimensional FVM formulation (control volumes are 1 mm thick). This FVM model has been validated against the well-known commercial software COMSOL Multiphysics [21].

3.4.4. LATENT HEAT THERMAL ENERGY STORAGE

Two types of LHTES system are considered in this study: PCM wallboards placed on the inner surface of walls and ceilings; PCM integrated on one side of the furnishing elements. Both systems consist of Energain® stable form PCM arranged in thin slabs. Energain® is a well-known commercial product. It is composed of 60 %mass micro-encapsulated paraffin (organic PCM) blended with 40 %mass polyethylene [109]. The thickness of the PCM panel is 1.5 cm. This sizing is a reasonable choice to insure an optimum activation of the PCM slab and a maximum additional effective thermal storage capacity with the minimum amount of material [21]. Guarded Hot Plate Apparatus and Differential Scanning Calorimetry measurements were conducted on Energain® samples. The results are combined with the information provided by the manufacturer to determine the thermophysical properties of the LHTES system. The PCM thermal conductivity varies between 0.18 W/m.K and 0.22 W/m.K as function of temperature. Its density is 1000 kg/m³, its specific heat capacity is 2000 J/kg.K, and its latent heat of fusion is 120 kJ/kg with a phase transition temperature of 22 °C [21].

Many PCM numerical models for building applications use an apparent specific heat capacity function to simulate the latent heat of the phase transition. Nevertheless, this approach does not represent the real physics of the phase transition but only its apparent thermal behaviour. In this study, the PCM model is based on an enthalpy formulation which accounts properly for the isothermal melting/solidification phase transition process [138][139].

The stable form PCM is assumed to be homogenous and set in thin layers. The heat transfer is thus considered one-dimensional. The temperature dependent density, specific (non-latent) heat capacity and thermal conductivity are modelled with linear functions fitting experimental test data. From these material properties, an enthalpy / temperature function accounting for the isothermal phase transition is built (see *Figure 3-9*). A fully implicit one-dimensional FVM formulation (control volumes are 1 mm thick) is then used to perform the calculation of the heat transfer within the PCM slab. In each control volume, the variation of internal energy (enthalpy) is then used with the enthalpy / temperature function to obtain the new temperature of the PCM cell.

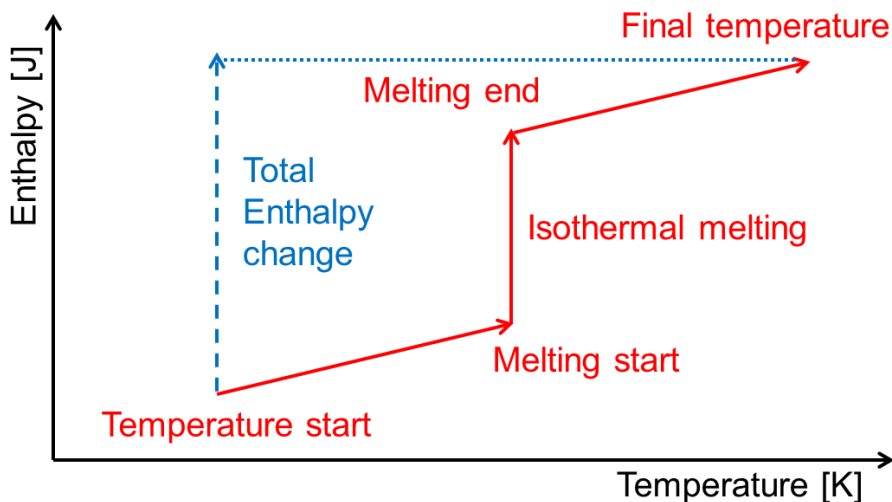


Figure 3-9: Enthalpy / temperature function for modelling phase change materials [21].

This PCM model can have distinct melting and solidification temperatures which allows it to account for hysteresis phenomena. However it is chosen to not introduce hysteresis for this study. The main limitation of this numerical model is that it cannot account for multiple phase transition temperatures. This situation can occur when the PCM is a mixture of several compounds with dissimilar melting temperatures. In the current case, it is thereby considered that the PCM presents only one definite phase transition temperature.

This PCM model has been validated against experimental tests performed on Energain® samples with a Guarded Hot Plate Apparatus [21].

For further information, please refer to Appendix B. Paper II, Appendix C. Paper III and Appendix F. Technical Report I: “Numerical analysis of the impact of thermal inertia from the furniture / indoor content and phase change materials on the building energy flexibility”, “Integration of a magnetocaloric heat pump in a low-energy residential building” and “Description and Validation of a MATLAB - Simulink Single Family House Energy Model with Furniture and Phase Change Materials (Update)”.

CHAPTER 4. HEATING ENERGY FLEXIBILITY POTENTIAL OF RESIDENTIAL BUILDINGS

As mentioned before, a paradigm shift is operating in the building energy sector and the interest for demand-side management strategies is increasing. Among the different building energy flexibility measures, passive thermal energy storage in the indoor environment has been found to be a cost effective solution to facilitate the management of Smart Energy Grid systems. This clever usage of the building thermal inertia can generate a larger reduction of excess RES electricity production and fuel consumption with a lower total cost compared to heat storage in water tanks [39]. The built environment presents a large thermal storage potential. The indoor temperature set point can be increased to store heat when the electricity is available and cheap, and it can be decreased when the power production is insufficient. Nonetheless, the building operative temperature should always be kept within the limits of the occupants' thermal comfort. Besides, building heating energy flexibility solutions are matter of great interested because heating demand remains the dominating energy need for cold winter countries, despite the continuous building regulation tightening of the latter. In Denmark, for instance, indoor space heating accounts for 25% of the annual national energy use [140].

With 75% of the total building surface area in Europe, the residential building stock is a major target. Moreover, single-family houses represent 64% of the residential heated surface area in Europe [17] and 60% in Denmark [141]. The focus of this study is therefore put on the heating energy flexibility potential of single-family dwellings in Denmark using an indoor temperature set point modulation strategy for TES in the built environment.

Previous studies have investigated the influence of different building parameters on the ability to modulate heating use. For TES in the build environment, the structural thermal mass defines the maximum storage capacity of the building. The larger the activated thermal mass, the more heat can be stored during off-peak periods and partly recovered during peak periods [142][143].

Other studies have shown that the building storage effectiveness and heating energy flexibility ability mainly depend on the level of envelope insulation and air tightness [144]. Poorly insulated buildings can only sustain short term heating load shifting of 1 to 5 hours. On the other hand, high performance envelope buildings can turn off their heaters in winter for more than 24 hours after a heat accumulation period without compromising thermal comfort [35].

The type of heat emitter also plays an important role in the effective storage capacity of a building and thus its energy flexibility potential. On the one hand, radiators have mainly convective heat emission which results in a quick air temperature rise. The ventilation and infiltration heat losses are augmented and the heat storage in the heavier building structural elements is limited. On the other hand, radiant terminals such as under-floor heating or thermally activated building systems (TABS) induce a direct thermal activation of construction floor elements with high thermal storage capacity. The indoor air temperature is maintained lower than in the case of convective terminal. The ventilation heat losses are thus reduced and a more effective heat storage is achieved [35][142][145][146].

Phase change materials can offer a significant improvement of the building TES potential within the narrow temperature span corresponding to the human comfort [67]. LHTES can easily be integrated as wallboard on the inner surfaces of the indoor environment to improve the heat storage capacity and therefore heating energy flexibility of light structure buildings. Some publications reported the benefit of PCM wallboards [147] and PCM under-floor heating systems [148] for space heating load shifting with a temperature set point modulation controller. Finally, the large surface area of furnishing elements which is exposed to the indoor environment could also be employed for the integration of PCMs and thus extend the applicability of the TES strategies [67].

The current numerical study aims at exploring further and quantifying the impact of the main building parameters (insulation level, thermal inertia, type of heat emitter) on the indoor space heating energy flexibility potential of Danish single-family dwellings. A particular attention is put on role of the structural thermal inertia and the influence of additional thermal mass from the indoor content / furniture or passive LHTES systems such as PCM wallboards and furniture with integrated PCM.

4.1. BUILDING ENERGY FLEXIBILITY INDEX

The building energy flexibility is a recent concept which is gaining a lot of attention nowadays. This research topic is very active and several different definitions and indicators have been created to determine what is “building energy flexibility” and how to quantify it. However, no scientific agreement has been reached yet. The on-going IEA EBC Annex Project 67 [38] is aiming to tackle these problems. Lopes et al. [149] and Reynders et al. [150] published thorough reviews and evaluations of the existing definitions and quantification methodologies for the energy flexibility of the building sector. It appears that publications usually define the energy flexibility as the ability for a building to adapt its profile of energy use without jeopardizing technical and comfort constraints [150].

In this study, the energy flexibility is defined as the ability for the building to shift in time its indoor space heating use from high energy price to low price energy periods whilst insuring a good indoor thermal comfort. In other words, a building is considered to be energy flexible if it manages to maximize its heating usage during low energy price periods and minimize it during high energy price periods [151]. Consequently, the energy flexibility index of this study is calculated as the change of heating use during medium and high price periods when the energy is accumulated during low price periods compared to a reference scenario without any heating load shifting strategy:

$$F = \left[\left(1 - \frac{\%High}{\%High_{ref}} \right) + \left(1 - \frac{\%Medium}{\%Medium_{ref}} \right) \right] \times \frac{100}{2}$$

(Equation 4-1)

Where F is the building energy flexibility index, $\%High$ and $\%Medium$ are the percentages of yearly heating energy (relatively to the total yearly heating needs) used during high and medium energy price periods respectively when the TES strategy is operational. Equivalently, $\%High_{ref}$ and $\%Medium_{ref}$ are the percentages of yearly heating energy use for the reference scenario (no TES strategy). The flexibility index takes the value of zero if the repartition of the energy use is the same as in the reference case. In that situation, the building did not provide any energy flexibility. The index becomes negative if the share of high and medium energy price periods is larger than the reference values. In that case, the building is performing worse than the reference scenario in terms of energy flexibility. The flexibility index reaches 50% if the energy share of the medium energy price period does not change and if all the energy share of the high energy price period is shifted to the low energy price period. Similarly, the flexibility index reaches 50% if the energy share of the high energy price period does not change and if all the energy share of the medium energy price period is shifted to the low energy price period. If both the high and the medium energy price period shares are decreased by half, the flexibility index also takes the value of 50%. If there is no remaining energy usage during the periods of high and medium energy price, the flexibility index takes the maximum value of 100%. In that situation, the building is fully energy flexible [151].

Several comments can be addressed to this building energy flexibility index. Firstly, a reference energy usage scenario is required for the index calculation, which is not necessary possible or convenient. Secondly, the limits and number of categories for the energy price are set arbitrarily. Moreover, the index is linked to a specific energy price profile. Different spot energy price profiles with shorter or longer price periods

could have a significant impact on the flexibility index. Similarly, the local climate and occupants' behaviour can seriously influence the results of the building energy flexibility index [152].

4.2. HEAT STORAGE CONTROL STRATEGY

The indoor space heat storage strategy which is implemented for this study is similar to the one used by Le Dréau et al. [35] and Péan et al. [153]. The end-goal of the energy flexibility measures is to allow the integration of a larger share of intermittent RES in a Smart Grid system. The building should therefore be able to accumulate energy when there is an excess of RES production, and reduce its energy usage when the RES production is low. The scope of that study is the indoor space heating energy flexibility for Danish detached houses where the primary heating source is an electrically driven heat pump. In Denmark, a large share of the electrical RES production is coming from wind turbines. The electricity spot price is thus a good indicator of the RES availability and the energy demand in Denmark. Consequently, the "Nord Pool" electricity spot price (hourly market price observed in the Nordic electricity market in the year 2009 [154]) is used here to control the heat storage strategy. The building accumulates heat energy during low energy price periods and save heat energy during high energy price periods.

As illustrated in *Figure 4-1*, limits for low price period and for high price period are calculated every hour as the lowest and highest quartile of the electricity market spot price over the last 14 days. The house temperature set point is then modulated accordingly:

- For high price periods, the temperature set point is set to minimum at 20 °C to save thermal energy.
- For medium price periods, the temperature set point is set to neutral at 22 °C.
- For low price periods, the temperature set point is set to maximum at 24 °C to accumulate thermal energy.

The temperature span of 4 K between the minimum set point and the maximum set point corresponds to a normal level of thermal comfort with less than 10% of dissatisfied occupants [155]. In addition, the transient indoor temperature variation is always kept below the thermal comfort limit of 2.1 K/h [156].

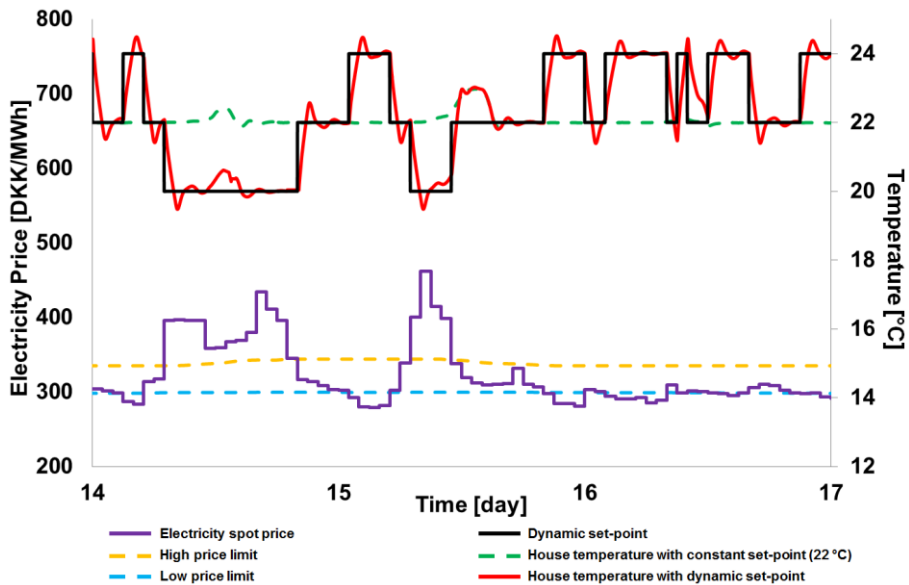


Figure 4-1: Example of indoor temperature set point modulation with price control and maximum activation time of 6 hours for low-insulation light structure house with radiator [151].

The occupants of a residential building might not agree with the change of the indoor temperature set point by an external signal for an extended period of time. The longer the set point deviates from the neutral level and the more disturbance could be caused to the occupants. In order to study the impact of different occupants' disturbance levels on the building energy flexibility, a maximum activation (high or low set point) time is defined between 30 minutes and 24 hours. When the activation period reaches the maximum activation time, the set point is put back to its neutral level of 22 °C. The temperature set point is then maintained at the neutral point for a period of time equal to the maximum activation time before the same activation can occur again [151].

4.3. RESULTS AND DISCUSSION

4.3.1. IMPACT OF ADDITIONAL INDOOR THERMAL MASS ON THE BUILDING TIME CONSTANT

The time constant of six building cases (three different structural thermal inertia classes: light 30 Wh/K.m², medium 50 Wh/K.m², heavy 100 Wh/K.m²; two envelope insulation levels: low-insulation house from the 80's, high-insulation passive house)

is calculated with and then without any additional indoor content / furniture or PCM element thermal mass. For that purpose, the outdoor temperature is kept constant whilst all radiation and internal gains are set to zero. Once the house’s temperature has reached a steady state, the convective radiator power is increased to maximum until the temperature reaches a new steady state at a higher temperature. The building time constant is then calculated as the time needed to reach 63.21% of the temperature change between the two steady states [157].

One can observe in *Figure 4-2* the influence of the different types of additional thermal mass on the building time constant. The time constant and the daily effective thermal inertia of the reference empty buildings are stated in the table below the figure. Results show that the PCM wallboards and the PCM integrated in furniture increase significantly the time constant of all the buildings. Concerning the indoor content / furniture elements, their effect is limited for medium and heavy structure cases but not negligible for light structure houses [151].

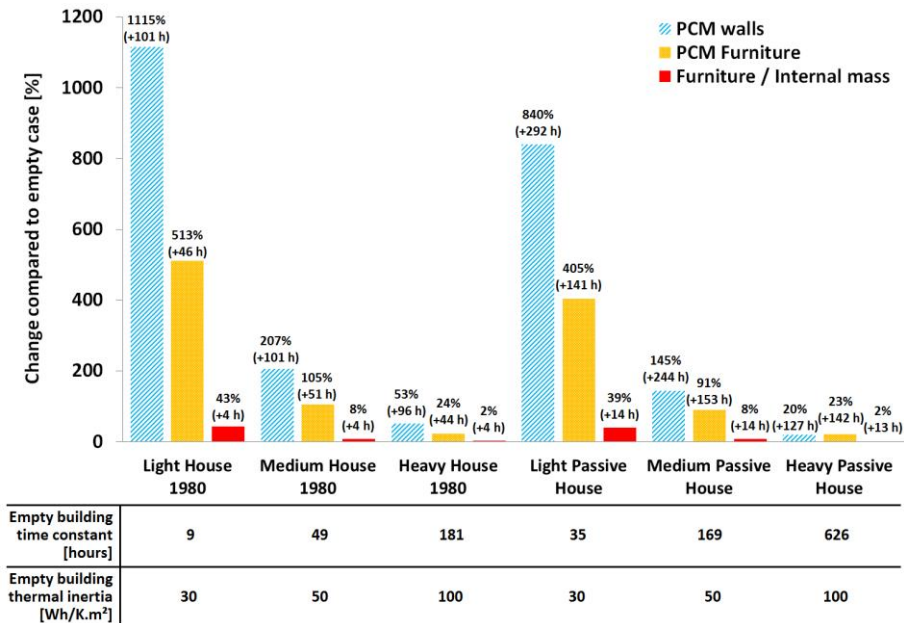


Figure 4-2: Change of building time constant with additional internal thermal mass [151].

4.3.2. INFLUENCE OF THE MAXIMUM ACTIVATION TIME ON THE BUILDING ENERGY FLEXIBILITY

48 different building configurations (two envelope insulation levels; three structural thermal inertia classes: light 30 Wh/K.m², medium 50 Wh/K.m², heavy 100 Wh/K.m²; four kinds of additional indoor thermal mass; two types of heating system) with 8 different maximum activation times each are compared. One can see in *Figure 4-3* an example of the indoor space heating energy usage distribution over the different price categories for increasing maximum activation time. High price periods are minimized together with a significant low price periods increase. There is no action to decrease energy use during medium price periods. The latter are therefore only marginally reduced as a secondary effect of the thermal storage during high price periods. Similar patterns can be observed for all the building cases [151].

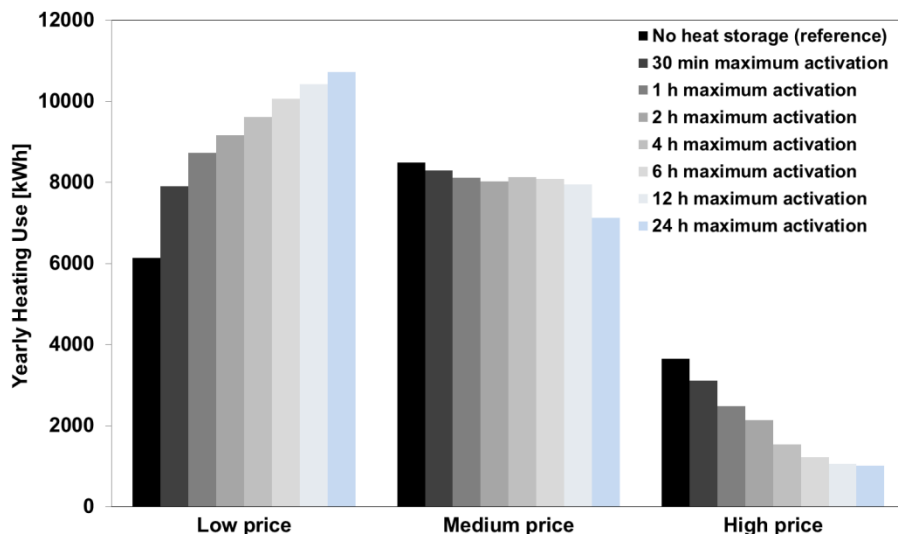


Figure 4-3: Example of yearly indoor space heating use repartition as function of maximum activation time (light-weight structure low-insulation house with PCM wallboard) [151].

The thermal storage in the indoor space by increasing the temperature of the built environment necessarily induces an augmentation of the building heat losses through the envelope and the ventilation system. In the current study, the average increase of the yearly energy use due to the heat accumulation strategy (24 hours of maximum activation) is 3.3% and 6.3% for houses from the 80's and passive houses, respectively. This observation is in agreement with previous studies [35].

Figure 4-4 presents the variation of the building energy flexibility index in function of the maximum activation time. The flexibility index increases quickly and then stabilizes for activation times above 6 hours. This saturation can be caused by two phenomena. Firstly, the building thermal storage capacity reaches its maximum limit and no more energy can be accumulated to improve the flexibility. Secondly, the maximum activation time is different from the effective activation time due to the variation frequency of the price signal. A Fourier analysis of the latter shows that its main components have an oscillation period of 12 hours, 24 hours and 1 week. Consequently, the available low price periods for storage are rarely lasting more than 6 hours and the average effective activation time has a maximum of 4.7 hours. These results are coherent with the previous study of Le Dréau et al. [35].

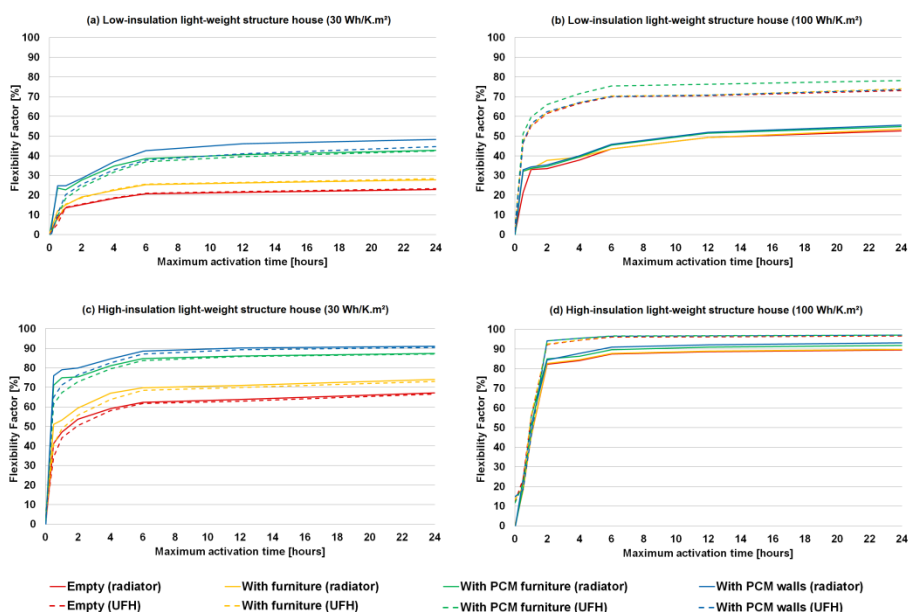


Figure 4-4: Building energy flexibility as function of maximum activation time (radiator: convective radiator; UFH: under-floor heating) [151].

4.3.3. IMPACT OF THE BUILDING PARAMETERS ON THE ENERGY FLEXIBILITY

One can see in Figure 4-5 the building energy flexibility of 144 different cases (two envelope insulation levels, three classes of structural thermal inertia with three different sub-variations, two types of heating system and four additional indoor thermal mass configurations: empty room, indoor content / furniture, PCM furniture, PCM wallboards) as function of the total effective building thermal inertia

(including structural and additional thermal mass). The maximum activation time is 24 hours.

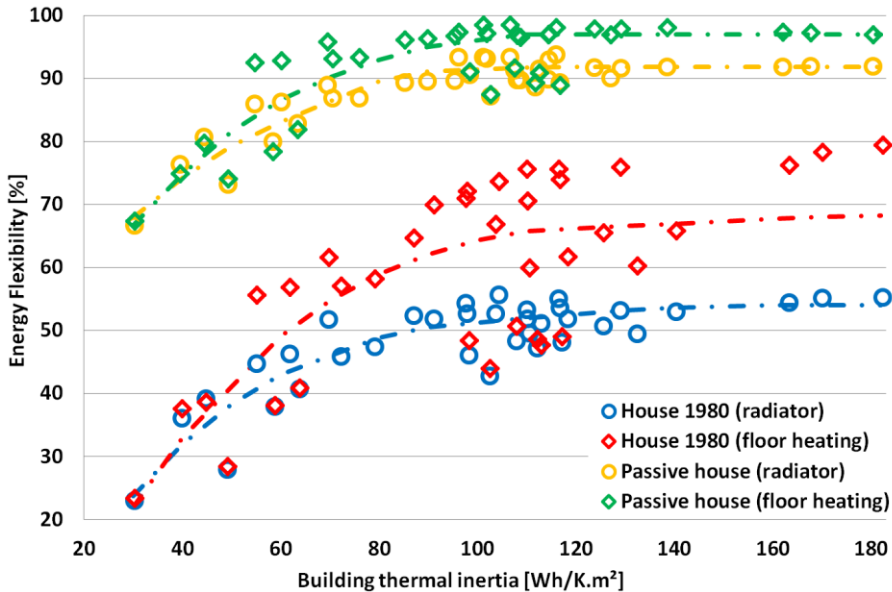


Figure 4-5: Evolution of the building energy flexibility as function of the thermal inertia for different insulation levels and heating systems [151].

Compared to the low-insulation dwelling, the passive house has lower indoor space heating needs and can therefore shift it with a smaller thermal storage capacity. In addition, high efficiency envelope maximizes the retrieval of the accumulated thermal energy. Passive houses thus present much larger heating energy flexibility potential than low-insulation dwellings. However, the latter have an absolute amount of energy shifted in time which is about 4 times more important than the high-insulation houses. Consequently, the low-insulation houses could be the main energy flexibility providers to the energy grids [151].

Above 80 Wh/K.m² of total daily effective thermal inertia, the heating energy flexibility stagnates, especially for well-insulated houses. Medium and heavy structure passive houses reach the maximum energy flexibility index: there is no remaining indoor space heating energy usage to be shifted in time and increasing thermal storage capacity further is ineffective. For low-insulation dwellings, additional thermal mass does not compensate for the poor envelope performance limiting the recovery of the accumulated thermal energy [151].

Concerning heat emitters, the UFH system presents greater performance compared to radiators in the case of medium and heavy structure houses. The concrete screed where the UFH hydronic circuit is laid is highly activated, allowing larger heat storage. Moreover, radiant UFH system can provide the same level of thermal comfort with a lower indoor air temperature. Ventilation and infiltration thermal losses are thus decreased and the heat accumulation efficiency is improved together with the energy flexibility. The employment of UFH can thus increase the building heating energy flexibility by up to 44% and 8% for low-insulation and high-insulation dwellings, respectively. However, the UFH was integrated in a wooden floor for light structure house. Consequently, the limited activated thermal mass of the latter does not improve the building heating energy flexibility [151].

4.3.4. IMPACT OF ADDITIONAL INDOOR THERMAL MASS ON THE BUILDING ENERGY FLEXIBILITY

The impact of three different types of additional indoor thermal mass element on the building heating energy flexibility is present in *Figure 4-6*. The energy flexibility and daily effective thermal inertia of the reference empty buildings are stated in the table below the figure. The relative values of the flexibility improvement are indicated as percentage and the absolute values of the flexibility change are in between parentheses.

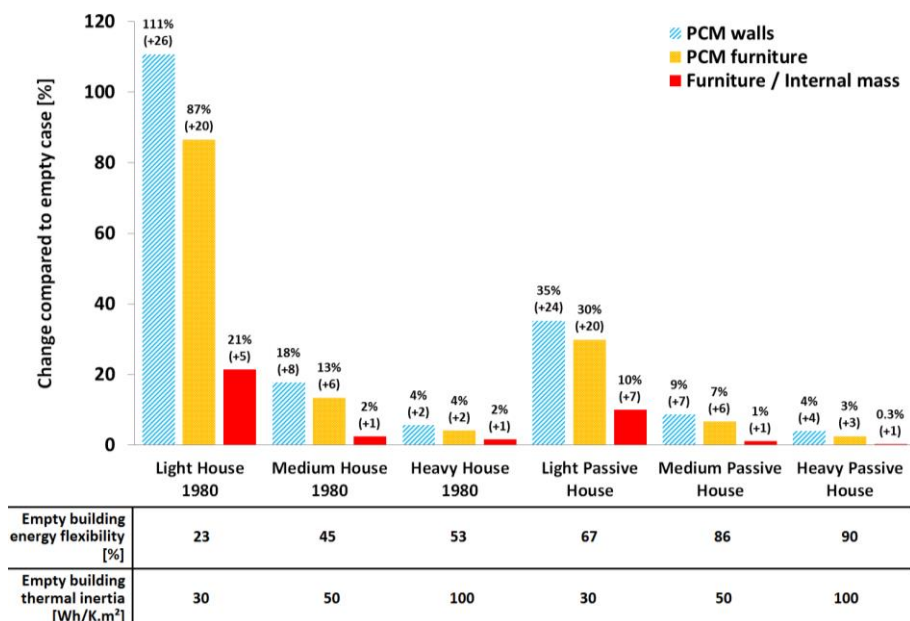


Figure 4-6: Change of building heating energy flexibility with additional indoor thermal mass (radiator heating system cases with maximum activation time of 24 hours) [151].

One can see that PCM wallboards and furniture with integrated PCM can appreciably increase the energy flexibility potential of dwellings with low insulation and low structural thermal inertia. However, the improvement is reduced for well-insulated houses and very limited for buildings with medium and heavy structures [151].

It should be noted that PCMs and consequently PCM wallboards have a relatively low thermal conductivity. When positioned on the inner surface of construction elements in the built environment, the PCM wallboards obstruct the activation of the thermal mass underneath them. This is a problem in the case of buildings with heavy structure such as concrete or brick walls. The large heat storage capacity of these construction elements is nullified by the presence of the PCM wallboards and is barely compensated by the latter [151].

Concerning furniture and indoor content, they only account for a small share of the total effective thermal inertia of medium and heavy structure houses [67]. It is thus not surprising that their impact on the building energy flexibility is almost negligible. Nevertheless, in the case of light structure dwellings, the influence of the indoor items is significant and should therefore be taken into account [151].

4.3.5. PARAMETRIC SENSITIVITY ANALYSIS

A statistical analysis of the previously presented results is performed to rank the different building parameters by order of significance regarding the heating energy flexibility. The parameter significance is assessed by the mean of consecutive ANOVA (analysis of variance) tests on linear regression models with iterative deletion of the least significant term [158]. The results are presented in *Table 4-1* with the most significant building parameter (highest F-value) on the top. It is clear that the envelope insulation level has the main role in the heating energy flexibility compared to the building thermal inertia, the type of heat emitter or the kind of additional indoor thermal mass.

Table 4-1: Significance ranking of the building parameters regarding heating energy flexibility [151].

Significance ranking	Building parameter	F-value
1	Envelope insulation level	685.4
2	Thermal inertia	91.4
3	Heating system type	42.3
4	Additional indoor thermal mass type	14.6

A sensitivity analysis is performed on the influence of the additional indoor thermal mass parameters regarding the heating energy flexibility of light-weight structure dwellings. One can see in *Table 4-2* the change of the flexibility index for realistic variations of the additional indoor thermal mass characteristics.

Table 4-2: Sensitivity analysis of the additional indoor thermal mass parameters [151].

Indoor items / furniture	Parameter variation			Variation of building energy flexibility			
				House 80's		Passive House	
	Low	Reference	High	Low	High	Low	High
Surface heat transfer coefficient [W/K.m ²]	5	7.7	10	-8.4%	18.4%	-5.1%	10.1%
Mass [kg/m ² floor area]	20	60	100	-11.6%	10.6%	-6.0%	4.7%
Surface area [m ² /m ² floor area]	0.8	1.8	2.8	-8.8%	7.8%	-4.3%	3.1%
Material density [kg/m ³]	150	715	1500	1.5%	-2.7%	0.5%	-1.0%
Material thermal conductivity [W/m.K]	0.1	0.3	0.5	2.3%	-0.5%	2.3%	-0.7%

PCM furniture parameters	Parameter variation			Variation of building energy flexibility			
				House 80's		Passive House	
	Low	Reference	High	Low	High	Low	High
Surface heat transfer coefficient [W/K.m ²]	5	7.7	10	-7.0%	12.2%	-3.1%	3.2%
Furniture mass [kg/m ² floor area]	20	60	100	-0.3%	2.6%	-0.2%	1.1%
PCM furniture surface area [m ² /m ² floor area]	0.8	1.8	2.8	-16.5%	9.3%	-10.6%	4.5%
Furniture material density [kg/m ³]	150	715	1500	-0.4%	0.9%	-0.2%	0.5%
Furniture material thermal conductivity [W/m.K]	0.1	0.3	0.5	-0.4%	0.3%	-1.0%	0.5%
PCM layer thickness [cm]	0.5	1.5	3	-13.7%	4.2%	-5.1%	1.2%
PCM average thermal conductivity [W/m.K]	0.1	0.2	0.4	-11.4%	10.6%	-2.3%	1.3%
PCM latent heat of fusion [kJ/kg]	60	120	180	-19.4%	11.3%	-6.5%	1.2%

PCM Wallboard parameters	Parameter variation			Variation of building energy flexibility			
				House 80's		Passive House	
	Low	Reference	High	Low	High	Low	High
Surface heat transfer coefficient [W/K.m ²]	5	7.7	10	-3.1%	1.3%	-1.2%	0.7%
PCM layer thickness [cm]	0.5	1.5	3	-15.7%	7.8%	-5.4%	1.2%
PCM average thermal conductivity [W/m.K]	0.1	0.2	0.4	-16.1%	8.0%	-5.3%	0.9%
PCM latent heat of fusion [kJ/kg]	60	120	200	-24.1%	9.8%	-8.5%	2.4%

An ANOVA statistical analysis is performed on the results of *Table 4-2*. The *Table 4-3* summarizes the significance ranking of the different parameters of the three types of additional indoor thermal mass. The surface heat transfer coefficient, the mass and the surface area of the elements play the main roles for indoor items/furniture. However, the material density and the thermal conductivity have little significance. For PCM furniture, the exposed surface area, the surface heat transfer coefficient and the PCM properties are the most significant parameters. For PCM wallboards, the PCM layer characteristics have dominant impacts.

Table 4-3: Significance ranking of the additional thermal mass parameters regarding heating energy flexibility [151].

Indoor items / furniture		
Significance ranking	Parameter	F-value
1	Surface heat transfer coefficient	30.1
2	Mass	18.3
3	Surface area	18
4	Material density	1.7
5	Material thermal conductivity	1.2
PCM furniture		
Significance ranking	Parameter	F-value
1	Surface area	45.1
2	PCM latent heat of fusion	27.9
3	Surface heat transfer coefficient	13.8
4	PCM thermal conductivity	11.8
5	PCM layer thickness	10.9
6	Furniture mass	0.5
7	Furniture material density	0.1
8	Furniture material thermal conductivity	0.1
PCM wallboard		
Significance ranking	Parameter	F-value
1	PCM latent heat of fusion	29
2	PCM layer thickness	12.6
3	PCM thermal conductivity	12.1
4	Surface heat transfer coefficient	0.5

4.4. CONCLUSION

The numerical study presented in this chapter has identified the role and quantified the impact of different building parameters concerning the heating energy flexibility potential of a Danish single-family house with a TES strategy based on indoor temperature set point modulation according to a price signal. The index assessing the building energy flexibility is defined as the ability of the dwelling to shift its indoor space heating use in time by accumulating thermal energy in the build environment during low electricity price periods, and conserve energy during high electricity price periods to reduce its heating use at that moment.

The maximum TES capacity of a building is mainly determined by its total effective thermal inertia. However, the results of a parametric sensitivity analysis show that the envelope insulation level is the most important building parameter with respect to the heating energy flexibility potential. Therefore, well-insulated dwellings can efficiently store thermal energy in their built environment and retrieve a large share of it later, allowing them to shift heating loads over long periods of time. Nevertheless, poorly insulated houses, despite their limited energy flexibility index, can have an important impact on the energy grids. The absolute amount of thermal energy they can shift is much larger than the one of highly insulated houses, but it can only be carried out over short periods of time. To a lesser extent, radiant under-floor heating system can improve the energy flexibility of buildings when the hydronic circuit is embedded in a dense material layer such as a concrete screed. The UFH decreases ventilation losses and benefits from the large activation of the floor thermal mass which increases the effective TES capacity and the building energy flexibility potential.

Phase change materials integrated in wallboards or in furniture elements can significantly increase the total effective thermal storage capacity of light-weight structure houses and therefore improve their heating energy flexibility potential. However, PCM wallboards should not be employed on heavy construction elements. They screen the thermal activation of the material layers placed beneath them and barely provide the same heat storage capacity as traditional concrete or brick walls.

Finally, it was demonstrated that the empty space assumption for dynamic energy simulations is not appropriate for houses with low structural thermal inertia. Transient thermal behaviour, building time constant, total heat storage capacity and heating energy flexibility can be significantly influenced by the presence of indoor content / furniture in the built environment.

For further information, please refer to Appendix B. Paper II and Appendix D. Paper IV: “Numerical analysis of the impact of thermal inertia from the furniture / indoor content and phase change materials on the building energy flexibility” and “Influence of envelope, structural thermal mass and indoor content on the building heating energy flexibility”.

CHAPTER 5. INTEGRATION OF A MAGNETOCALORIC HEAT PUMP IN RESIDENTIAL BUILDINGS WITH ENERGY FLEXIBILITY CONTROL STRATEGY

In this chapter, it is numerically demonstrated that a magnetocaloric heat pump can be used to provide for the space heating needs of a low-energy house in Denmark. A description of the device implementation in the building is firstly given, followed by the performance test results of the whole heating system with a simple controller. Finally, a new control strategy taking advantage of the building heating energy flexibility potential is implemented and evaluated on its capacity to improve the performance of the magnetocaloric heating system.

5.1. IMPLEMENTATION OF THE MAGNETOCALORIC HEAT PUMP IN THE HYDRONIC HEATING SYSTEM

For heat pump systems in general, the COP is largely improved by minimizing the temperature span between the heat source and the heat sink [119]. Moreover, in the case of magnetocaloric devices, the active magnetic regenerators are designed for an optimum operation temperature. Indeed, the magnetocaloric effect of the solid refrigerant is maximum in the vicinity of its Curie temperature. For some MCM, the latter can be finely adjusted to match the operation temperatures of the AMR [159] and its inherent temperature gradient (graded regenerator) [29]. Consequently, a ground source heat exchanger (horizontal collector or vertical borehole) is chosen as high and relatively stable temperature heat source for the integration of the MCHP in a low-energy house. In addition, a radiant under-floor heating system is chosen as low temperature heat sink (heat emitter) [31].

The MCHP operates at temperatures and fluid flow rates which are compatible with direct use in the UFH and in the ground source. The GSHE and the UFH are thereby directly coupled to the MCHP inside a single hydronic loop without any intermediate heat exchanger or hot water storage tank (see *Figure 5-1*). In that configuration, the same heat transfer fluid is circulated through the heat source, the heat sink and the MCHP by a single circulation pump. Such implementation reduces the effective temperature span between the heat source and the heat sink. It also simplifies the whole hydronic circuit which can lead to lower installation and operation costs [31].

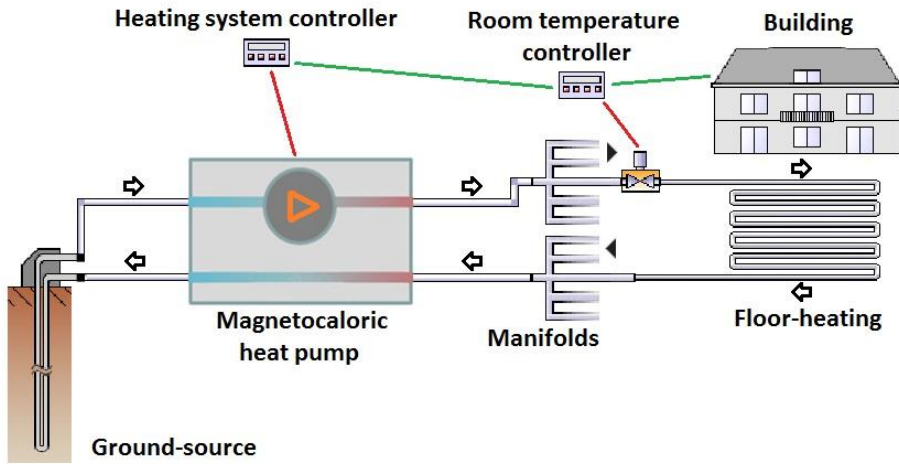


Figure 5-1: Integration of a magnetocaloric heat pump in single hydronic loop with ground source and under-floor heating system [31].

5.2. PERFORMANCE OF THE MAGNETOCALORIC HEAT PUMP WITH SIMPLE CONTROLLER

All the results presented hereafter correspond to a four-month heating test period (from the 1st of January to the 30th of April) for the low-energy house base case equipped with UFH and horizontal or vertical GSHE under Danish weather conditions (DRY 2013 [128]).

Two different coefficients of performance are defined to assess the MCHP operation efficiency. The COP_{AMR} is calculated with the useful heating power output $Q_{heating}$ delivered by the heat pump and the work due to the AMR internal operation: regenerator hydraulic pressure losses $W_{pressureloss}$ and magnetic work $W_{magnetic}$. This calculation is equivalent to considering that the motor and the pump of the MCHP have a 100% efficiency:

$$COP_{AMR} = \frac{Q_{heating}}{W_{pressureloss} + W_{magnetic}}$$

(Equation 5-1)

The COP_{system} is calculated with the useful heating power output of the heat pump and all the heating system operation works: circulation pump work W_{pump} ($W_{pressureloss}$ including the losses due to inefficiency), motor work W_{motor} ($W_{magnetic}$ including the losses due to inefficiency) and valves work W_{valves} :

$$COP_{system} = \frac{Q_{heating}}{W_{pump} + W_{motor} + W_{valves}}$$

(Equation 5-2)

A first test is performed with the magnetocaloric heating system supplying space heating to only one thermal zone: the living room. The heating system is controlled by a simple ON/OFF controller with a constant fluid flow rate during the 4 months of the test period. One can see in *Figure 5-2* and *Figure 5-3* the results of 150 simulations where average heating output, power usage and seasonal COPs are calculated for different constant fluid flow rates, rotation frequencies and types of GSHE [31].

The MCHP heating output and power need increase rather linearly with the nominal fluid flow rate. Most of the power use is due to pump work. At the lowest rotation frequency of 0.5 Hz, the MCHP heating output drops dramatically for fluid flow rates above 1600 L/h. Compared to the vertical borehole GSHE, the power output of the MCHP is sensibly diminished when connected to the horizontal GSHE because the average fluid temperature provided by the latter is significantly lower than the one of the vertical ground source. If coupled with a vertical borehole GSHE, the magnetocaloric heating system can deliver up to 2600 W of useful thermal power when operating at a rotation frequency of 1 Hz with a fluid flow rate of 2100 L/h. In this case, the average seasonal COP_{system} is 3.93 [31].

Concerning the efficiency of the AMR cycle only, the COP_{AMR} is maximum at rather low fluid flow rates and for low rotation frequency. However, in that case, even if the COP_{AMR} is significantly high, the heating power output is very limited while the energy use of the circulation pump remains high. Consequently, the COP_{system} of the overall heating system is maximum at the highest fluid flow rates with rotation frequency of 1 Hz or 2 Hz. Finally, the vertical borehole GSHE configuration presents better performance in terms of both COPs because of its higher fluid temperature supply [31].

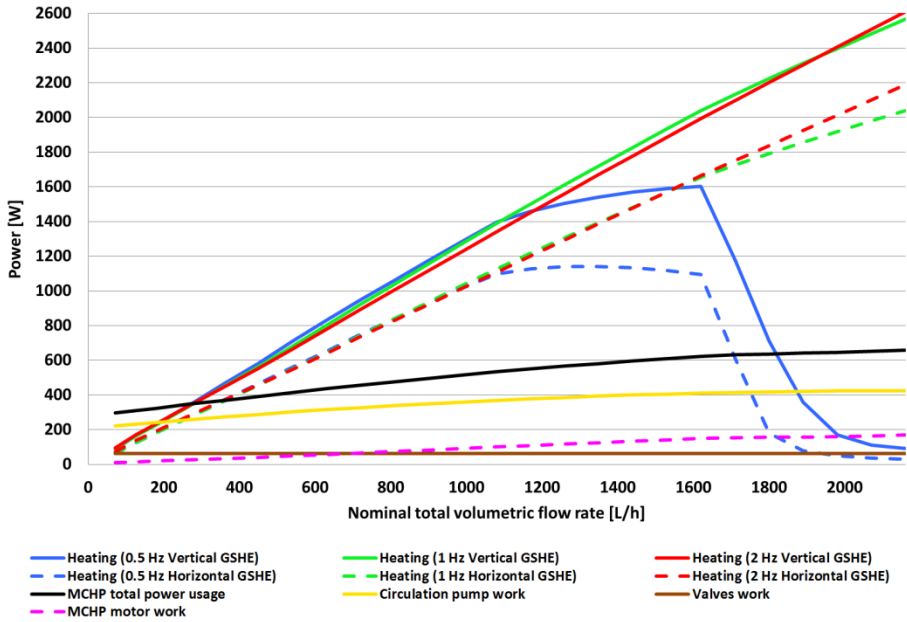


Figure 5-2: Heating power output and power usage of the magnetocaloric heat pump as function of fluid volumetric flow rate [31].

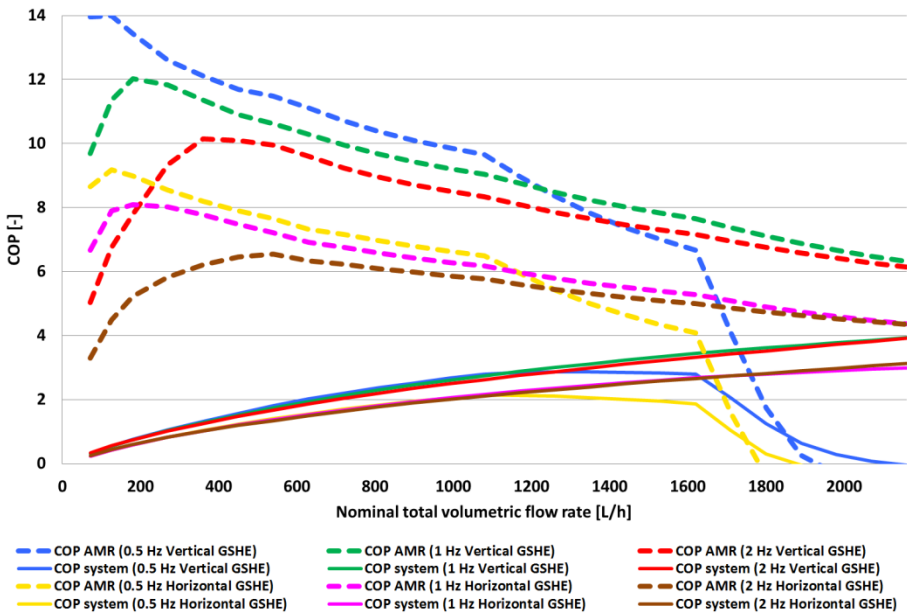


Figure 5-3: COP of the magnetocaloric heat pump and the entire heating system as function of the fluid volumetric flow rate [31].

A second test is performed with the magnetocaloric heating system supplying space heating to the entire house. According to the previous test results, the best performance for the MCHP over the whole fluid flow rate operation range is achieved for a rotation frequency of 1 Hz. This parameter is thus fixed to 1 Hz for the rest of the study. The heat pump controller is a basic flow rate regulation. The speed of the circulation pump is adjusted to keep a nominal fluid flow rate of around 220 L/h in each UFH sub-circuits. There are 9 UFH hydronic loops for the 8 thermal zones of the house. Each thermal zone has a thermostat adjusting the indoor temperature to a given set point by opening/closing the valve of the corresponding sub-loop. The speed of the MCHP circulation pump is varied accordingly. If all the valves of each floor heating sub-circuit are closed, the circulation pump and the MCHP are turned off [31].

One can see in *Figure 5-4* the temperature of the different building systems over the four-month heating test period. The magnetocaloric heating system successfully manages to provide inlet fluid to the UFH at an average temperature of 25.42 °C (maximum of 28.50 °C) allowing the operative temperature of the house to reach the set point of 22 °C at all time. In addition, one can observe that the outlet fluid temperature of the vertical borehole GSHE is higher (8.17 °C in average) and more stable than the one of the horizontal GSHE (2.42 °C in average). The temperature span between the heat source and sink is 17.25 °C and 23.00 °C in average for the vertical GSHE and the horizontal GSHE, respectively. Such results were expected as horizontal collectors are closer to the cold top surface of the ground and therefore more exposed to the outdoor air temperature variations [31].

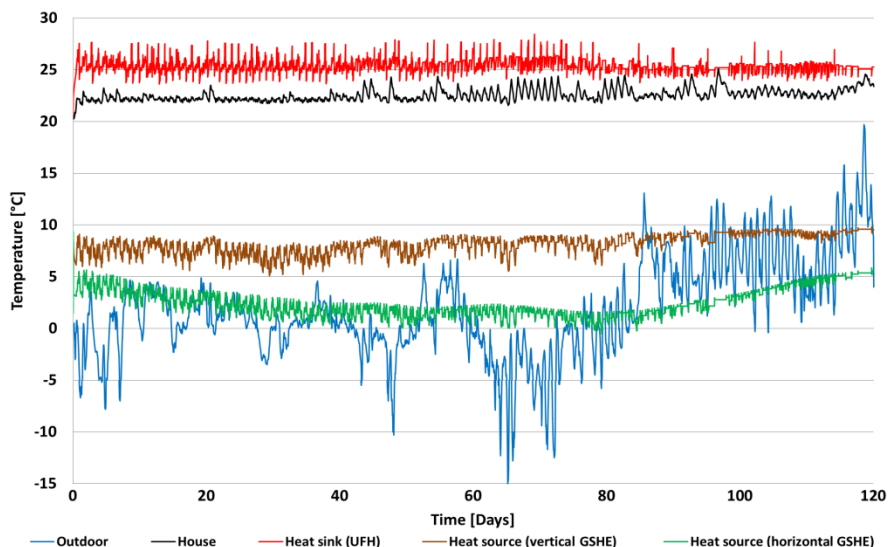


Figure 5-4: Temperatures of the building system as function of time during the four-month heating test period [31].

The *Figure 5-5* presents the variations of the daily running average COPs during the heating test period. Once again, the vertical borehole GSHE configuration shows better performance in terms of COPs (seasonal average COP_{AMR} of 9.19 and seasonal average COP_{system} of 1.84) compared to the horizontal GSHE one (seasonal average COP_{AMR} of 6.39 and seasonal average COP_{system} of 1.59). This is due to the fact that the warmer brine supplied by the vertical borehole GSHE improves the performance of the overall magnetocaloric heating system. However, the COP of the entire heating system is rather low compared to the previous results of the single room test. This can be explained by the fact that the magnetocaloric device, when heating up the entire house, operates part-load most of the time. As emphasized before, running the MCHP at low fluid flow rates leads to modest performance of the whole heating system [31].

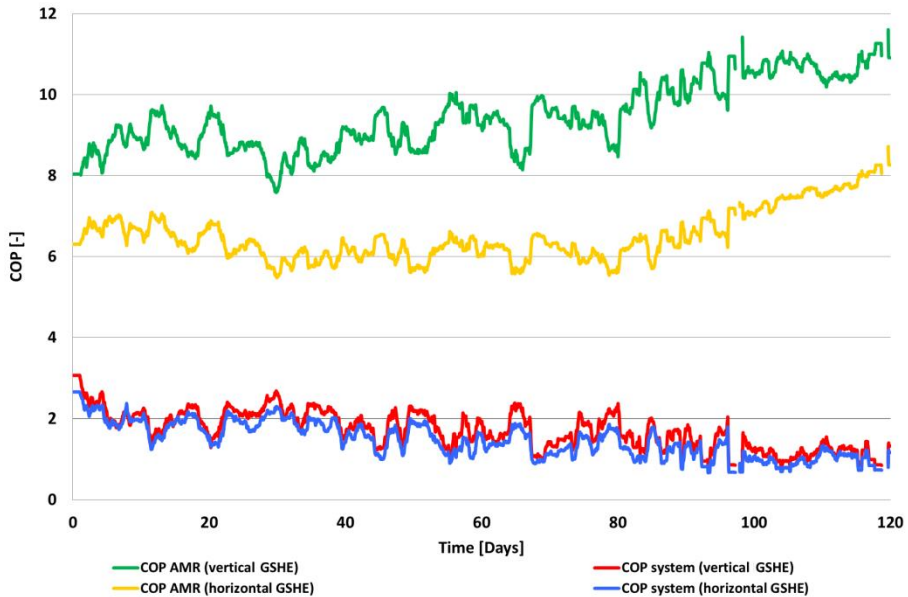


Figure 5-5: Daily average COPs of the magnetocaloric heat pump as function of time during the four-month heating test period [31].

5.3. ENERGY FLEXIBILITY CONTROL STRATEGY

The test results presented before showed that the MCHP controlled with a simple fluid flow rate regulation performs modestly. Because each room in the house has very different heating need time profiles, it is very rare that all rooms require maximum heating power at the same time. Consequently, the MCHP does not operate at the optimum fluid flow rate and highest COP most of the time [32].

In order to tackle this problem, the building heating energy flexibility, presented in the previous chapter, can be ingeniously employed to develop a new and more efficient control strategy for the magnetocaloric device. As mentioned before, indoor temperature set point modulation can allow efficient thermal energy storage in the built environment without jeopardizing the occupants' thermal comfort. A new MCHP controller is therefore created based on that principle. When the heating system is activated, it runs at maximum fluid flow rate with optimum COP to store thermal energy in the indoor space and structural thermal mass, leading to a slight increase of the indoor temperature. When the building is fully thermally charged, the heating system is completely turned off and the indoor temperature freely decreases until reaching a critical threshold for re-activation of the heat pump. The goal of this strategy is to maximize the MCHP operation time at optimum fluid flow rate and COP in order to improve the overall performance of the heating system [32].

Figure 5-6 illustrates the TES strategy and compares it to the simple fluid flow controller, in the case of a well-insulated house with high thermal inertia (100 Wh/K.m²). Similarly to the building energy flexibility strategy employed in the previous chapter, a minimum, a maximum and a neutral indoor temperature set points are defined. *Figure 5-6(a)* shows that the indoor temperature is allowed to vary around the neutral temperature set point of 22 °C. When the coldest room in the house reaches the minimum temperature limit (set between 20 °C and 22 °C), the MCHP is activated (see *Figure 5-6(b)*) and heats up all rooms at maximum power. When the temperature of a particular room reaches the maximum temperature limit (set between 22 °C and 24 °C), the room's thermostat adjusts the fluid flow in the corresponding UFH loop to keep the temperature at the maximum limit. The MCHP fluid flow rate is thus decreased accordingly. When the average temperature of the house (defined as the floor area weighted average temperature of all rooms) reaches the maximum temperature limit, the whole heating system is turned off [32].

One can see in *Figure 5-6(c)* a clear change in the MCHP fluid flow rate profile between the two control strategies. With the energy flexible control strategy, the MCHP fluid flow rate is kept at its maximum most of the time when the heating system is activated. Consequently, the COP during operation periods is greatly improved (see *Figure 5-6(d)*) [32].

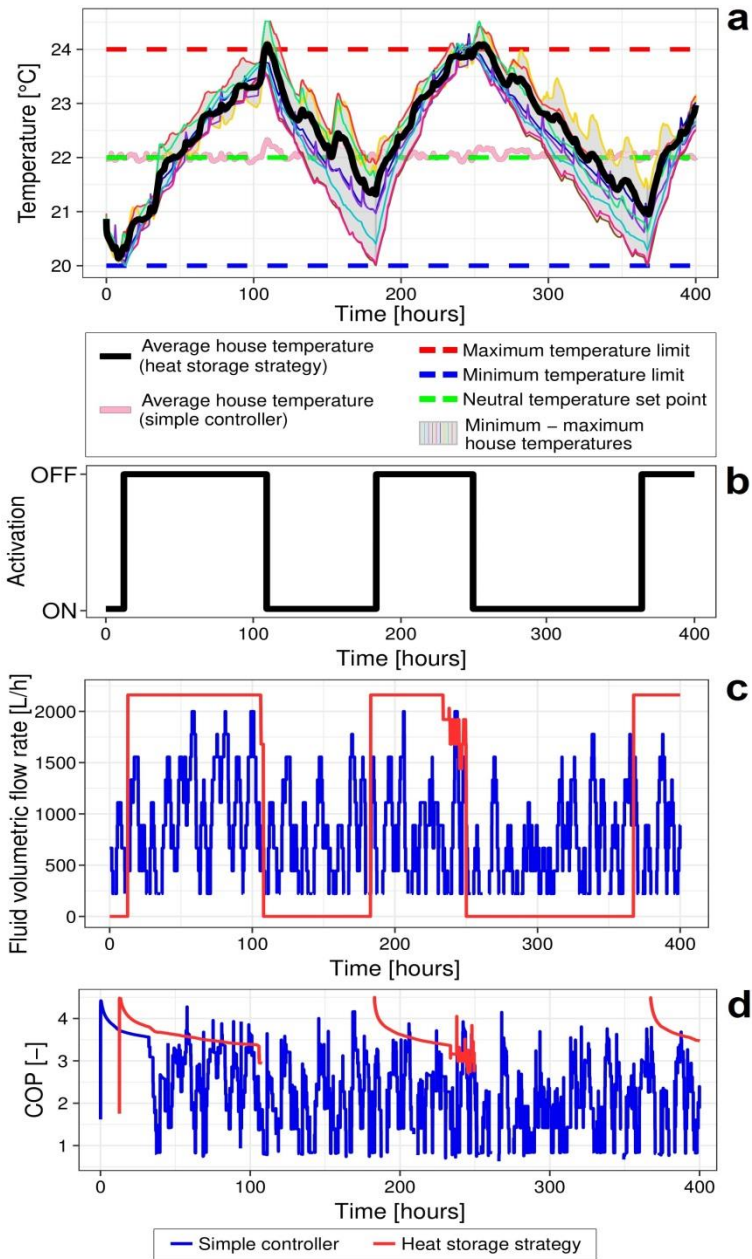


Figure 5-6: Example of heat storage strategy control for MCHP: (a) temperatures in the house (with and without heat storage strategy); (b) activation of the MCHP (with heat storage strategy); (c) fluid volumetric flow rate of the MCHP (with and without heat storage strategy); (d) COP of the MCHP (with and without heat storage strategy) [32].

5.4. PERFORMANCE OF THE MAGNETOCALORIC HEAT PUMP WITH ENERGY FLEXIBILITY CONTROL STRATEGY

All the results presented hereafter correspond to a four-month heating test period (from the 1st of January to the 30th of April) for the low-energy house base case equipped with UFH and a vertical GSHE under Danish weather conditions (DRY 2013 [128]). Three different classes of building thermal inertia are tested: light-weight structure (30 Wh/K.m²), medium-weight structure (60 Wh/K.m²) and heavy-weight structure (100 Wh/K.m²). In addition, the heat storage temperature span (difference between the maximum and the minimum temperature limit / set point) of the TES strategy is varied from 0 K to 4 K. The simple fluid flow control cases, corresponding to the 0 K temperature span scenario, are used as references to assess the improvement caused by the energy flexibility control strategy. Finally, the performance of the MCHP can be compared with the one of a conventional vapour-compression heat pump integrated in the same building cases [32].

The performances of the heat pump systems are assessed here by calculating the coefficient of performance of the entire heating system. In the case of the magnetocaloric device, COP_{MCHP} is calculated with the useful heating power $Q_{heating}$ delivered to the UFH, the work of circulation pump W_{pump} , the work of the motor W_{motor} , and the work of the valves W_{valves} :

$$COP_{MCHP} = \frac{Q_{heating}}{W_{pump} + W_{motor} + W_{valves}}$$

(Equation 5-3)

For the conventional vapour-compression heat pump, COP_{VCHP} is calculated with the useful heating power $Q_{heating}$ delivered to the UFH, the work of the compressor $W_{compressor}$, and the work of the 3 circulation pumps W_{pump} :

$$COP_{VCHP} = \frac{Q_{heating}}{W_{compressor} + W_{pump}}$$

(Equation 5-4)

One can see in *Figure 5-7* that both the heat storage temperature span and the thermal inertia have a positive impact on the maximization of the time duration at which the MCHP runs full-load with optimum COP. In the first part of the heating system activation period, the MCHP runs at full capacity and highest COP. The second phase of the heating system activation period starts when the warmest room in the house reaches the maximum temperature limit. From that moment, the MCHP operates part-load with diminished COP until the whole heating system is turned off. It is quite clear that if the heat storage temperature span and the structural thermal inertia increase, the first part of the activation period at continuous full heating capacity will last longer relatively to the part-load period [32].

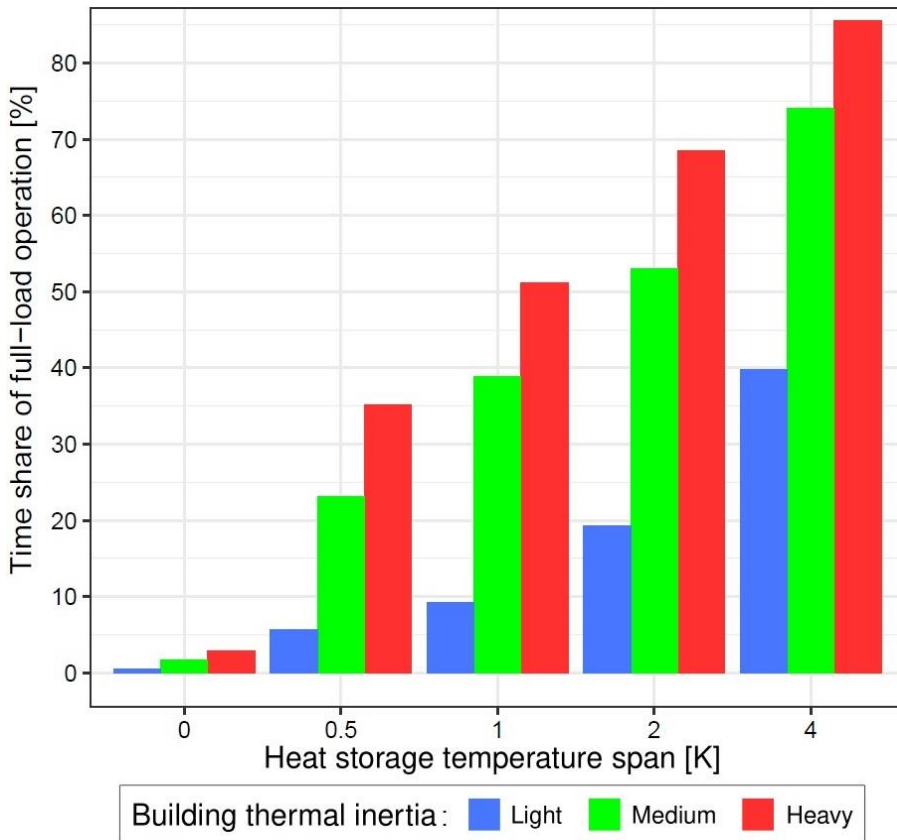


Figure 5-7: Full-load operation time share of the MCHP during the four-month heating test period [32].

One can observe in *Figure 5-8* the consequences of this optimization of the MCHP fluid flow rate in terms of COP for the heating system. Larger thermal inertia and heat storage temperature span lead to significant improvements of the COP. Even a moderate heat storage temperature span of 0.5 K can increase the average COP by 40%, 74% and 78% for light-weight, medium-weight and heavy-weight structure dwellings, respectively. With a maximum heat storage temperature span of 4 K, the COP reaches an average of 2.90 for the light thermal inertia house, 3.48 for the medium thermal inertia house, and 3.51 for the heavy thermal inertia house. In the cases of medium and heavy houses, the MCHP with heat storage strategy presents performances which are comparable to those of the conventional vapour-compression heat pump system. Nevertheless, the COP improvement of the magnetocaloric heating system is very limited for a heat storage temperature span above 2 K. Moreover, medium and heavy thermal mass houses have very similar performances. The latter can be explained by the fact that the light-weight house cases have their UFH circuits embedded in a light-weight structure wooden floor, whereas it is a concrete screed UFH for medium and heavy-weight houses. As explained before, the UFH loops enable an important thermal activation of the floor elements. Consequently, a concrete floor provides a much larger thermal storage potential than a wooden one. However, additional structural thermal mass such as concrete or brick walls and ceilings are not directly activated by the UFH. Therefore, its benefit in terms of heat pump operation improvement is limited [32].

Because no building envelope insulation is perfect, thermal energy storage in the indoor space by increasing the building's internal temperature will necessarily induce higher heat losses by transmission and ventilation. However, the test results show that the improvement of the heating system COP largely over-compensates the additional heat losses due to the increased indoor temperature. This leads to a substantial decrease of the total energy use during the heating period of about 28% to 41% compared to the reference cases. For medium and heavy-weight houses, the total energy usage of the magnetocaloric heating system with energy flexible control strategy is thereby similar to the one of the conventional vapour-compression heat pump [32].

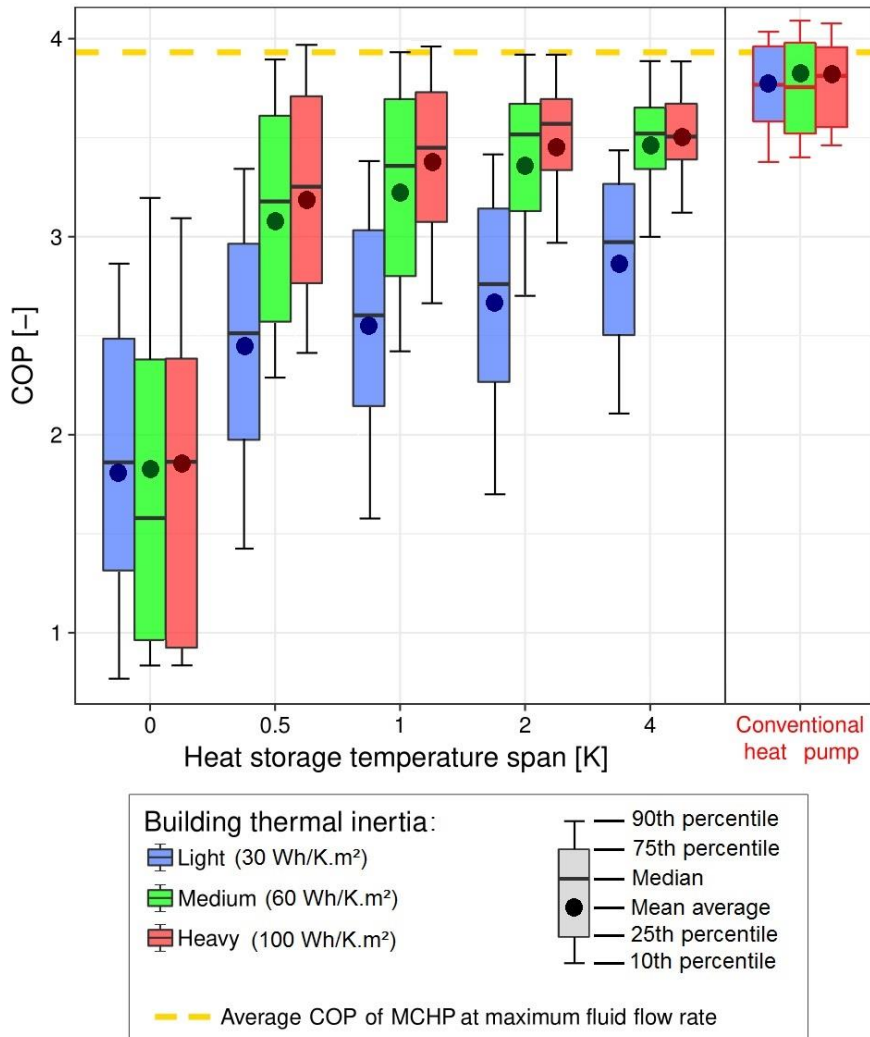


Figure 5-8: Box plot diagram of the heat pump COP as a function of heat storage temperature span and building thermal inertia (MCHP on the left, conventional vapour-compression heat pump on the right) [32].

The main constraint of thermal storage in the built environment by means of temperature set point modulation is the variability of the indoor operative temperature. The increase of the temperature set point to 24 °C in well-insulated south-oriented rooms with large windows could increase the risks of discomfort due to over-heating during sunny days [32].

In order to account for the indoor temperature variability of buildings with the TES strategy, the difference between the 5th and 95th percentile of all rooms operative temperatures during the heating test period is calculated and presented in *Figure 5-9*. Naturally, the temperature variability increases with the heat storage temperature span and decreases with the building thermal inertia. One can notice that in the case of medium and heavy-weight structure dwellings, the temperature variability with energy flexibility strategy never exceeds the one of the reference case with a simple fluid flow controller, even for a maximum heat storage temperature span of 4 K [32].

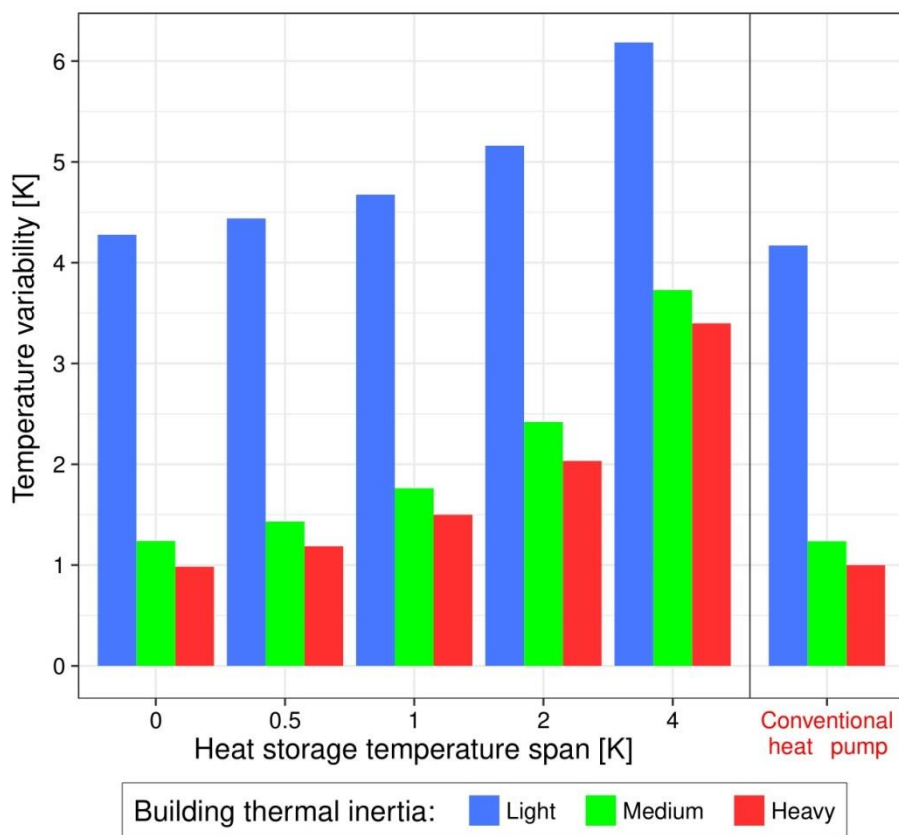


Figure 5-9: Temperature variability (difference between 5th and 95th percentile of the house temperature) during the four-month heating test period (MCHP on the left, conventional vapour-compression heat pump on the right) [32].

5.5. CONCLUSION

In this chapter, it was numerically demonstrated that a magnetocaloric heat pump can be implemented in a low-energy single-family house and provide for its indoor space heating needs under cold weather climate conditions. The MCHP can be integrated in a single hydronic loop including a high temperature ground source heat exchanger and a low temperature radiant under-floor heating without the need for intermediate heat exchanger or hot water storage tank. When coupled with a vertical borehole GSHE and if always running at maximum load, the magnetocaloric heating system can deliver up to 2600 W of useful heating power with an appreciable average seasonal COP of 3.93.

However, when implemented in a multi-zone building with a simple fluid flow regulation and independent thermostats in each room, the MCHP operates partial-load most of the time, which leads to modest performances. To tackle this problem, a new controller based on thermal storage in the built environment by means of indoor temperature set point modulation is implemented. This strategy takes advantage of the heating energy flexibility potential of the building to minimize the MCHP part-load operation time. Heating needs are shifted in time and concentrated over longer periods where the magnetocaloric device can run at full capacity with highest COP.

Test results show that with a maximum temperature set point modulation of 4 K, such energy flexibility strategy can improve the MCHP average seasonal COP up to 2.90, 3.48 and 3.51 for light, medium and heavy structure houses, respectively. These performances are comparable with the ones of conventional vapour-compression heat pumps. Despite the increase of transmission and ventilation losses due to higher indoor temperatures, the TES strategy can decrease the total heating energy use by about 28% to 41% during the heating period, reaching the same energy consumption level as conventional vapour-compression heat pumps.

Finally, it is shown that both the building thermal inertia and the heat storage temperature span have large positive impacts on the magnetocaloric system performance with such energy flexibility controller. However, it was found that the concrete screed of the UFH is the most contributing thermal mass element for this TES strategy. In addition, temperature spans above 2 K do not improve the heat pump operation much, whereas it significantly increases the temperature variability in the dwelling.

For further information, please refer to Appendix C. Paper III and Appendix E. Paper V: “Integration of a magnetocaloric heat pump in a low-energy residential building” and “Integration of a magnetocaloric heat pump in an energy flexible residential building”.

CHAPTER 6. CONCLUSIONS OF THE THESIS

The main objective of this research study is to investigate and demonstrate the possibility to integrate a magnetocaloric heat pump in a single-family house under Danish weather conditions. In addition, numerical analysis is carried out to increase the understanding of the heating energy flexibility potential of residential buildings using thermal storage in the indoor environment.

The magnetocaloric heat pump is an innovative technology employing the magnetocaloric effect of certain materials in active magnetic regenerator thermodynamic cycles generating a heat transfer from a heat source to a heat sink. In addition to silent operation, absence of greenhouse or toxic gases and possibility of recycling its components, this magnetic heating device has the potential for higher coefficient of performance than conventional vapour-compression systems. The current study made the numerical demonstration that a magnetocaloric heat pump can be coupled to a ground source heat exchanger (heat source) and a radiant under-floor heating system (heat sink) to successfully provide for the indoor space heating needs of a low-energy house in Denmark. These three components are integrated in a single hydronic loop without any intermediate heat exchanger or hot water storage tank. This configuration simplifies the hydronic circuit which can thus benefit from lower installation and operation costs. At maximum capacity, the magnetocaloric system delivers up to 2600 W of useful heating power with an appreciable average seasonal COP of 3.93.

However, when implemented in a multi-zone building with a simple fluid flow controller, the magnetocaloric heat pump presents modest performance with an average seasonal COP of 1.84 at best. This is due to the fact that the heating system does not run often at maximum capacity with optimum COP. To tackle this problem, this research study presented and tested a magnetocaloric heat pump control strategy based on thermal storage in the built environment by means of indoor temperature set point modulation. This controller takes advantage of the heating energy flexibility potential of the building to store thermal energy and shift the heating loads of each room in time. Heating usage is concentrated so that the magnetocaloric heat pump maximizes its full-load running time and therefore optimizes its average seasonal COP. This energy flexibility control strategy was found to increase the performance of the magnetic heating system up to COPs ranging from 2.90 to 3.51, which is comparable with conventional vapour-compression heat pumps. However, thermal storage in the built environment induces indoor temperature instability. It is therefore very important to always keep the building temperature in the vicinity of the occupants' thermal comfort range.

Indoor temperature set point modulation and thermal storage in the built environment are part of a larger set of demand side management strategies which are commonly designated as Building Energy Flexibility measures. These strategies can be used to adapt the energy usage of buildings to the energy grid requirements. The building sector can thus become an important active and interactive actor of the regulation of Smart Energy Grid systems. It can therefore enable the integration of a larger share of intermittent renewable energy sources.

This research study focussed on the heating energy flexibility potential of residential buildings in Denmark. This energy flexibility is defined here as the dwelling's ability to shift its indoor space heating use in time by accumulating thermal energy in the built environment during low energy price periods, and conserve it during high energy price periods. The results of the numerical analysis showed that even though effective thermal inertia determines the maximum heat storage capacity of the building, the insulation level of the envelope sets the storage efficiency and is the most important building parameter with respect to heating energy flexibility potential. Well-insulated dwellings can thereby efficiently store thermal energy in the indoor environment and shift heating loads over long periods of time. Poorly insulated buildings can only shift heating use over short periods of time. However, they can move a total amount of energy four times larger than high-insulation houses. Low-insulation dwellings can thus have a greater impact on the energy grids.

To a lesser extent, radiant under-floor heating system can also improve the building heating energy flexibility when the hydronic circuit is embedded in a dense material layer such as a concrete screed. Indeed, compared to a convective emitter, the under-floor heating decreases ventilation losses and benefits from the large activation of the floor thermal mass which increases the effective thermal storage capacity and consequently the flexibility potential.

Passive latent heat thermal storage solutions such as phase change materials integrated in wallboards or in furniture elements were found to significantly increase the total effective heat storage capacity of light-weight structure buildings. The heating energy flexibility capability of the latter could thus be improve by up to 111% and 87% when employing phase change materials in wallboards or furnishing, respectively. However, when positioned on heavy construction elements, phase change material wallboards are inefficient because of their limited thermal conductivity.

Finally, it was demonstrated that assuming the indoor space to be an empty volume is not appropriate for dynamic energy simulations of houses with low structural thermal inertia. Transient thermal behaviour, building time constant, total heat storage capacity and therefore heating energy flexibility can be significantly influenced by the presence of indoor content and furniture in the built environment.

To address that matter, this study reviewed the different methods for modelling items and furnishing elements present in the building indoor space. In addition, suggestions were made for choosing the representative material characteristics of these indoor content elements.

CHAPTER 7. FUTURE WORK

This research study presented promising findings on the application of the magnetocaloric heat pump technology for indoor space heating, the heating energy flexibility potential of dwellings, and the modelling of indoor content and its impact on the building thermodynamics. However, further work is required to assess and optimize the performance of these different technical solutions.

Concerning the magnetic heat pump itself, new magnetocaloric materials should be developed to enhance the magnetocaloric effect of the refrigerant. New magnet assembly configurations and regenerator geometries should be tested to optimize the magnetic field and heat transfer in the refrigerant, and minimize pressure losses and magnetic work. Novel designs of the magnetocaloric machines should be invented to improve its overall performances and reduce parasitic losses.

Further investigations should be carried out to understand the implications of the building design and the hydronic loop configurations on the magnetocaloric heating system performances. New control strategies, such as the ones taking advantage of the heating energy flexibility potential of the dwellings, should be tested. In addition, cascading implementation of the active magnetic regenerators could be an interesting solution to increase the temperature span between the heat source and the heat sink and therefore expand the magnetocaloric heat pump applications. The latter could thus be coupled with higher temperature heat emitters in poorly insulated buildings or be used for domestic hot water production.

Concerning demand side management strategies, novel methodologies for the assessment of the energy flexibility potential of buildings should be developed. The acceptability of such measures should also be thoroughly studied as building occupants might not agree with domestic heat storage strategies driven by external control signals. In the case of thermal accumulation in the indoor environment, the elaboration of new phase change materials with enhanced thermal conductivity could benefit to passive latent heat storage systems.

Finally, a better understanding of the complex interactions between the built environment and the indoor content / furniture elements should be established. Different models of entirely furnished buildings should be compared and full-scale experiments should be performed to measure the impact of additional indoor elements on the building time constant, HVAC systems efficiency, and thermal storage capacity. More accurate dynamic building energy models will benefit to energy flexibility and demand side management strategies with precise prediction of the transient indoor comfort. Moreover, the performance of furniture systems integrating phase change materials could be properly evaluated and optimized.

REFERENCES

- [1] Core Writing Team: Pachauri, R. K., & Meyer, L. A. (Ed.). (2014). *Climate Change 2014: Synthesis Report, Contribution of Working Groups I, II and III to the Fifth Assessment Report of the Intergovernmental Panel on Climate Change*. IPCC. Geneva. Retrieved from http://ar5-syr.ipcc.ch/ipcc/resources/pdf/IPCC_SynthesisReport.pdf
- [2] Rojas-Avellaneda, D. (2007). Fossil Fuels Pollution and Air Quality Modeling. In: Chávez, J. F. Alcalá (eds), Klapp, J., & Cervantes-Cota, J. L., *Towards a Cleaner Planet, Environmental Science and Engineering (Environmental Science)*. Berlin: Springer. <https://doi.org/10.1007/978-3-540-71345-6>
- [3] Wilson, C., & Tisdell, C. A. (2003). *Conflicts Over Natural Resources and the Environment: Economics and Security, Working Paper No. 86*. The University of Queensland. Retrieved from <http://ageconsearch.umn.edu/bitstream/48967/2/WP86.pdf>
- [4] World Health Organization. (2003). *Climate change and human health – risks and responses, summary chapter 6: Climate change and infectious diseases*. Retrieved from <http://www.who.int/globalchange/climate/en/chapter6.pdf>
- [5] The Clean Air Task Force. (2010). *The toll from coal – an updated assessment of death and disease from America’s dirtiest energy source*. Retrieved from http://www.catf.us/resources/publications/files/The_Toll_from_Coal.pdf
- [6] Lobell, D. B., Schlenker, W., & Costa-Roberts, J. (2011). Climate Trends and Global Crop Production Since 1980. *Science*, 333, 616-620. <https://doi.org/10.1126/science.1204531>
- [7] Creighton, C., Hobday, A. J., Lockwood, M., & Pecl, G. T. (2016). Adapting Management of Marine Environments to a Changing Climate: A Checklist to Guide Reform and Assess Progress. *Ecosystems*, 19, 187-219. <https://doi.org/10.1007/s10021-015-9925-2>
- [8] Rademaker, M., Jans, K., Frattina della Frattina, C., Rööds, H., Slingerland, S., Borum, A., & Van Schaik, L. (2016). *The Economics of Planetary Security – Climate Change as an Economic Conflict Factor*. Netherlands Institute of International Relations ‘Clingendael’, The Hague Centre for Strategic Studies. Retrieved from https://hcss.nl/sites/default/files/files/reports/economics_of_planetary_security.pdf
- [9] Eurostat. (2017). *Energy production and imports*. Retrieved from http://ec.europa.eu/eurostat/statistics-explained/index.php/Energy_production_and_imports
- [10] Reuveny, R. (2007). Climate change-induced migration and violent conflict. *Political Geography*, 26, 656-673. <https://doi.org/10.1016/j.polgeo.2007.05.001>
- [11] Schleussner, C. F., Donges, J. F., Donner, R. V., & Schellnhuber, H. J. (2016). Armed-conflict risks enhanced by climate-related disasters in ethnically fractionalized countries, *Proceedings of the National Academy of Sciences of the United States of America*, 113(33), 9216-9221. <https://doi.org/10.1073/pnas.1601611113>
- [12] International Energy Agency. (2017). *Statistics from the International Energy Agency*. Retrieved from <http://www.iea.org/statistics/>
- [13] United Nations Framework Convention on Climate Change. (2015). *Report of the Conference of the Parties on its twenty-first session, held in Paris from 30 November to 13 December 2015 - Adoption of the Paris Agreement*. Retrieved from <https://unfccc.int/resource/docs/2015/cop21/eng/10.pdf>
- [14] European Climate Foundation. (2010). *Roadmap 2050: a practical guide to a prosperous, low-carbon Europe, Technical report*. Retrieved from http://www.roadmap2050.eu/attachments/files/Volume1_fullreport_PressPack.pdf
- [15] © OECD/IEA International Energy Agency. (2014). *Renewable Energy, Medium-Term Market Report 2014 – Executive Summary*. IEA Publishing,. Licence: www.iea.org/t&c. Retrieved from <https://www.iea.org/Textbase/npsum/MTrenew2014sum.pdf>

- [16] International Energy Agency. (2013). *Transition to Sustainable Buildings: Strategies and Opportunities to 2050*. Retrieved from https://www.iea.org/publications/freepublications/publication/Building2013_free.pdf
- [17] Building Performance Institute Europe (BPIE). (2011). *Europe's Buildings under the Microscope, Executive Summary 2011*. Retrieved from http://bpie.eu/wp-content/uploads/2015/10/HR_EU_B_under_microscope_study.pdf
- [18] The European Parliament and the Council of the European Union. (2010). Directive 2010/31/EU on the energy performance of buildings. *Official Journal of the European Union*. Retrieved from <http://eur-lex.europa.eu/LexUriServ/LexUriServ.do?uri=OJ%3AL%3A2010%3A153%3A0013%3A0035%3AEN%3APDF>
- [19] Marszal, A. J., Heiselberg, P., Bourrelle, J. S., Musall, E., Voss, K., Sartori, I., & Napolitano, A. (2011). Zero Energy Building – A review of definitions and calculation methodologies. *Energy and Buildings*, 43, 971-979. <https://doi.org/10.1016/j.enbuild.2010.12.022>
- [20] Almeida, M., & Ferreira, M. (2017). Cost effective energy and carbon emissions optimization in building renovation (Annex 56). *Energy and Buildings*, 152, 718-738. <https://doi.org/10.1016/j.enbuild.2017.07.050>
- [21] Johra, H., & Heiselberg, P. K. (2018). *Description and Validation of a MATLAB - Simulink Single Family House Energy Model with Furniture and Phase Change Materials (Update)*. Aalborg: Aalborg University, Department of Civil Engineering. DCE Technical Reports, No. 238. Retrieved from http://vbn.aau.dk/files/270078674/Description_and_Validation_of_a_MATLAB_Simulink_Single_Family_House_Energy_Model_with_Furniture_and_Phase_Change_Materials_Update.pdf
- [22] Lund, H., Möller, B., Mathiesen, B. V., & Dyrrelund, A. (2010). The role of district heating in future renewable energy systems. *Energy*, 35(3), 1381-90. <https://doi.org/10.1016/j.energy.2009.11.023>
- [23] Palzer, A., & Henning, H. M. (2014). A comprehensive model for the German electricity and heat sector in a future energy system with a dominant contribution from renewable energy technologies – Part II: Results. *Renewable and Sustainable Energy Reviews*, 30, 1019-1034. <https://doi.org/10.1016/j.rser.2013.11.032>
- [24] Cockroft, J., & Kelly, N. (2006). A comparative assessment of future heat and power sources for the UK domestic sector. *Energy Conversion and Management*, 47, 2349-2360. <https://doi.org/10.1016/j.enconman.2005.11.021>
- [25] Self, S. J., Reddy, B. V., & Rosen, M. A. (2013). Geothermal heat pump systems: Status review and comparison with other heating options. *Applied Energy*, 111, 341-348. <https://doi.org/10.1016/j.apenergy.2012.01.048>
- [26] Fischer, D., & Madani, H. (2017). On heat pumps in smart grids: A review. *Renewable and Sustainable Energy Reviews*, 70, 342-357. <https://doi.org/10.1016/j.rser.2016.11.182>
- [27] Nowak, T., & Westring, P. (2015). *European heat pump market and statistics report 2015*. The European Heat Pump Association AISBL (EHPA). Retrieved from http://www.ehpa.org/fileadmin/red/07_Market_Data/2014/EHPA_European_Heat_Pump_Market_and_Statistics_Report_2015_-_executive_Summary.pdf
- [28] Bahl, C. R. H. (2015). *ENOVHEAT project summary: development of efficient novel magnetocaloric heat pumps*. Retrieved from <http://www.enovheat.dk/Research/ProjectSummary>
- [29] Smith, A., Bahl, C. R. H., Bjørk, R., Engelbrecht, K., Nielsen, K. K., & Pryds, N. (2012). Materials challenges for high performance magnetocaloric refrigeration devices. *Advanced Energy Materials*, 2, 1288-1318. <https://doi.org/10.1002/aenm.201200167>
- [30] Eriksen, D., Engelbrecht, K., Bahl, C. R. H., & Bjørk, R. (2016). Exploring the efficiency potential for an active magnetic regenerator. *Science and Technology for the Built Environment*, 22(5), 527-533. <https://doi.org/10.1080/23744731.2016.1173495>

- [31] Johra, H., Filonenko, K., Heiselberg, P., Veje, C., Lei, T., Dall'Olio, S., Engelbrecht, K., & Bahl, C. (2018). Integration of a magnetocaloric heat pump in a low-energy residential building. *Building Simulation: An International Journal*.
<https://doi.org/10.1007/s12273-018-0428-x>
- [32] Johra, H., Filonenko, K., Heiselberg, P., Veje, C., Dall'Olio, S., Engelbrecht, K., & Bahl, C. (2018). Integration of a magnetocaloric heat pump in an energy flexible residential building, *Renewable Energy* (under review).
- [33] Beurskens, W. M., Hekkenberg, M., & Vethman, P. (2011). *Renewable energy projections as published in the national energy action plans of the European member states, Report no. ECN-E-10-069*. ECN and European Environment Agency. Retrieved from <https://www.ecn.nl/docs/library/report/2010/e10069.pdf>
- [34] Energistyrelsen, Klima Energi og Bygningsministeriet. (2014). *Denmark's National Energy Efficiency Action Plan (NEEAP)*. Retrieved from https://ec.europa.eu/energy/sites/ener/files/documents/2014_neeap_en_denmark.pdf
- [35] Le Dréau, J., & Heiselberg, P. (2016). Energy flexibility of residential buildings using short term heat storage in the thermal mass. *Energy*, 111, 991-1002.
<https://doi.org/10.1016/j.energy.2016.05.076>
- [36] Lund, H., Werner, S., Wiltshire, R., Svendsen, S., Thorsen, J. E., Hvelplund, F., & Mathiesen, B. V. (2014). 4th Generation District Heating (4GDH): integrating smart thermal grids into future sustainable energy systems. *Energy*, 68, 1-11.
<https://doi.org/10.1016/j.energy.2014.02.089>
- [37] Mathiesen, B. V., Lund, H., Connolly, D., Wenzel, H., Østergaard, P. A., Möller, B., Nielsen, S., Ridjan, I., Karnøe, P., Sperling, K., & Hvelplund, F. K. (2015). Smart Energy Systems for coherent 100% renewable energy and transport solutions. *Applied Energy*, 145, 139-154.
<https://doi.org/10.1016/j.apenergy.2015.01.075>
- [38] Østergaard, S. J., Marszal-Pomianowska, A., Lollini, R., Pasut, W., Knotzer, A., Engelmann, P., Stafford, A., & Reynders, G. (2017). IEA EBC Annex 67 Energy Flexible Buildings. *Energy and Buildings*, 155, 25-34.
<https://doi.org/10.1016/j.enbuild.2017.08.044>
- [39] Hedegaard, K., Mathiesen, B. V., Lund, H., & Heiselberg, P. (2012). Wind power integration using individual heat pumps – Analysis of different heat storage options. *Energy*, 47, 284–93.
<https://doi.org/10.1016/j.energy.2012.09.030>
- [40] Clement-Nyns, K., Haesen, E., & Driesen, J. (2010). The impact of charging plug-in hybrid electric vehicles on a residential distribution grid. *IEEE Trans Power Syst*, 25, 371-380.
<https://doi.org/10.1109/tpwrs.2009.2036481>
- [41] Marszal, A. J., & Heiselberg, P. (2016). Household electricity demand profiles - a high-resolution load model to facilitate modelling of energy flexible buildings. *Energy*, 103, 487-501.
<https://doi.org/10.1016/j.energy.2016.02.159>
- [42] Kitanovski, A., Tušek, J., Tomc, U., Plaznik, U., Ožbolt, M., & Poredoš, A. (2015). *Magnetocaloric Energy Conversion: From Theory to Applications*. New York: Springer International Publisher, New York.
<https://doi.org/10.1007/978-3-319-08741-2>
- [43] Engelbrecht, K., Eriksen, D., Bahl, C. R. H., Bjørk, R., Geyti, J., Lozano, J. A., Nielsen, K. K., Saxild, F., Smith, A., & Pryds, N. (2012). Experimental results for a novel rotary active magnetic regenerator. *International Journal of Refrigeration*, 35, 1498-1505.
<https://doi.org/10.1016/j.ijrefrig.2012.05.003>
- [44] Lei, T., Engelbrecht, K., Nielsen, K. K., & Veje, C. T. (2017). Study of the geometries of active magnetic regenerators for room temperature magnetocaloric refrigeration. *Applied Thermal Engineering*, 111, 1232-1243.
<https://doi.org/10.1016/j.applthermaleng.2015.11.113>
- [45] Weiss, P., & Piccard, A. (1918). Sur un nouveau phénomène magnétocalorique. *Comptes Rendus Acad. Sci. (Paris)*, 166, 352-354.

- [46] Weiss, P., & Forrer, R. (1926). Aimantation et phénomène magnetocalorique du nickel. *Annales de Physique (Paris)*, 5, 153-213.
- [47] Debye, P. (1926). Einige Bemerkungen zur Magnetisierung bei tiefer Temperatur. *Annalen der Physik (Leipzig)*, 386, 1154-1160.
- [48] Giauque, W. F. (1927). A thermodynamic treatment of certain magnetic effects. A proposed method of producing temperatures considerably below 1 absolute. *Journal of the American Chemical Society*, 49, 1864-1870.
<https://doi.org/10.1021/ja01407a003>
- [49] Giauque, W. F., & MacDougall, D. P. (1935). The production of temperatures below one degree absolute by adiabatic demagnetization of gadolinium sulfate. *Journal of the American Chemical Society*, 57, 1175-1185.
<https://doi.org/10.1021/ja01310a007>
- [50] Urbain, G., Weiss, P., & Trombe, F. (1935). Un nouveau métal ferromagnétique, le gadolinium, *Comptes Rendus*, 200, 2132-2134.
- [51] Brown, G. V. (1976). Magnetic heat pumping near room temperature. *Journal of Applied Physics*, 47, 3673.
<https://doi.org/10.1063/1.323176>
- [52] Barclay, J. A., & Steyert, W. A. (1985). *US Patent US4332135*. Retrieved from <https://patentimages.storage.googleapis.com/6a/12/44/22460fdd3f9faf/US4332135.pdf>
- [53] Chen, F. C., Murphy, R. W., Mei, V. C., & Chen, G. L. (1992). Thermodynamic Analysis of Four Magnetic Heat-Pump Cycles. *Journal of Engineering for Gas Turbines and Power*, 114(4), 715-720.
<https://doi.org/10.1115/1.2906647>
- [54] Zimm, C., Jastrab, A., Sternberg, V., Pecharsky, V., Gschneidner Jr, K., Osborne, M., & Anderson, I. (1998). Description and performance of a near room temperature magnetic refrigerator. *Advances in Cryogenic Engineering*, 43, 1759-1766.
https://doi.org/10.1007/978-1-4757-9047-4_222
- [55] Okamura, T., & Hirano, N. (2013). Improvement of the performance of a room temperature magnetic refrigerator using Gd-alloy. *Journal of the Japan Society of Applied Electromagnetics and Mechanics*, 21 (1), 10-14.
<https://doi.org/10.14243/jsaem.21.10>
- [56] Jacobs, S., Auringer, J., Boeder, A., Chell, J., Komorowski, L., Leonard, J., Russek, S., & Zimm, C. (2014). The performance of a large-scale rotary magnetic refrigerator. *International Journal of Refrigeration*, 37(1), 84-91.
<https://doi.org/10.1016/j.ijrefrig.2013.09.025>
- [57] Lozano, J. A., Capovilla, M. S., Trevizoli, P. V., Engelbrecht, K., Bahl, C. R. H., Barbosa Jr, J. R. (2016). Development of a novel rotary magnetic regenerator. *International Journal of Refrigeration*, 68, 187-197.
<https://doi.org/10.1016/j.ijrefrig.2016.04.005>
- [58] Aprea, C., Greco, A., Maiorino, A., & Masselli, C. (2015). The energy performances of a rotary permanent magnet magnetic refrigerator. *International Journal of Refrigeration*, 61, 1-11.
<https://doi.org/10.1016/j.ijrefrig.2015.09.005>
- [59] Pecharsky, V. K., Cui, J., & Johnson, D. D. (2016). (Magneto)caloric refrigeration: is there light at the end of the tunnel? *Philosophical Transaction of the Royal Society A*, 374, 20150305.
<https://doi.org/10.1098/rsta.2015.0305>
- [60] Neves Bez, H., Bahl, C. R. H., Nielsen, K. K., & Smith, A. (2016). *Magnetocaloric materials and first order phase transitions*. Roskilde: Department of Energy Conversion and Storage: Technical University of Denmark. Retrieved from http://orbit.dtu.dk/files/127446068/Magnetocaloric_materials_and_first_order_phase_transitions.pdf
- [61] Mugica, I., Roy, S., Poncet, S., Bouchard, J., & Nesreddine, H. (2017). Exergy analysis of a parallel-plate active magnetic regenerator with nanofluids. *Entropy*, 19, 464.
<https://doi.org/10.3390/e19090464>

- [62] Insinga, A. R., Bjørk, R., & Smith, A. (2016). Optimally segmented permanent magnet structures. *IEEE Transactions on Magnetics*, 52, 7210306. <https://doi.org/10.1109/TMAG.2016.2593685>
- [63] Insinga, A. R., Bahl, C. R. H., Bjørk, R., & Smith, A. (2016). *Optimising magnetostatic assemblies*. Roskilde: Department of Energy Conversion and Storage: Technical University of Denmark. Retrieved from http://orbit.dtu.dk/ws/files/127592268/Optimising_Magnetostatic_Assemblies.pdf
- [64] Dall'Olio, S., Lei, T., Engelbrecht, K., & Bahl, C. (2017). The effect of tapering on a magnetocaloric regenerator bed. *International Journal of Refrigeration*, 84, 300-308. <https://doi.org/10.1016/j.ijrefrig.2017.08.012>
- [65] Lei, T., Engelbrecht, K., Nielsen, K. K., & Veje, C. T. (2017). Study of geometries of active magnetic regenerators for room temperature magnetocaloric refrigeration. *Applied Thermal Engineering*, 111, 1232-1243. <https://doi.org/10.1016/j.applthermaleng.2015.11.113>
- [66] Trevizoli, P. V., Nakashima, A. T., Peixer, G. F., & Barbosa Jr, J. R. (2017). Performance assessment of different porous matrix geometries for active magnetic regenerators. *Applied Energy*, 187, 847-861. <https://doi.org/10.1016/j.apenergy.2016.11.031>
- [67] Johra, H., & Heiselberg, P. (2017). Influence of internal thermal mass on the indoor thermal dynamics and integration of phase change materials in furniture for building energy storage: A review. *Renewable and Sustainable Energy Reviews*, 69, 19-32. <https://doi.org/10.1016/j.rser.2016.11.145>
- [68] Plaisance, H., Blondel, A., Desauziers, V., & Mocho, P. (2014). Hierarchical cluster analysis of carbonyl compounds emission profiles from building and furniture materials. *Building and Environment*, 75, 40-45. <https://doi.org/10.1016/j.buildenv.2014.01.014>
- [69] Athlaye, R. A., Xie, Y., Liu, B., & Rosenberg, M. I. (2013). *Analysis of daylighting requirements within ASHRAE standard 90.1*. US Department of Energy. Retrieved from https://www.pnnl.gov/main/publications/external/technical_reports/pnnl-22698.pdf
- [70] Brüel & Kjær Sound & Vibration Measurement A/S. (1988). *Measurements in Building Acoustics*. Retrieved from <https://www.bksv.com/media/doc/br0178.pdf>
- [71] Mortensen, L. H., Rode, C., & Peuhkuri, R. (2008). Investigation of airflow patterns in a microclimate by particle image velocimetry (PIV). *Building and Environment*, 43(11), 1929-1938. <https://doi.org/10.1016/j.buildenv.2007.11.012>
- [72] Yang, X., Fazio, P., Ge, H., & Rao, J. (2012). Evaluation of moisture buffering capacity of interior surface materials and furniture in a full-scale experimental investigation. *Building and Environment*, 47, 188-196. <https://doi.org/10.1016/j.buildenv.2011.07.025>
- [73] Horikiri, K., Yao, Y., & Yao, J. (2015). Numerical optimisation of thermal comfort improvement for indoor environment with occupants and furniture. *Energy and Buildings*, 88, 303-315. <https://doi.org/10.1016/j.enbuild.2014.12.015>
- [74] Bojic, M., Yik, F., Lo, T. Y. (2002). Locating air-conditioners and furniture inside residential flats to obtain good thermal comfort. *Energy and Buildings*, 34, 745-751. [https://doi.org/10.1016/S0378-7788\(01\)00143-8](https://doi.org/10.1016/S0378-7788(01)00143-8)
- [75] Babiak, J., Olesen, B. W., & Petráš, D. (2009). *Low temperature heating and high temperature cooling – Guidebook No. 7*. Brussels: REHVA - Federation of European Heating, Ventilation and Air Conditioning Associations.
- [76] Zhao, K., Lui, X. H., & Jiang, Y. (2013). Application of radiant floor cooling in a large open space building with high-intensity solar radiation. *Energy and Buildings*, 66, 246-257. <https://doi.org/10.1016/j.enbuild.2013.07.014>
- [77] Corcione, M., Fontana, L., & Moncada Lo Giudice, G. (2001). A parametric analysis on the effects of furnishings upon the performance of radiant floor-panel heating systems. *In Proceedings of the CLIMA 2000 International Congress (pp. 59-68)*. Naples.

- [78] Fontana, L. (2011). Thermal performance of radiant heating floors in furnished enclosed spaces. *Applied Thermal Engineering*, 31, 1547-1555.
<https://doi.org/10.1016/j.applthermaleng.2010.12.014>
- [79] Antonopoulos, K. A., & Koronaki, E. P. (2000). Effect of indoor mass on the time constant and thermal delay of buildings. *International Journal of Energy Research*, 24, 391-402.
[https://doi.org/10.1002/\(SICI\)1099-114X\(200004\)24:5<391::AID-ER585>3.0.CO;2-L](https://doi.org/10.1002/(SICI)1099-114X(200004)24:5<391::AID-ER585>3.0.CO;2-L)
- [80] Wolisz, H., Kull, T. M., Streblov, R., & Müller, D. (2015). The effect of furniture and floor covering upon dynamic thermal building simulations. *Energy Procedia*, 78, 2154-2159.
<https://doi.org/10.1016/j.egypro.2015.11.304>
- [81] Johra, H., Heiselberg, P., & Le Dréau, J. (2017). Numerical analysis of the impact of thermal inertia from the furniture / indoor content and phase change materials on the building energy flexibility. In *Proceedings of 15th IBPSA Conference, International Building Performance Simulation Association, San Francisco, CA, USA. Aug. 7-9, 2017*.
<https://doi.org/10.26868/25222708.2017.012>
- [82] International Organization for Standardization. (2008). *ISO 13790:2008 - Energy performance of buildings – Calculation of energy use for space heating and cooling*. Geneva.
- [83] Berthou, T., Stabat, P., Salvazet, R., & Marchio, D. (2014). Development and validation of a gray box model to predict thermal behavior of occupied office buildings. *Energy and Buildings*, 74, 91-100.
<https://doi.org/10.1016/j.enbuild.2014.01.038>
- [84] University of Wisconsin-Madison Solar Energy Laboratory, TRANSSOLAR Energietechnik GmbH, CSTB, & TESS. (2012). Type 56 and TRNBuild: Multizone building modeling. In: *TRNSYS 17 - Technical Documentation Vol. 5*.
- [85] Bacher, P., & Madsen, H. (2011). Identifying suitable models for the heat dynamics of buildings. *Energy and Buildings*, 43(7), 1511-1522.
<https://doi.org/10.1016/j.enbuild.2011.02.005>
- [86] Li, W., Xu, P., Wang, H., & Lu, X. (2016). A new method for calculating the thermal effects of irregular internal mass in buildings under demand response. *Energy and Buildings*, 130, 761-772.
<https://doi.org/10.1016/j.enbuild.2016.08.057>
- [87] Ma, P., & Wang, L. S. (2012). Effective heat capacity of interior planar thermal mass (IPTM) subject to periodic heating and cooling. *Energy and Buildings*, 47, 44-52.
<https://doi.org/10.1016/j.enbuild.2011.11.020>
- [88] Gao, M., Reid, C. N., Jahedi, M., & Li, Y. (2000). Estimating equilibration times and heating/cooling rates in heat treatment of workpieces with arbitrary geometry. *Journal of Materials Engineering and Performance*, 9, 62-71.
<https://doi.org/10.1361/105994900770346295>
- [89] Zhou, J., Zhang, G., Lin, Y., & Wang, H. (2011). A new virtual sphere method for estimating the role of thermal mass in natural ventilated buildings. *Energy and Buildings*, 43, 75-81.
<https://doi.org/10.1016/j.enbuild.2010.08.015>
- [90] University of Illinois, & Ernest Orlando Lawrence Berkeley National Laboratory. (2014). *Energy Plus Engineering Reference Manual*. Retrieved from https://energypplus.net/sites/default/files/pdfs_v8.3.0/EngineeringReference.pdf
- [91] EQUA Simulation AB. (2013). *User Manual IDA Indoor Climate and Energy – version 4.5*. Retrieved from <http://www.equaonline.com/iceuser/pdf/ICE45eng.pdf>
- [92] Raftery, P., Lee, E., Webster, T., Hoyt, T., & Bauman, F. (2014). Effects of furniture and contents on peak cooling load. *Energy and Buildings*, 85, 445-457.
<https://doi.org/10.1016/j.enbuild.2014.09.081>
- [93] Hand, J. (2016). Performance implications of fully participating furniture and fittings in simulation models. In *Proceedings of the BSO Conference, Newcastle, UK*. Retrieved from <http://www.ibpsa.org/proceedings/BSO2016/p1133.pdf>
- [94] Zalba, B., Marin, J. M., Cabeza, L. F., & Mehling, H. (2003). Review on thermal energy storage with phase change: materials, heat transfer analysis and applications. *Applied Thermal Engineering*, 23, 251-283.

- [https://doi.org/10.1016/S1359-4311\(02\)00192-8](https://doi.org/10.1016/S1359-4311(02)00192-8)
- [95] A. Sharma, V.V. Tyagi, C.R. Chen, & Buddhi, D. (2009). Review on thermal energy storage with phase change materials and applications. *Renewable and Sustainable Energy Reviews*, 13, 318-345. <https://doi.org/10.1016/j.rser.2007.10.005>
- [96] Pardiñas, Á. A., Alonso, M. J., Diz, R., Kvalsvik, K. H., & Fernández-Seara, J. (2017). State-of-the-art for the use of phase-change materials in tanks coupled with heat pumps. *Energy and Buildings*, 140, 28-41. <https://doi.org/10.1016/j.enbuild.2017.01.061>
- [97] Kee, S. Y., Munusamy, Y., & Ong, K. S. (2018). Review of solar water heaters incorporating solid-liquid organic phase change materials as thermal storage. *Applied Thermal Engineering*, 131, 455-471. <https://doi.org/10.1016/j.applthermaleng.2017.12.032>
- [98] Kuznik, F., Virgone, J., & Roux, J. J. (2008). Energetic efficiency of room wall containing PCM wallboard: a full-scale experimental investigation. *Energy and Buildings*, 40, 148-156. <https://doi.org/10.1016/j.enbuild.2007.01.022>
- [99] Athienitis, A. K., Liu, C., Hawes, D., Banu, D., & Feldman, D. (1997). Investigation of the thermal performance of a passive solar test-room with wall latent heat storage. *Building and Environment*, 32(5) 405-410. [https://doi.org/10.1016/S0360-1323\(97\)00009-7](https://doi.org/10.1016/S0360-1323(97)00009-7)
- [100] Diaconu, B. M., & Cruceru, M. (2010). Novel concept of composite phase change material wall system for year-round thermal energy savings. *Energy and Buildings*, 42(10), 1759-1772. <https://doi.org/10.1016/j.enbuild.2010.05.012>
- [101] Medina, M. A., King, J. B., & Zhang, M. (2008). On the heat transfer rate reduction of structural insulated panels (SIPs) outfitted with phase change materials (PCMs). *Energy*, 33(4), 667-678. <https://doi.org/10.1016/j.energy.2007.11.003>
- [102] Pomianowski, M., Heiselberg, P., & Zhang, Y. (2013). Review of thermal energy storage technologies based on PCM application in buildings. *Energy and Buildings*, 67, 56-69. <https://doi.org/10.1016/j.enbuild.2013.08.006>
- [103] Weinläder, H., Beck, A., & Fricke, J. (2005). PCM-facade-panel for daylighting and room heating. *Solar Energy*, 78(2), 177-186. <https://doi.org/10.1016/j.solener.2004.04.013>
- [104] Weinlaeder, H., Koerner, W., & Heidenfelder, M. (2011). Monitoring results of an interior sun protection system with integrated latent heat storage. *Energy and Buildings*, 43(9), 2468-2475. <https://doi.org/10.1016/j.enbuild.2011.06.007>
- [105] Alawadhi, E. M. (2012). Using phase change material in window shutter to reduce the solar heat gain. *Energy and Buildings*, 47, 421-429. <https://doi.org/10.1016/j.enbuild.2011.12.009>
- [106] Alfonsi, J. L., Duthu, N., Gavilan, J., & Albanés Saénz De Tejada, A. (2010). *Xx-PCM - thermoregulating panel for office furniture, "Au frais de mon arbre" project*. Seed-collectif.
- [107] Sapporo, J. (2015). *Abaisser les factures énergétiques en changeant de mobilier*. LE MONITEUR.FR. Retrieved from <http://www.lemoniteur.fr/article/abaisser-les-factures-energetiques-en-changeant-de-mobilier-28816549>
- [108] Rathod, M. K., & Banerjee, J. (2013). Thermal stability of phase change materials used in latent heat energy storage systems: A review. *Renewable and Sustainable Energy Reviews*, 18, 246-258. <https://doi.org/10.1016/j.rser.2012.10.022>
- [109] DuPont (2012). *Energain®*, Technical Datasheet. Retrieved from http://www.cse.fraunhofer.org/hs-fs/hub/55819/file-14736951-pdf/docs/energain_flyer.pdf
- [110] Grundfos Product Center. (2013). *GRUNDFOS Data Booklet - CRI-9 A-FGJA-E-HQQE 3x230/400 50Hz - Grundfos Pump 96478872*. Retrieved from <http://product-selection.grundfos.com/product-detail.product-detail.html?lang=ENU&productnumber=96478872&productrange=gma&qcid=228594986>

- [111] Engelbrecht, K. (2008). *A Numerical Model of an Active Magnetic Regenerator Refrigerator with Experimental Validation*. Madison: University of Wisconsin. Retrieved from <https://minds.wisconsin.edu/bitstream/handle/1793/7596/engelbrecht05.pdf>
- [112] Engelbrecht, K., & Bahl, C. R. H. (2010). Evaluating the effect of magnetocaloric properties on magnetic refrigeration performance. *Journal of Applied Physics*, 108(12), 123918. <https://doi.org/10.1063/1.3525647>
- [113] Engelbrecht, K., Tušek, J., Nielsen, K. K., Kitanovski, A., Bahl, C. R. H., & Poredoš, A. (2013). Improved modelling of a parallel plate active magnetic regenerator. *Journal of Physics D: Applied Physics*, 46(25), 255002. <https://doi.org/10.1088/0022-3727/46/25/255002>
- [114] Nielsen, K. K., Nellis, G. F., & Klein, S. A. (2013). Numerical modeling of the impact of regenerator housing on the determination of Nusselt numbers. *International Journal of Heat and Mass Transfer*, 65, 552-560. <https://doi.org/10.1016/j.ijheatmasstransfer.2013.06.032>
- [115] The MathWorks, Inc. (2018). *MATLAB software*. Retrieved from <https://se.mathworks.com/products/matlab.html>
- [116] Lei, T., Navickaitė, K., Engelbrecht, K., Barcza, A., Vieyra, H., Nielsen, K. K., & Bahl, C. (2017). Passive characterization and active testing of epoxy bonded regenerators for room temperature magnetic refrigeration. *Applied Thermal Engineering*, 128, 10-19. <https://doi.org/10.1016/j.applthermaleng.2017.08.152>
- [117] The Danish Ministry of Economic, Business Affairs Enterprise, and Construction Authority. (2010). *Building Regulations*. Retrieved from http://byggningsreglementet.dk/file/155699/BR10_ENGLISH.pdf
- [118] Larsen, T. S., & Brunsgaard, C. (2010). *Komfort Husene: erfaringer, viden og inspiration*. Saint-Gobain Isover a/s.
- [119] Jensen, J. B. (Dansk Energi), Hvenegaard, C. M. (Teknologisk Institut), Pedersen, S. V. (Teknologisk Institut), & Lindholm, D. (Dansk Energi). (2011). *Den lille blå om Varmepumper*. Dansk Energi. Retrieved from https://www.byggeriogenergi.dk/media/1380/den_lille_blaa_om_varmepumper_low.pdf
- [120] Uponor GmbH. (2012). *Ground Energy - Technical Information*. Retrieved from <https://issuu.com/uponoruk/docs/ground-energy-technical-information>
- [121] Verlag des Vereins Deutscher Ingenieure. (2001). *VDI 4640:2001, Thermal use of the underground-Ground source heat pump systems*. Berlin.
- [122] RETScreen International. (2005). *Ground-Source Heat Pump Project Analysis*. Minister of Natural Resources Canada. Retrieved from <http://publications.gc.ca/collections/Collection/M39-111-2005E.pdf>
- [123] Uponor GmbH. (2008). *Heating and cooling solutions - Technical guidelines - Uponor Uderfloor Heating Home Comfort System*.
- [124] European Committee for Standardization. (2011). *EN 1264:2011 - Water based surface embedded heating and cooling systems*. Brussels.
- [125] International Organization for Standardization. (2012). *ISO 11855:2012 - Building environment design. Design, dimensioning, installation and control of embedded radiant heating and cooling systems*. Geneva.
- [126] ClimateMaster. (2012). *Tranquility Water-to-Water (TMW) Series Submittal Data Model TMW036 - 340 50Hz - HFC-410A*. Retrieved from <http://lenergy.hu/dokuk/termek/103/98caovp2.pdf>
- [127] Grundfos Product Center. (2015). *GRUNDFOS Data Booklet - ALPHA2 L 15-40 130 - 95047560*. Retrieved from <https://product-selection.grundfos.com/product-detail.product-detail.html?productnumber=95047560&qcid=323188257>
- [128] Wang, P. G., Scharling, M., Nielsen, K. P., Wittchen, K. B., & Kern-Hansen, C. (2013). *2001-2010 Danish Design Reference Year - Reference climate dataset for technical dimensioning in building, construction and other sectors, Technical Report 13-19*. Danish Ministry of Climate, Energy and Building. Retrieved from https://www.dmi.dk/fileadmin/user_upload/Rapporter/TR/2013/TR13-19.pdf

- [129] Jensen, R. L., Nørgaard, J., Daniels, O., & Justesen, R. O. (2011). *Person- og forbrugsprofiler: bygningsintegreret energiforsyning. Aalborg: Department of Civil Engineering, Aalborg University. DCE Technical Reports, No. 69.* Retrieved from http://vbn.aau.dk/files/63284701/Person_og_Forbrugsprofiler.pdf
- [130] Kalagasidis, A. S., Rode, C., & Woloszyn, M. (2008). HAM-Tools – a whole building simulation tool in Annex 41. In: C. Rode, H. Hens, & H. Janssen (Eds.), *Proceedings of the IEA ECBCS Annex 41 Closing Seminar* (pp. 21-35). Copenhagen, Denmark: Technical University of Denmark, Department of Civil Engineering. Retrieved from <http://orbit.dtu.dk/files/3606165/ST1Bclosing.pdf>
- [131] Danish Building Research Institute – Sbi. (2013) *BSim software - User's Guide - tsbi5*.
- [132] ANSI/ASHRAE Standard. (2011). *Standard 140-2011: Standard method of test for the evaluation of building energy analysis computer programs*. Atlanta.
- [133] Adams, S., & Holmes, M. (1977). *Determining time constants for heating and cooling coils*. Building Services Research & Information Association. United Kingdom.
- [134] University of Wisconsin-Madison Solar Energy Laboratory, TRANSSOLAR Energietechnik GmbH, CSTB, & TESS. (2012). Type 31: Pipe or duct model. In: *TRNSYS 17 – Mathematical Reference* (pp. 186-188).
- [135] Scarpa, M., Grau, K., & Olesen, B. W. (2009). Development and validation of a versatile method for the calculation of heat transfer in water-based radiant systems. In: *Proceedings of the Eleventh International IBPSA Conference, Glasgow, Scotland*, (pp. 27-30). Retrieved from http://www.ibpsa.org/proceedings/BS2009/BS09_0688_695.pdf
- [136] Diersch, H. J. G., Bauer, D., Heidemann, W., Rahaak, W., & Schätzl, P. (2011). Finite element modeling of borehole heat exchanger systems - Part 1. Fundamentals. *Computers and Geosciences*, 37(8), 1122-1135. <https://doi.org/10.1016/j.cageo.2010.08.003>
- [137] Angrisani, G., Canelli, M., Roselli, C., & Sasso, M. (2014). Calibration and validation of a thermal energy storage model: influence on simulation results. *Applied Thermal Engineering* 67, 190-200. <https://doi.org/10.1016/j.applthermaleng.2014.03.012>
- [138] Prapainop, R., & Maneeratana, K. (2004). Simulation of ice formation by the finite volume method. *Songklanakarinn J. Sci. Technol.*, 26, 55-70. Retrieved from <http://www.thaiscience.info/journals/Article/SONG/10462408.pdf>
- [139] Verma, P., Varun, & Singal, S. K. (2008). Review of mathematical modeling on latent heat thermal energy storage systems using phase-change material. *Renewable and Sustainable Energy Reviews*, 12, 999-1031. <https://doi.org/10.1016/j.rser.2006.11.002>
- [140] Energistyrelsen, Klima Energi og Bygningsministeriet. (2012). *Danmarks Energifremskrivning 2012*. Retrieved from https://ens.dk/sites/ens.dk/files/Basisfremskrivning/danmarks_energifremskrivning_2012_endelig_v_1.2.pdf
- [141] Krag, J., & Wittchen, K. B. (2014). Development of two Danish building typologies for residential buildings. *Energy and Buildings*, 68 (Part A), 79-86. <https://doi.org/10.1016/j.enbuild.2013.04.028>
- [142] Reynders, G., Diriken, J., & Saelens, D. (2015). A generic quantification method for the active demand response potential of structural storage in buildings. In: *Proceedings of the 14th IBPSA conference, Building Simulation 2015, Hyderabad, India*. Retrieved from <https://lirias.kuleuven.be/bitstream/123456789/506774/1/p1510.pdf>
- [143] Favre, B., & Peupertier, B. (2014). Application of dynamic programming to study load shifting in buildings. *Energy and Buildings*, 82, 57-64. <https://doi.org/10.1016/j.enbuild.2014.07.018>
- [144] Masy, G., Georges, E., Verhelst, C., Lemort, V., & André, P. (2015). Smart grid energy flexible buildings through the use of heat pumps and building thermal mass as energy storage in the Belgian context. *Science and Technology for the Built Environment*, 21, 800-811. <https://doi.org/10.1080/23744731.2015.1035590>

- [145] Reynders, G., Nuytten, T., & Saelens, D. (2013). Potential of structural thermal mass for demand-side management in dwellings. *Building and Environment*, 64, 187-199.
<https://doi.org/10.1016/j.buildenv.2013.03.010>
- [146] Arteconi, A., Costola, D., Hoes, P., & Hensen, J. L. M. (2014). Analysis of control strategies for thermally activated building systems under demand side management mechanisms. *Energy and Buildings*, 80, 384-393.
<https://doi.org/10.1016/j.enbuild.2014.05.053>
- [147] Bastani, A., Haghighat, F., & Manzano, C. J. (2015). Investigating the effect of control strategy on the shift of energy consumption in a building integrated with PCM wallboard. *Energy Procedia*, 78, 2280-2285.
<https://doi.org/10.1016/j.egypro.2015.11.365>
- [148] Barzin, R., Chen, J. J. J., Young, B. R., & Farid, M. M. (2015). Application of PCM underfloor heating in combination with PCM wallboards for space heating using price based control system. *Applied Energy*, 148, 39-48.
<https://doi.org/10.1016/j.apenergy.2015.03.027>
- [149] Lopes, R. A., Chambel, A., Neves, J., Aelenei, D., & Martins, J. (2016). A literature review of methodologies used to assess the energy flexibility of buildings. *Energy Procedia*, 91, 1053-1058.
<https://doi.org/10.1016/j.egypro.2016.06.274>
- [150] Reynders, G., Lopes, R. A., Marszal-Pomianowska, A., Aelenei, D., Martins, J., & Saelens, D. (2018). Energy flexible buildings: An evaluation of definitions and quantification methodologies applied to thermal storage. *Energy and Buildings*, 166, 373-390.
<https://doi.org/10.1016/j.enbuild.2018.02.040>
- [151] Johra, H., Heiselberg, P., Le Dréau, J. (Under review). Influence of envelope, structural thermal mass and indoor content on the building heating energy flexibility. *Energy and Buildings*.
- [152] Le Dréau, J. (2016). Demand-side management of heating need in residential buildings. In: *Proceedings of the 12th REHVA world congress - CLIMA 2016, Aalborg, Denmark*. Retrieved from http://vbn.aau.dk/files/233817803/paper_499.pdf
- [153] Péan, T. Q., Salom, J., & Ortiz, J. (2017). Potential and optimization of a price-based control strategy for improving energy flexibility in Mediterranean buildings. *Energy Procedia*, 122, 463-468.
<https://doi.org/10.1016/j.egypro.2017.07.292>
- [154] EnergiNet.dk. (2009). *Market data, elspot price in Western Denmark*. Retrieved from www.energinet.dk/en/el/engrosmarked/udtraek-af-markedsdata/Sider/default.aspx
- [155] International Organization for Standardization. (2005). *ISO 7730 - Ergonomics of the thermal environment-analytical determination of thermal comfort by using calculation of the PMV and PPD indices and local thermal comfort criteria*. Geneva.
- [156] ASHRAE Standard. (2004). *Standard 55 – 2004. Thermal environmental conditions for human occupancy*. Atlanta.
- [157] Holman, J. P. (1994). *Experimental methods for engineers* (Sixth edition). USA: McGraw-Hill, Inc.
- [158] Montgomery, D. C. (2012). *Design and Analysis of Experiments* (Eighth edition). John Wiley & Sons Incorporated.
- [159] Basso, V., Küpferling, M., Curcio, C., Bennati, C., Barzca, A., Katter, M., Bratko, M., Lovell, E., Turcaud, J., & Cohen, L. (2015). Specific heat and entropy change at the first order phase transition of La(Fe-Mn-Si)₁₃-H compounds. *Journal of Applied Physics*, 118, 053907.
<https://doi.org/10.1063/1.4928086>

PUBLICATIONS FOR THE THESIS

Thesis Title: Integration of a magnetocaloric heat pump in energy flexible buildings.

Name of Ph.D. Student: Hicham Johra

Name of Supervisor: Professor Per K. Heiselberg

List of Publications:

- 1) Johra, H., & Heiselberg, P. (2017). Influence of internal thermal mass on the indoor thermal dynamics and integration of phase change materials in furniture for building energy storage: A review. *Renewable and Sustainable Energy Reviews*, 69, 19-32.
<http://dx.doi.org/10.1016/j.rser.2016.11.145>
- 2) Johra, H., Heiselberg, P., & Le Dréau, J. (2017). Numerical analysis of the impact of thermal inertia from the furniture / indoor content and phase change materials on the building energy flexibility. In: *Proceedings of the 15th IBPSA Conference, International Building Performance Simulation Association, San Francisco, CA, USA. Aug. 7-9, 2017.*
<https://doi.org/10.26868/25222708.2017.012>
- 3) Johra, H., Filonenko, K., Heiselberg, P., Veje, C., Lei, T., Dall'Olio, S., Engelbrecht, K., & Bahl, C. (2018). Integration of a magnetocaloric heat pump in a low-energy residential building. *Building Simulation: An International Journal*.
<https://doi.org/10.1007/s12273-018-0428-x>
- 4) Johra, H., Heiselberg, P., & Le Dréau, J. (Under review). Influence of envelope, structural thermal mass and indoor content on the building heating energy flexibility. *Energy and Buildings*.
- 5) Johra, H., Filonenko, K., Heiselberg, P., Veje, C., Dall'Olio, S., Engelbrecht, K., & Bahl, C. (Under review). Integration of a magnetocaloric heat pump in an energy flexible residential building. *Renewable Energy*.
- 6) Johra, H., & Heiselberg, P. K. (2018). *Description and Validation of a MATLAB - Simulink Single Family House Energy Model with Furniture and Phase Change Materials (Update)*. Aalborg: Aalborg University, Department of Civil Engineering, DCE Technical Reports, No. 238.
http://vbn.aau.dk/files/270078674/Description_and_Validation_of_a_MATLAB_Simulink_Single_Family_House_Energy_Model_with_Furniture_and_Phase_Change_Materials_Update_.pdf

Other Publications:

- 1) Karlsen, L., Heiselberg, P., Bryn, I., & Johra, H. (2015). Verification of simple illuminance based measures for indication of discomfort glare from windows. *Building and Environment*, 92, 615-626.
<https://doi.org/10.1016/j.buildenv.2015.05.040>
- 2) Karlsen, L., Heiselberg, P., Bryn, I., & Johra, H. (2016). Solar shading control strategy for office buildings in cold climate. *Energy and Buildings*, 118, 316-328.
<https://doi.org/10.1016/j.enbuild.2016.03.014>
- 3) Østergaard, M. B., Petersen, R. R., König, J., Johra, H., & Yue, Y. (2017). Influence of foaming agents on solid thermal conductivity of foam glasses prepared from CTR panel glass. *Journal of Non-Crystalline Solids*, 465, 59-64.
<https://doi.org/10.1016/j.jnoncrysol.2017.03.035>
- 4) Filonenko, K., Lei, T., Veje, C., Engelbrecht, K., Johra, H., Heiselberg, P. K., & Bahl, C. R. H. (Under review). Magnetocaloric heating modules for scalable and efficient heating. *International Journal of Thermal Sciences*.

This thesis has been submitted for assessment in partial fulfilment of the Ph.D. degree. The thesis is based on the submitted or published scientific papers which are listed above. Parts of the papers are used directly or indirectly in the extended summary of the thesis. As part of the assessment, co-author statements have been made available to the assessment committee and are also available at the Faculty.

APPENDICES

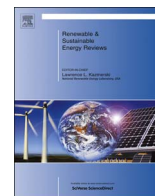
Appendix A. Paper I	114
Appendix B. Paper II	129
Appendix C. Paper III	138
Appendix D. Paper IV	165
Appendix E. Paper V	198
Appendix F. Technical Report I	231

Appendix A. Paper I

Johra, H., & Heiselberg, P. (2017). Influence of internal thermal mass on the indoor thermal dynamics and integration of phase change materials in furniture for building energy storage: A review. *Renewable and Sustainable Energy Reviews*, 69, 19-32.

<http://dx.doi.org/10.1016/j.rser.2016.11.145>

Reprinted by permission from Elsevier.



Influence of internal thermal mass on the indoor thermal dynamics and integration of phase change materials in furniture for building energy storage: A review



Hicham Johra*, Per Heiselberg

Aalborg University, Division of Architectural Engineering, Department of Civil Engineering, Thomas Manns Vej 23, DK-9220 Aalborg Øst, Denmark

ARTICLE INFO

Keywords:

Furniture
Thermal mass
Indoor thermal dynamics
Thermal energy storage
Phase change material
Building energy flexibility

ABSTRACT

The increasing share of intermittent renewable energy on the grid encourages researchers to develop demand-side management strategies. Passive heat storage in the indoor space is a promising solution to improve the building energy flexibility. It relies on an accurate control of the transient building temperature. However, many of the current numerical models for building energy systems assume empty rooms and do not account entirely for the internal thermal inertia of objects like furniture. This review article points out that such assumption is not valid for dynamic calculations. The furnishing elements and other internal content can have a significant impact on the indoor thermal dynamics and on the occupants' comfort. There is a clear lack of guidance and studies about the thermo-physical properties of this internal mass. Therefore, this paper suggests representative values for the furniture/indoor thermal mass parameters and presents the different available modelling technics. In addition, the large exposed surface area of furniture pieces offers a good potential for the integration of phase change materials. It can highly increase the effective thermal inertia of light frame buildings without any construction work.

1. Introduction

Climate change, pollution and fossil fuel shortage have been designated by many as some of the most important challenges of the 21st century. To prevent major energy crisis and reduce CO₂ emissions, significant efforts are required in increasing the renewable energy production while enhancing the energy efficiency of buildings [1]. With about 40% of the total final energy use in Europe, buildings are indeed the largest end-use energy sector, followed by transportation with 33%. Similar repartitions can be observed in the rest of the world [2]. On the production side, a significant expansion of wind and photovoltaic power is planned in many European countries [3]. In Denmark, for example, the energy mix is characterized by a large share of wind power which is expected to reach 50% on an annual basis in 2020. The energy development strategy of countries like Denmark relies on the implementation of a smart grid with high number of wind turbines coupled with district heating for buildings in cities, heat pumps outside urban areas and extensive use of electric cars [4] and [5].

Studies suggest that flexible technologies and demand-side management can improve the integration of renewable energies and facilitate operation of a smart grid system with high intermittent power

penetration [6]. Indoor space heating accounts for 75% of the energy demand of a building in Europe [2]. Analyses showed that individual heat pumps and district heating form the best heat supply solutions in relation to costs, fuel consumption and CO₂ emissions [7]. This thermal energy can be stored efficiently in the building indoor environment or in heat accumulation water tanks. It can thereby decouple the energy need from the intermittent availability of renewable energies, reduce excess wind electricity production and allow optimum use of the free internal and solar gains [8].

Low temperature, water-based radiant heating systems can accumulate heat in buildings with noticeable flexibility. They can be controlled according to a price signal and contribute to shaving of load peaks on the grid without affecting indoor comfort. A research indicated that passive heat storage in the indoor space can be more efficient for the reduction of excess electricity production and fuel consumption compared to heat accumulation water tanks [9]. Passive thermal energy storage (TES) aims to accumulate a maximum amount of heat in the building thermal mass and indoor volume. The operative temperature in the building increases when the electricity is available and cheap, and decreases when the power production is too low. However, the temperature must be kept within the limits of occupants'

* Corresponding author.

E-mail address: hj@civil.aau.dk (H. Johra).

thermal comfort.

The study, implementation and optimization of such strategy for energy flexible buildings need accurate dynamic thermal building models. Nevertheless, many of the current numerical models take into account solely the thermal inertia of the envelope, the floors and the internal walls. The indoor thermal zone is considered as an empty space filled with air only. Furniture and additional mass present in a real occupied building are not included. This assumption is reasonable for classic design and energy analysis of buildings based on steady state or simplified long-term calculations. However, it could lead to noticeable errors for short-term transient temperature prediction, especially in residential buildings with light structure and a lot of furnishing, appliances or objects. This model simplification is thus worth investigating to quantify the role of furniture/indoor thermal mass and develop passive TES with optimum predictive control.

The large surface area of the furniture exposed to the indoor environment can be ingeniously used for latent heat thermal energy storage (LHTES) with the integration of phase change materials (PCMs). Their appreciable energy storage density is an interesting asset for increasing the thermal inertia of light structure buildings and for extending the applicability of the TES strategy. PCM furniture could allow integration of LHTES in low thermal inertia dwellings without the need for building renovation.

This paper aims to review the different scientific studies dealing with the influence of the indoor mass on the building thermal dynamics and emphasises the opportunities for coupling with the PCM technology. The article will first define the thermal mass in buildings. This is followed by a review on the interaction between the internal elements and the indoor environment. Representative thermo-physical characteristics for indoor content will be suggested based on published data and a simple building survey in Denmark. The article will then present different internal element modelling technics. The two last parts of this paper will discuss the different kinds of PCMs and the potential for their integration in furniture. The paper closes with conclusions and proposal for further investigations.

2. Definition

From the thermodynamics point of view, a building is usually considered as an assembly of sub-systems or thermal zones. Each of them is composed of elements with specific conductance and thermal inertia [10]. This section suggests distribution of these thermal inertia elements into three categories: thermal zone envelope, indoor air volume and furniture/indoor thermal mass. Construction parts such as external walls, floors, ceilings, roofs or partition walls form the envelope of the thermal zones. They often integrate heavy materials from the building's structure and have a significant thermal inertia [11]. The external thermal mass of the building envelope is exposed to the outdoor and indoor environment. It is not isothermal and its internal energy varies slowly. On another hand, the air volume contained inside a thermal zone is usually considered as one single node with homogenous temperature. The indoor air temperature can vary quickly because of its limited thermal inertia [10].

If many numerical models only account for the indoor air volume and the zones' envelope thermal mass, the real occupied buildings are actually not empty spaces. The additional furniture/indoor thermal mass of a building is defined as all the matter in a room with the following characteristics:

- It is not defined in the construction elements of the building envelope, floor, ceilings or partition walls.
- It is permanent in the thermal zone. It can move inside the same zone, but it does not leave it.
- It does not emit noticeable heat.
- Its temperature is driven by convection heat exchange with the indoor air and long-wave radiation heat exchange with the envelope

inner surfaces, plus the internal heat gains (sun, HVAC systems, equipment and people loads).

According to that definition, the furniture/indoor thermal mass is composed of all the furnishing elements (sofa, bed, table, chair, desk, cupboard, closet, shelves and boards), the finishing parts or accessories that are not directly integrated in the envelope or walls and the aggregate of the other objects present in a room (plants, books, clothes, paper and small appliances). It excludes the body of living beings, movable objects, which enter and leave the zone several times a day, HVAC terminals (radiators, air handling units) and all equipment emitting heat energy (computer, ventilator, engines, lighting, lamps).

3. Influence of furniture and internal mass on the indoor environment

The furniture/indoor thermal mass elements present a large surface area for interaction with the indoor environment.

They exchange heat and moisture by convection with the indoor air and by diffusion with direct contact surfaces such as floors or walls. They also exchange heat by long wave radiation with the surrounding surfaces and can cover and hinder heating or cooling radiant systems. They can change air flow pattern in the room and affect ventilation efficiency and convection heat transfer. They can also reflect, diffuse and absorb solar radiation or internal gain and release it quickly to the surrounding air.

The furniture/indoor thermal mass is thus highly activated and coupled to the other elements. It is legitimate to wonder if this additional internal mass can be neglected in numerical models. This simplification could lead to significant errors especially for light structure houses or radiant systems. Some researchers have investigated this question. Most of the building related publications about internal mass and furniture study the chemical compounds emission of the different materials of furnishing parts and its impact on the indoor air quality [12]. Building numerical analysis including details of interior partitions and furniture has pointed out that they have a significant impact on daylight conditions [13]. However, the following discussion will only focus on the indoor thermal comfort and the thermal dynamics issues.

3.1. Micro-climate, indoor humidity and local discomfort

Mortensen et al. [14] investigated the local micro-climate created by furnishing elements close to cold walls. A piece of furniture placed near a poorly insulated external wall can lead to condensation on the inner side of the building envelope. The authors used particle image velocimetry to perform a two-dimensional experimental analysis of the airflow pattern in a small air gap between a chilled wall and a closet placed next to it. Two air gap widths were tested: 25 and 50 mm. Length of legs of the furniture varied from 0 to 200 mm. The study indicated that vertical flow dominates with similar behaviour as in between vertical plates heated asymmetrically. The flow in the air gap was not fully developed and maximum velocities were found near the cold wall. Finally, the flow rate increased when the gap was expanded or if the furniture was elevated from the floor.

The humidity buffering effect of materials located in the thermal zone can reduce humidity variation. It improves thermal comfort and decreases energy consumption of the mechanical systems for humidification or dehumidification. Yang et al. [15] conducted full-scale experiments on moisture buffering capacity of interior surface materials and impact of the presence of furniture in the interior space. The results showed that the indoor humidity variation decreased by up to 12% and the total moisture buffering potential of the room increased by up to 54.6% for a fully furnished case. The authors explained that furnishing elements present much more surface area for moisture exchange and buffering than envelope inner surfaces. Furniture

materials can also hold more water vapour than interior surface ones. In addition, the variation of moisture contents of walls screened by furnishing is not always the same as in an empty room. The results also indicated that a bookshelf with books and a bed with mattress present higher moisture buffering capacity than tables, chairs and curtains.

In [16], Horikiri et al. used computational fluid dynamics (CFD) to assess the effect of room occupancy and furniture arrangement with and without heat generation in terms of local thermal comfort. Three different configurations of furniture and occupants were compared with the empty room case. The study pointed out that addition of non-heat generating furnishing in the ventilated room can induce complicated flow re-circulations and high local air velocities around edges of the furniture. However, it has little influence on room temperature and airflow buoyancy strength, compared with that of unfurnished room case. Finally, the heat generation from the TV did not have important impact on the thermal comfort and heat transfer.

Another CFD analysis [17] looked into the interaction of ventilation and air-conditioning emitters with furniture in a bedroom. It concluded that the location of air-conditioner unit should take into account the existence of the room's furniture to avoid cold air re-circulation and local draft. Furniture obstruction can indeed lead to the air jet to not fully develop and bounce directly to the occupants.

These different publications emphasised that the existence of furniture in the indoor environment can have a significant impact on the internal air dynamics, local and global humidity conditions and comfort.

3.2. Impact of indoor elements on HVAC systems performance

Furnishing, carpets and interior decoration elements are often laid directly on the rooms' internal surfaces. They produce sensitive changes in radiative and convective heat exchange processes and impact the performance of heating and cooling radiant systems. It is therefore stated in the REHVA Guidebook [18] that additional surface thermal resistance should be applied in order to account for carpets and finishing layers covering radiant floor systems.

Zhao et al. [19] performed detailed calculations and field tests, which emphasised the effect of chairs and benches on the performance of radiant floor cooling systems, exposed to high solar load in a large building. These furnishing elements can overshadow the cooling surface and produce local lower surface temperatures. The floor surface under the benches was 3.8–7.5 °C colder than the unsheltered one. Consequently, the cooling effect of the covered radiant floor was decreased by 83%. The risks of moisture condensation on these cold shaded zones are also much higher. This should be taken into account for the system's design to insure that the lowest surface temperature is kept higher than the dew point of the local surrounding air.

Corcione et al. [20] published numerical studies showing a non-negligible decrease in the heat transfer from radiant surface systems to the furnished indoor space in comparison to an empty room case. The air and mean radiant temperature were also impacted. Fontana [21] extended this work with experimental investigations using a small-scale test setup to look at the impact of furniture pieces with different surface areas, locations and distance from the floor. The author concluded that 40% of floor covering with different kinds of furniture can reduce the heat flux from the radiant floor to the room by 25–30%.

Pomianowski et al. [22] conducted a full-scale experiment concerning the influence of an internal obstacle on the overall heat transfer in a room when using displacement night time ventilation. The presence of a table changed the average convective heat transfer coefficient in the test chamber and the mean heat flux at the ceiling by 3.96% and 9.84% respectively, when applying an air change rate of 6.6 h⁻¹. The only noticeable drops in the temperature efficiency caused by the presence of the table were observed at low air change rates.

The studies presented above pointed out that the influence of furniture cannot be neglected when designing a radiant floor system.

Surprisingly, it has been found that Fontana [21] was the only one to publish the results of an experiment investigating the impact of furniture on radiant systems. As mentioned by Le Dréau [23], further experimental researches are required to quantify the effect of furniture on the effectiveness of radiant systems.

3.3. Building thermal dynamics

The transient thermal behaviour of buildings mainly depends on the heat load admission rate and the activated thermal capacity. The building effective thermal capacitance quantifies its practical energy storage potential. It can considerably differ from the apparent thermal capacitance, which is the sum of specific heat capacities of the building elements [24]. Many different studies looked into the impact of the thermal inertia on the building dynamics, the reduction of temperature swings and cooling peak shaving with night time ventilation strategies [25–27] and [28]. However, most of them only consider the thermal mass of the building envelope and partition walls.

Antonopoulos and Koronaki [24,29] and [30] characterized the thermal capacitance, time constant and thermal delay of typical Greek detached houses with a one-dimensional finite-difference model. The authors took into account the presence of furniture thermal mass and modelled it as an equivalent one-side wooden slab of 6 m² per m² of floor area and a thickness of 5 cm, which gives an internal mass density of about 180 kg per m² of floor area. No justification was given for the choice of this value. Solar load and internal heat gains were applied to the air node only. The results showed that the envelope, partition walls and furniture represented 78.1%, 14.5% and 7.4% respectively, of the total effective building thermal capacitance. The authors concluded that furniture/indoor mass can increase the building time constant and thermal delay by up to 40% (25% for interior wall partitions and 15% for the furnishings).

Yam et al. [31] developed a simplified building model with adiabatic envelope and no internal sun load to inspect the nonlinear coupling between internal thermal mass and natural ventilation. They found that a maximum indoor temperature phase shift of 6 h can be achieved if the fresh air is directly supplied from the outdoor environment, presenting periodic temperature variations. The authors suggested that an appropriate amount of thermal mass should be used in building passive design because further increase above an optimum point does not change the phase shift of the system. Zhou et al. [32] extended the aforementioned study by adding the envelope thermal mass into consideration. The results showed that increasing the internal thermal mass of a building with a large time constant to adjust the indoor air temperature is not an effective solution.

Wolisz et al. [8] carried out a numerical analysis on the impact of modelling furniture and floor covering in thermal building simulations with temperature set point modulation control. The study cases were a massive building and a light frame building, both with very good insulation levels and under-floor heating systems. The furniture element was represented by an equivalent horizontal board of wood or metal. Long-wave radiation heat exchanges were modelled by coupling inner surfaces to a fictive massless black body node in a star network scheme [33]. One internal wall had 50% of its surface area covered by furniture. It was found that after 4 h of increased set point, an empty massive room was 1.2 °C warmer than the one with flooring and furniture. A fully equipped massive room can have a time delay of more than 7 h to raise its temperature by 5 °C, compared to an empty room. Furnishing and floor covers can change cool-down times by up to 2 h in the case of periodic set point control. The floor covering presented more significant effect on the heating time than the furniture element because the under-floor radiant system was used as a heating source. However, the effect of furniture became more important for the lightweight room with periodic set point scenario. The authors concluded that both the furniture and the floor covering of a room have a distinct and significant impact on the indoor temperature for

dynamic set point control.

If the influence of furniture is negligible in the case of steady state building thermal calculation, it is clearly not the case for the evaluation of dynamic strategies such as night time ventilation cooling or passive TES. The previously reviewed publications showed that the empty thermal zone assumption will necessarily lead to a noticeable underestimation of the building thermal capacitance and thus higher internal temperature swing. Consequently, such simplification can produce deviation of few degrees in the calculation of dynamic indoor temperature, which is significant for set point modulation control and TES in the indoor space.

3.4. Impact of internal mass on building energy needs

Only one publication focusing on the effect of furnishing on the building energy need has been found. Raftery et al. [34] performed a sensitivity analysis on the influence of furniture on the peak cooling load of a large open space multi-story office building located in San Francisco. The authors used the Energy Plus software and varied multiple parameters such as type of HVAC system, building orientation, window to wall ratio, envelope thermal inertia and amount and surface area of the internal mass element. Two different furniture models were tested: a simplified non-geometric furniture element, which is not taken into account for solar radiation and long-wave heat exchange and a new model with a geometric representation of an equivalent furniture slab located in the centre of the room, 0.5 m above the floor. With the latter, direct and diffuse solar radiation repartition can be executed accordingly with shading effect of the planar element on the floor. Long-wave radiation heat exchange can also be calculated with correct view factors. Results were presented using the median value following by the lower and upper quartiles in parentheses. The study found that internal mass can change peak cooling load by -2.28% (-5.45%, -0.67%). The geometric modelling changed peak cooling load by -0.25% (-1.02%, +0.23%) when compared to the non-geometric model. This geometric modelling had a larger effect in cases with high direct solar radiation and almost no effect for low solar loads. The impact was also found more important for HVAC radiant systems, which yield a surface temperature asymmetry. The thickness of the internal mass element had a relatively large impact on results. Very thin elements with a small time constant convert the solar load into a convective load quickly and can thus increase the peak cooling load. The authors concluded that the choice of modelling method is not significant compared to the uncertainty on the internal mass characteristics such as surface area, material properties, weight and thickness.

4. Internal thermal mass characteristics

As pointed in [34], there has not been found any survey, study or clear guidance concerning reasonable or typical values for furnishing/indoor mass parameter in buildings. This section treats this issue by presenting the results of a simple survey performed on residential and single office buildings in Denmark. Since the total amount of internal mass in each room and building can vary significantly from case to case, only a survey with a large sampling could pretend to provide statistically representative data. Therefore, the following study only intends to suggest reasonable boundaries for the internal mass and furniture parameters.

4.1. Internal mass materials

Multiple sources such as international standards, software documentation, industrial technical reports and scientific publications have been combined [35–41] and [42] to assess the thermal properties variation span of common building materials.

Density and thermal conductivity are two parameters, which are

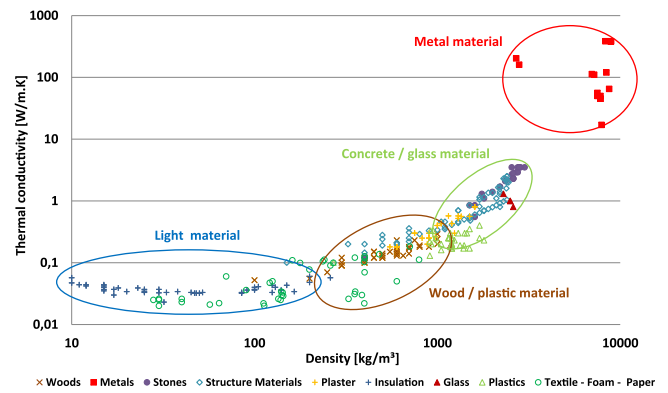


Fig. 1. Thermal conductivity of building materials in function of density.

relatively easy to measure precisely. They are well defined in different catalogues. In Fig. 1, one can see a clear correlation between material density and thermal conductivity. Several researchers have already studied this point [43–47] and [48]. Apart from metal, most of the building materials are porous media and compound of plastic, natural cellulose fibres or minerals. Their thermal conductivity is mainly determined by the air and water content, which is directly related to their porosity and, therefore, to their density. On the other hand, the specific heat capacity of the material is more difficult to assess. It has been noted that the same value is often given for the whole class of a material in the sources. As shown in Fig. 2, there is no clear relation between the density and the specific heat capacity of construction materials.

The mass and volume of objects are rather simple parameters to estimate. Therefore, it is suggested to classify the different materials in function of their density and deduct the thermal conductivity and specific heat capacity from this first characteristic. One can see this simple classification and representative thermal properties in Table 1.

4.2. Element thickness

Most of the building and internal mass elements have a planar shape. It is, therefore, possible to measure their thickness and surface area systematically. The simple survey on the Danish buildings showed that the surface weighted average thickness of indoor wood elements is 1.8 cm. Minimum and maximum thicknesses are 1 and 5 cm respectively. Metallic elements have a thickness between 1 and 3 mm. Ceramic and glass pieces have a thickness between 0.2 and 2 cm. Light material elements have a thickness from 0.5 to 24 cm.

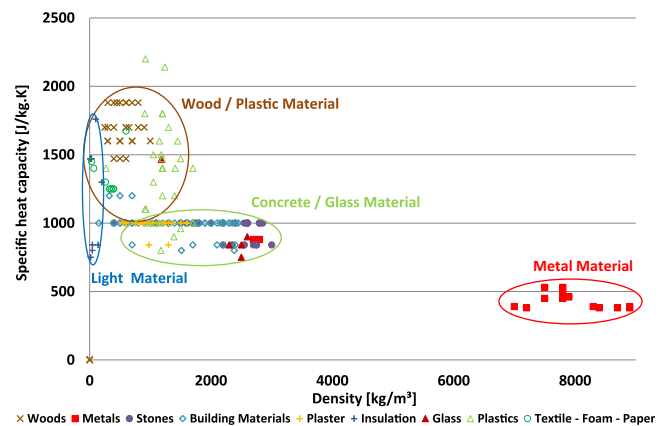


Fig. 2. Specific heat capacity of building materials in function of density.

Table 1
Representative building material categories and their characteristics. The average value is followed by the lower and upper range limits in parentheses.

Material/ Properties	Density (kg/ m ³)	Thermal conductivity (W/ m K)	Specific heat capacity (J/ kg K)
Light material	80 (20–140)	0.03	1400
Wood/plastic material	800 (400–1200)	0.2 (0.1–0.3)	1400
Concrete/glass material	2000 (1500–2500)	1.25 (0.5–2)	950
Metal material	8000	60	450

4.3. Quantification of the internal thermal mass

The total amount of internal mass in a building is not a trivial parameter to find. Unfortunately, professional removal companies do not estimate nor measure it. In [34], it is stated that the Californian non-residential alternative calculation method manual (2005) prescribes the value of 391 kg/m² of total floor area. It corresponds to about 470 kg/m² of net floor area. This value is very high because it probably takes into account the total amount of thermal mass including the envelope and the partition walls. The US benchmark commercial buildings from the PPNL (2013) and the DOE (2010) models use an amount of internal mass corresponding to 177 kg/m² of wood spread over twice the floor area. In the parametric study of Raftery et al. [34], the internal mass is varied from 0 up to 300 kg/m² of floor area. Antonopoulos et al. [30] used around 180 kg of wood per m² of floor area. In order to assess which of these values are realistic, the mass and dimensions of each piece of internal elements have been measured in 6 different bedrooms, 3 living rooms and 3 single office rooms in buildings located in Denmark. Fig. 3 presents the results of this simple survey.

As seen in Fig. 4, the total internal mass is often over-estimated. It is suggested that a reasonable range for the internal mass density in office and residential buildings would be 10–100 kg/m² of the net floor surface area.

4.4. Internal mass effective heat capacity

The thermal inertia of the different building elements can also be evaluated according to their effective heat capacity. It can be represented as the thermal storage capacity of a system subject to variable boundary conditions. It is chosen to use 24-h period sinusoidal variations to assess the effective heat capacity of a building in the case of daily indoor TES. It can be calculated with a one-dimensional numerical model such as finite control volume method or with a matrix

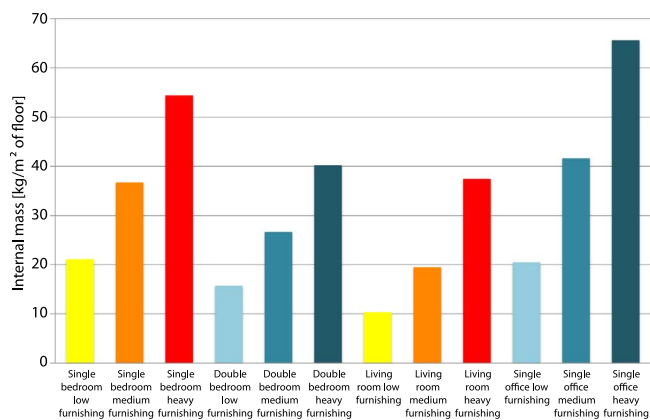


Fig. 3. Internal mass of the building survey.

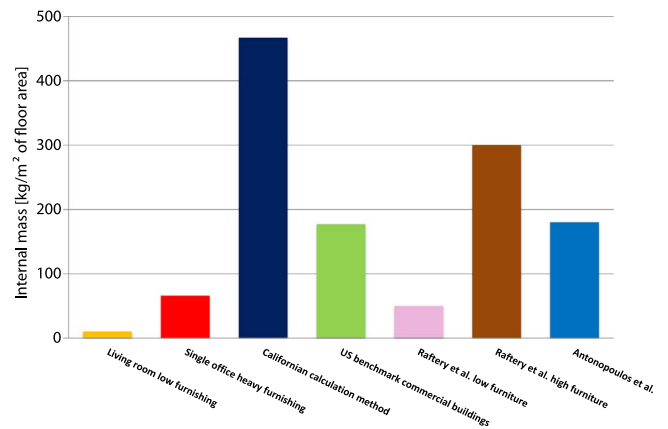


Fig. 4. Comparison between results of the survey and other published values from Antonopoulos et al. [29] and Raftery et al. [34].

calculation procedure defined in international standards [49]. However, such calculation requires a detailed description of every element present in the indoor space, which is rarely the case. To overcome this problem, Wang et al. [50] modelled the internal mass of a thermal zone as a lumped thermal capacitance and identified this parameter from the HVAC operation data with a genetic algorithm estimator.

It is stated in the French energy building regulation that the effective daily heat storage capacity of furniture is 20 kJ/K.m² of floor area [11]. Antonopoulos et al. calculated a value of 45 kJ/K.m² for a typical Greek residential house [30]. In [23] and [51], the indoor air volume thermal capacitance is multiplied by 5 and 8 respectively, in order to account for the furniture thermal mass. This is equivalent to about 17 and 27 kJ/K.m² respectively. Based on the detailed description of the internal mass survey in Danish buildings, the effective daily heat capacity of each construction and internal element is calculated with the matrix calculation method [49]. Furniture elements, metal pieces, lightweight material, clothes, books, paper, appliances and other objects are aggregated in different equivalent planar elements with appropriate material thermal properties. The same constant surface resistance of 0.13 K m²/W is assumed on both sides of the equivalent planar elements. Internal radiation gains are not taken into account.

The results from the survey presented in Fig. 5 are in good agreement with the other survey. The same matrix method is then used to calculate the daily effective thermal capacitance of the inner surfaces of the rooms for buildings with different class of envelope thermal mass.

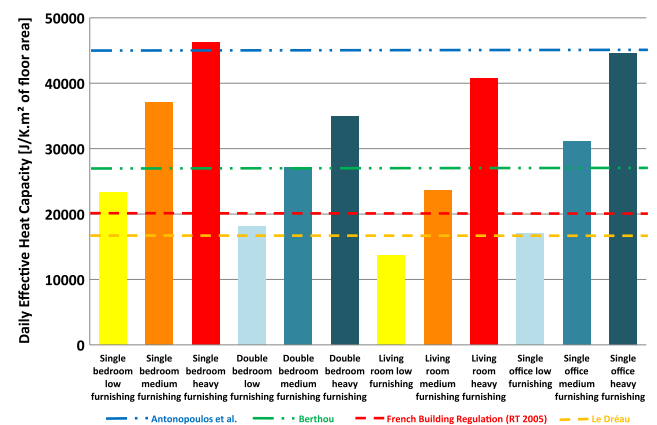


Fig. 5. Daily effective heat capacity of internal thermal mass in buildings. Comparison with published values from Le Dréau [23], Antonopoulos et al. [29], French building regulation (RT 2005) [11] and Berthou [51].

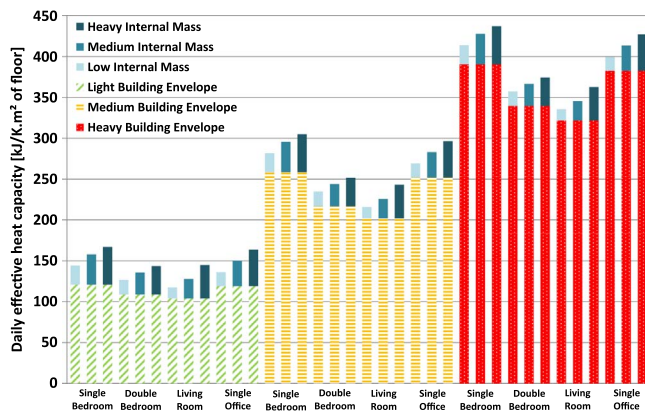


Fig. 6. Total daily effective heat capacity of buildings.

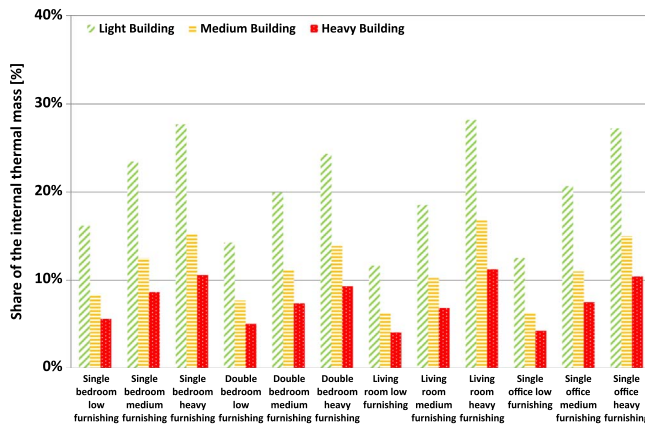


Fig. 7. Share of the internal thermal mass in the total daily effective heat capacity of the building.

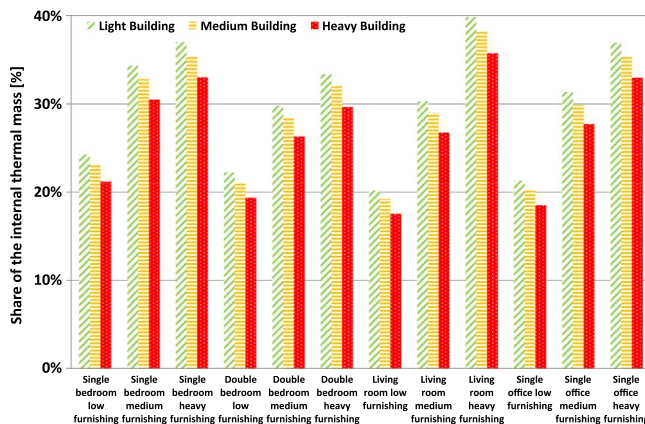


Fig. 8. Share of the internal thermal mass in the total hourly effective heat capacity of the building.

As seen in Figs. 6 and 7, the daily effective heat capacity of the internal mass holds a significant share of the total room thermal inertia. It is particularly important in the case of lightweight structure buildings. Because the internal mass is quickly activated, the impact on the total inertia is even more visible when considering the hourly effective thermal capacity (see Fig. 8).

4.5. Impact of internal mass properties on daily effective heat capacity

A simple parametric sensitivity analysis of the daily effective heat capacity is performed for four different materials with the matrix

calculation method. Density, heat conductivity and surface thermal resistance are varied within reasonable limits. The daily thermal mass activation percentage (ratio of effective heat capacity on apparent heat capacity) is calculated in function of the element thickness.

As shown in Fig. 9, all parameters of the equivalent planar elements have a significant impact on their effective thermal capacity. However, in the case of daily boundary condition variations, the slab elements are almost totally activated, meaning that their effective thermal capacitance is very close to their apparent maximum thermal capacitance. However, this is not the case for light material elements thicker than 10 cm with density higher than 80 kg/m³. Lightweight elements thicker than 10 cm are generally mattresses and cushions. According to retailer documentation, their density is always lower than 60 kg/m³. It is, therefore, reasonable for a simple calculation to assume that the daily effective thermal capacity of the indoor mass is equal to its apparent thermal capacity Fig. 10.

5. Internal mass modelling

The furniture/indoor thermal mass forms a set of complicated geometries with various materials. It is necessary to simplify such complex system in a proper way so that it grasps the dominant aspects of the indoor physics. This section reviews different approaches found in publications and software documentation.

5.1. First order thermal network

Simplified thermal network or resistance – capacitance (RC) models with the *xRIC* configuration aggregate all the effective thermal inertia of the thermal zone (indoor air, interior walls, furniture and building envelope) in a single capacitance [52]. It is assumed that this thermal mass is perfectly isothermal with homogenous equivalent properties. An example of such model is described by a *5RIC* scheme in the ISO 13790:2008 standard [53].

5.2. Higher degree thermal network

In order to refine the dynamic response of building models, the thermal mass elements with dissimilar thermal diffusivities are segregated into different lumped capacitances. Two clearly distinct thermal masses are the indoor air volume and the construction elements. In *xR2C* schemes and higher degree models, the indoor air temperature is coupled to the air volume heat capacitance. The building envelope temperature is coupled to an equivalent wall capacitance [51]. The question is thus to decide where to include the furniture and other indoor items.

One way is to assume that objects in the indoor zone are perfectly isothermal and always in thermal equilibrium with the indoor air node. In this situation, all the indoor content capacitance is added to the one of the air. This configuration can be found in TRNSYS multi-zone building model (type 56) [54] or in the *xR2C* schemes described in ref [51]. The air capacitance is simply multiplied by a constant value to account for the additional furniture inertia. Nevertheless, no requirement or indication concerning this parameter has been found. The TRNSYS software uses a default value of 1.2 times the air volume heat capacitance, but some guided examples advise using a value of 3 [54]. In Refs. [23] and [51] the coefficient is set to 5 and 8 respectively. Another solution, presented in the *6R3C* model of ref [51], is to couple the furniture thermal capacitance to the inner surface envelope temperature node. It is also possible to aggregate interior walls, furniture and other indoor mass into a lumped capacitance which is distinct from air and external walls one [52]. This internal mass subsystem can be expanded into a *2R2C* scheme to account for the temperature gradient in the equivalent element [50].

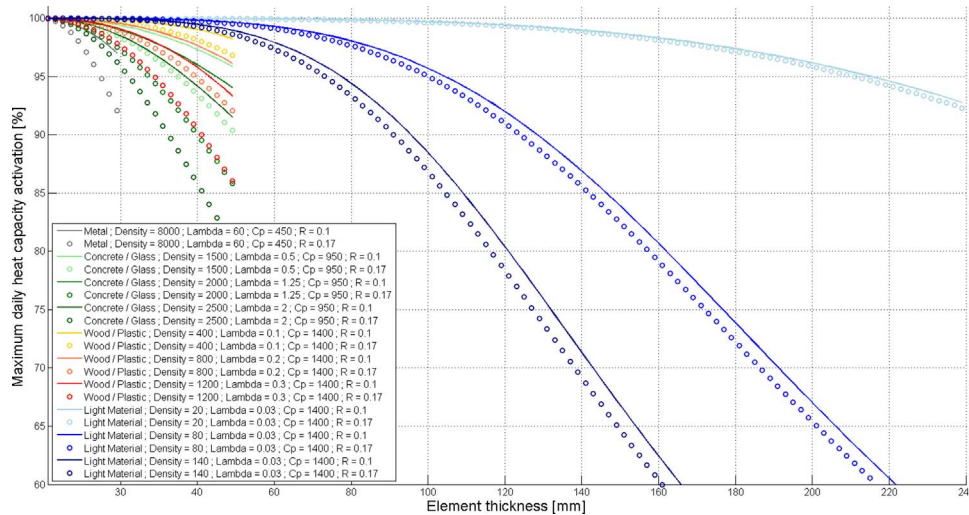


Fig. 9. Daily activation of the equivalent material elements thermal mass.

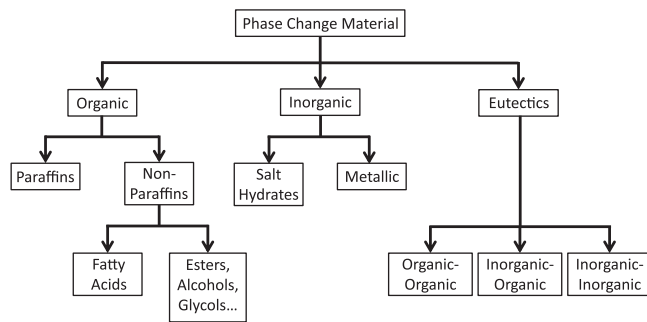


Fig. 10. General categorization of PCMs [69].

5.3. Distinct internal mass capacitance

One could consider that the thickness, thermal diffusivity and heat exchanges of internal mass elements differ significantly from the ones of the air volume and wall inner surfaces. The temperature difference between the furniture node and the other elements would justify an indoor mass modelling with its own lumped capacitance. The TRNSYS Type 56 model is a non-geometrical heat balance [54]. The room furnishings can easily be included in the star network for radiation and convection heat exchange [33] and [54] as a new lumped capacitance like an ordinary wall element. The location of the internal mass is not required, but a proper representative surface area must be specified [55]. The effective thermal mass area is defined in international standards [53] as $A_m = C_m^2 / \sum (A_i \times \kappa_i^2)$. Where C_m , A_i , κ_i represent total effective heat capacity of the zone [J/K], area of the i element [m²], areal effective heat capacity of the i element [J/K m²], respectively.

5.4. Virtual sphere model

In models presented before where an element is represented by a single node, the temperature distribution is assumed to be uniform. The element is isothermal, and heat exchanges are treated as quasi-static processes. This assumption is acceptable if the thermal diffusion within the thermal mass is much faster than the heat transfer at the volume surface. It is the case when the *Biot* number is smaller than 0.1. For wooden plate element, this condition would be fulfilled if the thickness is smaller than 2 mm. However, most of the internal mass and furniture elements are thicker than 2 mm. Therefore, the lumped method should not be used to model the interior thermal mass [56]. The *Biot* number calculations for planar elements with different

materials presented in Table 2 clearly show that only metal elements can be modelled realistically with the lumped method.

In order to overcome this problem, Zhou et al. [57] presented a building model where the effect of intern mass is calculated by the virtual sphere method. The latter was first proposed by Gao et al. [58]. It aggregates different shapes of solid body into a single sphere with a radius equal to the characteristic length of the element. It is appropriate for systems with *Biot* number in the range of 0–20, which is typically the case for internal building content. Zhou et al. published a new formulation for unsteady heat transfer of the indoor mass. The total heat capacity for N internal thermal mass elements is $C = \sum_{i=1}^N M_i C_{m,i}$ [J/K]. The radius of the virtual sphere is $R = 3 \sum_{i=1}^N V_i / \sum_{i=1}^N S_i$ [m]. Where M_i , $C_{m,i}$, V_i , S_i represent mass [kg], heat capacity [J/kg K], volume [m³], area [m²] of i internal thermal mass, respectively. The heat balance equation between the virtual sphere and the indoor air is then developed with the external and average temperature of the sphere. The temperature of the solid can be calculated from analytical solution of the heat equation in spherical coordinates. Moreover, an effective convection heat transfer coefficient is introduced to account for the uneven distribution of internal mass temperature. Nevertheless, the current model does not include radiation heat exchanges.

5.5. Virtual equivalent planar element

In the Energy Plus and IDA ICE software, there is a possibility to insert furniture elements as a one-dimensional multi-layer planar element [59,60] and [61]. The same approach is used in ref [30], [8] and [56]. The energy balance and temperature distribution of this simple system is easy to solve by the mean of numerical methods. However, these internal mass equivalent slab elements do not have a geometric representation in the thermal zone. This means that the presence of the planar elements in the room is not taken into account for the internal solar distribution or the long-wave heat exchanges in between inner surfaces. The equivalent furniture element only interacts with the air node by convection.

5.6. Geometric equivalent planar element

As mentioned before, Raftery et al. [34] developed and implemented into Energy Plus an internal mass equivalent planar element model with a geometric representation and location inside the thermal zone. This object is thus fully taken into account for the computation of the direct light beam reaching internal surfaces, diffuse solar repartition and radiant mean temperature. The long-wave radiation heat exchange

Table 2
Biot number of different material elements.

Material	Metal	Metal	Metal	Concrete	Concrete	Concrete	Plaster	Plaster	Plaster	Plastic	Plastic	Plastic	Wood	Wood	Wood	PUR Foam	PUR Foam	PUR Foam
Thickness (cm)	1	3	5	1	3	5	1	3	5	1	3	5	1	3	5	1	3	5
Biot number	0.001	0.002	0.002	0.030	0.076	0.109	0.090	0.227	0.327	0.180	0.455	0.655	0.240	0.606	0.873	12,000	3,032	4,365

can be calculated by radiosity method with correct view factors affected by the furniture element in the middle of the room. Shading effect on the floor is modelled properly which adds a more realistic physical behaviour to radiant systems.

5.7. Heat balance modelling

The energy balance of an internal mass element depends on the three heat transfer modes. The dynamic conduction in a solid is a well-known problem which is handled by solving the heat equation with numerical methods such as finite difference, finite volume, finite element methods or transfer functions [23]. One-dimensional heat flux with constant thermal properties and homogenous surface temperatures are convenient assumptions, which are reasonable in the case of slabs such as equivalent internal mass elements.

Solar radiation distribution to the internal mass can be modelled in a simple way with the “solar to air factor” or “sol-air coefficient”. It is defined in the standard ISO 15265:2007 [62] as the fraction of the radiation entering through a glazing which is immediately delivered as a convective heat flow to the indoor air. This fraction depends on the presence of internal elements with very small time constant such as carpets or furniture. These thin elements can be illuminated by direct solar radiation and reach thermal equilibrium with the indoor environment within one simulation time step. This coefficient is assumed to be time independent and set to the default value of 10%. However, this factor does not exist in the simplified modelling method described in the ISO 13790:2008 [53]. BSim software documentation [10] advises to fix this factor between 10% and 30%.

If the internal elements have a real geometry in the indoor space, various calculation methods can determine the shadow and direct solar beam trajectory striking internal surfaces with a certain number of reflections and diffuse re-emission. The diffuse sun radiation distribution is performed separately with a simple absorptance weighted area ratios or from view factors between internal surfaces and the windows (Gebhart Method) [54]. The ray tracing method gives very accurate results for the solar repartition of direct and diffuse sun gain on inner surfaces but it is computationally demanding. The values are thus pre-calculated for different positions of the sun in the sky and then interpolated during the actual simulation [23].

Straightforward long-wave radiative exchange models have been developed for simple geometries with 2 or 3 interacting surfaces and infinite reflection [23]. Concave configurations with more surfaces can be transformed in a simplified start network with coupling to a central fictive massless black body node [33] and [54]. The radiosity method gives the exact solution to long-wave radiation heat exchange, but it needs higher computation resources, especially when surface temperatures are unknown [23]. This method is based on the calculation of the view factor matrix. The latter can be determined in a furnished enclosure by the mean of correlations taking into account the obstruction of an object by another one [63] or with the ray tracing method.

The convection is the least well understood and thus the most difficult thermal transfer mode to simulate in building physics. It has not been accurately modelled yet and many simplified models use constant convective or combined convective/radiative indoor heat transfer coefficients ranging from 0.7 to 5 W/m² K and from 5.88 to 10 W/m² K, respectively [64]. However, the review paper of Peeters, Beausoleil-Morrison and Novoselac [65] presents detailed empirical correlations for various indoor configurations and surface orientations.

6. Phase change materials for building energy storage

In recent years, the use of phase change materials to enhance the thermal capacity of the buildings is becoming an attractive solution [66]. Indeed, PCM’s latent heat can store 5–14 times more thermal energy per unit volume than sensible storage materials such as water or concrete [67]. Moreover, this high storage density can be employed

with a small temperature change. This section gives an overview of the state-of-the-art of materials with solid-liquid phase transition which are the most commonly used PCMs for building applications [68].

6.1. PCMs characteristics

A good PCM for building TES should have the following properties:

- Melting temperature in the desired operating range to assure useful heat storage and extraction. Building application temperatures range from 15 °C (cold storage) to 70 °C (heat storage).
- High latent heat of phase transition per unit volume to achieve high storage density.
- High specific heat to provide additional sensible heat storage.
- High thermal conductivity of both solid and liquid phases to assist the energy charging and discharging process.
- Small volume change on phase transformation (less than 10%) and small vapour pressure at operating temperature to reduce the containment problem.
- Congruent melting for a constant storage capacity with each freezing/melting cycle.
- Complete reversible freeze/melt cycle. Stable and reproducible phase change over time. No degradation after a large number of freeze/melt cycles.
- High nucleation rate to avoid sub-cooling of the liquid phase and to assure that melting and solidification proceed at the same temperature.
- No corrosiveness to the construction and containment materials.
- Non-toxic, non-flammable and non-explosive material for environmental and safety reasons.
- Abundant, available and cost-effective to be economically competitive with other storage options.

Relevant PCMs for building TES are paraffin, fatty acids, salt hydrates and their eutectic mixtures. Their price varies from 0.5 to 10 €/kg. Different technics allow change in their chemical composition and combination with other substances in order to tune the melting temperature to a desirable one, improve the thermal conductivity and incorporate them into common construction elements [70].

The paraffins are very popular organic PCMs. They have a wide range of melting temperatures with a density of around 900 kg/m³. Most of commercial products are extracted from oil. They are cheap with good thermal storage densities (around 200 J/g or 180 MJ/m³). They undergo negligible sub-cooling during the freezing process and provide congruent melting. They are non-corrosive, chemically inert and stable with no phase segregation and low vapour pressure. However, their flammability and low heat conductivity (around 0.2 W/m K) are certain limitations of their effectiveness [71].

Other organic PCMs are generally found in the form of fatty acids. Their melting temperatures vary from 5 to 70 °C. They possess appreciable latent heat ranging from 45 to 210 J/g but usually around 150 J/g (140 MJ/m³). They have the advantages of congruent melting, low sub-cooling and vapour pressure, non-toxicity, good thermal and chemical stability, small volume change, self-nucleating behaviour and biodegradability. They are also capable of thousands of thermal (melting/freezing) cycles without any notable degradation in thermal properties. The raw materials of fatty acids can be obtained from cheap sources such as the fat of animals and vegetables. They are divided into six groups: caprylic, capric, lauric, myristic, palmitic and stearic. They can be combined together in different proportion to form binary and ternary fatty acids eutectic mixture. The phase change temperature of these eutectic mixtures can be tuned to desirable ranges. Their high surface tension improves their capability of integration in a porous material matrix. However, like paraffins, the major drawback of fatty acids is their low thermal conductivity (around 0.17 W/m K) [71] and [72].

Esterification of fatty acids with alcohols is a common method to shift the phase transition temperature. It enables decreasing the melting point of fatty acids with high thermal capacity. The production of binary and ternary PCMs by mixing fatty acids with fatty alcohols, polyethylene oxide, oleic acid, pentadecane or other products with low melting temperature is another possible tuning technic [72].

Other organic PCMs have received less attention by researchers such as sugar alcohol. Some of the polyalcohols have latent heat almost double than that of the other organic PCMs but their melting point ranges from 90 to 200 °C, which is too high for building applications. Among them, erythritol is especially noticeable with a latent heat of fusion of 339.8 J/g at 120 °C.

Bio-based PCMs are organic materials produced from the biomass: soybean oils, coconut oils, palm oils and beef tallow. Like the other organic product, they have an interesting latent heat with good chemical stability and phase transition temperatures ranging from –22.77 to 77.83 °C. Nevertheless, they suffer from the same problems as other organic materials [71].

Inorganic PCMs are classified into two main material groups: hydrated salts and metallic products. Metallic PCMs have too high melting temperatures for building applications. Like previously mentioned PCMs, the salt hydrates possess a significant storage capacity and operate phase transition at ambient temperature. Many studies focused on the calcium chloride hexahydrate, sodium sulphate and magnesium chloride hexahydrate because of their availability, moderate costs and non-flammability. Salt hydrates have a density of around 1700 kg/m³, which is twice higher than for paraffins. With a maximum latent heat of around 200 J/g, their heat storage on a per volume basis is around 350 MJ/m³, which is much higher than organic products. Another significant advantage is their thermal conductivity (around 0.5 W/m K), which is also higher compared to organic materials. However, these products become chemically instable at high temperature. Heating cycles cause continuous dehydration of the PCM and the heat storage capacity usually degrades over time. Moreover, most salt hydrates melt incongruently with the formation of a lower form product. This irreversible process is an additional drawback for their long term performance. The liquid phase separation and segregation can be prevented by addition of gelling or thickening agents. Sub-cooling is another problem associated with salt hydrates. The phenomenon is characterized by a solidification of the product below its phase transition temperature. It can be reduced by inducing heterogeneous nucleation in the salt hydrates thanks to nucleators or direct contact with an immiscible heat transfer fluid [70].

One can see that there is no perfect product for LHTES in the temperature range 19–25 °C. Fig. 11 shows that very few of them present latent heat above 200 J/g. Organic PCMs offer better chemical and thermal stability with congruent melting and they exhibit little or no sub-cooling. On the other hand, inorganic products suffer from

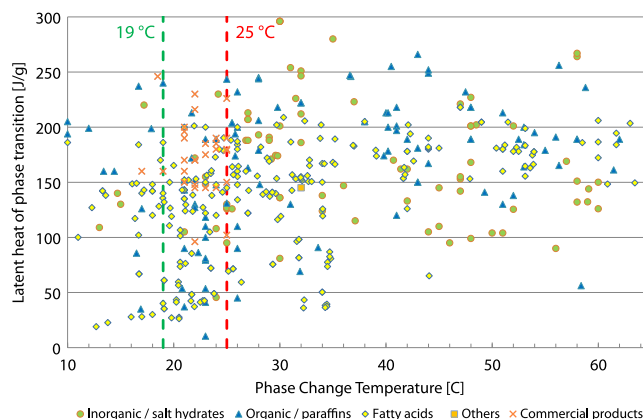


Fig. 11. Compilation of PCM thermal properties found in the literature [70–88] and [89].

cycling instability, require nucleating and thickening agents to minimize sub-cooling and are highly reactive to metal materials. Therefore, the organic PCMs seem to be the most appropriate for low temperature building TES application.

6.2. PCMs containment

For building applications, a PCM should be contained or mechanically stabilized so that the liquid phase cannot flow away. A good integration within passive LHTES system has to prevent direct contact between the product and its environment to avoid deterioration of the PCM by its surrounding and vice versa.

PCMs can be integrated into conventional building materials by direct incorporation or immersion methods. The first method is the simplest and the cheapest. The PCM is directly mixed with construction materials such as gypsum, concrete or plaster during their production. For the immersion method, the porous construction material is immersed into the melted PCM. The porous media absorbs the product by capillarity. However, leakage and incompatibility with building materials may occur in the both cases [66].

PCMs can be encapsulated before incorporation into building elements. The containment should provide strength, flexibility, resistance to corrosion, structural and thermal stability. It should also separate properly the material from its environment but have sufficient surface area for optimum heat transfer [90].

The micro-encapsulation method involves small (less than 1 mm) spherical or rod-shaped PCM particles coated with a thin polymeric film. This film must be compatible with both the PCM and the matrix. This technique improves heat transfer to the surrounding through its large surface-to-volume ratio. It also provides a good cycling stability since phase segregation is restricted to microscopic distances [91]. Even though microencapsulation is a relatively expensive process, micro-encapsulated paraffin is a popular solution such as the commercial product Energain® [92] which contains 60% PCM and presents a latent heat of around 70 J/g [93].

It is also possible to encapsulate PCMs at nano-scale. A study suggested that the nano-capsules are more stable than micro-capsules. Paraffin was successfully encapsulated in 100 nm diameter formaldehyde spheres. With a PCM mass content of 60%, this product showed an appreciable latent heat of 134.61 J/g [94].

Macro-encapsulation is a simple containment method. The PCM placed in bulk storage reservoirs such as tubes, pouches, spheres or panels which are usually larger than 1 cm. The first historical macro-encapsulation systems were too large and suffered from the poor thermal conductivity of most PCMs to insure an efficient energy loading. The product solidifies at the edges of the containers preventing effective heat transfer. The containers can serve directly as heat exchangers to overcome this problem. Aluminium profiles with fins or heat exchanger with finned tubes filled with PCM can thus significantly increase the heat transfer rate and reduce phase segregation [70] and [95].

In recent years, shape-stabilized PCMs were attracting a lot of attention. They have a large apparent heat storage capacity, suitable thermal conductivity, chemical and mechanical long-term stability [95]. Stable form PCMs without any leakage can be obtained by impregnation of porous material matrices. Direct impregnation technic is simple, but the vacuum impregnation method is more effective in loading very fine mesh porous matrix with a maximum amount of product. The latent heat of these compounds increases almost linearly with the PCM fraction mass [96]. For example, a shape-stabilized PCM composed of 80% mass paraffin and 20% styrene-butadiene-styrene can reach 80% of pure paraffin's latent heat [97]. Because of their high surface tension and chemical stability, organic PCMs are the most appropriate for integration in porous matrices [96]. Many researchers tested incorporation, stability and thermal properties of PCMs in various porous materials such as expanded perlite [98], halloysite

nanotubes [99], montmorillonite [100], vermiculite [101], expanded graphite [102], porous silica matrix [103], expanded clay aggregate [104] and diatomite [105].

6.3. PCMs thermal transfer enhancement

PCMs are employed to accumulate energy within short periods. Fast loading and unloading capability is therefore a problem for LHTES systems because of their low thermal conductivity. Numerous technics for heat transfer enhancement have been tested in order to increase the activation depth of the material layer and consequently improve the energy storage capacity. High conductivity structures in bulk PCM reservoir such as copper, aluminium, nickel, stainless steel and carbon in various forms of fins, plates, honeycomb, wool, foam, fibres or brush have been employed as thermal conductivity promoters. The presence of metal fins in PCM macro-containers significantly hinders natural convection in the liquid phase but strongly enhances the conduction [106]. The integration of PCMs in highly conductive porous matrices or the dispersion of high conductivity particles (expanded graphite, fibrous materials, macro, micro or nano capsules) has been widely studied as containment and heat transfer enhancement [107]. Direct exposition to solar radiation, high radiation absorptivity of the finishing surface and augmented convective heat transfer can highly improve LHTES capacity as well [110] and [111]. The performances of some thermal conductivity enhancement technics are presented in Table 3.

6.4. Passive latent heat storage applications in buildings

LHTES has found many practical applications from solar energy storage to space satellite thermal regulation or cooling of the electronics. This discussion focuses on low temperature passive LHTES systems in buildings, loaded and unloaded by the only mean of indoor temperature variations and internal radiation.

Macro-encapsulated PCMs were found inadequate to deliver accumulated heat due to their limited surface of exchange. Therefore, most studies focused on PCM integrated into building elements such as walls, ceilings and floors. They offer a larger surface of exchange with the indoor space and thus a greater storage capacity [107]. Wallboards are cheap, commonly used in building construction and thus appropriate for the integration of PCMs. Many numerical and experimental studies assessed the performance of these enhanced wallboards [66]. A full-scale experiment with summer conditions showed that 5 mm PCM wallboard is equivalent to 8 cm of concrete with regards to indoor air temperature fluctuations and overheating [112]. Comparative in situ studies in a renovated building equipped with similar PCM wallboards concluded that the heat storage capacity of rooms was doubled [113]. A wallboard with 25% mass butyl stearate could reduce heat load by 15% for a building located in Montreal [114]. The energy savings of a sandwich-type PCM/insulating wallboard integrated in a building under continental climate were evaluated at 12.8% for heating and 1% for cooling. Cooling and heating peak loads were reduced by 35.4% [115]. Another experiment demonstrated that PCM insulation wall can decrease daily heat transfer across the envelope by 38% and diminish peak heat flux by up to 62% under summer conditions [116].

Researchers tried to incorporate PCM into concrete for effective heat capacity augmentation. The latest analyses concluded that concrete LHTES was not a suitable solution because the maximum amount of mixed PCM cannot be higher than 5–6% by weight. The thermal inertia improvement due to the PCM itself is thus very little. In addition, it significantly deteriorates the thermal conductivity of the concrete and consequently the overall activated thermal mass [107].

The translucent properties of some PCMs can be employed to manufacture translucent bulk containment panel in windows [107]. The product is in direct sun exposure and can be fully activated. The PCM filters out the solar radiation and reduces the amount of heat gains until it is completely melted. The system can provide homo-

Table 3
Performance of different thermal heat transfer enhancement methods.

PCM type	Containment	Thermal enhancement method	Performance	Reference
Deionized water	Macro-container	Addition of copper tubes and graphite matrices	Reduce melting time by factor 2.5	[106]
Pure eicosane and commercial wax	Macro-container	Addition of aluminium honeycombs and thin-strip matrices	Reduce solidification time by factor 7	[106]
Paraffin	Macro-container	Addition of 20% volume of lessing rings	Reduce solidification time by factor 9	[106]
Paraffin RT58	Stable form PCM	Integration in copper foam matrix	Increase heat transfer by factor 10	[107]
Eicosane	Stable form PCM	Integration in 95% porosity copper foam matrix	Thermal conductivity from 0.423 to 3.06 W/m K	[102]
Eicosane	Stable form PCM	Integration in 97% porosity nickel foam matrix	Thermal conductivity from 0.423 to 9 W/m K	[102]
Paraffin	Stable form PCM	Integration in compressed expanded graphite matrix	Thermal conductivity from 0.24 to 4 or up to 70 W/m K	[108]
Paraffin	Macro-container	Addition of 0.5% mass of 80 μ m aluminium particles	Reduce melting time by 60%	[107]
Fatty acid	Stable form PCM	Addition of 2% mass EG in expanded perlite matrix	Thermal conductivity from 0.25 to 0.5 W/m K	[73]
Fatty acid	Stable form PCM	Addition of 7% mass EG in expanded perlite matrix	Thermal conductivity from 0.25 to 2.51 W/m K	[73]
Paraffin	Stable form PCM	Addition of 10% mass exfoliated graphite nano-platelet	Increase heat transfer by factor 10	[109]

geneous illumination with light transmittances in the range of 0.4 and reduce heat losses by 30%. These PCM panels can be good supplements to conventional windows where there is no need for visual contact to the environment [117]. Internal shutters and solar shadings can also contain PCM and be integrated in window facades. The systems should operate cyclically to enable sun energy storage during the day and release towards the indoor space at night. Tests showed that rooms equipped with PCM interior sun protections had air temperature 1–2 °C lower than rooms with conventional blinds [118]. Numerical results indicated that 23% reduction of heat gain through a window can be reached with 3 cm thick PCM shutter with regards to the same shutter made of foam and aluminium [119]. Finally, the introduction of PCMs in Trombe walls could contribute to the development of light and portable systems adapted to the lightweight buildings [66].

7. Integration of phase change materials into furniture

As discussed previously, PCM systems located in the inner surfaces of the indoor space, such as wallboards, offer the best thermal mass enhancement. However, their use is limited to the internal surface area of rooms. Furniture parts are often neglected in energy building investigations, but they also possess a large surface of exchange with the indoor environment. The furnishing can be an interesting location for LHTES which could therefore be installed without the need for extra space or construction works. This section is reviewing the few projects involving furniture and PCMs. A simple calculation is then presented to give an idea of the potential for PCM furniture in terms of TES. Finally, the section will discuss modelling and optimization of LHTES systems.

7.1. PCMs furniture systems

Passive cooling by direct contact with human body such as cooling seats or cooling blankets are the most common products available on the market. “Smart textile” with integrated PCM is also commercialized. However, these solutions are not TES systems and only have a limited effect on occupants’ thermal comfort.

Many papers focus on the study or the review of the different PCM applications, but no specific publication was found on the integration of PCM in furniture. Very few articles mention the PCM furnishing option and if they do, they do not provide any concrete examples [120].

Only one publication presented the first PCM active application located in furniture. It consists of an air heat exchanger (electric fan)

with macro-encapsulated PCM. The system is placed underneath box-type furniture for living rooms or bedrooms. The concept was proposed for the American Solar Decathlon in 2007, but no further documentation or characteristics could be found [121].

The company EPS Ltd has elaborated the “PlusICE furniture” for office passive cooling. This product is actually not available, and the company only provides bulk containment or stable form PCM to be placed under the furnishing parts [122].

One architecture group suggested the use of paraffin in an aluminium frame to mount various office furniture pieces for the 2012 “adream” competition. A simple performance assessment in office buildings concluded that the cooling and heating energy needs can be decreased by up to 40% and 34%, respectively [123].

A similar solution was presented in the French press by the engineering company Egis in 2015. The PCM is encapsulated and located below a wooden office table. The bottom face of the furniture is covered with an aluminium corrugated sheet in order to increase the heat exchange rate. According to the designers, this PCM table can reduce cooling and heating needs by up to 30% and 60%, respectively [124].

7.2. Potential for furniture PCMs integration

The simple survey on Danish building indoor content provided an estimation of the available furniture, wall, floor and ceiling surface area in direct contact with the air. One can see on Fig. 12 that the furniture surface, which is available for PCM integration can represent up to 50% of the room’s inner surface.

An optimization study on a wallboard containing 60% of micro-encapsulated paraffin showed that the optimum daily activated PCM thickness is 1 cm [125]. This value is used to get a simple estimation of the daily effective thermal capacity of internal wall and furniture covered by a layer of PCM. The latent heat of the product is chosen to be 180 MJ/m³. It is assumed that the 1 cm of PCM is fully activated within a 24-h cycle, which is equivalent to 1.8 MJ/m². The sensible heat of the other building elements is calculated with the daily effective heat capacity of each element and a temperature variation of 4 °C.

As seen on Fig. 13, the furnishing elements covered with PCM can significantly improve the daily thermal capacity of a room.

7.3. Modelling and optimization of LHTES systems

PCM mathematical models are needed for the study and optimum

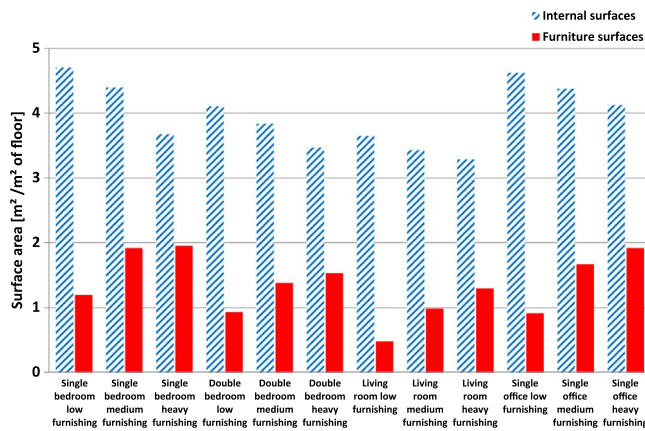


Fig. 12. Surface area available in buildings for integration of phase change materials.

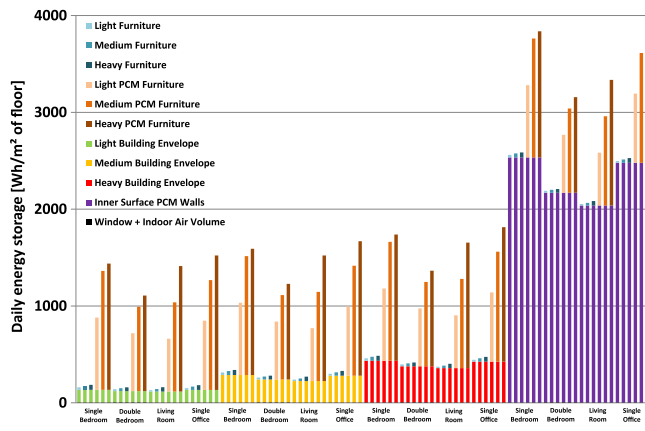


Fig. 13. Daily thermal storage capacity of building elements.

design of LHTES systems. In their review paper, Soares et al. [66] discussed the different modelling technics. It is stated that solving a phase change problem numerically is difficult because of the moving boundary on which heat and mass transfer have to be solved. The two phases of the PCM have different thermo-physical properties. Because of this non-linear behaviour, the position of the moving interface cannot be determined a priori. This solid–liquid interface boundary system is named “Stefan problem”.

The authors report that most of the current numerical models are based on the first or the second law of thermodynamics and use fixed or adaptive meshing. The first law models do not consider the effect of time duration for heat storage and release nor the temperature at which the heat is supplied. The second law models take these parameters into account. The time variant meshing method offers good accuracy, but it is limited to simple problems and geometries. On the other hand, the fixed mesh approach is much simpler to use for multidimensional problems.

LHTES equations are usually solved with finite difference, finite control volume or finite element methods. The phase transition can be modelled by introducing an equivalent specific heat of the PCM in function of temperature. The material's latent heat of fusion is transformed into a peak on the sensible specific heat capacity curve over the whole phase transition temperature interval. The system is simplified into a non-linear single phase conduction problem. The latent heat of fusion can also be described with an enthalpy formulation. The enthalpy of the system becomes the state variable which has to comply with the energy conservation equation. The temperature is then calculated from the enthalpy and the thermal properties of the PCM.

The performance of passive LHTES systems is highly affected by the indoor environmental conditions such as internal heat loads, ventila-

tion rate, convection heat transfer coefficient, solar radiation and ambient temperature. The type of PCM, its melting temperature, layer thickness, location and orientation should be determined within an optimization process to increase the storage/release capacity using as little material as possible [125]. Charging and discharging time should also be taken into account. The effective energy storage capacity is proportional to the PCM volume, which has melted and solidified during a complete TES cycle. If the material amount is overestimated, the time needed for the heat to penetrate the PCM layer could become larger than the charging period, and the melting process cannot be completed [126]. Similarly, the design of passive LHTES furniture systems should be performed according to a specific TES strategy and account for the difference in radiative and convective conditions on the each side of the elements.

8. Conclusion

This article intended to attract readers' attention on what many consider a negligible detail in the field of energy and buildings. Most of the building models assume empty rooms without furniture or indoor content, but very few people have tried to understand if such simplification is reasonable or not. Some publications emphasised the strong interaction of the furniture/indoor thermal mass with the internal air node and HVAC systems. It can have a significant impact on the local indoor humidity and thermal comfort. Because of its large surface for heat exchange, the internal content is highly activated and can account for up to 40% of the total hourly effective heat capacity of a room, and increase its time constant by several hours. Although it does not play a major role in the energy consumption of buildings with a static controller, several studies showed that indoor mass cannot be ignored when using set point modulation for passive TES or night time cooling.

There is a clear lack of guidance in publications for the assessment of the indoor thermal mass characteristics. This paper suggested a simple classification of these elements with representative thermal properties. In addition, the results of a survey on Danish buildings were presented to give some insight into reasonable variation for the mass and heat capacity of furnishing and items in a room.

Different furniture modelling technics were described in scientific articles and software documentation. Most of them introduce an additional lumped capacitance in a RC network while some use an equivalent fictitious planar or spherical element. Only one model was found with a geometric description of an equivalent slab for proper solar radiation distribution and long-wave radiation heat exchange. Very little methodology was found concerning the way to aggregate internal content with various sizes and thermal properties into equivalent simplified elements.

Furnishing elements offer a large surface area exposed to the indoor environment, which makes them a good candidate for PCM integration. It can be an interesting solution for the implementation of passive LHTES systems without construction work and thereby improving thermal inertia and energy flexibility of light buildings.

Further investigations are needed to assess the complex effects of furniture/indoor thermal mass on building systems. A large survey on occupied buildings would give statistical insight into rooms' content. Full-scale experiments should be performed to measure the impact of internal mass on building's time constant, HVAC systems efficiency, and passive TES potential. Realistic models and aggregation methodologies have to be developed for indoor mass elements. Finally, the integration of PCM in furniture raises new issues concerning their compliance with fire regulation, recycling process and total life cycle analysis.

Acknowledgements

This work was financed by the ENOVHEAT project, which is funded

by Innovation Fund Denmark (contract no 12-132673).

References

- [1] The European Parliament and the Council of the European Union . Directive 2010/31/EU on the energy performance of buildings. Off J Eur Union 2010;19.
- [2] Building Performance Institute Europe (BPIE) . Europe's buildings under the microscope. Exec Summ 2011.
- [3] Beurskens WM, Hekkenberg M, Vethman P. Renewable energy projections as published in the national energy action plans of the European member states. Report no. ECN-E-10-069. ECN and European Environment Agency; 2011.
- [4] The Danish Government. Energy Strategy 2050 – from coal, oil and gas to green energy; February 2011
- [5] Danskeenergi, energinet.dk. Smart Grid in Denmark; February 2011.
- [6] Mathiesen BV, Lund H, Connolly D, Wenzel H, Østergaard PA, Möller B, et al. Smart energy systems for coherent 100% renewable energy and transport solutions. *Appl Energy* 2015;145:139–54.
- [7] Lund H, Möller B, Mathiesen BV, Dyrrelund A. The role of district heating in future renewable energy systems. *Energy* 2010;35(3):1381–90.
- [8] Wolisz H, Kull T.M, Streblov R, Müller D. The effect of furniture and floor covering upon dynamic thermal building simulations. 6th International Building Physics Conference, IBPC; 2015.
- [9] Hedegaard K, Mathiesen BV, Lund H, Heiselberg P. Wind power integration using individual heat pumps – analysis of different heat storage options. *Energy* 2012;47:284–93.
- [10] tsbi5 – Bsim User's Guide.
- [11] French Building Energy and Thermal Regulation 2005, CSTB FR.
- [12] Plaisance H, Blondel A, Desauziers V, Mocho P. Hierarchical cluster analysis of carbonyl compounds emission profiles from building and furniture materials. *Build Environ* 2014;75:40–5.
- [13] Athlaye RA, Xie Y, Liu B, Rosenberg MI. Analysis of daylighting requirements within ASHRAE standard 90.1. US Dep Energy 2013.
- [14] Mortensen LH, Rode C, Peuhkuri R. Investigation of airflow patterns in a microclimate by particle image velocimetry (PIV). *Build Environ* 2008;43:1929–38.
- [15] Yang X, Fazio P, Ge H, Rao J. Evaluation of moisture buffering capacity of interior surface materials and furniture in a full-scale experimental investigation. *Build Environ* 2012;47:188–96.
- [16] Horikiri K, Yao Y, Yao J. Numerical optimisation of thermal comfort improvement for indoor environment with occupants and furniture. *Energy Build* 2015;88:303–15.
- [17] Bojic M, Yik F, Lo TY. Locating air-conditioners and furniture inside residential flats to obtain good thermal comfort. *Energy Build* 2002;34:745–51.
- [18] REHVA. Low temperature heating and high temperature cooling guidebook No 7; 2009.
- [19] Zhao K, Lui XH, Jiang Y. Application of radiant floor cooling in a large open space building with high-intensity solar radiation. *Energy Build* 2013;66:246–57.
- [20] Corcione M, Fontana L, Moncada Lo Giudice G. A parametric analysis on the effects of furnishings upon the performance of radiant floor-panel heating systems. Proceedings of the Clima 2000 international congress, Naples; 2001. p. 59–68.
- [21] Fontana L. Thermal performance of radiant heating floors in furnished enclosed spaces. *Appl Therm Eng* 2011;31:1547–55.
- [22] Pomianowski MZ, Khalegi F, Domarks G, Taminskas J, Bandurski K, Madsen KK, et al. Experimental investigation of the influence of obstacle in the room on passive night-time cooling using displacement ventilation. In: Vinha J, Piironen J, Salminen K, (Eds.), Proceedings of the 9th nordic symposium on building physics: NSB 2011. (Vol. 1, p. 499–506. Tampere, Finland: Tampere, University Press.
- [23] Le Dréau J. Energy flow and thermal comfort in buildings – comparison of radiant and air-based heating and cooling systems[Ph.D. thesis]. Denmark: Aalborg University; 2014.
- [24] Antonopoulos KA, Koronaki EP. Thermal parameter components of building envelope. *Appl Therm Eng* 2000;20:1193–211.
- [25] Balaras CA. The role of thermal mass on the cooling load of buildings. *Overv Comput Methods Energy Build* 1996;24:1–10.
- [26] Al-Sanea SA, Zedan MF, Al-Hussain SN. Effect of thermal mass on performance of insulated building walls and the concept of energy savings potential. *Appl Energy* 2012;89:430–42.
- [27] Yang L, Li Y. Cooling load reduction by using thermal mass and night ventilation. *Energy Build* 2008;40:2052–8.
- [28] Artmann N, Manz H, Heiselberg P. Parameter study on performance of building cooling by night-time ventilation. *Renew Energy* 2008;33:2589–95.
- [29] Antonopoulos KA, Koronaki EP. Envelope and indoor thermal capacitance of buildings. *Appl Therm Eng* 1999;19:743–56.
- [30] Antonopoulos KA, Koronaki EP. Effect of indoor mass on the time constant and thermal delay of buildings. *Int J Energy Res* 2000;24:391–402.
- [31] Yam J, Li Y, Zheng Z. Nonlinear coupling between thermal mass and natural ventilation in buildings. *Int J Heat Mass Transf* 2003;46:1251–64.
- [32] Zhou J, Zhang G, Lin Y, Li Y. Coupling of thermal mass and natural ventilation in buildings. *Energy Build* 2008;40:979–86.
- [33] Felgner F, Agustina S, Cladera Bohigas R, Merz R, Litz L. Simulation of Thermal Building Behaviour in Modelica. In: Proceedings of the 2nd International Modelica Conference; 2002.
- [34] Raftery P, Lee E, Webster T, Hoyt T, Bauman F. Effects of furniture and contents on peak cooling load. *Energy Build* 2014;85:445–57.
- [35] EN ISO 10456:1999 – Building material and products. Procedure for determining design value.
- [36] EN ISO 12524:2000 – Building materials and products.
- [37] Catalogue of material properties. Report Annex 14. Volume 3. IEA.
- [38] Stanković SB, Popović D, Poparić GB. Thermal properties of textile fabrics made of natural and regenerated cellulose fibers. *Polym Test* 2008;27:41–8.
- [39] Shabaridharan, Das A. Study on heat and moisture vapour transmission characteristics through multilayered fabric ensembles. *Fibers and Polymers* 13. p. 522–8.
- [40] Selvakumar B, Prabhu Raja V, Senthil Kumar AP, Karthikeyan P. Investigation on effective thermal conductivity of foams using transient plane heat source method. *Int J Res Eng Technol* 2014;3:249–51.
- [41] Jarfelt U, Ramnäs O. Thermal conductivity of polyurethane foam – best performance. In: Proceedings of the 10th international symposium on district heating and cooling; September 3-5, 2006
- [42] Abdel-Rehim ZS, Saad MM, El-Shakankery M, Hanafy I. Textile fabrics as thermal insulators. *AUTEX Res J* 2006:6.
- [43] Kiran MC, Nandanwar A, Venugopal Naidu M, Varada Rajulu KC. Effect of density on thermal conductivity of bamboo mat board. *Int J Agric For* 2012;2:57–61.
- [44] Ganjian Esmail. The relationship between porosity and thermal conductivity of concrete [Ph.D thesis]. University of Leeds; 1990.
- [45] Garcia Ten J, Orts MJ, Saburit A, Silva G. Thermal conductivity of traditional ceramics. Part I: influence of bulk density and firing temperature. *Ceram Int* 2010;36:1951–9.
- [46] Sugawara A, Yoshizawa Y. An investigation on the thermal conductivity of porous materials and its application to porous rock. CSIRO; 1961.
- [47] Hongmei Gu. Structure based, two-dimensional, anisotropic, transient heat conduction model for wood. [Ph.D. thesis], Faculty of the Virginia Polytechnic Institute; August 2001.
- [48] Kaiser G. Thermal Conductivity of Insulating Materials by Means of HFM Measurements. NETZSCH-Gerätebau GmbH.
- [49] ISO 13786:2007, Thermal performance of building components – dynamic thermal characteristics – calculation methods
- [50] Wang S, Xu X. Parameter estimation of internal thermal mass of building dynamic models using genetic algorithm. *Energy Convers Manag* 2006;47:1927–41.
- [51] Berthou T, Stabat P, Salvazet R, Marchio D. Development and validation of a gray box model to predict thermal behavior of occupied office buildings. *Energy Build* 2014;74:91–100.
- [52] Bacher P, Madsen H. Identifying suitable models for the heat dynamics of buildings. *Energy Build* 2011;43:1511–22.
- [53] ISO 13790:2008 Energy performance of buildings – calculation of energy use for space heating and cooling
- [54] TRNSYS 17 Technical Documentation Vol. 5, Multizone Building modeling with Type56 and TRNBuild.
- [55] Carlson SW. Modeling of heat transfer in buildings using comprehensive room transfer function [Master thesis]. USA: University of Wisconsin-Madison; 1988.
- [56] Ma P, Wang LS. Effective heat capacity of interior planar thermal mass (IPTM) subject to periodic heating and cooling. *Energy Build* 2012;47:44–52.
- [57] Zhou J, Zhang G, Lin Y, Wang H. A new virtual sphere method for estimating the role of thermal mass in natural ventilated buildings. *Energy Build* 2011;43:75–81.
- [58] Gao M, Reid CN, Jahedi M, Li Y. Estimating equilibration times and heating/cooling rates in heat treatment of workpieces with arbitrary geometry. *J Mater Eng Perform* 2000;9:62–71.
- [59] Energy Plus Engineering Reference Manual.
- [60] User Manual. IDA Indoor Climate and Energy, Version 4.5; February 2013
- [61] Getting Started. IDA Indoor Climate and Energy, Version 4.5; February 2013
- [62] ISO 15265 . Energy performance of buildings. calculation of energy needs for space heating and cooling using dynamic methods. Gen Criteria Valid Proceed 2007.
- [63] Vorre MH, Jensen RL, Le Dréau J. Radiation exchange between persons and surfaces for building energy simulations. *Energy Build* 2015;101:110–21.
- [64] ISO 6946:2007 Building components and building elements – thermal resistance and thermal transmittance – calculation method.
- [65] Peeters L, Beausoleil-Morrison I, Novoselac A. Internal convective heat transfer modeling: critical review and discussion of experimentally derived correlations. *Energy Build* 2011;43:2227–39.
- [66] Soares N, Costa JJ, Gaspar AR, Santos P. Review of passive PCM latent heat thermal energy storage systems towards buildings' energy efficiency. *Energy Build* 2013;59:82–103.
- [67] Sharma A, Tyagi VV, Chen CR, Buddhi D. Review on thermal energy storage with phase change materials and applications. *Renew Sustain Energy Rev* 2009;13:318–45.
- [68] Zalba B, Marin JM, Cabeza LF, Mehling H. Review on thermal energy storage with phase change: materials, heat transfer analysis and applications. *Appl Therm Eng* 2003;23:251–83.
- [69] Rathod MK, Banerjee J. Thermal stability of phase change materials used in latent heat energy storage systems: a review. *Renew Sustain Energy Rev* 2013;18:246–58.
- [70] Cabeza LF, Castell A, Barreneche C, de Garcia A, Fernández AI. Materials used as PCM in thermal energy storage in buildings: a review. *Renew Sustain Rev* 2011;15:1675–95.
- [71] Sharma RK, Ganesan P, Tyagi VV, Metselaar HSC, Sandaran SC. Developments in organic solid-liquid phase change materials and their applications in thermal energy storage. *Energy Convers Manag* 2015;95:193–228.
- [72] Yuan Y, Zhang N, Tao W, Cao X, He Y. Fatty acids as phase change materials: a review. *Renew Sustain Energy Rev* 2014;29:482–98.

- [73] Liu C, Yuan Y, Zhang N, Cao X, Yang X. A novel PCM of lauric–myristic–stearic acid/expanded graphite composite for thermal energy storage. *Mater Lett* 2014;120:43–6.
- [74] Sari A, Karaipekli A. Preparation, thermal properties and thermal reliability of palmitic acid/expanded graphite composite as form-stable PCM for thermal energy storage. *Sol Energy Mater Sol Cells* 2009;93:571–6.
- [75] Chen Z, Shan F, Cao L, Fang G. Synthesis and thermal properties of shape-stabilized lauric acid/activated carbon composites as phase change materials for thermal energy storage. *Sol Energy Mater Sol Cells* 2012;102:131–6.
- [76] Fang G, Li H, Chen Z, Liu X. Preparation and characterization of stearic acid/expanded graphite composites as thermal energy storage materials. *Energy* 2010;35:4622–6.
- [77] Yang X, Yuan Y, Zhang N, Cao X, Liu C. Preparation and properties of myristic–palmitic–stearic acid/expanded graphite composites as phase change materials for energy storage. *Sol Energy* 2014;99:259–66.
- [78] Pan L, Tao Q, Zhang S, Wang S, Zhang J, Wang S, et al. Preparation, characterization and thermal properties of micro-encapsulated phase change materials. *Sol Energy Mater Sol Cells* 2012;98:66–70.
- [79] Shilei L, Neng Z, Guohui F. Eutectic mixtures of capric acid and lauric acid applied in building wallboards for heat energy storage. *Energy Build* 2006;38:708–11.
- [80] Zhang N, Yuan Y, Yuan Y, Cao X, Yang X. Effect of carbon nanotubes on the thermal behavior of palmitic–stearic acid eutectic mixtures as phase change materials for energy storage. *Sol Energy* 2014;110:64–70.
- [81] Karaipekli A, Sari A. Preparation, thermal properties and thermal reliability of eutectic mixtures of fatty acids/expanded vermiculite as novel form-stable composites for energy storage. *J Ind Eng Chem* 2010;16:767–73.
- [82] Sari A, Biçer A. Preparation and thermal energy storage properties of building material-based composites as novel form-stable PCMs. *Energy Build* 2012;51:73–83.
- [83] Feldman D, Banu D, Hawes D. Low chain esters of stearic acid as phase change materials for thermal energy storage in buildings. *Sol Energy Mater Sol Cells* 1995;36:311–22.
- [84] Xu S, Zou L, Ling X, Wei Y, Zhang S. Preparation and thermal reliability of methyl palmitate/methyl stearate mixture as a novel composite phase change material. *Energy Build* 2014;68:372–5.
- [85] Jeong SG, Jeon J, Cha J, Kim J, Kim S. Preparation and evaluation of thermal enhanced silica fume by incorporating organic PCM, for application to concrete. *Energy Build* 2013;62:190–5.
- [86] Wang W, Yang X, Fang Y, Ding J, Yan J. Preparation and thermal properties of polyethylene glycol/expanded graphite blends for energy storage. *Appl Energy* 2009;86:1479–83.
- [87] Kim S, Drzal LT. High latent heat storage and high thermal conductive phase change materials using exfoliated graphite nanoplatelets. *Sol Energy Mater Sol Cells* 2009;93:136–42.
- [88] Sun D, Wang L, Li C. Preparation and thermal properties of paraffin/expanded perlite composite as form-stable phase change material. *Mater Lett* 2013;108:247–9.
- [89] Rastogi M, Chauhan A, Vaish R, Kishan A. Selection and performance assessment of phase change materials for heating, ventilation and air-conditioning applications. *Energy Convers Manag* 2015;89:260–9.
- [90] Regin AF, Solanki SC, Saini JS. Heat transfer characteristics of thermal energy storage system using PCM capsules: a review. *Renew Sustain Energy Rev* 2008;12:2438–58.
- [91] Khudhair AM, Farid MM. A review on energy conservation in building applications with thermal storage by latent heat using phase change materials. *Energy Conserv Manag* 2004;45:263–75.
- [92] Navarro L, de Garcia A, Niall D, Castell A, Browne M, McCormack SJ, et al. Thermal energy storage in building integrated thermal systems: a review. Part 2. Integration as passive system. *Renewable Energy*. In Press, Corrected Proof; 2015.
- [93] DuPont Energain®, Technical Datasheet.
- [94] Sukhorukov G, Fery A, Möhwalld H. Intelligent micro- and nanocapsules. *Prog Polym Sci* 2005;30:885–97.
- [95] Zhou D, Zhao CY, Tian Y. Review on thermal energy storage with phase change materials (PCMs) in building applications. *Appl Energy* 2012;92:593–605.
- [96] Zhang D, Zhou J, Wu K, Li Z. Granular phase changing composites for thermal energy storage. *Sol Energy* 2005;78:471–80.
- [97] Xiao M, Feng B, Gong K. Thermal performance of a high conductive shape-stabilized thermal storage material. *Sol Energy Mater Sol Cells* 2001;69:293–6.
- [98] Lu Z, Xu B, Zhang J, Zhu Y, Sun G, Li Z. Preparation and characterization of expanded perlite/paraffin composite as form-stable phase change material. *Sol Energy* 2014;108:460–6.
- [99] Mei D, Zhang B, Liu R, Zhang Y, Liu J. Preparation of capric acid/halloysite nanotube composite as form-stable phase change material for thermal energy storage. *Sol Energy Mater Sol Cells* 2011;95:2772–7.
- [100] Cai Y, Song L, He Q, Yang D, Hu Y. Preparation, thermal and flammability properties of a novel form-stable phase change materials based on high density polyethylene/poly(ethylene-co-vinyl acetate)/organophilic montmorillonite nanocomposites/paraffin compounds. *Energy Convers Manag* 2008;49:2055–62.
- [101] Chung O, Jeong SG, Kim S. Preparation of energy efficient paraffinic PCMs/expanded vermiculite and perlite composites for energy saving in buildings. *Sol Energy Mater Sol Cells* 2015;137:107–12.
- [102] Luo JF, Yin HW, Li WY, Xu ZJ, Shao ZZ, Xu XJ, et al. Numerical and experimental study on the heat transfer properties of the composite paraffin/expanded graphite phase change material. *Int J Heat Mass Transf* 2015;84:237–44.
- [103] Wu Y, Wang T. Preparation and characterization of hydrated salts/silica composite as shape-stabilized phase change material via sol–gel process. *Thermochim Acta* 2014;591:10–5.
- [104] Nepomuceno MCS, Silva PD. Experimental evaluation of cement mortars with phase change material incorporated via lightweight expanded clay aggregate. *Constr Build Mater* 2014;63:89–96.
- [105] Xu B, Li Z. Paraffin/diatomite composite phase change material incorporated cement-based composite for thermal energy storage. *Appl Energy* 2015;105:229–37.
- [106] Fan L, Khodadadi JM. Thermal conductivity enhancement of phase change materials for thermal energy storage: a review. *Renew Sustain Energy Rev* 2011;15:24–46.
- [107] Pomianowski M, Heiselberg P, Zhang Y. Review of thermal energy storage technologies based on PCM application in buildings. *Energy Build* 2013;67:56–69.
- [108] Py X, Olives R, Mauran S. Paraffin/porous-graphite-matrix composite as a high and constant power thermal storage material. *Int J Heat Mass Transf* 2001;44:2727–37.
- [109] Shi JN, Ger MD, Liu YM, Fan YC, Wen NT, Lin CK, et al. Improving the thermal conductivity and shape-stabilization of phase change materials using nanographite additives. *Carbon* 2013;51:365–72.
- [110] Susman G, Dehouche Z, Cheechern T, Craig S. Tests of prototype PCM ‘sails’ for office cooling. *Appl Therm Eng* 2011;31:717–26.
- [111] David D, Kuznik F, Roux JJ. Numerical study of the influence of the convective heat transfer on the dynamical behavior of a phase change material wall. *Appl Therm Eng* 2011;31:3117–24.
- [112] Kuznik F, Virgone J, Roux JJ. Energetic efficiency of room wall containing PCM wallboard: a full-scale experimental investigation. *Energy Build* 2008;40:148–56.
- [113] Kuznik F, Virgone J, Johannes K. In-situ study of thermal comfort enhancement in a renovated building equipped with phase change material wallboard. *Renew Energy* 2011;36:1458–62.
- [114] Athienitis AK, Liu C, Hawes D, Banu D, Feldman D. Investigation of the thermal performance of a passive solar test-room with wall latent heat storage. *Build Environ* 1997;5:405–10.
- [115] Diaconu BM, Cruceru M. Novel concept of composite phase change material wall system for year-round thermal energy savings. *Energy Build* 2010;42:1759–72.
- [116] Medina MA, King JB, Zhang M. On the heat transfer rate reduction of structural insulated panels (SIPs) outfitted with phase change materials (PCMs). *Energy* 2008;33:667–78.
- [117] Weindlader H, Beck A, Fricke J. PCM-facade-panel for daylighting and room heating. *Sol Energy* 2005;78:177–86.
- [118] Weindlader H, Koerner W, Heidenfelder M. Monitoring results of an interior sun protection system with integrated latent heat storage. *Energy Build* 2011;43:2468–75.
- [119] Alawadhi EM. Using phase change material in window shutter to reduce the solar heat gain. *Energy Build* 2012;47:421–9.
- [120] Kalnaes SE, Jelle BP. Phase change materials and products for building applications: a state-of-the-art review and future research opportunities. *Energy Build* 2015;94:150–76.
- [121] Rodriguez-Ubinas E, Ruiz-Valero L, Vega S, Neila J. Applications of phase change material in highly energy-efficient houses. *Energy Build* 2012;50:49–62.
- [122] PlusIce, Passive Cooling Furniture, Brochure, EPS Ltd.
- [123] Xx-PCM, thermoregulating panel for office furniture, Au frais de mon arbre project, Brochure, Seed-collectif. Jean-Luc Alfonsi, Nicolas Duthu, Juan Gavilan, Antonio Albanés Saénz De Tejada.
- [124] Sapporo J. Abaisser les factures énergétiques en changeant de mobilier (in French). LE MONITEUR.FR; 2015. (<http://www.lemoniteur.fr/article/abaisser-les-factures-energetiques-en-changeant-de-mobilier-28816549>) [accessed 17.09.15].
- [125] Kuznik F, Virgone J, Noel J. Optimization of a phase change material wallboard for building use. *Appl Therm Eng* 2008;28:1291–8.
- [126] Rostamizadeh M, Khanlarkhani M, Mojtaba Sadrameli S. Simulation of energy storage system with phase change material (PCM). *Energy Build* 2012;49:419–22.

Appendix B. Paper II

Johra, H., Heiselberg, P., & Le Dréau, J. (2017). Numerical analysis of the impact of thermal inertia from the furniture / indoor content and phase change materials on the building energy flexibility. In: *Proceedings of the 15th IBPSA Conference, International Building Performance Simulation Association, San Francisco, CA, USA. Aug. 7-9, 2017.*

<https://doi.org/10.26868/25222708.2017.012>

Reprinted by permission from IBPSA-USA

Numerical Analysis of the Impact of Thermal Inertia from the Furniture / Indoor Content and Phase Change Materials on the Building Energy Flexibility

Hicham Johra¹, Per Kvols Heiselberg¹, Jérôme Le Dréau²

¹Department of Civil Engineering, Aalborg University, Aalborg, Denmark

²LaSIE UMR CNRS 7356, La Rochelle University, La Rochelle, France

Abstract

Many numerical models for building energy simulation assume empty rooms and do not account for the indoor content of occupied buildings. Furnishing elements and indoor items have complicated shapes and are made of various materials. Therefore, most of the people prefer to ignore them. However, this simplification can be problematic for accurate calculation of the transient indoor temperature. This article firstly reviews different solutions to include the indoor content in building models and suggests typical values for its characteristics. Secondly, the paper presents the results of a numerical study investigating the influence of the different types of thermal inertia on buildings energy flexibility. Although the insulation level and thermal mass of a building envelope are the dominant parameters, it appears that indoor content cannot be neglected for lightweight structure building simulations. Finally, it is shown that the integration of phase change materials in wallboards or furniture elements can appreciably improve the energy flexibility of buildings.

Introduction

A significant deployment of renewable energy sources (RES) is foreseen in numerous European countries. The increasing share of intermittent RES may decouple instantaneous energy use and production, affecting the stability of the grids (Beurskens et al. 2011). In order to face this problem, recent projects are developing energy flexible technologies and demand-side management strategies to facilitate the operation of a smart grid system with high intermittent power penetration, (Mathiesen et al. 2015).

Buildings can bear flexible energy use to a certain extent. Moreover, the building sector is the largest energy end-user in many countries and can therefore play an important role in the management of the energy grid. Passive thermal energy storage (TES) in the indoor space was found to be a promising solution for building energy flexibility and more cost effective than heat accumulation water tanks (Hedegaard et al. 2012). Le Dréau and Heiselberg (2016) evaluated the potential of residential buildings for set point modulation in order to shift the energy use from high price to low price periods. It was shown that power modulation could be achieved without compromising the indoor thermal comfort: from

a couple of hours for poorly insulated houses and up to 24 hours for well-insulated buildings.

This strategy relies on an accurate control of the transient building temperature. However, many of the current numerical models for building energy systems assume empty rooms and do not account for the internal content thermal inertia of objects like furniture. Such simplification is sufficient for energy calculations with constant set point but could be problematic for light buildings with dynamic set point modulation.

Some researchers emphasized the role of furniture in the indoor thermodynamics. Antonopoulos and Koronaki (2000) evaluated that furniture represented 7.4% of the total effective thermal capacitance of a typical Greek house, and can increase the building time constant and thermal delay by up to 15%. Wolisz et al. (2015) carried out a numerical analysis on the impact of modelling furniture and floor covering for building simulations with temperature set point modulation. The study showed that a fully equipped room can present a temperature increase time delay of more than 7 hours compared to an empty room. In the case of periodic set point control, the furnishing and floor covers can change the cool-down time by up to 2 hours.

In a first part, this article reviews different suggestions for the modelling of the furniture / indoor content thermal mass in building energy simulations. In a second part, the impact of different thermal inertia elements, and in particular the furniture / indoor content, is evaluated regarding short-term indoor heat storage for building energy flexibility.

Quantification and characterisation of the indoor content thermal mass

The amount of items in the indoor space can vary considerably in each room and building. No study or clear guidance concerning typical values for the furnishing / indoor content parameters in buildings could be found. It is therefore complicated to tackle the problem of indoor thermal mass modelling without having an idea of what are its physical properties. In order to address this issue, a simple survey has been performed on residential and single office buildings in Denmark (Johra and Heiselberg 2017). The quantification and characterisation of the building indoor content is a tedious task and only a study with a large sampling could pretend to provide statistically

representative data. This is not the aim of this survey as it only proposes reasonable boundaries for the furniture / indoor content parameters based on systematic measurements of mass and dimensions of each piece of internal elements in 6 different bedrooms, 3 living rooms and 3 single office rooms.

One can see on Figure 1 that a reasonable range for the internal mass density in office and residential buildings would be 10–100 kg/m² of the net floor surface area (Johra and Heiselberg 2017). The few publications providing a value for internal content mass tend to over-estimate it compared to the results of the current survey (Raftery et al. 2014; Antonopoulos and Koronaki 2000).

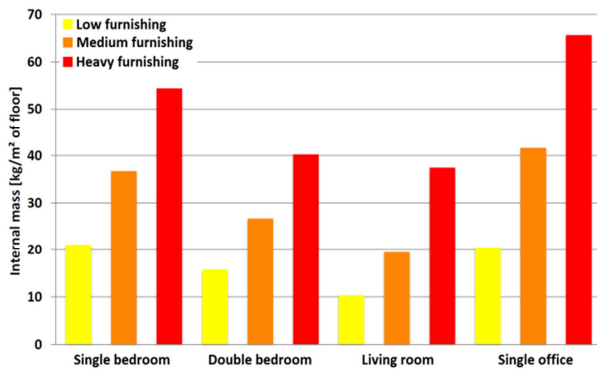


Figure 1: Internal mass of the building survey.

In addition, it has been found that most of the indoor content elements have a planar shape and can be classified into 4 distinct representative material categories.

Based on the results of the survey, suggestions for the thermo-physical properties of these 4 representative categories and an equivalent fictitious indoor content material are presented in Table 1 (Johra and Heiselberg 2017). They can be used to model the indoor content in

Table 1: Properties of the representative indoor content material categories.

Material category	Room mass content (kg/m ² floor area)	Surface area (m ² /m ² floor area)	Material density (kg/m ³)	Material thermal conductivity (W/m.K)	Material specific heat capacity (J/kg.K)	Planar element thickness (cm)	Daily effective thermal inertia (kJ/K.m ² floor area)
Light material	7 (0.5–14)	0.3 (0.1–0.6)	80 (20–140)	0.03	1400	10 (0.5–24)	3 (0.2–7)
Wood / plastic material	30 (8–80)	1.4 (0.5–2)	800 (400–1200)	0.2 (0.1–0.3)	1400	1.8 (1–5)	26 (9–45)
Concrete / glass material	1 (0.5–2)	0.03 (0.01–0.04)	2000 (1500–2500)	1.25 (0.5–2)	950	1 (0.2–2)	0.1 (0.05–0.2)
Metal material	2 (1–5)	0.02 (0.01–0.03)	8000	60	450	0.2 (0.1–0.3)	0.1 (0.05–0.4)
Equivalent indoor content material	40 (10–100)	1.8 (0.8–2.8)	600 (150–1500)	0.3 (0.1–0.5)	1400	4 (1–10)	30 (10–50)

building energy simulations as thin planar elements. In Table 1, the average value of each parameter is followed by its minimum and maximum limits in parentheses.

From these measurements and material assumptions, the effective thermal capacitance of each indoor element is calculated according to the standard method ISO 13786:2007. Their summation gives the total daily effective thermal inertia of each room's internal content.

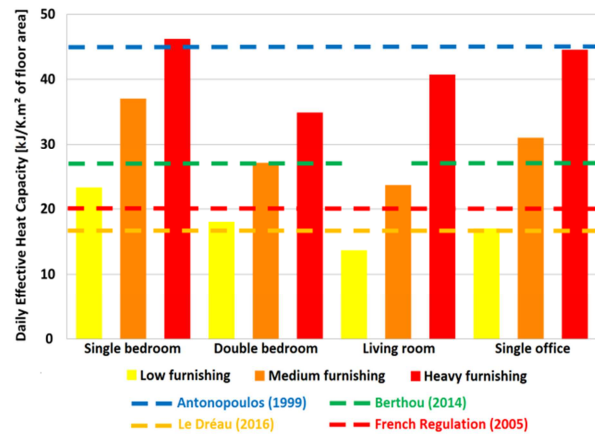


Figure 2: Daily effective heat capacity of indoor content / furniture thermal mass in buildings.

One can observe on Figure 2 that the results of the survey are in good agreement with the values found in different publications.

Modelling of the indoor content thermal mass for building energy simulations

The indoor content and furnishing elements often have complicated geometries with various types of material. The following section presents the different modelling technics found in publications attempting to represent the indoor thermodynamics in details.

First order thermal network building model

Simplified thermal network or resistance – capacitance (RC) models with the $xRIC$ (x resistances and 1 capacitance) configuration aggregate all the effective thermal inertia of a thermal zone in a single capacitance. The latter includes the indoor air volume, interior walls, inner envelope walls and the furniture / indoor content effective thermal capacitance. This simplified model assumes that the entire thermal mass is perfectly isothermal with homogenous equivalent properties and constant thermal resistances. A $5RIC$ model is described in the standard ISO 13790:2008.

Higher order thermal network building model

A RC network building model with more a realistic dynamic behaviour can be achieved by increasing the number of lumped capacitance nodes and dissociating the thermal mass elements with dissimilar thermal diffusivities. The indoor air volume and the construction elements can be separated to form a $xR2C$ model. The RC network can be expanded further to a $xR3C$ or $xRyC$ configuration (x resistances and y capacitances) by segregating the internal separation walls, the envelope walls and the heavy concrete floors or ceilings.

The furniture / indoor content effective thermal mass can then be integrated into these different lumped capacitances. Berthou et al. (2014) and TRNSYS type 56 models assume that items in the indoor zone are perfectly isothermal and in thermal equilibrium with the indoor air. The indoor content capacitance is therefore added to the one of the indoor air.

On the contrary, if it is assumed that the indoor content is not at the same temperature as the indoor air, the furniture / indoor content thermal mass can be merged with the one of the inner surface envelope walls or the interior partition walls (Berthou et al. 2014; Bacher and Madsen 2011). Moreover, the internal mass sub-system can be extended into a $2R2C$ network to account for the temperature gradient in the equivalent element.

Distinct furniture / indoor content thermal mass capacitance

The thickness, thermal diffusivity and heat exchange coefficients of the furnishing elements may differ significantly from the ones of the wall inner surfaces. Therefore, a noticeable temperature difference could remain between the indoor content and the other building elements or the indoor air node. This would justify to model the indoor thermal mass with its own lumped capacitance.

The TRNSYS Type 56 model allows the inclusion of an additional fictitious furniture thermal mass node in the star network scheme for radiation and convection heat exchange calculations. The specific location of the internal mass is not required, but a proper equivalent surface area must be specified.

The ISO 13790:2008 standard provides a simplified formulation for the calculation of this equivalent indoor content surface area. Li et al. (2016) proposed a new method to transform the furniture items with irregular

shape into a single lumped capacitance node with an appropriate effective area.

It should be kept in mind that the aggregation of the indoor objects into a single lumped capacitance is a non-geometrical heat balance calculation. Consequently, the correct assessment of solar radiation reaching the furniture node and the long-wave radiation heat exchanges with radiant surfaces can influence significantly the simulation results.

Equivalent virtual sphere model

The resistance – capacitance models represent the building system with a reduced number of nodes. Each of these node sub-systems is thus assumed to be isothermal. This assumption is acceptable if the Biot number of the element is smaller than 0.1. For plastic and wooden plates constituting most of the furnishing, this condition would imply elements thinner than 2 mm. However, most of the internal mass and furniture elements are thicker than 2 mm. Consequently, the indoor thermal mass cannot be considered isothermal and the lumped capacitance method should not be used to model it (Ma and Wang 2012).

To overcome this problem, Gao et al. (2000) and Zhou et al. (2011) suggested the virtual sphere method to model the internal mass. It aggregates different shapes of solid body into a single sphere with a radius equal to the characteristic length of the element. It is suitable for systems with Biot number in the range of 0 to 20, which is typically the case for the indoor content. Moreover, an effective convection heat transfer coefficient is introduced to account for the uneven distribution of indoor items' temperature. Nevertheless, this model does not currently include the radiation heat exchange.

Equivalent virtual planar element model

Antonopoulos and Koronaki (2000), Ma et al. (2012) and Wolisz et al. (2015) have chosen to concentrate the entire indoor content into a single equivalent planar element. This slab is made of an homogeneous material with constant properties which are representative of the items found in the indoor space. Because the length and width of the slab are much larger than its thickness, the conduction heat transfers and temperature distribution inside the element can be easily calculated with a one-dimensional finite difference or finite volume method formulation.

However, this equivalent slab element does not have a geometric representation in the thermal zone. Therefore, the presence of the planar element in the room is not taken into account for the calculation of internal solar distribution or long-wave heat exchange in between inner surfaces.

Energy Plus and IDA ICE software also allow the insertion of an equivalent furniture element as a fictitious one-dimensional multi-layer planar element which interacts solely with the air node by convection.

Equivalent geometric planar element model

Raftery et al. (2014) developed and implemented into Energy Plus software an equivalent planar element

model with a geometric representation and location inside the thermal zone. The slab is thus taken into account for the computation of the direct light beam reaching internal surfaces, diffuse solar repartition and radiant mean temperature. The long-wave radiation heat exchange can be calculated by radiosity method with correct view factors affected by the planar element in the middle of the room. Shading effect on the floor is modelled properly which adds a more realistic thermal behaviour to radiant systems.

Detailed explicit furniture model

The aforementioned indoor content modelling technics aggregate the items of the indoor space into a single equivalent element. This choice is justified by the complexity and the unknowns of what is inside an occupied building. Nonetheless, some numerical studies investigated the implications of the detailed modelling of furniture and indoor content with explicit locations in the building.

Athlaye et al. (2013) conducted an analysis with Radiance software and concluded that including details of interior partitions and furnishing has a significant impact on the indoor daylight conditions.

Bojic et al. (2002) and Horikiri et al. (2015) used CFD models of fully furnished ventilated rooms and showed that indoor items can create complex air flow patterns leading to local thermal discomfort.

Hand (2016) presented a library of pre-existing components such as office chairs, bookcases, light fittings, stairs or monitors, which can be easily integrated into ESP-r building models. These components have realistic geometries and thermo-physical properties. They can be positioned precisely in the indoor space. Exact solar distribution, shadowing and surface-to-surface view-factors can therefore be calculated for every surface in rooms with arbitrary complexity. Comparative simulations showed that the presence of indoor elements can have a significant impact on local discomfort due to their influence on local radiant temperature and radiant asymmetry. Moreover, it was found that additional thermal mass and lightweight pieces of furniture placed close to facades affect the heating and cooling demand profile of a building.

Current challenges for the indoor content modelling

A number of issues have to be addressed concerning the integration of simplified or complex modelling of the indoor content in buildings. Additional experimental investigations, such as the twin room tests conducted by Li et al. (2016), should be conducted to validate and improve the methodologies to aggregate complex items with various shapes and thermo-physical properties into simple equivalent elements. Great unknowns still remain regarding what typical amount of indoor thermal mass is present in buildings, what part of internal and solar gains are directly absorbed by these elements, what are the convection heat transfer conditions on their surfaces, how does furniture interact with radiant systems and how it influences the thermal comfort evaluation.

Building energy flexibility

The energy flexibility is often defined as the ability for a building to control its energy demand and generation according to local climate conditions, user needs and grid requirements. However, there is currently no agreement on an exact definition for the energy flexibility index and consequently no overview of the flexibility potential for the different types of building, Lopes et al. (2016). The on-going IEA EBC Annex Project 67 aims at defining precisely the energy flexibility concept and increasing knowledge on how building energy demand management can improve the operation of energy grids.

The rest of this article focuses on the capacity of a building to shift its heating energy use from high price periods to low price periods by the mean of indoor temperature set point modulation. One can see on the Figure 3 an example from the current numerical study of the heating energy shift induced by the heat storage strategy.

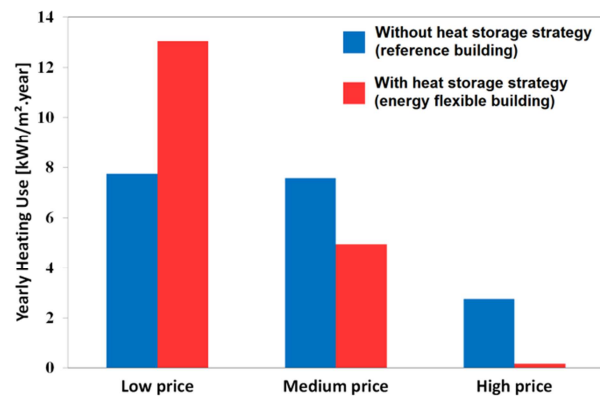


Figure 3: Variation of the yearly heating use profile for light structure passive house with heat storage strategy.

The performance of heat storage in the indoor environment highly depends on the amount of building thermal mass which can be activated and the efficiency of the envelope. The current study emphasizes the impact of the envelope thermal mass and additional thermal mass such as furniture and phase change material (PCM) on the energy flexibility capacity.

Methodology

Numerical model of the building case study

A MATLAB-Simulink multi-zone building model of a typical Danish single family house has been created within the framework of the EnovHeat project. It is used here to investigate the influence of detached houses' characteristics on their capacity to shift in time heating use under Danish weather conditions (Denmark Design Reference Year 2013). Envelope performance, construction thermal mass, heating system and additional indoor thermal mass parameters are varied to generate 48 different study cases. Two different classes of insulation are considered (low insulation house from the 80's and high insulation passive house) with three levels of envelope thermal mass each (light structure: 30

Wh/K.m², medium structure: 55 Wh/K.m², heavy structure: 100 Wh/K.m²). In addition to the empty room cases, three kinds of additional internal thermal mass are modelled (furniture / indoor content, PCM integrated in furniture elements and PCM wallboards placed on inner walls and ceilings). Two types of heating system are tested (radiators and water based under-floor heating).

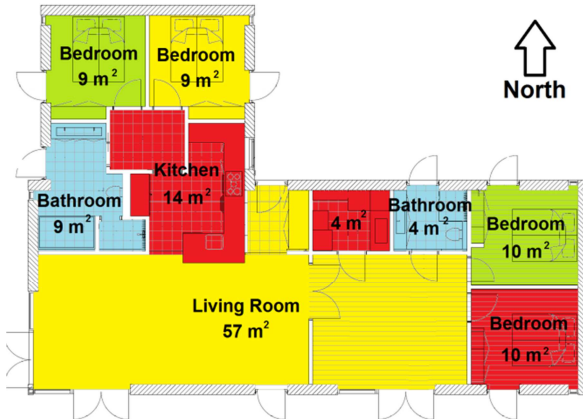


Figure 4: Scheme of the house case study: a typical 150 m² single family house in Denmark.

The furniture / indoor content is represented as a fictitious equivalent planar element and modelled with a one-dimensional implicit finite control volume formulation. The mass of each element is 60 kg/m² of the room's floor surface area concentrated in a 4.7 cm thick slab. The equivalent homogeneous material of the element is chosen to be with a density of 715 kg/m³, a thermal conductivity of 0.3 W/m.K and a specific heat capacity of 1400 J/kg.K. It is assumed that 50% of the internal radiative heating gains and solar radiation are absorbed by the surfaces of the planar elements.

The PCM wallboards are modelled with an enthalpy formulation coupled to a one-dimensional implicit finite control volume model. The 1.5 cm thick PCM slab elements are considered made of Energain®. The latter is a common commercial product composed of 60 w% micro-encapsulated paraffin incorporated into 40 w% polyethylene matrix. The material is set to be with a melting temperature of 22 °C, a total latent heat of fusion of 120 kJ/kg, a density of 1000 kg/m³, a thermal conductivity ranging from 0.18 to 0.22 W/m.K and a specific heat capacity of 2000 J/kg.K.

Furniture with integrated PCM are represented by a PCM wallboard element attached on one side of a fictitious equivalent furniture planar element.

The building numerical model has been validated with a BESTEST procedure. Each sub-component of the building model has been validated against commercial software (COMSOL Multiphysics and BSim) or experimental test data.

Validation test results and detailed description of the building model and its sub-components can be found in a DCE technical report (Johra and Heiselberg 2016).

Heat storage control strategy

The main objective of developing energy flexible buildings in a smart grid system is to allow the

integration of a larger share of intermittent RES. The electricity spot price is a good indicator of the availability of RES in Denmark. Consequently, a price control strategy based on the 2009 Danish electricity spot price is used for this study.

As shown on Figure 5, the indoor temperature set point is increased to 24 °C when the electricity price is low to accumulate thermal energy. When the electricity price is high, the temperature set point is decreased to 20 °C to save thermal energy. If the electricity price is within the medium price range, the temperature set point is maintained at 22 °C.

Low price and a high price limits are defined for each hour as the lowest and highest quartile of the hourly electricity market price over the last 14 days.

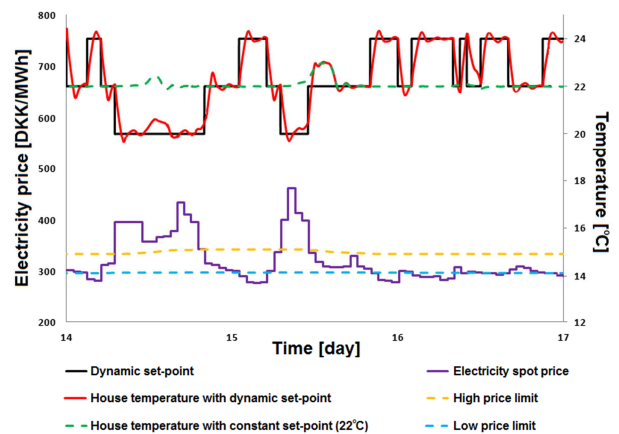


Figure 5: Temperature set point modulation with price control for a low insulation and light structure house.

Building energy flexibility index

Similarly to Le Dréau and Heiselberg (2016), the energy flexibility of a building is defined here as its capacity to reduce heating need during medium and high electricity price periods by storing heat during low electricity price periods (see example on Figure 3). The flexibility index is then calculated with equation (1).

$$F = \left[\left(1 - \frac{\%High}{\%High_{ref}} \right) + \left(1 - \frac{\%Medium}{\%Medium_{ref}} \right) \right] \times \frac{100}{2} \quad (1)$$

%High and %Medium are the percentages of the yearly thermal energy used during high and medium price periods respectively when set point modulation with price control is activated. Similarly, %High_{ref} and %Medium_{ref} account for the reference case which does not have any heating storage strategy.

If the energy usage repartition with heat accumulation is the same as the reference case, the flexibility index is zero. If the energy share of high and medium price period increases, the flexibility index is negative. If all the energy share of the high price period is shifted to the low price period, the flexibility index is 50%. If all the energy share of the high and medium period is shifted to the low price period, the flexibility index reaches the maximum value of 100%.

Results

A total of 48 different building scenarios were simulated with the same weather conditions and heat accumulation strategy: two different insulation levels, three different classes of envelope thermal mass, two types of heating system (radiators and under-floor heating) and four different configurations of additional thermal mass (empty room, furniture / indoor content, furniture with PCM, PCM wallboards). The building cases equipped with convective radiators and no TES strategy are taken as references for the calculation of the energy flexibility index.

During the entire heating period, the indoor operative temperature is maintained between 20 °C and 24 °C. This temperature span corresponds to a normal level of thermal comfort with less than 10% of dissatisfied occupants (ISO 7730). Moreover, the time variation of the house temperature is always kept below the thermal comfort limit of 2.1 K/h (ASHRAE Standard 55 - 2004).

Figure 6 illustrates the increase of the building energy flexibility in function of its total effective thermal mass including the thermal mass of the envelope and the indoor content. It appears that activated thermal mass, regardless of its nature and location, contributes to increase the total storage capacity and therefore the energy shifting ability of the building. However, the impact of this parameter is smaller for low energy buildings compared to houses with poor envelope performance. Above 80 Wh/K.m² of total daily effective thermal mass, low energy buildings reach the maximum flexibility potential: there is no more energy to shift in time. It is therefore useless to increase the thermal mass of these buildings further more.

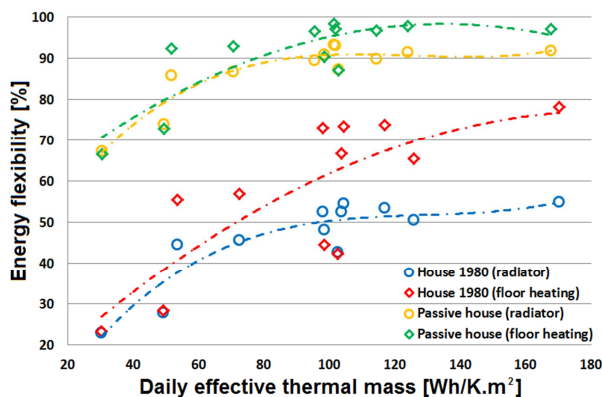


Figure 6: Effect of building effective thermal mass on energy flexibility.

Moreover, the insulation level seems to play a dominant role in the improvement of the building energy flexibility compared to its thermal inertia. Indeed, only poorly insulated house cases with a very large heating storage capacity and under-floor heating system are able to reach the same flexibility potential as passive houses.

Finally, the type of heat emitter has a limited effect on the building energy flexibility. Nevertheless, under-floor heating can improve the activation of the thermal mass

of poorly insulated houses and noticeably improve their energy flexibility.

One can see on Figure 7 the impact of the different types of additional thermal mass on the building energy flexibility potential. The empty room building cases with no PCM are used as reference.

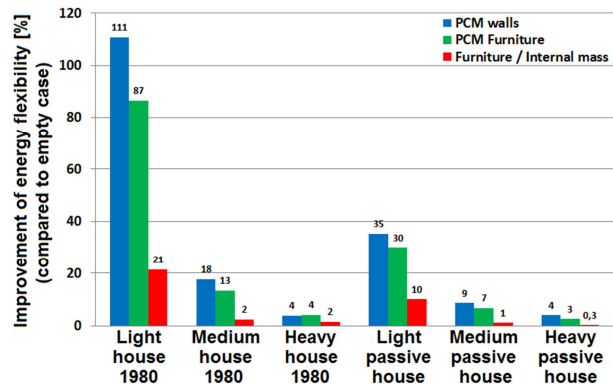


Figure 7: Influence of internal thermal mass on energy flexibility for houses equipped with radiators.

The results indicate that PCM integrated in wallboards or furniture elements can significantly improve the energy flexibility potential of low insulation light structure buildings. However, the benefit is lower for well-insulated dwellings and very limited in the case of medium and heavy structure buildings. Because of their low thermal conductivity, PCM wallboards positioned on inner surfaces of thermal zones tend to screen the activation of the thermal mass underneath them. It thus nullifies the storage capacity of the structural elements which is counterproductive in the case of heavy construction elements such as masonries.

In the case of houses with large effective thermal mass, the share of additional thermal inertia of indoor items and furniture is very small. Therefore, the impact of the latter on the building energy flexibility index appears to be almost negligible. Nevertheless, the influence of the furniture / indoor content for the light structure buildings should be taken into account.

Conclusion

This article presented a numerical study assessing the influence of different building parameters (effective thermal mass, insulation level and type of heating emitter) on the heating energy flexibility potential of a single family house in Denmark.

The energy flexibility index is here defined as the capacity of the building to shift its heating use from high and medium electricity price periods to low electricity price periods by the mean of temperature set point modulation.

Although the effective thermal mass of a building determines its maximum energy storage capacity, results indicate that the envelope performance is the most important parameter concerning the ability of a house to shift heating use. Under-floor heating systems present better performance in that matter, especially for low

insulation level buildings. It is therefore more interesting to improve the building envelope and storage efficiency rather than increasing its thermal inertia or changing heating systems.

Nevertheless, the integration of phase change materials in wallboards or furniture elements appears to be a good solution to increase the effective thermal mass of lightweight structure buildings and consequently significantly improve their energy flexibility potential. It should be noted that PCM wallboards should not be employed in heavy masonry constructions because they screen the thermal mass activation underneath them and do not provide more heat capacity than thick concrete walls.

Finally, it has been clearly shown that the empty room assumption is not valid for the simulation of low thermal mass buildings with dynamic indoor temperature set point. The indoor content of such buildings can change the assessment of its energy flexibility by up to 21%. The modelling of the indoor content is therefore significant for detailed and realistic building simulations. This should be taken as a motivation to explore further the different modelling techniques reviewed in this article. More theoretical and experimental investigations should be performed to have a better knowledge of what is present inside occupied buildings and how these objects interact with the rest of the building thermal systems.

Acknowledgement

This work was financed by the ENOVHEAT project, which is funded by Innovation Fund Denmark (contract no 12-132673) and was carried out partly within the framework of IEA EBC Annex 67 Energy Flexible Buildings.

References

- Antonopoulos, K.A. and Koronaki, E.P (1999). Envelope and indoor thermal capacitance of buildings. *Appl Therm Eng* 19, 743–56.
- Antonopoulos, K.A. and Koronaki, E.P (2000). Effect of indoor mass on the time constant and thermal delay of buildings. *Int J Energy Res* 24, 391–402.
- ASHRAE Standard, Standard 55 – 2004. Thermal environmental conditions for human occupancy. 2004.
- Athlaye, R.A. et al (2013). Analysis of Daylighting Requirements within ASHRAE Standard 90. US Department of Energy.
- Bacher, P. and Madsen, H (2011). Identifying suitable models for the heat dynamics of buildings. *Energy Build* 43, 1511–22.
- Berthou, T, Stabat, P, Salvazet, R. and Marchio, D (2014). Development and validation of a gray box model to predict thermal behavior of occupied office buildings. *Energy Build* 74, 91–100.
- Beurskens, W.M, Hekkenberg, M. and Vethman, P (2011). Renewable energy projections as published in the national energy action plans of the European member states. Report no. ECN-E-10-069. *ECN and European Environment Agency*.
- Bojic, M, Yik, F. and Lo, T.Y (2002). Locating air-conditioners and furniture inside residential flats to obtain good thermal comfort. *Energy and Buildings* 34, 745–51.
- DuPont Energain®, Technical Datasheet.
- Energy Plus Engineering Reference Manual.
- EnovHeat project: development of efficient novel magneto-caloric heat pumps.
www.enovheat.dk/Research/ProjectSummary
- French Building Energy and Thermal Regulation (2005), CSTB FR.
- Gao M, Reid C.N, Jahedi M, Li Y (2000). Estimating equilibration times and heating/ cooling rates in heat treatment of workpieces with arbitrary geometry. *J Mater Eng Perform* 9, 62–71.
- Hand. J (2016). Performance implications of fully participating furniture and fittings in simulation models. Conference: BSO August 2016, Newcastle, UK.
- Hedegaard, K, Mathiesen, B.V, Lund, H. and Heiselberg, P (2012). Wind power integration using individual heat pumps – Analysis of different heat storage options. *Energy* 47, 284–93.
- Horikiri, K, Yao, Y. and Yao, J (2015). Numerical optimisation of thermal comfort improvement for indoor environment with occupants and furniture. *Energy and Buildings* 88, 303–15.
- International Energy Agency: EBC project “Annex 67: Energy Flexible Buildings”. <http://www.iea-ebc.org/projects/ongoing-projects/ebc-annex-67/>
- ISO 7730:2005, Ergonomics of the thermal environment – analytical determination of thermal comfort by using calculations of the PMV and PPD indices and local thermal comfort criteria.
- ISO 13786:2007, Thermal performance of building components – dynamic thermal characteristics – calculation methods.
- ISO 13790:2008, Energy performance of buildings – calculation of energy use for space heating and cooling.
- Johra, H. and Heiselberg, P (2016). Description and Validation of a MATLAB: Simulink Single Family House Energy Model with Furniture and Phase Change Materials. Aalborg: Department of Civil Engineering, Aalborg University. (DCE Technical Reports; No. 187).
[vbn.aau.dk/en/publications/description-and-validation-of-a-matlab\(5614a2bf-a32f-493f-9b11-95a2ee033243\).html](http://vbn.aau.dk/en/publications/description-and-validation-of-a-matlab(5614a2bf-a32f-493f-9b11-95a2ee033243).html)
- Johra, H. and Heiselberg, P (2017). Influence of internal thermal mass on the indoor thermal dynamics and

- integration of phase change materials in furniture for building energy storage: A review. *Renewable and Sustainable Energy Reviews* 69, 19–32.
- Le Dréau, J. and Heiselberg, P (2016). Energy flexibility of residential buildings using short term heat storage in the thermal mass. *Energy* 111, 991–1002.
- Li, W, Xu, P, Wang, H. and Lu, X (2016). A new method for calculating the thermal effects of irregular internal mass in buildings under demand response. *Energy and Buildings* 130, 761–772
- Lopes, R.A, Chambel, A, Neves, J, Aelenei, D. and Martins, J (2016). A literature review of methodologies used to assess the energy flexibility of buildings. *Energy Procedia* 91, 1053–1058.
- Ma, P. and Wang, L.S (2012). Effective heat capacity of interior planar thermal mass (IPTM) subject to periodic heating and cooling. *Energy Build* 47, 44–52.
- Mathiesen, B.V, Lund, H, Connolly, D, Wenzel, H, Østergaard, P.A, Möller, B, et al. (2015). Smart Energy Systems for coherent 100% renewable energy and transport solutions. *Applied Energy* 145, 139–54.
- Raftery, P, Lee, E, Webster, T, Hoyt, T. and Bauman, F (2014). Effects of furniture and contents on peak cooling load. *Energy Build* 85, 445–57.
- TRNSYS 17 Technical Documentation Vol. 5, Multizone Building modeling with Type56 and TRNBuild.
- User Manual IDA Indoor Climate and Energy – version 4.5 (2013). EQUA Simulation AB.
- Wolisz, H, Kull, T.M, Streblov, R. and Müller, D (2015). The effect of furniture and floor covering upon dynamic thermal building simulations. *6th International Building Physics Conference, IBPC*.
- Zhou J, Zhang G, Lin Y, Wang H (2011). A new virtual sphere method for estimating the role of thermal mass in natural ventilated buildings. *Energy Build* 43, 75–81.

Appendix C. Paper III

Johra, H., Filonenko, K., Heiselberg, P., Veje, C., Lei, T., Dall'Olio, S., Engelbrecht, K., & Bahl, C. (2018). Integration of a magnetocaloric heat pump in a low-energy residential building. *Building Simulation: An International Journal*.

<https://doi.org/10.1007/s12273-018-0428-x>

Reprinted by permission from Building Simulation: An International Journal, Springer Nature (License Number: 4302530729362). Building Simulation: An International Journal, Integration of a magnetocaloric heat pump in a low-energy residential building, Hicham Johra, Konstantin Filonenko, Per Heiselberg, Christian Veje, Tian Lei, Stefano Dall'Olio, Kurt Engelbrecht, Christian Bahl, © Tsinghua University Press and Springer-Verlag GmbH Germany, part of Springer Nature (2018), advance online publication, 13 January 2018 (doi: 10.1007/s12273-018-0428-x Build. Simul.).

Integration of a magnetocaloric heat pump in a low-energy residential building

Hicham Johra ^{a,*}, Konstantin Filonenko ^b, Per Heiselberg ^a,
Christian Veje ^b, Tian Lei ^c, Stefano Dall'Olio ^c, Kurt
Engelbrecht ^c, Christian Bahl ^c,

^a *Aalborg University, Division of Architectural Engineering, Department of Civil Engineering, Thomas Manns Vej 23, DK-9220 Aalborg Øst, Denmark*

^b *University of Southern Denmark, Center for Energy Informatics, Campusvej 55, DK-5230 Odense M, Denmark*

^c *Technical University of Denmark, Department of Energy Conversion and Storage, Frederiksborgvej 399, DK-4000 Roskilde, Denmark*

** Corresponding author. Tel.: +45 9940 7234. E-mail address: hj@civil.aau.dk (H. Johra).*

Abstract

The EnovHeat project aims at developing an innovative heat pump system based on the magnetocaloric effect and active magnetic regenerator technology to provide for the heating needs of a single family house in Denmark. Unlike vapor-compression devices, magnetocaloric heat pumps use the reversible magnetocaloric effect of a solid refrigerant to build a cooling/heating cycle. It has the potential for high coefficient of performance, more silent operation and efficient part-load control. After presenting the operation principles of the magnetocaloric device and the different models used in the current numerical study, this article demonstrates for the first time the possibility to utilize this novel heat pump in a building. This device can be integrated in a single hydronic loop including a ground source heat exchanger and a radiant under-floor heating system. At maximum capacity, this magnetocaloric heat pump can deliver 2600 W of heating power with an appreciable average seasonal system COP of 3.93. On variable part-load operation with a simple fluid flow controller, it can heat up an entire house with an average seasonal system COP of 1.84.

Keywords

Magnetocaloric heat pump, magnetic heating, active magnetic regenerator, innovative heating system

1. Introduction

In many countries, heat pumps now represent a key component of the energy development strategies. Consequently, researchers and industry strive to bring new cost-effective technical solutions to market. Conventional heat pumps and air-conditioner units are based on vapor compression technologies. They transfer thermal energy from a low-temperature to a high-temperature environment by means of irreversible thermodynamic cycles. In recent years, several research groups investigated the potential of the magnetocaloric effect for ambient temperature cooling applications. This innovative technology uses magnetocaloric materials (MCM) as solid refrigerants in magnetic cooling/heating cycle. Because of the reversible nature of the magnetocaloric effect, magnetic heating/cooling devices have a potential for high coefficient of performance (COP). In addition, they could also present the advantage of a more silent operation, efficient part-load control, a lack of toxic or greenhouse contributing gases, and the possibility for recycling the MCM and magnets at end-of-life (Smith et al. 2012). However, it has yet to prove its competitiveness compared to mature vapor compressor technologies (Eriksen et al. 2016).

The history of the active magnetocaloric regenerator cooling system started in 1982 with the proposal by Barclay of the active magnetic regenerator (AMR) cycle which is the basis for magnetocaloric heat pump (MCHP) systems (Barclay 1982). In 1998, an AMR device using superconducting magnets reached COPs above 6 (Zimm et al. 1998). Since then, different research groups have reported the performances of their AMR prototypes using permanent magnets for near-room temperature cooling. In 2012, Engelbrecht et al. (2012) presented a rotary AMR device operating with a maximum cooling capacity of 1010 W and a no-load temperature span of 25.4 K (Engelbrecht et al. 2012). In 2013, a Japanese group presented a device operating at a temperature span of 5 K with a COP of 2.5 (Okamura and Hirano 2013). In 2014, Jacobs et al. (2014) reported the performances of a prototype achieving a zero temperature span cooling power of 3042 W and cooling power of 2502 W at a temperature span of 12 K with a COP above 2 (Jacobs et al. 2014). In 2016, several research teams have published the performances of their AMR device. A group from the Federal University of Santa Catarina reported a maximum no-load temperature span of 12 K, a maximum zero-span cooling power of 150 W and a thermal load of 80.4 W for a temperature span of 7.1 K and a COP of 0.54 (Lozano et al. 2016). A group from the University of Salerno reported a maximum no-load temperature span of 11.9 K and a maximum COP of 2.5 for a thermal load of 200 W (Aprea et al. 2016). A research team from the Technical University of Denmark published the

study of an AMR device capable of 81.5 W of cooling power at a temperature span of 15.5 K and with a COP of 3.6 (Eriksen et al. 2016).

Some key topics are being investigated to improve the performance of magnetocaloric devices: development, characterization and modelling of new magnetocaloric materials (Pecharsky et al. 2016; Neves Bes et al. 2016), using nanofluids to improve heat transfer in regenerators (Mugica et al. 2017), optimization of permanent magnet configurations (Insinga et al. 2016a; Insinga et al. 2016b), different regenerator geometries for efficient heat transfer and minimum pressure losses (Dall’Olio et al. 2017; Lei et al. 2017; Trevizoli et al. 2017), and novel designs for optimum operation and reduced parasitic losses of the whole machine (Eriksen et al. 2016; Lozano et al. 2016).

The “EnovHeat” project aims to tackle the aforementioned questions and develop the prototype of an innovative magnetocaloric heat pump (see **Fig. 1**) able to provide for the heating needs of a single family house in Denmark (excluding domestic hot water production) with a higher COP than conventional systems (Bahl 2015).

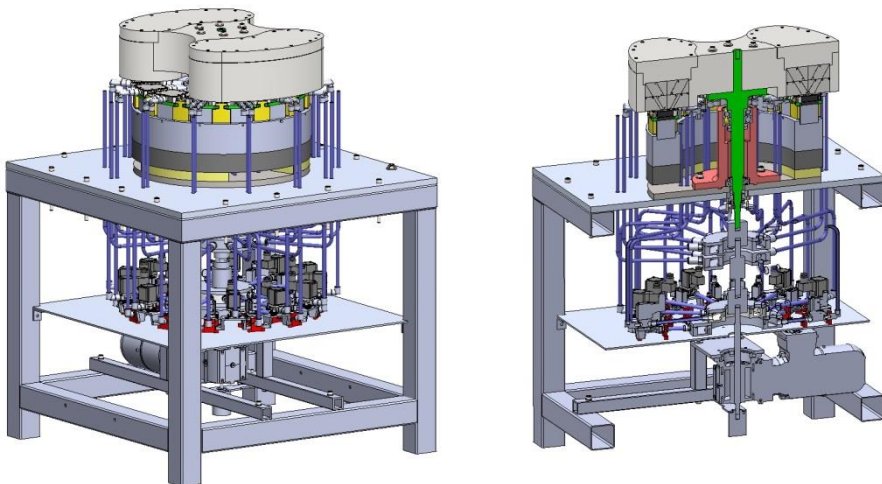


Fig. 1 CAD model of the magnetocaloric heat pump prototype of the EnovHeat project: “MagQueen”

This article firstly introduces the operation principles of this novel MCHP and presents the numerical models of this device and the building case study used in this project. For the first time, the integration of this innovative heat pump as heating system in a building is discussed. The results of this numerical study are presented and the operation performance of the MCHP in a low-energy house is assessed. Finally, suggestions for further research on efficient control of this device are made.

2. Magnetocaloric heat pump

2.1. Operation of the magnetocaloric heat pump

A magnetocaloric heat pump transforms a low-quality thermal energy supplied by a low-temperature heat source into a high-quality thermal energy utilized by a high-temperature heat sink. This heat transfer is performed by means of several magnetic cooling/heating cycles, also known as the active magnetic regenerator (AMR) cycle. The refrigerant here is a solid material which exhibits a thermal response when the applied magnetic field changes. The magnetization (applying a magnetic field) of the refrigerant material induces an increase of its temperature and a decrease of its entropy. Reciprocally, the demagnetization (removing a magnetic field) of the refrigerant material leads to a decrease of its temperature and an increase of its entropy. This phenomenon is often nearly reversible and is named the “magnetocaloric effect”. Materials exhibiting this effect are called “magnetocaloric materials” and present a maximum magnetocaloric response at the ferro-to-paramagnetic phase transition called the “Curie temperature”. The reference material for the magnetocaloric effect at room-temperature is Gadolinium. More information about the magnetocaloric effect and magnetocaloric materials can be found in Smith et al. (2012) and Kitanovski et al. (2015).

The AMR cycle, at the core of the operation of this innovative heat pump, makes use of the magnetocaloric effect by alternatively magnetizing and demagnetizing a MCM with an external magnetic field source. The MCM solid refrigerant is contained as a porous media in a regenerator allowing bi-directional circulation of the coolant fluid transferring the thermal energy from the cold side to the warm side of the device. **Fig. 2** illustrates in details the AMR cycle. At the beginning of the cycle, there is a temperature gradient over the regenerator length and no magnetic field is applied: **Fig. 2(a)**. The cycle starts with an adiabatic magnetization of the MCM leading to a uniform temperature increase over the length of the regenerator: **Fig. 2(b)**. The heat transfer fluid is pushed from the cold side to the warm side of the AMR (cold-to-hot blow). The hotter fluid rejects the heat to the heat sink and the regenerator is cooled down at constant magnetic field: **Fig. 2(c)**. The magnetic field is removed and the regenerator operates an adiabatic demagnetization leading to a uniform temperature decrease over the length of the AMR: **Fig. 2(d)**. At the end of the cycle, the fluid is pushed back from the warm side to the cold side of the AMR (hot-to-cold blow) under zero-magnetic field, re-heating the bulk of the regenerator: **Fig. 2(e)**. Once the heat transfer fluid and the MCM reached local thermal equilibrium, the temperature distribution across the regenerator length is the same as at the initial state of the AMR cycle **Fig. 2(f)**. A detailed description of the AMR cycle can be found in the papers published by Lei et al. (2017) and Engelbrecht et al. (2012).

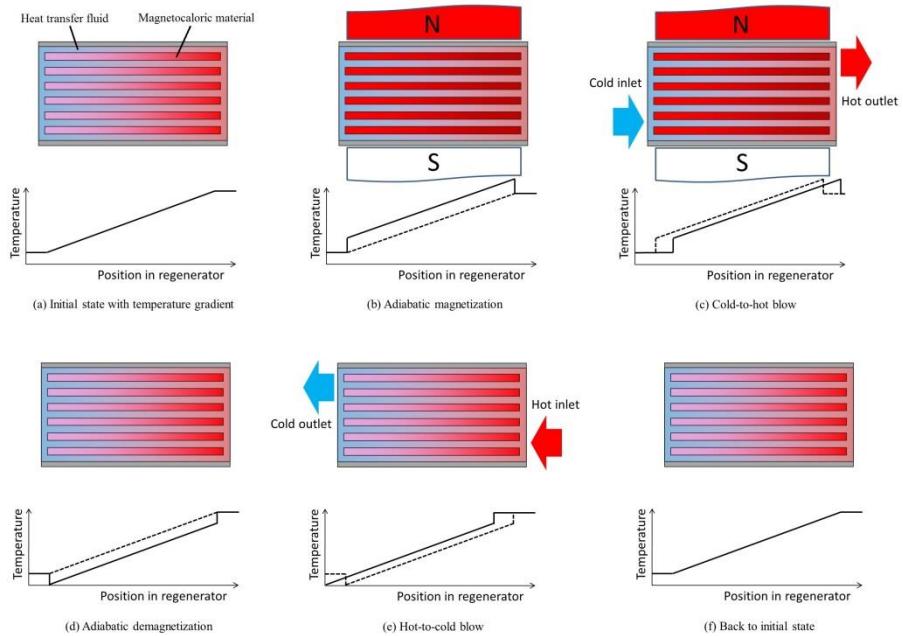


Fig. 2 Active magnetic regenerator cycle consisting of four processes: (b) adiabatic magnetization; (c) cold-to-hot blow; (d) adiabatic demagnetization; (e) hot-to-cold blow

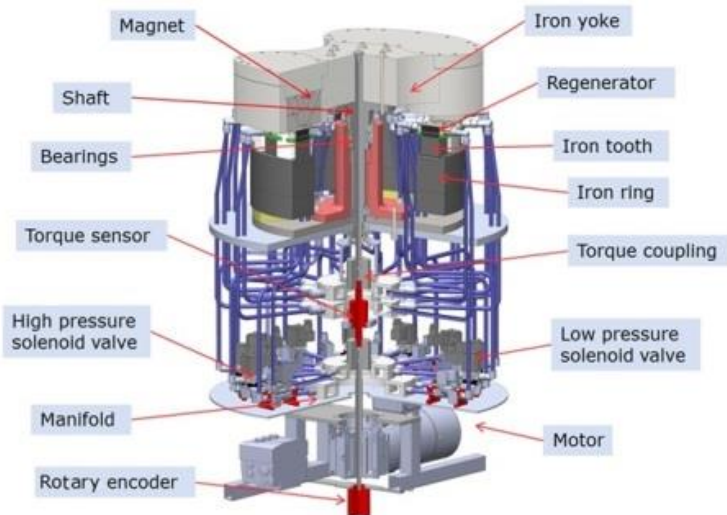


Fig. 3 Detailed description of the magnetocaloric heat pump prototype of the EnovHeat project: “MagQueen”

The MCHP prototype of the EnovHeat project is a rotary device with 13 packed bed spheres active magnetic regenerators placed on the stator and a two-pole permanent magnet assemblies placed on the rotor (see **Fig. 3**). The regenerators consist of trapezoidal shaped-cassettes (see **Fig. 4**) filled with MCM having a spherical shape with an average diameter of $450\ \mu\text{m}$. The spheres are kept together by an epoxy layer and the total amount of MCM is around 2.8 kg for the entire prototype. The rotor is mounted on a vertical axis connected to an electric motor, and supports the two-pole magnet composed of 28 permanent magnet elements each. The rotation of the magnet creates a varying magnetic field having a maximum value of 1.4 T in the air gap. The 13 regenerators are connected to 2 manifold collectors and 2 manifold distributors: one of each on the cold side and on the hot side respectively. 13 high pressure and 13 low pressure solenoid valves allow synchronized regulation of the fluid flow through each of the regenerators. The circulation of the heat transfer fluid is performed by a single centrifugal pump (GRUNDFOS Data Booklet 2013).

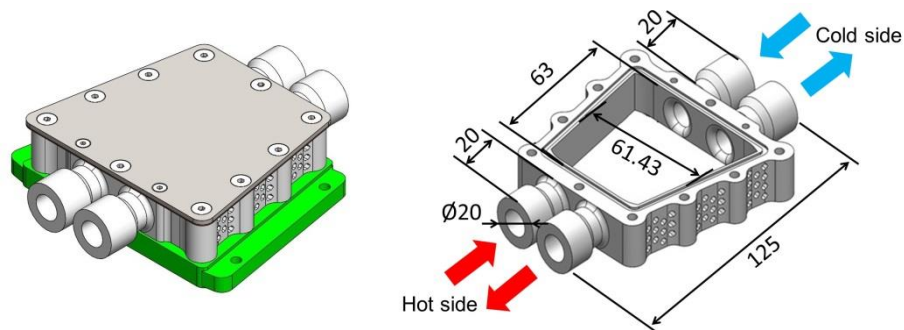


Fig. 4 CAD model of the regenerator for the magnetocaloric heat pump prototype (dimensions are indicated in millimeters)

2.2. Numerical modelling of the magnetocaloric heat pump

The core of the magnetocaloric heat pump modelling process is the original one-dimensional numerical model created by Engelbrecht (2008) and further developed by Lei et al. (2017). Heat losses inside the regenerator, such as internal axial conduction, are taken into account, as indicated in the governing equations. External heat losses through the walls of the regenerators are neglected. The demagnetization losses are assessed by calculating the internal magnetic field in the MCM using an average demagnetization factor, which is calculated to be 0.58, for the entire regenerator bed which is assumed to be a rectangular solid. The demagnetization is implemented in the model as described in Engelbrecht et al. 2013. This leads to two coupled partial differential equations describing the fluid temperature distribution in the AMR with regards of time:

$$\begin{aligned} & \frac{\partial}{\partial x} \left(k_{\text{disp}} A_c \frac{\partial T_f}{\partial x} \right) - \dot{m}_f c_f \frac{\partial T_f}{\partial x} - \frac{Nuk_f}{d_h} a_s A_c (T_f - T_s) + \left| \frac{\partial P}{\partial x} \frac{\dot{m}_f}{\rho_f} \right| \\ & = A_c \varepsilon \rho_f c_f \frac{\partial T_f}{\partial t} \end{aligned} \quad (1)$$

$$\begin{aligned} & \frac{\partial}{\partial x} \left(k_{\text{stat}} A_c \frac{\partial T_s}{\partial x} \right) + \frac{Nuk_f}{d_h} a_s A_c (T_f - T_s) \\ & = A_c (1 - \varepsilon) \rho_s \times \left[c_H \frac{\partial T_s}{\partial t} + T_s \left(\frac{\partial s_s}{\partial H} \right)_{T_s} \frac{\partial H}{\partial t} \right] \end{aligned} \quad (2)$$

Where k , T , ρ , c and s are the thermal conductivity, temperature, density, specific heat, and specific entropy; A_c , d_h , a_s , ε , x , t , \dot{m}_f , and H are the cross sectional area, hydraulic diameter, specific surface area, porosity of the regenerator bed, axial position, time, fluid mass flow rate and internal magnetic field; $\partial P / \partial x$ and Nu are the pressure drop and the Nusselt number. The subscripts f and s represent fluid and solid refrigerant, respectively. k_{disp} is the thermal conductivity of the fluid due to axial dispersion, k_{stat} is the static thermal conductivity of regenerator and fluid, and c_H is the specific heat capacity of the MCM at constant magnetic field. The Nusselt number, k_{disp} and k_{stat} are calculated using correlations which are described in detail by Nielsen et al. (2013). These equations are solved using implicit finite volume method implemented in MATLAB calculation programming software. This numerical model has been tested against experimental data and showed very good capabilities to predict the performances of real MCHP prototypes (Lei et al. 2018). However, this model is too computationally demanding to be used as is in building simulations. Because of the relatively fast operation of the MCHP, the numerical model outputs can be approximated by a series of quasi-steady states suitable for building simulations with time step size of 60 seconds. Therefore, the detailed MCHP model is run with the parameters of the EnovHeat prototype in order to generate around 1600 output points for building a set of 5-dimensional lookup tables. These lookup tables are implemented in MATLAB-Simulink function blocks and provide output fluid temperatures, heating and cooling powers, COP, magnetic work and fluid pressure losses as functions of the inlet fluid temperatures, operation frequency and fluid mass flow rate to the heat pump for very little computation time.

The additional elements of the MCHP are modelled in a simple way. The average electrical power usage of the set of valves (\dot{W}_{valves}) has been measured directly on the prototype and has been found to be 63 W. It should be noted that some heat from the solenoid valves' operation would be absorbed by the fluid on the hot end of the regenerator. This would therefore slightly increase the heating power of the MCHP. However, this amount is limited and neglecting it is a conservative assumption to avoid over predicting the system performance. The electrical power usage of the device's motor (\dot{W}_{motor}) is calculated from the magnetic work of the AMR with the assumption of a motor efficiency factor equal to 0.65. Finally, the pump work (\dot{W}_{pump}) is calculated with a polynomial function fitting the operation data provided by the manufacturer (GRUNDFOS Data Booklet 2013).

3. Building systems

The EnovHeat project aims at developing a novel heat pump system and demonstrating that it can provide for the heating needs of a low-energy single family house in Denmark. The following sections present the building case study chosen to test the integration of the MCHP, and the detailed dynamic building energy model developed for that purpose.

3.1. Building case study

A single-story house with 126 m² of heated floor area and a typical geometry for dwellings in Denmark is chosen as case study (see **Fig. 5**). With a yearly heating need of 16 kWh/m², the design fulfills the low-energy requirements of a new building “class 2020” of the Danish building regulation (Building Regulation 2010) and almost reaches the “Comfort House” standard (Larsen and Brunsgaard 2010). The main characteristics of the house case study can be found in **Table 1**.

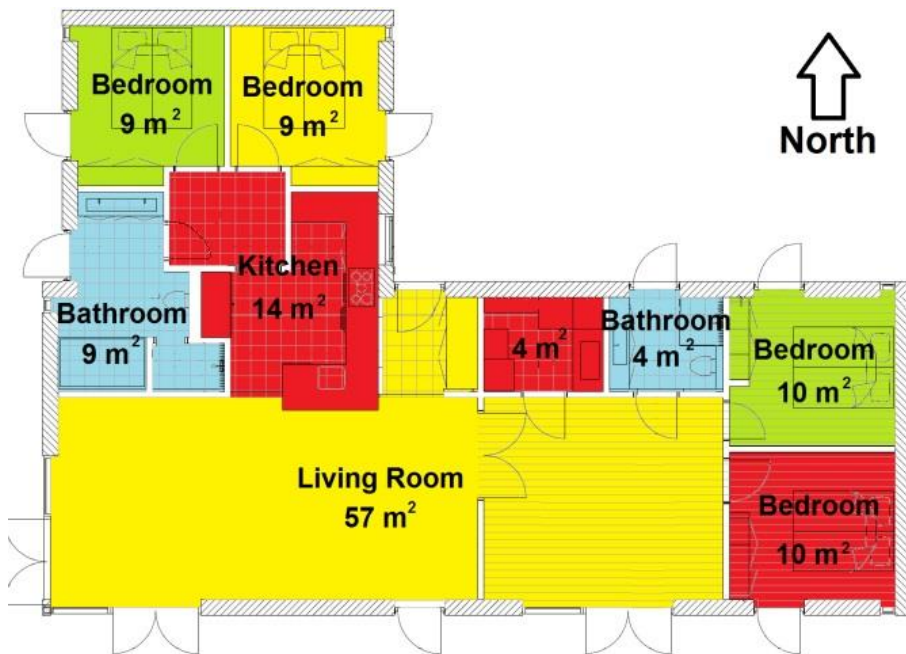


Fig. 5 Plan view of the house case study: a typical single family house in Denmark

Table 1 Parameters of the building case study

Total ground floor area including walls [m ²]	150
Heated floor area [m ²]	126
Heated net volume [m ³]	309
External walls <i>U</i> -value [W/(m ² ·K)]	0.11
Floor <i>U</i> -value [W/(m ² ·K)]	0.071
Roof <i>U</i> -value [W/(m ² ·K)]	0.081
Doors and windows <i>U</i> -value [W/(m ² ·K)]	1
Glazing transmittance [%]	0.63
Infiltration rate [h ⁻¹]	0.1
Air change rate (without infiltration) [h ⁻¹]	1.2
Ventilation heat recovery [%]	85
Heating temperature set point [°C]	22
Heating energy need (set point = 20 °C) [kWh/(m ² ·year)]	16

In the case of Danish dwellings, the most energy efficient configuration for heat pump systems is to couple a ground source heat exchanger (GSHE) with a hydronic radiant under-floor heating (UFH) (Den lille blå om Varmepumper 2011). The water-brine heat transfer fluid is chosen to be 20% vol ethylene glycol and 80% vol water.

Two types of GSHE are considered in this case study: a horizontal GSHE and a vertical borehole GSHE. The ground loops are designed according to international standards and manufacturer's guidelines (VDI 4640:2001; Uponor Ground Energy Technical Information 2012; Ground Source Heat Pump Project Analysis 2005) with the assumption that the soil is a humid clayey sand: thermal conductivity of 1.5 W/m.K; density of 1900 kg/m³; specific heat capacity of 1400 J/kg.K. The grouting material is chosen to be with a thermal conductivity of 1.4 W/m.K, a density of 1500 kg/m³ and a specific heat capacity of 1670 J/kg.K. Consequently, the horizontal GSHE is a 194 m long single collector with a serpentine layout. It is composed of PEX pipes with 40 mm outer diameter and 33 mm inner diameter. They are placed at a depth of 1.5 m with a pipe spacing of 1.5 m. The collector covers 291 m² of ground surface area. The vertical borehole GSHE is a single collector consisting of a double U-tube PEX pipe with outer diameter of 44 mm and inner diameter of 37

mm. The borehole has a depth of 100 m and a diameter of 160 mm. The spacing between the 2 U-tube legs is 80 mm. The total pipe collector length is 200 m.

The hydronic under-floor heating system is designed according to international standards and manufacturer's guidelines (EN 1264:2011; ISO 11855:2012; Uponor Heating and cooling solutions – Technical guidelines 2008). Each room has a 100 mm thick concrete screed with embedded PE-Xa pipes with outer diameter of 16 mm and inner diameter of 13 mm. They lay 60 mm below the surface of the concrete screed. The spacing between the pipe legs is 300 mm.

The outdoor conditions and solar gains are extracted from the national reference Danish weather file DRY 2013. The building is therefore assumed to be located in an open field around Copenhagen. It is considered that 4 persons are occupying the house according to a fixed weekly schedule. The equipment and people load schedules are based on typical Danish equipment use and people schedule for a residential house (Jensen et al. 2011). A detailed description of the building case study can be found in a DCE technical report (Johra and Heiselberg 2016).

3.2. Modelling of the building systems

A detailed multi-zone numerical model of the building case study is created with the MATLAB-Simulink software. Similarly to the HAM-tools (Kalagasidis et al. 2008), this model calculates heat transfer through building elements with a one-dimensional explicit finite volume method (FVM) formulation comprising a small number of control volumes. This formulation is also known as “Resistance-Capacitance” network (RC network). External walls, internal walls, ceilings and roof elements are subdivided into 5 thermal nodes for the 3 different material layers (external panel, insulation layer, internal panel). Floor elements are subdivided into 9 nodes for the 3 different material layers and the hydronic UFH system (underground layer, insulation layer, UFH concrete screed).

Inside each thermal zone, the inner surfaces and the indoor air temperature nodes are connected within a star network configuration with constant mixed convection/radiation surface thermal resistance coefficients. Thermal bridges, ventilation, air infiltration and windows heat losses are modelled using constant thermal resistances.

Direct and diffuse solar radiation and long-wave radiation to the sky are calculated for external surfaces as a function of the local weather conditions and the surface orientation. The internal loads and the indoor solar gains are distributed over the air nodes and the internal surfaces according to constant ratio factors. 70% of the internal gains are modelled as purely convective and the remaining 30% are distributed over all the indoor surfaces according to their surface area. Concerning

the internal solar loads, 15% are modelled to go directly to the air node, 55% to go to the floor and 30% to go to the vertical walls of the thermal zone.

The hydronic UFH system and the horizontal GSHE are modelled similarly as horizontal heat exchangers embedded in a multilayer slab by coupling a “plug flow” model in a pipe with the ε -NTU method. The plug flow principle model accounts for the dynamics of the fluid pushed into the pipes when the flow rate is changing over time (TRNSYS 17 – Mathematical Reference). The ε -NTU method collapses the three-dimensional domain of a horizontal heat exchanger into a one-dimensional Resistance-Capacitance star network. The effectiveness of the heat exchanger is calculated by taking into account the equivalent interaction thermal resistance in the layer of the slab where the hydronic pipes are laid (ISO 11855:2012; Scarpa et al. 2009). The vertical borehole GSHE is simulated by coupling two plug flow pipe models in a triangular thermal RC network representing the complex thermal interaction between the U-pipe of the heat exchanger, the grout of the borehole and the surrounding soil domain (Diersch et al. 2011). The ground around the GSHE systems is simulated as a one-dimensional finite domain in a MATLAB state space function. Boundary conditions are defined by the weather condition and the undisturbed deep ground constant temperature. The constant deep ground temperature is set to 9.4 °C at a depth of 30 m for the horizontal GSHE, and 10.1 °C at a depth of 100 m for the vertical borehole GSHE. All the fluid properties of the brine, the convective heat transfer coefficient in the pipes and the pressure losses are calculated according to brine composition, fluid velocity, temperature and Reynolds number.

The 10 different thermal zones of the dwelling (9 rooms and an attic) are connected together in order to form the house case study multi-zone model. No direct air exchange between thermal zones is considered. Because the heat equation is solved here with an explicit scheme, the simulation time step size is set constant to 60 seconds to avoid numerical instability. This time step size is fine enough to satisfy the stability criteria (see **Eq. (3)**) in every finite control volume of the model.

$$\Delta t \leq \frac{1}{2} \times \frac{\rho \cdot C_p \cdot \Delta x^2}{k} \quad (3)$$

Where Δt is the time step size and Δx , k , ρ , and C_p are the thickness, the thermal conductivity, the density and the specific heat capacity of a finite control volume.

The building numerical model has been validated with a BESTEST procedure. In addition, each sub-component of the building model has been validated against commercial software (COMSOL Multiphysics and BSim) or experimental test data.

Validation test results and detailed description of the building model and its sub-components can be found in a DCE technical report (Johra and Heiselberg 2016).

4. Integration of the magnetocaloric heat pump in the building

In order to achieve a high COP with heat pump systems, it is crucial to minimize the temperature span between the heat source and the heat sink. For that purpose, it is recommended to use ground source heat exchangers such as horizontal collectors or vertical boreholes in countries like Denmark. Although they have a significant investment cost, large amounts of thermal energy can be extracted from them at a higher and more stable temperature than outdoor air source systems, especially during the winter periods (Den lille blå om Varmepumper 2011). Concerning heat emitters, radiant under-floor heating systems offer a large surface of exchange with the indoor environment. They can therefore deliver an appreciable heating power with low inlet fluid temperature and keep the indoor air temperature lower than with radiator systems for an equivalent thermal comfort (Le Dréau 2014). As mentioned before, the magnetocaloric effect of a MCM is maximum around its Curie temperature. For some of these materials, the Curie temperature can be finely adjusted to match the temperatures inside the regenerator (Basso et al. 2015), taking into account its inherent temperature gradient (graded regenerator) (Smith et al. 2012). Consequently, the MCHP is designed for fixed optimum inlet and outlet temperatures which increases the importance of using a ground heat source which can provide a stable inlet fluid temperature.

The principle of the AMR technology is to circulate the same fluid from one side of the system to the other. It is therefore possible to integrate the MCHP in a single hydronic loop without intermediate heat exchangers between the different sections of the circuit (see **Fig. 6**). Because this heat pump can provide fluid flow rates and temperatures which are directly usable in a UFH system, a storage hot water tank is not needed. Such implementation has the potential of decreasing the effective temperature span between the heat source and the heat sink, but also simplifies the piping network and can therefore reduce the total installation costs and storage hot water tank heat losses. As mentioned before, the heat transfer fluid is circulated through the ground source loop, the UFH loops and the regenerators with only one circulation pump which can run at volume flow rates ranging from 100 L/h up to 2100 L/h with a net positive suction head ranging from 20 to 41 kPa (GRUNDFOS Data Booklet 2013).

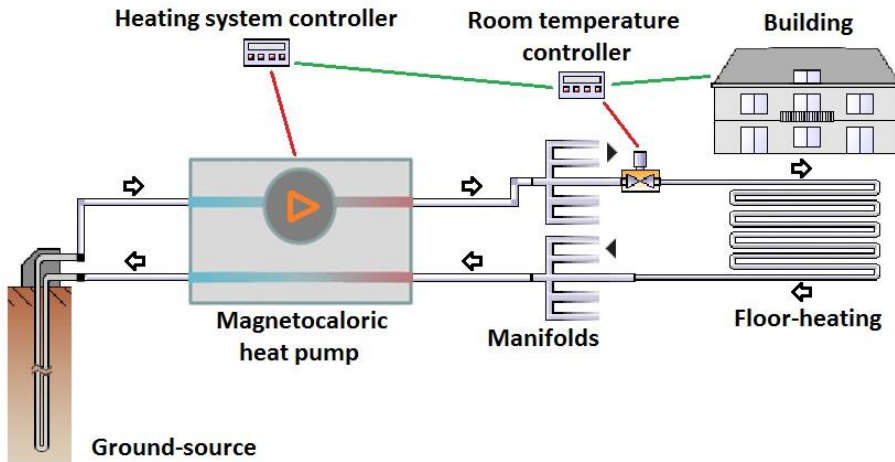


Fig. 6 Integration of a magnetocaloric heat pump in single hydronic loop with ground source and under-floor heating system

The control of the MCHP in this case study is based on a simple volume flow rate regulation. Each of the 9 UFH hydronic loops of the house is equipped with a valve regulated by an ON/OFF controller connected to a room temperature sensor. If the room temperature is above the temperature set point of 22 °C, the valve of the corresponding UFH loop is closed. If the room temperature drops below the temperature set point, the valve is fully open to provide a nominal fluid volume flow of 220 L/h. The speed of the circulation pump and the total heat pump flow rate are varied accordingly. If all the UFH loop valves are closed, the circulation pump and the MCHP are turned off.

In addition, this heat pump device can operate at different rotation frequencies from 0.5 Hz up to 2 Hz. This allows additional control capabilities for optimizing the COP in function of the fluid flow rate.

5. Results

All the results presented hereafter are calculated for a four-month heating period from the 1st of January to the 30th of April under Danish weather conditions (Danish Design Reference Year DRY 2013).

The COP is a common performance assessment index used for heat pump and refrigeration systems. Two different COPs are defined here to study the efficiency of the MCHP. The COP_{AMR} is calculated with the useful heating power $Q_{heating}$ delivered by the heat pump and only considering the work due to the AMR internal

operation: regenerator hydraulic pressure losses $W_{pressureloss}$ and magnetic work $W_{magnetic}$. This calculation is similar to considering that the device is working with a perfect motor and a perfect pump. The COP_{system} is calculated with the heating power of the heat pump and considering all the work power which is necessary to operate the building heating system: circulation pump work W_{pump} ($W_{pressureloss}$ including the losses due to inefficiency), MCHP motor work W_{motor} ($W_{magnetic}$ including the losses due to inefficiency) and MCHP valves work W_{valves} . The heat losses through the heat distribution piping network of the house are not taking into account because they are included in the total heating output of the UFH system (Georges et al. 2017).

$$COP_{AMR} = \frac{Q_{heating}}{W_{pressureloss} + W_{magnetic}} \quad (4)$$

$$COP_{system} = \frac{Q_{heating}}{W_{pump} + W_{motor} + W_{valves}} \quad (5)$$

Another commonly used performance indicator to compare heat pump technologies is the second-law efficiency, noted η_{2nd} . It is defined as the ratio between the COP of a real device and the COP of an ideal reversible device (Carnot heating cycle) operating within the same temperature span between the hot and cold environments (Lozano et al. 2016).

$$\eta_{2nd} = \frac{COP_{system}}{COP_{ideal}} \quad (6)$$

Where COP_{ideal} is the COP of the reversible heat pump system. It is defined according to the hot and cold environment absolute temperatures T_h and T_c (Lozano et al. 2016).

$$COP_{ideal} = \frac{T_h}{T_h - T_c} \quad (7)$$

The hot environment is the house indoor space which has an absolute temperature of 295.15 K. The cold environment is the undisturbed underground soil in Denmark

which is assumed to have an average absolute temperature of 283.15 K. The COP of an ideal reversible heat pump operating in these conditions is thus 24.6.

Initial tests are performed with the MCHP heating up only one thermal zone in the house case study: the living room. The total nominal flow of the heat pump is kept constant during the 4 months of the heating test period. Figure 7, Figure 8 and Figure 9 present the results of 150 simulations where the average heating production, system power usage, seasonal COPs and temperature span have been calculated for different constant total nominal heat pump fluid flows, 3 different AMR rotation frequencies and 2 kinds of ground loop heat source (horizontal GSHE and vertical borehole GSHE). It has to be noted that for low nominal volume flow rates, the heat pump does not provide enough heating power output to warm the living room up to the set point temperature of 22 °C. In these cases, the MCHP runs continuously during the whole test period and the indoor temperature is always below the target set point.

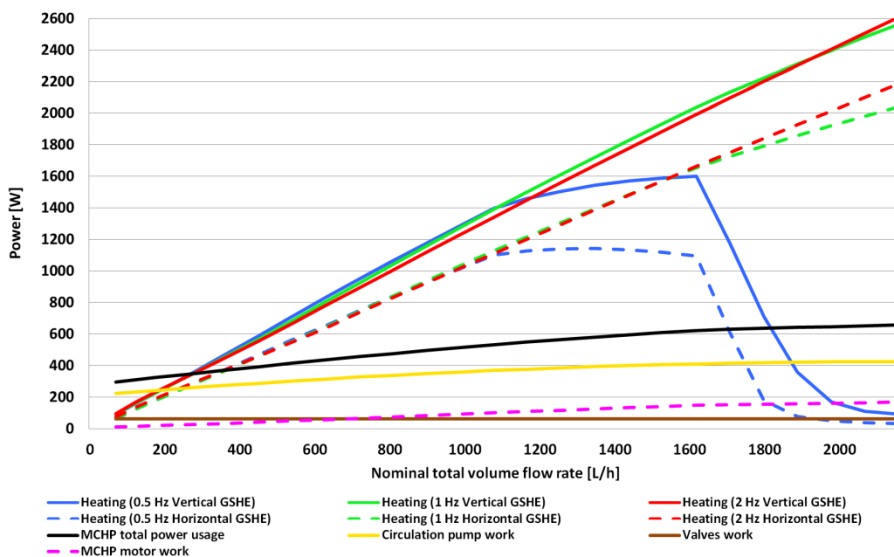


Fig. 7 Heating power production and power usage of the magnetocaloric heat pump as function of fluid volume flow rate

One can see on **Fig. 7** that the MCHP heating production and its power usage increase rather linearly with the total fluid flow. However, for the lowest operation frequency of 0.5 Hz, the performances of the MCHP drop for fluid mass flow rates above 1600 L/h. In addition, when the heat pump is connected to a horizontal GSHE, its heating capacity is significantly diminished because of the lower fluid inlet temperature provided by this ground loop heat source. One can notice that the major part of the MCHP power usage is due to the pump work.

If the MCHP system is coupled with a vertical borehole GSHE, it can deliver up to 2600 W of heating power when operating at a maximum fluid flow rate of 2100 L/h and with a rotation frequency of 1 Hz. In this case, the average seasonal system COP is 3.93 (10% and 90% percentile of the system COP are 3.72 and 4.12 respectively) for an average temperature span between the cold and hot side of the AMR of 19.9 K. If the MCHP system is coupled with a horizontal GSHE, it can deliver up to 2200 W of heating power when operating at a maximum fluid flow rate of 2100 L/h and with a rotation frequency of 2 Hz. In this case, the average seasonal system COP is 3.13 (10% and 90% percentile of the system COP are 2.92 and 3.34 respectively) for an average temperature span of 25.5 K.

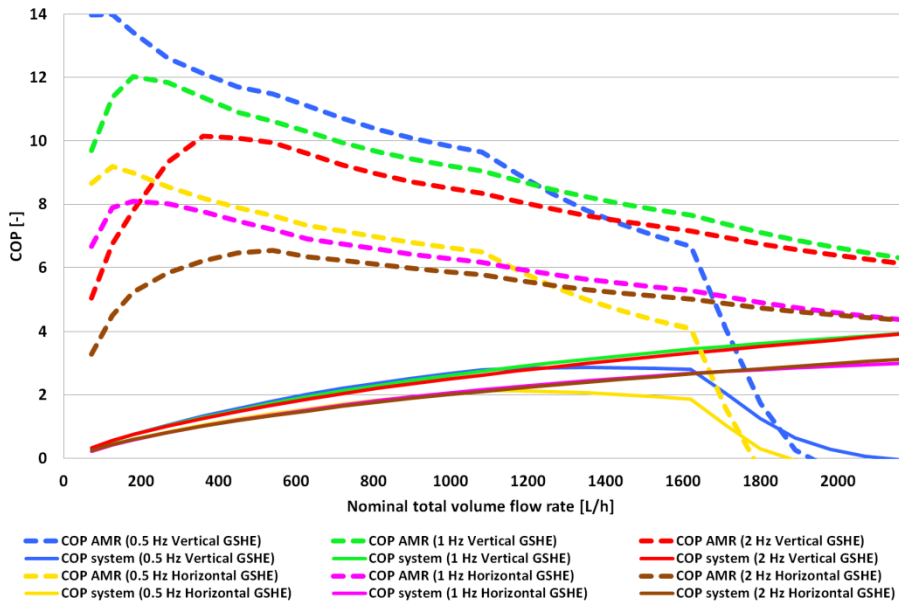


Fig. 8 COP of the magnetocaloric heat pump and the entire heating system as function of fluid volume flow rate

The **Fig. 8** illustrates the change of the average seasonal COP_{AMR} and COP_{system} in function of the total nominal mass flow rate. Concerning solely the AMR, its performance (COP_{AMR}) is maximum for low fluid flow rates and low operation frequency. However, even if the COP_{AMR} is significant, the heating power output is very limited at low flow rates while the energy usage of the circulation pump remains high. Therefore, the performance of the overall heating system (COP_{system}) is maximum at high fluid flow rates with operation frequency of 1 or 2 Hz. Here again, one can see that vertical borehole GSHE allows better MCHP performance compared to the horizontal GSHE. These results can be compared to conventional

vapour-compression ground source heat pumps which have COPs typically ranging from 3 to 5 (Self et al. 2013).

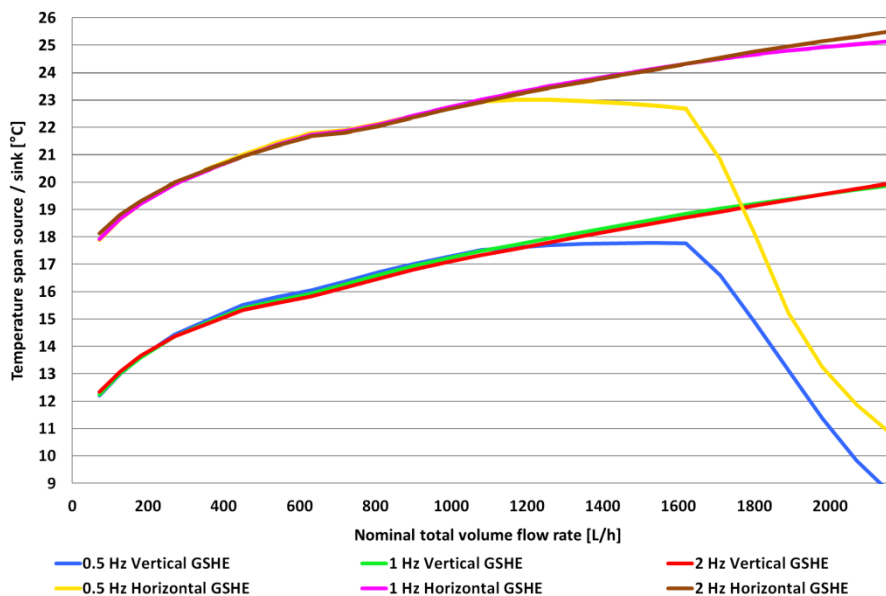


Fig. 9 Average temperature span between the cold and hot side of the AMR as function of fluid volume flow rate

Fig. 9 shows the variation of the average temperature span between the cold and hot side of the AMR as a function of the nominal total volume flow rate of the MCHP. One can see that the temperature span of the horizontal GSHE configuration is significantly larger than the one of the vertical borehole GSHE configuration. This is due to the fact that the vertical borehole GSHE can supply a significantly warmer input fluid to the MCHP compared to the horizontal GSHE.

In a second case study, the MCHP is tested to heat the whole house. According to the aforementioned results, the operation frequency is kept constant at 1 Hz as it shows the best performance for the considered range of fluid flow rates. **Fig. 10** presents the temperature of the different building systems as function of time during the four-month tests of heating up the house case study with the MCHP. The first test has a vertical borehole GSHE as the heat source, and the second test has a horizontal GSHE as the heat source. One can see that the heating system always manages to keep the operative temperature of the house above the set point of 22 °C. The average temperature and maximum temperature inlet to the under-floor heating system are 25.42 °C and 28.50 °C respectively. The average temperature outlet of the vertical borehole GSHE is 8.17 °C (10% and 90% percentile of the temperature outlet are 6.89 °C and 9.30 °C respectively). The average temperature outlet of the

horizontal GSHE is 2.42 °C (10% and 90% percentile of the temperature outlet are 0.93 °C and 4.51 °C respectively). The average total volume flow rate of the system coupled with the vertical borehole GSHE is 689 L/h (10% and 90% percentile of the total volume flow rate are 222 L/h and 1333 L/h respectively). The average total volume flow rate of the system coupled with the horizontal GSHE is 775 L/h (10% and 90% percentile of the total volume flow rate are 222 L/h and 1555 L/h respectively). One can see that the vertical borehole GSHE is a more stable heat source which can provide higher brine outlet temperature to the heat pump compared to the horizontal GSHE. The average temperature span between the heat source and the heat sink is 17.25 °C and 23.00 °C for the vertical borehole GSHE and the horizontal GSHE respectively.

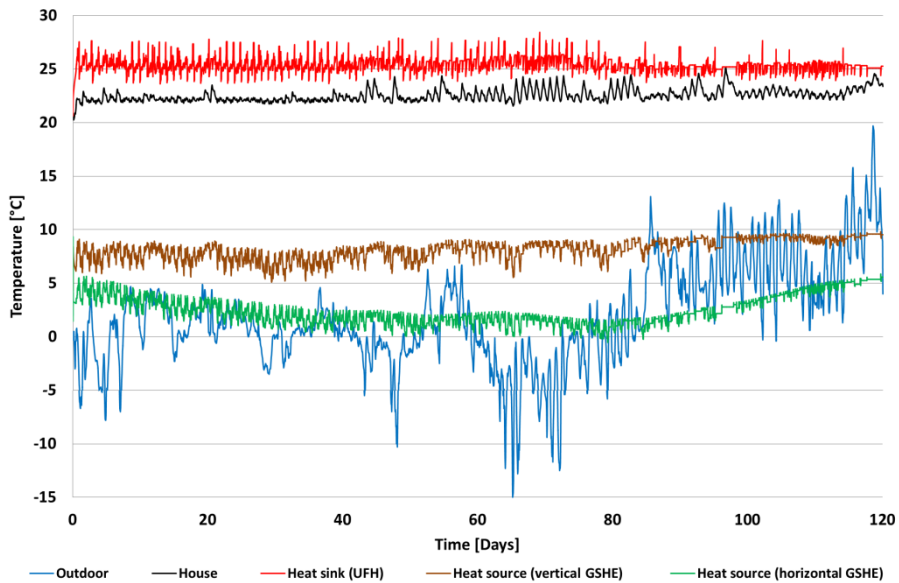


Fig. 10 Temperatures of the building system as function of time during the four-month test of heating up a house with a magnetocaloric heat pump

The **Fig. 11** shows the evolution of the COPs during the four month heating test period. All these results are daily running average. For the vertical borehole GSHE case, the seasonal average COP_{AMR} is 9.19 (10% and 90% percentile of the COP_{AMR} are 7.69 and 10.60 respectively) and the seasonal average COP_{system} is 1.84 (10% and 90% percentile of the COP_{system} are 0.84 and 2.96 respectively). For the horizontal GSHE case, the seasonal average COP_{AMR} is 6.39 (10% and 90% percentile of the COP_{AMR} are 5.31 and 7.48 respectively) and the seasonal average

COP_{system} is 1.59 (10% and 90% percentile of the COP_{system} are 0.67 and 2.55 respectively). Once again, one can see that the higher heat source temperature provided by the vertical borehole GSHE allows better operation performances of the MCHP compared to the horizontal GSHE. However, it is noticeable that the total system COP is rather low compared to the results of the single room test. This is due to the fact that the MCHP does not often run at maximum fluid flow rate where the coefficient of performance of the device is greater.

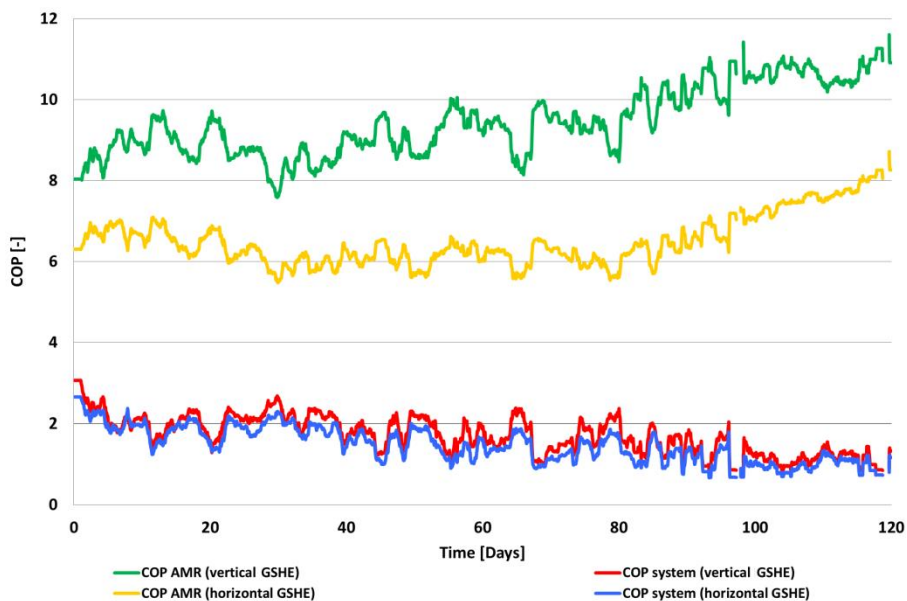


Fig. 11 Daily average COPs of the magnetocaloric heat pump as function of time during the four-month heating test period

Finally, **Fig. 12** presents the daily average second-law efficiency of the MCHP system as a function of time. The second-law efficiency of a conventional ground source heat pump system with a COP of 3 is also indicated on the figure for comparison. For the vertical borehole GSHE case, the seasonal average second-law efficiency is 6.99% (10% and 90% percentile of the second-law efficiency are 4.47% and 9.31% respectively). For the horizontal GSHE case, the seasonal average second-law efficiency is 6.02% (10% and 90% percentile of the second-law efficiency are 3.74% and 8.24% respectively).

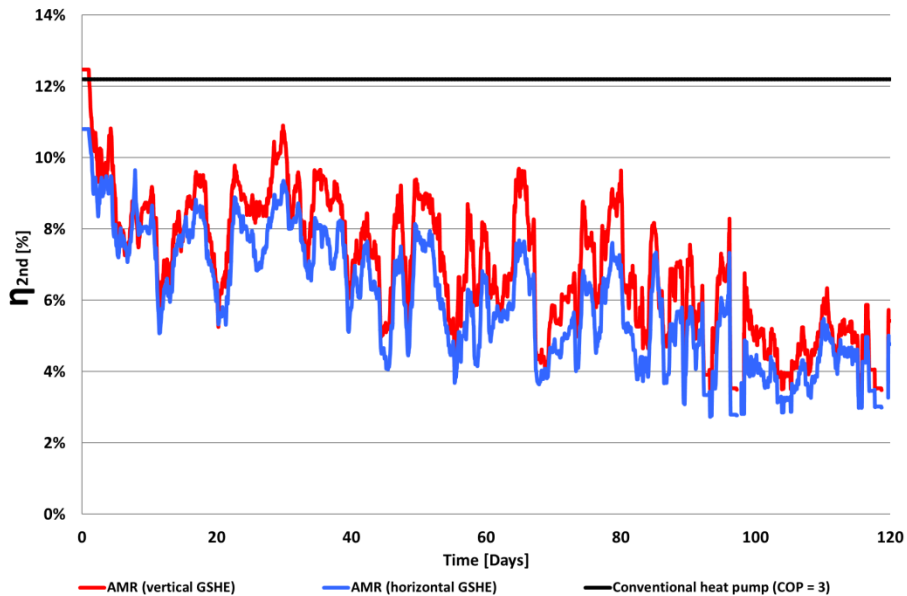


Fig. 12 Daily average second-law efficiency of the magnetocaloric heat pump as function of time during the four-month heating test period

6. Conclusions

This article demonstrates for the first time the possibility to utilize a magnetocaloric heat pump for heating an entire building. This innovative heating device has been modelled as multi-dimensional lookup tables derived from a detailed numerical model in order to be tested with dynamic building energy simulations. It has been shown that it can be integrated in a single hydronic loop including a ground source heat exchanger and a radiant under-floor heating system. Such implementation does not require a storage hot water tank or additional circulation pumps or intermediate heat exchangers. At a constant maximum fluid flow rate of 2100 L/h, this magnetocaloric heat pump, when coupled to a vertical borehole heat source, can deliver up to 2600 W of heating power with an appreciable average seasonal system COP of 3.93. Moreover, the use of a vertical borehole as a heat source allows better performance of the heat pump because it can provide a more stable and higher fluid temperature inlet compared to a horizontal ground source heat exchanger.

However, when the magnetocaloric device is used to heat an entire house with several thermal zones regulated by simple ON/OFF controllers, the heating system often operates at part-load capacity which leads to low COPs. Therefore, the magnetocaloric heat pump average seasonal system COP implemented in a low-energy house under Danish weather conditions is 1.84 and 1.59 for a vertical borehole GSHE heat source and a horizontal GSHE heat source respectively.

Advanced control strategies used in demand side management for building energy flexibility such as indoor temperature set point modulation, could be an interesting solution to improve the operation performance of this magnetocaloric heat pump. This question will be addressed in further research.

Acknowledgements

This work was financed by the ENOVHEAT project, which is funded by Innovation Fund Denmark (contract no 12-132673).

References

- Apra C, Greco A, Maiorino A, Masselli C (2016). The energy performances of a rotary permanent magnet magnetic refrigerator. *International Journal of Refrigeration* 61: 1–11.
- Bahl CRH (2015). EnovHeat project summary: development of efficient novel magnetocaloric heat pumps. Available at <http://www.enovheat.dk/Research/ProjectSummary>. Accessed 30 Aug 2017.
- Barclay JA (1982). Use of a ferrofluid as a heat exchange fluid in a magnetic refrigerator. *Journal of Applied Physics* 53, 4: 2887–2894.
- Basso V, K upferling M, Curcio C, Bennati C, Barzca A, Katter M, Bratko M, Lovell E, Turcaud J, Cohen L (2015). Specific heat and entropy change at the first order phase transition of La(Fe-Mn-Si)₁₃-H compounds. *Journal of Applied Physics* 118(5): 053907.
- Dall’Olio S, Lei T, Engelbrecht K, Bahl CRH (2017). The effect of tapering on a magnetocaloric regenerator bed. *International Journal of Refrigeration*, 84: 300–308.
- Diersch HJG, Bauer D, Heidemann W, R ahaak W, Sch atzl P (2011). Finite element modeling of borehole heat exchanger systems - Part 1. Fundamentals. *Computers and Geosciences*, 37: 1122–1135.
- Engelbrecht K (2008). A Numerical Model of an Active Magnetic Regenerator Refrigerator with Experimental Validation. PhD Thesis, University of Wisconsin, Madison, USA.
- Engelbrecht K, Eriksen D, Bahl CRH, Bj ork R, Geyti J, Lozano JA, Nielsen KK, Saxild F, Smith A, Pryds N (2012). Experimental results for a novel rotary active magnetic regenerator. *International Journal of Refrigeration* 35: 1498–1505.

Engelbrecht K, Tušek J, Nielsen KK, Kitanovski A, Bahl CRH, Poredoš A (2013). Improved modelling of a parallel plate active magnetic regenerator. *Journal of Physics D: Applied Physics* 46(25): 255002.

Eriksen D, Engelbrecht K, Bahl CRH, Bjørk R (2016). Exploring the efficiency potential for an active magnetic regenerator. *Science and Technology for the Built Environment* 22: 527–533.

European Committee for Standardization (2011). EN 1264:2011 - Water based surface embedded heating and cooling systems. Brussels: European Committee for Standardization.

Georges L, Iwanek T, Thalfeldt M (2017). Energy efficiency of hydronic space-heating distribution systems in super-insulated residential buildings. In: Proceedings of the 15th IBPSA Building Simulation Conference (BS2017), San Francisco, USA, pp.1852–1861.

Grundfos Product Center (2013). GRUNDFOS Data Booklet - CR1-9 A-FGJA-E-HQQE 3x230/400 50Hz - Grundfos Pump 96478872. Available at <http://product-selection.grundfos.com/product-detail.product-detail.html?lang=ENU&productnumber=96478872&productrange=gma&qcid=228594986>. Accessed 30 Aug 2017.

Insinga AR (2016). Optimising magnetostatic assemblies. PhD thesis, Technical University of Denmark, Denmark.

Insinga AR, Bjørk R, Smith A (2016). Optimally segmented permanent magnet structures. *IEEE Transactions on Magnetics* 52(12): 7210306.

ISO (2012). ISO 11855:2012 - Building environment design. Design, dimensioning, installation and control of embedded radiant heating and cooling systems. Geneva: International Organization for Standardization.

Jacobs S, Auringer J, Boeder A, Chell J, Komorowski L, Leonard J, Russek S, Zimm C (2014). The performance of a large-scale rotary magnetic refrigerator. *International Journal of Refrigeration* 37: 84–91.

Dansk Energi (2011). Den lille blå om Varmepumper. Jensen JB (Dansk Energi), Hvenegaard CM (Teknologisk Institut), Pedersen SV (Teknologisk Institut), Lindholm D (Dansk Energi). (in Danish).

Jensen RL, Nørgaard J, Daniels O, Justesen RO (2011). Person-og forbrugsprofiler: bygningsintegreret energiforsyning (DCE Technical Reports; Nr. 69). Aalborg University, Denmark.

Johra H, Heiselberg P (2016). Description and Validation of a MATLAB-Simulink Single Family House Energy Model with Furniture and Phase Change Materials (DCE Technical Reports; No. 187). Aalborg University, Denmark.

Kalagasidis AS, Rode C, Woloszyn M (2008). HAM-Tools, a whole building simulation tool in Annex 41. In: Proceedings of the IEA ECBCS Annex 41 Closing Seminar, Copenhagen, Denmark, pp. 21–35.

Kitanovski A, Tusek J, Tomc U, Plaznik U, Ozbolt M, Poredos A (2015). Magnetocaloric Energy Conversion: From Theory to Applications. New York: Springer International Publisher.

Larsen TS, Brunsgaard C (2010). Komfort Husene: erfaringer, viden og inspiration. Saint-Gobain Isover a/s, Denmark.

Le Dréau J (2014). Energy flow and thermal comfort in buildings - comparison of radiant and air-based heating and cooling system. PhD thesis, Aalborg University, Denmark.

Lei T, Engelbrecht K, Nielsen KK, Veje TC (2017). Study of the geometries of active magnetic regenerators for room temperature magnetocaloric refrigeration. *Applied Thermal Engineering*, 111: 1232–1243.

Lei T, Navickaite K, Engelbrecht K, Barcza A, Vieyra H, Nielsen KK, Bahl CRH (2018). Passive characterization and active testing of epoxy bonded regenerators for room temperature magnetic refrigeration. *Applied Thermal Engineering*, 128: 10–19.

Lozano JA, Capovilla MS, Trevizoli PV, Engelbrecht K, Bahl CRH, Barbosa Jr JR (2016). Development of a novel rotary magnetic regenerator. *International Journal of Refrigeration*, 68: 187–197.

Mugica I, Roy S, Poncet S, Bouchard J, Nesreddine H (2017). Exergy analysis of a parallel-plate active magnetic regenerator with nanofluids. *Entropy* 19(9): 464.

Neves Bez H, Bahl CRH, Nielsen KK, Smith A (2016). Magnetocaloric materials and first order phase transitions. PhD thesis, Technical University of Denmark, Denmark.

Nielsen KK, Nellis GF, Klein SA (2013). Numerical modeling of the impact of regenerator housing on the determination of Nusselt numbers. *International Journal of Heat and Mass Transfer*, 65: 552–560.

Okamura T, Hirano N (2013). Improvement of the performance of a room temperature magnetic refrigerator using Gd-alloy. *Journal of the Japan Society of Applied Electromagnetics and Mechanics* 21: 10–4.

Pecharsky VK, Cui J, Johnson DD (2016). (Magneto)caloric refrigeration: is there light at the end of the tunnel? *Philosophical Transaction of the Royal Society A*, 374: 20150305.

RETScreen International (2005). Ground-Source Heat Pump Project Analysis. Canada, Minister of Natural Resources Canada.

Scarpa M, Grau K, Olesen BW (2009). Development and validation of a versatile method for the calculation of heat transfer in water-based radiant systems. In: Proceedings of the 11th IBPSA Building Simulation Conference, Glasgow, USA, pp. 27–30.

Self SJ, Reddy BV, Rosen MA (2013). Geothermal heat pump systems: Status review and comparison with other heating options. *Applied Energy*, 101: 341–348.

Smith A, Bahl CRH, Bjork R, Engelbrecht K, Nielsen KK, Pryds N (2012). Material challenges for high performance magnetocaloric refrigeration devices. *Advanced Energy Materials*, 2: 1288–1318.

The Danish Ministry of Economic (2010). Building Regulations. Business Affairs Enterprise, and Construction Authority. Available at http://byggningsreglementet.dk/file/155699/BR10_ENGLISH.pdf. Accessed 30 Aug 2017.

Trevizoli PV, Nakashima AT, Peixer GF, Barbosa Jr JR (2017). Performance assessment of different porous matrix geometries for active magnetic regenerators. *Applied Energy*, 187: 847– 861.

TRNSYS (2012). TRNSYS 17 - Mathematical Reference. Type 31: Pipe Or Duct, University of Wisconsin-Madison Solar Energy Laboratory, TRANSSOLAR Energietechnik GmbH, CSTB, TESS, pp.186–188.

Uponor GmbH (2008). Heating and cooling solutions - Technical guidelines. Uponor GmbH, Germany.

Uponor GmbH (2012). Ground Energy Technical Information. Uponor GmbH, Germany.

Verlag des Vereins Deutscher Ingenieure (2001). VDI 4640:2001, Thermal use of the underground-Ground source heat pump systems. Verlag des Vereins Deutscher Ingenieure, Germany.

Zimm C, Jastrab A, Sternberg V, Pecharsky V, Gschneidner Jr K, Osborne M, Anderson I (1998). Description and performance of a near room temperature magnetic refrigerator. In: Kittel P (ed), *Advances in Cryogenic Engineering*, Vol 43. Boston, MA, USA: Springer, pp. 1759–1766.

Appendix D. Paper IV

Johra, H., Heiselberg, P., & Le Dréau, J. (Under review). Influence of envelope, structural thermal mass and indoor content on the building heating energy flexibility. *Energy and Buildings*.

Reprinted by permission from Elsevier.

Energy and Buildings

(Under review)

Influence of envelope, structural thermal mass and indoor content on the building heating energy flexibility

Hicham Johra ^{a, *}, Per Heiselberg ^a, Jérôme Le Dréau ^b^a *Aalborg University, Division of Architectural Engineering, Department of Civil Engineering, Thomas Manns Vej 23, DK-9220 Aalborg Øst, Denmark*^b *LaSIE UMR CNRS 7356, La Rochelle University, FR-17 000 La Rochelle, France*** Corresponding author. Tel.: +45 9940 7234. E-mail address: hj@civil.aau.dk (H. Johra).*

Abstract

This article presents the results of a numerical study investigating the influence on the heating energy flexibility of a Danish house of different thermal mass types located in the building envelope or in the indoor space. The heating energy flexibility is defined here as the dwelling's ability to shift heating use in time. A heat storage strategy with indoor temperature set point modulation based on a price signal is implemented in the building model. The impact of additional indoor thermal mass elements (indoor items/furniture, PCM integrated in furnishing, PCM wallboards) is then compared to the main building parameters (envelope insulation level, structural thermal mass, heating system type). It is shown that the insulation level of the envelope is the building's characteristic with the largest effect on the heating energy flexibility. To a lesser extent, the total thermal inertia also presents a significant influence. Moreover, it is found that indoor items and furniture must not be ignored in the case of dwellings with low structural thermal mass. Finally, phase change materials integrated in wallboards or in furnishing elements can increase substantially the time constant and heating energy flexibility of a house.

Keywords: *Building energy flexibility; demand-side management; space heating; indoor thermal mass; envelope thermal inertia; phase change material; furniture.*

1. Introduction

Most of the current national energy development strategies involve a large expansion of renewable energy sources (RES). A significant deployment of wind and photovoltaic power is planned in numerous European countries [1]. In Denmark, for example, the share of wind power is expected to reach 50% on an annual basis in 2020. In 2050, Denmark aims at covering its entire energy needs with RES [2].

The major drawback of RES is that their production is intermittent and difficult to modulate. The important expansion of these intermittent RES may thus induce a serious mismatch between instantaneous energy use and production. Consequently, the stability of electrical grids can be significantly compromised. In the recent years, increasing efforts have been dedicated to develop demand-side management technologies allowing a modulation of the end-users' energy need and consumption. These so-called "energy flexible" solutions can counter-balance the irregularities of RES production in an integrated Smart Grid system. It improves the controllability of the energy grids and therefore eases the integration of RES [3].

In many countries, buildings hold the largest share of the total energy needs. Moreover, 75% of the buildings energy use in Europe is dedicated to indoor space heating [4]. To a certain extent, the energy used for the conditioning of the indoor environment can be shifted in time without jeopardizing indoor comfort. To that matter, the thermal heat capacity of the buildings' envelope and structural elements can present large potential for energy storage. Therefore the building sector should not be perceived as a passive energy end-user. On the contrary, it can be an important interactive actor, modulating its energy utilisation to facilitate the management of energy grids. The passive thermal energy storage (TES) in the indoor environment of buildings can be a cost effective key component for the management strategies of a smart energy grid system. A research study indicated that this clever usage of the building thermal inertia allows a larger reduction of excess electricity production and fuel consumption with a lower total cost compared to the heat accumulation water tanks solution [5]. The building set point indoor temperature can be increased to accumulate heat when the electricity is available and cheap and can be decreased when the power production is too low. However, the operative temperature should always be kept within the limits of the occupants' thermal comfort.

Some previous studies investigated the influence of different building parameters on the ability to modulate heating needs. In the case of TES in the indoor environment, the available structural thermal mass defines the maximum storage capacity of the system. The larger the activated thermal mass, the more heat energy can be stored during off-peak periods and partly recovered during peak periods [6] [7].

The effectiveness of the storage mainly depends on the envelope performance: level of insulation and air tightness. The higher the insulation level is, the better the building energy flexibility potential is [8]. Poorly insulated buildings can only sustain short term load shifting. In winter, after a heat accumulation period, they can

maintain thermal comfort without any heating need for a maximum of 1 – 5 hours whereas high performance envelope buildings can turn off their heaters for more than 24 hours. Consequently, a large amount of thermal energy can be shifted over a short period of time for low-insulation buildings while the well-insulated ones can shift a small quantity of energy over a long period of time [9].

Moreover, it was found that the heat emitter type has a significant influence on the flexibility potential. On the one hand, radiator terminals have mainly convective heat emission which results in a quick activation of the low capacitive indoor air. Therefore, the ventilation and infiltration heat losses are increased and the heat storage in the structural heavy building elements is limited. On the other hand, radiant emitters such as under-floor heating (UFH) or thermally activated building systems (TABS) activate directly the high thermal capacity of the floor elements. The time constant of the building increases and the indoor air temperature is lower. Consequently, the ventilation heat losses are reduced and the effective heat storage capacity is improved [6] [9] [10] [11].

Phase change materials (PCMs) offer an appreciable energy storage density within narrow temperature span. Latent heat thermal energy storage (LHTES) can be integrated in the inner surfaces of the indoor environment in order to increase the heat storage capacity of light structure buildings. Some researchers demonstrated the benefit of PCM wallboards and PCM UFH for space heating load shifting with set point temperature modulation control [12] [13]. Furniture pieces present a large surface area exposed to the indoor environment. It can also be used for the integration of PCMs and thus extend the applicability of the TES strategy [14].

Even if regulations tend to improve the energy efficiency of buildings, the heating demand remains dominating in cold winter countries. In Denmark, for example, 25% of the annual national energy use is dedicated to heating up buildings [15]. Moreover, single family houses represent 60% of the heated area of Danish residential buildings [16]. This paper will thus focus on the capacity of single family dwellings to shift in time their heating energy use by the mean of set point temperature modulation under Danish weather conditions. The current numerical study aims at exploring further the influence the building's structural thermal inertia and different types of additional indoor thermal mass elements on the energy flexibility potential of houses. Two other building parameters are also investigated; namely, the envelope performance level and the type of heating system.

Firstly, the methodologies for calculation of the energy flexibility factor and the building thermal inertia are explained. The different study cases and the numerical building model and its sub-components are then presented in details. A discussion follows about the results of this numerical investigation, including a parametric sensitivity analysis. Finally, a conclusion and suggestions for further research close the article.

2. Methodology

2.1. Definition of the building energy flexibility

With the recent paradigm shift in the building energy research sector from energy efficiency to demand-side management, several different energy flexibility indicators have been created. A review of these different metrics has been published by Rui et al. [19]. However, there is presently no scientific agreement about a clear definition of what is the “building energy flexibility”. Consequently, there is no standard way to assess it. The on-going IEA EBC Annex Project 67 [17] [18] is aiming to tackle these two problems by providing guidelines and increasing knowledge on the building energy flexibility concepts.

In this study, the approach is similar to the one of a recent publication by Le Dréau et al. [9]. The energy flexibility is defined as the ability for the building to minimize the heating energy usage during high price periods and maximize it during low price periods. In other words, the building energy flexibility index assesses the capacity to shift in time heating use from high price to low price periods whilst insuring good indoor thermal comfort (see example on **Fig. 1**). The flexibility index is calculated according to equation (1). It represents the change of heating use during medium and high price periods when the energy is accumulated during low price periods compared to a reference scenario without any thermal storage strategy.

$$F = \left[\left(1 - \frac{\%High}{\%High_{ref}} \right) + \left(1 - \frac{\%Medium}{\%Medium_{ref}} \right) \right] \times \frac{100}{2} \quad (1)$$

Where $\%High$ and $\%Medium$ are the percentages of yearly heating energy (relatively to the total yearly heating needs) used during high and medium price periods respectively when the heat storage strategy is operational. Equivalently, $\%High_{ref}$ and $\%Medium_{ref}$ are the percentages of yearly heating energy for the reference scenario (no heat storage strategy). The flexibility index takes the value of zero if the repartition of the energy use is the same as in the reference case. The building did not provide any energy flexibility. The index becomes negative if the share of high and medium price periods is larger than the reference values. In that case, the building is performing worse than the reference scenario in terms of energy flexibility. The flexibility index reaches 50% if the energy share of the medium price period does not change and if all the energy share of the high price period is shifted to the low price period. Similarly, the flexibility index reaches 50% if the energy share of the high price period does not change and if all the energy share of the medium price period is shifted to the low price period. If both the high and the medium price period shares are decreased by half, the flexibility index also takes the value of 50%. If there is no remaining energy usage during the periods of high and medium price, the flexibility index takes the maximum value of 100%. In that situation, the building presents a total energy flexibility.

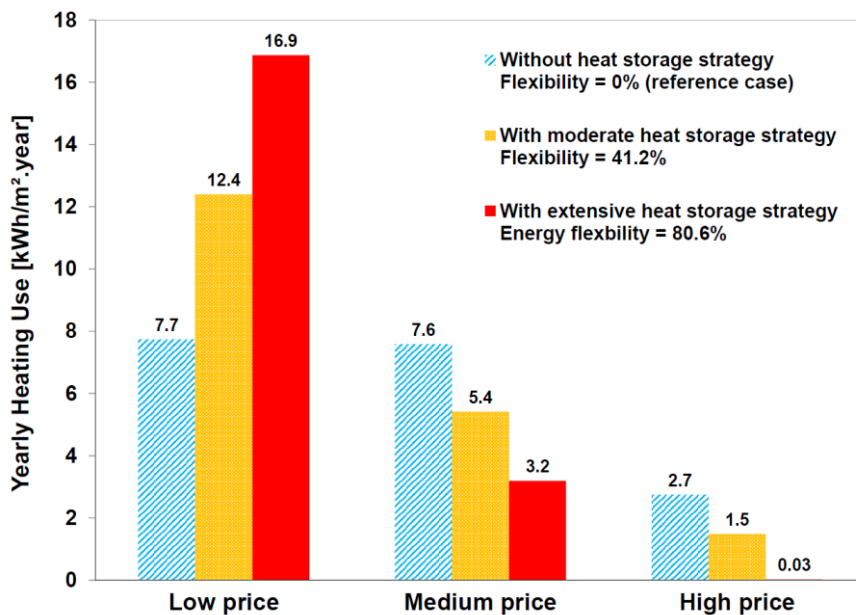


Fig. 1. Variations of yearly heating use for light structure passive house with heat storage strategy (results from the current study).

Several comments can be made about the definition of this flexibility factor. Firstly, it is necessary to obtain a reference energy usage scenario of the building to calculate its flexibility factor. Secondly, the energy price categories are established with an arbitrary definition (see following section) and are based on a specific electricity spot price profile. Different spot price profiles with shorter or longer price periods can have a significant impact on the flexibility factor calculation results. Similarly, the building's local climate and occupants' behaviour can largely influence the building energy flexibility potential [20].

2.2. Evaluation of the thermal inertia of building components with PCM

As this numerical study focuses its attention on the different types of thermal mass elements in dwellings, it is important to assess the thermal inertia of each building component in a consistent way. The “effective thermal inertia” (expressed in $J/K.m^2$ or in $Wh/K.m^2$) is therefore chosen as a common metric for the different construction elements. This metric is not present in the numerical model, but only used to compare the study cases.

The effective thermal inertia of a building element can be evaluated numerically for different variation periods; typically 1 hour (hourly effective thermal inertia) or

24 hours (daily effective thermal inertia) [21]. Because the most important boundary conditions driving the transient response of a building (outdoor temperature, solar radiation, internal load, etc) present a clear daily variation profile, it is very common to characterize the building effective thermal inertia with a 24 hours variation periods, which is the case in the current study.

The total daily effective thermal inertia of a building is calculated as the sum of the daily effective thermal inertia of each of its construction component, including internal partition walls. For the sake of convenience, in the rest of this article, the total daily effective thermal inertia of the building study cases is reported with respect of the gross floor surface area of the house and noted “building thermal inertia” (Wh/K.m²).

The calculation of the daily effective thermal inertia of planar building elements can be performed according to the detailed matrix method described in the standard EN ISO 13786 [21]. This matrix method is based on the quadrupole formalism presented by Maillet et al. [22]. It is straightforward and can easily be implemented in calculation software to evaluate multi-layered material elements. However, it is based on the analytical solution of a simplified thermodynamic system assuming one-dimensional heat transfer through infinitely large planar solids. The dynamic boundary conditions are restricted to following a sinusoidal function. This assumption is nonetheless reasonable as sinusoidal functions are a common way to model indoor and outdoor temperature time variations [23]. For a given surface orientation and exposure, the surface heat transfer coefficient is assumed to be constant. The latter is set according to common values used in building energy calculations [24]. Another limitation of this methodology is that it only considers materials with constant thermal properties. Consequently, it cannot be used for materials in which phase transition occurs.

In order to evaluate the effective thermal inertia of building elements including PCM, a one-dimensional finite volume method (FVM) numerical model of the planar element with PCM layers is developed (see description of the models for building elements with PCM in the following sections). It is then used for the calculation of the total internal energy variations when dynamic boundary conditions are applied. Kuznik et al. [23] employed a similar approach for the optimization of a PCM wallboard. From the point of view of a single side of the planar element, its areal effective thermal inertia κ (J/K.m²) is the capacity to store energy when subjected to periodically varying boundary conditions [21]. It is equal to the amplitude of internal energy variation ΔE (Joule) of a half volume element divided by the amplitude of temperature change $\Delta\theta$ (K) at the boundaries, and the element’s surface area A (m²):

$$\kappa = \frac{\Delta E}{\Delta\theta \times A} \quad (2)$$

Similarly to the matrix method for daily effective thermal inertia calculation, a 24-hour period sinusoidal function is used to define the boundary conditions. The

average boundary conditions temperature is equal to the melting/solidification temperature of the PCM. Once the system reaches periodic steady state, the areal effective thermal inertia is calculated. This numerical method has been validated against the detailed matrix method. It shows very good agreement for non-PCM materials: average deviation of 0.09% in the case of a concrete wall modelled with 100 control volumes (see **Fig. 2**).

One can also see on **Fig. 2** the evolution of the areal effective thermal inertia of PCM wallboard element with a variable thickness and different amplitudes of sinusoidal temperature variation. These results are coherent with previous investigations [23], but no clear maximum effective thermal inertia could be found in the current case. For materials with constant thermal properties, such as concrete, the amplitude of the boundary conditions temperature variation has no effect on the calculation of the effective thermal inertia. But in the case of PCMs, it can induce noticeable discrepancies: average divergence of 4%. This can be explained by the fact that the PCM latent heat and temperature dependent thermal conductivity induce a non-linear correlation between temperature variation and internal energy variation.

In the rest of this study, the detailed matrix method is used for normal (non-PCM) materials and the numerical model method with 5 K temperature variation scheme is used for PCM elements.

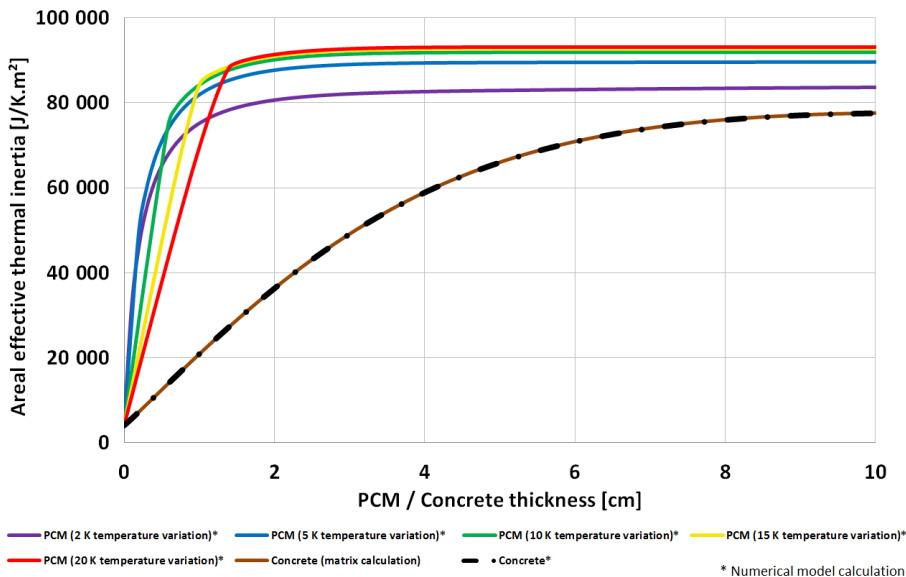


Fig. 2. Areal effective thermal inertia of PCM wallboard and concrete wall as function of the thickness of the construction element.

3. Description of the building study cases

A single-story building with 126 m² of heated space and a typical geometry for dwellings in Denmark is chosen as base case study. As the structural thermal inertia, the additional indoor thermal mass, the envelope performance level and the heating system type are under study in this paper, a total of 144 different versions of the single family house presented on **Fig. 3** are generated with variations of these four building parameters.

Two categories of building envelope performance are considered; namely, low-insulation house from the 80's and high-insulation passive house. The low-insulation case corresponds to a Danish house built in the years 1980 with relatively poor thermal performances: yearly heating need around 160 kWh/m². The high-insulation case corresponds to a "KomfortHus" and has been designed according to the Passive House standard [25]: yearly heating need around 13 kWh/m². For both categories, the insulation thickness and thermal conductivity, the infiltration and ventilation rate, the windows' characteristics and surface area, and the HVAC systems' performance are chosen accordingly.

The material properties of the external and internal surfaces of the house's walls, ceilings and floors are set in order to generate three structural thermal inertia building classes with three different sub-variations in each of them [26]:

- Light-weight structure house; building thermal inertia: 30 Wh/K.m², 40 Wh/K.m² and 45 Wh/K.m².
- Medium-weight structure house; building thermal inertia: 50 Wh/K.m², 60 Wh/K.m² and 70 Wh/K.m².
- Heavy-weight structure house; building thermal inertia: 90 Wh/K.m², 100 Wh/K.m² and 110 Wh/K.m².

In addition, four indoor thermal mass configurations are considered: empty rooms filled with air only; additional indoor items/furniture present in the rooms; PCM integrated in furnishing elements; PCM wallboards placed on the inner surfaces of the house's walls and ceilings.

Finally, two types of heating system are integrated in the different building scenarios: convective radiator (30% of heat output by radiation and 70% by convection) and water-based under floor heating system. The design of the heating systems has been made according to the Danish and international standards and manufacturer's technical guidelines [27] [28] [29] [30] [31] [32]. It is assumed that the primary energy source of the heating system is electricity with the use of a heat pump for example.

The outdoor conditions correspond to the typical weather data in Denmark (Danish Design Reference Year 2013) [33]. The buildings are therefore assumed to be located in an open field around Copenhagen. People load and equipment internal gains are set according to a typical Danish appliance usage and dwellings occupancy schedule for four habitants [34].

The main information about the building cases is summarized in **Table 1**. More details can be found in a technical report [35].

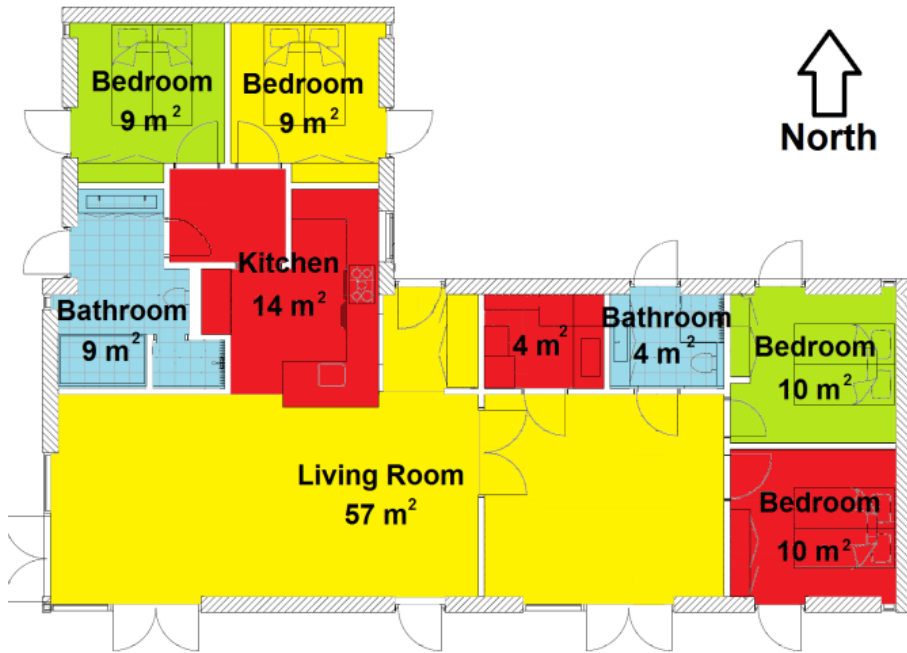


Fig. 3. Plan view of the house case study.

Table 1: Characteristics of the building cases.

Building envelope category	House 1980's			Passive House		
Structural thermal mass category	Light	Medium	Heavy	Light	Medium	Heavy
Effective thermal mass: Cm 24h (Wh/K.m ² gross floor)	30 - 40 - 45	50 - 60 - 70	90 - 100 - 110	30 - 40 - 45	50 - 60 - 70	90 - 100 - 110
Building envelope heat losses (W/K.m ² gross floor)	1.12	1.13	1.13	0.37	0.37	0.37
U-value windows (W/m ² .K)	1.7			0.78		
g-value windows (-)	0.63			0.5		
Ratio windows / gross floor area (m ²)	16.70%			26.90%		
Windows area (m ²)	25.1			40.39		
Air infiltration (ACH)	0.2			0.07		
Ventilation (ACH)	0.4			0.4		
Heat recovery (-)	0			0.8		
Air flow heat losses (W/K)	64			15.6		
Air flow heat losses (W/K.m ² gross floor)	0.43			0.1		
Yearly radiator heating need with set-point at 22°C (kWh/m ² net floor.year)	164	160	155	14	13	12
Maximum radiator heating power (W/m ²)	75			25		
Under-floor heating type	Type G wood floor	Concrete screed	Concrete screed	Type G wood floor	Concrete screed	Concrete screed
Yearly under-floor heating need with set-point at 22 °C (kWh/m ² net floor.year)	160	151	157	15	13.5	13
Nominal water flow per UFH loop (l/h)	170			125		
UFH maximum inlet water temperature (°C)	47	43	43	35	30	30

4. Description of the building numerical model

Within the framework of the EnovHeat project [36], a detailed building energy model of a single family house has been developed. This model is used in the present study. The following section presents succinctly the different elements of the MATLAB - Simulink numerical model and the main results of the validation test procedures. More information about the building model and all validation test results can be found in a detailed technical report [35].

4.1. Multi-zone building model

Similarly to the HAM-tools [38] the heat transfer through planar construction elements is calculated with a one-dimensional finite control volume method (FVM) with explicit formulation comprising a small number of control volumes (commonly named “Resistance-Capacitance network” or “RC network”). External wall, internal wall, ceiling and roof elements are subdivided into 5 thermal nodes along the direction normal to the main plan surface: 2 nodes for the external panels (plaster,

wood, brick or concrete) and 3 nodes for the insulation layer (stone wool). Floor elements (including the soil layer under the house, the expanded polystyrene insulation layer and the concrete or wood slab containing the UFH system) are subdivided into 9 nodes.

For the external surfaces, the direct and diffuse solar radiation and the long-wave radiation to the sky are calculated as a function of the local weather conditions and the surface orientation. Inside each thermal zone, the inner surfaces and the indoor air temperature nodes are connected within a star network configuration with constant mixed convection/radiation surface thermal resistance coefficients. Thermal bridges, ventilation, air infiltration and windows heat losses are modeled using constant thermal resistances. The ventilation heat recovery is activated during the heating season and turned off for an air inlet temperature above 22 °C. In case of over-heating during summer period, natural ventilative cooling is simulated by increasing the ventilation rate without any heat recovery.

70% of the people load and equipment internal heat gains are considered fully convective and therefore applied directly to the air node of the thermal zone. The remaining 30% are modeled as radiative and distributed over all the indoor surfaces with respect to their surface area. Concerning the internal solar loads, 15% are modeled to go directly to the air node, 55% to go to the floor and 30% to go to the vertical walls of the thermal zone [37]. Concerning additional indoor items/furniture present in the indoor space, they can account for a large share of the surfaces exposed to radiations [14]. However, in this model, these elements do not have any real geometrical representation or position in the room and it is assumed that 50% of the radiative share of equipment, people, solar and radiator gains is absorbed by these elements' surfaces.

The 10 different thermal zones of the dwelling (9 rooms and an attic) are connected together to form the house multi-zone model. Doors in between the rooms are considered closed all the time and therefore there is no direct air exchange between the different thermal zones. Because the heat equation is solved with an explicit scheme, the simulation time step size is chosen to be 60 seconds in order to avoid numerical instability.

4.2. Heating systems

Two types of heating emitters are investigated in this study: convective radiator and water-based under floor heating system. The paper focuses on the house heating demand and therefore only considers the emitted energy and not the total energy consumption of the system. Consequently, the primary systems for heat generation are not modeled.

The radiator heating system is modeled with a first order transfer function which has a time constant of 10 minutes [39]. The radiator is regulated by a PI controller and emits 30% of its heat output by radiation and 70% by convection.

The water-based UFH system is modeled as a horizontal heat exchanger embedded in a slab by coupling a “plug flow” model in a pipe with the ϵ -NTU

method. The plug flow principle model accounts for the dynamics of the incompressible brine moving inside a pipe at variable flow rate. At each time step, an additional fluid cell is queued and pushed at the inlet/beginning of the pipe. The size of this new fluid cell is calculated according to the brine volume flow rate and the diameter of the pipe. Because of conservation of the total volume in the pipe, all the other queued fluid cells are pushed forward towards the pipe's outlet. The outlet fluid temperature is calculated as the volume-weighted average temperature of the fluid cells exiting the pipe at each time step. The plug flow model assumes a no-mixing condition between adjacent fluid cells. This is a reasonable assumption as the brine is circulating with a fairly high velocity in the pipes and the temperature difference between each cell remains small. Therefore the fluid cells solely exchange heat by convection with the walls of the surround pipe [40]. The ϵ -NTU method is used to calculate the heat transfer between each fluid cell in the pipe and the walls of the pipe and, consequently, with the rest of the UFH slab. This methodology collapses the complex heat transfers in the three-dimensional domain of a horizontal embedded heat exchanger into a simplified one-dimensional Resistance – Capacitance star network. The effectiveness of the heat exchanger takes into account the equivalent interaction thermal resistance in the layer of the slab where the water pipes are laid [30] [41]. The convective heat transfer coefficient of the brine in the pipe is calculated according to the fluid velocity, Reynolds number, temperature and other temperature dependent thermo-physical properties. The conductive slab surrounding the UFH pipe circuit is sub-divided into 3 thermal nodes. A PI controller regulates the water temperature provided to the UFH distribution manifold.

4.3. Latent heat thermal energy storage

Phase change materials have found interesting applications for TES in buildings. One of the most promising solutions is the integration of PCM in wallboard panels on the internal surfaces of the indoor environment such as walls and ceilings. Moreover, the large surface area of furnishing elements which are exposed to the indoor environment is also a good candidate for the integration of PCMs [14].

Many LHTES numerical models for building systems are using an apparent heat capacity function to account for the latent heat of the phase transition. However, this approach does not really represent the physics of the PCM but only its apparent behaviour with regards of temperature. The PCM model for this study is based on an enthalpy formulation which really simulates the melting/solidification phase transition process at constant temperature [42] [43].

The stable form PCM is considered to be a homogenous material set in thin layers so that the heat transfer can be assumed one-dimensional. Density, specific (non-latent) heat capacity and thermal conductivity of each control volume are calculated as function of its current temperature. These material properties and melting/solidification temperatures are used to build an enthalpy/temperature function curve. A fully implicit one-dimensional FVM formulation with 1 mm thick

control volumes performs the heat transfer calculation in between the PCM layers. The variation of internal energy in each control volume is then used with the enthalpy/temperature function to get the corrected temperature.

One limitation of this numerical model is that it cannot account for multiple phase transition temperatures. This situation can occur for PCMs which are made of several compounds with dissimilar melting temperatures. It is thus assumed that the PCM has only one specific melting temperature and one specific solidification temperature. These temperatures can be different to take into account hysteresis phenomena. However, in this model, it is chosen to not introduce any hysteresis effect and therefore both melting and solidification temperatures are fixed to 22 °C.

Two types of LHTES system are tested in this study: PCM wallboards for the inner surfaces of walls and ceilings, and PCM integrated in furniture elements. Both systems consist of Energain® stable form PCM arranged in thin slabs. Energain® is a well-known commercial product. It is composed of 60 w% micro-encapsulated paraffin (organic PCM) mixed with 40 w% polyethylene [44]. The thickness of the PCM panel is chosen to be 1.5 cm. This value seems to be a reasonable choice to insure a significant increase of the heat capacity for daily temperature variations with an optimum amount of material. Indeed, one can see on **Fig. 2** that PCM wallboards only present marginal improvement of the effective thermal inertia for PCM thickness above 1.5 cm. For thicker LHTES systems, the time needed for the heat to penetrate the PCM layer becomes larger than the charging period, and the melting process cannot be completed.

Guarded Hot Plate Apparatus and Differential Scanning Calorimetry measurements have been conducted in order to determine precisely the thermal characteristics of the Energain® product. Some dissimilarity has been found between the current measurements and the results from a previous study of Kuznik et al. [23]. This discrepancy is probably due to the variability of the Energain® manufacturing process. Based on these experimental data and the information provided by the manufacturer, realistic PCM parameters (presented in **Table 2**) are chosen for the LHTES systems which are implemented in the building model. In particular, the PCM thermal conductivity is constant at 0.22 W/m.K for temperatures below 16 °C, constant at 0.18 W/m.K for temperatures above 28 °C, and varies linearly from 0.22 W/m.K to 0.18 W/m.K within the temperature range of 16 °C to 28 °C.

The additional daily effective thermal inertia of the PCM integrated in furniture elements is around 71.4 Wh/K.m² of gross floor surface area in average. The additional daily effective thermal inertia of the PCM wallboards ranges from 6.4 to 68 Wh/K.m² of gross floor surface area.

Table 2: *Characteristics of the phase change material.*

	PCM characteristics
Paraffin mass content (%)	60
Paraffin latent heat of fusion (kJ/kg)	200
Melting temperature (°C)*	22
Thermal conductivity (W/m.K)*	0.22 – 0.18
Density (kg/m ³)*	1000
Specific heat capacity (J/kg.K)*	2000
Latent heat of fusion (kJ/kg)*	120
Total heat storage for $\Delta\theta = 30$ K (kJ/kg)*	180

* For stable form PCM product: 60 w% paraffin in polyethylene matrix

4.4. Indoor items/furniture elements

The additional thermal mass of the indoor items and furniture elements inside occupied buildings can be accounted in different ways with various degrees of details: from simple virtual thermal node aggregating all elements, to detailed modelling with explicit location of each item in the building space [14]. In the current study, the additional indoor thermal mass is modelled as an equivalent fictitious planar element which aggregates all indoor items into an homogenous representative material. The thermo-physical properties of this equivalent element are chosen according to a previous study on the indoor content of dwellings in Denmark [14] and are presented in **Table 3**.

In each of the dwelling's thermal zones, the indoor thermal mass element is 60 kg/m² of the room's floor surface area concentrated in a 4.7 cm thick slab. Consequently, the surface area of one side of the planar element is equal to 1.8 times the room's floor surface area. The equivalent planar element does not have any real geometrical representation or position in the room. It is therefore assumed that 50% of the radiative share of the equipment, people, solar and radiator heating loads are distributed on its surfaces. The element is coupled to the rest of the thermal zone in the same way as if it was an additional internal wall. The mixed convection/radiation surface thermal resistance coefficient is set constant and equal to 0.13 m².K/W. The additional daily effective thermal inertia of the equivalent element is around 18.1 Wh/K.m² of gross floor surface area in average.

In the case of PCM integrated on furniture elements, the two models for indoor thermal mass/furniture and for PCM are combined together. The 1.5 cm thick layer of Energain® stable form PCM is added on the upper part of the equivalent planar element.

Table 3: *Equivalent indoor thermal mass/furniture properties.*

	Equivalent planar element
Thickness (mm)	47
Density (kg/m³)	715
Thermal conductivity (W/m.K)	0.3
Specific heat capacity (J/kg.K)	1400
Space discretization (nodes)	20

4.5. Validation of the numerical models

The FVM formulation for the construction elements has been tested and validated against the commercial software COMSOL Multiphysics. The other sub-components of the model and the entire multi-zone building model have been tested and validated against the commercial software BSim. The average absolute difference between the MATLAB - Simulink model and the BSim reference model is 0.12 °C for indoor temperature, 0.5 W/m² for the heating power need and 0.88% for the cumulative energy consumption over 2000 hours of the heating period. In addition, a BESTEST procedure has been performed and shows that the MATLAB – Simulink building model can calculate correctly the indoor temperature and the heating/cooling needs of a light or heavy structure building. Finally, The PCM model has been validated against experimental Guarded Hot Plate Apparatus tests on Energain® samples.

4.6. Heat storage control strategy

The indoor space heat accumulation strategy which is implemented in the building model is the same as the one used by Le Dréau et al. [9] and similar to the one of Péan et al. [45]. In principle, the end-goal of the energy flexibility and demand-side management strategies is to allow the integration of a larger share of intermittent RES in a Smart Grid system. For that purpose, the building should be able to accumulate energy when there is an excess of RES production, and reduce its energy usage when the RES production is low. In countries like Denmark, where a large share of the electrical energy production mix is coming from wind turbines, the

electricity spot price is a good indicator of the RES availability and the energy demand. Consequently, the Danish electricity spot price (hourly market price observed in the Nordic electricity market “Nord Pool” in the year 2009 [46]) is used here to control the heating modulation strategy. The building accumulates heat energy during low price periods and save heat energy during high price periods.

As shown on **Fig. 4**, limits for low price and for high price are calculated every hour as the lowest and highest quartile of the electricity market price over the last 14 days. The house temperature set point is then modulated accordingly with three different values: minimum set point of 20 °C, neutral set point of 22 °C and a maximum set point of 24 °C. The temperature span between the minimum set point and the maximum set point is 4K. It corresponds to a normal level of thermal comfort with less than 10% of unsatisfied occupants [47]. Moreover, the transient indoor temperature change is always kept below the thermal comfort limit of 2.1 K/h [48]. When the spot price becomes low, the set point is increased to accumulate heat energy. When the spot price becomes high, the set point is decreased to save heat energy. When the spot price is within the medium category, the set point is kept at 22 °C.

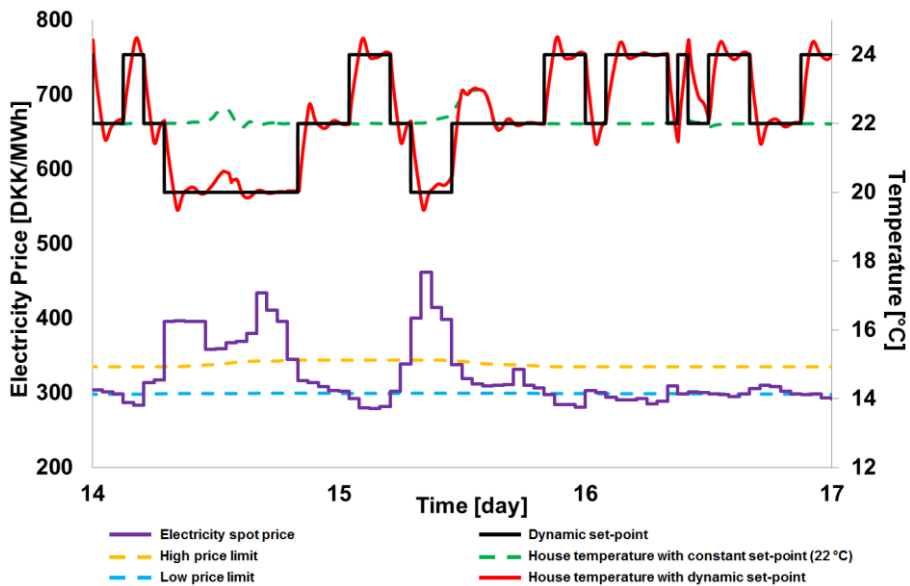


Fig. 4. *Temperature set point modulation with price control and maximum activation time of 6 hours for low-insulation light structure house with radiator.*

However, the occupants of a building might not necessary accept the change of the indoor temperature set point for an extended period of time based on an external signal. The longer the set point temperature is away from the neutral level and the more disturbance could be induced to the occupants. In order to study the impact of

different occupants' disturbance levels on the building energy flexibility, a maximum activation time is defined between 30 minutes and 24 hours. When the low or high activation period reaches the maximum activation time, the set point is put back to its neutral level of 22 °C. The temperature set point is then maintained at the neutral point for a duration equal to the maximum activation time before the same activation can occur again [9].

5. Results and discussion

5.1. Impact of additional indoor thermal mass on the building time constant

The impact of additional indoor thermal mass on the building's dynamics is investigated. Firstly, the time constant of six building cases from the three different structural thermal mass classes (light: 30 Wh/K.m², medium: 50 Wh/K.m², heavy: 100 Wh/K.m²) and the two envelope performance categories (low-insulation house from the 80's, high-insulation passive house) is calculated without any additional indoor thermal mass. The outdoor temperature is kept constant whilst all radiation and internal gains are set to zero. Once the house's temperature has reached a steady state (indoor temperature set point at 19 °C), the convective radiator power is increased to maximum until the temperature reaches a new steady state. The building time constant is then calculated as the time needed to reach 63.2% of the temperature change between the two steady states.

The **Fig. 5** presents the influence of the different types of additional thermal mass on the building's time constant compared to the empty room reference cases. The time constant and the thermal inertia of the reference empty buildings are stated in the table below the figure. One can observe that the PCM wallboards and the PCM integrated in the furniture increase significantly the time constant of all the buildings. Concerning the indoor items/furniture elements, their effect is limited for medium and heavy structure cases but not negligible for light structure buildings.

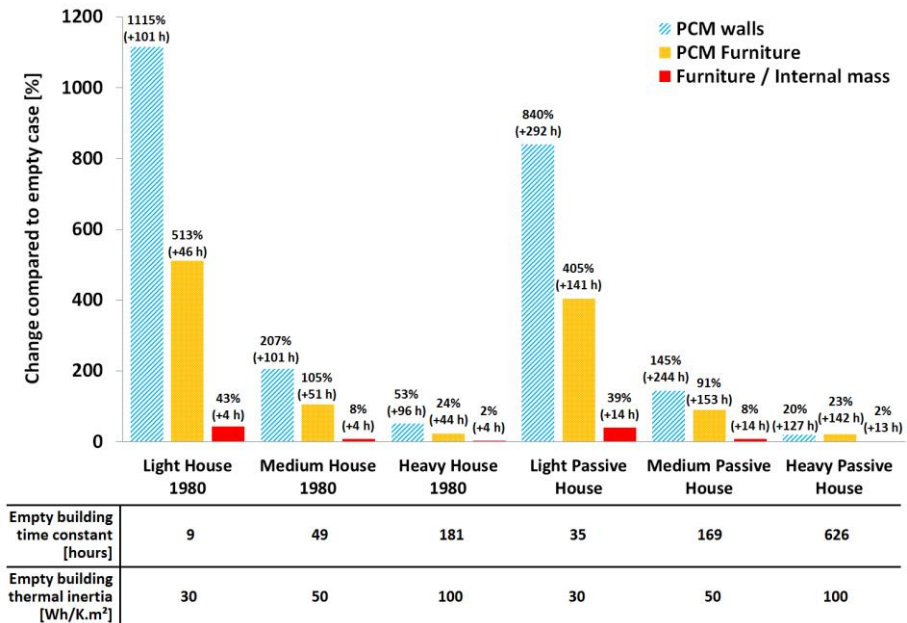


Fig 5. Change of building time constant with additional internal thermal mass.

5.2. Influence of the maximum activation time on the building energy flexibility

48 different building configurations (two envelope performance categories, three structural thermal mass classes, four kinds of additional indoor thermal mass and two types of heating system) are then simulated with 8 different maximum activation times for the heat storage strategy. One can see on **Fig. 6** an example of the distribution of the heating energy consumption over the different price categories when the maximum activation time for TES is increasing. The control strategy tries to maximize the energy use during low price period and minimize it during high price period. However, there is no particular action to decrease energy consumption during medium price period. Consequently, the accumulated thermal energy is firstly impacting the high price category and marginally decreasing the medium price category in a second time. Similar patterns can be observed for all the building cases. The average increase of yearly heating energy use due to heat accumulation strategy (24 hours of maximum activation) is 3.3% and 6.3% for houses from the 80's and passive houses respectively.

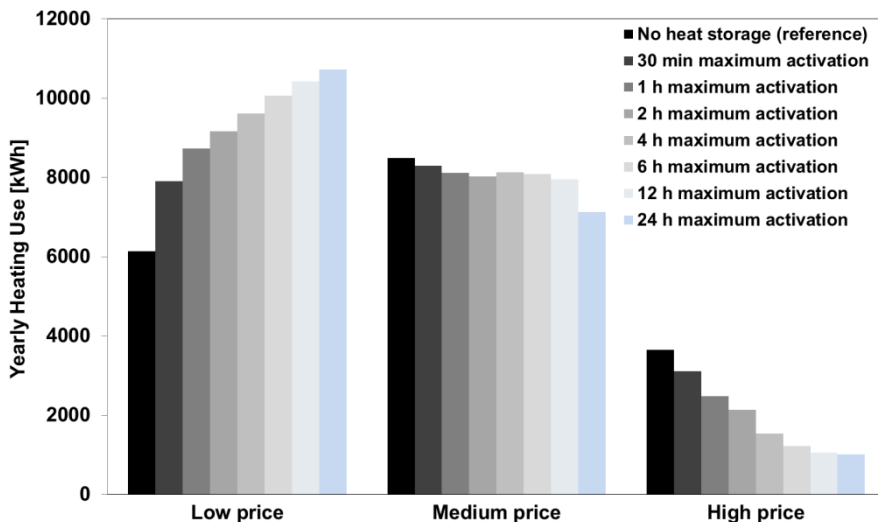
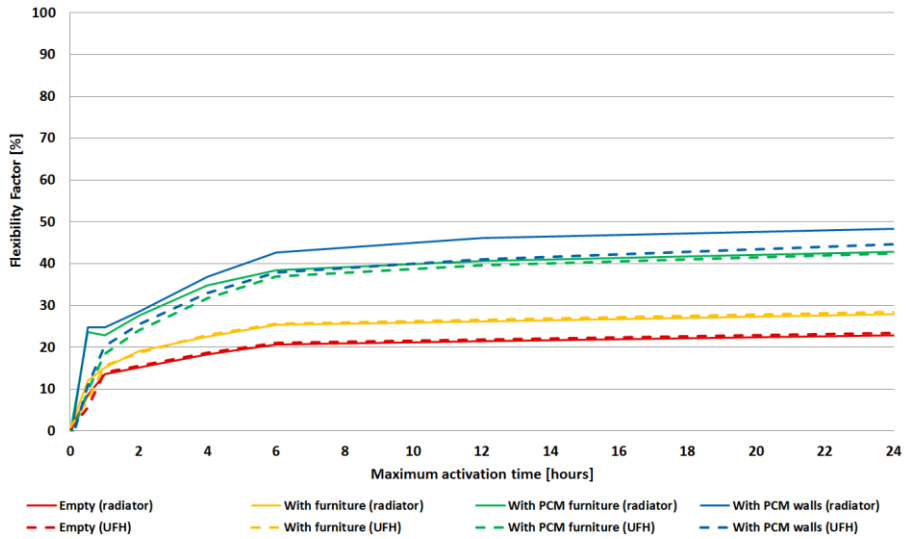
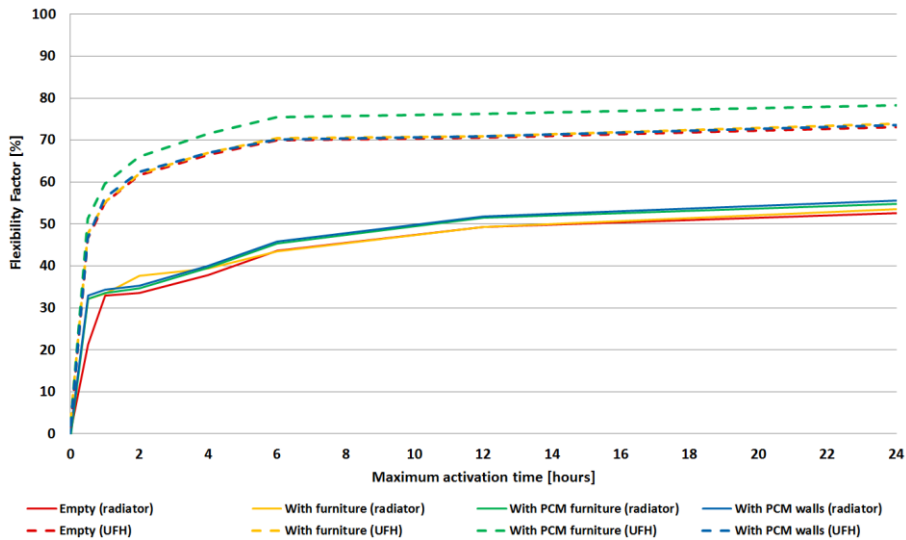


Fig 6. Yearly heating use variation of a light structure low-insulation house with PCM wallboard for different maximum activation times.

Fig. 7 and **Fig. 8** show the evolution of the building energy flexibility index as function of the maximum activation time. These results are coherent with the previous study of Le Dréau et al. [9]. The flexibility index increases quickly and then stabilizes for activation times above 6 hours. This saturation effect can be explained by two phenomena. First of all, the building thermal storage capacity reaches its maximum limit and cannot accumulate more energy to improve its flexibility. Secondly, the indicated maximum activation time which is allowed to the controller is different from the effective activation time due to the variation frequency of the price signal. A Fourier analysis of this price signal shows that its main components have an oscillation period of 12 hours, 24 hours and 1 week. Consequently, the available accumulation low price periods are rarely lasting more than 6 hours and thus the maximum yearly average activation time is 4.7 hours.

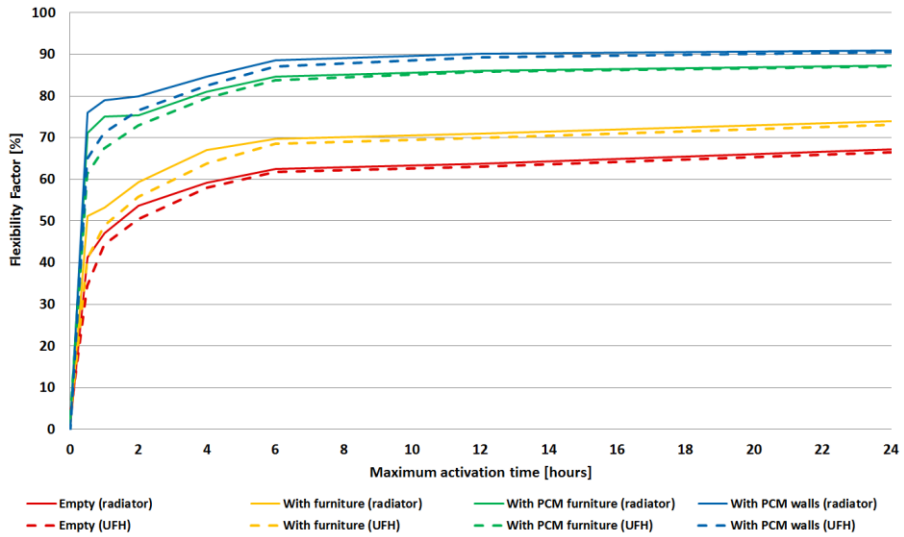


(a) Light structure: building thermal inertia = 30 Wh/K.m²

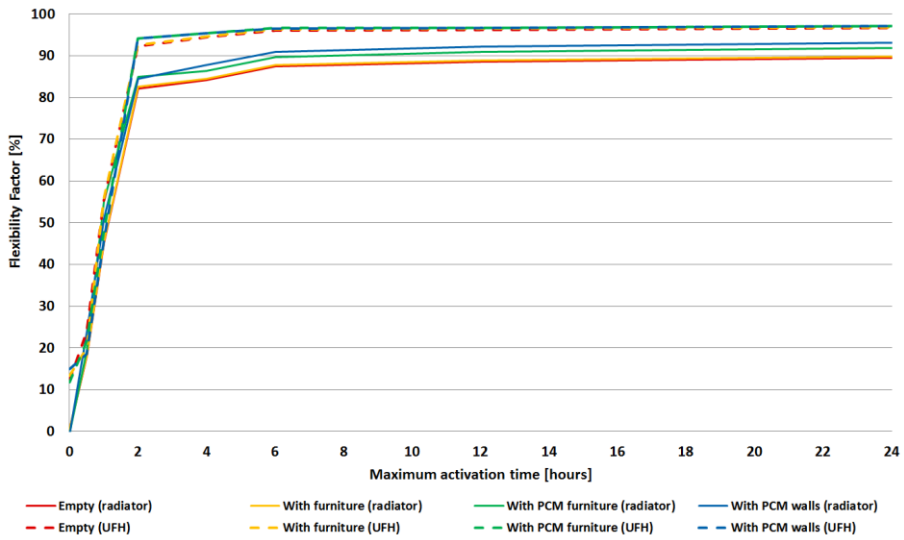


(b) Heavy structure: building thermal inertia = 100 Wh/K.m²

Fig 7. Building energy flexibility of low-insulation house 1980 with light structure (a) and heavy structure (b) as function of maximum activation time (radiator: convective radiator; UFH: under floor heating).



(a) Light structure: building thermal inertia = 30 Wh/K.m²



(b) Heavy structure: building thermal inertia = 100 Wh/K.m²

Fig 8. Building energy flexibility of high-insulation passive house with light structure (a) and heavy structure (b) as function of maximum activation time (radiator: convective radiator; UFH: under floor heating).

5.3. Impact of the building parameters on the energy flexibility

For the rest of this study, the maximum activation time of the heat accumulation strategy is kept at 24 hours. The building energy flexibility index has been calculated for 144 different study cases: two categories of building envelope performance, three classes of structural thermal inertia with three different sub-variations, two types of heating system and four additional indoor thermal mass configurations (empty room, furniture/indoor content, PCM furniture, PCM wallboards). The results are shown on the **Fig. 9** where one can see the increase of the energy flexibility as function of building total effective thermal inertia (including structural thermal mass from the envelope and additional indoor thermal mass, if any).

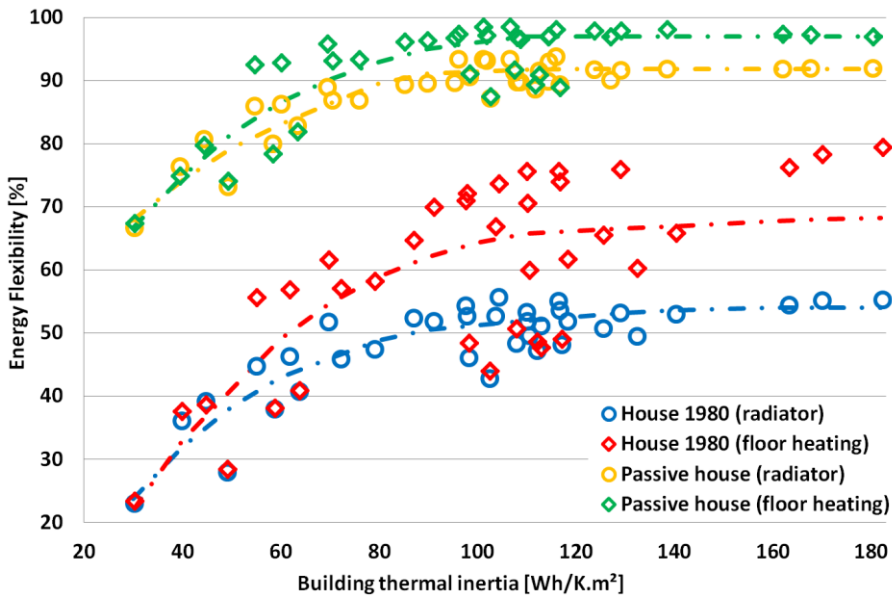


Fig 9. Evolution of the building energy flexibility as function of the thermal inertia.

It is clear that low-insulation houses present a significantly lower energy flexibility potential than high-insulation ones. Well-insulated dwellings have lower heating needs and can therefore shift it with a smaller storage capacity. Moreover, the efficiency of their envelope allows retrieval of a greater share of the accumulated thermal energy. However, one should keep in mind that low-insulation buildings can have a larger individual impact on the energy grid because the absolute amount of energy they are able to shift in time is about 4 times more important than high-insulation buildings.

Furthermore, the results show that all kinds of activated thermal masses, regardless of their nature or location in the house, contribute to increase the overall heat storage capacity and consequently building energy flexibility potential. However, this impact stagnates for effective thermal inertia above 80 Wh/K.m², especially for low energy buildings. Indeed, medium and heavy structure passive houses reach the maximum energy flexibility potential: there is no remaining heating energy use to be shifted in time and therefore increasing thermal inertia further for additional heat storage capacity is ineffective. In the case of medium and heavy structure low-insulation dwellings, additional thermal mass cannot compensate for the poor envelope performance which greatly limits the recovery of accumulated thermal energy and therefore the total energy flexibility potential.

Concerning heat emitters, the under floor heating system shows greater performance compared to convective radiators for medium and heavy structure buildings. The concrete screed where the under floor hydronic circuit is laid is highly activated, which allows a larger heat storage capacity. Moreover, radiant UFH system can provide the same level of thermal comfort with a lower indoor air temperature. This leads to a decrease of the ventilation and infiltration thermal losses and therefore improves the heat accumulation efficiency and the building energy flexibility. The employment of UFH can thus increase the building energy flexibility by up to 44% and 8% for low-insulation and high-insulation dwellings respectively. In the case of light structure house, the under floor heating was integrated in a wooden floor which does not have a significant heat capacity. Consequently, the flexibility potential of low thermal mass buildings is not improved by the use of UFH.

5.4. Impact of additional indoor thermal mass on the building energy flexibility

This numerical study also focused on assessing the influence of three different types of additional indoor thermal mass element on the building energy flexibility. The comparison results are presented on **Fig. 10**. The energy flexibility and the thermal inertia of the reference empty buildings are stated in the table below the figure. The relative values of the flexibility improvement are indicated as percentage and the absolute values of the flexibility change are in between parentheses. One can see that PCM wallboards and furniture with integrated PCM can appreciably increase the energy flexibility potential of dwellings with low insulation and low structural thermal inertia. However, the improvement is reduced for well-insulated houses and very limited for buildings with medium and heavy structures.

In addition, it should be noted that PCMs and consequently PCM wallboards have a relatively low thermal conductivity. When positioned on the inner surface of construction elements in the thermal zone, the PCM wallboards obstruct the activation of the thermal mass underneath them. This is a problem in the case of buildings with heavy structures such as concrete or brick walls. The large heat

storage capacity of these construction elements is nullified by the presence of the PCM wallboards and is barely compensated by the latter.

Concerning furniture and indoor content, they only account for a small share of the total effective thermal inertia of medium and heavy structure houses. It is thus not surprising that their impact on the building energy flexibility is almost negligible. Nevertheless, in the case of light structure dwellings, the influence of the indoor items is significant and should therefore be taken into account.

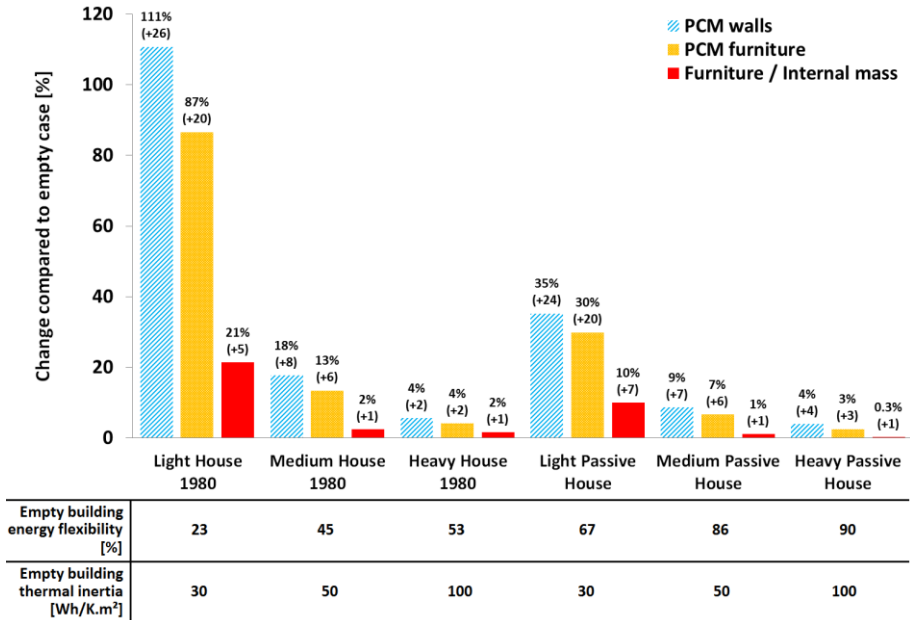


Fig 10. Change of building energy flexibility with additional internal thermal mass (radiator heating system and maximum activation time of 24 hours).

5.5. Parametric sensitivity analysis

A statistical analysis of the results presented in the previous section (see **Fig. 10**) is performed to rank the different building parameters by order of significance regarding the energy flexibility. The effect level of the parameters is assessed by the mean of consecutive ANOVA (analysis of variance) tests on linear regression models with iterative deletion of the least significant term [49]. The results are presented in **Table 4** with the most significant building parameter regarding energy flexibility (highest F-value) on the top. From this statistical analysis, it can be concluded that the insulation level of the house has the main role in the building energy flexibility compared to the building total thermal inertia, type of heat emitter or the kind of additional indoor thermal mass.

Table 4: *Significance ranking of the building parameters regarding energy flexibility.*

Significance ranking	Building parameter	F-value
1	Envelope insulation level	685.4
2	Thermal inertia	91.4
3	Heating system type	42.3
4	Additional indoor thermal mass type	14.6

Secondly, a sensitivity analysis of the influence of the additional indoor thermal mass parameters regarding the light-structure dwellings energy flexibility is conducted. The flexibility factor is calculated for realistic low and high additional indoor thermal mass characteristic variations (see **Table 5**). Relative changes of the flexibility factor from the reference cases are indicated in the colored boxes (red color for positive variations and blue color for negative variations). A similar ANOVA statistical analysis is then performed on these results. The **Table 6** sums up the significance ranking of the different parameters of the three types of additional indoor thermal mass element. One can see that for indoor items/furniture elements, the surface heat transfer coefficient, the mass and the surface area of the elements play the main role while material density and thermal conductivity have little significance. For PCM furniture, the exposed surface area, the heat transfer coefficient and the PCM properties are the most significant parameters. For PCM wallboards, the characteristics of the phase change material layer have the dominant effects.

Table 5: Sensitivity analysis of the additional indoor thermal mass parameters.

Indoor Items / furniture	Parameter variation			Variation of building energy flexibility			
				House 80's		Passive House	
	Low	Reference	High	Low	High	Low	High
Surface heat transfer coefficient [W/K.m ²]	5	7.7	10	-8.4%	18.4%	-5.1%	10.1%
Mass [kg/m ² floor area]	20	60	100	-11.6%	10.6%	-6.0%	4.7%
Surface area [m ² /m ² floor area]	0.8	1.8	2.8	-8.8%	7.8%	-4.3%	3.1%
Material density [kg/m ³]	150	715	1500	1.5%	-2.7%	0.5%	-1.0%
Material thermal conductivity [W/m.K]	0.1	0.3	0.5	2.3%	-0.5%	2.3%	-0.7%

PCM furniture parameters	Parameter variation			Variation of building energy flexibility			
				House 80's		Passive House	
	Low	Reference	High	Low	High	Low	High
Surface heat transfer coefficient [W/K.m ²]	5	7.7	10	-7.0%	12.2%	-3.1%	3.2%
Furniture mass [kg/m ² floor area]	20	60	100	-0.3%	2.6%	-0.2%	1.1%
PCM furniture surface area [m ² /m ² floor area]	0.8	1.8	2.8	-16.5%	9.3%	-10.6%	4.5%
Furniture material density [kg/m ³]	150	715	1500	-0.4%	0.9%	-0.2%	0.5%
Furniture material thermal conductivity [W/m.K]	0.1	0.3	0.5	-0.4%	0.3%	-1.0%	0.5%
PCM layer thickness [cm]	0.5	1.5	3	-13.7%	4.2%	-5.1%	1.2%
PCM average thermal conductivity [W/m.K]	0.1	0.2	0.4	-11.4%	10.6%	-2.3%	1.3%
PCM latent heat of fusion [kJ/kg]	60	120	180	-19.4%	11.3%	-6.5%	1.2%

PCM Wallboard parameters	Parameter variation			Variation of building energy flexibility			
				House 80's		Passive House	
	Low	Reference	High	Low	High	Low	High
Surface heat transfer coefficient [W/K.m ²]	5	7.7	10	-3.1%	1.3%	-1.2%	0.7%
PCM layer thickness [cm]	0.5	1.5	3	-15.7%	7.8%	-5.4%	1.2%
PCM average thermal conductivity [W/m.K]	0.1	0.2	0.4	-16.1%	8.0%	-5.3%	0.9%
PCM latent heat of fusion [kJ/kg]	60	120	200	-24.1%	9.8%	-8.5%	2.4%

Table 6: *Significance ranking of the additional thermal mass parameters regarding energy flexibility.*

Indoor items/furniture		
Significance ranking	Parameter	F-value
1	Surface heat transfer coefficient	30.1
2	Mass	18.3
3	Surface area	18.0
4	Material density	1.7
5	Material thermal conductivity	1.2
PCM furniture		
Significance ranking	Parameter	F-value
1	Surface area	45.1
2	PCM latent heat of fusion	27.9
3	Surface heat transfer coefficient	13.8
4	PCM thermal conductivity	11.8
5	PCM layer thickness	10.9
6	Furniture mass	0.5
7	Furniture material density	0.1
8	Furniture material thermal conductivity	0.1
PCM wallboard		
Significance ranking	Parameter	F-value
1	PCM latent heat of fusion	29.0
2	PCM layer thickness	12.6
3	PCM thermal conductivity	12.1
4	Surface heat transfer coefficient	0.5

5.6. Indoor thermal comfort

Concerning the indoor thermal comfort, it has been observed that the house's temperature stability (here assessed as the difference between the 5% quantile and the 90% quantile of the indoor temperatures during the heating period) is very dependent of the maximum activation time for the low-insulation dwellings. However, this parameter has a limited impact on high-insulation cases when the activation time is larger than 2 hours. Higher thermal inertia and better envelope performance improve significantly the indoor temperature stability. In the case medium and heavy structure houses, the UFH system also noticeably improves the indoor temperature stability compared to the convective radiator. These results are coherent with the previous study of Le Dréau et al. [9].

6. Conclusion

The numerical study presented in this article has investigated the role of different building parameters in the heating energy flexibility potential of a Danish single family house with a heat storage strategy based on indoor temperature set point modulation according to a price signal. The building energy flexibility index defined in this paper represents the capacity of the dwelling to shift its heating use in time by accumulating thermal energy in the indoor environment during low electricity price periods, and reducing its heating use during high electricity price periods.

The maximum thermal energy storage capacity of a building is mainly determined by its total effective thermal inertia. However, it was found that the envelope insulation level is the most important building parameter with respect to the capacity of a dwelling to shift its heating use in time. From the energy flexibility perspective, it is therefore more interesting to lower the building energy consumption and improve its storage efficiency rather than increasing the thermal inertia or changing the type of heating system. Nevertheless, it should be noted that poorly insulated houses, despite their limited energy flexibility potential, can have a larger individual impact on the energy grid because the absolute amount of energy they shift in time is more important than the one of highly insulated houses.

In order to increase the effective thermal inertia of lightweight structure dwellings and consequently improve their energy flexibility potential, the integration of phase change materials in inner surface wallboards or in furniture elements seems to be a good solution. In the current numerical study, the PCM wallboards could increase the energy flexibility index by up to 111% and 35% in the cases of low-insulation and high-insulation light-structure houses respectively. Similarly, furniture with integrated PCM could increase the energy flexibility index by up to 87% and 30% in the cases of low-insulation and high-insulation light-structure houses respectively. It should be pointed that PCM wallboards should not be placed on heavy construction elements. They screen the thermal activation of the material layers placed behind them and barely provide the same heat storage capacity as traditional concrete or brick walls. In the case of medium and heavy structure

houses, additional thermal inertia only marginally improves the energy flexibility potential. In addition, the use of UFH system instead of convective radiators can activate more of the building structural thermal mass with a reduced indoor air temperature. It can thus lead to a building energy flexibility improvement of up to 44% and 8% for low-insulation and high-insulation dwellings respectively.

This paper also demonstrated that the empty space assumption for dynamic energy simulations was not appropriate for lightweight structure buildings with less than 50 Wh/K.m² of thermal inertia. Transient thermal behaviour and total heat storage capacity can be significantly influenced by the presence of items and furniture in the indoor environment. It was found that the assessment of the time constant of such building can be increased by up to 43% and the energy flexibility index by up to 21% when indoor items are taken into account.

Demand side management and building energy flexibility are promising research topics. Further work is needed to develop novel methodologies for the assessment of the energy flexibility potential of buildings and their capacity to respond to the grid needs. More studies should also be made on the acceptability of users regarding domestic heat storage strategies with external control signals. Concerning numerical simulations, knowledge has to be gained about the interaction between the indoor content elements, such as furniture, and the indoor environment for a better prediction of the dynamic building thermal behaviour. Finally, the potential for phase change materials integrated in furnishing elements should be investigated further. The design of these latent heat thermal energy storage systems should be optimized in accordance to a certain heat accumulation strategy and precise boundary conditions.

Acknowledgements

This work was financed by the ENOVHEAT project which is funded by Innovation Fund Denmark (contract no 12-132673) and was carried out partly within the framework of IEA EBC Annex 67 Energy Flexible Buildings.

References

- [1] W.M. Beurskens, M. Hekkenberg, P. Vethman, Renewable energy projections as published in the national energy action plans of the European member states. Report no. ECN-E-10-069. ECN and European Environment Agency. <https://www.ecn.nl/docs/library/report/2010/e10069.pdf>. February 2011 (Accessed 17 October 2017).
- [2] Energy Strategy 2050 – from coal, oil and gas to green energy, The Danish Government. <http://www.kebmin.dk/sites/kebmin.dk/files/news/from-coal-oil-and-gas-to-green-energy/Energy%20Strategy%202050%20web.pdf>. February 2011 (Accessed 17 October 2017).
- [3] B.V. Mathiesen, H. Lund, D. Connolly, H. Wenzel, P.A. Østergaard, B. Möller, et al, Smart Energy Systems for coherent 100% renewable energy and transport solutions, Applied Energy 145 (2015) 139–154.
- [4] Building Performance Institute Europe (BPIE), Europe’s Buildings under the Microscope, Executive Summary 2011. http://bpie.eu/wp-content/uploads/2015/10/HR_EU_B_under_microscope_study.pdf. 2011 (Accessed 17 October 2017).
- [5] K. Hedegaard, B.V. Mathiesen, H. Lund, P. Heiselberg, Wind power integration using individual heat pumps – Analysis of different heat storage options, Energy 47 (2012) 284–93.
- [6] G. Reynders, J. Diriken, D. Saelens, A generic quantification method for the active demand response potential of structural storage in buildings, 14th IBPSA conference, Building Simulation 2015, Hyderabad, India (2015).
- [7] B. Favre, B. Peuportier, Application of dynamic programming to study load shifting in buildings, Energy Build 82 (2014) 57-64.
- [8] G. Masy, E. Georges, C. Verhelst, V. Lemort, P. André, Smart grid energy flexible buildings through the use of heat pumps and building thermal mass as energy storage in the Belgian context, Science and Technology for the Built Environment. 21 (2015) 800-811.
- [9] J. Le Dréau, P. Heiselberg, Energy flexibility of residential buildings using short term heat storage in the thermal mass, Energy 111 (2016) 991-1002.
- [10] G. Reynders, T. Nuytten, D. Saelens, Potential of structural thermal mass for demand-side management in dwellings. Build. Environ. 64 (2013) 187-199.
- [11] A. Arteconi, D. Costola, P. Hoes, J.L.M. Hensen, Analysis of control strategies for thermally activated building systems under demand side management mechanisms. Energy Build. 80 (2014) 384-393.
- [12] R. Barzin, J.J.J Chen, B.R. Young, M.M Farid, Application of PCM underfloor heating in combination with PCM wallboards for space heating using price based control system. Applied Energy 148 (2015) 39-48.
- [13] A. Bastani, F. Haghigat, C.J. Manzano, Investigating the effect of control strategy on the shift of energy consumption in a building integrated with PCM wallboard. In: 6th International Building Physics Conference, IBPC (2015).
- [14] H. Johra and P. Heiselberg, Influence of internal thermal mass on the indoor thermal dynamics and integration of phase change materials in furniture for building energy storage: A review, Renewable and Sustainable Energy Reviews 69 (2017) 19-32.
- [15] Energistyrelsen, Danmarks Energifremskrivning 2012 . https://ens.dk/sites/ens.dk/files/Basisfremskrivning/danmarks_energifremskrivning_2012_endelig_v1.2.pdf. October 2012 (Accessed 17 October 2017).

- [16] J. Krag, K.B. Wittchen, Development of two Danish building typologies for residential buildings, *Energy Build.* 68 Part A (2014) 79-86.
- [17] <http://www.iea-ebc.org/projects/ongoing-projects/ebc-annex-67/>
(Accessed 17 October 2017).
- [18] S.J. Østergaard, A. Marszal-Pomianowska, R. Lollini, W. Pasut, A. Knotzer, P. Engelmann, A. Stafford, G. Reynders, IEA EBC Annex 67 Energy Flexible Buildings, *Energy and Buildings* 155 (2017) 25-34.
- [19] R.A Lopes, A. Chambel, J. Neves, D. Aelenei and J. Martins, A literature review of methodologies used to assess the energy flexibility of buildings, *Energy Procedia* 91 (2016) 1053-1058.
- [20] J. Le Dréau, Demand-side management of heating need in residential buildings, CLIMA 2016 – proceedings of the 12th REHVA world congress.
- [21] ISO 13786:2007, Thermal performance of building components – Dynamic thermal characteristics – Calculation methods.
- [22] D. Maillat, S. André, J.-C. Batsale, A. Degiovanni, C. Moyne, *Thermal Quadrapoles*, Wiley, New York (2000).
- [23] F. Kuznik, J. Virgone, J. Noel, Optimization of a phase change material wallboard for building use, *Applied Thermal Engineering* 28 (2008) 1291–8.
- [24] ISO 6946:2007, Building components and building elements – thermal resistance and thermal transmittance – calculation method.
- [25] T.S. Larsen, C. Brunsgaard, *Komfort Husene: erfaringer, viden og inspiration*. Saint-Gobain Isover a/s (2010).
- [26] French Building Energy and Thermal Regulation 2012, CSTB FR (2012)
- [27] K. Ovesen, SBI Anvisning 175-Varmeanlæg med vand som medium. Danish Building Research Institute - SBI (2000).
- [28] EN 1264, Water based surface embedded heating and cooling systems.
- [29] EN 15377, Heating systems in buildings – Design of embedded water based surface heating and cooling system.
- [30] ISO 11855, Building environment design – Design, dimensioning, installation and control of embedded radiant heating and cooling systems.
- [31] Uponor, Heating and cooling solutions - technical guidelines. https://www.uponor.co.in/~media/countryspecific/international/download-centre/indoor_climate/underfloor-heating/brochures/technical-guidelines-home-comfort.pdf?version=1. March 2009 (Accessed 17 October 2017).
- [32] Uponor, Installation guide for underfloor heating systems - technical information (2016).
- [33] P.G. Wang, M. Scharling, K.P. Nielsen, K.B. Wittchen, C. Kern-Hansen, DMI Technical Report 13-19: 2001-2010 Danish Design Reference Year - Reference Climate Dataset for Technical Dimensioning in Building, Construction and other Sectors (2013).
- [34] R.L. Jensen, J. Nørgaard, O. Daniels, R.O. Justesen, Person og forbrugsprofiler: bygningsintegreret energiforsyning. Aalborg University, DCE Technical Reports No. 69 (2011).
- [35] H. Johra, P. Heiselberg, Description and validation of a MATLAB - Simulink single family house energy model with furniture and phase change materials. Aalborg University, DCE Technical Reports No. 187 (2016).
- [36] C.R.H. Bahl. EnovHeat project summary: development of efficient novel magnetocaloric heat pumps.

- <http://www.enovheat.dk/Research/ProjectSummary>. 2015 (Accessed 17 October 2017).
- [37] BSim software - User's Guide – tsbi5. Danish Building Research Institute - SBI (2013).
- [38] A.S. Kalagasidis, C. Rode, M. Woloszyn, HAM-Tools – a whole building simulation tool in Annex 41. Proceedings of the IEA ECBCS Annex 41 Closing Seminar (2008).
- [39] S. Adams, M. Holmes, Determining time constants for heating and cooling coils. Building Services Research & Information Association, UK (1977).
- [40] University of Wisconsin-Madison Solar Energy Laboratory, TRANSOLAR Energietechnik GmbH, CSTB, TESS. Type 31: Pipe or duct model. TRNSYS 17 – Mathematical Reference 2012, 186 – 188.
- [41] M. Scarpa, K. Grau, B.W. Olesen, Development and validation of a versatile method for the calculation of heat transfer in water-based radiant systems. Eleventh International IBPSA Conference, Glasgow, Scotland, 27-30 (July 2009).
- [42] R. Prapainop, K. Maneeratana, Simulation of ice formation by the finite volume method. Songklanakarin J. Sci. Technol. 26 (2004) 55-70.
- [43] P. Verma, Varun, S.K. Singal, Review of mathematical modeling on latent heat thermal energy storage systems using phase-change material. Renewable and Sustainable Energy Reviews 12 (2008) 999-1031.
- [44] DuPont Energain®, Technical Datasheet. http://www.cse.fraunhofer.org/hs-fs/hub/55819/file-14736951-pdf/docs/energain_flyer.pdf. 2012 (Accessed 17 October 2017).
- [45] T.Q. Péan, J. Salom, J. Ortiz, Potential and optimization of a price-based control strategy for improving energy flexibility in Mediterranean buildings. In: CISBAT 2017 International Conference – Future Buildings & Districts – Energy Efficiency from Nano to Urban Scale, 6-8 September 2017, Lausanne, Switzerland.
- [46] EnergiNet.dk. Market data (elspot price in Western Denmark). www.energinet.dk/en/el/engrosmarked/udtraek-af-markedsdata/Sider/default.aspx. 2009 (Accessed 17 October 2017).
- [47] EN ISO 7730. Ergonomics of the thermal environment-analytical determination of thermal comfort by using calculation of the PMV and PPD indices and local thermal comfort criteria (2005).
- [48] ASHRAE Standard, Standard 55 – 2004. Thermal environmental conditions for human occupancy.
- [49] D.C. Montgomery, Design and Analysis of Experiments, Eighth edition. John Wiley & Sons Incorporated (2012).

Appendix E. Paper V

Johra, H., Filonenko, K., Heiselberg, P., Veje, C., Dall'Olio, S., Engelbrecht, K., & Bahl, C. (Under review). Integration of a magnetocaloric heat pump in an energy flexible residential building. *Renewable Energy*.

Reprinted by permission from Elsevier.

Integration of a magnetocaloric heat pump in an energy flexible residential building

Hicham Johra ^{a,*}, Konstantin Filonenko ^b, Per Heiselberg ^a,
Christian Veje ^b, Stefano Dall'Olio ^c, Kurt Engelbrecht ^c,
Christian Bahl ^c

^a Aalborg University, Division of Architectural Engineering, Department of Civil Engineering, Thomas Manns Vej 23, DK-9220 Aalborg Øst, Denmark

^b University of Southern Denmark, Center for Energy Informatics, Campusvej 55, DK-5230 Odense M, Denmark

^c Technical University of Denmark, Department of Energy Conversion and Storage, Frederiksborgvej 399, DK-4000 Roskilde, Denmark

* Corresponding author. Tel.: +45 9940 7234. E-mail address: hj@civil.aau.dk (H. Johra).

Abstract

The main goal of the EnovHeat project is to develop, build and test a prototype of an innovative heat pump based on active magnetic regenerator technology. This device can be coupled to a ground source heat exchanger and an under-floor heating system to provide for the space heating needs of a low-energy house in Denmark. However, the use of a simple controller leads to modest performances because the heating system is running mostly part-load. This numerical study has tested the possibility of using heat storage in the indoor environment as an effective strategy to optimize the operation of the magnetocaloric heat pump. Indoor temperature set point modulation can take advantage of the building energy flexibility potential to maximize the full-load operation time of the heating system and therefore improve its overall COP. Results show that this new controller can significantly increase the average COP, ranging from 2.90 to 3.51 depending on the cases. Although the indoor temperature stability is reduced, it allows the magnetocaloric heat pump to reach energy use efficiencies which are similar to the ones of conventional vapour-compression heat pumps.

Keywords: *Magnetocaloric heat pump; magnetic heating; active magnetic regenerator; innovative heating system; building energy flexibility; demand-side management*

1. Introduction

In the recent years, global agreements have been reached concerning the necessity of decreasing our dependency on fossil fuels [1]. To meet these goals, a large deployment of renewable energy sources (RES) and a sharp improvement of our societies' energy efficiency are needed [2]. In many countries, the building sector is the largest energy end-user. In Europe, for instance, it accounts for around 40% of the total energy demand and indoor space heating represents 75% of the building energy needs [3]. Consequently, the development of sustainable low-energy buildings with efficient heating systems is essential.

1.1. Role of heat pump systems

Heat pumps are mechanical devices which transfer thermal energy from a cold reservoir with low exergy (heat source) to a warmer environment with higher exergy (heat sink) by means of heating/cooling thermodynamic cycles. Conventional heat pumps are typically electrically driven and operate with a vapour compression thermodynamic cycle. This mature technology for heating is cost effective, presents low CO₂ emission, and achieves high coefficient of performance (COP) ranging from 3 to 5 [4][5].

Heat pump systems are therefore an excellent solution to supply heating energy for indoor space conditioning and domestic hot water in countries where the heating demand is dominating. Indeed, in the case of Denmark, a study showed that district heating (in urban areas) and individual heat pumps (outside urban areas) are the best heating supply solutions with regards to costs, energy consumption and CO₂ emissions [6]. Similarly, it was found that heat pumps are an environmentally and economically optimum solution for heating supply in the future RES-dominated energy systems of Germany [7] and the U. K. [8].

Consequently, heat pumps are key components of the energy development strategies in many countries. It therefore leads to a rapid increase of the market demand. For example, in the European Union, between 2005 and 2014, an average of 720 000 units were installed each year. In 2014, the total European heat pump stock was of 7.5 million units. With the continuous tightening of the building energy efficiency regulations and the enthusiasm for the renovation sector, the heat pump market presents a significant growth perspective. It is estimated that, if all the European countries had the same market penetration as Sweden, there would be 36.9 million heat pump units running in Europe in 2020 and 85.9 million in 2030 [9].

1.2. EnovHeat project: the magnetocaloric heat pump

Responding to the large public interest for the heat pump technology, industries and research teams continuously endeavour to develop new cost-effective technical solutions to be production oriented. In that sense, the main goal of the EnovHeat project [10] is to develop, build and test the prototype of an innovative heat pump system based on active magnetic regenerator (AMR) technology (see **Fig. 1**). The cooling/heating thermodynamic cycle for heat transfer is generated from the reversible magnetocaloric effect of the materials used as solid refrigerants (the magnetocaloric materials). Due to the reversible nature of the magnetocaloric effect, this technology has great potential for high COP. Moreover, AMR devices have the benefit of a more silent operation, an absence of greenhouse or toxic gases, and the possibility for recycling the magnets and the magnetocaloric materials [11]. Comprehensive explanation of the magnetocaloric effect, materials and systems can be found in the publications of Smith et al. [11] and Kitanovski et al. [12]. The AMR system principle is described in detail in the articles of Engelbrecht et al. [13] and Lei et al. [14].

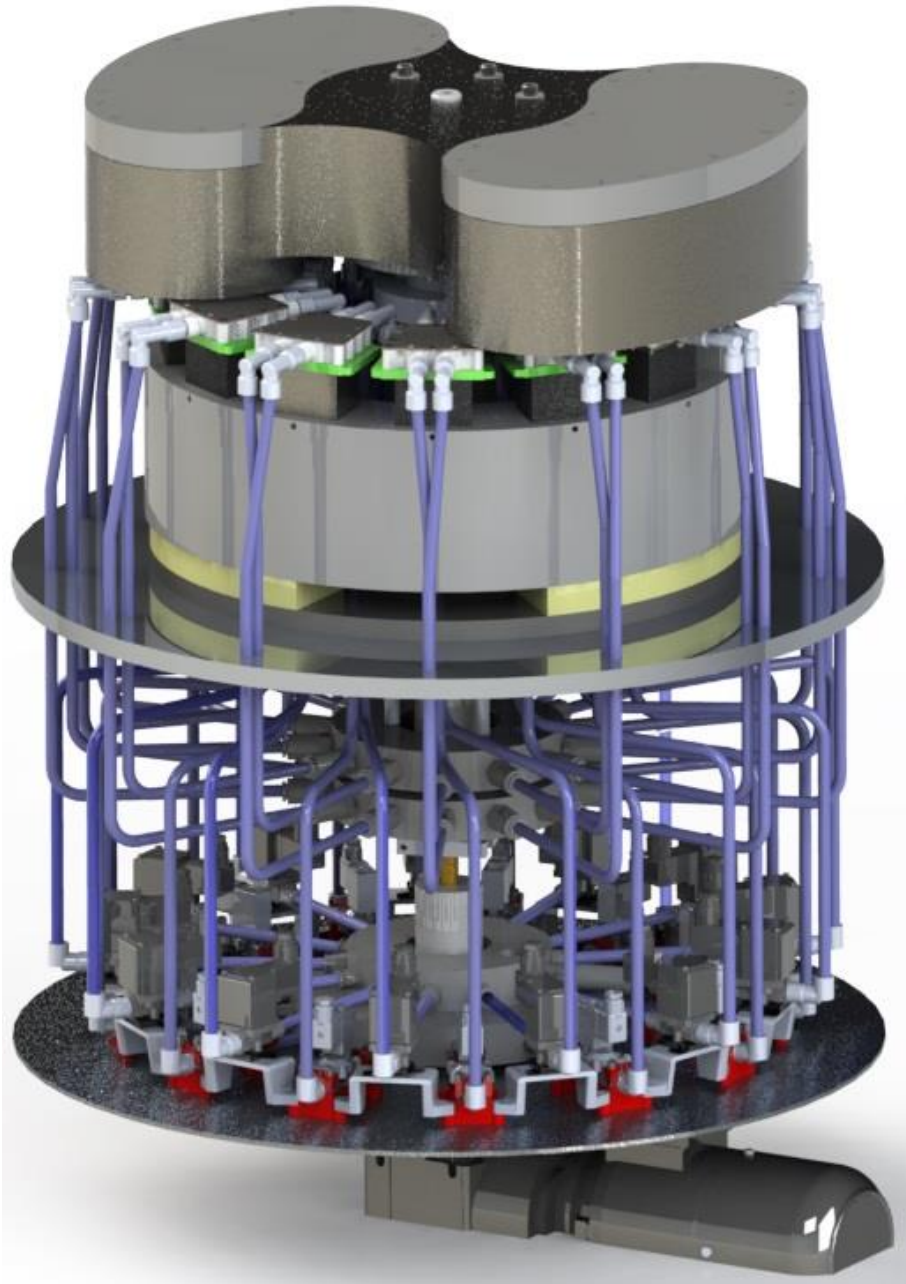


Fig. 1. CAD model of the magnetocaloric heat pump prototype of the EnovHeat project: “MagQueen”.

A previous study [15] numerically demonstrated for the first time that such a magnetocaloric heat pump (MCHP) can be implemented in a low-energy single family house and provide for its space heating needs under cold weather climate conditions (Denmark). In the EnovHeat project, the MCHP is used solely for indoor space heating because domestic hot water production requires a higher temperature span. Nevertheless, this is an encouraging starting point for the development of this promising technology.

The MCHP can be integrated in a single hydronic loop including a vertical borehole ground source heat exchanger (GSHE) and a radiant under-floor heating (UFH) without an intermediate heat exchanger or hot water storage tank. As shown in **Fig. 2**, this system configuration can run with appreciable COP. It can produce up to 2600 W of heating power with an average seasonal COP of 3.93 when operating at maximum capacity. However, if the MCHP is implemented in a multi-zone building with a simple fluid flow rate controller and independent thermostats in each thermal zone, the heating system operates on partial-load most of the time. As illustrated in **Fig. 3**, this leads to modest performances (average seasonal COP of 1.84).

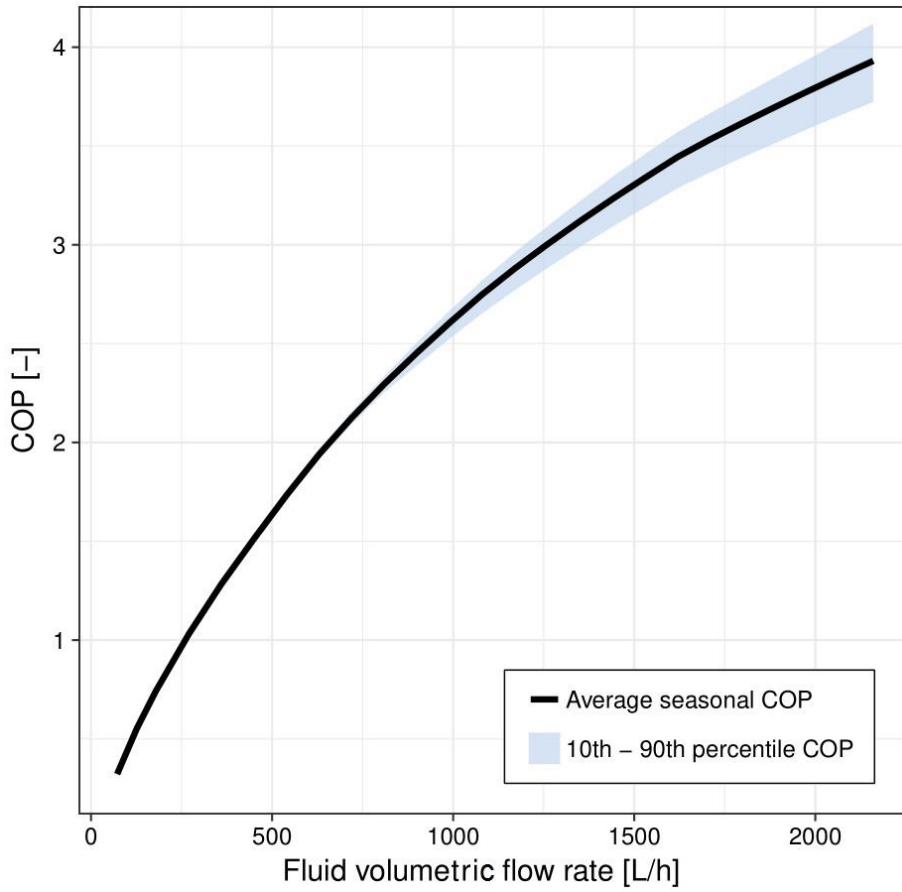


Fig. 2. COP of the entire heating system (comprising the MCHP, the vertical borehole GSHE and the UFH hydronic loops) as a function of the heat pump fluid volumetric flow rate [15].

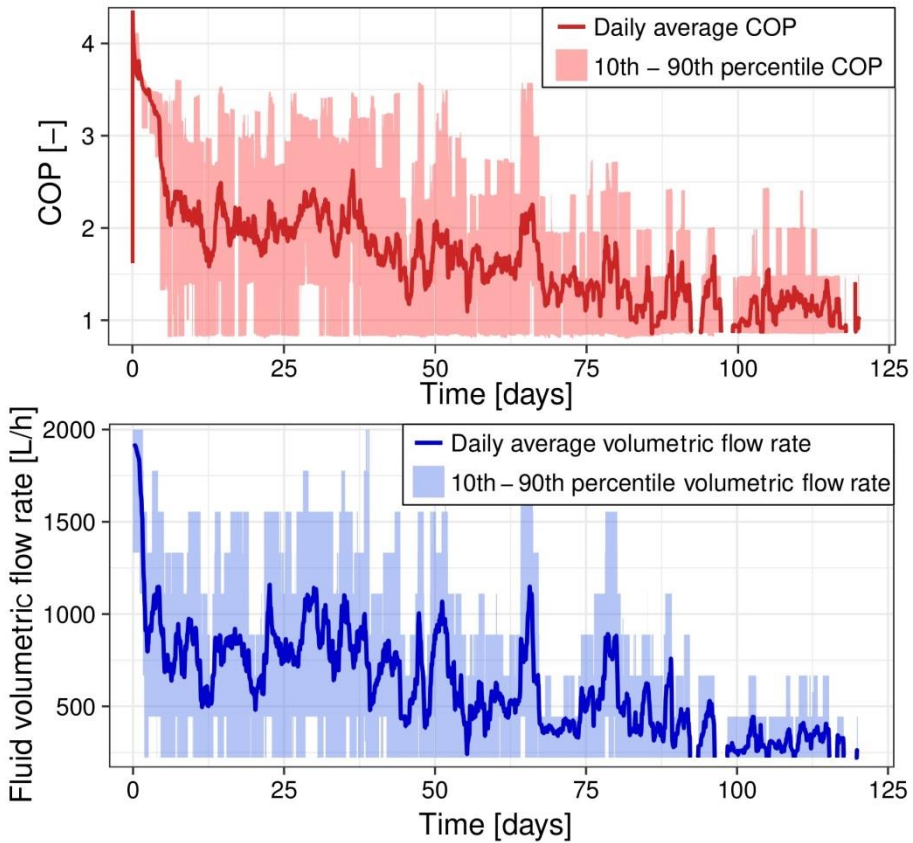


Fig. 3. COP and fluid volumetric flow rate of the MCHP heating system during a four-month winter test period [15].

1.3. Building energy flexibility

The major drawback of RES is the intermittence of power generation. The increasing share of RES in electricity grids can thus induce major mismatch between instantaneous energy use and production, leading to grid instability. A paradigm shift is occurring in the field of energy system management and the concept of Smart Grids with massive RES penetration is emerging. Consequently, there is an increasing demand for energy storage and energy end-user flexibility [16]. For that matter, the building sector should not be considered as a simple passive end-user but, on the contrary, as a major active player which can help regulating the electricity production and consumption. Buildings' energy demand can be modulated by means of thermal storage, HVAC usage adjustment, electric vehicles charging scheduling, plug-loads shifting, etc. These demand side management

measures are commonly denominated as “Building Energy Flexibility” strategies [17].

As mentioned before, the heating need for indoor space conditioning is a major target for building efficiency improvement. It is also the case for building energy flexibility strategies. The large potential for thermal energy storage (TES) in buildings can be cleverly employed to shift heating use in time and thus reshape the overall power profile. To that end, it was found that passive TES in the indoor environment and building structural thermal mass is more cost effective than enlarging storage water tanks [18]. In conventional vapour-compression heat pump (VCHP) systems, most of the flexibility is provided by an accumulation hot water tank. However, there is no water tank in the current MCHP system implementation [15]. Indoor temperature set point modulation for passive TES in the indoor space could therefore be a solution to enable building energy flexibility [19] and optimize the MCHP operation by increasing its running time at highest COP.

1.4. Aim of the current study

The current numerical study extends the previous research conducted on the integration of this innovative heat pump in dwellings [15] by implementing a new control strategy taking advantage of the building energy flexibility potential. Firstly, the MCHP system and the building study cases are described. The heat storage control strategy for optimized heating system performances is then presented. Finally, the benefits of this control strategy concerning the heat pump operation are discussed and followed by a conclusion and suggestions for further work on that research topic.

2. Magnetocaloric heat pump system

2.1. Characteristics of the magnetocaloric heat pump

The fundamental principle of a heat pump system is to transfer thermal energy from a cold source to a warmer sink. In order to achieve that, the magnetocaloric device (see **Fig. 4**) makes use of magnetic heating/cooling thermodynamic cycles, commonly named “active magnetic regenerator” (AMR) cycles. The refrigerant is a solid magnetocaloric material (MCM) arranged as packed bed spheres (450 μm diameter) in trapezoidal shaped-cassettes regenerators (63 mm by 61.43 mm). 13 of these regenerators are mounted on an iron ring that represents the vertical stator. A two-pole permanent magnet assembly is placed on the rotor to complete the rotary device which can create a varying magnetic field with a maximum value of 1.46 T. The rotation of the magnet subjects the beds filled with MCM to a time-varying magnetic field which, in return, exhibit a thermal response. When the MCM is magnetized, its temperature increases. When the MCM is demagnetized, its temperature decreases. The rotation frequency of the device is fixed at 1 Hz. For each of the regenerator beds there are two solenoid valves synchronized with the position of the magnet via an absolute encoder. These valves allow for bi-directional

circulation of the coolant fluid (20% vol ethylene glycol and 80% vol water) through the individual MCM porous media beds while the overall flow to the device is delivered by a continuously operating pump. The overall effect is to transfer thermal energy from the cold side to the warm side of the regenerators. A single centrifugal pump circulates the heat transfer fluid from the heat source to the two manifold distributors and from the two manifold collectors to the heat sink.

A detailed description of the EnovHeat MCHP device and its operation principle can be found in the paper published by Johra et al. [15].

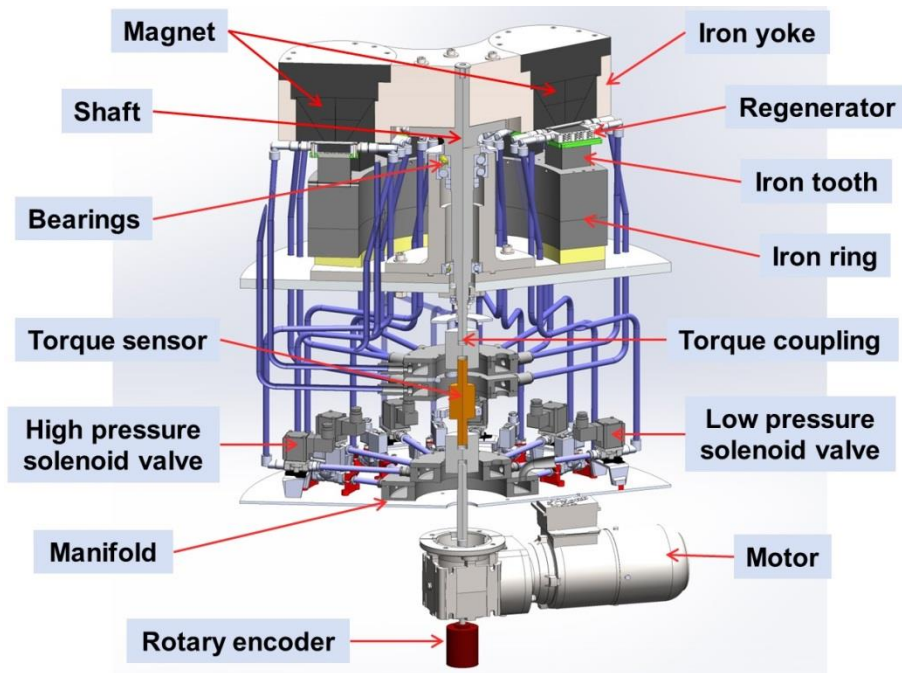


Fig. 4. Detailed description of the magnetocaloric heat pump prototype of the EnovHeat project: “MagQueen”.

2.2. Numerical modelling of the magnetocaloric heat pump

Originally, the MCHP has been modelled by Engelbrecht [20] and then further developed by Lei et al. [14]. If reasonable assumptions on regenerator's geometry, external heat losses and demagnetization losses are made, the time-dependent fluid temperature distribution in the AMR can be calculated with two coupled partial differential equations:

$$\begin{aligned} \frac{\partial}{\partial x} \left(k_{\text{disp}} A_c \frac{\partial T_f}{\partial x} \right) - \dot{m}_f c_f \frac{\partial T_f}{\partial x} - \frac{Nuk_f}{d_h} a_s A_c (T_f - T_s) + \left| \frac{\partial P}{\partial x} \frac{\dot{m}_f}{\rho_f} \right| \\ = A_c \varepsilon \rho_f c_f \frac{\partial T_f}{\partial t} \end{aligned} \quad (1)$$

$$\begin{aligned} \frac{\partial}{\partial x} \left(k_{\text{stat}} A_c \frac{\partial T_s}{\partial x} \right) + \frac{Nuk_f}{d_h} a_s A_c (T_f - T_s) \\ = A_c (1 - \varepsilon) \rho_s \times \left[c_H \frac{\partial T_s}{\partial t} + T_s \left(\frac{\partial s_s}{\partial H} \right)_{T_s} \frac{\partial H}{\partial t} \right] \end{aligned} \quad (2)$$

Where k , T , ρ , c and s are the thermal conductivity, temperature, density, specific heat, and specific entropy; A_c , d_h , a_s , ε , x , t , \dot{m}_f , and H are the cross sectional area, hydraulic diameter, specific surface area, porosity of the regenerator bed, axial position, time, fluid mass flow rate and internal magnetic field; $\partial P / \partial x$ and Nu are the pressure drop and the Nusselt number. The subscripts f and s represent fluid and solid refrigerant, respectively. k_{disp} is the thermal conductivity of the fluid due to axial dispersion, k_{stat} is the static thermal conductivity of regenerator and fluid, and c_H is the specific heat capacity of the MCM at constant magnetic field. An implicit finite volume method scheme is used to solve these equations within the MATLAB software environment. This numerical model has been successfully validated with experimental data of a real AMR device [21]. For the purpose of the numerical simulation of an entire building, the detailed MCHP model is approximated by a series of around 1600 quasi-steady states implemented in 5-dimensional lookup tables. These lookup tables are function blocks of the MATLAB-Simulink software environment which can generate the MCHP output values with minimum computation needs.

More details about the numerical modelling of the EnovHeat MCHP can be found in the paper published by Johra et al. [15].

3. Building systems

3.1. Building study case

The building study case of the EnovHeat project for testing the integration of the MCHP is a single family house in Denmark. This single-story dwelling has a heated floor surface area of 126 m² and a geometry which is typical for modern Danish houses (see **Fig. 5**). It is a low-energy building with a yearly heating need of 16 kWh/m² [22].

In the case of TES in the indoor environment, the building envelope performance and the structural thermal inertia are the main parameters determining the heat storage capacity and efficiency of a building and, consequently, its energy flexibility potential [23]. However, the current configuration of the MCHP is restricted to low-energy buildings. Therefore, only the structural thermal inertia of the house is varied to assess the influence of the energy flexibility on the MCHP performance. 3 different classes of structural thermal inertia are defined for this house:

- Light-weight structure building: daily effective thermal inertia of 30 Wh/K.m².
- Medium-weight structure building: daily effective thermal inertia of 60 Wh/K.m².
- Heavy-weight structure building: daily effective thermal inertia of 100 Wh/K.m².

The outdoor boundary conditions for air and ground temperature, solar gains, atmospheric pressure, cloud cover, relative humidity, wind speed and long wave radiation are extracted from the weather file of the Danish Reference Year (DRY 2013) [24]. It is assumed that 4 persons are living in the dwelling with occupancy following a representative weekly schedule for Denmark. The equipment and people load time distribution are set accordingly [25].

More details about the EnovHeat building study cases can be found in the paper published by Johra et al. [15] and in a DCE technical report [26].

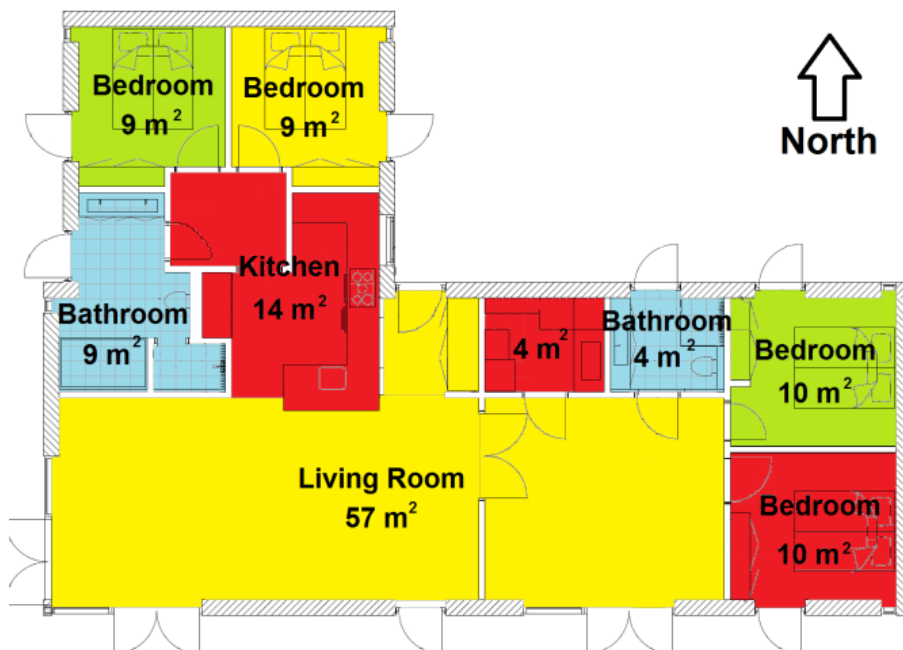


Fig. 5. Plan view of the house study case.

3.2. Heating systems

To maximize the performance of the heat pump system, a vertical borehole GSHE is used as high temperature heat source, and a hydronic radiant under-floor heating system is used as low temperature heat sink. The under-floor heating system consists of PE-Xa pipe (16 mm outer diameter) loops embedded in a 100 mm thick concrete screed in the case of the medium and heavy thermal inertia houses. For the light thermal inertia house cases, UFH pipes are embedded in the wooden floor. It has been sized according to international standards and manufacturer's guidelines [27][28][29]. The ground source loop is a vertical borehole heat exchanger consisting of a single collector double U-tube PEX pipe (44 mm diameter). The borehole is 100 m deep and has a diameter of 160 mm. The total pipe length of the ground loop is thus 200 m. The design and sizing of the GSHE has been made according to international standards and manufacturer's guidelines [30][31][32], and assuming that the soil is a humid clay sand.

The MCHP operates at temperatures and fluid flow rates which are compatible with direct use in the heat emitter. Therefore, the GSHE and the UFH are coupled to the MCHP inside a single hydronic loop without any intermediate heat exchanger or hot water storage tank (see **Fig. 6**). With that configuration, the same heat transfer fluid (20% vol ethylene glycol and 80% vol water) is circulated through the heat

source, the heat sink and the MCHP. The fluid flow is generated by the internal circulation pump of the MCHP which has a maximum volumetric flow rate of 2100 L/h.

The original controller for the MCHP heating system is a basic flow rate regulation. The speed of the circulation pump is adjusted to keep a nominal fluid volumetric flow rate of around 220 L/h in each UFH sub-circuits. There are 9 UFH hydronic loops arranged in the 8 thermal zones of the house. Each thermal zone has a thermostat adjusting the indoor temperature to a given set point by opening/closing a motorized valve with an ON/OFF controller.

The performance of the MCHP is compared with a conventional water-to-water VCHP implemented in the same building case with the same UFH system and vertical borehole GSHE. The VCHP has characteristics similar to the model TWM036 of ClimateMaster® [33]. With a nominal fluid flow rate of 2052 L/h in both heat source and heat sink, this ground source VCHP has a heating power output of 8.28 kW with a COP of 4.51 (heat source at 5 °C and heat sink at 35 °C). A 250 L hot water storage tank, 3 circulation pumps and a mixing valve are added to the heating system (see Fig. 7). The hot water accumulation tank has a temperature set point of 35 °C. The water temperature is measured in the top third of the water tank.

More details about the building heating systems can be found in the paper published by Johra et al. [15] and in a DCE technical report [26].

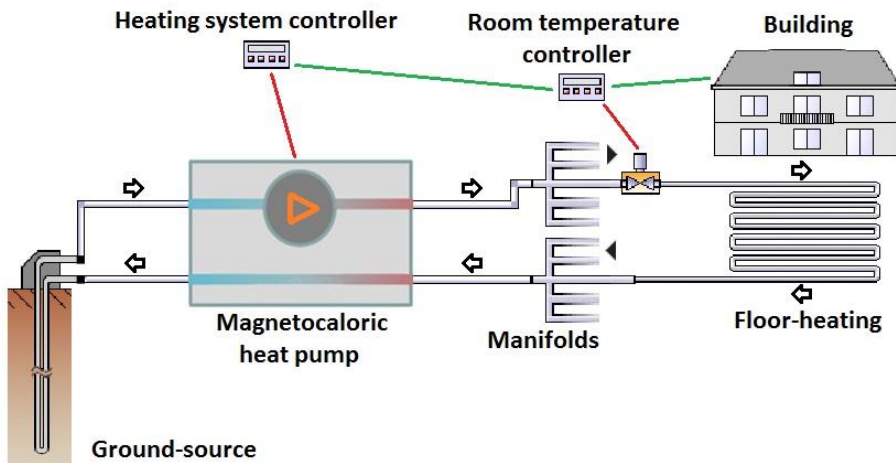


Fig. 6. Integration of a magnetocaloric heat pump in single hydronic loop with ground source heat exchanger and under-floor heating system.

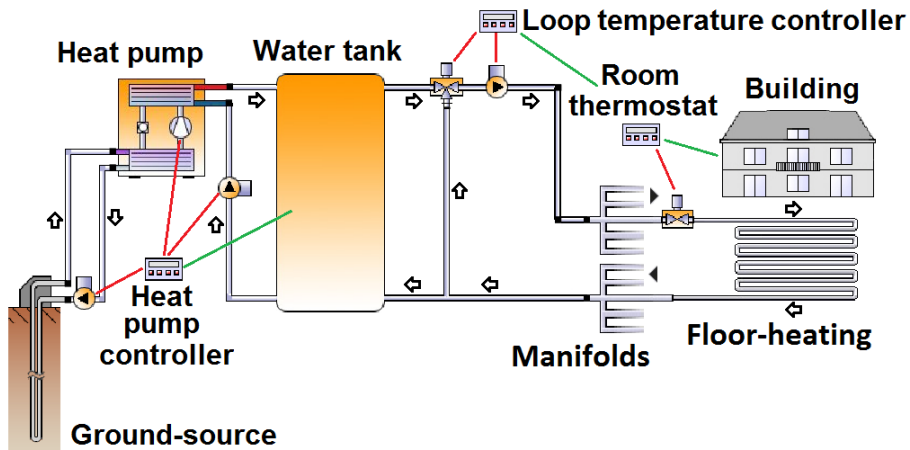


Fig. 7. Integration of a conventional vapour-compression heat pump with ground source heat exchanger, hot water storage tank and under-floor heating system.

3.3. Numerical modelling of the building systems

A thermodynamic multi-zone model of the building is created within the MATLAB-Simulink software environment. A one-dimensional explicit finite volume method with a limited number of control volumes is employed to calculate the heat transfer through the construction elements. Surfaces facing the indoor space are connected to the indoor air node within a star network configuration using constant mixed convection/radiation thermal resistance coefficients. Constant thermal resistances are used to model thermal bridges, ventilation, air infiltration and windows heat losses. Solar heat gains and long-wave radiation to the sky are calculated as a function of surface orientation and outdoor weather conditions.

The hydronic under-floor heating is modelled with the ϵ -NTU method [28][34] as a horizontal heat exchanger embedded in a multilayer slab. The dynamics of the fluid in the pipe network when the flow rate is varying are simulated with a “plug flow” model [35]. The vertical borehole GSHE component is created by coupling two straight pipe heat exchanger sub-models (ϵ -NTU method with “plug flow” model) in a triangular thermal network (Resistance-Capacitance network) [36]. The underground soil around the ground source is considered as a one-dimensional finite domain and implemented in a MATLAB state space function. Temperature boundary conditions are defined on the upper ground surface by the weather conditions. At a depth of 100 m, the ground temperature is set constant to 10.1 °C. The thermo-physical properties of the brine and the associated convective heat transfer coefficient in the pipes are calculated as a function of the fluid composition, velocity and temperature.

Similarly to the MCHP, the conventional VCHP is modelled with a collection of steady states implemented in a 4-dimensional lookup table function. The lookup

table data is obtained from documentation of the VCHP manufacturer [33]. The 250 L hot water storage tank has a cylindrical shape (radius of 29 cm; height of 95 cm) with 5 cm of polyurethane insulation (heat losses to the ambient are 1.356 W/K). The water tank model is a simplified version of that presented by Angrisani et al. [37].

The building model has been validated with a BESTEST procedure [38]. Sub-components of the building model have been validated against commercial software or experimental data. More details about the numerical models of the building systems can be found in the paper published by Johra et al. [15]. Validation test results and detailed description of the building sub-components can be found in a DCE technical report [26].

4. Heat storage control strategy

As mentioned before, the original MCHP controller is simple and causes the heating system to operate with modest performances. Because each room in the house has very different time profiles for heating need, it is very rare that all rooms need maximum heating power at the same time. Consequently, the MCHP does not run at the optimum fluid flow rate and highest COP most of the time.

A new control strategy is thus implemented. It takes advantage of the building energy flexibility potential by using indoor temperature set point modulation to allow TES in the indoor environment. When the heating system is activated, it operates at high capacity with optimum COP to store thermal energy in the house's thermal mass leading to a slight increase of the indoor temperature. When the building is fully charged, the heating system is completely turned off and the indoor temperature freely decreases until reaching a critical threshold for re-activation of the heat pump. The maximization of the MCHP operation time at optimum COP increases the overall performance of the heating system.

Fig. 8 illustrates in more details this new heat storage strategy and compares it to the simple controller (building case study with high thermal inertia: 100 Wh/K.m²). One can see in **Fig. 8(a)** that the house indoor temperature is allowed to vary around the “neutral temperature set point” of 22 °C. When the lowest temperature of the house (coldest room) reaches the “minimum temperature limit” (set between 20 °C and 22 °C), the heating system is activated (see **Fig. 8(b)**) and warms up all rooms at maximum power. If the temperature of a particular room is reaching the “maximum temperature limit” (set between 22 °C and 24 °C), the room's thermostat adjusts the fluid flow in the corresponding UFH loop to keep the temperature at the maximum temperature limit, which decreases accordingly the total fluid flow rate of the MCHP. When the average temperature of the house (defined as the floor area weighted average temperature of all rooms) reaches the maximum temperature limit, the whole heating system is turned off.

The temperature span between the minimum and maximum temperature limits centred on the neutral indoor temperature set point, cannot be greater than 4 K. These requirements maintain a normal thermal comfort level with less than 10% dissatisfied occupants [39].

One can see in **Fig. 8(c)** the clear change in the MCHP fluid flow rate profile. When the heating system is activated, the fluid flow rate is kept at its maximum most of the time. Consequently, the COP during operation time is greatly improved (see **Fig. 8(d)**).

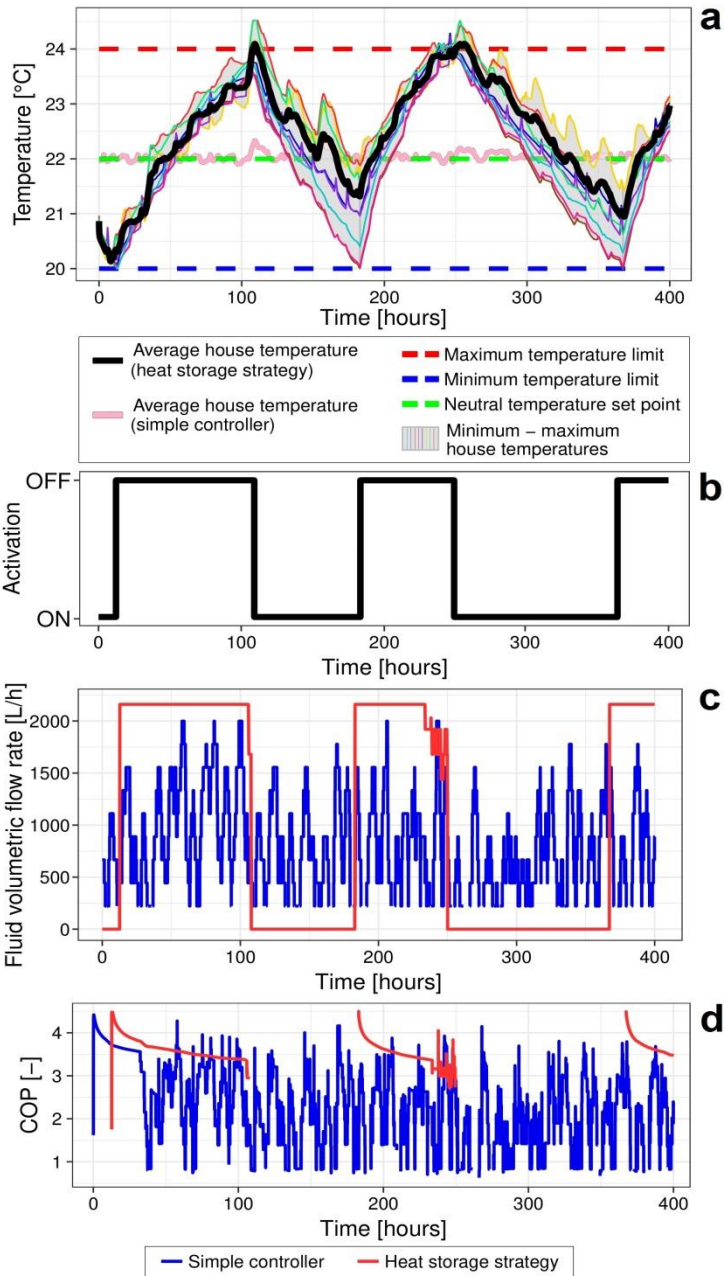


Fig. 8. Example of heat storage strategy control for MCHP: (a) temperatures in the house (with and without heat storage strategy); (b) activation of the MCHP (with heat storage strategy); (c) fluid volumetric flow rate of the MCHP (with and without heat storage strategy); (d) COP of the MCHP (with and without heat storage strategy).

5. Results and discussion

The simulation results presented hereafter correspond to a four-month heating period from the 1st of January to the 30th of April under Danish weather conditions [24]. The “heat storage temperature span” is defined as the difference between the minimum and the maximum temperature limits.

5.1. Performance metric

The performance of a heat pump system is commonly assessed by calculating its coefficient of performance (COP). In the case of the magnetocaloric device, COP_{MCHP} is calculated with the useful heating power $Q_{heating}$ delivered to the UFH, the circulation pump work W_{pump} , the motor work W_{motor} , and the valves work W_{valves} . In the case of the conventional vapour-compression heat pump, COP_{CVCHP} is calculated with the useful heating power $Q_{heating}$ delivered to the UFH, the compressor work $W_{compressor}$, and the work of the 3 circulation pumps W_{pump} .

$$COP_{MCHP} = \frac{Q_{heating}}{W_{pump} + W_{motor} + W_{valves}} \quad (3)$$

$$COP_{CVCHP} = \frac{Q_{heating}}{W_{compressor} + W_{pump}} \quad (4)$$

5.2. Example of magnetocaloric heat pump operation improvement with the heat storage strategy

In this section, we examine an example of magnetocaloric heat pump operation improvement by using a heat storage strategy. The building case has a medium thermal inertia of 60 Wh/K.m², and a heat storage temperature span of 4 K. One can clearly see in **Fig. 9** that the heat storage strategy enables a shift of most of the operation time towards maximum fluid flow rate. Consequently, the MCHP is activated less often and for shorter periods of time but with significantly improved COP (see **Fig. 10** and **Fig. 11**). In that case, the average COP of the heating system during the four-month heating period with a simple controller is of 1.81 (10th and 90th percentile of the COP are 0.83 and 3.20, respectively). The heat storage strategy improves the average COP to 3.48 (10th and 90th percentile of the COP are 3.00 and 3.89, respectively).

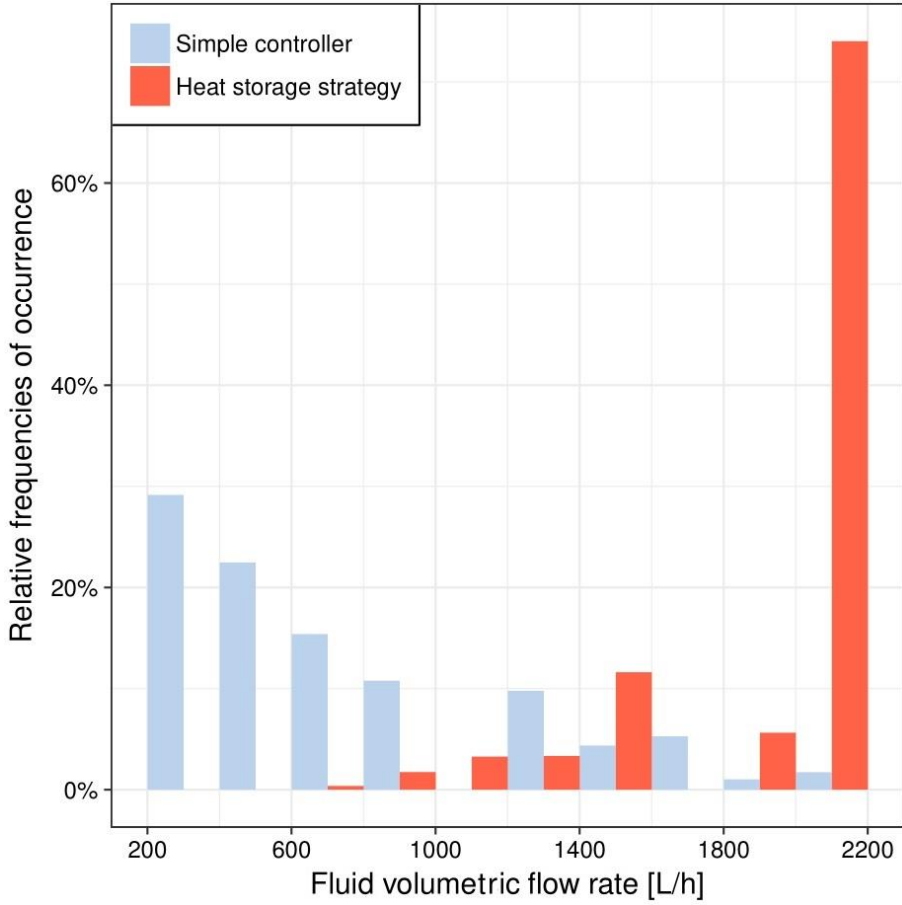


Fig. 9. Histogram of the MCHP heating system fluid volumetric flow rate during the four-month heating test period.

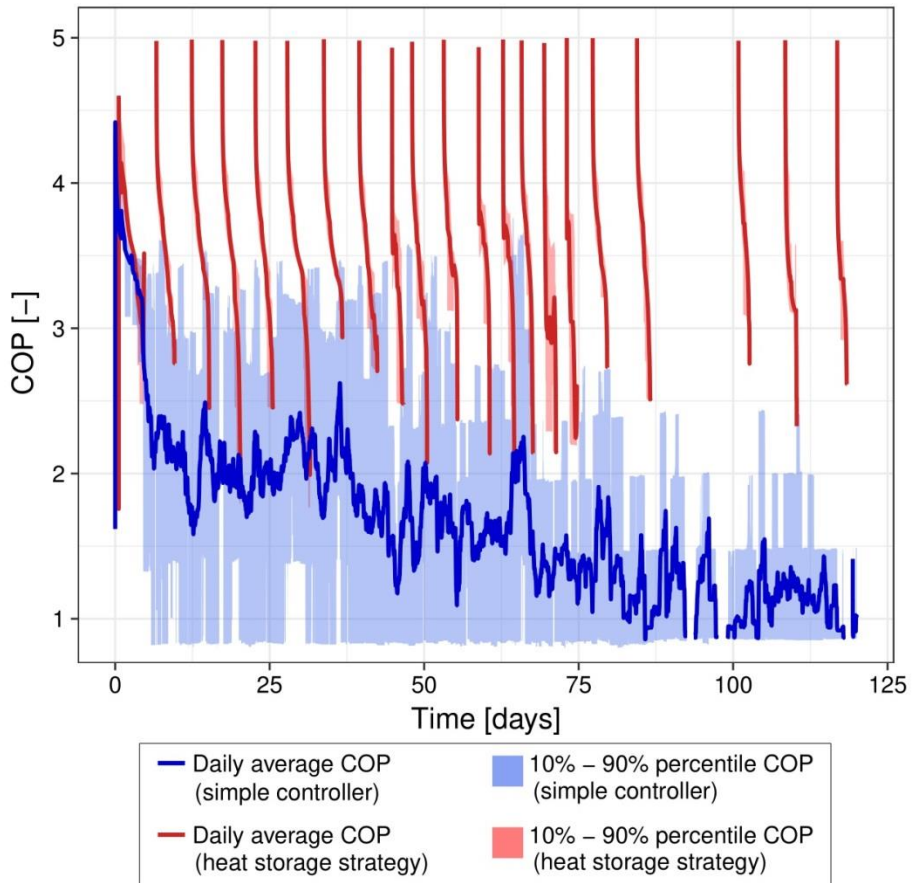


Fig. 10. COP of the MCHP system as a function of time during the four-month heating test period.

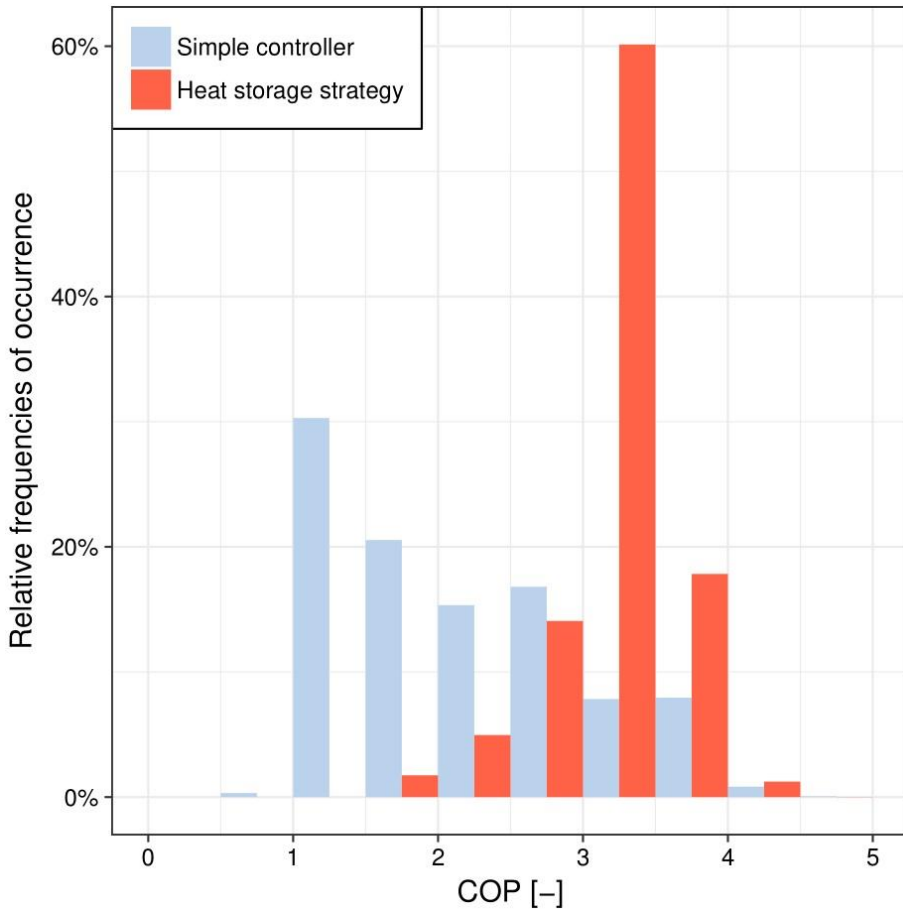


Fig. 11. Histogram of the MCHP heating system COP during the four-month heating test period.

5.3. Influence of building thermal inertia and heat storage temperature span on the magnetocaloric heat pump performance

In this section, the results of 18 different study cases are analysed. The MCHP system with a heat storage strategy is compared with the simple controller cases and the conventional VCHP cases. As mentioned before, 3 different classes of building thermal inertia are tested. The heat storage temperature span of the MCHP heat storage strategy is varied from 0 K to 4 K. The 0 K temperature span cases actually correspond to the simple controller cases.

One can see in **Fig. 12** that both the heat storage temperature span and the thermal inertia have a positive impact on the average fluid flow rate of the heat pump, which improves its performance. **Fig. 13** emphasizes the maximization of the time duration at which the heating system runs at full-load and optimum COP. In the first part of the MCHP activation period, the heating system runs at full capacity and highest COP. The second part of the MCHP activation period starts when the first room of the house reaches the maximum temperature limit. During that time, the heating system operates at part-load with lower COP until the MCHP is turned off. It is quite clear that the larger the heat storage temperature span and structural thermal inertia, the longer the first part of the activation period at continuous full heating capacity compared to the part-load period.

Fig. 14 presents the consequences of this maximization of the fluid flow rate in terms of COP for the heating system. Larger thermal inertia and heat storage temperature span lead to significant improvements of the COP. One can notice that even a moderate heat storage temperature span of 0.5 K can increase the average COP by 40%, 74% and 78% for light, medium and heavy structure houses, respectively. At a maximum heat storage temperature span of 4 K, the average COP reaches 2.90 (10th and 90th percentile of the COP are 2.11 and 3.44, respectively) for the light thermal inertia house, 3.48 (10th and 90th percentile of the COP are 3.00 and 3.89, respectively) for the medium thermal inertia house, and 3.51 (10th and 90th percentile of the COP are 3.12 and 3.89, respectively) for the heavy thermal inertia house. In the cases of medium and heavy houses, the MCHP with heat storage strategy presents performances which are comparable to those of the conventional VCHP system. However, the COP improvement of the MCHP is very limited for a heat storage temperature span above 2 K. In addition, it can be noted that medium and heavy thermal mass houses have very similar performances. The latter can be explained by the fact that the light-weight house cases have their UFH circuits embedded in a light-weight structure wooden floor, whereas it is a concrete screed UFH for medium and heavy-weight houses. The UFH loops enable an important thermal activation of the floor elements. Consequently, a concrete floor provides a much larger thermal storage potential than a wooden one. However, additional structural thermal mass such as concrete or brick walls and ceilings are not directly activated by the UFH. Therefore, its benefit in terms of MCHP operation improvement is limited.

Because no building envelope insulation is perfect, accumulating thermal energy in the indoor environment by increasing the building's internal temperature will necessarily lead to higher heat losses by transmission and ventilation. However, one

can see in **Fig. 15** that the improvement of the heating system COP over-compensates the envelope additional heat losses. This leads to a substantial decrease of the total energy use during the heating period of about 28% to 41%. In the cases of medium and heavy-weight houses, the total energy usage of the MCHP system with heat storage strategy is thereby similar to the conventional VCHP.

Another constraint of TES in the indoor space by means of temperature set point modulation is the variability of the operative temperature. To avoid thermal discomfort, the indoor temperature should not change faster than 2.1 K/h [40]. This requirement is fulfilled in every case here. However, the increase of temperature set point to 24 °C in well-insulated south-oriented rooms with large windows could increase the risks of discomfort due to over-heating during sunny days. **Fig. 16** illustrates this indoor temperature variability with the calculation of the difference between the 5th and 95th percentile of all rooms operative temperature during the four-month heating test period. Naturally, the temperature variability increases with the heat storage temperature span and decreases with building thermal inertia. It can be noted for medium and heavy-weight structure houses, the temperature variability with heat storage strategy never exceeds the one of the simple controller reference case, even with the maximum heat storage temperature span of 4 K.

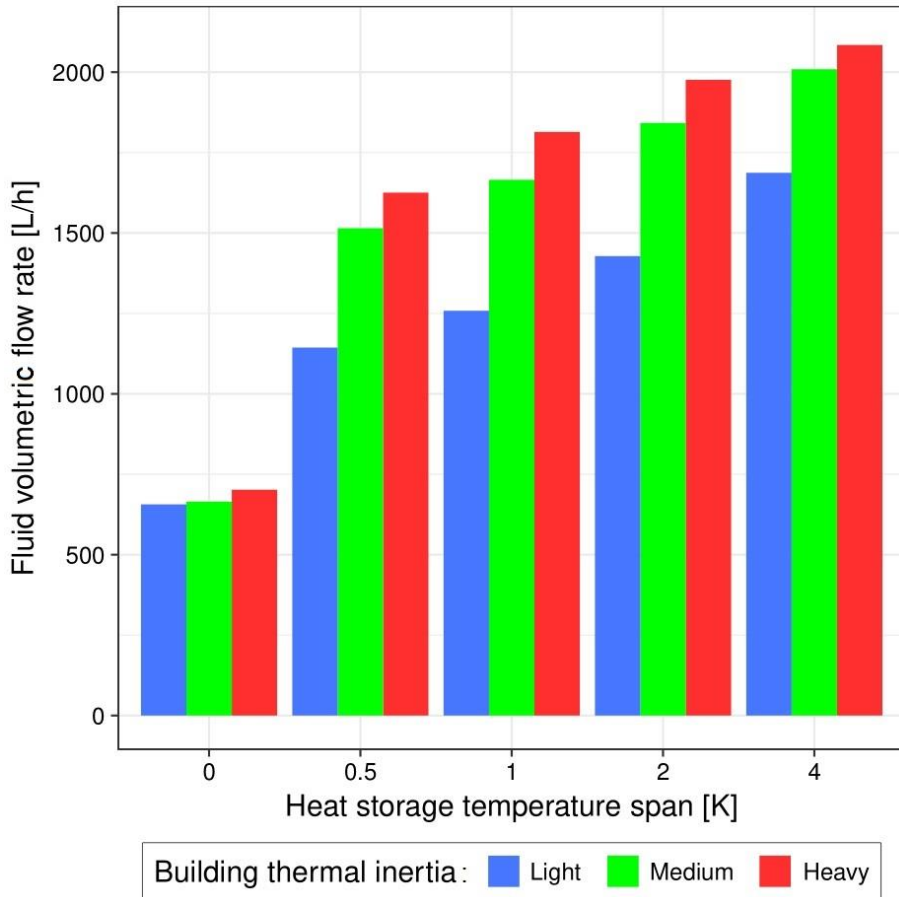


Fig. 12. Average fluid volumetric flow rates of the MCHP during the four-month heating test period.

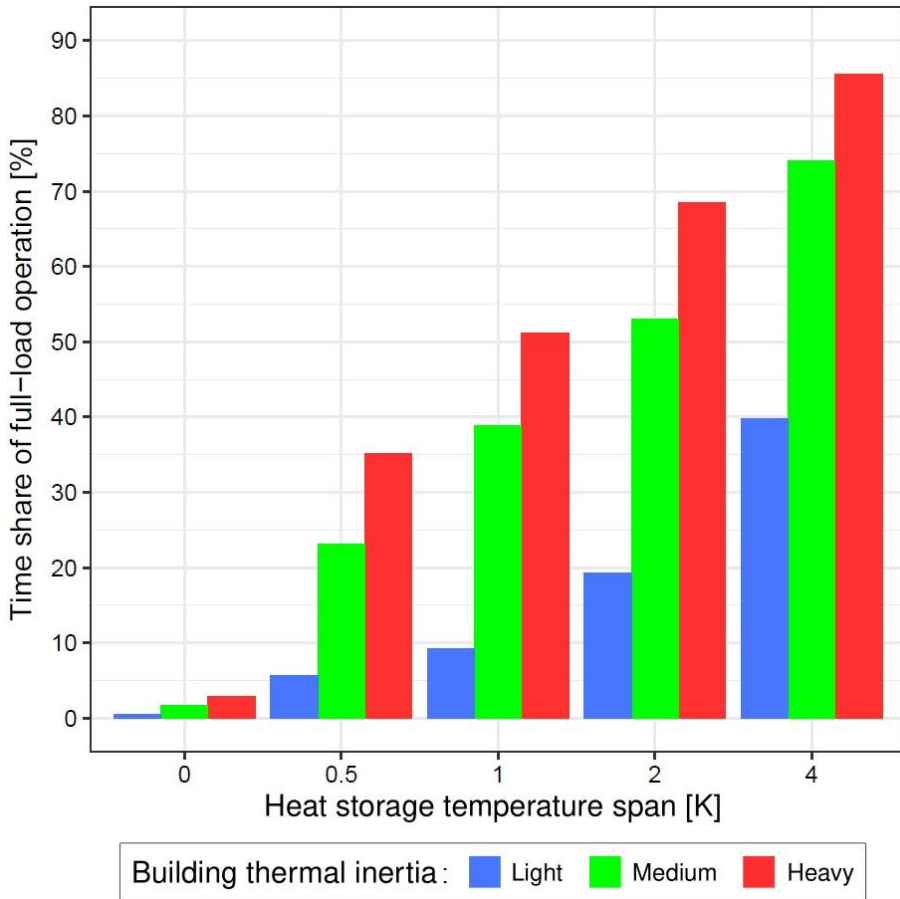


Fig. 13. Full-load operation time share of the MCHP during the four-month heating test period.

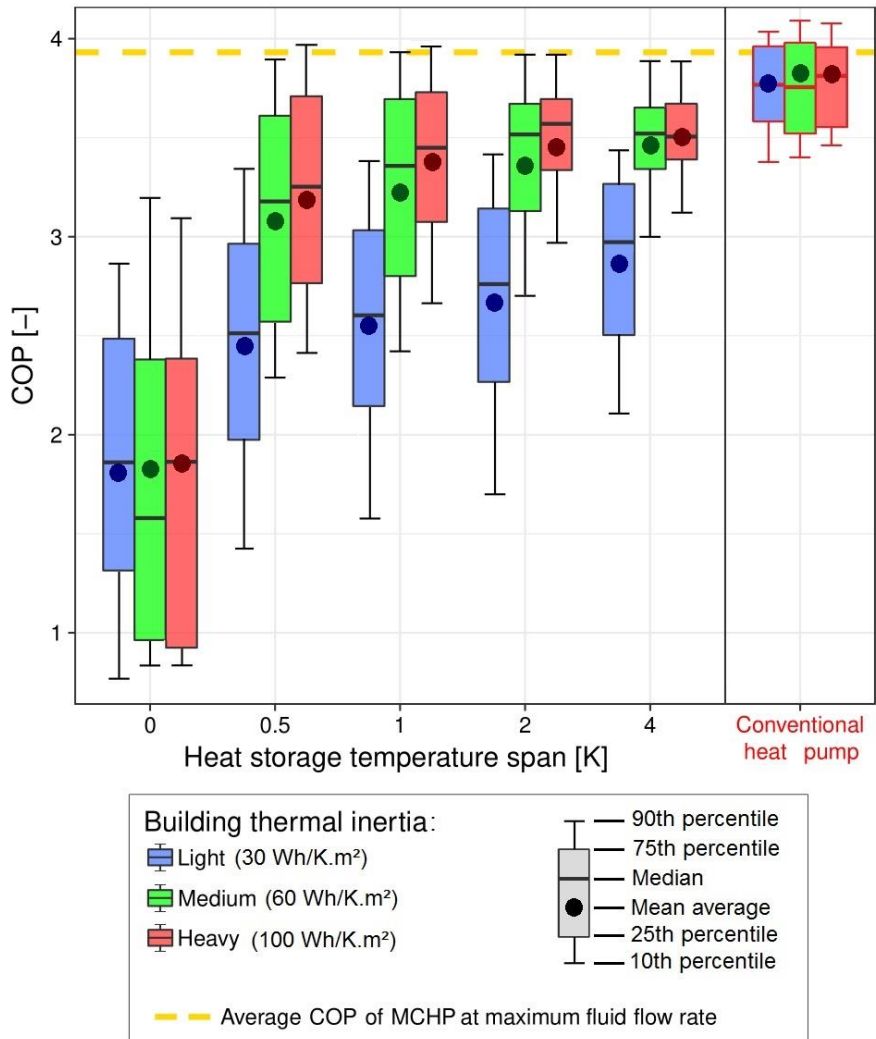


Fig. 14. Box plot diagram of the heat pump COP as a function of heat storage temperature span and building thermal inertia (MCHP on the left, conventional vapour-compression heat pump on the right).

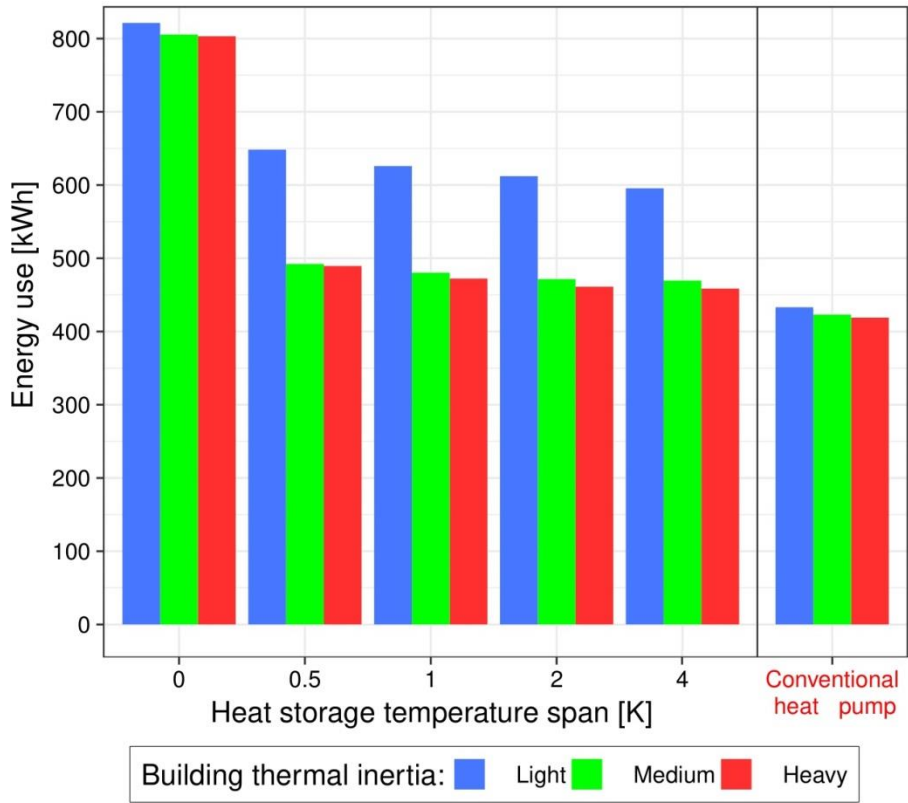


Fig. 15. Total heating use during the four-month heating test period (MCHP on the left, conventional vapour-compression heat pump on the right).

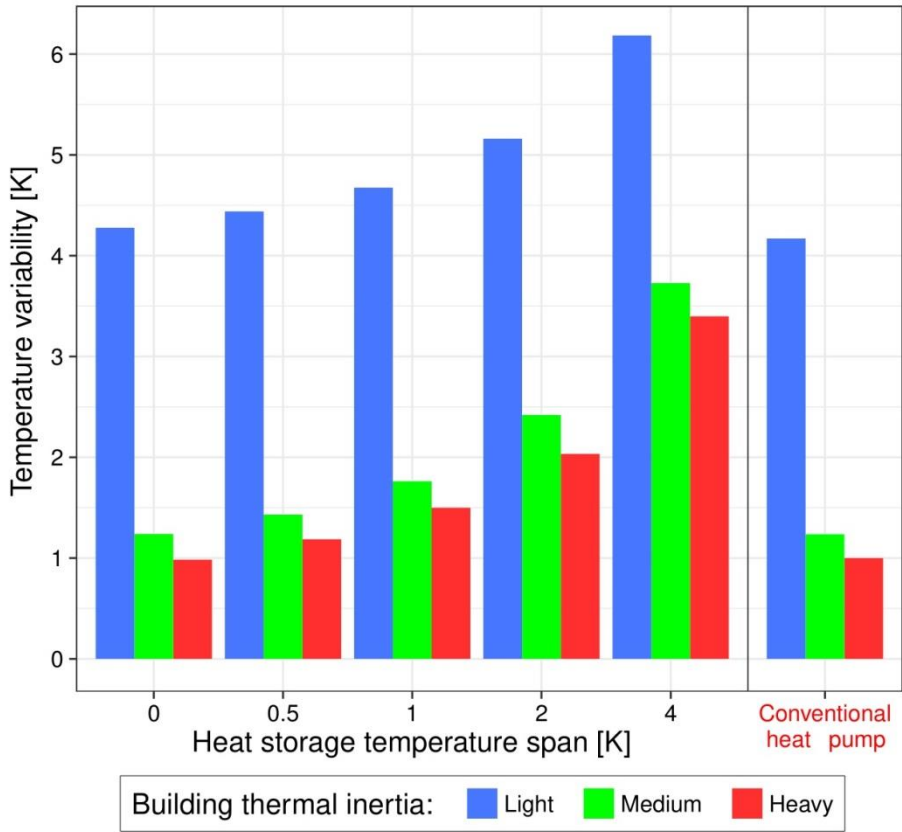


Fig. 16. Temperature variability (difference between 5th and 95th percentile of the house temperature) during the four-month heating test period (MCHP on the left, conventional vapour-compression heat pump on the right).

6. Conclusion

This numerical study has tested the use of a heat storage strategy in order to improve the operation performance of a magnetocaloric heat pump integrated in a low-energy Danish residential building. This innovative heating system can be implemented in a single hydronic loop including a vertical borehole ground source heat exchanger and a radiant under-floor heating without intermediate heat exchanger or hot water storage tank. Because the magnetocaloric heating system presents an optimum coefficient of performance at maximum fluid flow rate (average COP of 3.93), it is beneficial to minimize its part-load operation time. In conventional heat pump configurations, the hot water storage tank allows a certain power generation flexibility which reduces the number of ON/OFF cycles and improves global performances. In the case of the magnetocaloric system, the building thermal inertia is employed to enable energy flexibility. Indoor temperature set point modulation is used to store heat in the built environment and thus maximize the full-load operation time. Heating needs are shifted in time and concentrated over longer periods where the magnetocaloric device can run at full capacity with highest COP.

Both the building thermal inertia and the heat storage temperature span (difference between upper and lower limit for the temperature set point modulation controller) have positive impacts on the magnetocaloric system performance. A moderate heat storage temperature span of 0.5 K can increase the average COP by 40%, 74% and 78% for light, medium and heavy structure houses, respectively. With a maximum temperature set point modulation of 4 K, the average COP reaches 2.90, 3.48 and 3.51 for light, medium and heavy structure houses, respectively. These performances are comparable with conventional vapour-compression heat pump installations. Despite the increase of transmission and ventilation losses, the heat storage strategy decreased the total energy use by about 28% to 41% during the four-month heating test period.

Conclusions can be drawn about the impact of the building thermal mass and heat storage temperature span on the magnetocaloric heat pump performance. The thermal mass of the concrete screed where the under-floor heating circuit is laid, brings great benefits compared to a light-weight wooden floor. This large thermal inertia is well thermally activated and offers good heat storage for higher average heat pump COP. However, additional thermal mass of walls and ceilings has only limited impact because these construction elements are not directly activated by the under-floor heating system. Concerning the temperature set point modulation controller, a temperature span above 2 K does not improve the heat pump operation much, whereas it significantly increases the temperature variability in the dwelling.

This article has demonstrated the possibility of using heat storage in the indoor environment as an effective strategy to optimize the operation of the magnetocaloric heat pump. It can significantly improve the average COP of the entire heating system and reduce the energy usage, but, as a trade-off, decreases the building temperature stability, augmenting the risks of over-heating and thermal discomfort.

Further research should be carried out on new control strategies and building integration possibilities for this innovative magnetocaloric device. The heat storage

in the indoor environment is built upon the relatively large range of human thermal comfort. However, the acceptability of the occupants regarding automated temperature set point modulation should be tested, especially for dwellings. The robustness of such a control strategy should also be further studied in the case of buildings with critical rooms which cool down much faster than the others. Finally, cascading configurations for the magnetocaloric heat pump could generate much larger temperature span between heat source and heat sink, allowing its use domestic hot water production.

Acknowledgements

This work was financed by the ENOVHEAT project which is funded by Innovation Fund Denmark (contract no 12-132673) and was carried out partly within the framework of IEA EBC Annex 67 Energy Flexible Buildings.

References

- [1] United Nations Framework Convention on Climate Change, Report of the Conference of the Parties on its twenty-first session, held in Paris from 30 November to 13 December 2015 - Adoption of the Paris Agreement, 2015.
- [2] European Climate Foundation, Roadmap 2050: a practical guide to a prosperous, low-carbon Europe, Technical report, 2010.
- [3] Building Performance Institute Europe (BPIE), Europe's Buildings under the Microscope, Executive Summary 2011. http://bpie.eu/wp-content/uploads/2015/10/HR_EU_B_under_microscope_study.pdf, 2011 (accessed 24 January 2018).
- [4] S.J. Self, B.V. Reddy, M.A. Rosen, Geothermal heat pump systems: Status review and comparison with other heating options, *Applied Energy* 111 (2013) 341-348.
- [5] D. Fischer, H. Madani, On heat pumps in smart grids: A review, *Renewable and Sustainable Energy Reviews* 70 (2017) 342-357.
- [6] H. Lund, B. Möller, B.V. Mathiesen, A. Dyrelund, The role of district heating in future renewable energy systems, *Energy* 35 (3) (2010) 1381-90.
- [7] A. Palzer, H.M. Henning, A comprehensive model for the German electricity and heat sector in a future energy system with a dominant contribution from renewable energy technologies – Part II: Results, *Renewable and Sustainable Energy Reviews* 30 (2014) 1019-1034.
- [8] J. Cockroft, N. Kelly, A comparative assessment of future heat and power sources for the UK domestic sector, *Energy Conversion and Management* 47 (2006) 2349-2360.
- [9] T. Nowak, P. Westring, The European Heat Pump Association AISBL (EHPA), European heat pump market and statistics report 2015. http://www.ehpa.org/fileadmin/red/07_Market_Data/2014/EHPA_European_Heat_Pump_Market_and_Statistics_Report_2015_-_executive_Summary.pdf, 2015 (accessed 24 January 2018).

- [10] C.R.H. Bahl, EnovHeat project summary: development of efficient novel magnetocaloric heat pumps. <http://www.enovheat.dk/Research/ProjectSummary>, 2015 (accessed 24 January 2018).
- [11] A. Smith, C.R.H. Bahl, R. Bjørk, K. Engelbrecht, K.K. Nielsen, N. Pryds, Materials challenges for high performance magnetocaloric refrigeration devices, *Advanced Energy Materials* 2 (2012) 1288-1318.
- [12] A. Kitanovski, J. Tušek, U. Tomc, U. Plaznik, M. Ožbolt, A. Poredoš, *Magnetocaloric Energy Conversion: From Theory to Applications*, Springer International Publisher, New York, 2015.
- [13] K. Engelbrecht, D. Eriksen, C.R.H. Bahl, R. Bjørk, J. Geyti, J.A. Lozano, K.K. Nielsen, F. Saxild, A. Smith, N. Pryds, Experimental results for a novel rotary active magnetic regenerator, *International Journal of Refrigeration* 35 (2012) 1498-1505.
- [14] T. Lei, K. Engelbrecht, K.K. Nielsen, C.T. Veje, Study of the geometries of active magnetic regenerators for room temperature magnetocaloric refrigeration, *Applied Thermal Engineering* 111 (2017) 1232-1243.
- [15] H. Johra, K. Filonenko, P. Heiselberg, C. Veje, T. Lei, S. Dall'Olivo, K. Engelbrecht, C. Bahl, Integration of a magnetocaloric heat pump in a low-energy residential building, *Building Simulation* (2018).
- [16] B.V. Mathiesen, H. Lund, D. Connolly, H. Wenzel, P.A. Østergaard, B. Möller, S. Nielsen, I. Ridjan, P. Karnøe, K. Sperling, F.K. Hvelplund, Smart Energy Systems for coherent 100% renewable energy and transport solutions, *Applied Energy* 145 (2015) 139-154.
- [17] S.J. Østergaard, A. Marszal-Pomianowska, R. Lollini, W. Pasut, A. Knotzer, P. Engelmann, A. Stafford, G. Reynders, IEA EBC Annex 67 Energy Flexible Buildings, *Energy and Buildings* 155 (2017) 25-34.
- [18] K. Hedegaard, B.V. Mathiesen, H. Lund, P. Heiselberg, Wind power integration using individual heat pumps – Analysis of different heat storage options, *Energy* 47 (2012) 284-93.
- [19] J. Le Dréau, P. Heiselberg, Energy flexibility of residential buildings using short term heat storage in the thermal mass, *Energy* 111 (2016) 991-1002.
- [20] K. Engelbrecht, C.R.H. Bahl, Evaluating the effect of magnetocaloric properties on magnetic refrigeration performance, *Journal of Applied Physics* 108 (2010) 123918.
- [21] T. Lei, K. Navickaitė, K. Engelbrecht, A. Barcza, H. Vieyra, K.K Nielsen, C.R.H. Bahl, Passive characterization and active testing of epoxy bonded regenerators for room temperature magnetic refrigeration, *Applied Thermal Engineering* 128 (2018) 10-19.
- [22] The Danish Ministry of Economic, Business Affairs Enterprise, and Construction Authority, Building Regulations. http://bygningsreglementet.dk/file/155699/BR10_ENGLISH.pdf, 2010 (accessed 24 January 2018).
- [23] H. Johra, P. Heiselberg, J. Le Dréau, Influence of envelope, structural thermal mass and indoor content on the building heating energy flexibility, *Energy and Buildings* (under review).
- [24] P.G. Wang, M. Scharling, K.P. Nielsen, K.B. Wittchen, C. Kern-Hansen, Danish Ministry of Climate, Energy and Building, 2001-2010 Danish Design Reference Year – Reference climate dataset for technical dimensioning in building, construction and other sectors, Technical Report 13-19, 2013.
- [25] R.L. Jensen, J. Nørgaard, O. Daniels, R.O. Justesen, Person-og forbrugsprofiler: bygningsintegreret energiforsyning, DCE Technical Reports; Nr. 69.

- http://vbn.aau.dk/files/63284701/Person_og_Forbrugsprofil.pdf, 2011 (accessed 24 January 2018).
- [26] H. Johra, P. Heiselberg, Description and Validation of a MATLAB-Simulink Single Family House Energy Model with Furniture and Phase Change Materials, DCE Technical Reports; No. 187. http://vbn.aau.dk/files/244109005/Description_and_Validation_of_a_MATLAB_Simulink_Single_Family_House_Energy_Model_with_Furniture_and_Phase_Change_Materials.pdf, 2016 (accessed 24 January 2018).
- [27] European Committee for Standardization, EN 1264:2011 - Water based surface embedded heating and cooling systems, 2011.
- [28] International Organization for Standardization, ISO 11855:2012 - Building environment design. Design, dimensioning, installation and control of embedded radiant heating and cooling systems, 2012.
- [29] Uponor GmbH, Heating and cooling solutions - Technical guidelines, 2008.
- [30] Verlag des Vereins Deutscher Ingenieure, VDI 4640:2001, Thermal use of the underground-Ground source heat pump systems, 2001.
- [31] Uponor GmbH, Ground Energy Technical Information, 2012.
- [32] RETScreen International, Minister of Natural Resources Canada, Ground-Source Heat Pump Project Analysis. Canada, 2005.
- [33] ClimateMaster, Tranquility Water-to-Water (TMW) Series Submittal Data Model TMW036 – 340 50Hz - HFC-410A. <http://energy.hu/dokuk/termekek/103/98caovp2.pdf>, 2012 (accessed 24 January 2018).
- [34] M. Scarpa, K. Grau, B.W. Olesen, Development and validation of a versatile method for the calculation of heat transfer in water-based radiant systems, in: Proceedings of the 11th International Building Performance Simulation Association Conference and Exhibition (BS2009), Glasgow, Scotland, 2009.
- [35] University of Wisconsin-Madison Solar Energy Laboratory, TRANSSOLAR Energietechnik GmbH, CSTB, TESS, Type 31: Pipe Or Duct, in: TRNSYS 17 - Mathematical Reference, 2012, pp. 186-188.
- [36] H.J.G. Diersch, D. Bauer, W. Heidemann, W. Rühaak, P. Schätzl, Finite element modeling of borehole heat exchanger systems - Part 1. Fundamentals, Computers and Geosciences 37 (2011) 1122-1135.
- [37] G. Angrisani, M. Canelli, C. Roselli, M. Sasso, Calibration and validation of a thermal energy storage model: influence on simulation results, Applied Thermal Engineering 67 (2014) 190-200.
- [38] ANSI/ASHRAE Standard, Standard 140-2011: Standard method of test for the evaluation of building energy analysis computer programs, 2011.
- [39] European Committee for Standardization, EN ISO 7730 - Ergonomics of the thermal environment-analytical determination of thermal comfort by using calculation of the PMV and PPD indices and local thermal comfort criteria, 2005.
- [40] ASHRAE Standard, Standard 55 – 2004: Thermal environmental conditions for human occupancy, 2004.

Appendix F. Technical Report I

Johra, H., & Heiselberg, P. K. (2018). *Description and Validation of a MATLAB - Simulink Single Family House Energy Model with Furniture and Phase Change Materials (Update)*. Aalborg: Aalborg University, Department of Civil Engineering. DCE Technical Reports, No. 238.

[http://vbn.aau.dk/files/270078674/Description and Validation of a MATLAB Simulink Single Family House Energy Model with Furniture and Phase Change Materials Update .pdf](http://vbn.aau.dk/files/270078674/Description_and_Validation_of_a_MATLAB_Simulink_Single_Family_House_Energy_Model_with_Furniture_and_Phase_Change_Materials_Update_.pdf)



Aalborg Universitet

AALBORG UNIVERSITY
DENMARK

Description and Validation of a MATLAB - Simulink Single Family House Energy Model with Furniture and Phase Change Materials (Update)

Johra, Hicham; Heiselberg, Per Kvols

Publication date:
2018

Document Version
Publisher's PDF, also known as Version of record

[Link to publication from Aalborg University](#)

Citation for published version (APA):
Johra, H., & Heiselberg, P. K. (2018). Description and Validation of a MATLAB - Simulink Single Family House Energy Model with Furniture and Phase Change Materials (Update). Aalborg: Aalborg University, Department of Civil Engineering. DCE Technical Reports, No. 238

General rights

Copyright and moral rights for the publications made accessible in the public portal are retained by the authors and/or other copyright owners and it is a condition of accessing publications that users recognise and abide by the legal requirements associated with these rights.

- ? Users may download and print one copy of any publication from the public portal for the purpose of private study or research.
- ? You may not further distribute the material or use it for any profit-making activity or commercial gain
- ? You may freely distribute the URL identifying the publication in the public portal ?

Take down policy

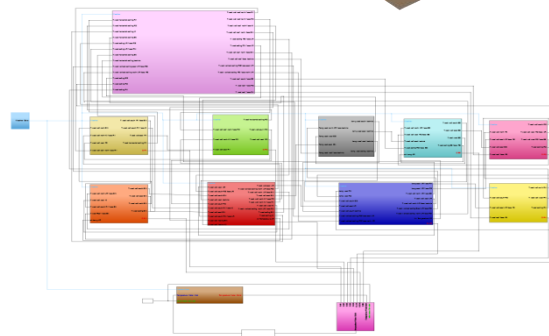
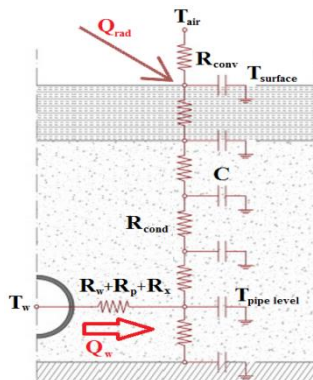
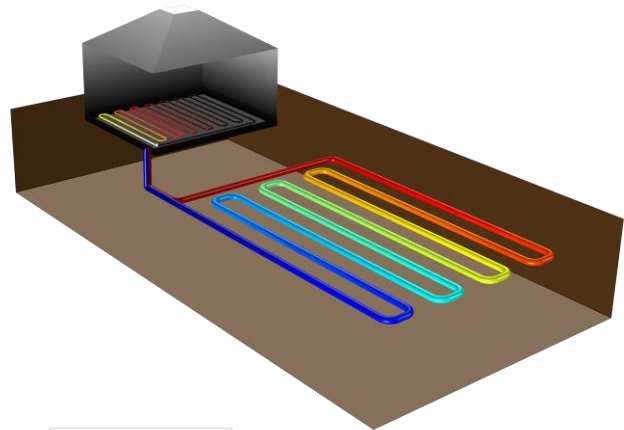
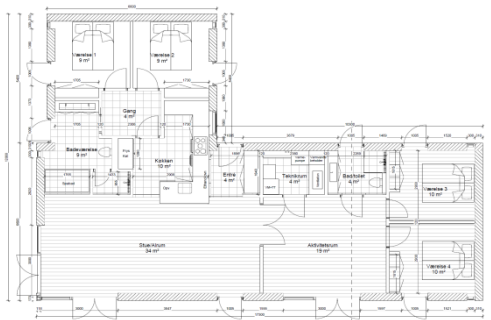
If you believe that this document breaches copyright please contact us at vbn@aub.aau.dk providing details, and we will remove access to the work immediately and investigate your claim.



DEPARTMENT OF CIVIL ENGINEERING
AALBORG UNIVERSITY

Description and Validation of a MATLAB - Simulink Single Family House Energy Model with Furniture and Phase Change Materials (Update)

Hicham Johra
Per Heiselberg



Aalborg University
Department of Civil Engineering
Architectural Engineering

DCE Technical Report No. 238

Description and Validation of a MATLAB - Simulink Single Family House Energy Model (Update)

by

Hicham Johra
Per Heiselberg

February 2018

© Aalborg University

Scientific Publications at the Department of Civil Engineering

Technical Reports are published for timely dissemination of research results and scientific work carried out at the Department of Civil Engineering (DCE) at Aalborg University. This medium allows publication of more detailed explanations and results than typically allowed in scientific journals.

Technical Memoranda are produced to enable the preliminary dissemination of scientific work by the personnel of the DCE where such release is deemed to be appropriate. Documents of this kind may be incomplete or temporary versions of papers—or part of continuing work. This should be kept in mind when references are given to publications of this kind.

Contract Reports are produced to report scientific work carried out under contract. Publications of this kind contain confidential matter and are reserved for the sponsors and the DCE. Therefore, Contract Reports are generally not available for public circulation.

Lecture Notes contain material produced by the lecturers at the DCE for educational purposes. This may be scientific notes, lecture books, example problems or manuals for laboratory work, or computer programs developed at the DCE.

Theses are monographs or collections of papers published to report the scientific work carried out at the DCE to obtain a degree as either PhD or Doctor of Technology. The thesis is publicly available after the defence of the degree.

Latest News is published to enable rapid communication of information about scientific work carried out at the DCE. This includes the status of research projects, developments in the laboratories, information about collaborative work and recent research results.

Published 2018 by
Aalborg University
Department of Civil Engineering
Thomas Manns Vej 23
DK-9220 Aalborg Øst, Denmark

Printed in Aalborg at Aalborg University

ISSN 1901-726X
DCE Technical Report No. 238

Contents

Contents	5
Introduction.....	7
1. Presentation of the Case Study Buildings.....	8
1.1. EnovHeat Case Study Building.....	8
1.2. Energy Flexibility Case Study Buildings.....	14
1.3. Conventional Heat Pump System	17
1.4. Magnetocaloric Heat Pump System	18
1.5. Under Floor Heating Systems	18
1.6. Ground Source Heat Exchangers	20
1.7. Phase Change Material.....	25
1.8. Phase Change Material Wallboard.....	28
1.9. Additional Indoor Thermal Mass / Furniture.....	30
1.8. Phase Change Material Integrated into Furniture Elements.....	30
2. Presentation of the Building Model	31
2.1. Construction Elements	31
2.2. Windows, Thermal Bridges, Ventilation and Infiltration Losses	36
2.3. Zone Air Node.....	37
2.4. Multi-Zone Building Model.....	38
2.5. Weather Data	39
2.6. Solar Gains and Internal Gains	41
2.7. Radiator Heating System	43
2.8. Hydronic Under-Floor Heating Systems	43
2.9. Horizontal Ground Source Heat Exchanger.....	47
2.10. Vertical Borehole Ground Source Heat Exchanger.....	48
2.11. Water-Based Brines of the Hydronic Networks	50
.....	56

2.13.	Heat Pump System	57
2.14.	Circulation Pump for Water-Based Heating System.....	58
2.15.	Hot Water Storage Tank	60
2.15.	Phase Change Material Wallboard	62
2.15.	Furniture / Indoor Content	65
3.	Validation of the Building Model.....	66
3.1.	Validation of the Construction Element with BSim Software	66
3.2.	Validation of the Multi-Zone Model with BSim Software	68
3.3.	Validation of the Building Model with BESTEST	71
3.4.	Validation of Under Floor Heating System and Horizontal Ground Source Heat Exchanger with BSim Software	77
3.5.	Validation of Vertical Borehole Ground Source Heat Exchanger with Experimental Data	80
3.6.	Validation of Phase Change Material Model with the COMSOL Software and the Guarded Hot Plate Apparatus Experimental Tests.....	81
	Conclusion	86
	References.....	87

Introduction

In recent years, significant efforts have been made to decrease the energy consumption of our societies. In heating dominated climates such as in Denmark, in Germany or in the U.K, individual heat pumps have been found to be the most efficient heat supply for buildings detached from district heating network [1][2][3]. This flexible technology can also improve the integration of intermittent renewable energy sources (RES). Heat pumps thus became a key component for the energy development policy of many countries, leading to a substantial increase of the market demand [4]. It is therefore important to bring new and cost effective technical solutions.

The “EnovHeat” project aims to develop an innovative magnetocaloric heat pump based on the active magnetic regenerator technology with a higher coefficient of performance (COP) than conventional vapour-compression heat pumps. It should be able to provide for the indoor space heating needs of a recently built single family house in Denmark [5].

The main task of the work package conducted at Aalborg University is to investigate how to integrate a magnetocaloric heat pump into a residential building, and assess its performance and impact on the overall system [6]. The objective is to demonstrate the feasibility and the advantages of using such magnetocaloric device compared to conventional solutions and develop an efficient control strategy for it.

A typical Danish single family house is used as case study. The magnetocaloric heat pump model has been developed within the MATLAB software environment. It must be tested in a versatile environment with the possibility for implementation of complex controller and small simulation time step resolution. A MATLAB - Simulink multi-zone model is therefore created for the dwelling with water-based under floor heating (UFH) system and two different types of ground source heat exchangers (GSHE): horizontal and vertical.

Passive heat accumulation or thermal energy storage (TES) in the indoor space is an efficient way to modulate house heating power usage [7]. Flexible demand side management was found to improve the operation of a smart energy grid systems with a large share of intermittent RES [8]. This building energy flexibility potential can also be employed to optimize the operation of the magnetocaloric heat pump. For that reason, the building model is also used to assess the impact of additional indoor content thermal mass on the house energy flexibility capacity [9]. A simplified model of furniture / indoor content is implemented together with a phase change material (PCM) model based on finite volume method and enthalpy formulation.

This report aims to present in details the numerical building model and each of its elements. In the second part, the results of different validation tests are presented to certify the reliability of the model and thus the results of numerical analyses using it.



1. Presentation of the Case Study Buildings

1.1. EnovHeat Case Study Building

The EnovHeat project aims to create a magnetocaloric heat pump which is able to provide 2 kW of heating power for a single family house with a temperature span of around 20 °C - 30 °C between the ground source and the heating emitter [5]. These objectives are only reachable for a well-insulated building.

The “iLiving Project” single storey house is chosen to be the case study of the EnovHeat project. It is a typical newly built low energy single family house located in Løkken, Denmark.



Figure 1: Location of the building case study in Denmark.

This house has been designed according to the Danish building regulation “BR10” [10] with the goal of achieving very low energy consumption . It is equipped with a heat recovery ventilation system and has a radiant under floor heating system connected to a ground source heat pump. The details about the building case study parameters are presented in **Table 1 - 3** and **Figure 2 - 5**.

Table 1: *EnovHeat building parameters.*

Total ground floor area including walls [m ²]	150
Heated floor area [m ²]	126
Heated net volume [m ³]	309
Building envelope area including ground [m ²]	545
Number of occupants	4
External walls U-value [W/m ² .K]	0,11
Floor U-value [W/m ² .K]	0,071
Roof U-value [W/m ² .K]	0,081
Doors and windows U-value [W/m ² .K]	1
Glazing transmittance [%]	0,63
Infiltration rate [h^{-1}]	0,1
Ventilation [m ³ /s]	0,103
Air change rate (without infiltration) [h^{-1}]	1,2
Ventilation heat recovery [%]	85
Design heat loss [kW]	3,78
Heating system max power [kW]	2,93
Heating temperature set point [C]	22
Heating energy need (SP = 20°C) [kWh/m ² .year]	16



Figure 2: *View of the EnovHeat house case study.*

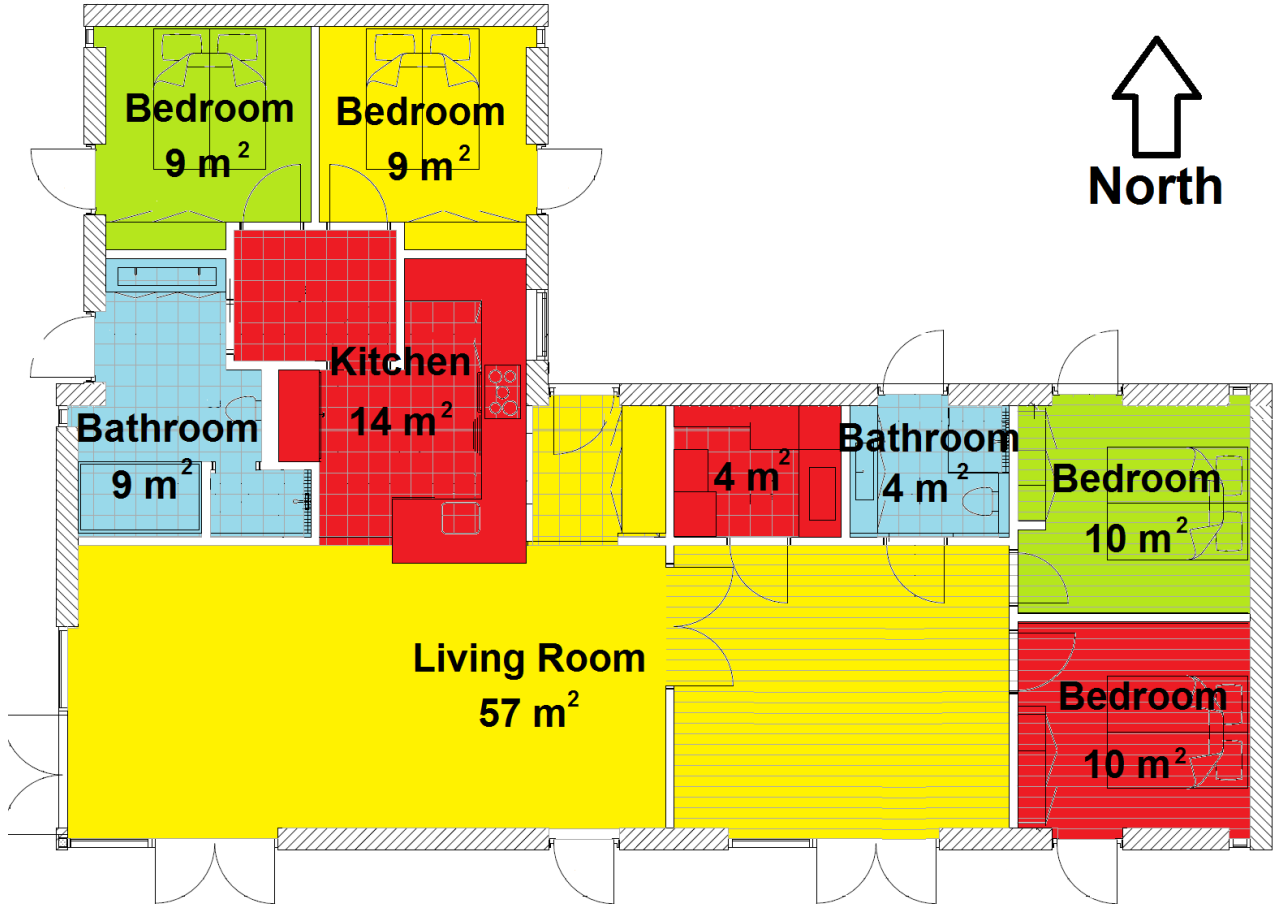
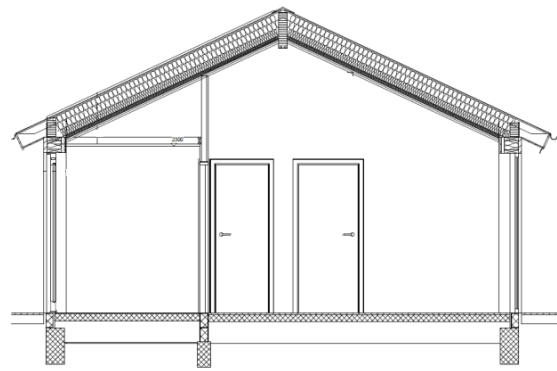
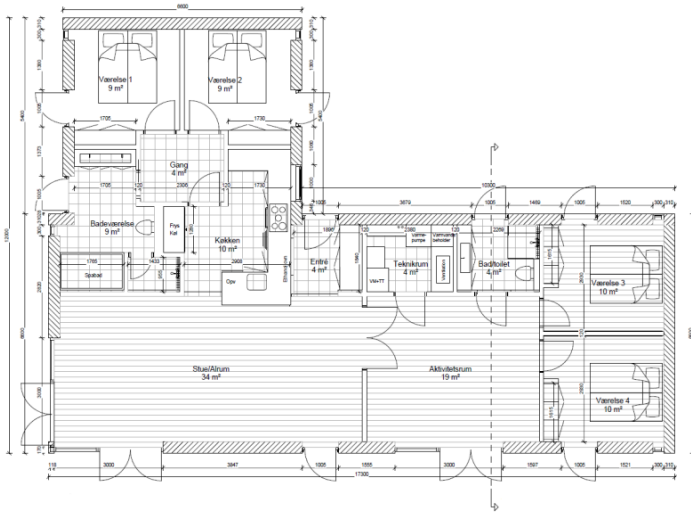


Figure 3: Plan view of the house case study.

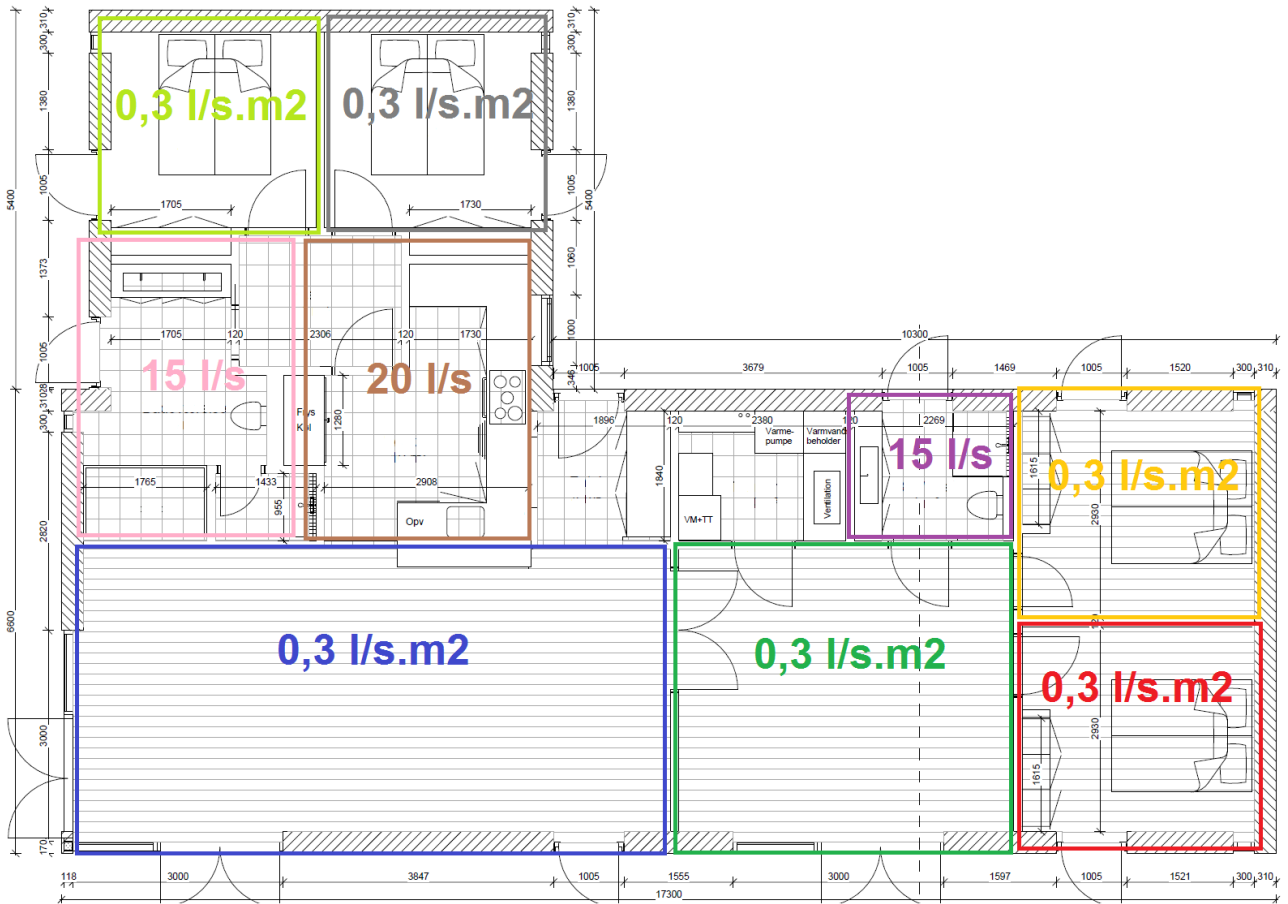


Figure 4: Ventilation rate of each thermal zone.

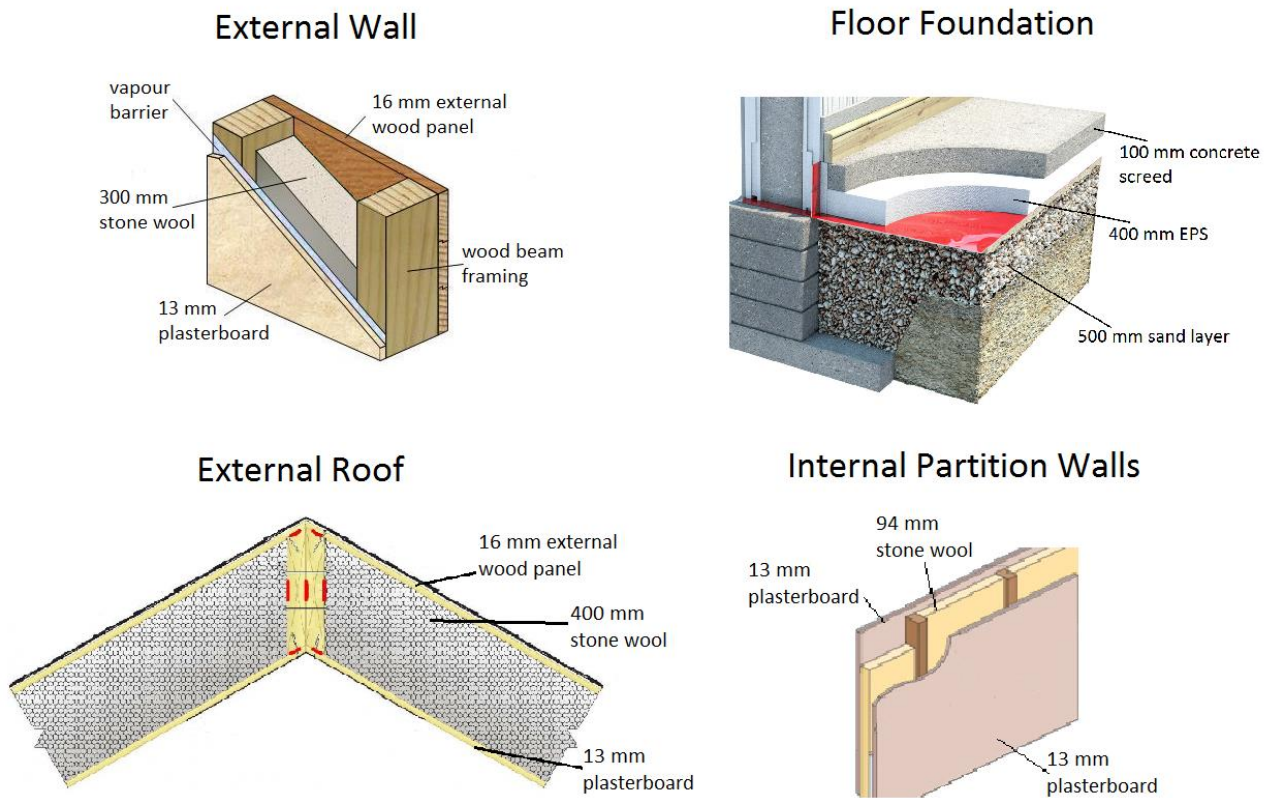


Figure 5: Description of the construction elements.

Table 2: Thermal properties of the construction materials.

	External Wood Panel	Plasterboard	Stone Wool	Concrete	EPS Insulation	Sand (house underground)	Brick
Thermal Conductivity [W/m.K]	0,12	0,2	0,033	2,1	0,03	0,68	0,68
Density [kg/m ³]	500	900	45	2400	17	800	1840
Heat Capacity [J/kg.K]	1800	1000	800	800	750	1600	800

Table 3: Radiation surface properties of the building elements.

	Light Grey Painting (internal surfaces/floor)	Wood (external surfaces)	Grass (outdoor surrounding)
Emissivity	0,9	0,9	0,9
Solar Absorptance	0,4	0,55	0,8
Reflectance	0,6	0,45	0,2
Albedo			0,25

One can see on **Figure 6 - 7** that the EnovHeat house case study has a very efficient thermal envelope which lies between “class 2020” and “Passive House” level according to the Danish building regulation [10] [11].

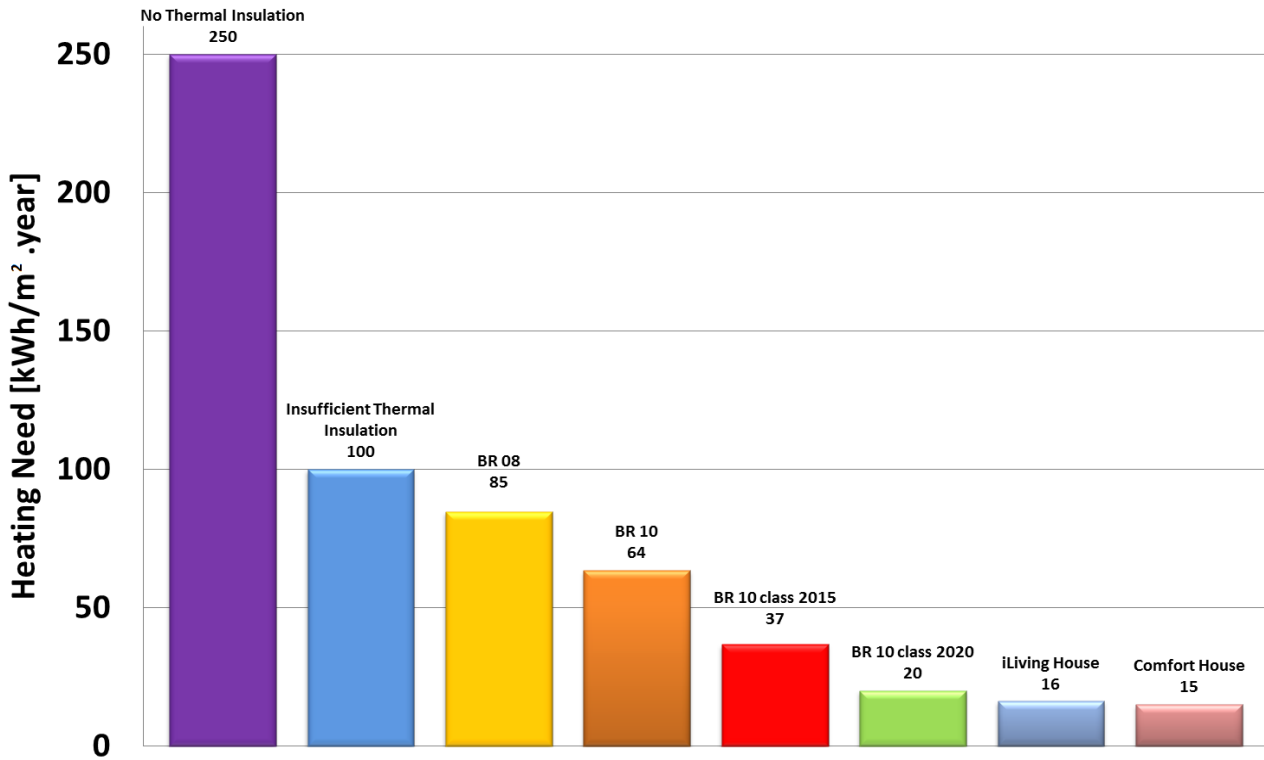


Figure 6: Total yearly heating need of detached residential houses in Denmark (Indoor temperature set point = 20 °C). Results from the iLiving project are obtained from a BSim model of the house.

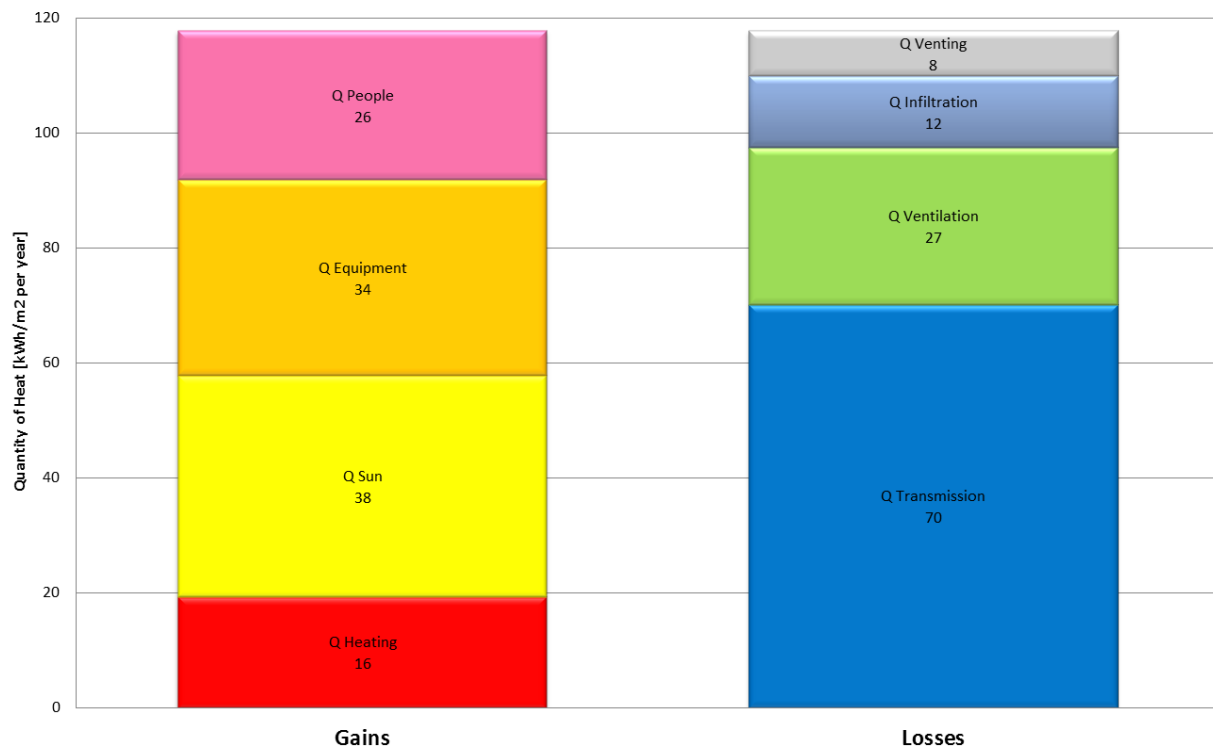


Figure 7: Yearly energy balance of the iLiving project house (Indoor temperature set point = 20 °C). Results are obtained from a BSim model of the house under Danish weather conditions.

1.2. Energy Flexibility Case Study Buildings

The EnovHeat case study building parameters are changed in order to generate different thermal mass and insulation level categories for further numerical investigations on the impact of thermal mass on the energy flexibility capacity of dwellings.

The insulation layer of the roof, external walls and floor, the infiltration, the windows and HVAC systems' performance are varied accordingly. The low insulation house category corresponds to the typical insulation level of a 1980's house in Denmark. The high insulation house category corresponds to the typical insulation level of a Passive House or "Komforthus" in Denmark. The original design of the EnovHeat house has a medium effective thermal capacity. The materials of the internal and external surfaces of the walls, roofs and floors are changed in order to vary the total thermal inertia of the building. 3 different building structure thermal mass categories are generated [12] with 3 different case variations in each categories (9 different building structure thermal mass cases in total):

- Light-weight structure house: 30 Wh/K.m², 40 Wh/K.m² and 45 Wh/K.m²
- Medium-weight structure house: 50 Wh/K.m², 60 Wh/K.m² and 70 Wh/K.m²
- Heavy-weight structure house: 90 Wh/K.m², 100 Wh/K.m² and 110 Wh/K.m².

The details of the construction elements of each thermal mass category are presented in **Figure 8**. Details of the different building parameters of the house study cases are presented in **Table 4**.

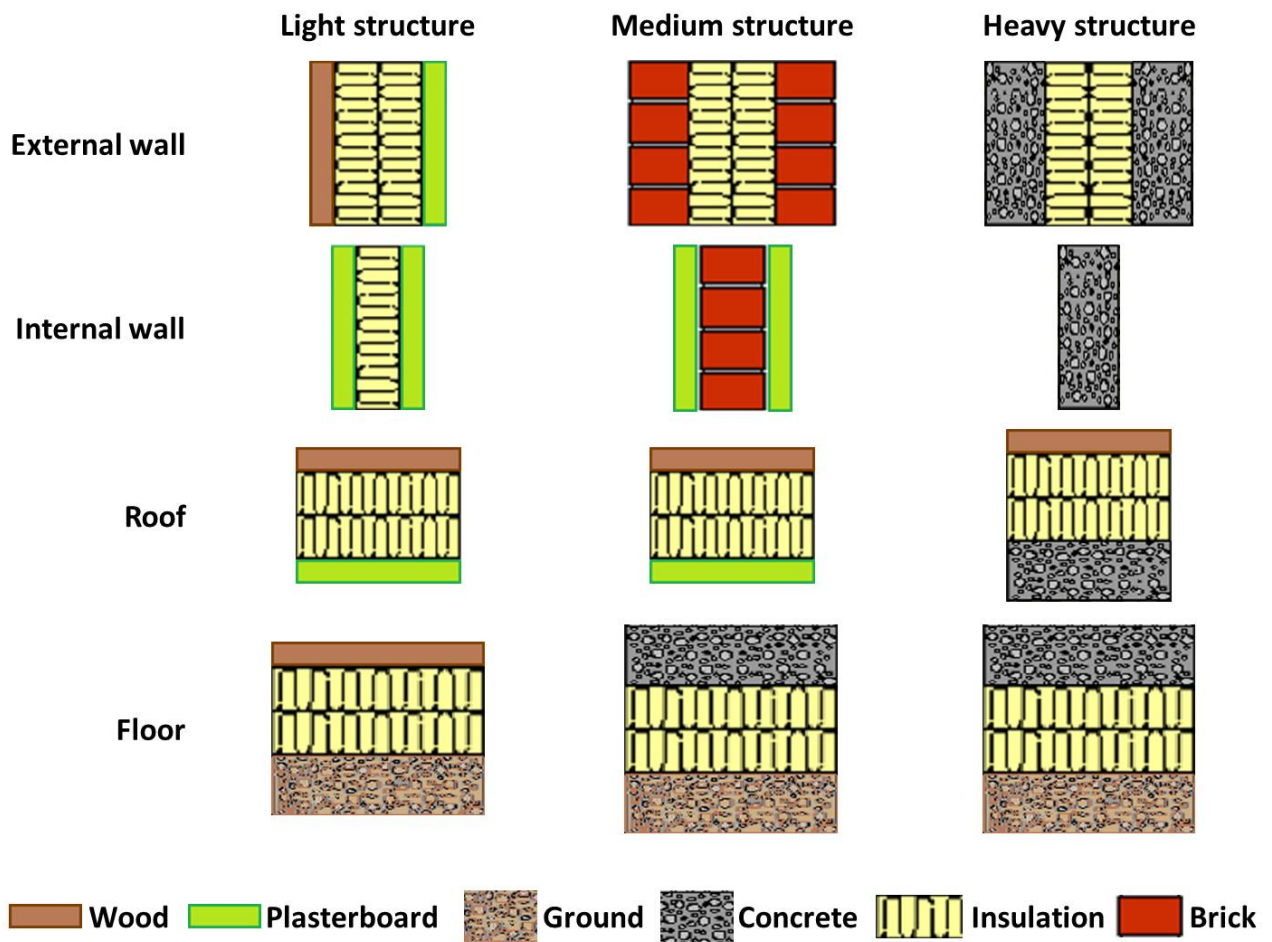


Figure 8: Details of the construction elements for each thermal mass category.

Table 4: Building parameters.

Building envelope category	House 1980's			Passive House		
Structural thermal inertia category	Light	Medium	Heavy	Light	Medium	Heavy
Building thermal inertia (Wh/K.m ²)	30 - 40 - 45	50 - 60 - 70	90 - 100 - 110	30 - 40 - 45	50 - 60 - 70	90 - 100 - 110
Building envelope heat losses (W/K.m ² gross floor)	1.12	1.13	1.13	0.37	0.37	0.37
U-value windows (W/m ² .K)	1.70			0.78		
g-value windows (-)	0.63			0.50		
Ratio windows / gross floor area (%)	16.7 %			26.9 %		
Windows area (m ²)	25.10			40.39		
Air infiltration (ACH)	0.2			0.07		
Ventilation (ACH)	0.4			0.4		
Heat recovery (-)	0			0.8		
Air flow heat losses (W/K)	64			15.6		
Air flow heat losses (W/K.m ² gross floor)	0.43			0.10		
Yearly radiator heating need with set-point at 22°C (kWh/m ² net floor)	164	160	155	14	13	12
Maximum radiator heating power (W/m ²)	75			25		
Under-floor heating type	Type G wood floor	Concrete screed	Concrete screed	Type G wood floor	Concrete screed	Concrete screed
Yearly under-floor heating need with set-point at 22 °C (kWh/m ² net floor)	160	151	157	15	13.5	13
Nominal water flow per UFH loop (l/h)	170			125		
UFH maximum inlet water temperature (°C)	47	43	43	35	30	30

1.3. Conventional Heat Pump System

The reference heat generation system of the building case study is a conventional vapor-compression water-to-water heat pump with characteristics similar to the model TWM036 of ClimateMaster® [13]. When running at nominal fluid volumetric flow rate of 2052 L/h in both heat source and heat sink loops, this heat pump delivers 8.28 kW of heating power with a COP of 4.51. The heat pump is coupled with a ground source heat exchanger and a hydronic low-temperature radiant under-floor heating system (see **Figure 9**). The hot water storage tank has a capacity of 250 L (cylindric shape tank with radius of 29 cm and height of 95 cm) with 5 cm of polyurethane insulation (heat losses to the ambient U-value of 1.356 W/K).

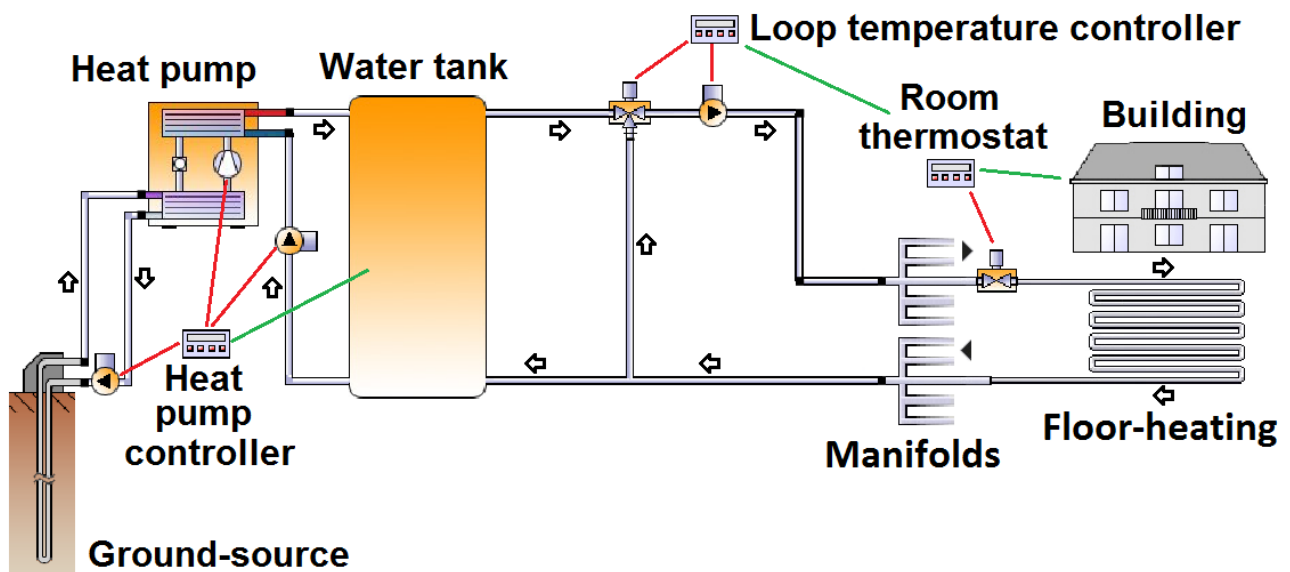


Figure 9: Schematic of the heating system implementation for the conventional heat pump.

Hydraulic circulation pumps are placed on the different sections or loops of the water/brine-based heating system in order to carry the heat-transfer fluid from the ground heat source to the under-floor manifolds and the different loops in each room.

To choose an appropriate hydraulic pump for that system, the pressure drop of the critical loop is calculated for the nominal mass flow and a water-brine with 20%vol ethylene glycol and 80%vol water. It is found that the critical loop on the side of the heat sink (under-floor heating) has a total pressure drop which is always below 15 kPa at nominal mass flow rate. It is therefore chosen to use an hydraulic circulation pumps Grundfos ALPHA2 L 15-40 [14]. These circulator pumps can operate with variable flow rate and constant pressure difference. It is therefore chosen to use the lowest constant pressure regulation (CP1) at 23 000 Pa. Similarly, the maximum pressure drop in ground source heat exchanger loop is always below 15 kPa at nominal mass flow. It is therefore also chosen to use an hydraulic circulation pumps Grundfos ALPHA2 L 15-40. The hot water storage tank circuit circulation pump is also a Grundfos ALPHA2 L 15-40.

1.4. Magnetocaloric Heat Pump System

The magnetocaloric heat pump is coupled with the ground source heat exchanger and the under floor heating system within a single hydronic loop without an intermediate heat exchanger or hot water storage tank (see **Figure 10**).

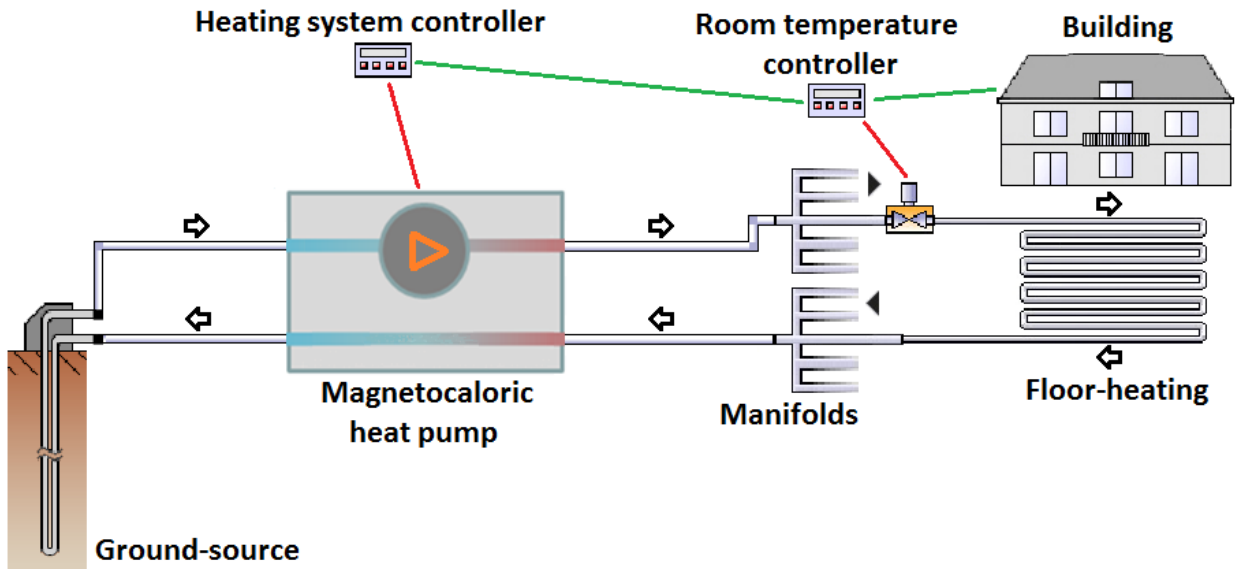


Figure 10: Schematic of the heating system implementation for the magnetocaloric heat pump.

The pressure drop in the packed bed sphere regenerator of the magnetocaloric heat pump is significantly higher than the pressure drop in the under floor heating loops or in the ground source heat exchanger loop. Consequently, an hydraulic pump able to generate enough pressure difference is chosen to circulate the heat transfer fluid in the single hydronic loop. The circulation pump is a Grundfos CR 1-9 A-FGJ-A-E-HQQE – 96478872 operating on the power curve P2 [15].

1.5. Under Floor Heating Systems

Two different types of water-based under floor heating systems are implemented in the building study cases. Light structure buildings are equipped with a “type G” wooden floor embedded pipe under floor heating (See **Figure 11**). Medium and heavy structure buildings are equipped with a concrete screed embedded pipe under floor heating (See **Figure 12**).

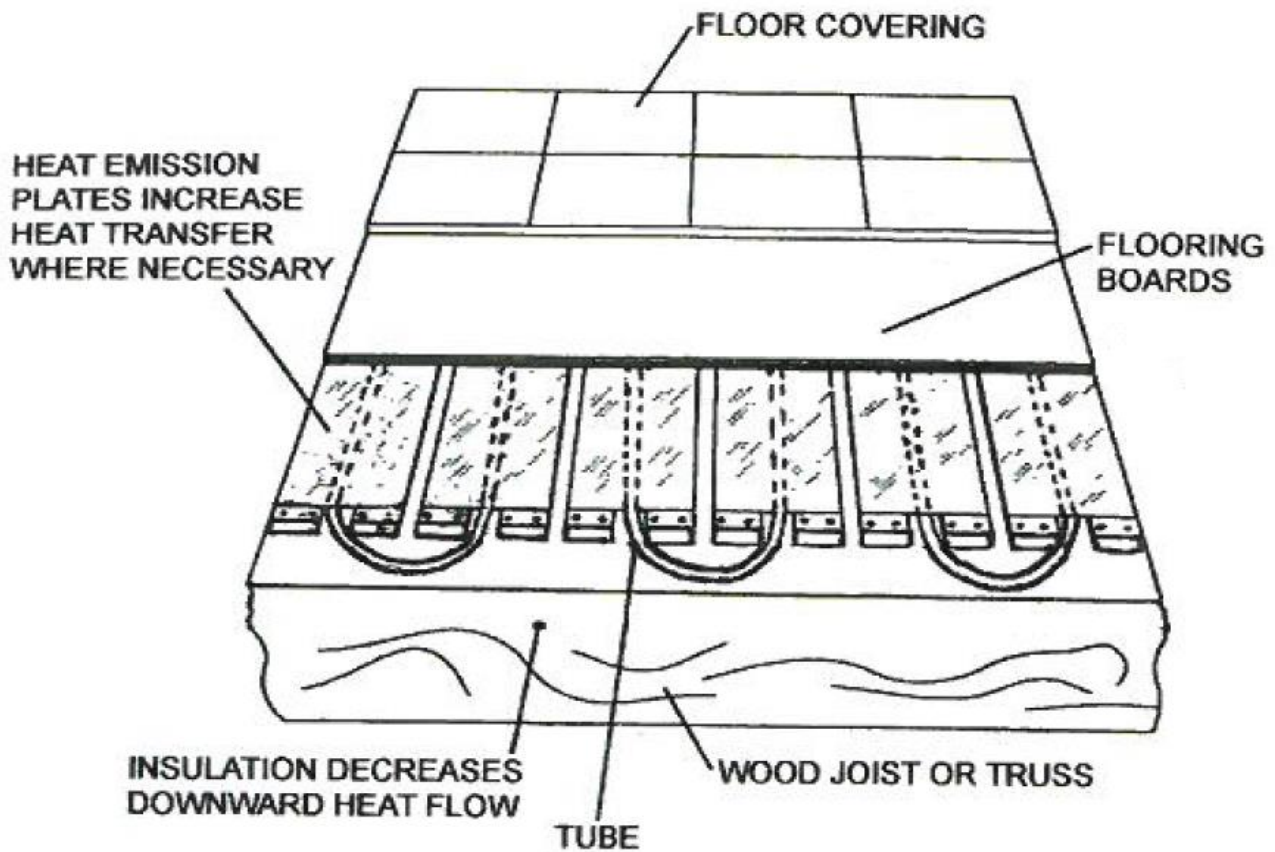


Figure 11: Type G under floor heating system with pipe embedded in wooden floor.

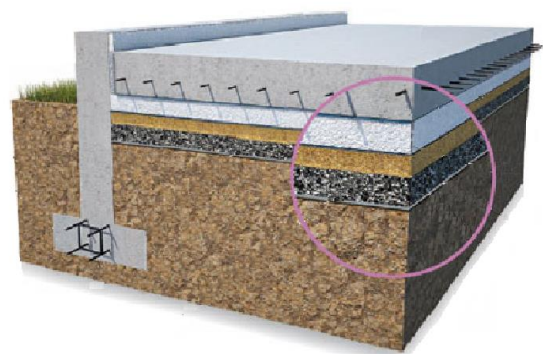
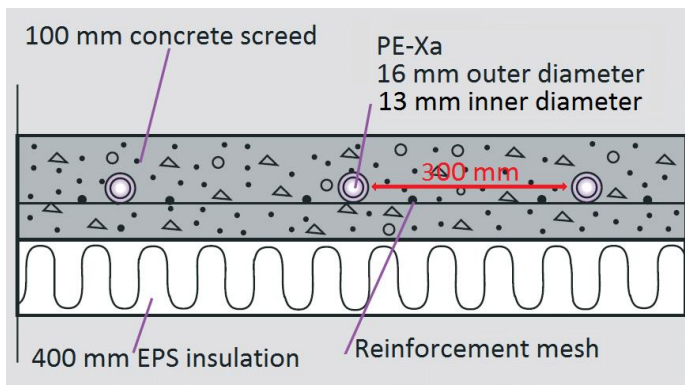


Figure 12: Concrete screed embedded pipe under floor heating (EnovHeat case study house).

The design and sizing of the under-floor heating systems are performed according to manufacturer's technical guidelines (Uponor) and international standards [16] [17] [18] [19] [20].

For concrete screed under floor heating system, the total thickness of the concrete layer is 100 mm. The center of the pipes network embedded in the concrete screed is 60 mm from the upper surface of the

concrete slab. The hydronic network is made of PE-Xa pipes with external diameter of 16 mm, internal diameter of 13 mm (wall thickness of 1.5 mm), thermal conductivity of 0.45 W/m.K, and inner surface pipe roughness (according to Prandtl and Colebrook) of 0.007 mm/m. The spacing in between the center of each pipe is of 200 mm for the houses of 1980's and 300 mm for the passive houses.

For the type G under floor heating system with pipe embedded in wooden floor, the total thickness of the wooden layer is 30 mm. The center of the pipes network embedded in the wooden floor is 12 mm from the upper surface of the wooden slab. The hydronic network is made of PE-Xa pipes with external diameter of 16 mm, internal diameter of 13 mm (wall thickness of 1.5 mm), thermal conductivity of 0.45 W/m.K, and inner surface pipe roughness (according to Prandtl and Colebrook) of 0.007 mm/m. The spacing in between the center of each pipe is of 200 mm for the houses of 1980's and 300 mm for the passive houses. The heat emission plates are made of aluminum. They are 1 mm thick with a thermal conductivity of 300 W/m.K. The gap between each plate is 5 mm.

1.6. Ground Source Heat Exchangers

The space heating needs of the case study buildings are provided by a water-to-water heat pump connected to a ground source heat exchanger (domestic hot water production is not in the scope of the study). Two types of ground source heat exchangers are therefore designed to insure enough heat supply to the building: a vertical borehole heat exchanger and a horizontal ground source heat exchanger.

First of all, representative characteristics of the ground properties in Denmark are evaluated from numerous measurement campaigns gathered into publically available database [21] [22] [23] [24] [25]. The soil parameters chosen for the case study are the ones of a humid clayey sand (humid winter conditions in Denmark) with a thermal conductivity of 1.5 W/m.K, a density of 1900 kg/m³ and a specific heat capacity of 1400 J/kg.K. The grouting material is chosen to be with a thermal conductivity of 1.4 W/m.K, a density of 1500 kg/m³ and a specific heat capacity of 1670 J/kg.K.

SOIL MAP OF DENMARK (National Soil Maps, EuDASM)

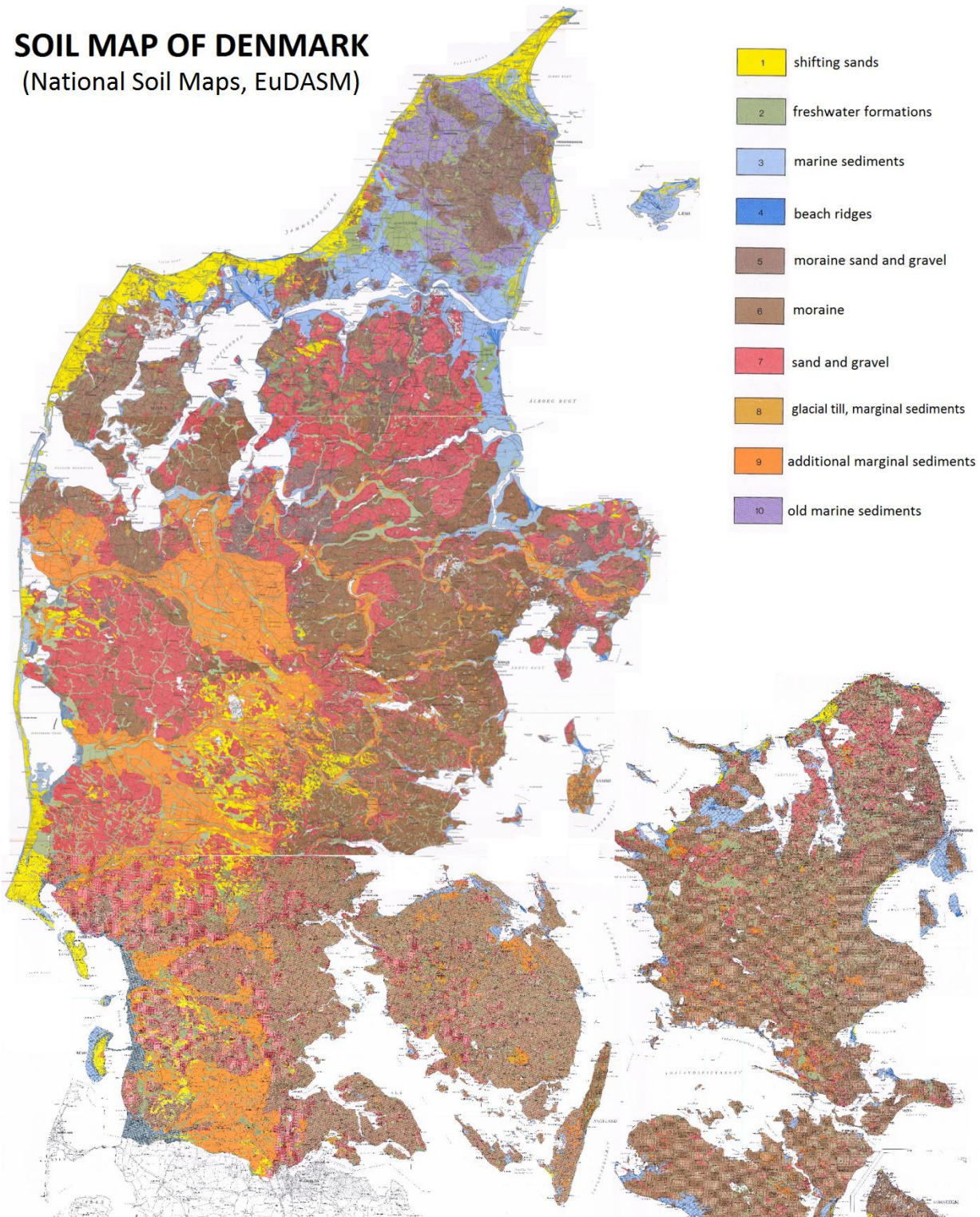


Figure 13: Soil map of Denmark.

The horizontal ground source heat exchanger is designed according to the VDI 4640 standard and the recommendations of manufacturers [26] [27] [28]. The hydronic network is made of PEX pipes with outer

diameter of 40 mm, wall thickness of 3.5 mm, inner diameter of 33 mm, thermal conductivity of 0.45 W/m.K and Inner roughness (according to Prandtl-Colebrook) of 0.007 mm/m. They are placed at a depth of 1.5 m from the ground surface according to a serpentine layout (See **Figure 14**). The spacing in between each pipe's leg is 1.5 m. The total length of the pipe collector is 194 m and it covers 291 m² of soil surface area.

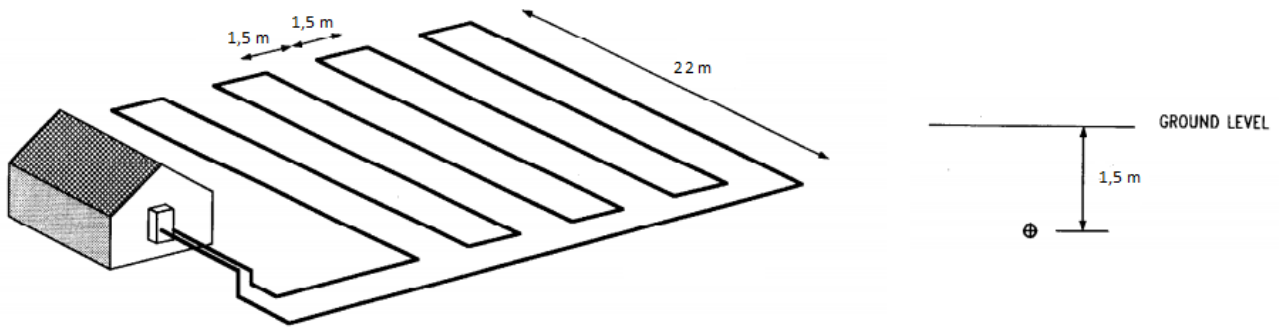


Figure 14: Serpentine layout of the horizontal ground source heat exchanger.

The vertical borehole ground source heat exchanger is designed according to the VDI 4640 standard and the recommendations of manufacturers [26] [27] [28]. The hydronic loop is made of single double U-tube PEX pipe with outer diameter of 44 mm, wall thickness of 3.5 mm, inner diameter of 37 mm, thermal conductivity of 0.45 W/m.K and Inner roughness (according to Prandtl-Colebrook) of 0.007 mm/m. The borehole has a depth of 100 m (see **Figure 15**) with a diameter of 160 mm. The spacing between the centers of the two legs of the U-pipe is 80 mm (see **Figure 16**). The total length of the pipe collector is 200 m.

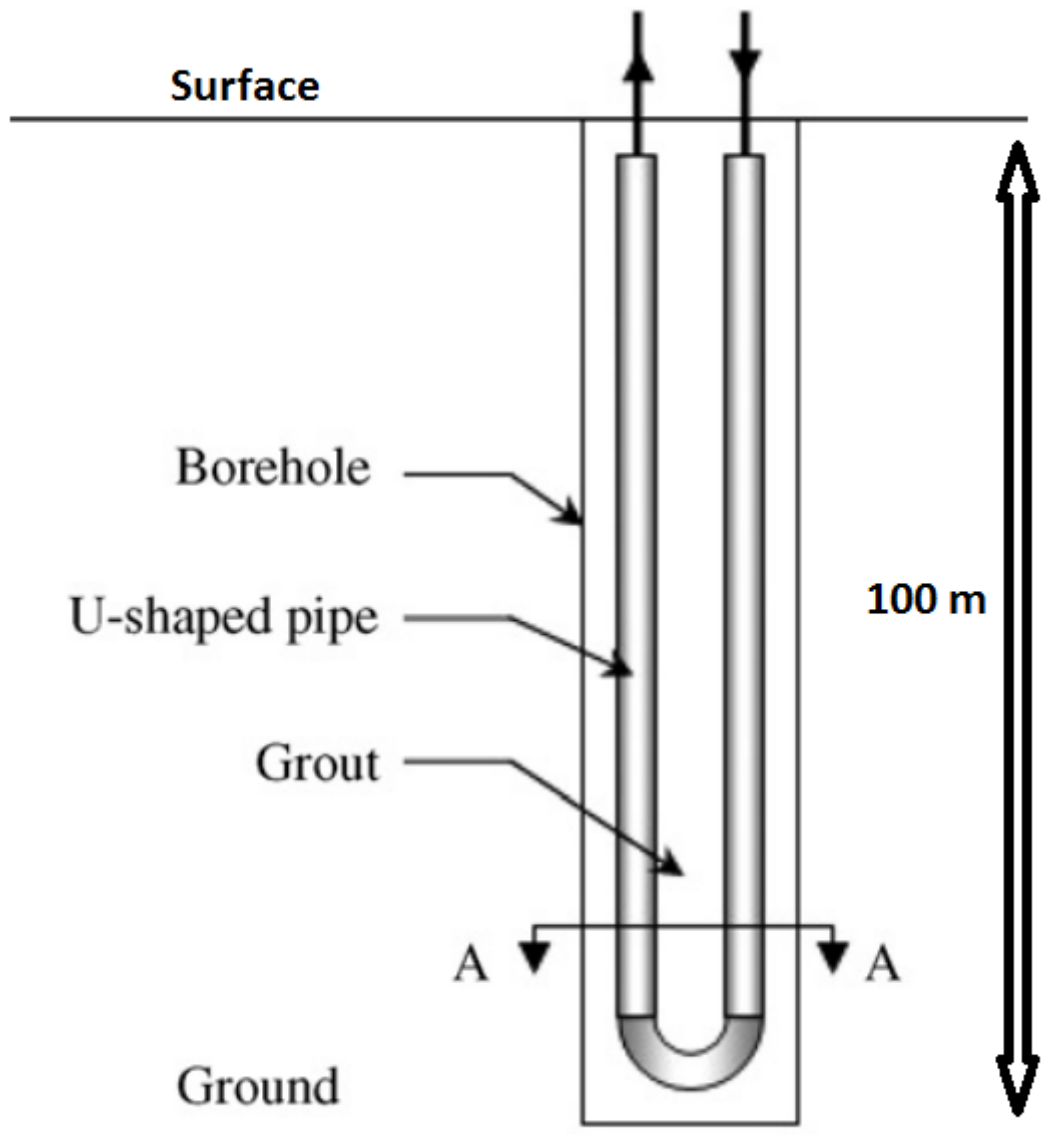
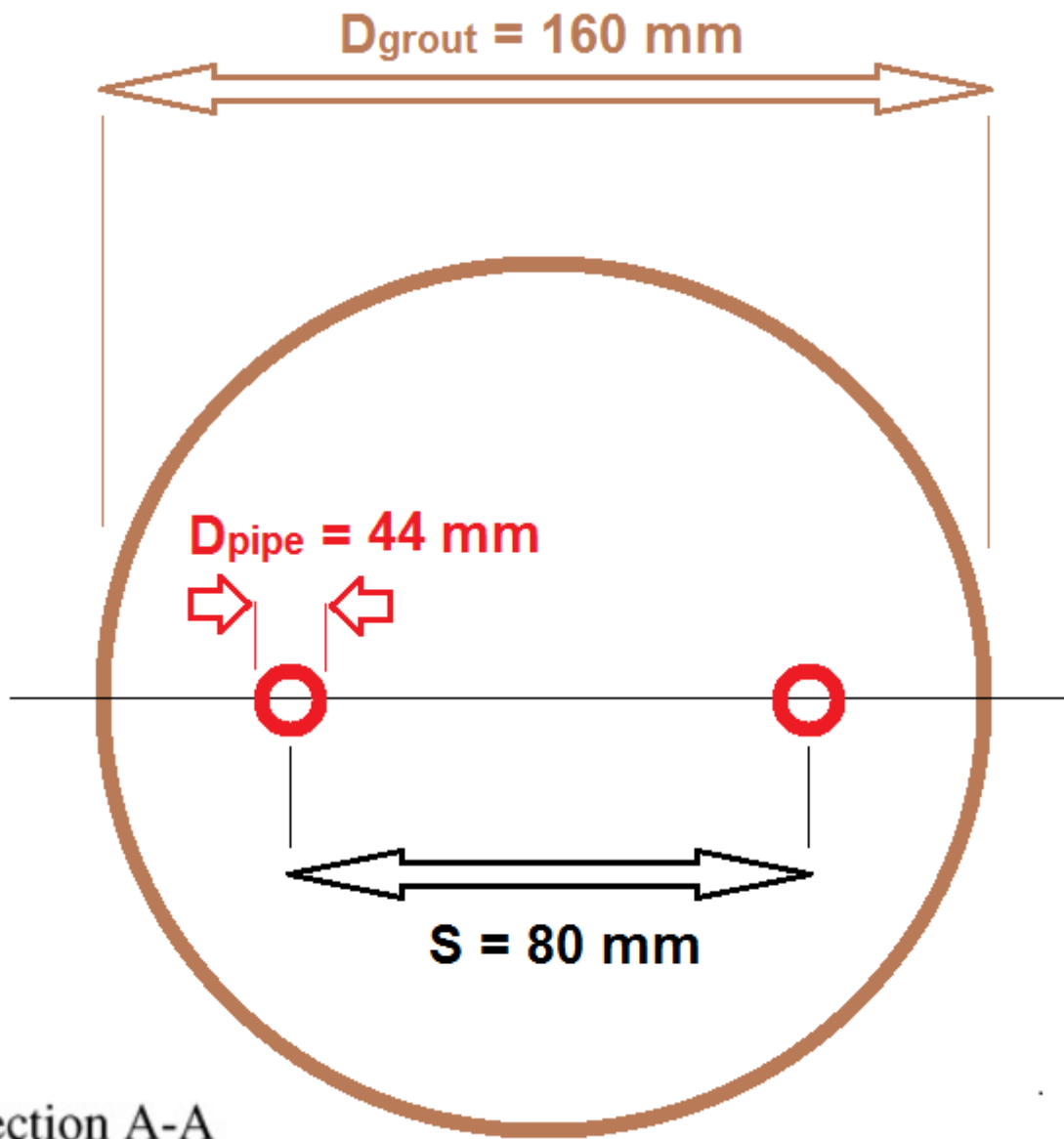


Figure 15: Schematic of a vertical borehole ground source heat exchanger with U-pipe.



Section A-A

Figure 16: horizontal cross section of the vertical borehole heat exchanger.

1.7.Phase Change Material

The thermal storage capacity of a building can be enhanced by the integration of phase change materials. Concerning passive latent heat storage in the indoor environment, studies found that the most efficient location for PCM is on the inner surfaces of the indoor space for a maximum thermal activation [29]. Consequently, some of the case study buildings are equipped with PCM panels fixed on the inner surfaces of the thermal zones: external walls, internal walls, ceiling and furniture surfaces.

The PCM wallboards used in the study are similar to the Energain® [30]. This is a common commercial product made of 60%mass micro-encapsulated paraffin incorporated into 40%mass polyethylene matrix.

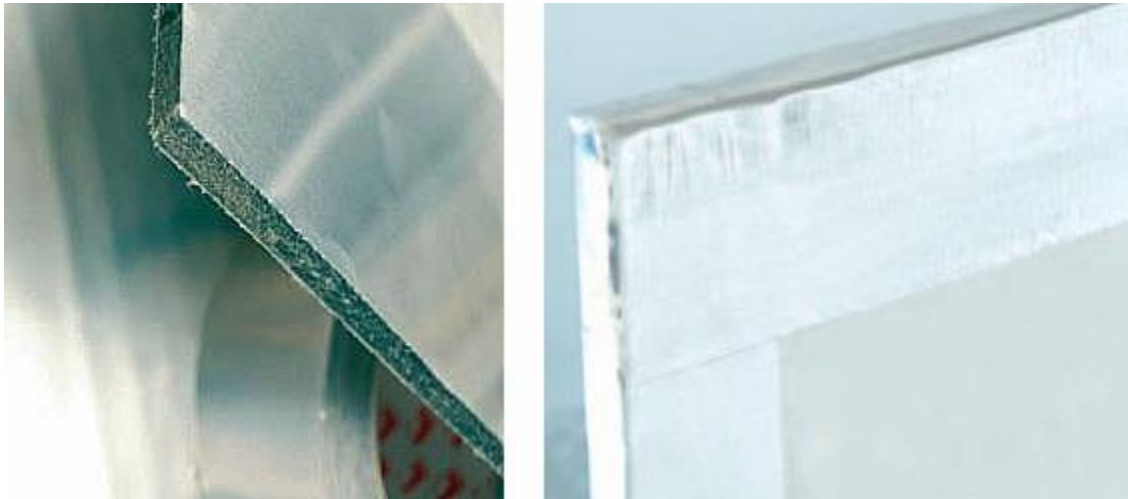


Figure 17: *Energain® PCM wallboards (DuPont).*

Experimental tests have been conducted at Aalborg University Laboratory in order to measure the thermal characteristics of this PCM. These characteristics are used in the numerical models of the study and presented hereafter.

The melting and solidification temperatures of the PCM are 22 °C and 21.8 °C respectively. The latent heat of fusion for the pure paraffin is 200 kJ/kg. This is a very common value compared to other products used for ambient temperature applications [29]. Therefore the latent heat of fusion for the 60 %mass paraffin stable form PCM is 120 kJ/kg.

The global thermal conductivity is assumed to follow the results found by Kuznik et al. in a previous study [31]. The PCM has a constant thermal conductivity of 0.22 W/m.K and 0.18 W/m.K below 16 °C and above 28 °C, respectively. It is assumed that the thermal conductivity varies linearly from 0.22 to 0.18 W/m.K in between 16 °C and 28 °C. These results have been confirmed by Guarded Hot Plate Apparatus measurements on Energain® test samples with different thicknesses (see **Figure 18**).

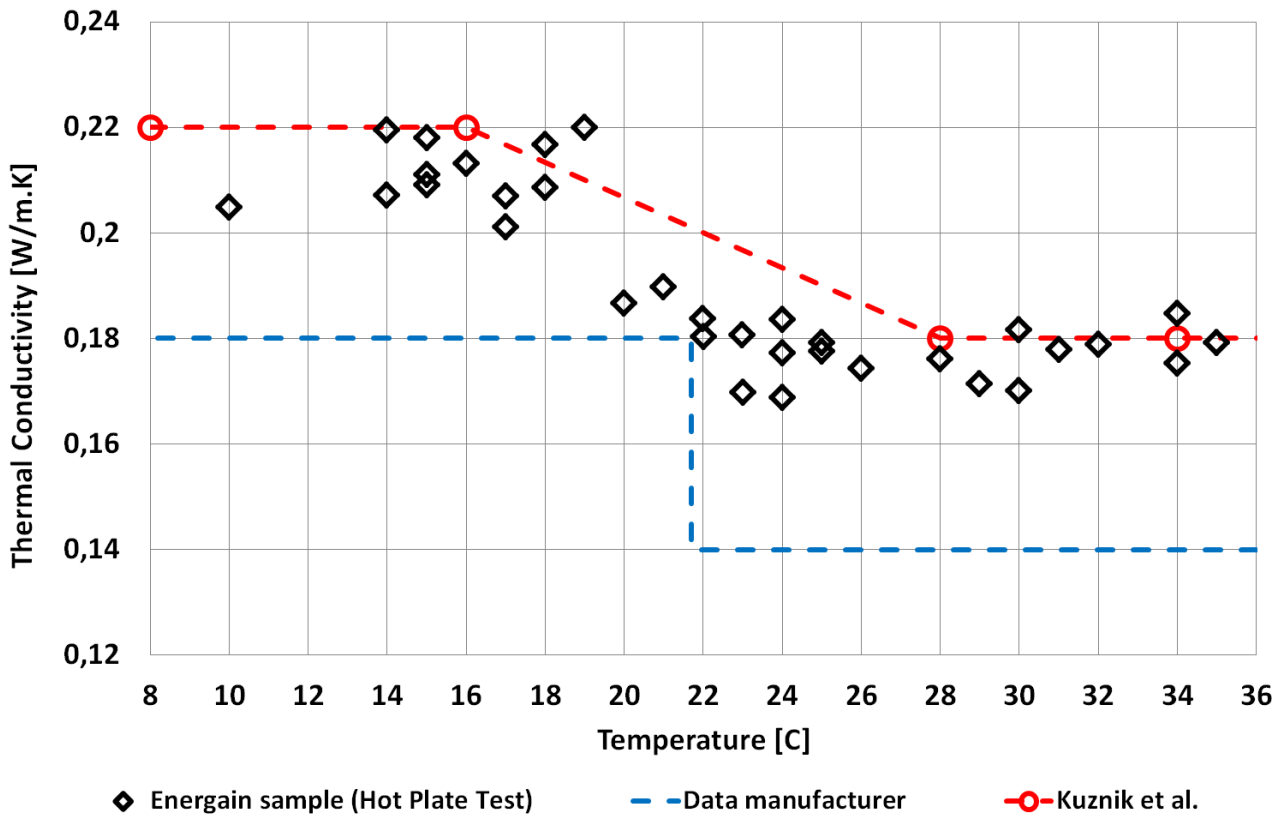


Figure 18: Guarded Hot Plate thermal conductivity measurements.

The specific heat capacity of the stable form PCM is 2000 J/kg.K. This value corresponds to the mass percentage content weighted sum of the specific heat capacity of paraffin and polyethylene. It fits very well with Differential Scanning Calorimetry (DSC) measurements of Energain® test samples above the melting temperature when no phase transition occurs (experimental tests performed at Aalborg University laboratory with temperature change of 2 K/min). One can see on **Figure 19** that there is a noticeable difference between the measurements of Kuznik et al. and the ones of Aalborg University. This dissimilarity could be due to the variability of the Energain® manufacturing process. Moreover, one can notice that the increase of apparent heat capacity forms a rather wide dome instead of a sharp peak. It seems that the phase transition occurs marginally all along the 0 °C to 30 °C temperature interval. This might be due to the fact that the micro-encapsulated paraffin of the PCM product is composed of different grades of hydrocarbon chains with different individual melting temperature. However, the main phase transition is at 22 °C.

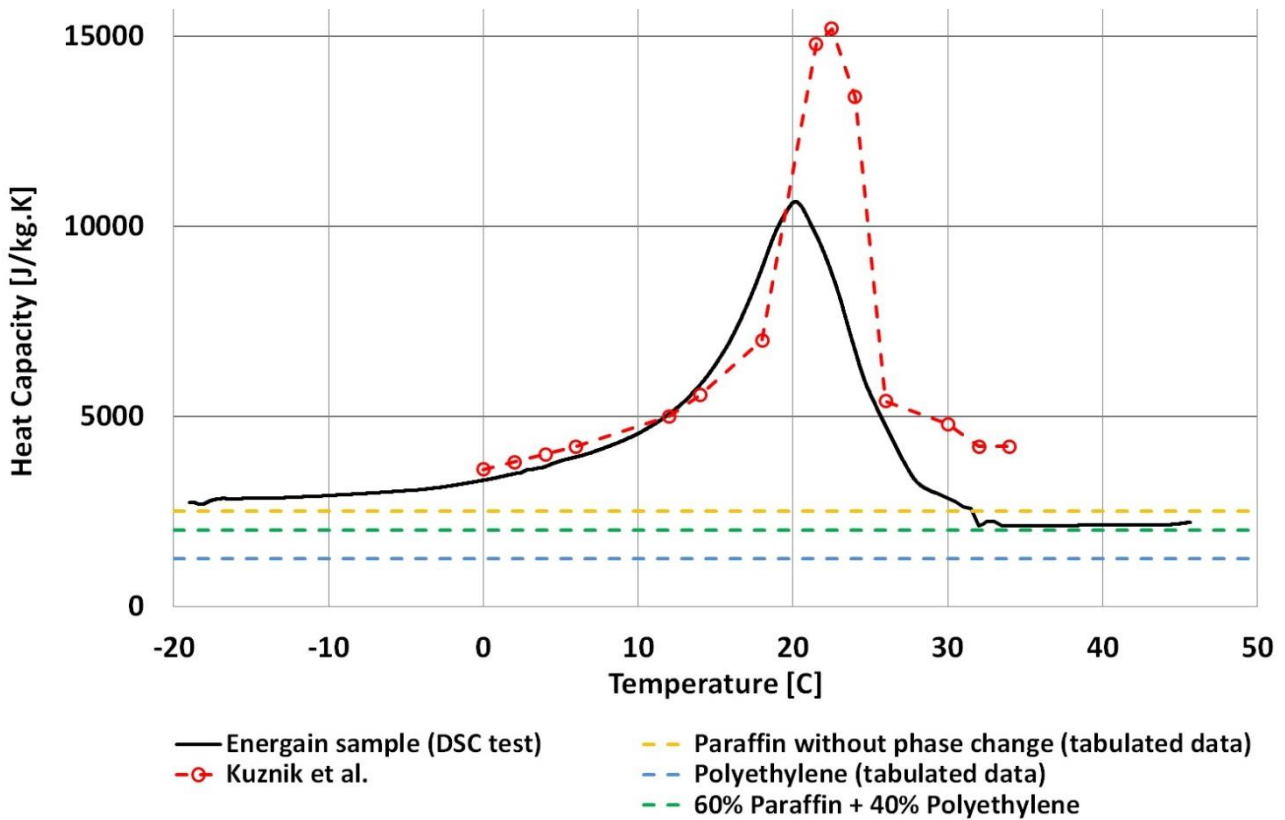


Figure 19: *Differential Scanning Calorimetry heat capacity measurements.*

The average density measured for the stable form PCM is 1000 kg/m^3 , which is close to the density of paraffin and polyethylene and in agreement with measurements of Kuznik et al. Moreover, the DSC test shows that the total heat storage capacity is 144 kJ/kg (temperature rising from $10 \text{ }^\circ\text{C}$ to $40 \text{ }^\circ\text{C}$). This result is in very good agreement with the technical documentation provided by the manufacturer [30].

All parameters of the PCM used in the study are summarized in **Table 5**.

	PCM model	Measurements (current study)	Energain® (data manufacturer)	Kuznik et al.
Paraffin mass content (%)	60	-	60	60
Paraffin latent heat of fusion (kJ/kg)	200	-	-	-
Melting temperature (°C)*	22	20	21,7	22
Thermal conductivity (W/m.K)*	0.22 - 0,18	0.22 – 0.17	0.18 – 0.14	0,22 – 0.18
Density (kg/m³)*	1000	900	800	1019
Specific heat capacity (J/kg.K)*	2000	2000	-	-
Latent heat of fusion (kJ/kg)*	120	-	> 70	-
Total heat storage for $\Delta\theta = 30$ K (kJ/kg)*	180	170	140	200

* For stable form PCM product: 60 % mass paraffin in polyethylene matrix

Table 5: Phase change material thermal properties.

1.8. Phase Change Material Wallboard

The stable form PCM boards are implemented in the case study buildings as passive latent heat thermal energy storage (LHTES) systems. These systems have to be sized to the optimum thickness to maximize the additional thermal inertia with the minimum amount of PCM possible. The effective energy storage capacity is proportional to the PCM volume which melted and solidified during a complete TES cycle. If the material amount is overestimated, the time needed for the heat to penetrate the PCM layer could become larger than the charging period, and the melting process cannot be completed.

The effective heat capacity optimization for normal material without phase transition is rather simple to perform. The daily effective heat capacity can be calculated with the detailed matrix method described in the standard EN ISO 13786 [32] with a 24 hour period of variations. This method is straightforward, robust and easy to implement for multilayer materials. Dynamic boundary conditions are restricted to sinusoidal variations, which is a common way to model indoor and outdoor temperature change over time.

As indicated by Ma and Wang [33], the change of effective thermal storage capacity of a normal material as function of its layer thickness presents a maximum. Increasing further the thickness of the material layer does not improve its effective thermal capacity and actually decreases it slightly.

However, this methodology is based on the analytical solution of one-dimensional heat transfers through solids with constant thermal properties. Therefore it cannot be used for materials presenting phase transition. In order to assess the effective thermal inertia of elements including PCM, a numerical model (described later in this report) is used for the calculation of internal energy variations. A similar approach is used by Kuznik et al. [31] for the optimization of a PCM wallboard. The areal effective thermal inertia κ on one side of a plane element is its ability to store energy when temperature varies periodically [32]. It is equal to the maximum variation of internal energy ΔE (Joule) of a half element divided by the maximum boundary temperature change $\Delta\theta$ (K) and the surface area A (m²):

$$\kappa = \frac{\Delta E}{\Delta \theta \times A}$$

Similarly to the matrix method, the temperature boundary conditions are changing as a 24 hour period sinusoidal function. After 10 cycles, the system reaches a periodic steady state and the effective heat capacity is calculated. This method has been compared to the detailed matrix one and presents very good agreement for normal materials: average deviation of 0.09% for concrete wall modeled with 100 control volumes (see **Figure 20**).

The **Figure 20** shows the evolution of the effective heat capacity of an internal wall element made of mineral wool and covered by a PCM layer with variable thickness. These results are coherent with the investigations of Kuznik et al. [31]. However no clear maximum effective thermal capacitance can be observed. The amplitude of boundary temperature variation does not influence the areal effective thermal inertia of material with constant thermal properties. However, one can see that it induces noticeable deviations of 4% in average for the PCM elements. Larger temperature swing increases non-linearly the maximum amount of melted PCM and stored energy because of latent heat and temperature dependent thermal conductivity. Nevertheless, the optimum PCM thickness with maximum heat capacity remains the about same.

The thickness of the PCM layer for the wallboard of the study case is chosen to be 1.5 cm. This value seems to be a reasonable choice to insure a maximum thermal heat capacity for daily temperature variations and it is in agreement with the results of Kuznik et al.

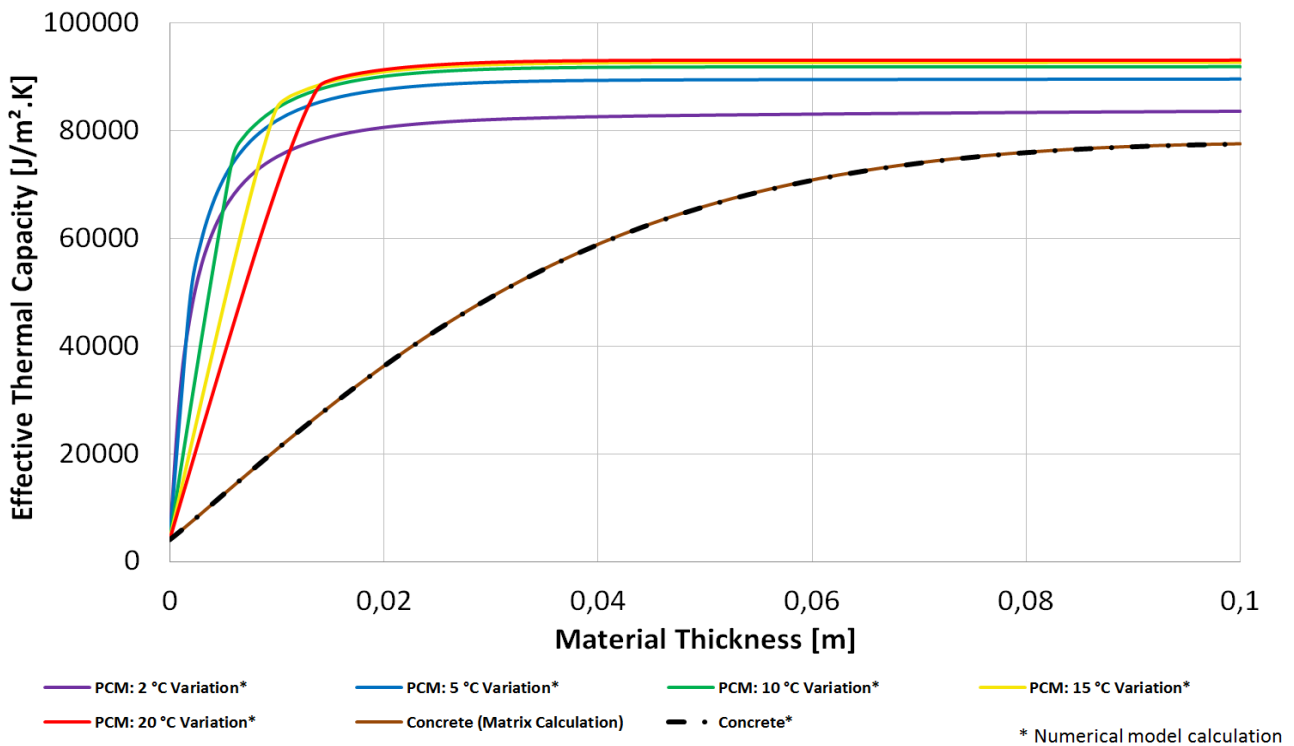


Figure 20: Phase change material effective thermal capacity in function of layer thickness.

The PCM wallboards are attached to the inner surface of the building's thermal zones: external walls, internal walls and ceiling. The average amount of PCM in the building is therefore about 40 kg/m² of floor surface area.

1.9. Additional Indoor Thermal Mass / Furniture

One of the aims of this study is to assess the influence of additional thermal mass in the indoor environment such as internal thermal mass or furniture. This additional indoor thermal mass is here considered to be representative of a house with a significant amount of items inside. The total mass of indoor thermal mass / furniture in the case study building is 60 kg/m² of floor surface area [29].

1.8. Phase Change Material Integrated into Furniture Elements

Another additional indoor thermal mass to be tested is the integration of PCM into furniture elements. The same PCM element used as wallboard is here placed on one surface of the furnishing directly exposed to the indoor space. The thickness of the PCM elements is also 1.5 cm.

2. Presentation of the Building Model

Similarly to the HAM-tools [34], the MATLAB - Simulink building model used in this study is based on an one-dimensional explicit finite volume method (FVM) formulation with a limited number of control volumes (also known as Resistance-Capacitance network or RC thermal network. The water-based under-floor heating system and the horizontal ground source heat exchanger are modeled with a MATLAB function. They couple a dynamic fluid “plug flow” model in a pipe with a ϵ -NTU method which accounts for the equivalent interaction thermal resistance in the layer of the slab where the heat exchanger is laid. The vertical borehole heat exchanger is modeled with a MATLAB function coupling two fluid plug flow pipes in a Resistance-Capacitance network. Both ground sources are integrated in a Simulink state space block function representing the soil surrounding the collector as a 1-D finite domain. The fluid of the hydronic systems can be chosen among 5 different brines. All flow regimes are taken into account for the calculation of the convective heat transfer and the pressure loss. Concerning additional indoor thermal mass, the furniture elements are modeled as an equivalent planar element. A PCM enthalpy model accounts for the LHTES system. The following section presents in details each part of the building model used in the study.

2.1. Construction Elements

The basic blocks of this building model are simulating the heat transfer through the construction elements: external walls, internal walls, internal ceiling, external roof, floor and ground. The building envelope and internal partitions are subdivided into a collection of planar elements. The thickness of these planar elements is considered very small in comparison to their length and width. Therefore it is possible to assume that all heat transfers occur in only one direction normal to the main plan surface of the element (See **Figure 21**).

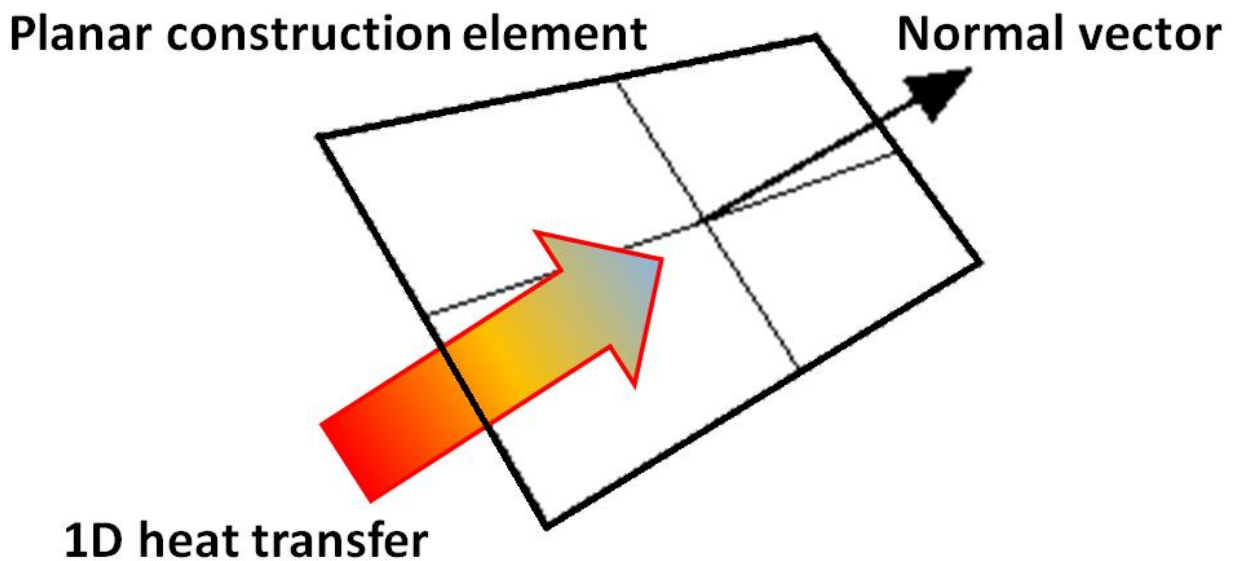


Figure 21: One-directional heat transfer through planar construction element.

Each construction element is then subdivided into finite control volumes (See **Figure 22**). It is assumed that within each time step, the temperature of each control volume is constant and homogeneous. Therefore the heat transfers are calculated based on the temperature in the center node of each control volume.

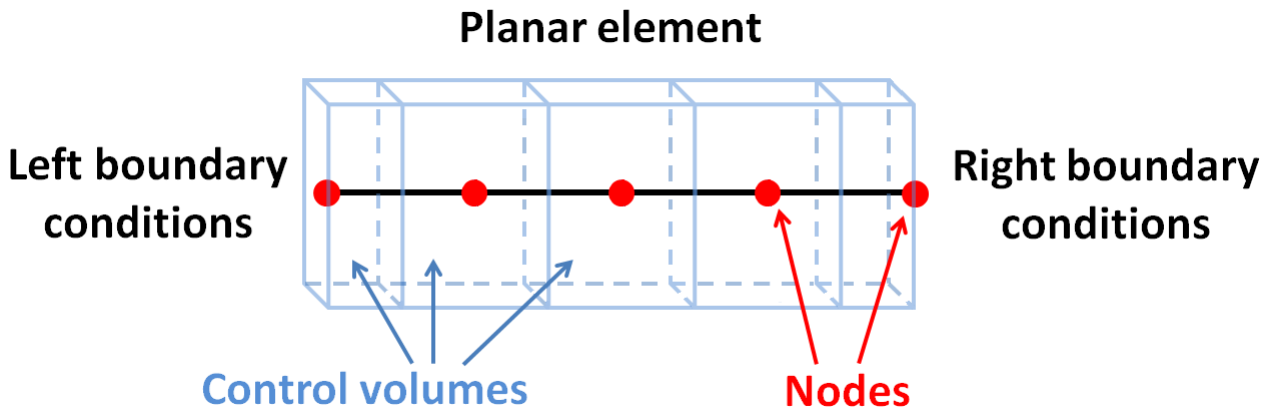


Figure 22: Space discretization of the planar construction element domain.

The heat transfers are calculated by solving the heat equation in each thermal node with an explicit finite volume formulation or Resistance-Capacitance network (See **Figure 23**).

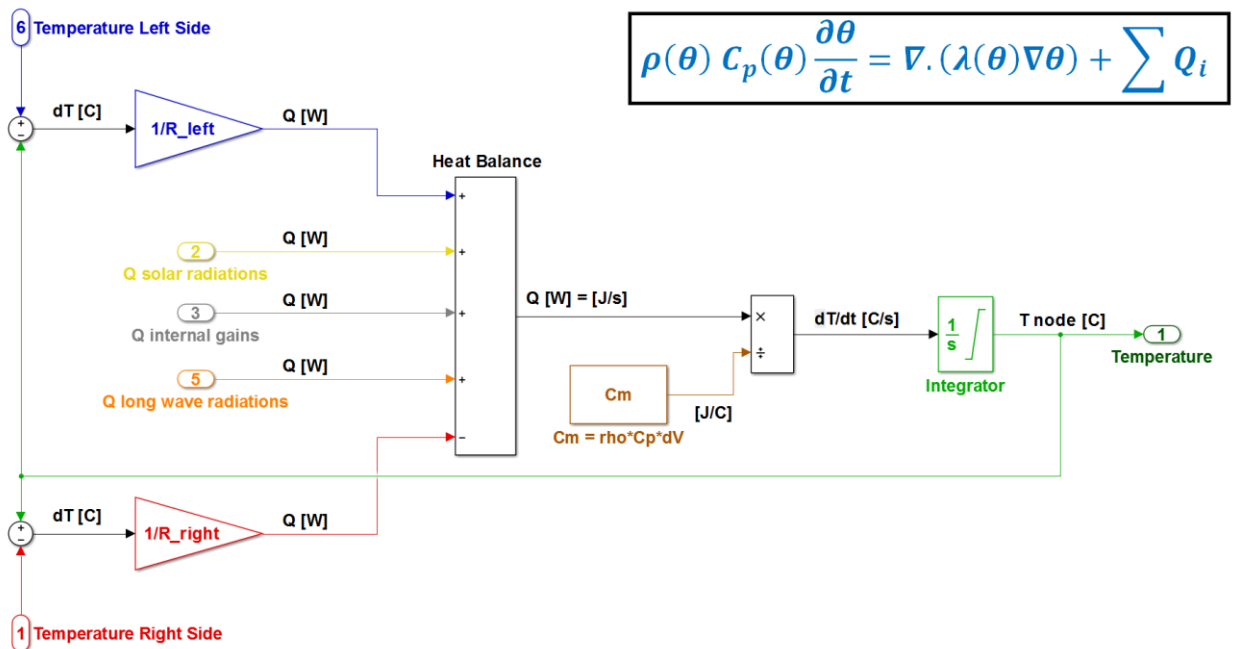


Figure 23: Explicit finite volume formulation (RC network) of the heat equation with Simulink.

The Simulink formulation for each thermal node is coupled together in order to solve the heat transfer of the whole construction element (See **Figure 24 -25**).

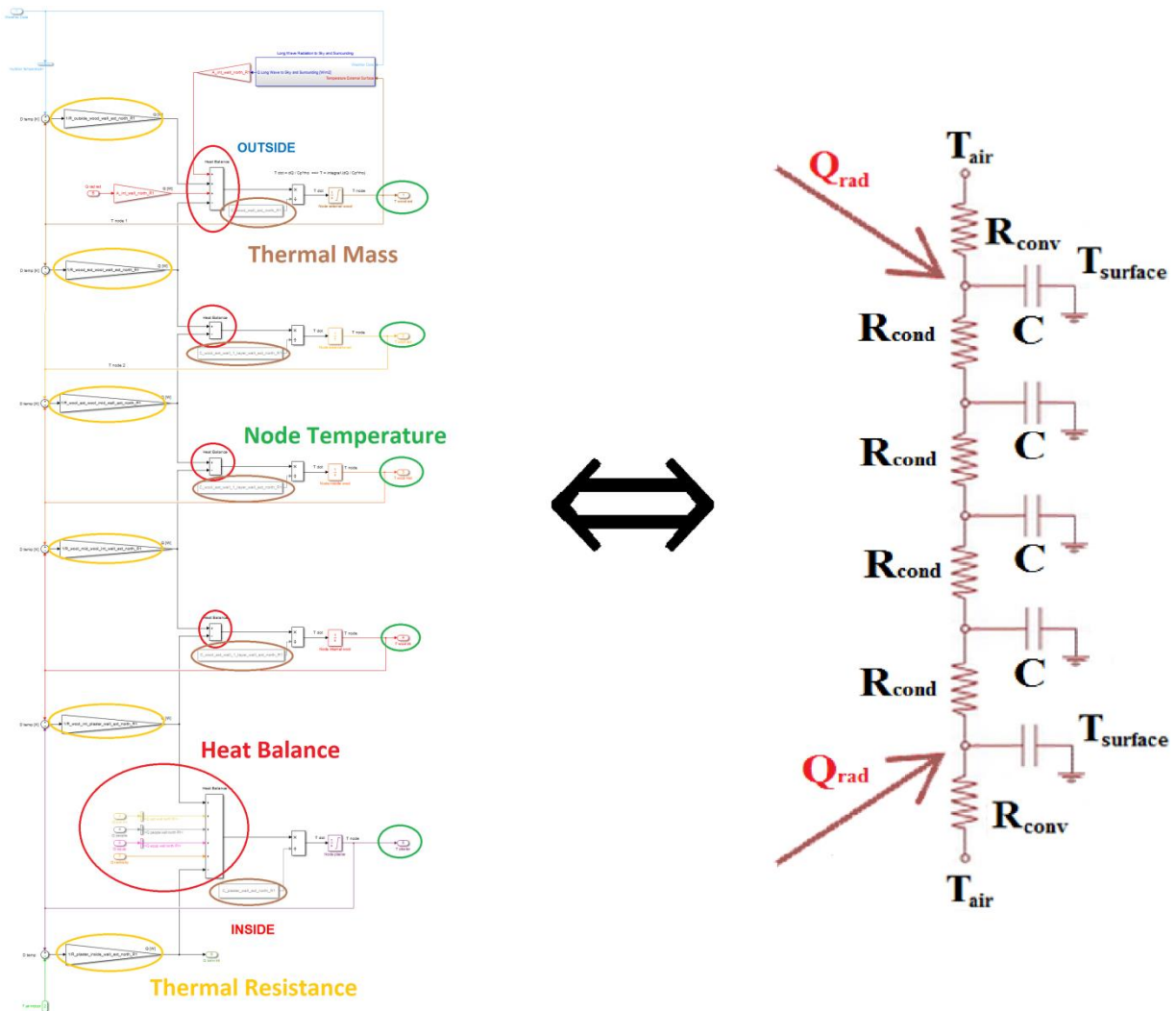


Figure 24: Implementation of a RC network into a Simulink explicit finite volume formulation.

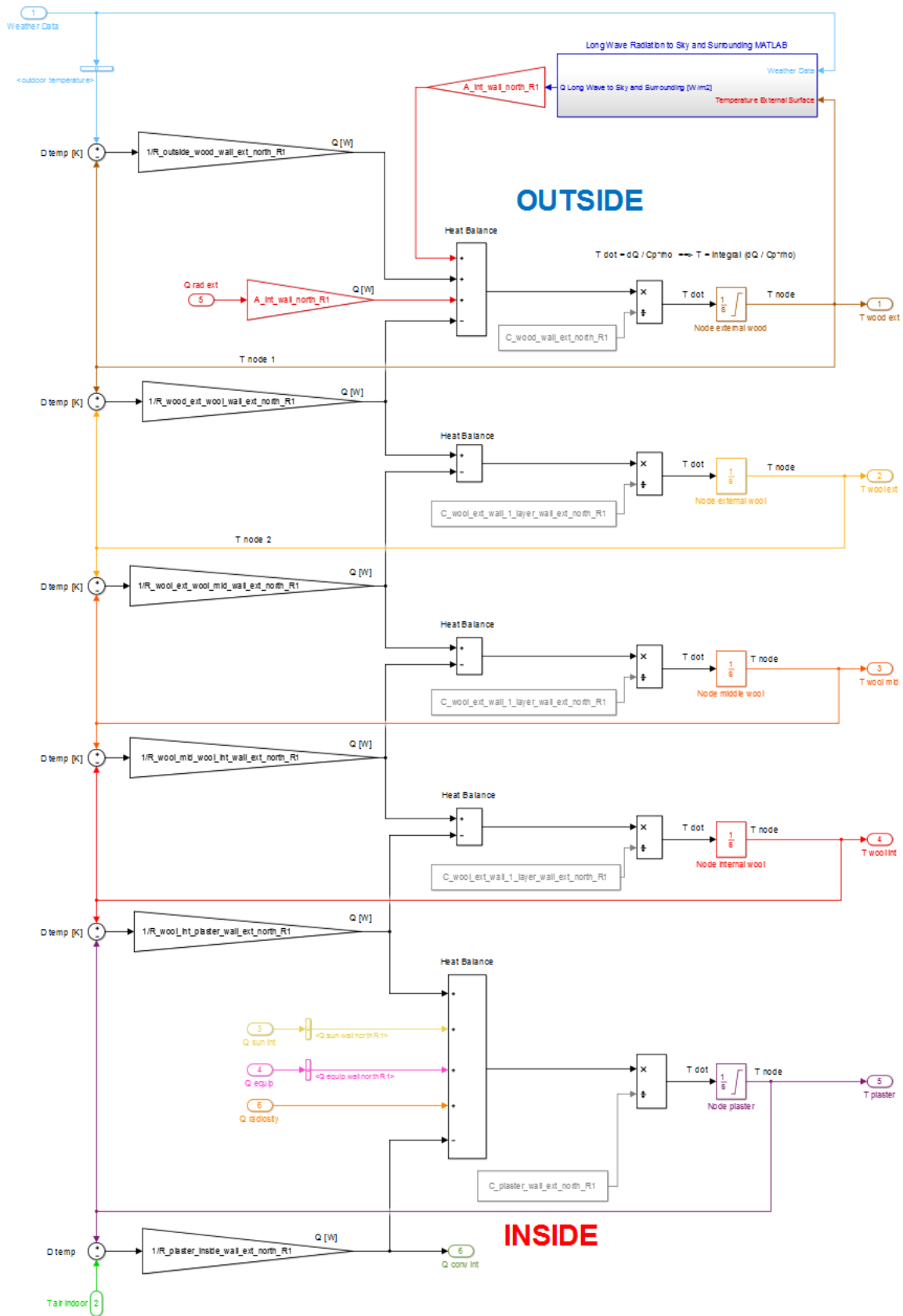


Figure 25: Finite volume formulation of an external wall element.

External walls, internal walls, ceiling and roof elements are subdivided into 5 thermal nodes: 1 node on the left hand side and 1 node on the right hand side for the external panels (plaster, wood, brick, concrete). 3 nodes in the middle of the domain for the insulation layer (stone wool). Floor elements are subdivided into 9 nodes. They include the soil layer under the house and the layers of the water-based under floor heating system.

Because the heat equation is solved in this model with an explicit formulation, the time step size of the simulation has to be chosen with great care so that there is no numerical instability. Therefore the time step size is chosen to be 60 seconds. This time step size is small enough to respect the stability criteria for every thermal node in the model:

$$\Delta t \leq \frac{1}{2} \times \frac{\rho \cdot C_p \cdot \Delta x^2}{\lambda}$$

Where Δt is the time step size and Δx , λ , ρ , and C_p are the thickness, the thermal conductivity, the density and the specific heat capacity of a finite control volume, respectively.

For the construction elements of the envelope, the long wave radiation to the sky and to the surrounding are calculated according to the tilt angle of the surface, the surface emissivity, the sky temperature, the surrounding temperature, the outdoor air temperature, cloud cover, atmospheric pressure, outdoor relative humidity and the position of the sun in the sky. The diffuse and direct short wave solar radiation reaching the external surfaces are directly extracted from a BSim reference model of the study case building.

For the nodes of the construction elements facing the indoor environment, the short wave radiations of the solar loads and the radiative part of the other internal gains are taken into account. The Surface nodes of each construction element is connected to the outdoor air node or to the appropriate thermal zone air node within a star network configuration with constant mixed convection/radiation surface thermal resistance coefficients (See **Table 6** and **Figure 26**) [35].

Name		Value	Unit
Internal, combined surface resistance	upward heat flow	0.10	m ² K/W
	vertical heat flow	0.13	
	downward heat flow	0.17	
External, combined surface resistance	upward heat flow	0.04	m ² K/W
	vertical heat flow	0.04	
	downward heat flow	0.04	
External, combined surface resistance for constructions facing ground		1,50	m ² K/W
Internal convective resistance	floors	0.40	m ² K/W
	ceilings	0.50	
	walls	0.33	

Table 6: Mixed convection / radiation surface thermal resistance coefficient [35].

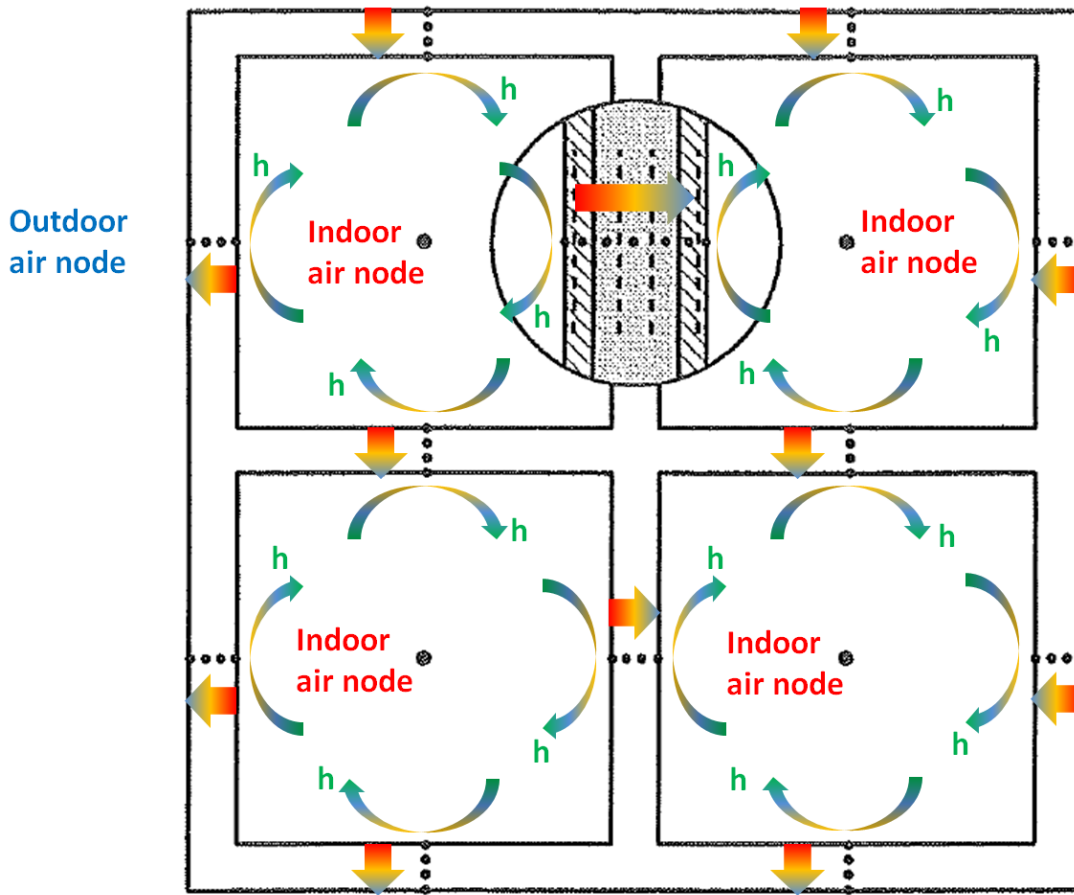


Figure 26: Coupling of thermal nodes in start network.

2.2.Windows, Thermal Bridges, Ventilation and Infiltration Losses

Heat losses through windows, thermal bridges, ventilation and air infiltration are modeled in a simple way. A constant U-value is used for windows and thermal bridges heat losses. It is assumed that there is no thermal mass in these elements.

Heat losses due to air infiltrations are also treated in a simple way with the following formula:

$$Q_{infiltration} = \dot{V}_{infiltration} \times \rho_{air} \times C_{p,air} \times (\theta_{outdoor} - \theta_{indoor})$$

Ventilation heat losses are calculated with the same formula but taking into account the heat recovery (if any):

$$Q_{ventilation} = \dot{V}_{ventilation} \times \rho_{air} \times C_{p,air} \times (\theta_{inlet} - \theta_{indoor})$$

with

$$\theta_{inlet} = \eta_{heat\ recov} \times (\theta_{exhaust} - \theta_{outdoor})$$

The inlet air temperature from the heat recovery ventilation unit is limited to 24 °C. Above that temperature, the heat recovery is turned off. Natural ventilation during summer period is simulated by increasing the ventilation rate without any heat recovery process.

2.3.Zone Air Node

All the element blocks of the different building systems are connected together to the air node of the thermal zone. One can see on the **Figure 27** that the thermal zone air node heat balance is made with the heat fluxes coming from the different elements interacting with it: building elements, solar gains, internal gains, convective heating system, ventilation, infiltration, windows and thermal bridges.

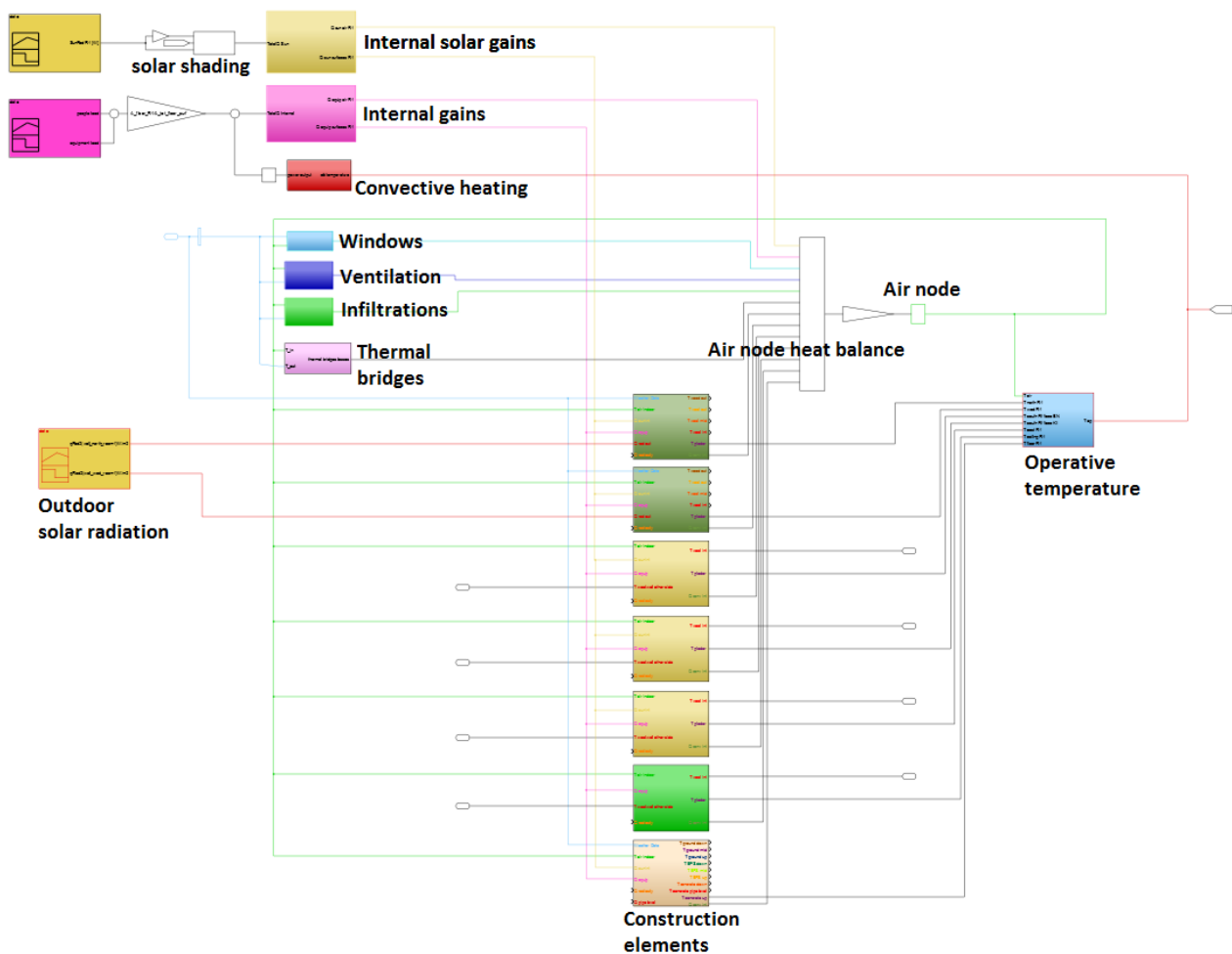


Figure 27: Thermal zone model – all element blocks connected to the air node of the zone.

The air temperature and the temperature of all thermal zone surface elements are taken into account for the calculation of the operative temperature. The latter is then used as process variable for the controller of the heating system.

2.4. Multi-Zone Building Model

The different thermal zones of the building model are connected together to form the multi-zone model of the building (See **Figure 28**). The temperature in the middle of a internal partition walls is used as boundary condition for the wall element adjacent to the thermal zone.

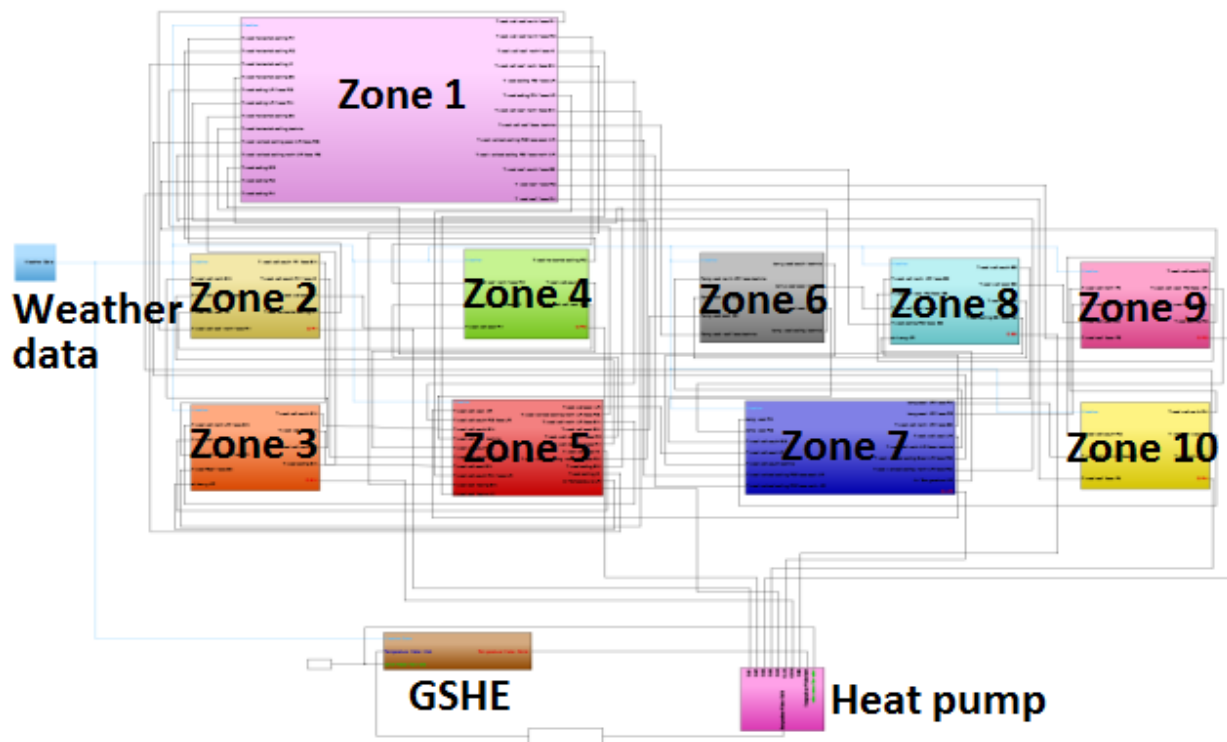


Figure 28: Overview of the multi-zone building model.

2.5. Weather Data

The weather data is taken from the national Danish Reference Year (DRY 2013) based on weather station measurements from 2001 to 2010 and updated in 2013 by the Danish Building Research Institute (SBI). These data has been selected to be used for energy performance calculations and building simulations in Denmark [36].

The parameters included in the dataset are temperature, relative humidity, wind speed and direction, atmospheric pressure, global radiation, cloud cover, soil temperature, sea temperature, diffuse irradiance and illuminance. The time resolution is hourly except for soil temperature where the resolution is daily values.

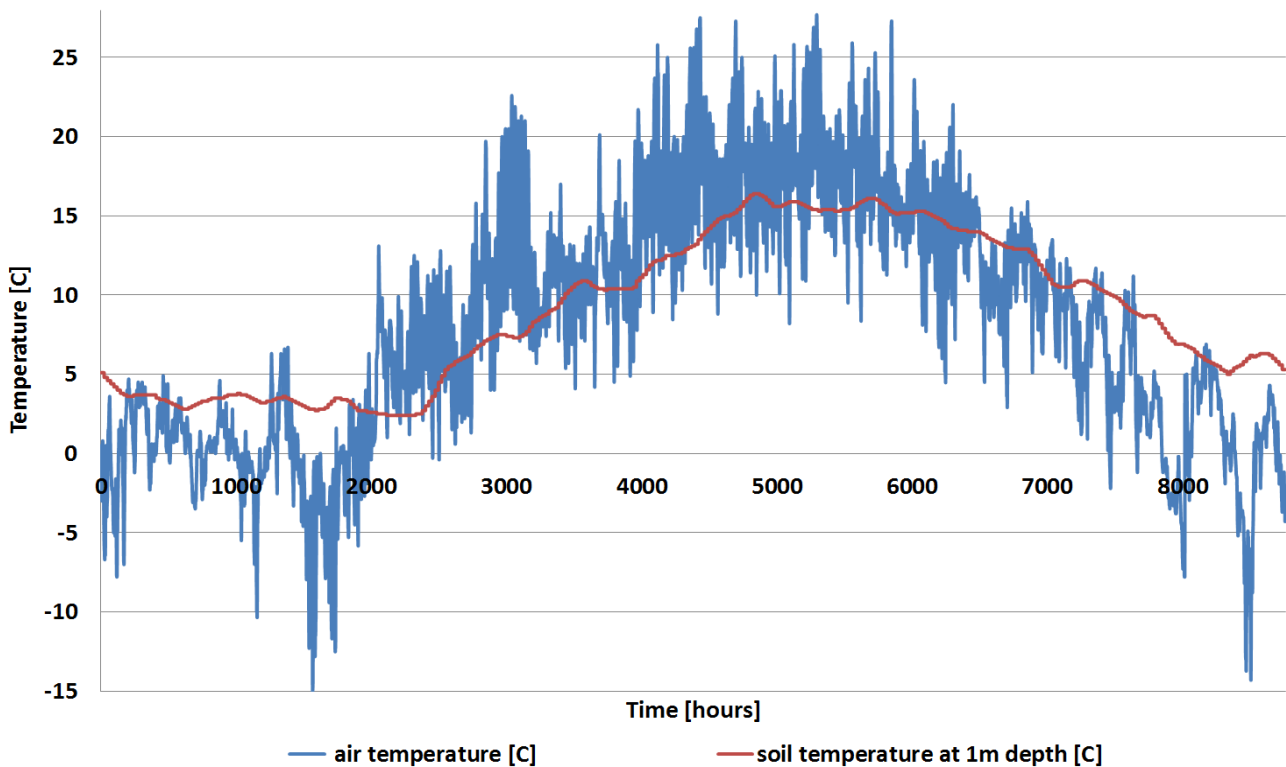


Figure 29: Outdoor air and ground temperature for the reference year in Denmark (DRY 2013).

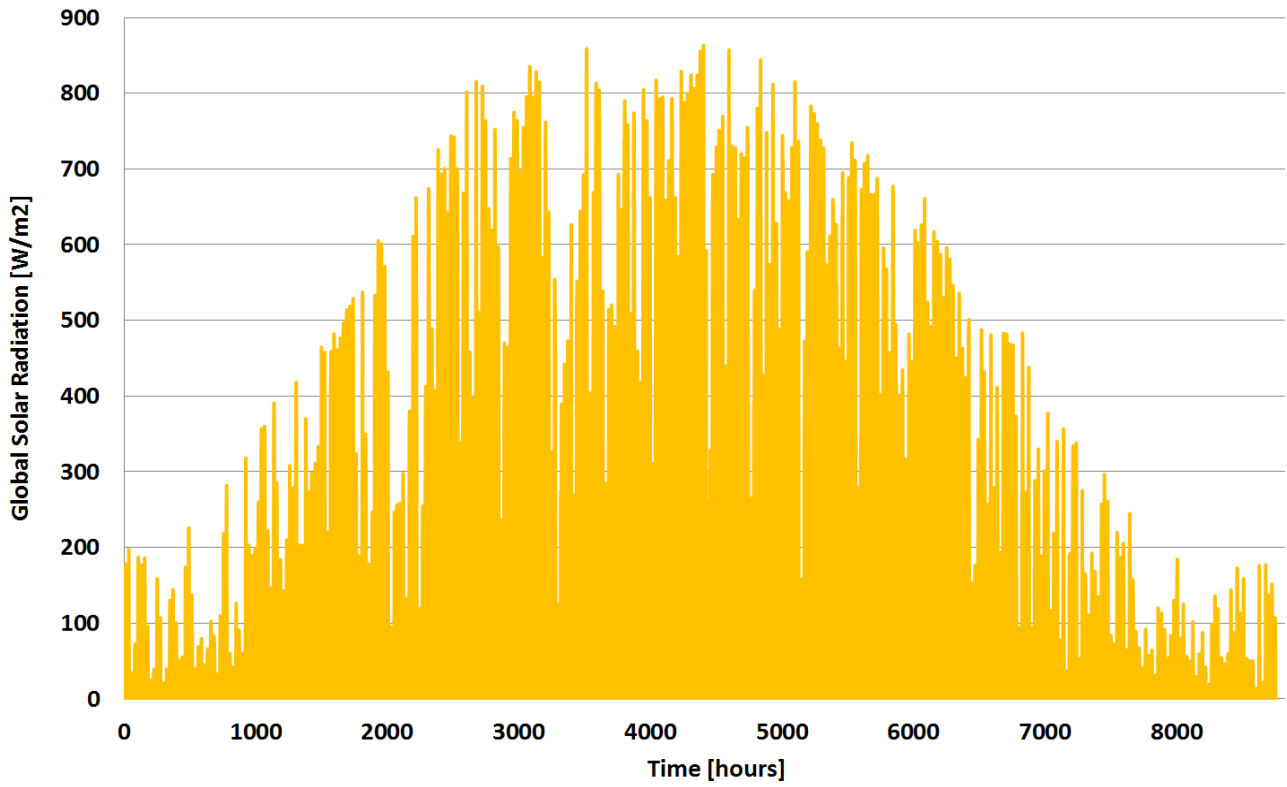


Figure 30: Global outdoor sun radiation for the reference year in Denmark (DRY 2013).

2.6.Solar Gains and Internal Gains

Internal thermal gains (excluding the heating system’s load) originate from the heat released by the occupants during occupying time and the heat released from the house equipment such as computers, lightning, oven, TV, etc. A standard person has heating power of around 100 W and generates 0,06 kg of moisture and 17 L of CO2 per hour.

The equipment and people load schedules are based on typical Danish equipment use and people schedule for a residential house [37]. The overall internal gains time profile of the house is presented in **Table 7** and **Figure 31**. Each type of room (living room, bedroom, bathroom) has a specific people/equipment loads weekly schedule accounting for realistic average internal loads to these rooms.

4 People Schedule							
Time \ Day	Monday	Tuesday	Wednesday	Thursday	Friday	Saturday	Sunday
1	4	4	4	4	4	4	4
2	4	4	4	4	4	4	4
3	4	4	4	4	4	4	4
4	4	4	4	4	4	4	4
5	4	4	4	4	4	4	4
6	4	4	4	4	4	4	4
7	2	2	2	2	2	4	4
8	2	2	2	2	2	4	4
9	0	0	0	0	0	2	2
10	0	0	0	0	0	2	2
11	0	0	0	0	0	2	2
12	0	0	0	0	0	2	2
13	0	0	0	0	0	2	2
14	0	0	0	0	0	2	2
15	0	0	0	0	2	2	2
16	0	0	0	0	2	2	2
17	2	2	2	2	4	4	4
18	4	4	4	4	4	4	4
19	4	4	4	4	4	4	4
20	4	4	4	4	4	4	4
21	4	4	4	4	4	4	4
22	4	4	4	4	4	4	4
23	4	4	4	4	4	4	4
24	4	4	4	4	4	4	4

Table 7: Schedule of the people load for a typical single family house in Denmark.

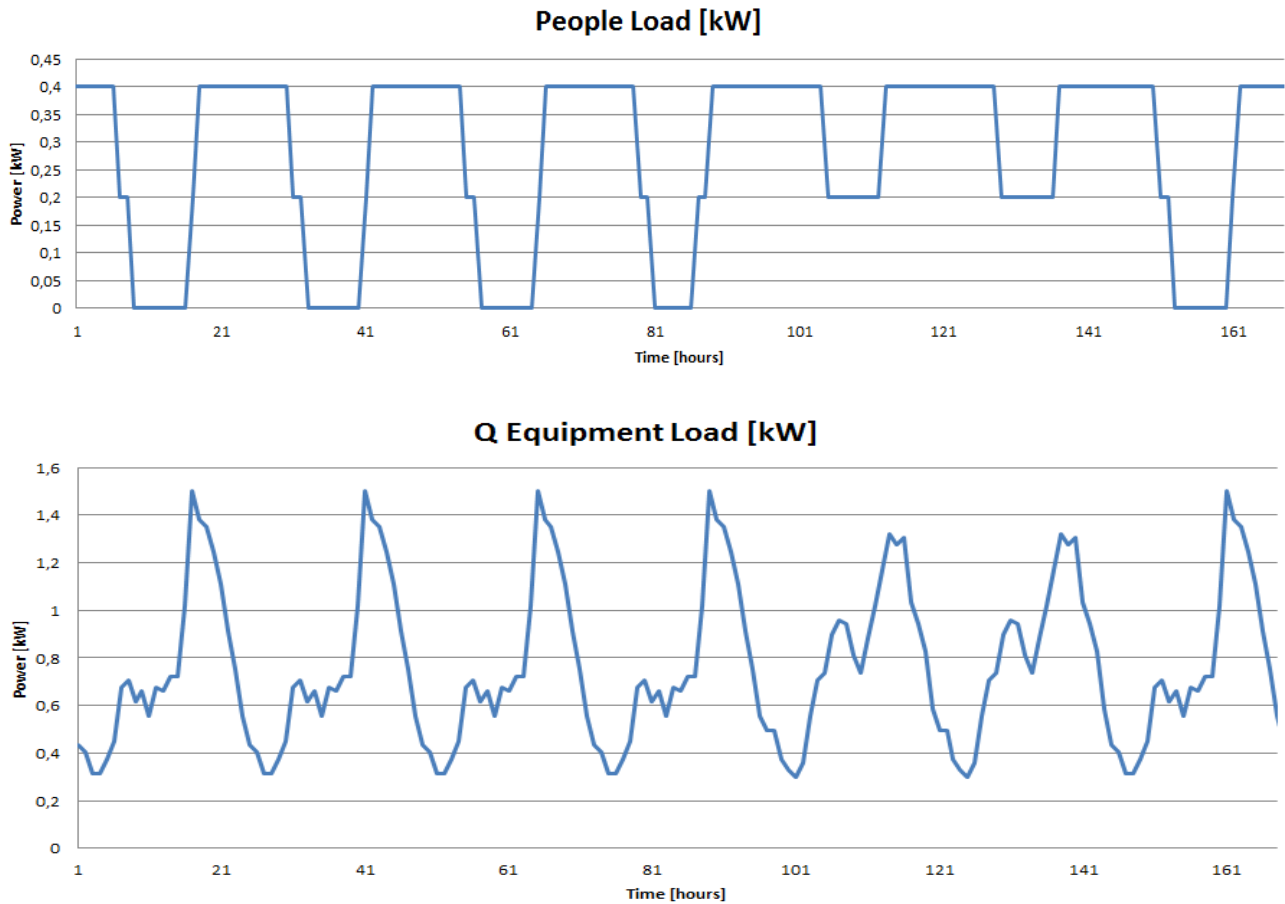


Figure 31: Time profile of the internal gains of a typical single family house in Denmark.

The internal solar gains (the direct, diffuse and reflected solar radiation entering the indoor environment and not leaving it) are directly extracted from the BSim reference model of the study case building for each thermal zone and for each hour of the year.

The distribution of the equipment, people and radiator heat load is as follow: 70% goes directly to the air node of the thermal zone; 30% goes to the internal surfaces of the thermal zone (long wave radiation share). The radiative share is equally distributed over all surfaces in function of their surface area weighing [35].

The distribution of the internal solar gain is as follow: 15% goes directly to the air node of the thermal zone; 55% goes to the floor; 30% goes to the vertical walls of the thermal zone and is equally distributed over these surfaces in function of their surface area weighing; no solar radiation goes to the ceiling [35].

In the case of additional indoor thermal mass / furniture in the indoor space, 50% of the radiative share of the equipment, people, solar and radiator heating loads is distributed on the surfaces of the equivalent planar element modeling the furniture.

2.7. Radiator Heating System

Two types of heating emitters are investigated in this study: radiator and water-based under floor heating system.

The radiator heating system is modeled in a simple way with a first order transfer function which has a time constant of 10 minutes [38]. The radiator is regulated with a PI controller. 30% of its heat output is transferred to the indoor environment by radiation and 70% by convection.

2.8. Hydronic Under-Floor Heating Systems

In most building energy software tools, the conductive heat transfer through the building construction is evaluated assuming a one-dimensional heat flow and homogenous surface temperature. For a hydronic radiant floor terminal, the correct modeling of the conductive flow is more difficult due to the three-dimensional heat transfers at the pipe level. The conductive flow at the activated surface (embedded pipe level) is mainly influenced by the type of pipe (diameter, wall thickness and material), the pipe spacing, the water flow (water velocity) and the resistance of the conducting layers. Different calculation methods have been developed to model the conductive flow from the pipe level to the surface with the objective of either calculating the heating/cooling capacity of the radiant systems or of simulating their dynamic behavior in building energy software tools:

- Glück B [39] [40] has developed an analytical solution of the thermal field due to the presence of pipes embedded in an infinitely long slab under steady-state conditions. However the consequent analytical solution is very complex, needs a significant computer calculation time to be obtained, does not take into account the different material layers (pipe, insulation, concrete screed) and therefore cannot be widely applied.
- Most of the models are based on a one-dimensional Resistance - Capacitance network, similar to the technique described in the standard EN 15377-1 [17]. The principle of this calculation method is to determine an equivalent resistance between the heating or cooling medium to the fictive core (or heat conduction layer) where the pipes are located. The variation of fluid temperature along the circuit is modeled considering the pipe circuit as a heat exchanger. The three-dimensional domain collapses into a simpler 1D problem and the efficiency of such heat exchanger is computed via the ϵ -NTU (effectiveness-Number of Transfer Units) method. Koschenz and Lehmann [41] [42] have developed the calculation procedure for TABS and this model has been extended for other systems by De Carli, Koschenz, Olesen and Scarpa in the standard EN 15377-1. Scarpa et al. [43] developed and validated the RC model for different geometries of radiant systems. It has to be noted that the accuracy of these RC models is greatly affected by the determination the thermal properties of the different RC components.
- Other methods have been developed such as the conduction transfer function method from Strand and Pedersen [44], the response factors technique from De Carli et al. or the universal single power function of the standard EN 1264-2 [16]. More detailed models, which are evaluating the conductive heat transfer based on two-dimensional calculations (FEM, FVM), are also available.

The modeling of the hydronic components in this study is based on the ϵ -NTU method developed by Scarpa et al. [43] to represent the complex interaction between the embedded pipes and the conductive slab, and a “plug-flow” principle model, similar to the Type 31 model from TRNSYS 17 software [45], in order to account for dynamics of the fluid pushed into the pipes.

For high fluid flow in hydronic system, the time needed for a fluid cell to go through the whole pipe’s length is smaller than the time step size of the model. In that case, it is assumed that the fluid subsystem in the pipe reaches a pseudo-steady state within the time step. Therefore the calculation of the fluid temperature profile is performed according to the ϵ -NTU method.

On the other hand, for low fluid flow, a fluid cell can take several simulation time steps before reaching the outlet of the hydronic loop. In that case, the calculation of the fluid temperature profile is performed according to the “plug flow” principle [45]. As shown on **Figure 32**, at each time step, one fluid cell is added at the beginning of the pipe (queuing in). The new fluid control volume “ T_i ” pushes all the other control volumes towards the exit of the pipe without any mixing in between adjacent cells (plug flow principle). Heat transfer in between adjacent cells could be considered if there would be some correlation of mixing and heat transfer in between these cells for a pipe, but this is not the case here. This no-mixing assumption is reasonable if the fluid is circulating with a fairly high velocity and if the temperature difference in between each cell is not too important.

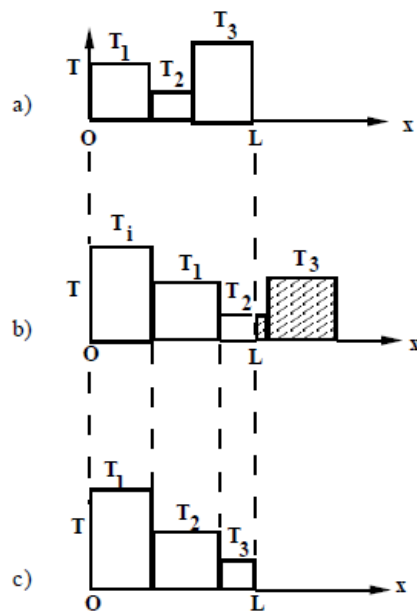


Figure 32: Plug flow principle.

The outlet temperature is calculated as volume weighted average temperature of the fluid cells exiting the hydronic system. If the pipe is very long and the flow is very small, a lot of small fluid cells will get stacked into the model queue. To avoid memory issues, the maximum number of fluid cells in the systems is limited

to 100. When the maximum number of fluid cells is reached, the 2 neighboring cells with the smallest temperature difference are merged together and assigned an appropriate new average temperature. The heat exchanger between the fictitious pipe level slab and each fluid cell is performed according to the ϵ -NTU method.

The water temperature change along the pipe is considered following an exponential decay function. The logarithmic mean fluid temperature along the pipe circuit may be assumed as a reference for the estimation of the heat exchange between the fluid and the inner surface of the pipe. The temperature of the pipe is assumed constant with respect of its length. The ϵ -NTU calculation is performed with the effectiveness of the equivalent heat exchanger formed by the embedded pipe in the conductive slab of the under-floor heating system. This effectiveness is determined by the thermal resistance of the fluid in the pipe, the thermal resistance of the pipe itself, the thermal resistance of the different layers of the slab and an equivalent thermal resistance. The latter accounts for the complex three-dimensional interactions between the different sections of the serpentine pipe layout network with the rest of the conductive slab where it is positioned [43] (See **Figure 33**).

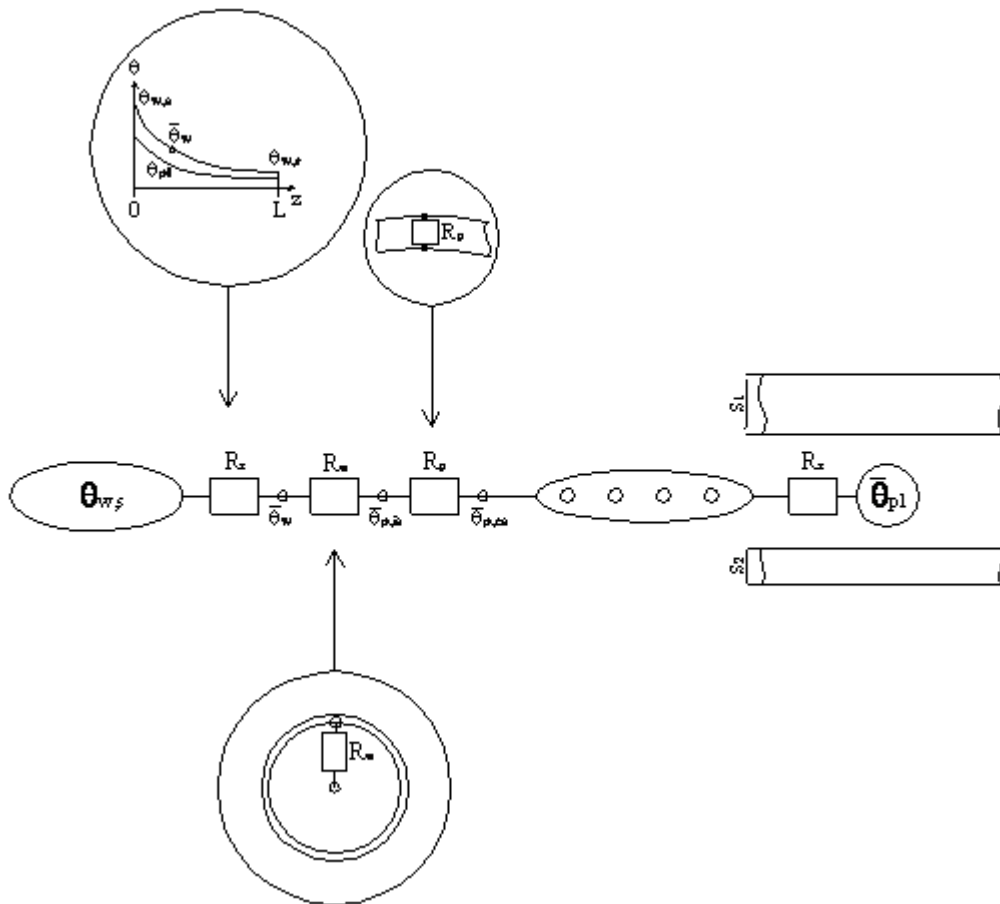


Figure 33: Schematic of the equivalent RC network of the hydronic floor heating system.

2.9. Horizontal Ground Source Heat Exchanger

Horizontal ground source heat exchangers are buried at depths ranging between 0.8 and 2 m and their performances are also influenced by weather conditions at the soil surface (See **Figure 35**).

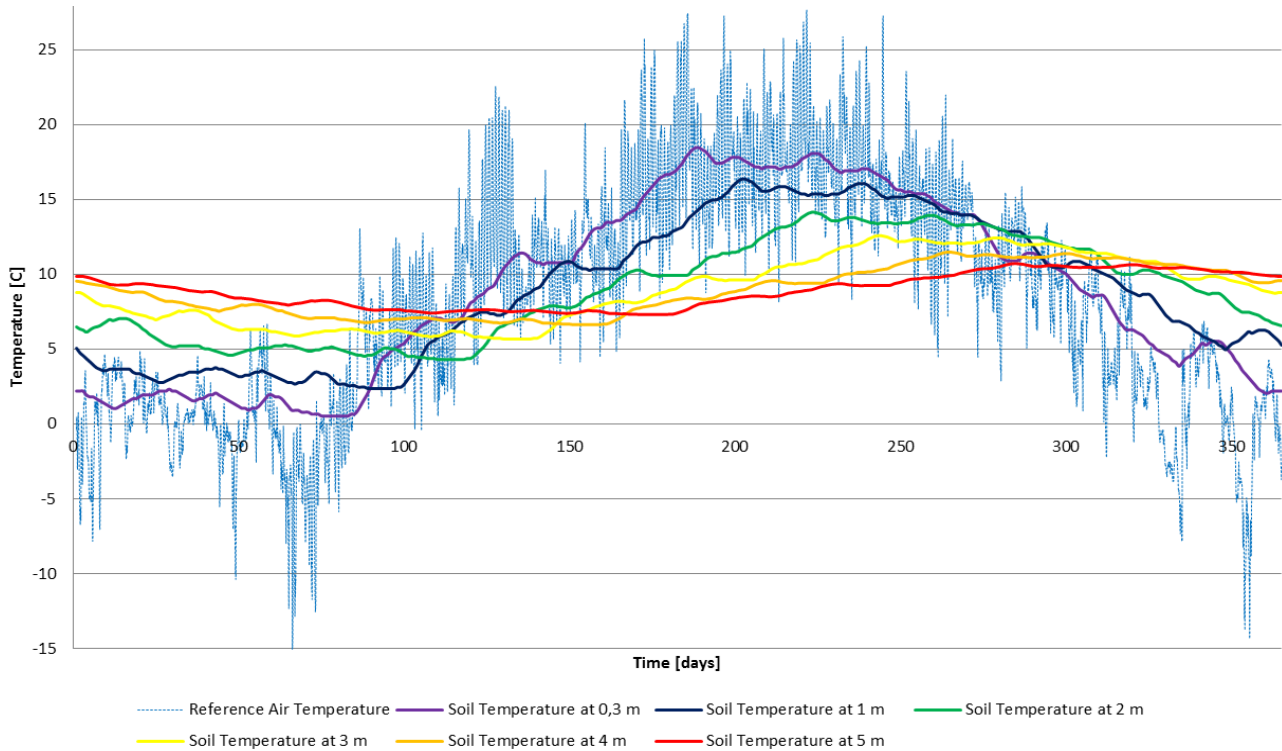


Figure 35: Ground temperature in Denmark.

Similarly to the under-floor heating system, the horizontal ground source heat exchanged is modeled with the plug flow / ϵ -NTU method function. The ground domain is modeled with a state-space function (See **Figure 36**) which represents a soil cube of 12 x 25 m with a depth of 30 m. The bottom boundary conditions of the ground domain are set as constant temperature of 9.4 °C. The boundary conditions of the top surface of the ground domain are determined by the weather data: outdoor air temperature, wind speed and global solar radiations. The temperature boundary conditions on the sides of the domain are following the temperature time variation of the undisturbed ground temperature in Denmark.

$$\{\dot{\theta}\} = [A] \cdot \{\theta\} + [B] \cdot \{u\}$$

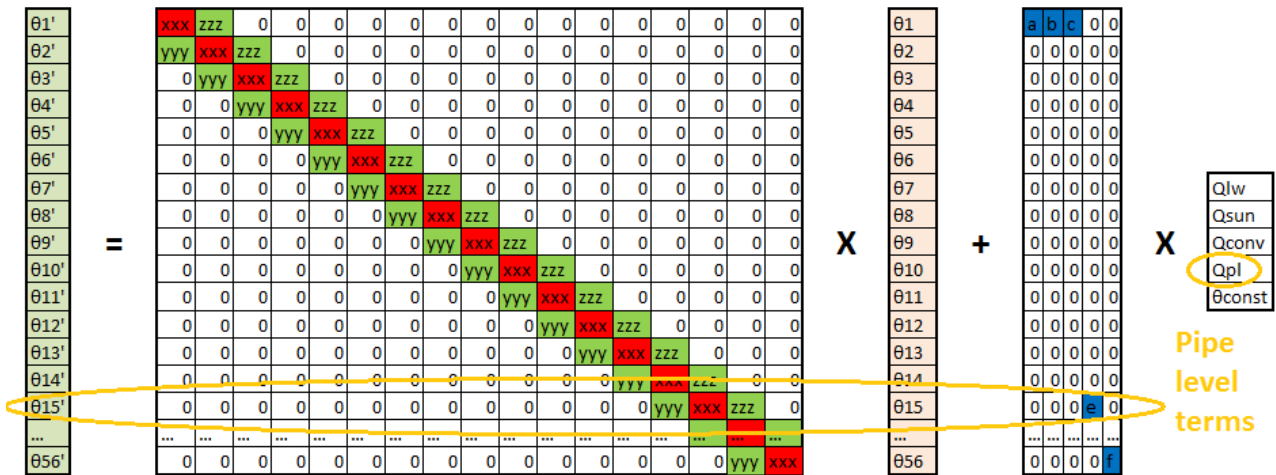


Figure 36: State space representation of the ground domain.

The soil domain reduced into a one-dimensional heat transfer system. It is discretized into ground 29 slices of 10 cm (on the top half), 27 slices of 1 m (on the bottom half) and slice of 20 cm for the fictitious pipe level.

2.10. Vertical Borehole Ground Source Heat Exchanger

The vertical borehole ground source heat exchanger is modeled with two plug flow / ϵ -NTU method MATLAB functions coupled together. The inlet section of the U-pipe is modeled with the first function and the outlet section of the U-pipe is modeled with the second function. The two pipe models are connected to the surrounding ground represented by a state-space model function with concentric cylindrical slices of ground. The ground slice subsystems are 100 m deep and 10 cm or 1 m thick. The ground domain is therefore discretized into 16 volumes accounting for the ground which is 10 m apart from the center of the GSHE.

The complex thermal interaction between the U-pipe of the heat exchanger, the grout and the ground is modeled with a triangular thermal network (RC network) (See **Figure 37**). This thermal network modeling is presented in details in a journal paper of Diersch et al. [46].

The initial temperature conditions for the ground domain are set as the yearly average temperature profile of an undisturbed soil in Denmark (See **Figure 38**). The bottom boundary conditions of the ground domain are set as constant temperature of 10.1 °C, while the boundary conditions of the top surface of the ground domain are determined by the weather data: outdoor air temperature, wind speed and global solar radiations.

Ground

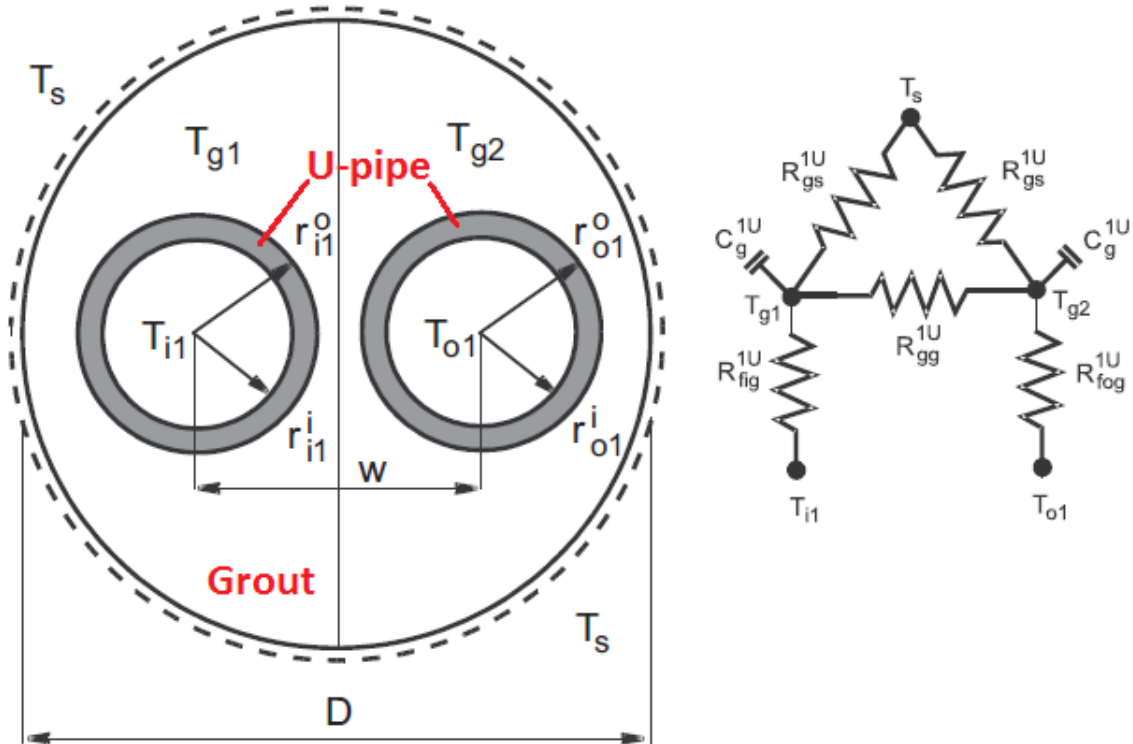


Figure 37: RC network modeling the heat transfer between the U-pipe, the grout and the surrounding ground domain [46].

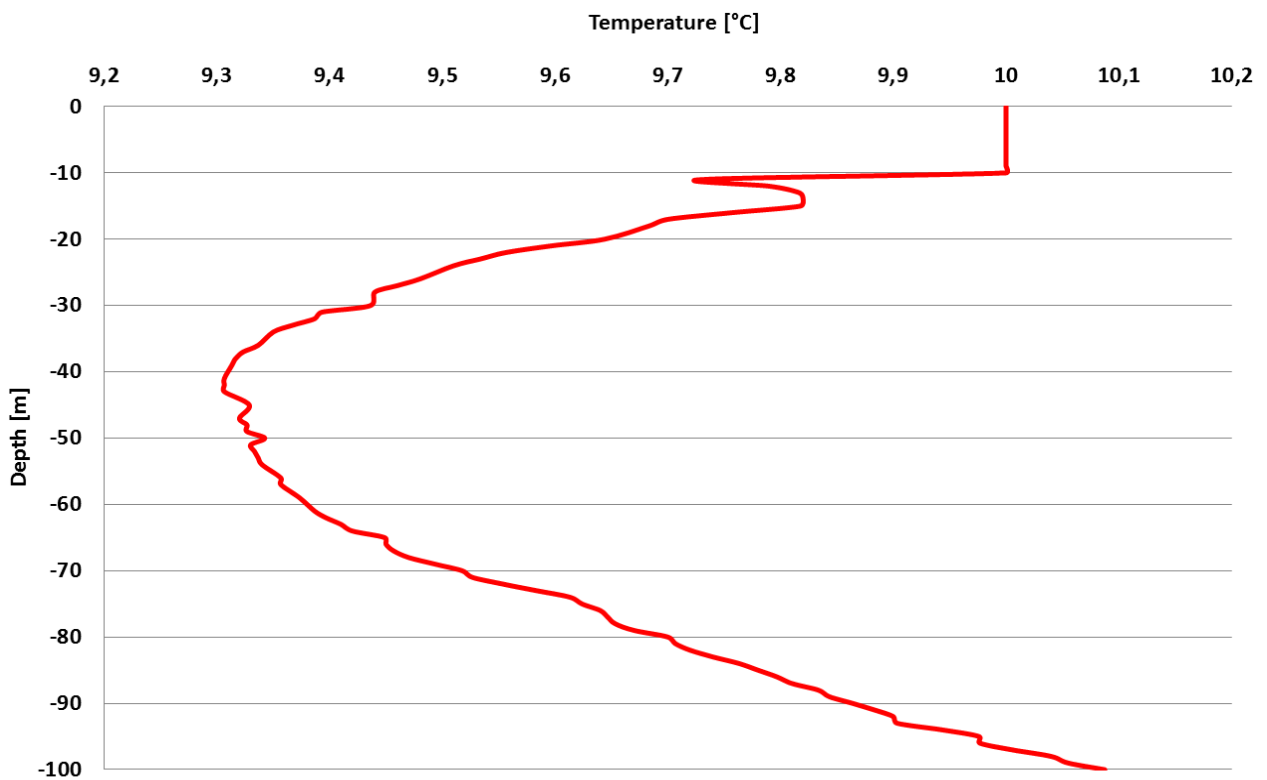


Figure 38: Yearly temperature profile of undisturbed soil in Denmark.

2.11. Water-Based Brines of the Hydronic Networks

In order to calculate precisely the heat transfer between the brine carrier fluid and the heat exchanger, all physical and thermal properties of 5 fluids have been modeled with polynomial correlations based on manufacturer's database. Density, thermal conductivity, specific heat capacity and dynamic viscosity are calculated in function of fluid temperature and brine product concentration for pure water, propylene glycol, ethylene glycol, ethanol or methanol. These 5 products are the most commonly used brine fluids in hydronic systems. One can see on **Figure 39 – 44** some of the polynomial correlations established from tabulated data of manufacturers and textbooks [47] [48] [49] [50] [51] [52] [53] [54] [55] [56] [57] [58] [59] [60] [61] [62] [63] [64] [65].

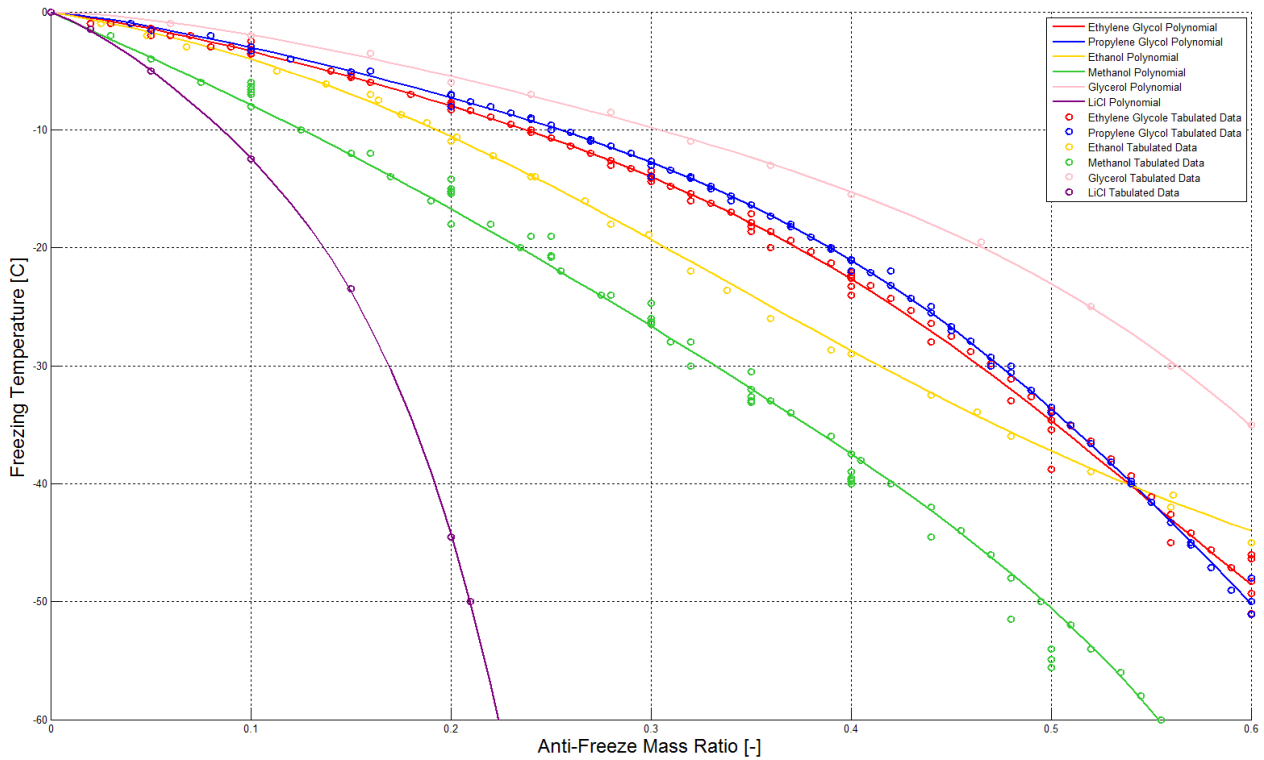


Figure 39: Water-based brine freezing temperature in function of product concentration.

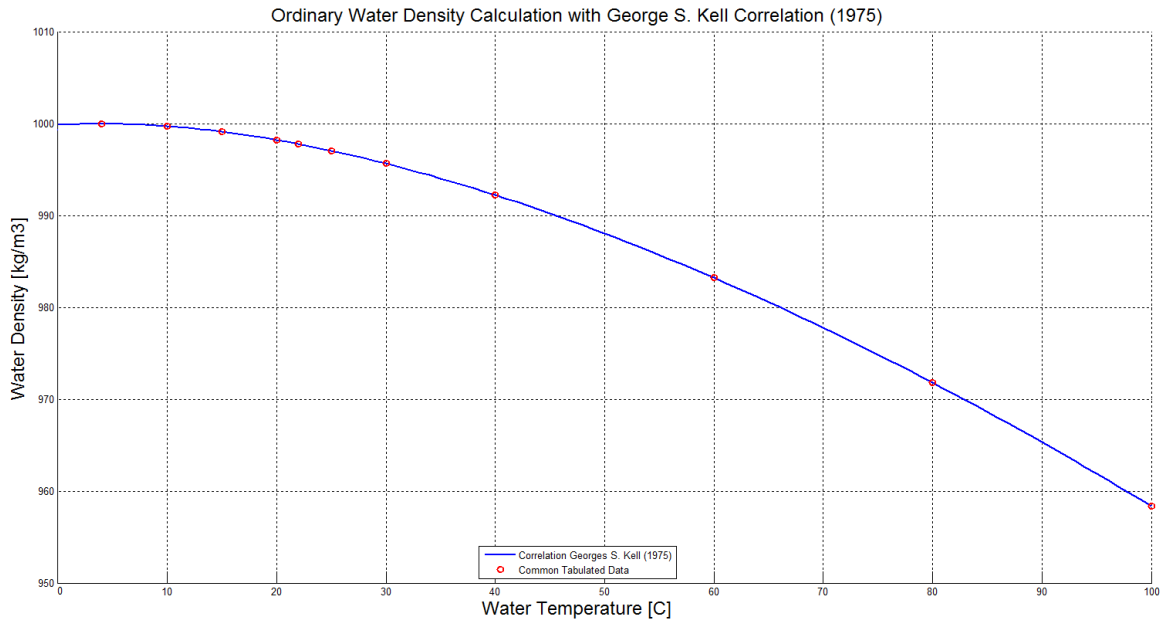


Figure 40: Ordinary water density in function of temperature.

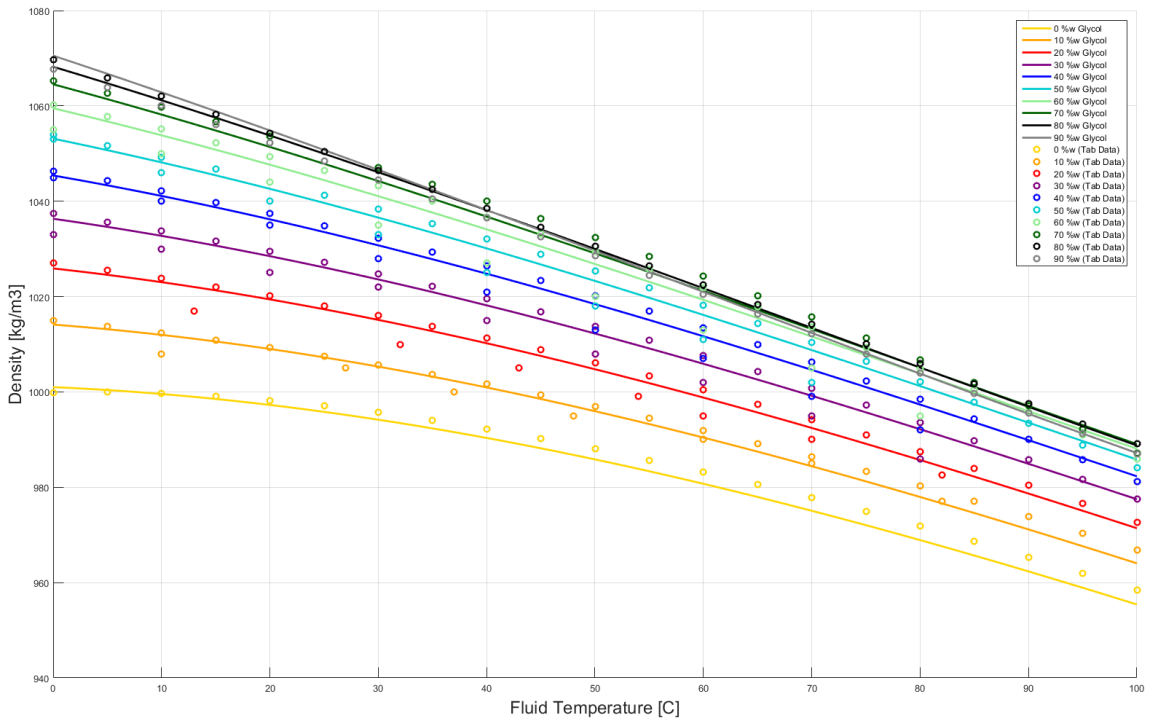


Figure 41: Propylene glycol density in function of temperature and concentration.

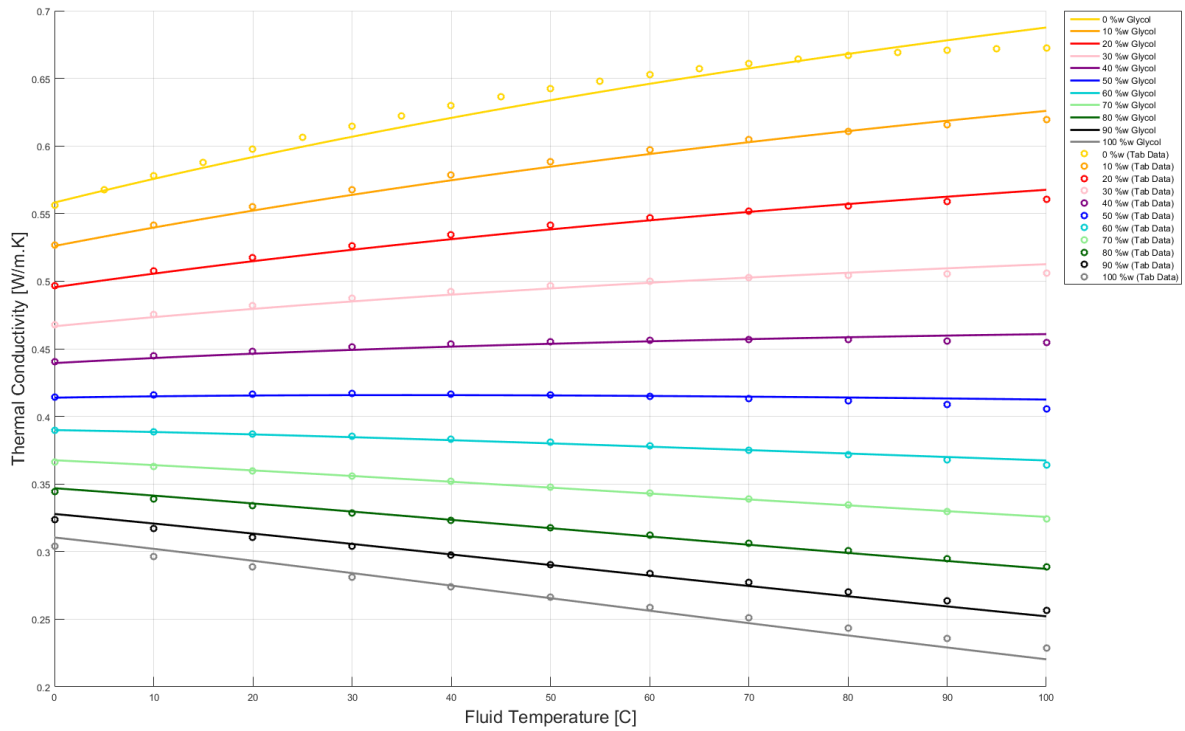


Figure 42: Ethylene glycol thermal conductivity in function of temperature and concentration.

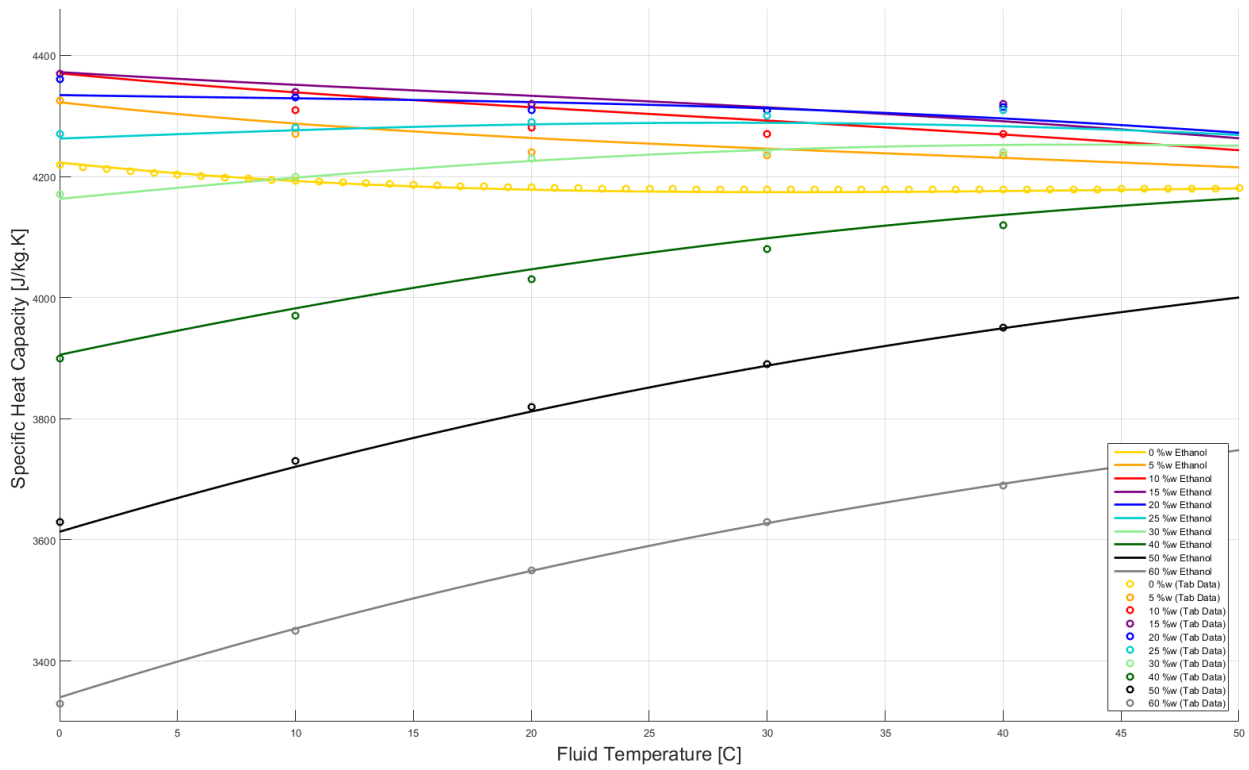


Figure 43: Ethanol specific heat capacity in function of temperature and concentration.

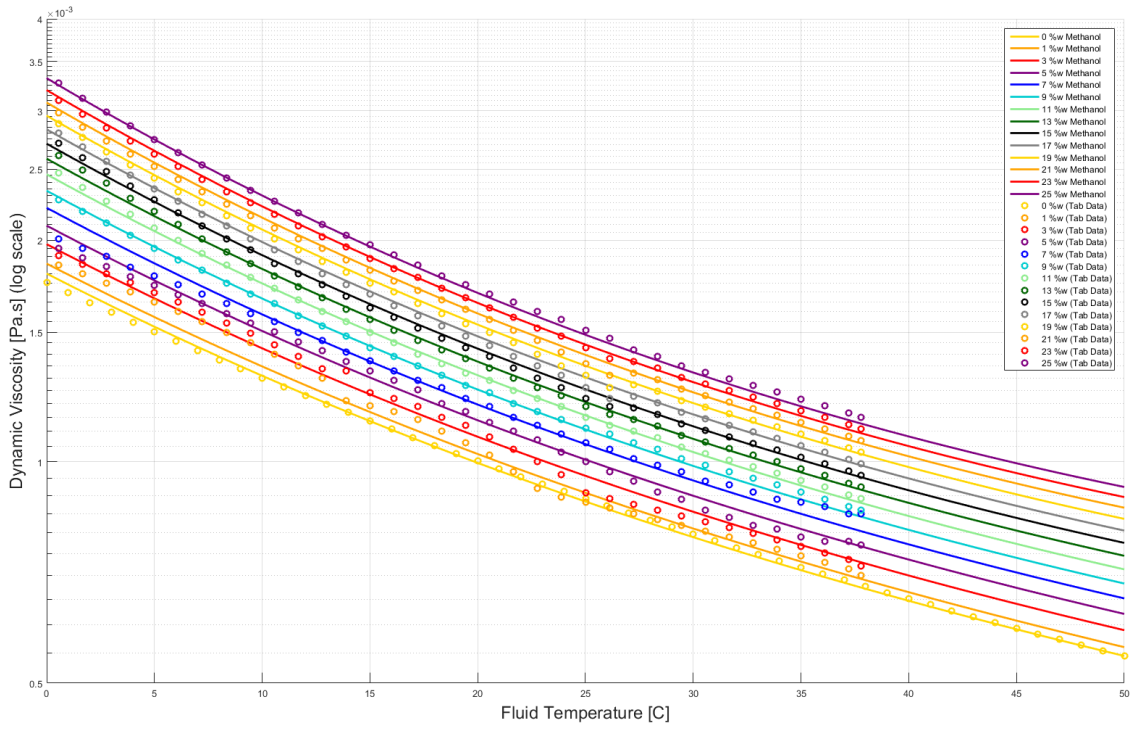


Figure 44: Methanol dynamic viscosity in function of temperature and concentration.

The Prandtl number, the Reynolds number, the Darcy friction factor (see **Figure 44**) and the Nusselt number are then derived from the thermo-physical properties of the brine.

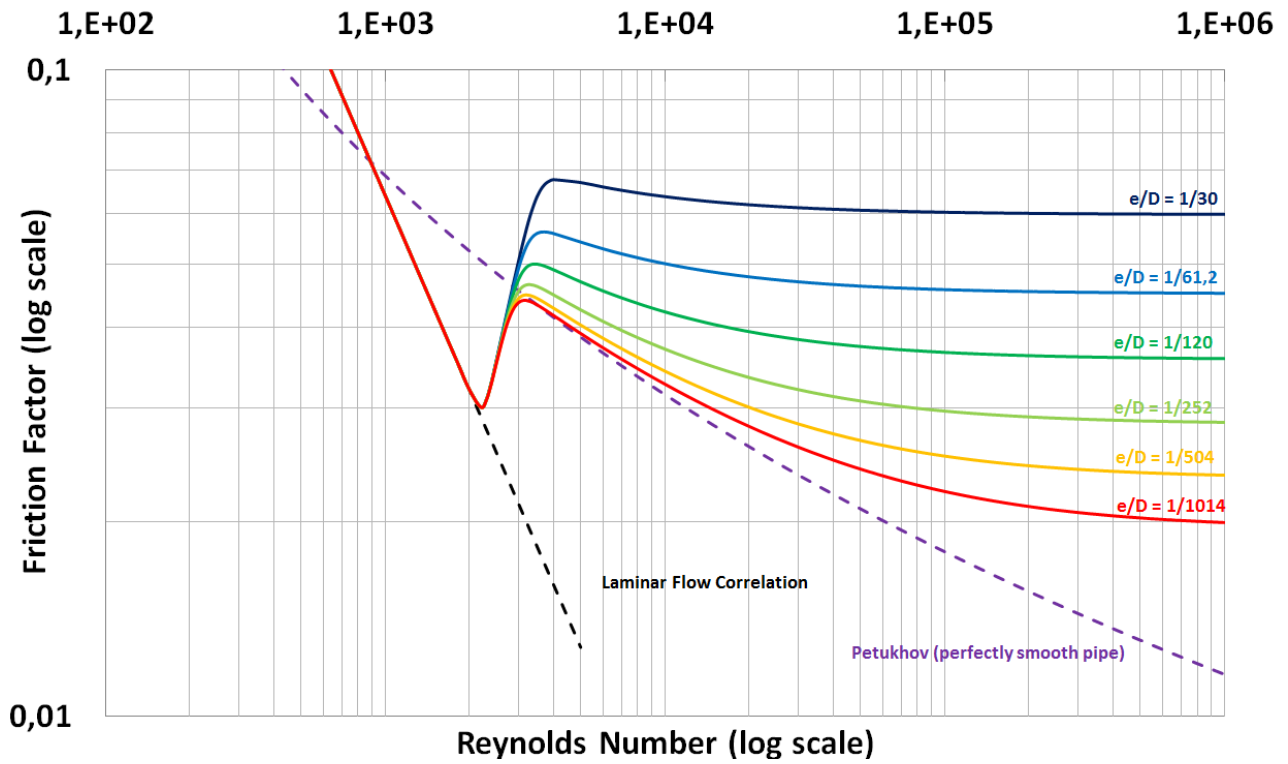


Figure 48: Darcy friction factor (correlation Churchill 1977).

Finally, the convective heat transfer coefficient and the convective thermal resistance are calculated for the circular pipe (See **Figure 46 – 47**).

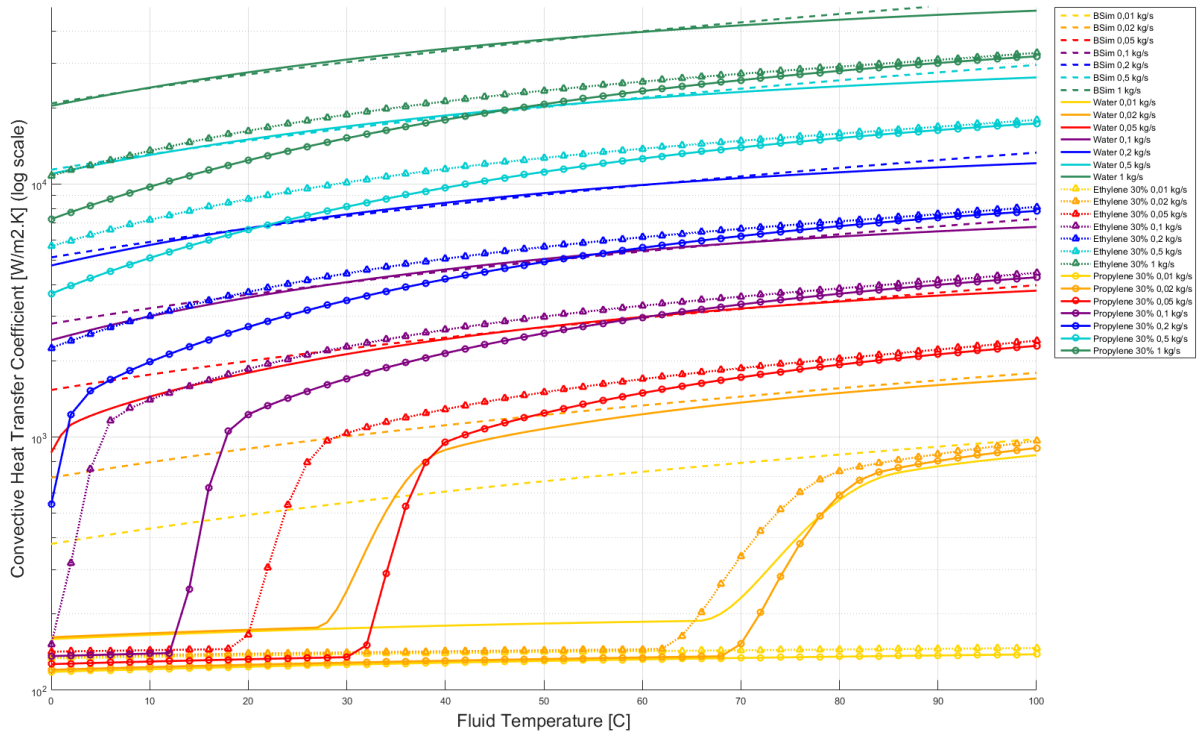


Figure 46: Convective heat transfer coefficient in circular pipe ($D_i = 13 \text{ mm}$, $e = 0.0015 \text{ mm}$, $L = 100 \text{ m}$).

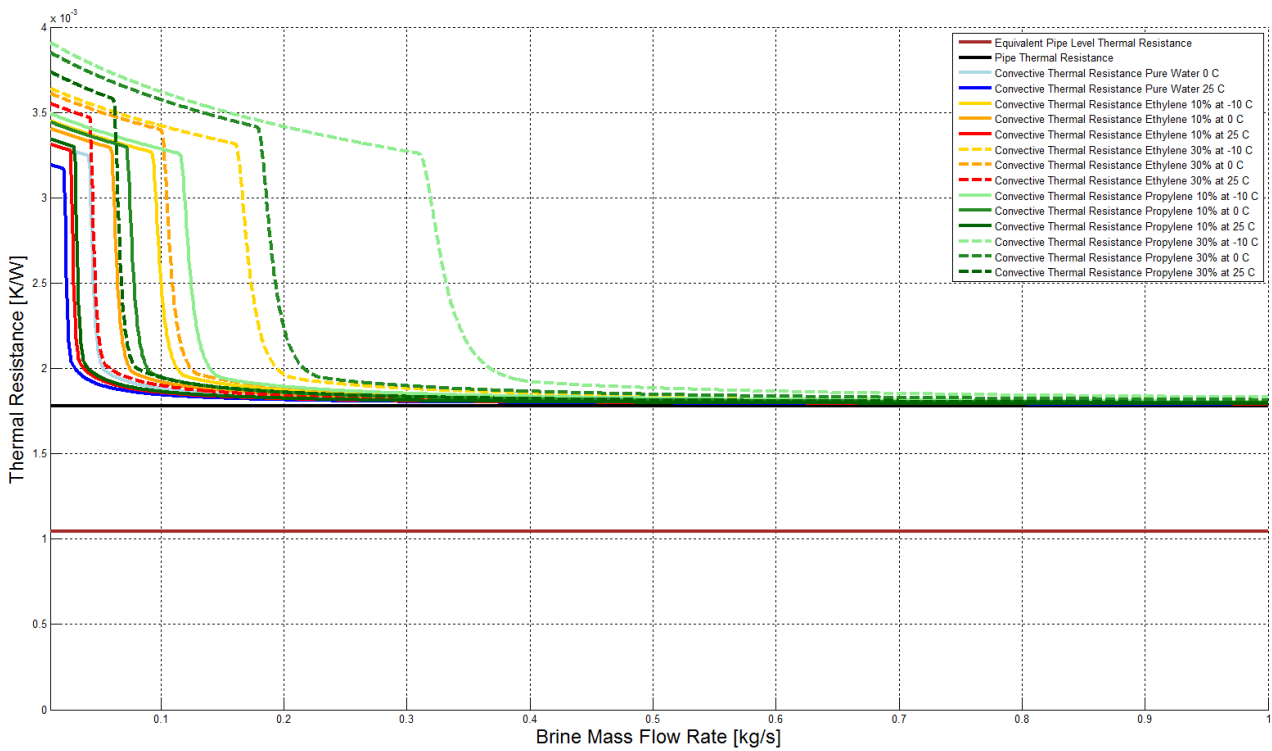


Figure 47: Floor heating heat exchanger thermal resistance ($D_i = 13 \text{ mm}$, $e = 0.0015 \text{ mm}$, $L = 100 \text{ m}$).

2.12 Pressure Loss in the Hydronic Systems

In order to evaluate the energy consumption of the entire system, the pumping workloads are assessed by calculating the total pressure drop of the whole hydronic system. The latter is obtained by adding the pressure drop across the piping loops, the manifold, the valves, the mixer the supply and return pipes. The system is a closed loop, therefore the inlet and the outlet are at the same altitude and so there is no pressure loss due to inlet and outlet height difference.

The pressure drop in straight pipes caused by fluid friction in fully developed flows of all “well-behaved” (Newtonian) fluids is described by the Darcy-Weisbach equation:

$$\Delta p = f \frac{L \rho v^2}{2D}$$

Valves and fittings cause singular pressure losses that can be greater than those caused by the pipe alone. They are expressed as:

$$\Delta p_i = K_i \frac{\rho v^2}{2}$$

5 different methods have been implemented to calculate the singular pressure drop of hydronic elements:

- Equivalent length method
- Excess head 1K method
- 2K method
- 3K method
- Babcock and Wilcox Co., 1978

2.13. Heat Pump System

The conventional water-to-water vapor-compressor heat pump system is modeled in a simple way with a collection of steady states implemented in a 4-dimensional lookup table function. The important hypothesis here (and therefore limitation of the model) is that it is assumed that the heat pump operation reaches quasi-steady state within each simulation time step of 60 sec. The data implemented in the lookup table function is obtained from documentation of the model TWM036 heat pump manufacturer [13].

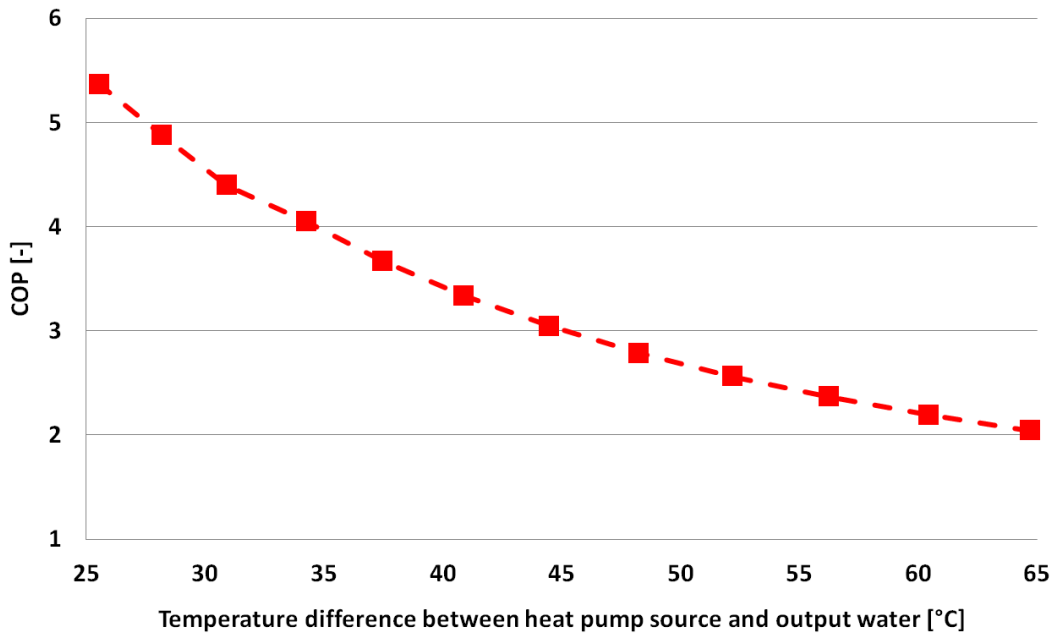


Figure 48: Heat pump COP in function of temperature difference between evaporator inlet and condenser outlet at steady state.

2.14. Circulation Pump for Water-Based Heating System

The modeling of the circulation pump Grundfos Alpha2 L 15-40 is made in a simple way with a second degree polynomial function fitting operation data provided by Grundfos manufacturer [14] (see **Figure 49 - 50**). The hydraulic circulation pumps are all set to constant pressure regulation (CP1) at 23 000 Pa.

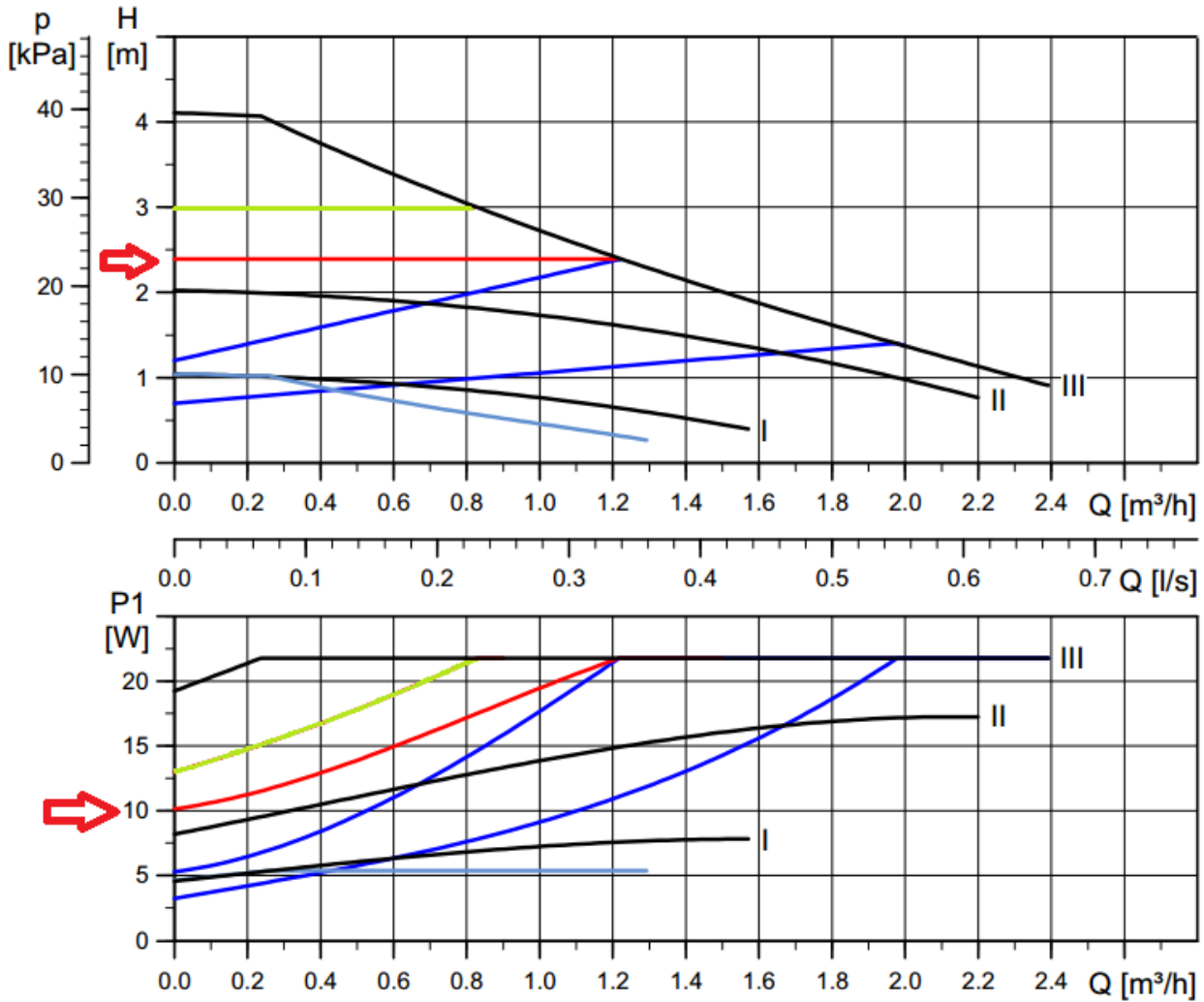


Figure 49: Performance curves of the pump circulator Grundfos Alpha2 L 15-40.

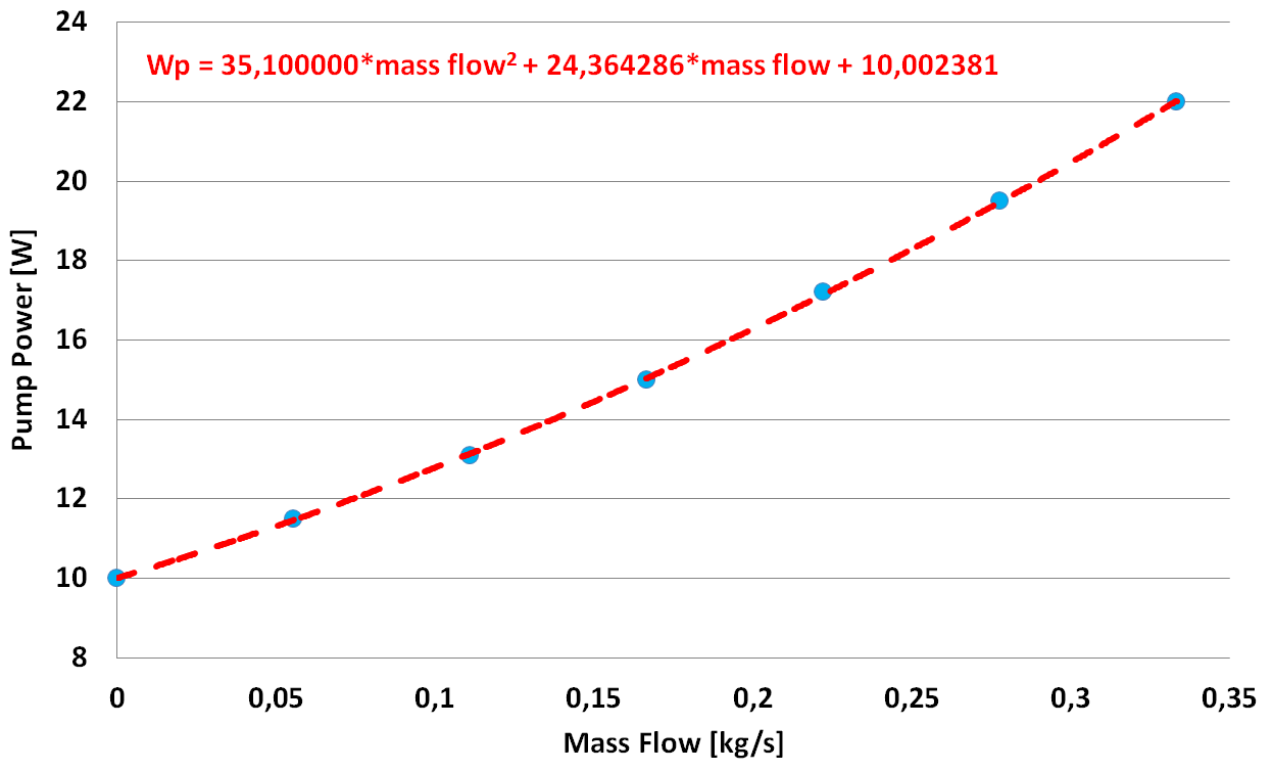


Figure 50: Empirical model of the pump circulator Grundfos Alpha2 L 15-40.

Similarly, the modeling of the circulation pump Grundfos CR 1-9 A-FGJ-A-E-HQQE – 96478872 is made with a second degree polynomial function fitting operation data provided by Grundfos manufacturer [15] (see **Figure 51 - 52**). The hydraulic circulation pumps is set to operate according to the power curve P2.

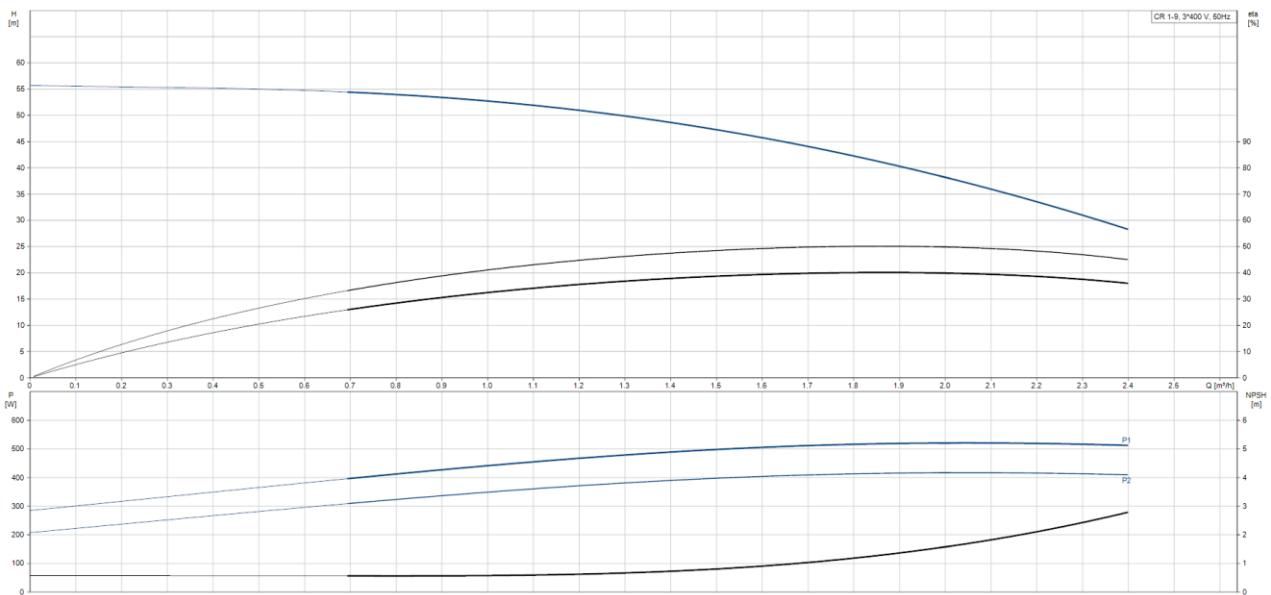


Figure 51: Performance curves of the pump circulator Grundfos CR 1-9 A-FGJ-A-E-HQQE – 96478872.

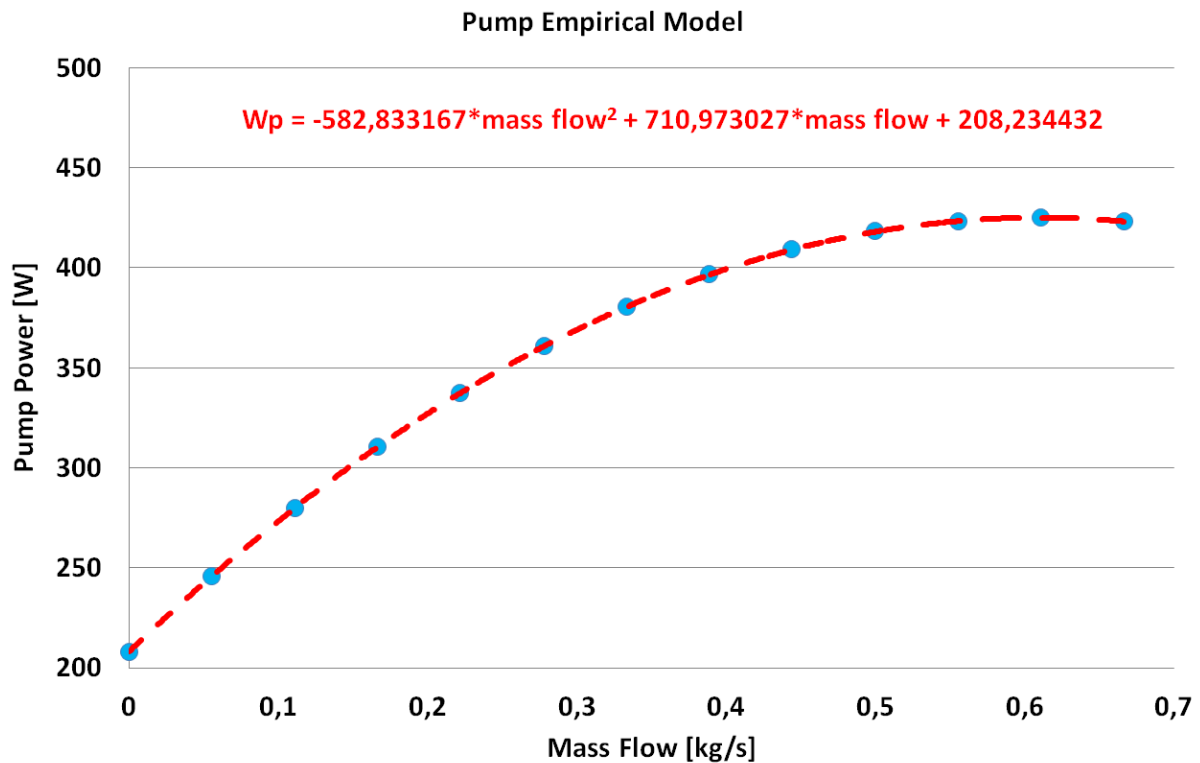


Figure 52: Empirical model of the pump circulator Grundfos CR 1-9 A-FGJ-A-E-HQQE – 96478872.

2.15. Hot Water Storage Tank

The 250 L stratified hot water storage tank has a cylindrical shape: radius of 29 cm and height of 95 cm. There is 5 cm of polyurethane insulation around the water tank (heat losses to the ambient are 1.356 W/K). The water tank model is a simplified version of that presented by Angrisani et al. [66]. Heat losses to the ambient are modelled with a constant heat transfer coefficient between the ambient indoor environment and the internal wall surface of the water tank. The convective and conductive heat transfer between brine circulating in cold and hot helical coil heat exchangers (heat pump condenser) and the water inside the buffer tank are calculated according to the fluid temperature and composition.

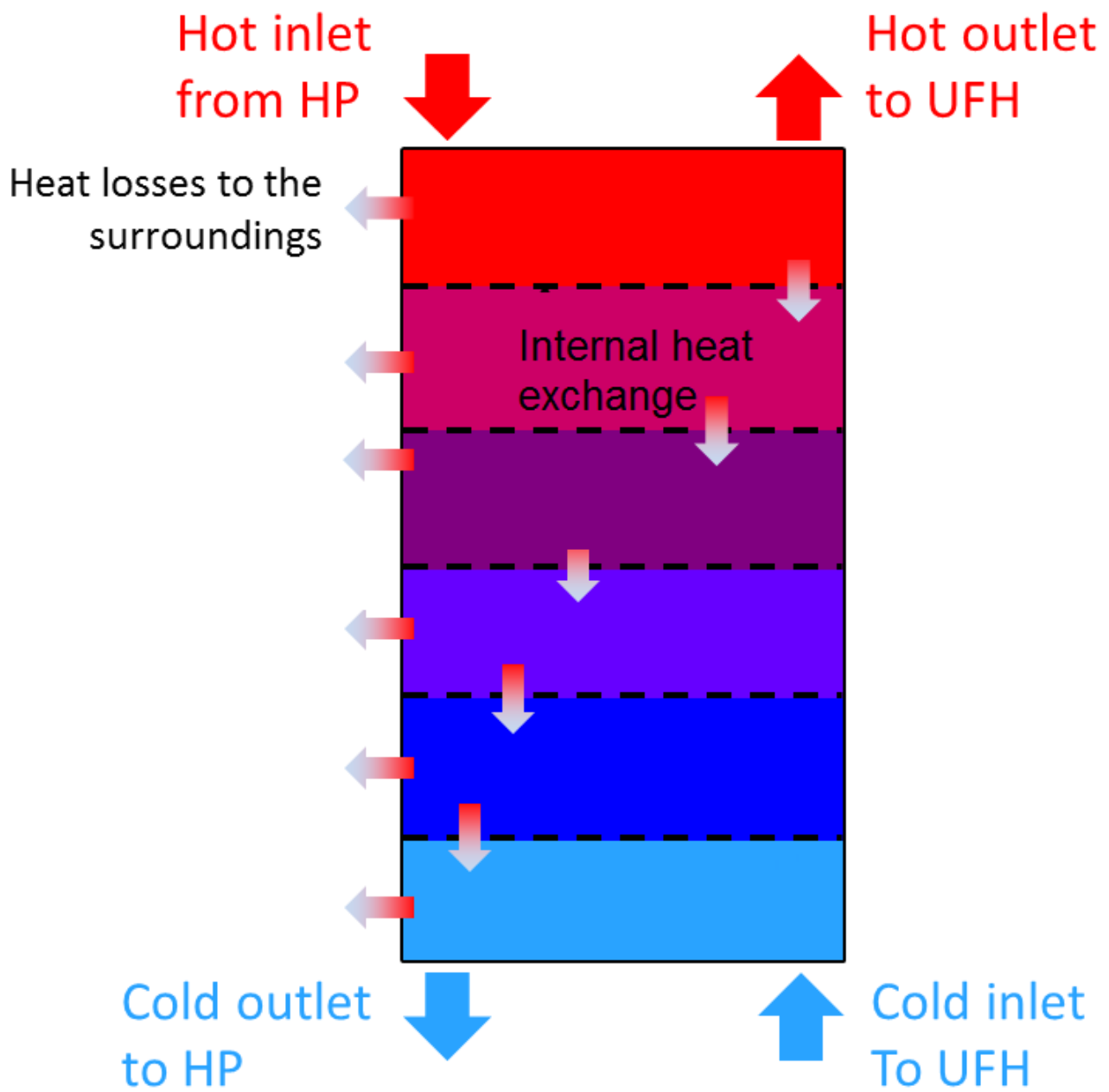


Figure 53: Hot water storage tank model.

2.15. Phase Change Material Wallboard

Many PCM numerical models are using an apparent heat capacity (C_p curve) formulation to take into account the latent heat of the phase transition. This variable C_p as function of temperature can be obtained from experimental tests such as differential scanning calorimetry (DSC) or T-history method. However, the apparent heat capacity modeling does not really represent the physics of the latent heat phase transition but only its apparent behavior. The shape of the C_p curve can change depending on the method used in the measurement. The size of the sample and the speed of temperature change rate are especially very sensitive parameters.

The PCM model of this study is based on an enthalpy formulation which really takes into account the phase transition process at constant temperature. The stable form PCM is considered to be a homogenous material set in thin layers so that the heat transfer can be reduced as a one-dimensional problem. The enthalpy formulation for the latent heat of the phase transition is coupled to a 1D implicit finite volume formulation to calculate the heat transfer between the PCM layers and change of internal energy. The implicit finite volume formulation is more complex to implement but has the great advantage of being unconditionally stable even with a very fine space discretization and large time step.

The density, specific heat capacity (not taking into account the latent heat) and thermal conductivity of each PCM control volume is calculated in function of its temperature based on the temperature-dependent characteristics of the PCM compounds: liquid PCM phase, solid PCM phase and non-PCM surrounding matrix. Therefore the characteristics of each compound, their proportions or the latent heat of the PCM can be changed independently and correctly taken into account in the model.

During the simulation, the PCM model calculates the heat transfers as follow: The thermo-physical properties of each PCM control volume are calculated according to the current local temperature. These properties are used to build the “stiffness matrix” for the implicit finite volume formulation. Solving the heat equation for each control volume gives the heat transfer in between each PCM layer. It is therefore possible to know what is the change of internal energy or enthalpy of each control volume.

For each PCM control volume, an enthalpy / temperature curve is built (see **Figure 54**). This function is inverted in order to find the new temperature at the next time step from the change of enthalpy and taking into account the phase transition at constant temperature. If the new temperature does not reach transition temperature, then the calculation is the same as a normal implicit FVM calculation.

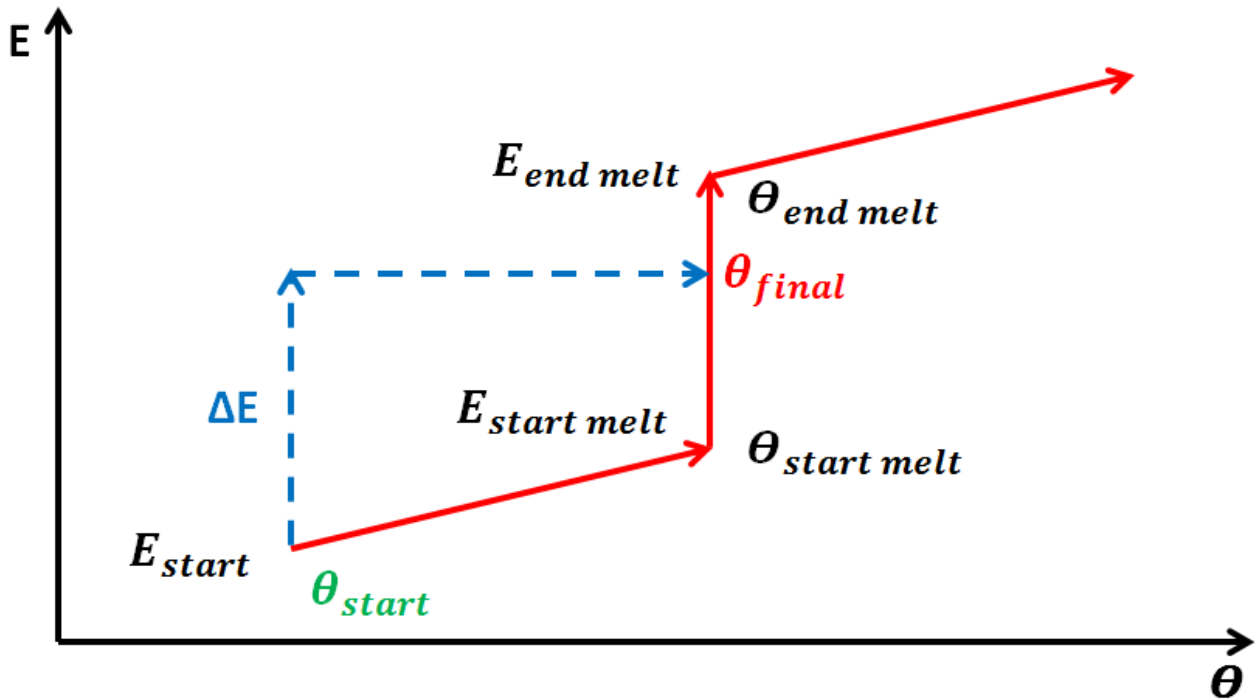


Figure 54: Enthalpy / temperature function.

The new temperature is then used in the next time step to re-calculate the thermo-physical material properties and the heat transfers [67] [68].

It is assumed that the PCM is pure and has only one specific melting temperature and one specific solidification temperature. These temperatures can be different to take into account hysteresis phenomena (see Figure 55). However, it not possible to simulate a PCM made of a mix of compounds which have different transition temperatures.

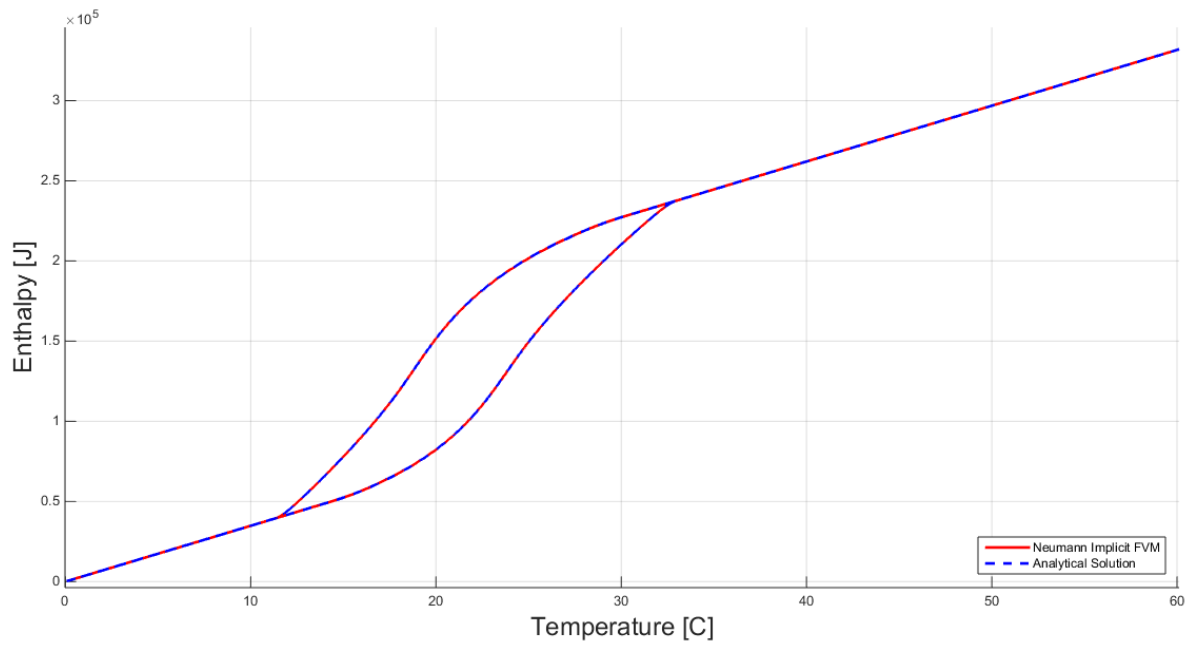


Figure 55: Heating / cooling PCM model test with hysteresis.

The PCM wallboard elements of the study are discretized in control volumes which are 1 mm thick.

2.15. Furniture / Indoor Content

The additional indoor thermal mass / furniture is modeled as an equivalent fictitious planar element which aggregates all indoor items into an homogenous representative material. The representative thermo-physical properties of this equivalent planar element are chosen according to a previous study about the indoor content of dwellings in Denmark [29] (see **Table 8**). The 60 kg/m² of additional indoor content are gathered in an equivalent slab which is 4.7 cm thick. The surface area of one side of the element is equal to 1.8 times the surface area of the floor in the thermal zone. The equivalent planar element does not have any real geometrical representation or position in the room. It is therefore assumed that 50% of the radiative share of the equipment, people, solar and radiator heating loads are distributed on its surfaces. The element is coupled to the rest of the thermal zone in the same way as if it was an internal wall only connected to the air node. The mixed convection/radiation surface thermal resistance coefficient t is constant and equal to 0.13 m².K/W.

	Equivalent planar element
Thickness [mm]	47
Density [kg/m³]	715
Thermal conductivity [W/m.K]	0,3
Specific heat capacity [J/kg.K]	1400
Space discretization [nodes]	20

Table 8: *Equivalent indoor thermal mass / furniture properties.*

In the case of PCM integrated on furniture elements, the two models for indoor thermal mass / furniture and for PCM are combined together. A 1.5 cm thick layer of stable form PCM is added on the upper part of the equivalent planar element.

3. Validation of the Building Model

This section presents different validation tests performed to demonstrate the usefulness of the models presented before.

3.1. Validation of the Construction Element with BSim Software

The first step for validating a building model is to make sure that the basic construction element blocks are calculating the heat transfer properly. One can see on **Figure 56**, the validation test in steady state of a MATLAB Simulink block modeling an external wall for the building model of the study. The 5 temperatures of the 5 thermal nodes fit perfectly with the analytical solution. Average absolute error of the model is 0.0015 °C.

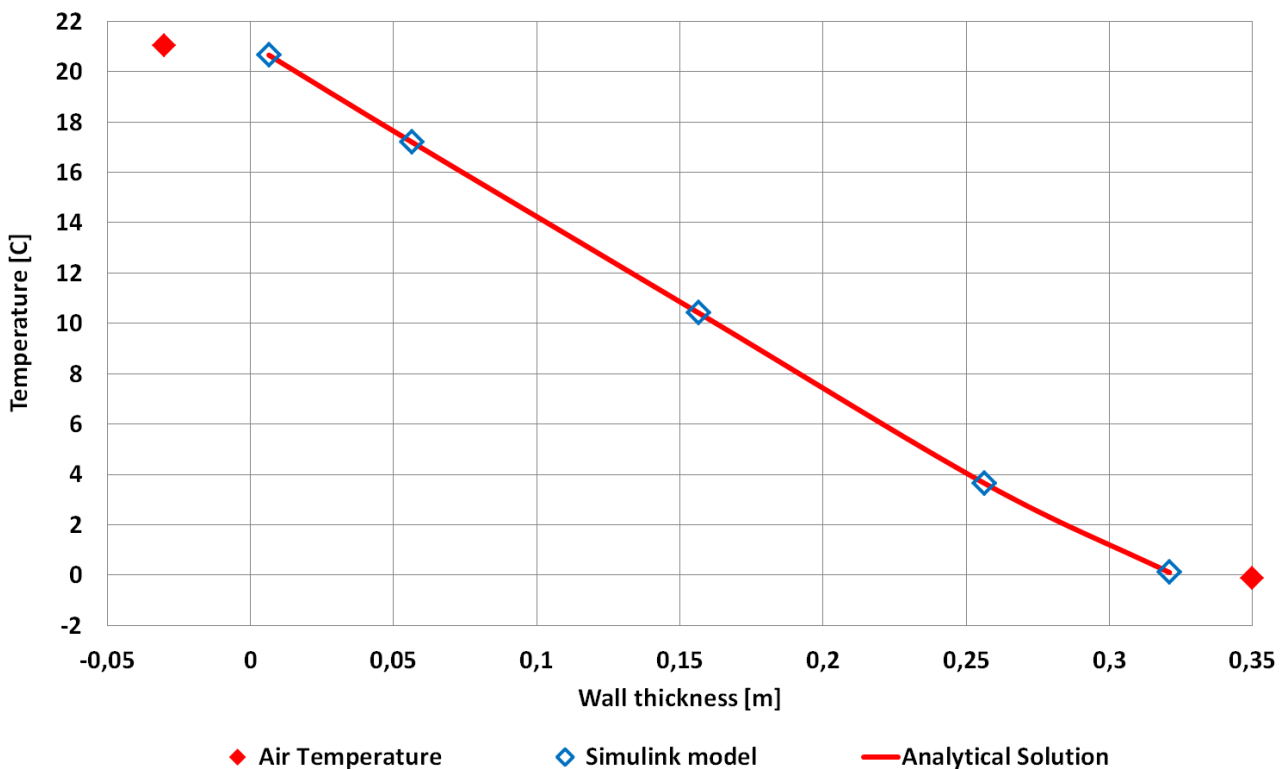


Figure 56: Steady state temperature profile of external test wall.

The construction element block for wall elements is then tested with dynamic boundary conditions (weather data DRY 2013) including varying outdoor temperature, solar radiation, wind, long-wave radiations to the sky and constant indoor air temperature and internal radiation loads. The temperatures of the different thermal nodes in de MATLAB – Simulink model are compared with the temperature of a BSim reference model. BSim software is a well-known and validated building energy software. One can see on

Figure 57 – 59, that the temperatures of the MATLAB –Simulink model fit very well the ones of the BSim reference model for dynamic boundary conditions.

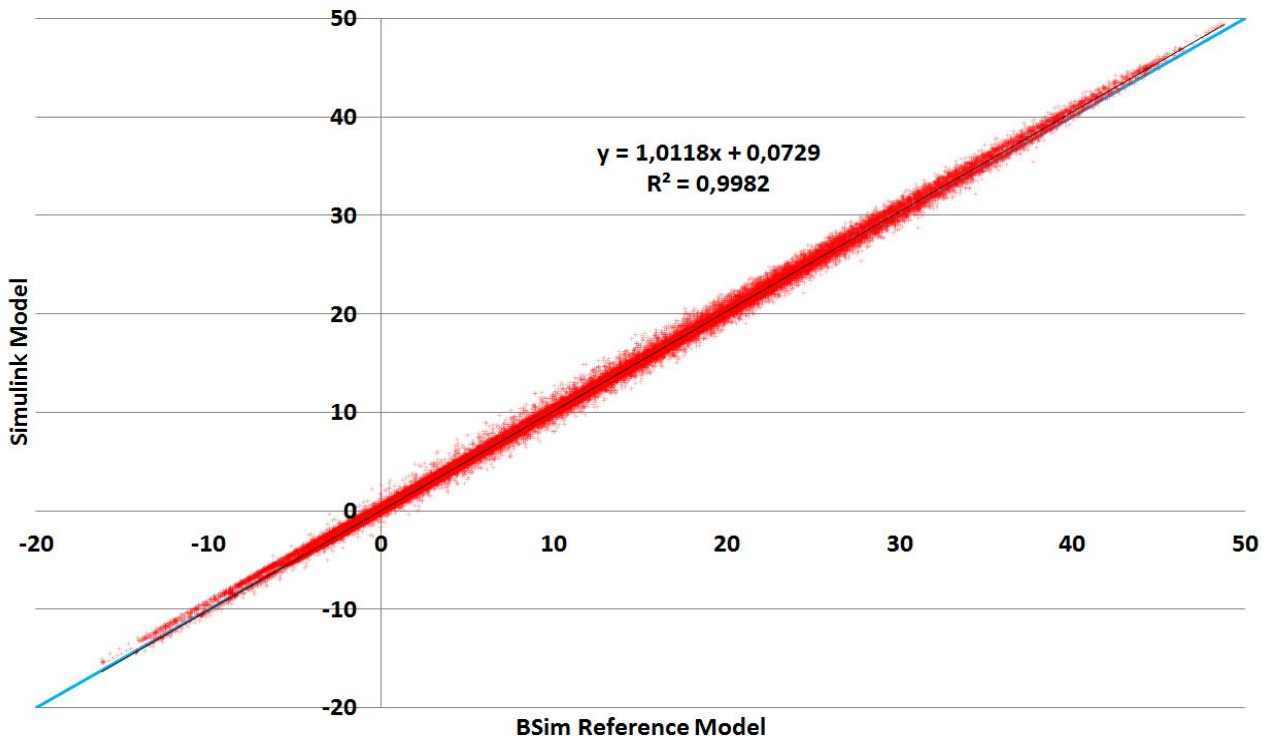


Figure 57: Wall external surface temperature BSim reference model vs MATLAB-Simulink model.

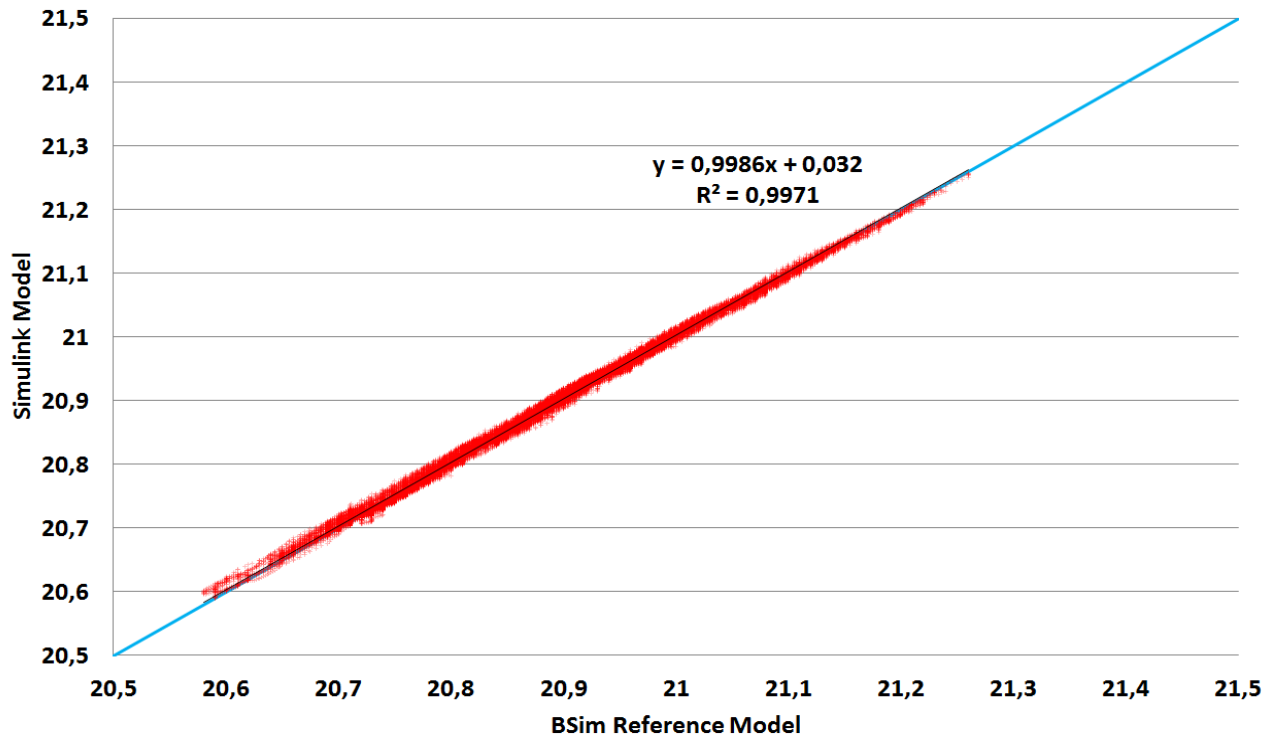


Figure 58: Wall internal surface temperature BSim reference model vs MATLAB-Simulink model.

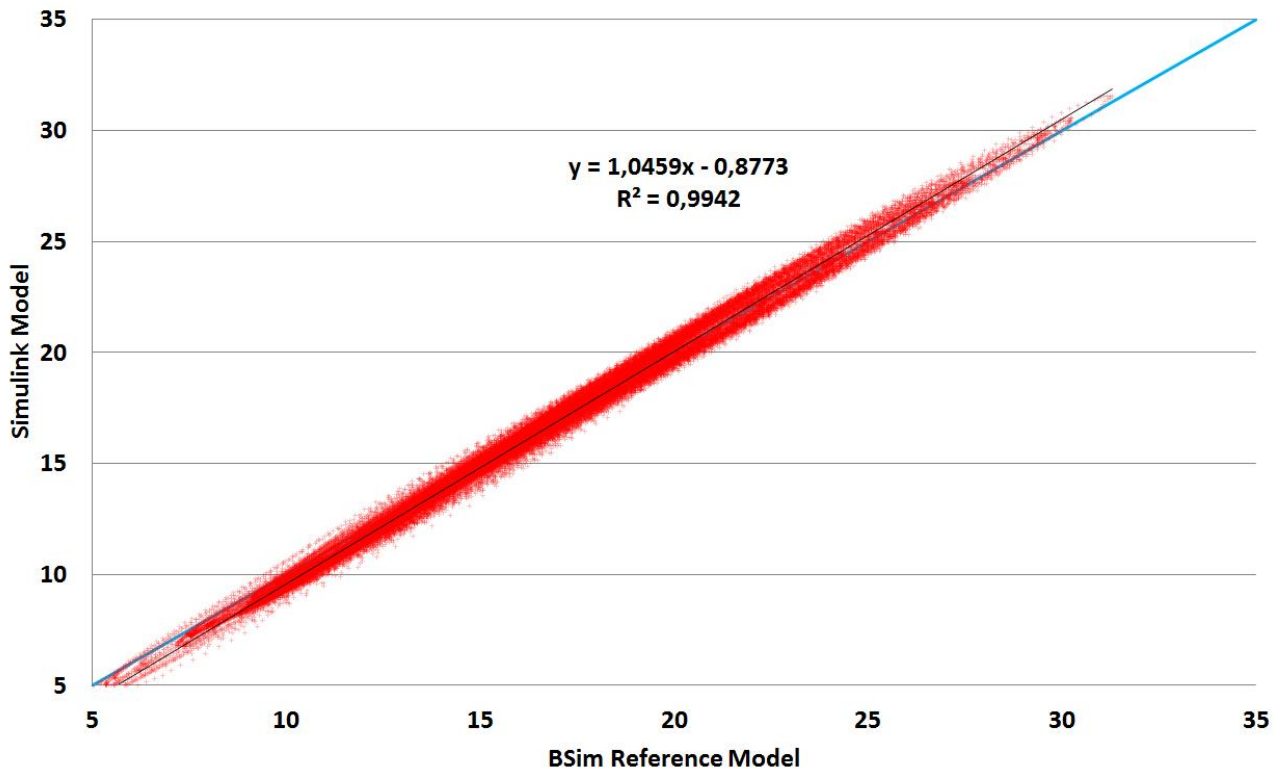


Figure 59: Wall insulation layer temperature BSim reference model vs MATLAB-Simulink model.

The average absolute temperature difference between the MATLAB-Simulink model and the BSim reference model is 0.3 °C.

3.2.Validation of the Multi-Zone Model with BSim Software

The full multi-zone MATLAB-Simulink building model is then tested against the BSim reference model of the same building for the same weather data and building parameters. The building type tested here is a well-insulated house (Passive House) with medium structural thermal mass and radiator heating system.

One can see on **Figure 60 – 62** that the building temperatures and heating power needs of the MATLAB-Simulink model fit very well with the ones of the BSim reference model. The average absolute building temperature difference between the MATLAB-Simulink model and the BSim reference model is 0.12 °C. The average absolute building heating power need difference between the MATLAB-Simulink model and the BSim reference model is 82 W (0.54 W/m²) which represents 3% of the maximum heating power need of the house. The difference in cumulative energy consumption over 2000 hours of heating period is 10.42 kWh, which represents a relative difference of 0.88%.

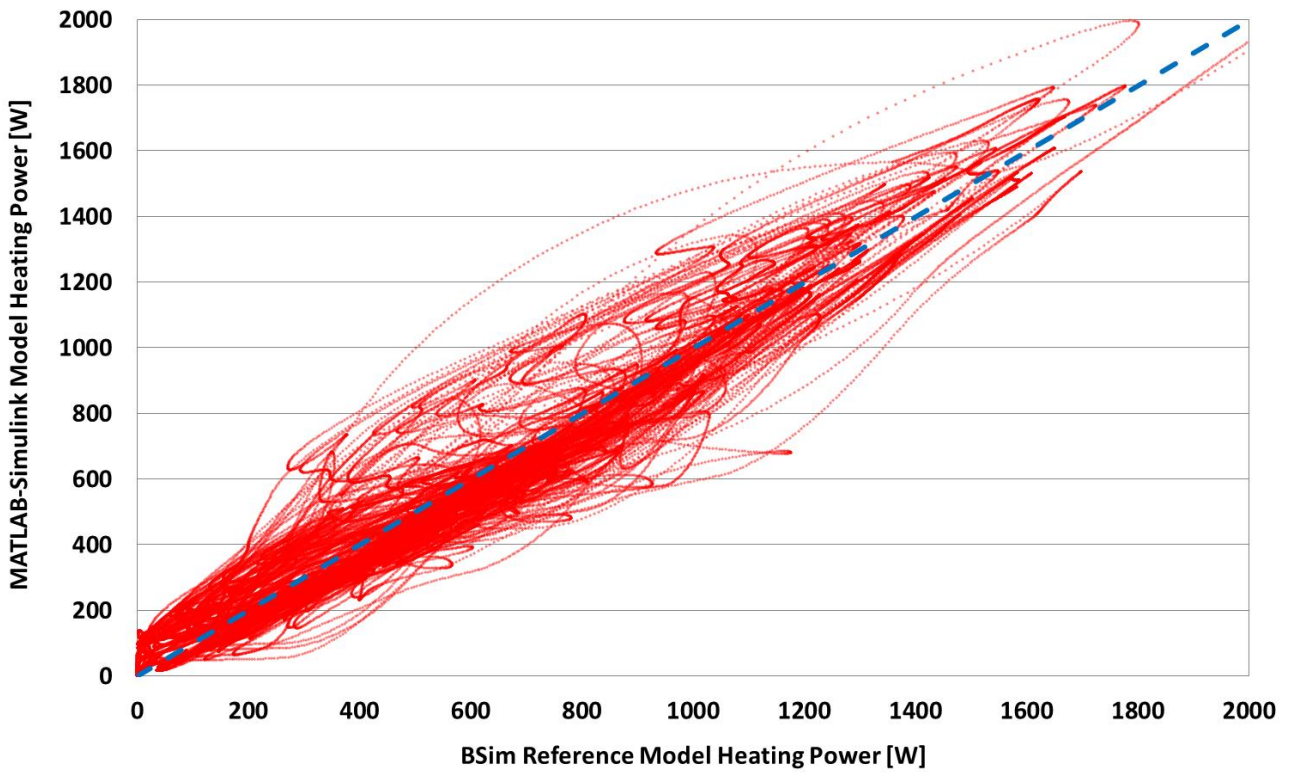


Figure 60: Multi-zone heating power need BSim reference model vs MATLAB-Simulink model.

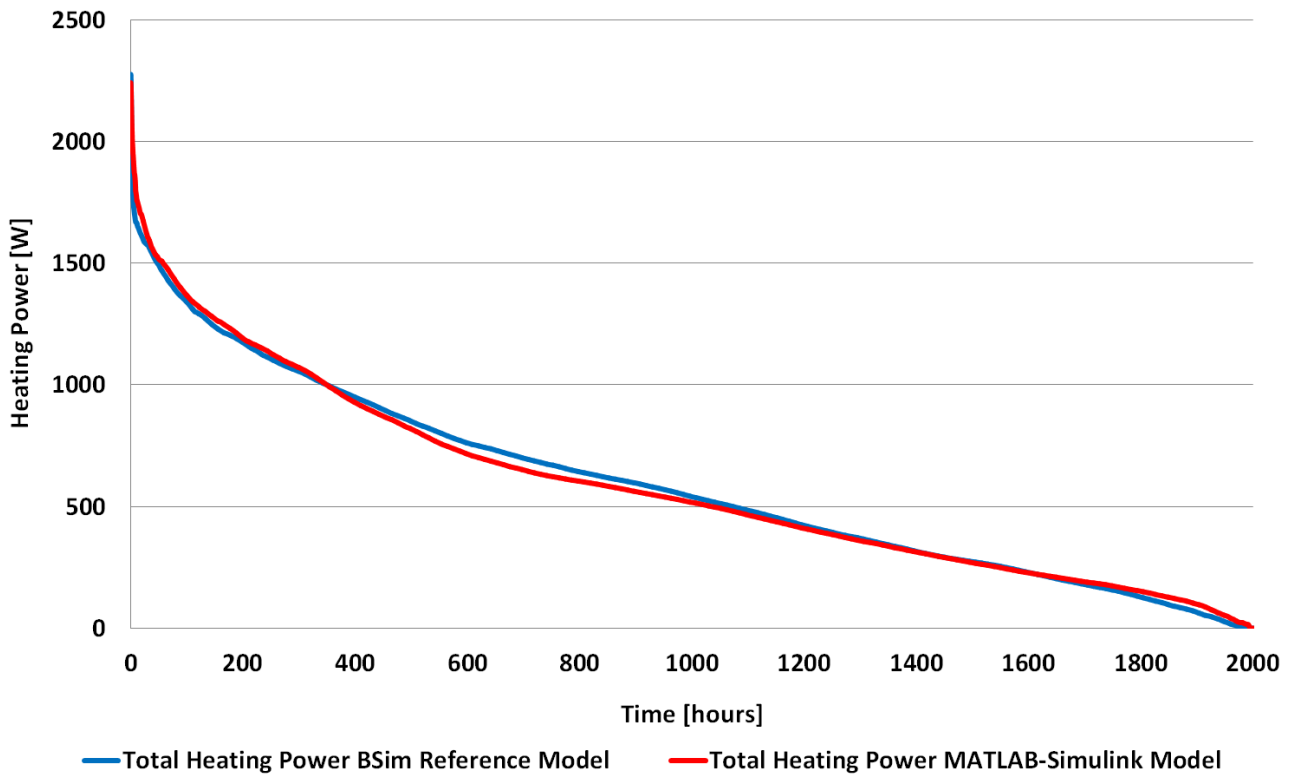


Figure 61: Ordered heating power need of the multi-zone building models.

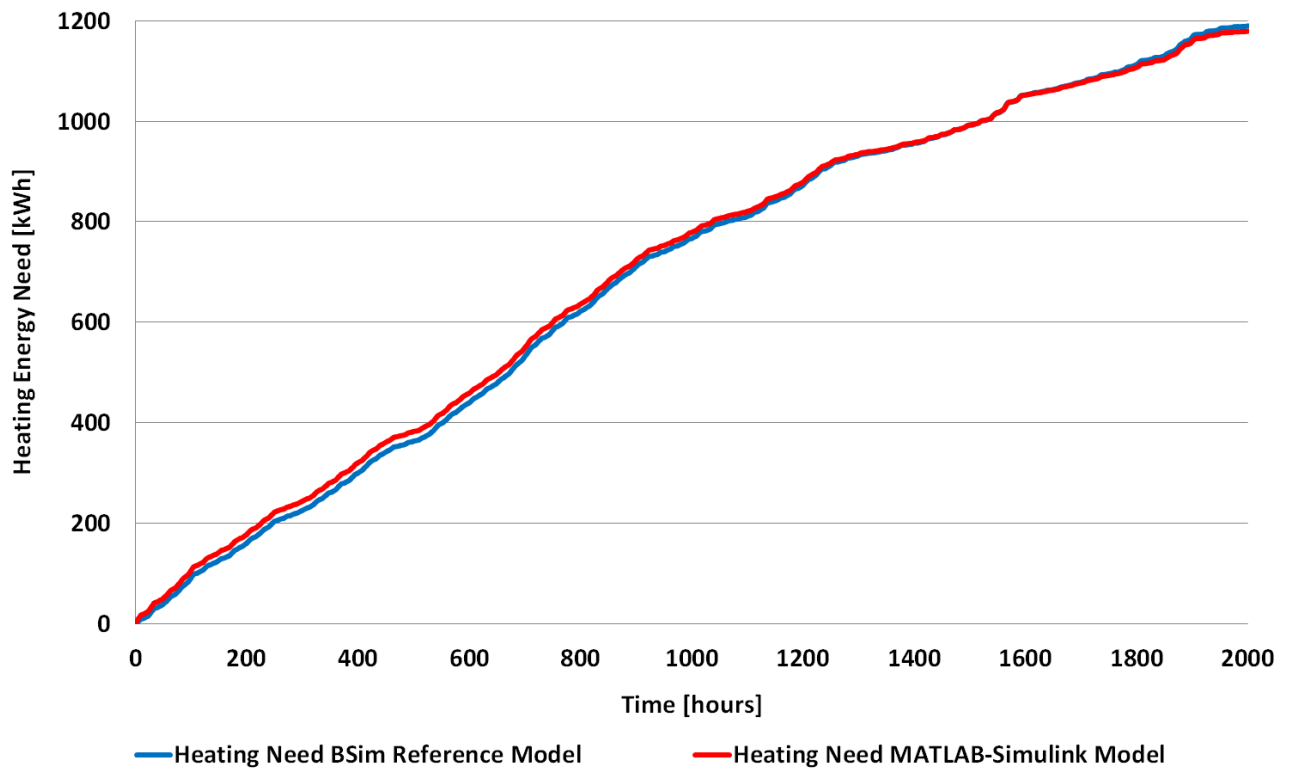


Figure 62: Cumulative heating need of the multi-zone building models.

3.3. Validation of the Building Model with BESTEST

In addition to the previously presented validation tests for the building numerical model used in this study, the BESTEST validation method is used to certify its correctness and consistency. The BESTEST procedure is a comparison method used to evaluate building simulation models. It is based on benchmark test cases generated by the IEA-EBC Annex 43: IEA Building Energy Simulation Test (BESTEST) [69]. The BESTEST method is described in details in ASHRAE standard [70].

6 different BESTEST cases are tested with the MATLAB-Simulink building model and presented hereafter. The basis of the different test cases is a rectangular room (see **Figure 63**).

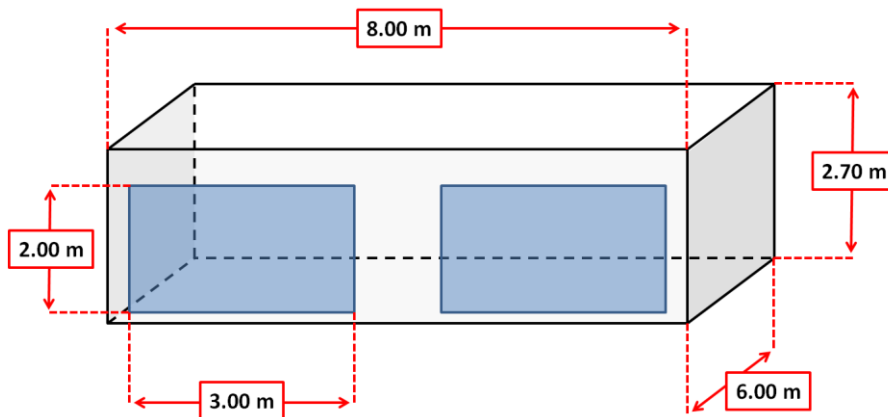


Figure 63: BESTEST test cell.

The envelope characteristics, orientation of windows and temperature set points vary between the different test cases. The main characteristics of the test cell are given in **Table 9** for the base test-case C600.

Test cell dimensions	8 x 6 x 2.7 m
Walls U-value	0.514 W/m².K
Roof U-value	0.318 W/m².K
Floor U-value	0.039 W/m².K
Windows dimensions	2 x 6 m² (south oriented)
Windows U-value	3 W/m².K
Windows solar factor	0.78
Infiltration rate	0.5 vol/h
Internal gains	200 W (60% radiative, 40% convective)
Heating / cooling system	Perfect unlimited system (100% convective)

Table 9: Test cell description – C600.

In addition to the base case C600, the case C620 (C600 with on window East oriented and one window West oriented), the case C640 (C600 with night set back to 10 °C between 23:00 and 7:00), the case C900 (C600 with heavy walls and outdoor insulation), the case C920 (C620 with heavy walls and outdoor insulation) and the case C940 (C640 with heavy walls and outdoor insulation) are also tested. These BESTEST cases are chosen to focus especially on the correctness of the calculation for solar internal gains and the proper behavior of a building with indoor temperature set point modulation and variation of envelope thermal mass.

The output results of the different test cases are presented hereafter on **Figures 64 – 72**. The MATLAB – Simulink numerical model is compared with the results of other commercial software: ESP, BLAST 3.0, DOE – 2.1 D 14, SERIRES / SUNCODE 5.7, SERIRES 1.2, S3PAS, TRNSYS 13.1 and TASE.

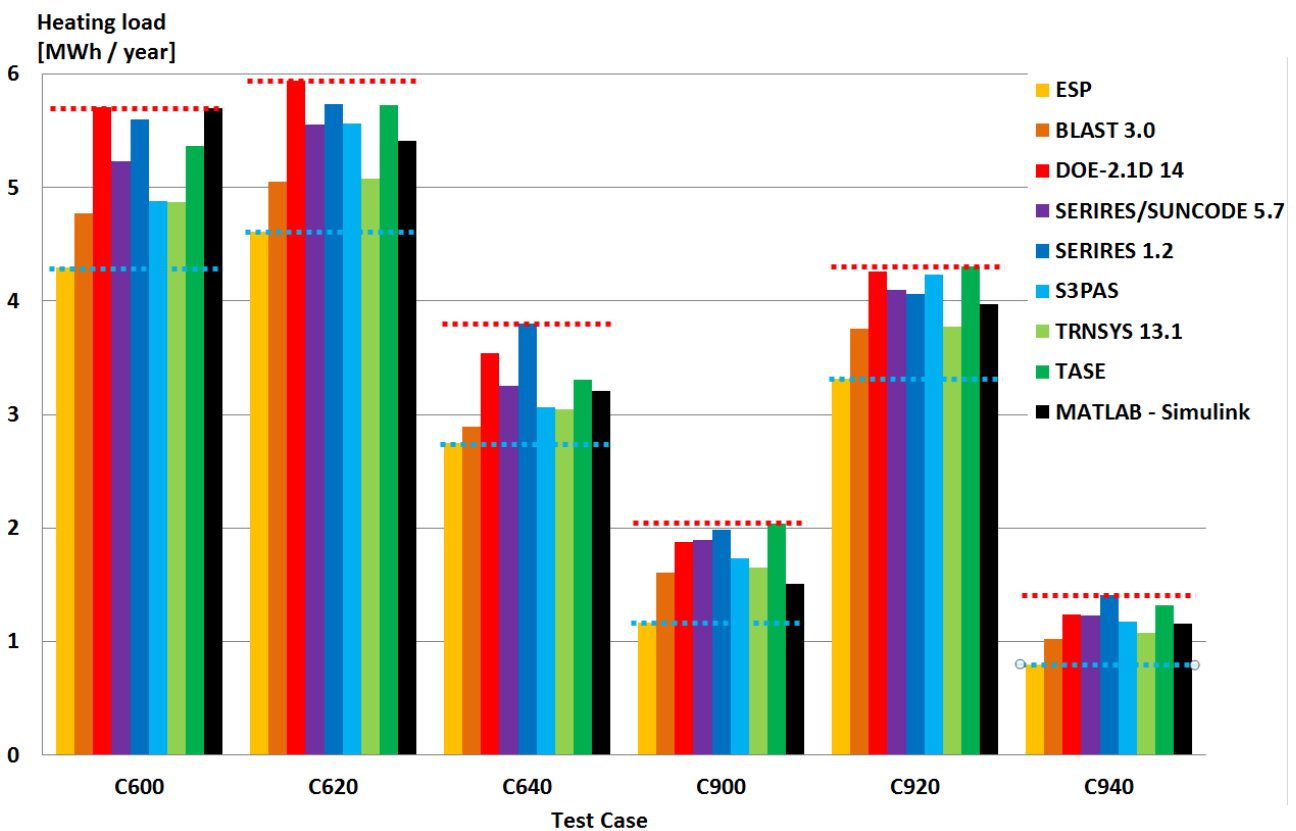


Figure 64: BESTEST heating needs comparison.

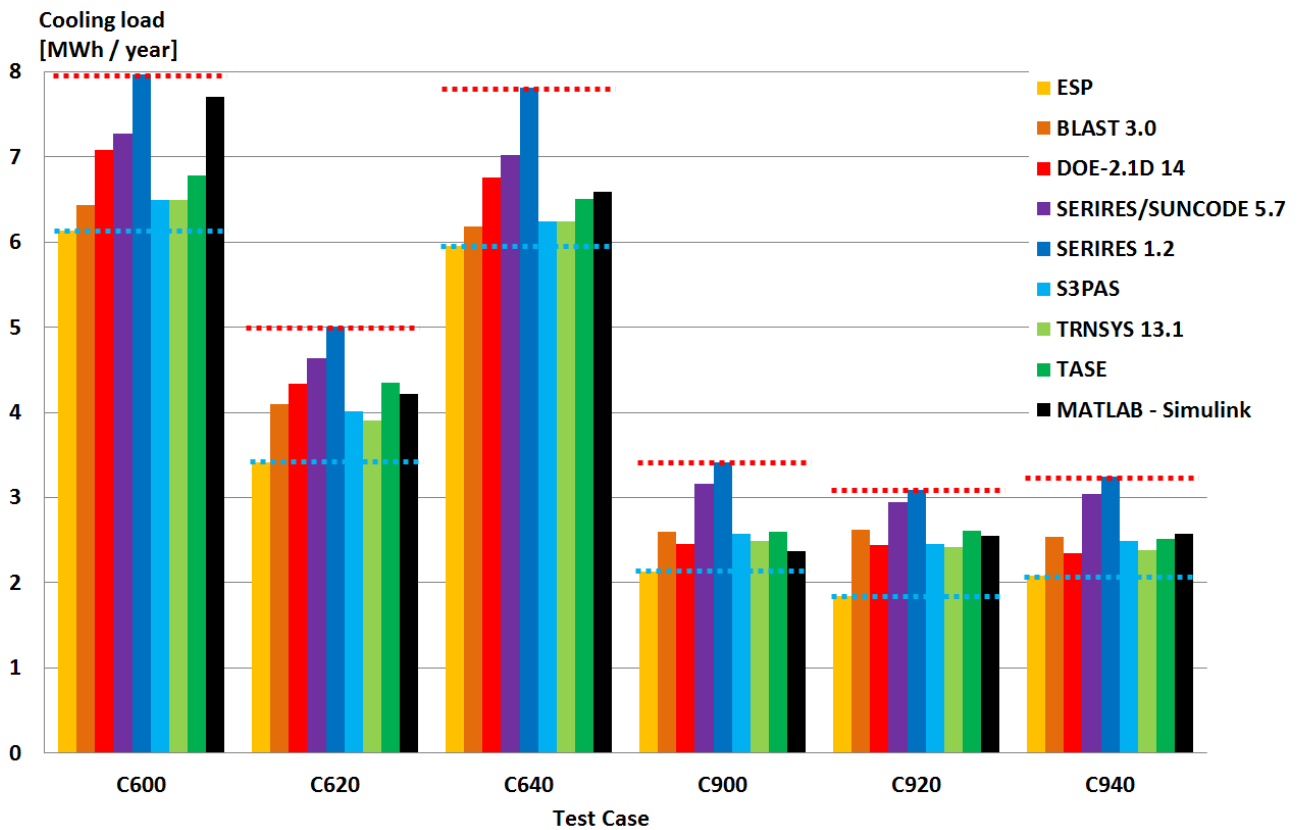


Figure 65: BESTEST cooling needs comparison.

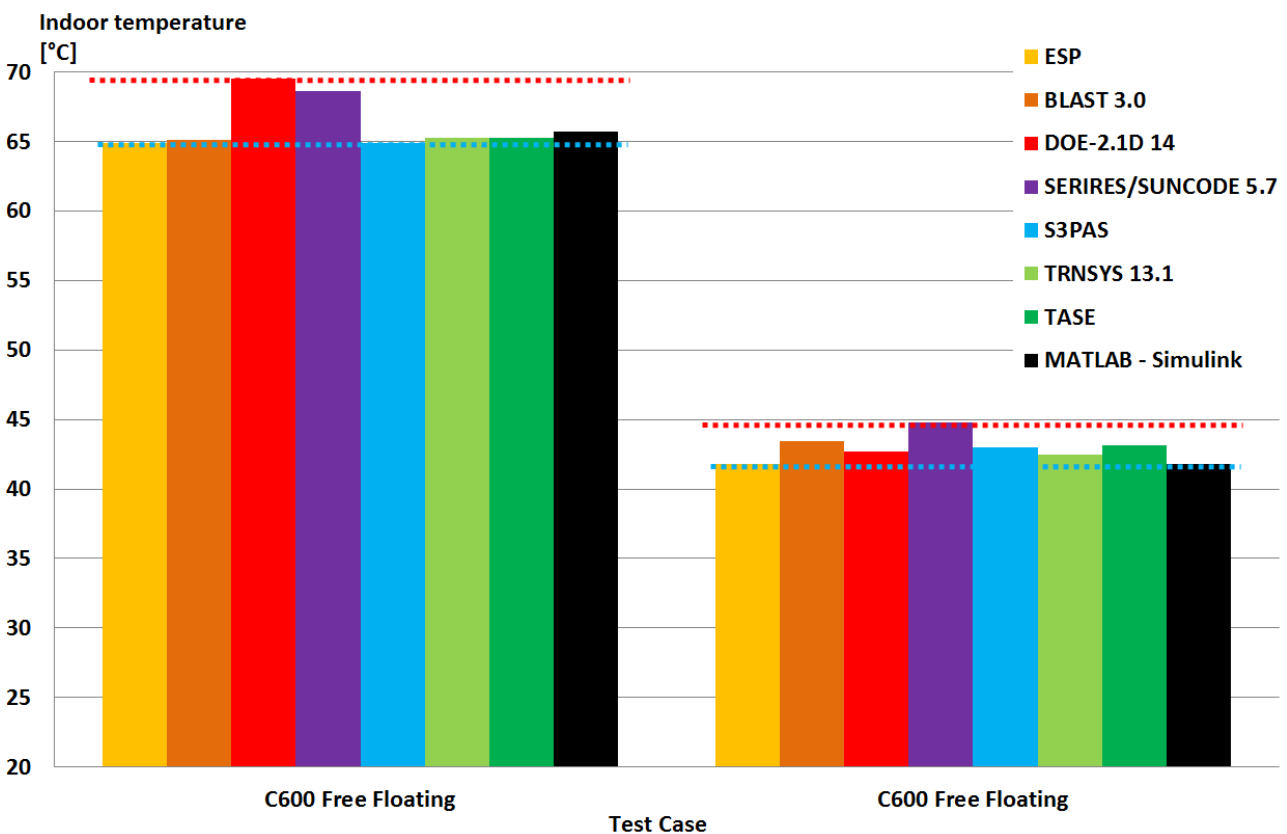


Figure 66: BESTEST maximum indoor temperature comparison.

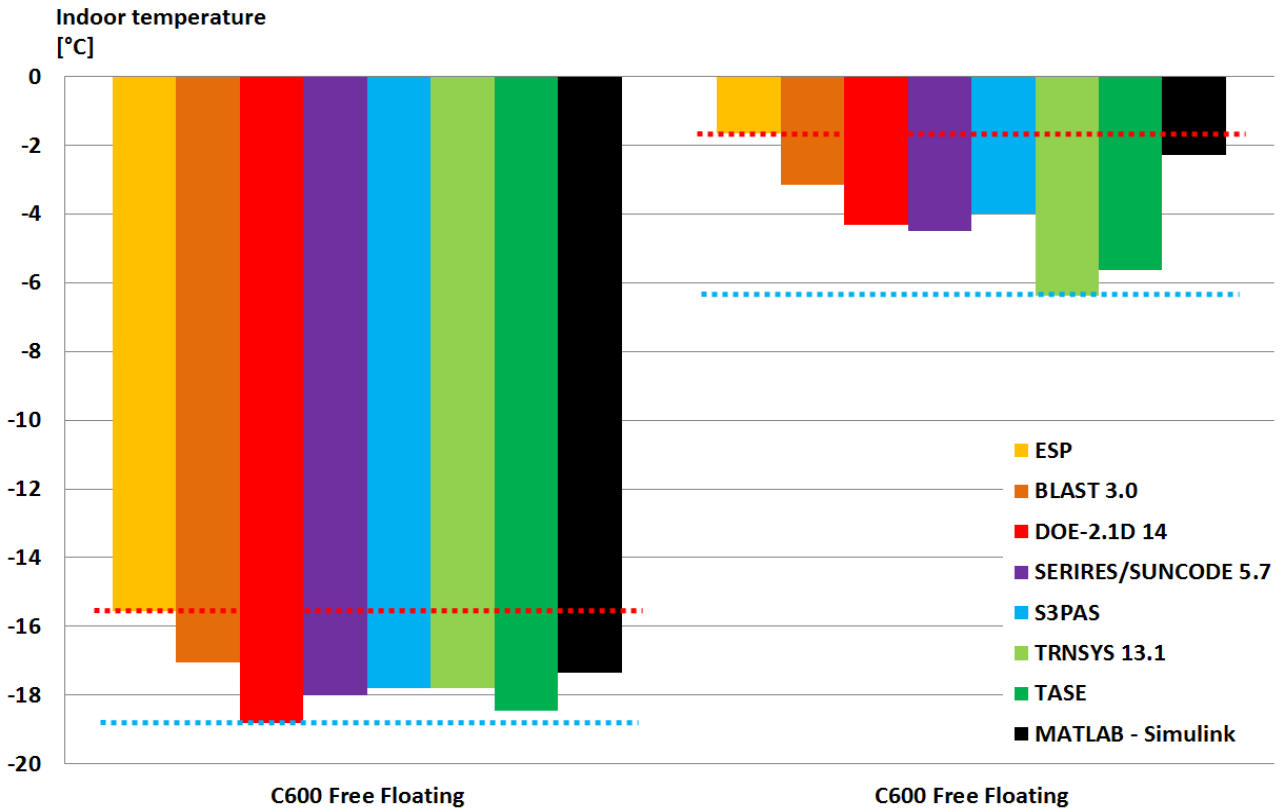


Figure 67: BESTEST minimum indoor temperature comparison.

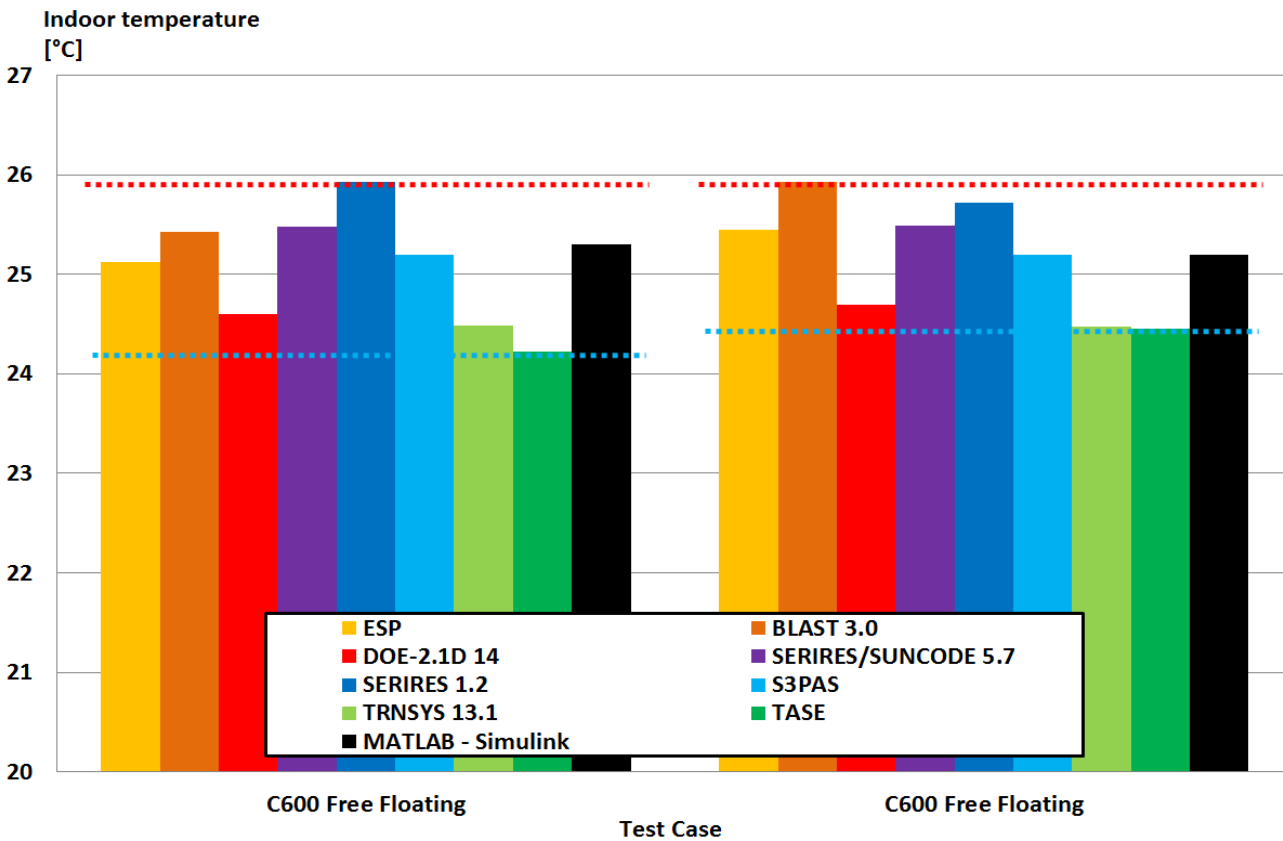


Figure 68: BESTEST average indoor temperature comparison.

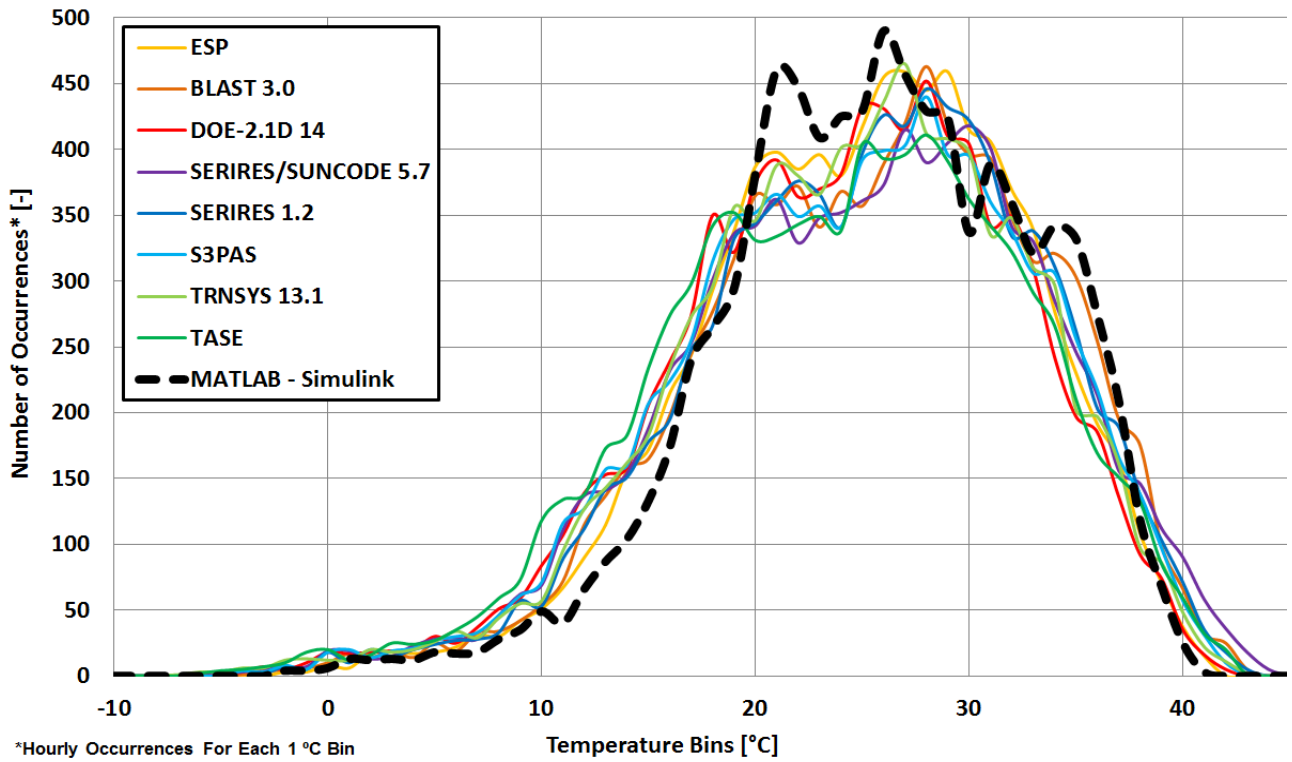


Figure 69: BESTEST C900 Free Floating annual hourly temperature frequency comparison.

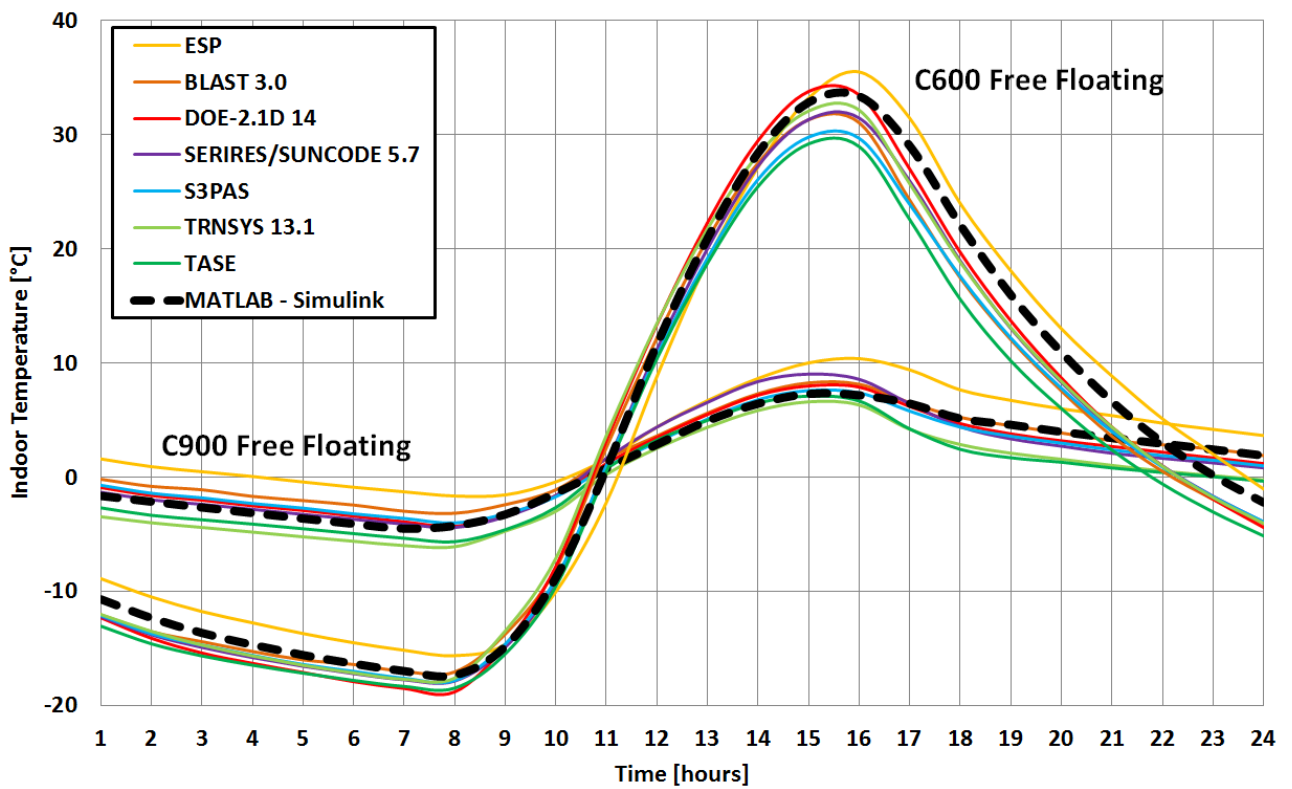


Figure 70: BESTEST free floating temperature profiles of a clear cold day.

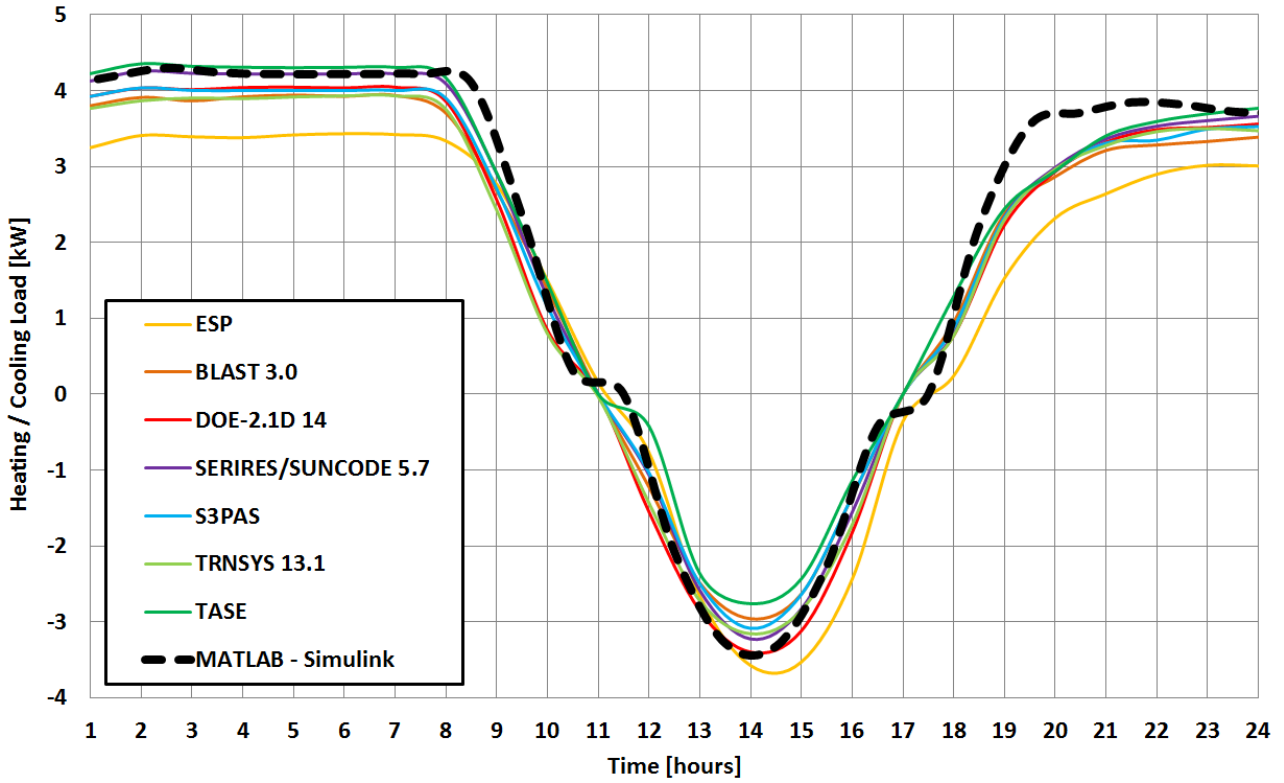


Figure 71: BESTEST C600 heating / cooling needs during a clear cold day.

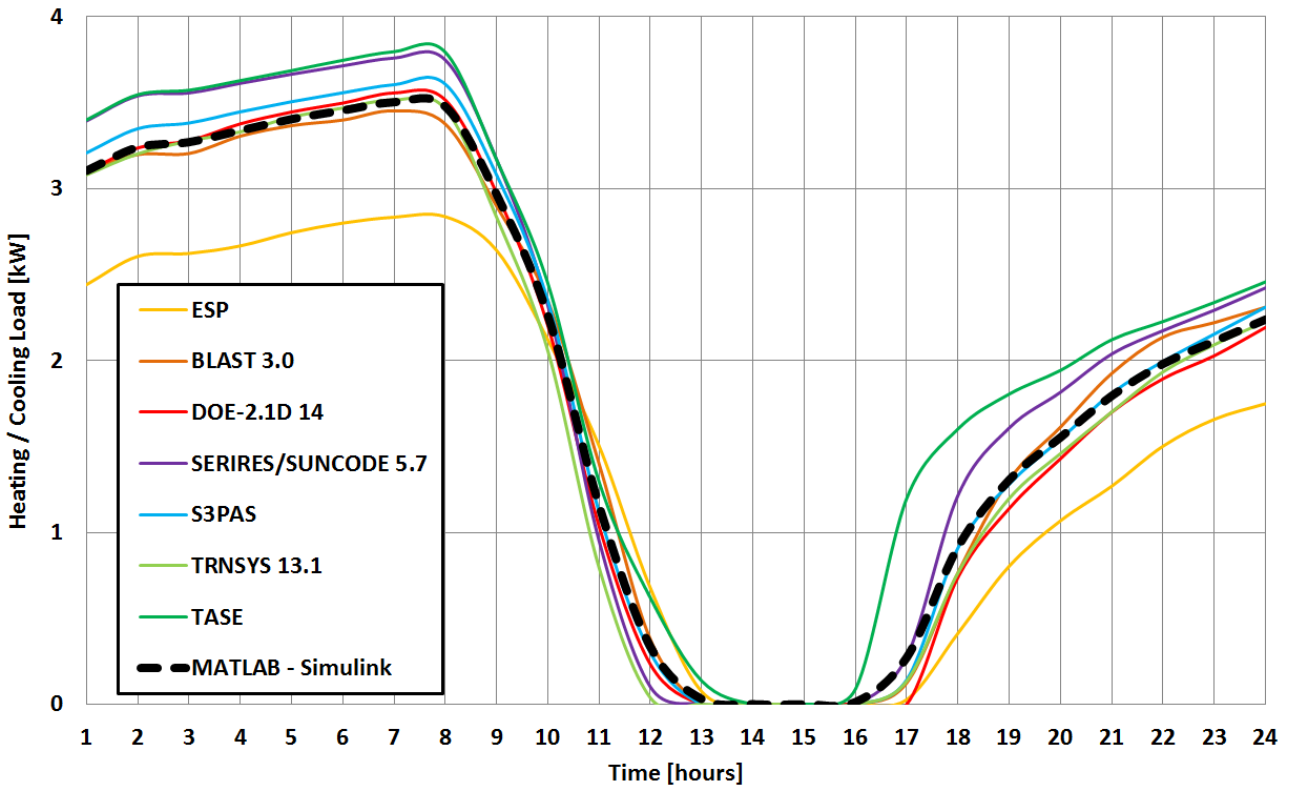


Figure 72: BESTEST C900 heating / cooling needs during a clear cold day.

One can see on the previous figures that the MATLAB - Simulink model gives output results which are always within the results of the other software for the different test cases. It can therefore be considered that the MATLAB – Simulink building model is validated and can be used for numerical studies.

3.4. Validation of Under Floor Heating System and Horizontal Ground Source Heat Exchanger with BSim Software

The hydronic under floor heating system and the horizontal ground source heat exchanger are modeled in the same way. In the case of the floor heating system, the bottom surface is in contact with the underground temperature of the building and the upper surface is exposed to the indoor environment of the building. In the case of horizontal ground source heat exchanger, the bottom surface is in contact with the deep ground temperature and the upper part is exposed to the outdoor conditions. Apart from the number of layers, the thermal properties of the layers and the size of the pipes, the heat exchanger model itself is the same.

The MATLAB-Simulink hydronic heat exchanger model is firstly tested in steady state conditions against the BSim reference model. One can see on **Figure 73** that the temperature profile of the MATLAB-Simulink heat exchanger’s slab fits very well with the one of the BSim reference model. The average absolute temperature difference between the two models is 0.07 °C.

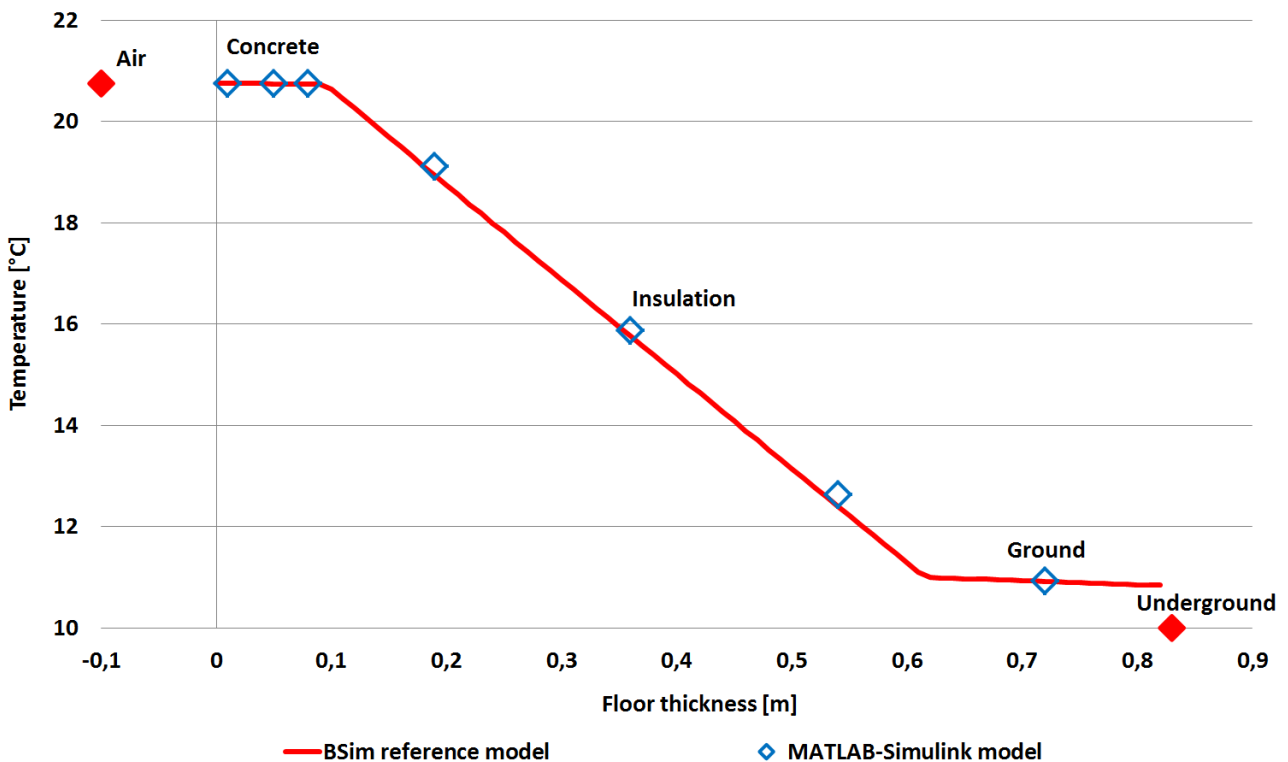


Figure 73: Steady state temperature profile of a floor heat exchanger.

The MATLAB-Simulink heat exchanger model is then tested in heating and cooling mode as a floor heating heat exchanger in a test room with dynamic boundary conditions. The temperatures of the different thermal nodes and the heat transfer from the fluid to the slab in de MATLAB – Simulink model are compared with ones of the BSim reference model. One can see on **Figure 74 – 76**, that the temperatures and heat transfer of the MATLAB –Simulink model fit very well the ones of the BSim reference model for dynamic boundary conditions.

The average absolute difference in heat transfer between the MATLAB – Simulink model and the BSim reference model is 3.2 W. The average absolute temperature difference in air temperature and pipe level temperature between the two models is 0.07 and 0.1 °C respectively.

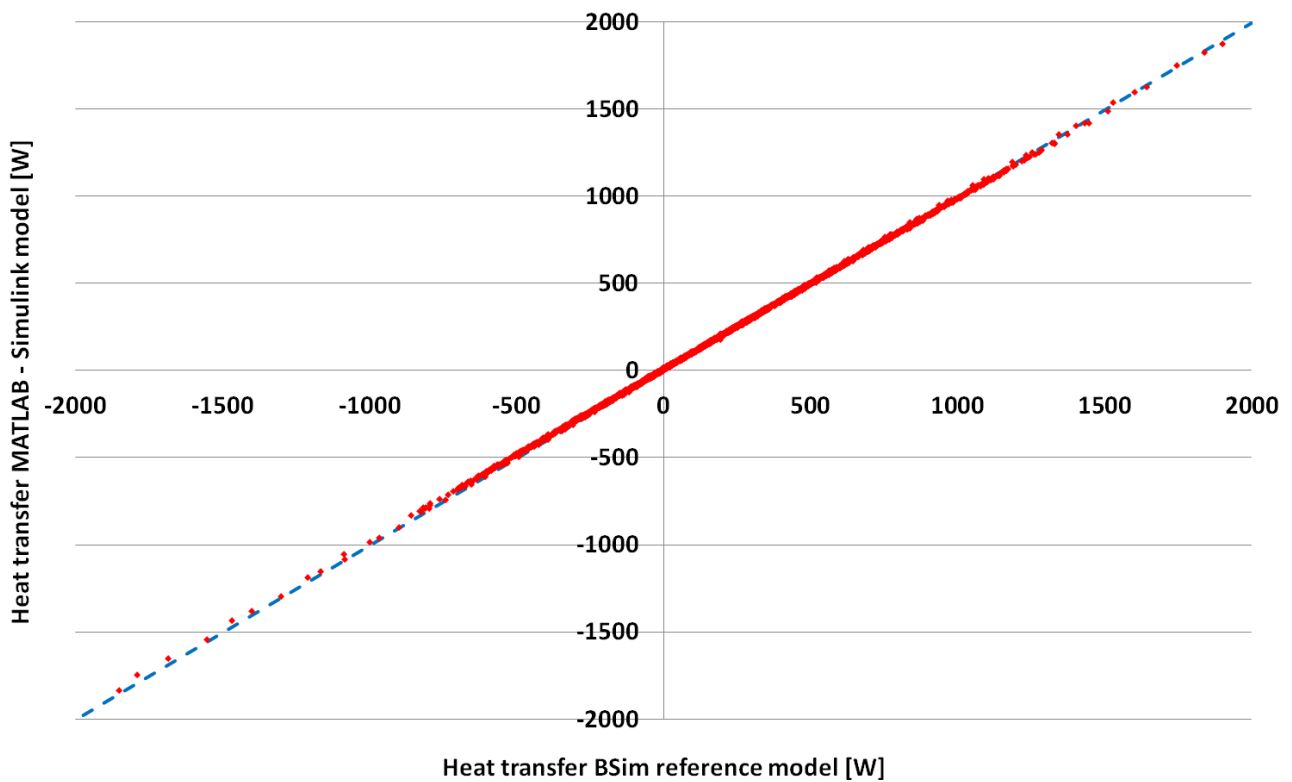


Figure 74: Floor heat exchanger heat transfer BSim reference model vs MATLAB-Simulink model.

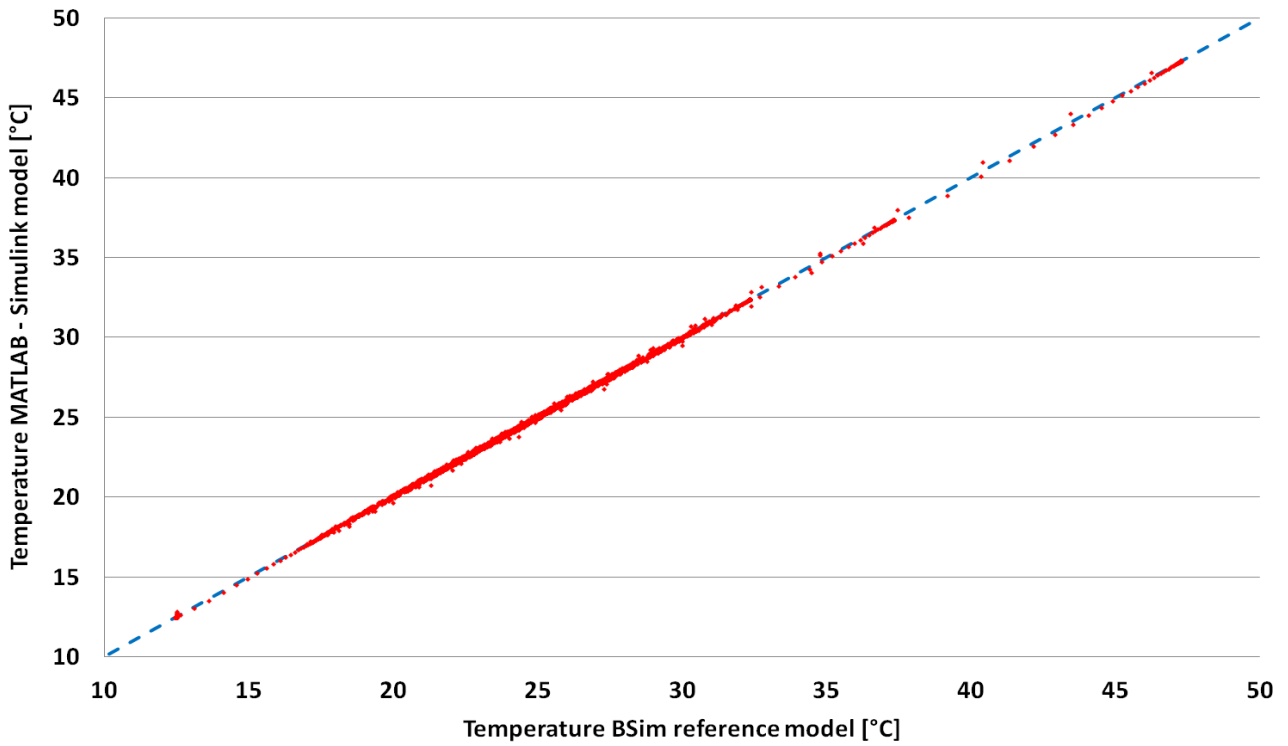


Figure 75: Operative temperature in test room with floor heat exchanger BSim reference model vs MATLAB-Simulink model.

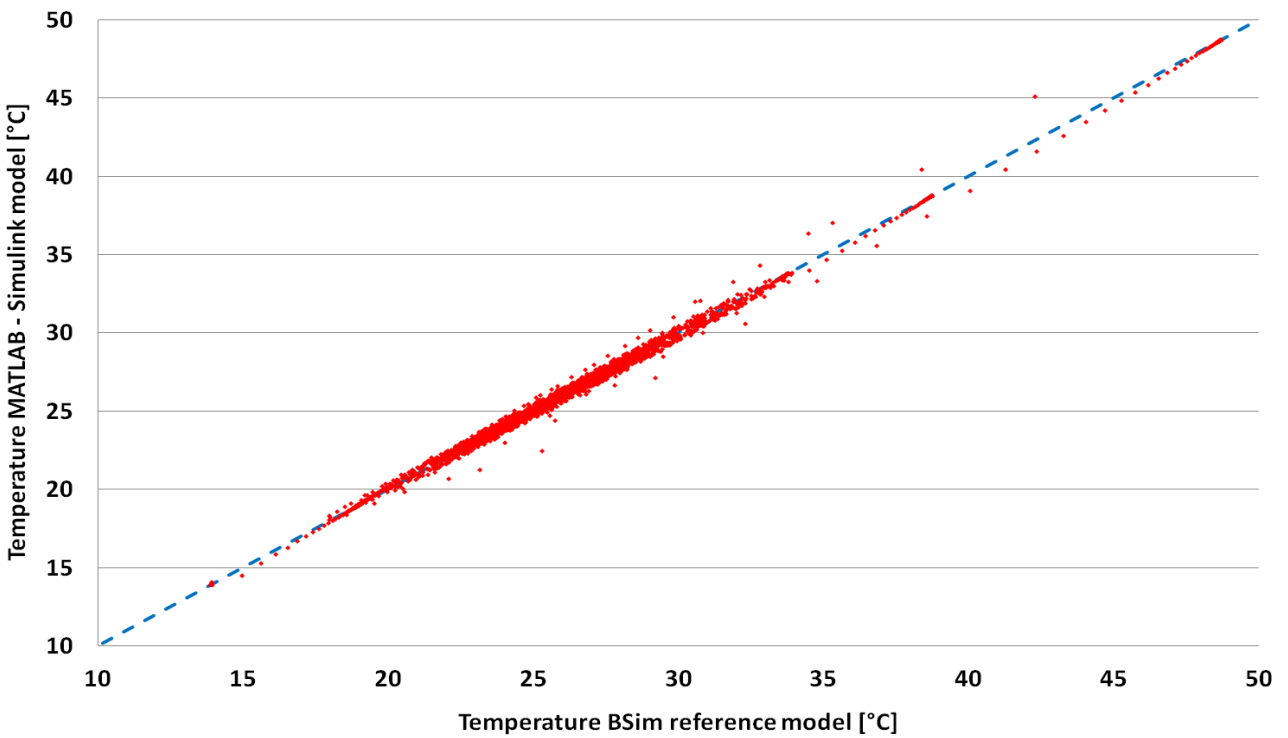


Figure 76: Pipe level temperature in test room with floor heat exchanger BSim reference model vs MATLAB-Simulink model.

3.5. Validation of Vertical Borehole Ground Source Heat Exchanger with Experimental Data

The vertical borehole ground source heat exchanger model is validated with the experimental data of 5 different thermal response tests performed on real borehole heat exchangers in Denmark [71][72][73]. Different geometries, length and types of brine are tested (See **Table 10**). The input data are inlet flow and inlet temperature. The outlet temperature is compared between the experiment and the MATLAB-Simulink model.

	Blaavand	Glud	Ordruggaard	VIA 12	VIA 14
Borehole depth [m]	102	100	102	103	100
Borehole diameter [m]	0,22	0,16	0,2	0,16	1,6
Pipe external diameter [m]	0,04	0,04	0,04	0,04	0,04
Pipe internal diameter [m]	0,0326	0,0326	0,0326	0,0326	0,0326
Pipe thermal conductivity [W/m.K]	0,42	0,42	0,42	0,42	0,42
Pipe spacing [m]	0,1	0,08	0,11	0,08	0,08
Undisturbed ground temperature [C]	9,3	9,5	9,8	10,23	9,59
Ground thermal conductivity [W/m.K]	2,11	1,43	1,8029	2,04	2,14
Borehole thermal resistance [m.K/W]	0,184	0,11	0,16842	0,123	0,114
Fluid type	Water	11 % IPA Sprit (Ethanol)	Water	Water	Water

Table 10: Validation thermal response tests parameters.

One can see on **Figure 77 – 78** that the MATLAB-Simulink vertical borehole ground source heat exchanger model fits very well the validation experimental data. The difference between the model and the experimental data is most of the time below 0.2 °C.

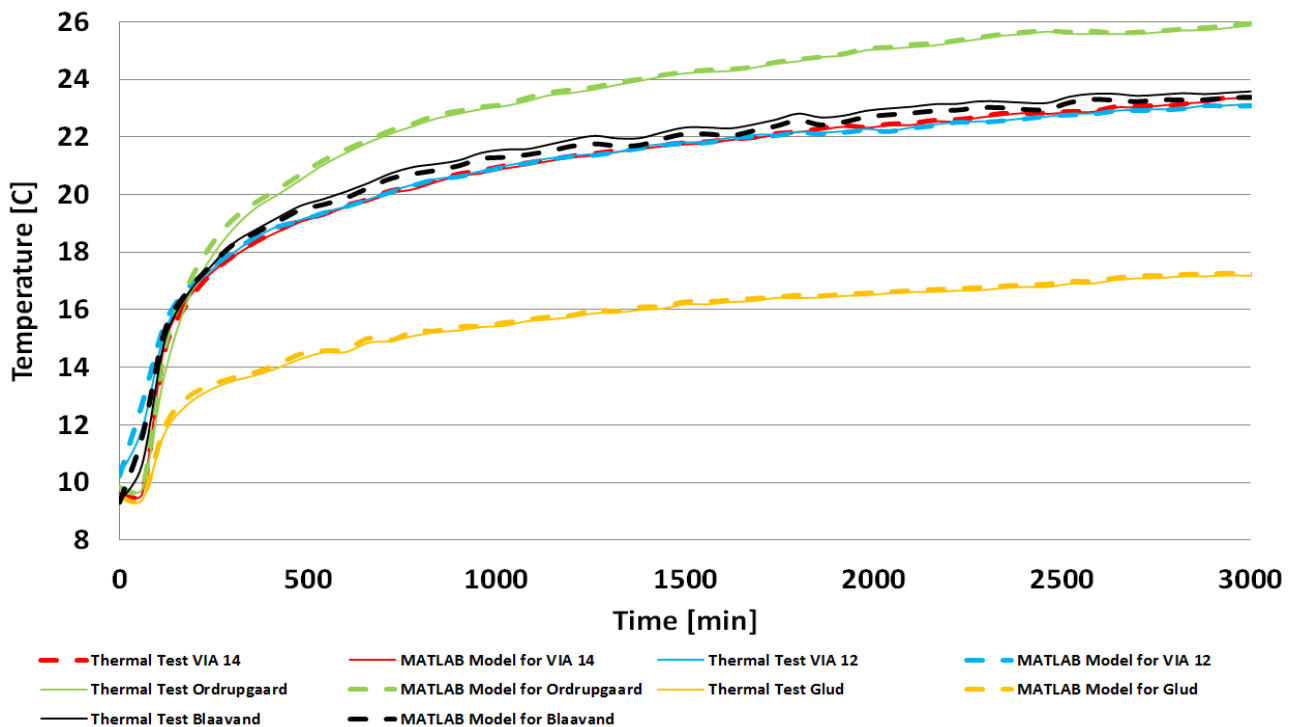


Figure 77: Vertical borehole GSHE thermal response test temperature profiles.

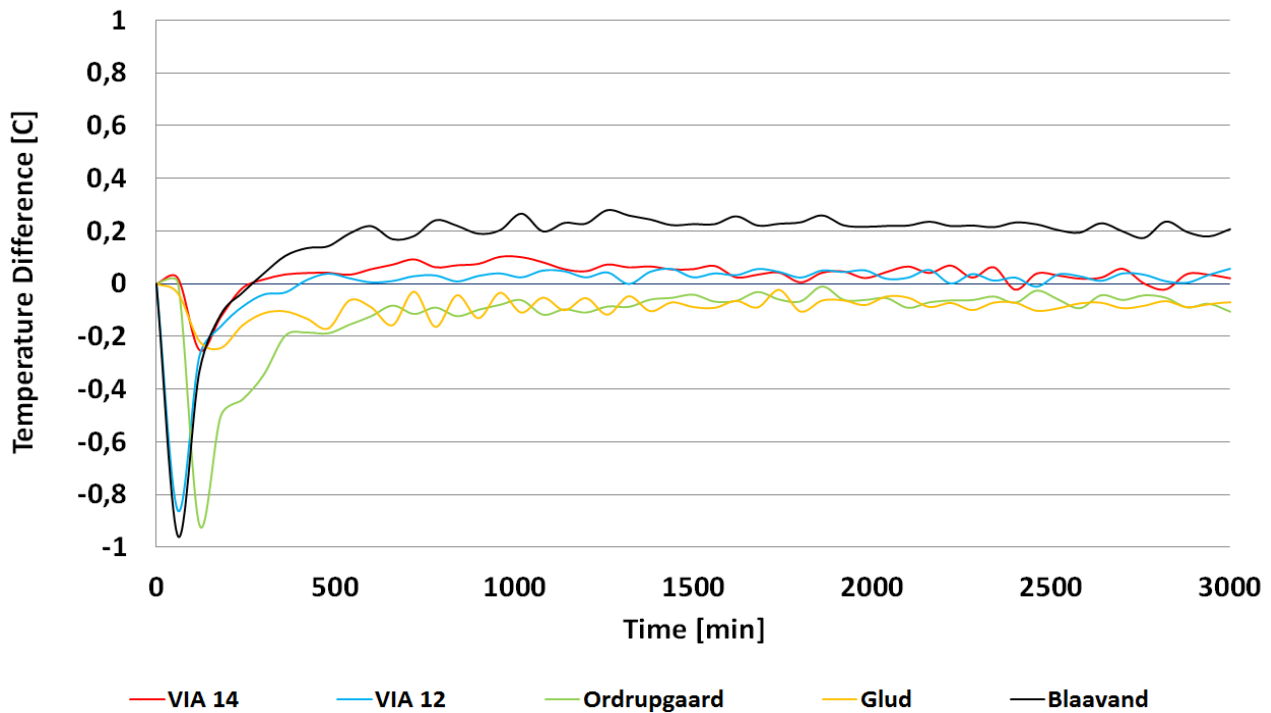


Figure 78: Difference between MATLAB-Simulink model and validation experimental data.

3.6. Validation of Phase Change Material Model with the COMSOL Software and the Guarded Hot Plate Apparatus Experimental Tests

First of all, the MATLAB implicit finite volume model with enthalpy formulation is tested for steady state conditions against the well-known and validated finite element method software COMSOL Multi-physics and analytical solution. The test sample is a 45 cm thick multi-layer wall made of concrete, stone wool, wood and metal. Each control volume is 1 cm thick. One can see on **Figure 79 – 80** that the MATLAB-Simulink model fits perfectly with the steady state analytical solution and the COMSOL reference model.

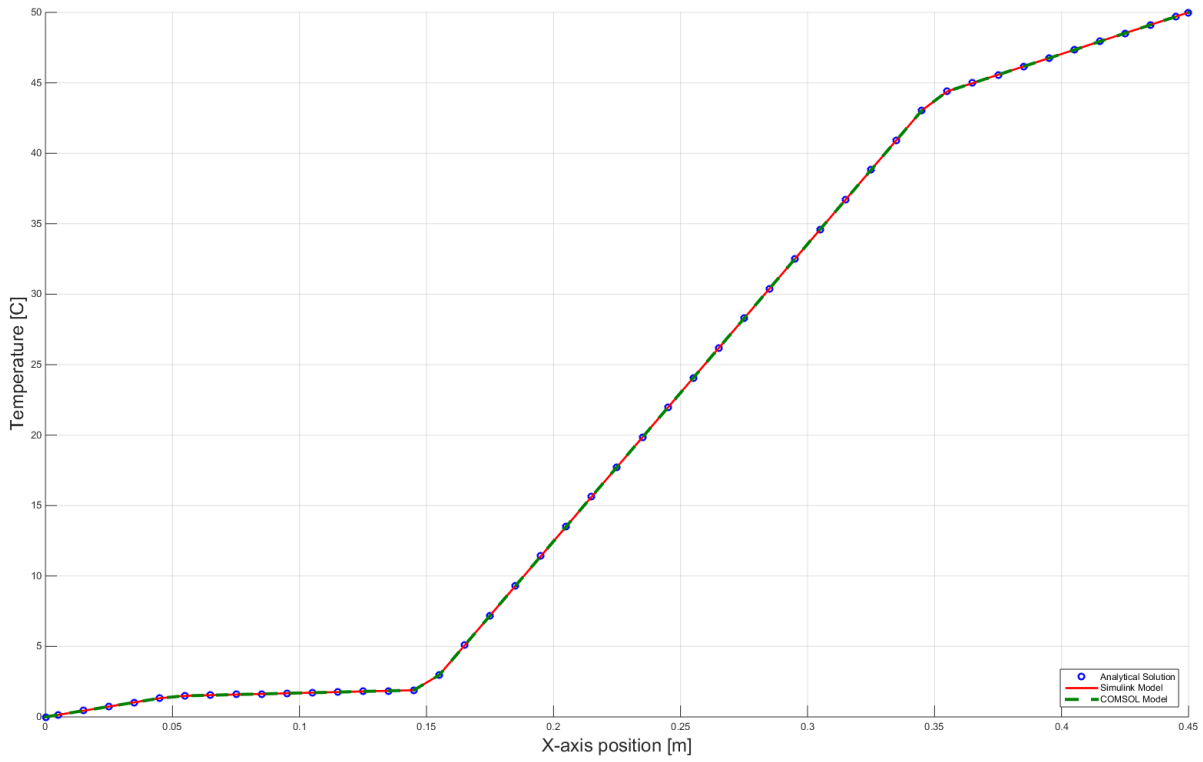


Figure 79: Steady state multi-layer wall temperature profile.

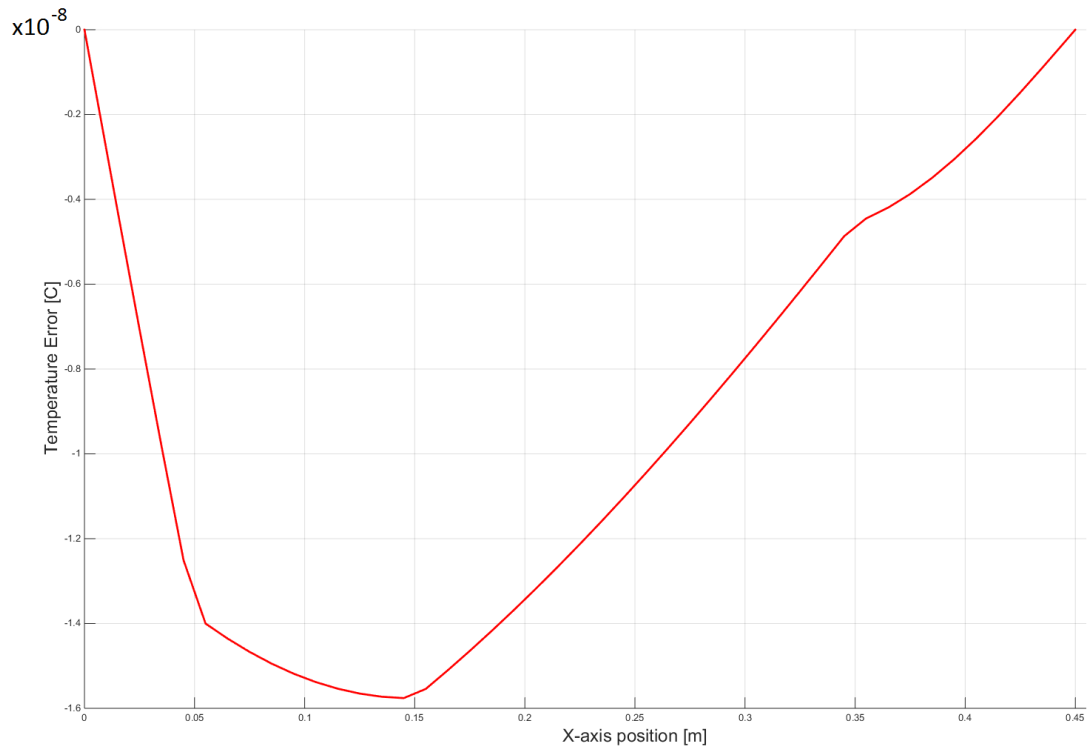


Figure 80: Absolute temperature difference between MATLAB-Simulink model and steady state analytical solution.

The MATLAB-Simulink model is then tested with dynamic boundary conditions against the COMSOL reference model. The surface heat transfer coefficients are kept constant while the surrounding temperatures are varying with time as sinusoidal functions. There is no phase transition in this test. One can see on **Figure 81 – 82** that the MATLAB-Simulink model fits very well to the COMSOL reference model. The temperature difference between the two models is most of the time below 0.02

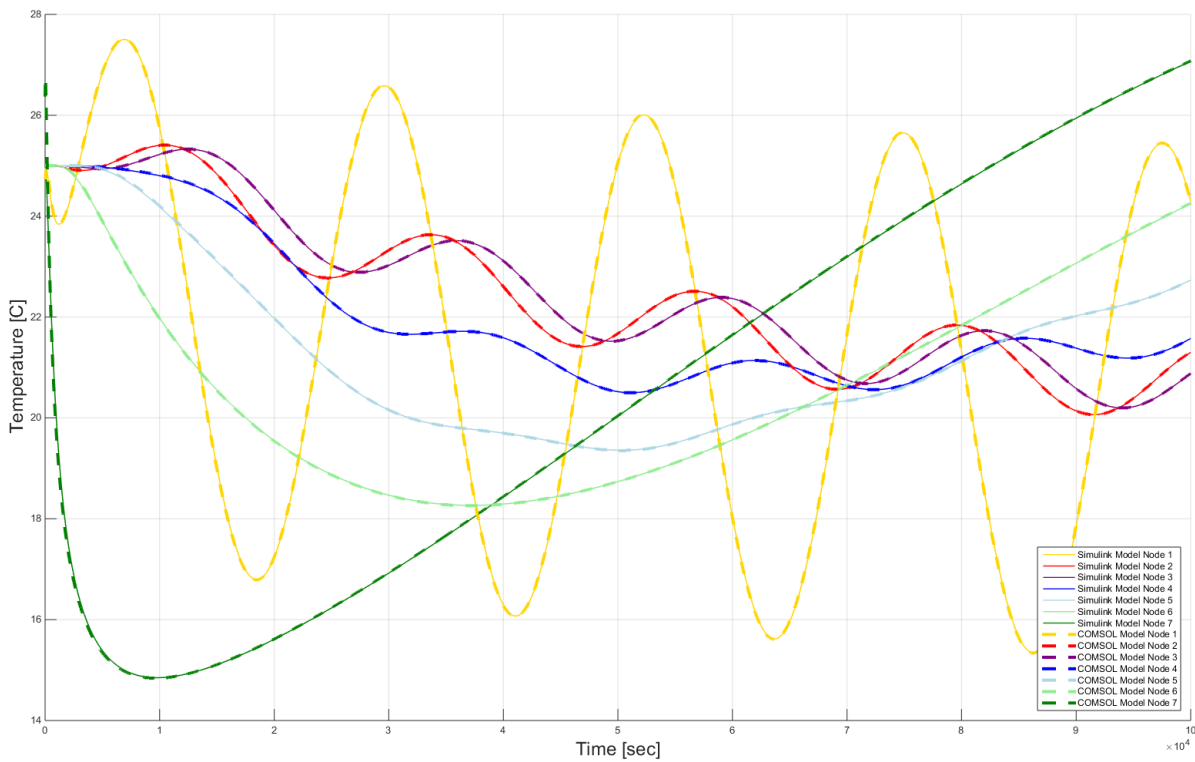


Figure 81: Temperature of the multi-layer sample test with dynamic boundary conditions.

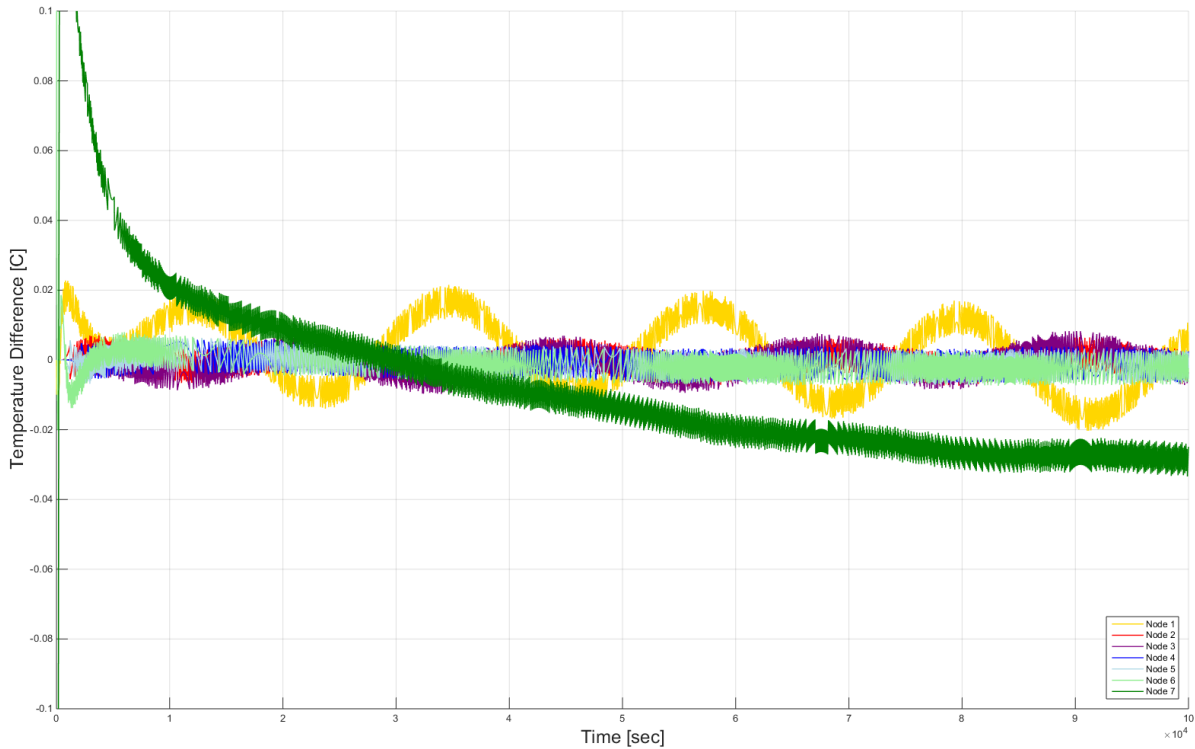


Figure 82: *Temperature difference between MATLAB-Simulink model and COMSOL reference model during the dynamic boundary conditions validation test.*

The PCM numerical model is then tested against experimental measurements performed with the hot plate apparatus in dynamic mode. 3 different PCM samples with different thickness and properties are prepared: BASF Micronal PCM paste, DuPont Energain PCM wall board and PCM plasterboard. Type K thermocouples are inserted inside the samples in order to record the temperature change in function of time. The uncertainty of the temperature measurement with the Type K Thermocouples is 0.15 °C [74]. The thermal conductivity of the samples is measured with the guarded hot plate apparatus, the heat capacity is measured with a DSC and the latent heat of fusion is taken from manufacturer's documentation. The PCM samples are placed in the guarded hot plate and a temperature increase ramp is applied while recording the temperature inside the center of the sample.

One can see on **Figure 83** that the model has good agreement for the 3 different PCM samples tested with the dynamic hot plate apparatus. However, at low temperature, the model and the experimental data have some divergence. This is due to the fact that the phase transition of the organic PCMs in tested samples occurs within a certain range of temperature while the model can only account for a phase transition at a fixed temperature. Therefore, the model underestimates the apparent total heat capacity of the material at temperatures below the average phase transition temperature.

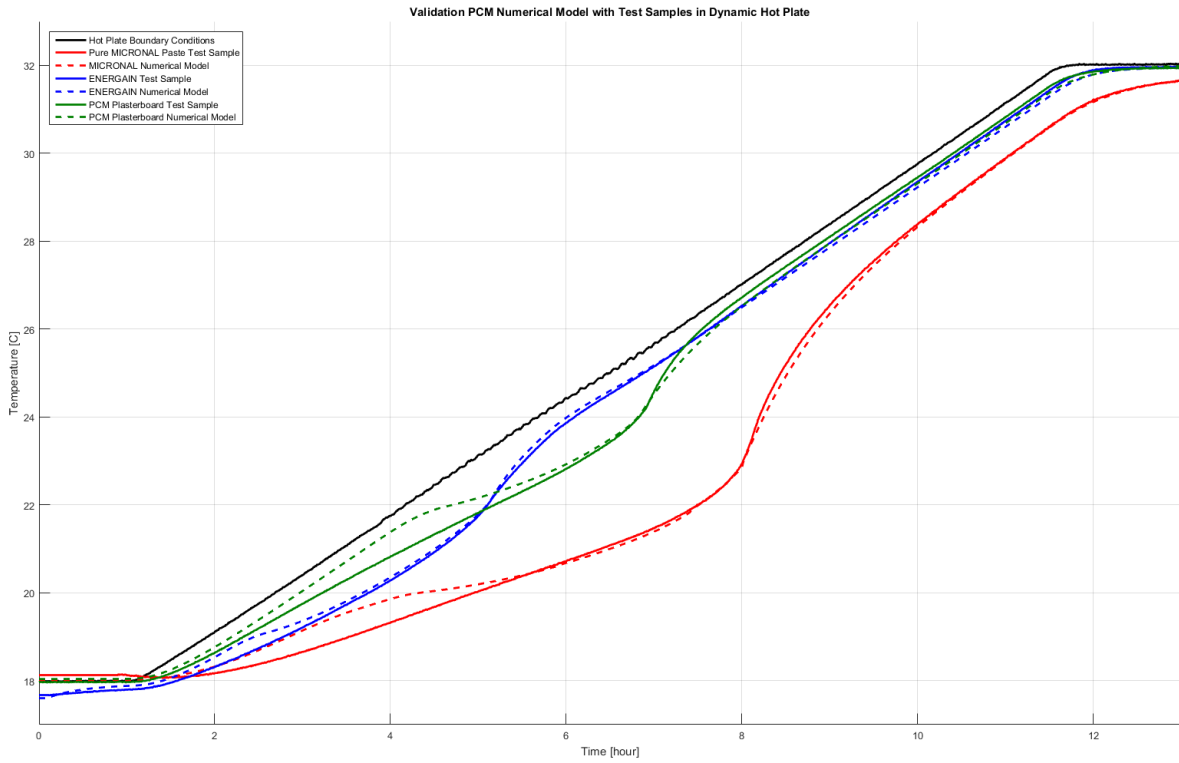


Figure 83: Guarded hot plate validation test for PCM numerical model.

Conclusion

This report presented in details the energy building numerical model used for the EnovHeat project, its different parameters and sub-systems. It has been demonstrated that this building model is able to simulate correctly the physics of dwellings with different levels of insulation and thermal masses, indoor content / furniture elements, phase change materials, heat pump systems with different heat sources and emitter configurations.

References

- [1] H. Lund, B. Möller, B.V. Mathiesen, A. Dyrelund, The role of district heating in future renewable energy systems, *Energy* 35 (3) (2010) 1381-90.
- [2] A. Palzer, H.M. Henning, A comprehensive model for the German electricity and heat sector in a future energy system with a dominant contribution from renewable energy technologies – Part II: Results, *Renewable and Sustainable Energy Reviews* 30 (2014) 1019-1034.
- [3] J. Cockroft, N. Kelly, A comparative assessment of future heat and power sources for the UK domestic sector, *Energy Conversion and Management* 47 (2006) 2349-2360.
- [4] T. Nowak, P. Westring, The European Heat Pump Association AISBL (EHPA), European heat pump market and statistics report 2015. http://www.ehpa.org/fileadmin/red/07_Market_Data/2014/EHPA_European_Heat_Pump_Market_and_Statistics_Report_2015_-_executive_Summary.pdf, 2015.
- [5] C.R.H. Bahl, EnovHeat project summary: development of efficient novel magnetocaloric heat pumps, <http://www.enovheat.dk/Research/ProjectSummary>, 2015.
- [6] H. Johra, K. Filonenko, P. Heiselberg, C. Veje, T. Lei, S. Dall'Olio, K. Engelbrecht, C. Bahl, Integration of a magnetocaloric heat pump in a low-energy residential building, *Building Simulation* (2017). <https://doi.org/10.1007/s12273-018-0428-x>
- [7] J. Le Dréau, P. Heiselberg, Energy flexibility of residential buildings using short term heat storage in the thermal mass, *Energy* 111 (2016) 991-1002.
- [8] B.V. Mathiesen, H. Lund, D. Connelly, H. Wenzel, P.A. Østergaard, B. Möller, S. Nielsen, I. Ridjan, P. Karnøe, K. Sperling, F.K. Hvelplund, Smart energy systems for coherent 100% renewable energy and transport solutions, *Applied Energy* 145 (2015) 139-154.
- [9] H. Johra, P. Heiselberg, J. Le Dréau, Numerical Analysis of the Influence of Thermal Mass, Phase Change Materials and Furniture/Indoor Content on Building Energy Flexibility, the 15th International Conference of IBPSA, San Francisco, 2017. http://www.ibpsa.org/proceedings/BS2017/BS2017_012.pdf
- [10] The Danish Ministry of Economic, Business Affairs Enterprise, and Construction Authority, Building Regulations. http://bygningsreglementet.dk/file/155699/BR10_ENGLISH.pdf, 2010.
- [11] Larsen T.S, Brunsgaard C, Komfort Husene: erfaringer, viden og inspiration. Saint-Gobain Isover a/s; 2010.
- [12] CSTB, French Building Energy and Thermal Regulation, 2012.
- [13] ClimateMaster, Tranquility Water-to-Water (TMW) Series Submittal Data Model TMW036 – 340 50Hz - HFC-410A. <http://lenergy.hu/dokuk/termekek/103/98caovp2.pdf>, 2012.
- [14] Grundfos Product Center, GRUNDFOS Data Booklet – ALPHA2 L 15-40 130 – 95047560, <https://product-selection.grundfos.com/product-detail.product-detail.html?productnumber=95047560&qcid=323188257>, 2015.
- [15] Grundfos Product Center, GRUNDFOS Data Booklet – CR1-9 A-FGJ-A-E-HQQE 3x230/400 50Hz – Grundfos Pump 96478872, <http://product-selection.grundfos.com/product-detail.product-detail.html?lang=ENU&productnumber=96478872&productrange=gma&qcid=233560216>, 2013.
- [16] European Committee for Standardization, EN 1264:2011, - Water based surface embedded heating and cooling systems, 2011.
- [17] European Committee for Standardization, EN 15377:2007 - Heating systems in buildings – Design of embedded water based surface heating and cooling system, 2007.
- [18] International Organization for Standardization, ISO 11855:2012 - Building environment design – Design, dimensioning, installation and control of embedded radiant heating and cooling systems, 2012.
- [19] Uponor GmbH, Heating and cooling solutions - Technical guidelines, 2008.
- [20] Uponor GmbH, Installation guide for underfloor heating systems - Technical information, 2013.
- [21] Energiteknologisk Udviklings og Demonstrations Program (EUDP), GeoEnergi project, <http://geoenergi.org/>, 2014.
- [22] EuroGeoSurveys, ThermoMap project, <http://www.eurogeosurveys.org/projects/thermomap/>, 2010.
- [23] Geological Survey of Denmark and Greenland, GEUS, <http://www.geus.dk/DK/Sider/default.aspx>
- [24] C. Ditlefsen, I. Sørensen, M. Slott, M. Hansen, Geological Survey of Denmark and Greenland, VIA University College, Estimating thermal conductivity from lithological descriptions – a new web-based tool for planning of ground-source heating and cooling, 2013.
- [25] D. Bertermann (FAU), C. Bialas (FAU), M. Psyk (REHAU), L. Morper-Busch (PLUS), ThermoMap MapViewer Technical Guidelines, 2011.
- [26] Verlag des Vereins Deutscher Ingenieure, VDI 4640: 2001, Thermal use of the underground - Ground source heat pump systems, 2001.
- [27] Uponor GmbH, Ground Energy Technical Information, 2012.

- [28] RETScreen International, Minister of Natural Resources Canada, Ground-Source Heat Pump Project Analysis, 2005.
- [29] H. Johra, P. Heiselberg, Influence of internal thermal mass on the indoor thermal dynamics and integration of phase change materials in furniture for building energy storage: A review, *Renewable and Sustainable Energy Reviews* 69 (2017) 19-32.
<https://doi.org/10.1016/j.rser.2016.11.145>
- [30] DuPont, Energain® - Technical Datasheet.
- [31] F. Kuznik, J. Virgone, J. Noel, Optimization of a phase change material wallboard for building use, *Applied Thermal Engineering* 28 (2008) 1291–1298.
- [32] International Organization for Standardization, ISO 13786:2007 - Thermal performance of building components – Dynamic thermal characteristics – Calculation methods, 2007.
- [33] P. Ma, L.S. Wang, Effective heat capacity of interior planar thermal mass (IPTM) subject to periodic heating and cooling, *Energy and Buildings* 47 (2012) 44-52.
- [34] A.S. Kalagasidis, C. Rode, M. Woloszyn, HAM-Tools – a whole building simulation tool in Annex 41, *Proceedings of the IEA ECBCS Annex 41 Closing Seminar*, 2008.
- [35] Danish Building Research Institute – Sbi, BSim software - User's Guide – tsbi5, 2013.
- [36] P.G. Wang, M. Scharling, K.P. Nielsen, K.B. Wittchen, C. Kern-Hansen, DMI Technical Report 13-19: 2001-2010 Danish Design Reference Year – Reference Climate Dataset for Technical Dimensioning in Building, Construction and other Sectors, 2013.
- [37] R.L. Jensen, J. Nørgaard, O. Daniels, R.O. Justesen, Person- og forbrugsprofiler: bygningsintegreret energiforsyning, DCE Technical Reports 69, [http://vbn.aau.dk/da/publications/person-og-forbrugsprofiler\(8c95574a-5bc0-4d41-9363-19932b7d9394\).html](http://vbn.aau.dk/da/publications/person-og-forbrugsprofiler(8c95574a-5bc0-4d41-9363-19932b7d9394).html), 2011.
- [38] S. Adams, M. Holmes, Determining time constants for heating and cooling coils, *Building Services Research & Information Association*, UK, 1977.
- [39] B. Glück, *Strahlungsheizung – Theorie und Praxis*, Verlag C.F Müller, Karlsruhe, 1982.
- [40] B. Glück, *Wärmeübertragung, Wärmeabgabe von Raumheizflächen und Rohren*, VED Verlag für Bauwesen, Berlin, 1989.
- [41] M. Koschenz, B. Lehmann, *Thermoaktive Bauteilsysteme*, EMPA, Dübendorf (CH), 2000.
- [42] B. Lehmann, V. Dorer, M. Koschenz, Application range of thermally activated building systems TABS, *Energy and Buildings* 39 (2007) 593-598.
- [43] M. Scarpa, K. Grau, B.W. Olesen, Development and validation of a versatile method for the calculation of heat transfer in water-based radiant systems, 11th International IBPSA Conference, Glasgow, Scotland, July 27-30, 2009.
- [44] Energy Plus Engineering Reference Manual.
- [45] University of Wisconsin-Madison Solar Energy Laboratory, TRANSSOLAR Energietechnik GmbH, CSTB, TESS, Type 31: Pipe Or Duct, in: TRNSYS 17 - Mathematical Reference, 2012, pp. 186-188.
- [46] H.J.G. Diersch, D. Bauer, W. Heidemann, W. Rühak, P. Schätzl, Finite element modeling of borehole heat exchanger systems - Part 1. Fundamentals, *Computers & Geosciences* 37 (2011) 1122-1135.
- [47] G.S. Kell, Density, thermal expansivity, and compressibility of liquid water from 0 to 150 C: correlations and tables for atmospheric pressure and saturation reviewed and expressed on 1968 temperature scale", *J Chem Eng Data* 1975 (20) 97-105.
- [48] J.B. Patterson, E.C. Morris, Measurement of absolute water density, 1–40 C, *Metrologia* 31 (1994) 277-288.
- [49] M. Tanaka, G. Girard, R. Davis, A. Peuto, N. Bignell, Recommended table for the density of water between 0 and 40 C based on recent experimental reports, *Metrologia* 38 (2001) 301-309.
- [50] Engineering tool box, http://www.engineeringtoolbox.com/ethylene-glycol-d_146.html
- [51] J.V. Sengers, J.T.R. Watson, Improved international formulations for the viscosity and thermal conductivity of water substance, *J. Phys. Chem. Ref. Data*, 15 (1986) 1291.
- [52] American Institute of Physics and American Chemical Society (IUPAC), Standard Reference Data for the Thermal Conductivity of Water, 1995.
- [53] M. Conde Engineering, Thermophysical properties of brines – Models, 2011.
- [54] K.N. Marsh, *Recommended Reference Materials for the Realization of Physicochemical Properties*, Blackwell Scientific Publications, Oxford, 1987.
- [55] Incropera, DeWitt, Bergman, Lavine, *Fundamentals of Heat and Mass Transfer*", seventh edition.
- [56] Lange's Handbook of Chemistry, 10th ed.
- [57] DOW Chemical Company, Guide to Glycols (Propylene Glycols).
- [58] DOW Chemical Company, Engineering and Operating Guide for DOWFROST, Inhibited Propylene Glycol-based Heat Transfer Fluid.
- [59] DOW Chemical Company, Engineering and Operating Guide for DOWTHERM, Inhibited Ethylene Glycol-based Heat Transfer Fluid.
- [60] MEGlobal Company, Ethylene Glycol Product Guide.
- [61] Dow Chemical Database, 2001.
- [62] ASHRAE Handbook Fundamentals, 2005.
- [63] Freezing points of methanol solutions, novosolution.ca

- [64] Å. Melinder, Thermophysical properties of aqueous solutions used as secondary working fluids, PhD Thesis, Royal Institute of Technology, Stockholm, Sweden, 2007.
- [65] GeoPro. Inc, Borehole Heat Exchanger Head Loss Calculation Excel Sheet.
- [66] G. Angrisani, M. Canelli, C. Roselli, M. Sasso, Calibration and validation of a thermal energy storage model: influence on simulation results, *Applied Thermal Engineering* 67 (2014) 190-200.
- [67] R. Prapainop, K. Maneeratana, Simulation of ice formation by the finite volume method, *Songklanakarin J. Sci. Technol.*, 26(1) (2004) 55-70.
- [68] Verma P, Varun, Singal S.K. Review of mathematical modeling on latent heat thermal energy storage systems using phase-change material. *Renewable and Sustainable Energy Reviews* 12 (2008) 999-1031.
- [69] IEA-EBC Annex 43 Project, <http://www.ecbcs.org/annexes/annex43.htm>
- [70] ANSI/ASHRAE Standard 140-2011. Standard method of test for the evaluation of building energy analysis computer programs, 2011.
- [71] S.E. Poulsen, M. Alberdi-Pagola, Thermal Response Test and temperature profiles at Kongestien 45, Virum (Denmark), Research output report, [http://vbn.aau.dk/en/publications/thermal-response-test-and-temperature-profiles-at-kongestien-45-virum-denmark\(243a4fef-e879-47db-9246-99b3cb487e8a\).html](http://vbn.aau.dk/en/publications/thermal-response-test-and-temperature-profiles-at-kongestien-45-virum-denmark(243a4fef-e879-47db-9246-99b3cb487e8a).html), 2015.
- [72] S.E. Poulsen, M. Alberdi-Pagola, Thermal Response Test at Ordrupgaard Museum, Ordrupgaard (Denmark), [http://vbn.aau.dk/en/publications/thermal-response-test-at-ordrupgaard-museum-ordrupgaard-denmark\(490330c0-790e-4a38-9c37-43c1bd85ec7a\).html](http://vbn.aau.dk/en/publications/thermal-response-test-at-ordrupgaard-museum-ordrupgaard-denmark(490330c0-790e-4a38-9c37-43c1bd85ec7a).html), 2015.
- [73] S.E. Poulsen, M. Alberdi-Pagola, Interpretation of ongoing thermal response tests of vertical (BHE) borehole heat exchangers with predictive uncertainty based stopping criterion, *Energy* 88 (2015) 157-167.
<https://doi.org/10.1016/j.energy.2015.03.133>
- [74] J. Le Dreau, P. Heiselberg, R.L. Jensen, Experimental data from a full-scale facility investigating radiant and convective terminals: Uncertainty and sensitivity analysis, Description of the experimental data, DCE Technical Reports 168, [http://vbn.aau.dk/da/publications/experimental-data-from-a-fullscale-facility-investigating-radiant-and-convective-terminals\(1ce46b33-cfa8-4979-b112-cd9ab487f9c7\).html](http://vbn.aau.dk/da/publications/experimental-data-from-a-fullscale-facility-investigating-radiant-and-convective-terminals(1ce46b33-cfa8-4979-b112-cd9ab487f9c7).html), 2014.

ISSN 1901-726X

DCE Technical Report No. 238

SUMMARY

To prevent future energy crisis and tackle the problems of climate change, modern society must promote a radical evolution in our energy systems. The building sector, and in particular its heating needs, have clearly been identified as one of the main targets for the reduction of the global energy usage. In addition, buildings are a key actor for the development of renewable energy sources. The main objective of this research study is to investigate and demonstrate the possibility of integrating an innovative magnetocaloric heat pump in a single-family house under Danish weather conditions. Moreover, the study includes a numerical analysis to increase the understanding of the heating energy flexibility potential of residential buildings using thermal storage in the indoor environment.